QA: QA

MDL-NBS-HS-000023 REV 01

May 2007

Simulation of Net Infiltration for Present-Day and Potential Future Climates

THIS DOCUMENT CONTAINS THE FOLLOWING, LOCATED AT THE BACK OF THE DOCUMENT:
1) ADDENDUM 001, DATED 01/28/2008

Prepared for:
U.S. Department of Energy
Office of Civilian Radioactive Waste Management
Office of Repository Development
1551 Hillshire Drive
Las Vegas, Nevada 89134-6321

Prepared by:
Sandia National Laboratories
OCRWM Lead Laboratory for Repository Systems
1180 Town Center Drive
Las Vegas, Nevada 89144

Under Contract Number:
DE-AC04-94AL85000

DISCLAIMER

This report was prepared as an account of work sponsored by an agency of the United States Government. Neither the United States Government nor any agency thereof, nor any of their employees, nor any of their contractors, subcontractors or their employees, makes any warranty, express or implied, or assumes any legal liability or responsibility for the accuracy, completeness, or any third party's use or the results of such use of any information, apparatus, product, or process disclosed, or represents that its use would not infringe privately owned rights. Reference herein to any specific commercial product, process, or service by trade name, trademark, manufacturer, or otherwise, does not necessarily constitute or imply its endorsement, recommendation, or favoring by the United States Government or any agency thereof or its contractors or subcontractors. The views and opinions of authors expressed herein do not necessarily state or reflect those of the United States Government or any agency thereof.

QA: QA

Simulation of Net Infiltration for Present-Day and Potential Future Climates

MDL-NBS-HS-000023 REV 01

May 2007

ACKNOWLEDGMENTS

This work relied on the expertise and hard work from a list of individuals too long to list here. The main technical contributors including their areas of responsibility are listed below:

Joshua Stein (SNL)	Lead author, project integrator, and team lead.
Al Reed (SNL)	Conceptual model development, MASSIF model developer, model validation (comparison to streamflow measurements)
Dan Levitt (LANL)	Conceptual model development and model validation (comparison to site-specific datasets)
John Stormont (UNM)	Conceptual model development
David Groeneveld (HydroBio)	Evapotranspiration model development and satellite measurement of vegetation
Bob Walsh (Apogen)	Stochastic precipitation model development, Parameter and model uncertainty
John Del Mar (Apogen)	Parameter and model uncertainty
Cedric Sallaberry (SNL)	Stochastic precipitation model development, uncertainty and sensitivity analysis
Rick Allen (UI)	Evapotranspiration model development (FAO-56 consultation and model development of solar radiation on slopes)
Kaylie Rasmuson (BSC)	Evapotranspiration model development (Site specific vegetation)
Elena Kalinina (GRAM)	Model validation (Lysimeter simulations and HYDRUS comparisons)
Joseph Kanney (SNL)	Model validation (comparison to regional net infiltration estimates)

INTENTIONALLY LEFT BLANK

Model Signature Page/Change History

Complete only applicable items.

1. Total Pages: ~~944~~ 942
CNH 5/24/07

2. Type of Mathematical Model

☒ Process Model ☐ Abstraction Model ☐ System Model

Describe Intended Use of Model

The purpose of the model documented in this report is to provide a spatial representation, including uncertainty, of the predicted average annual net infiltration at the Yucca Mountain site during three climates scenarios predicted for the next 10,000 years.

3. Title

Simulation of Net Infiltration for Present-Day and Potential Future Climates

4. DI (including Revision No. and Addendum No.):

MDL-NBS-HS-000023 REV 01

	Printed Name	Signature	Date
5. Originator	Joshua S. Stein	Joshua S. Stein	5/24/2007
6. Independent Technical Reviewer	Charles Haukwa	[signature]	5/24/07
7. Checker	Earl Mattson	Earl D. Mattson	5/24/07
8. QCS/Lead Lab QA Reviewer	Brian Mitcheltree	[signature]	5/24/07
9. Responsible Manager/Lead	Cliff Ho	Clifford K. Ho	5/24/2007
10. Responsible Manager	Stephanie Kuzio	[signature]	5/24/2007

11. Remarks

Change History

12. Revision No. and Addendum No.	13. Description of Change
REV 00	Initial Issue This report is a revision of the report by the same title, Document Identifier ANL-NBS-HS-000032 (USGS 2003 [DIRS 166518]). In this new model report, changes were made in response to recommendations from the Regulatory Integration Team/Natural Systems Team. The entire model documentation was revised. Changes were too extensive to use Step 5.8f)1) per AP-SIII.10Q, REV 02, ICN 07.

REV 01	This report is an extensive rework of the previous revision. A new model, MASSIF (Mass Accounting System for Soil Infiltration and Flow) was developed. Changes were too extensive to use change bars. Upon completion of this report, the following 14 Condition Reports (CRs) are closed: CRs 2842, 3551, 5071, 5222, 5356, 5698, 5907, 6312, 6334, 6938, 7184, 7589, 7729, and 9227. There are no actions associated with this report for the following open CRs: 7626—is an opportunity for improvement. The reevaluation of input data for CR 7627 was considered exemplary and therefore a lessons-learned is required so the method used might be generally applied to other License Application documents. 7627—requires reevaluation of 68 DTNs that were shown as "Qualified" in the TDMS and were used as direct input to the previous version of this report. However, none are used as direct input to this revision. If appropriate, the qualification status of some DTNs will be changed, but that will not affect this revision. CR 9580—identifies preliminary output files from this document as containing errors; however, this revision shows these output files were rerun with errors corrected. A separate in-process data qualification report is qualifying the preliminary data for use as the errors were tolerably small. CR 10472—concerns a suspected error in streamflow measurements used to validate the MASSIF model. The model has been validated successfully with the existing streamflow data; if the resolution of the CR confirms this suspected error, it would provide further support to validation of the MASSIF model.

CONTENTS

Page

CONTENTS (Continued)

Page

CONTENTS (Continued)

Page

CONTENTS (Continued)

Page

CONTENTS (Continued)

Page

INTENTIONALLY LEFT BLANK

FIGURES

Page

FIGURES (Continued)

Page

FIGURES (Continued)

Page

FIGURES (Continued)

Page

FIGURES (Continued)

Page

FIGURES (Continued)

Page

FIGURES (Continued)

Page

FIGURES (Continued)

Page

FIGURES (Continued)

Page

FIGURES (Continued)

Page

FIGURES (Continued)

Page

INTENTIONALLY LEFT BLANK

TABLES

Page

TABLES (Continued)

Page

TABLES (Continued)

Page

TABLES (Continued)

Page

TABLES (Continued)

Page

TABLES (Continued)

Page

TABLES (Continued)

Page

TABLES (Continued)

Page

TABLES (Continued)

Page

INTENTIONALLY LEFT BLANK

ACRONYMS AND ABBREVIATIONS

B.P.	before present
BSC	Bechtel SAIC Company
CDF	cumulative distribution functions
cm	centimeter
CMB	chloride mass balance
COL	*Coleogyne* vegetation association
COTS	commercial-off-the-shelf
DEM	digital elevation model
DIRS	Document Input Reference System
DOE	U.S. Department of Energy
DOQQ	Digital Ortho-Quarterquad (from U.S. Geological Survey)
DOS	dark object subtraction
DOY	day of the year
DTN	data tracking number
E	amount of water evaporated from a unit cell
ENVI	Environment for Visualizing Images
EPA	U.S. Environmental Protection Agency
EROS	Earth Resources Observation and Science
ESF	Exploratory Studies Facility
ESP	ecological study plot
ESRI	Environmental Systems Research Institute
ET	evapotranspiration
ET_0	reference evapotranspiration
FACE	(Nevada) Free-Air CO_2 Enrichment Facility
FAO	Food and Agricultural Organization of the United Nations
FAO-56	Food and Agricultural Organization of the United Nations [FAO] Irrigation and Drainage Paper 56
fc	fraction covered
FC	field capacity
FEP	feature, event, or process
few	fraction exposed and wetted
GCP	ground control point
GFM	geologic framework model
GIS	geographic information system
GTC	Glacial Transition Climate
HC	holding capacity
HELP	Hydrologic Evaluation of Landfill Performance
IBP	International Biological Program

ACRONYMS AND ABBREVIATIONS (Continued)

IHU	infiltration hydrogeologic unit
IWCF	initial water content fraction
KTI	key technical issue
LA	*Larrea-Ambrosia* vegetation association
LAI	leaf area index
LG	*Lycium-Grayia* vegetation association
LHS	Latin Hypercube Sampling
LLG	*Larrea-Lycium-Grayia* vegetation association
LN m	lognormal mean
LSC	Lower Sheep Creek
LSCE	Lower Sheep Creek East
LSCW	Lower Sheep Creek West
LU	loguniform
m	meter
MAP	mean annual precipitation
MASSIF	Mass Accounting System for Soil Infiltration and Flow
MAT	mean annual temperature
MC	Monsoon Climate
MCMC	Markov Chain Monte Carlo
ME	Maxey-Eakin
mm	millimeter
MME	modified Maxey-Eakin
MPa	mega Pascal
MRC	moisture retention curve
MS	Microsoft
N	normal
NDVI	Normalized Difference Vegetation Index
NDVI'	NDVI corrected for the Yucca Mountain environment
NED	national elevation dataset
NIR	near infrared
NOAA	National Oceanic and Atmospheric Administration
NRC	U.S. Nuclear Regulatory Commission
NTS	Nevada Test Site
NWRC	Northwest Watershed Research Center
PC	personal computer
PET	potential evapotranspiration
PT	potential transpiration
PVR	potential vegetation response

ACRONYMS AND ABBREVIATIONS (Continued)

QA	Quality Assurance
RAW	readily available water
RCEW	Reynolds Creek Experimental Watershed
REW	readily evaporated water
RH	relative humidity
RMS	root mean square
ROI	region of interest
RWMS	Radioactive Waste Management Site
SRC	Standardized Regression Coefficients
SRRC	Standardized Rank Regression Coefficients
SRTM	Shuttle Radar Topography Mission
STN	software tracking number
SZ	saturated zone
TAW	total available water
TDMS	Technical Data Management System
TEW	total amount of water available for evaporation
TM	thematic mapper
TSPA	total system performance assessment
TWP	technical work plan
U	uniform
USDA	U.S. Department of Agriculture
USGS	United States Geological Survey
UTM	Universal Transverse Mercator
UZ	unsaturated zone
WB	water budget
WHC	water holding capacity
WY	water year
WYDOY	water year day of year
YM	Yucca Mountain
YMP	Yucca Mountain Project
YMRP	*Yucca Mountain Review Plan, Final Report*
ZFP	zero flux plane

INTENTIONALLY LEFT BLANK

1. PURPOSE

1.1 INTENDED USE

This model report documents the development and validation of a conceptual, mathematical, and numerical model for predicting net infiltration of water into the unsaturated zone. The model applies a simple water mass-balance approach to the near surface layer that is influenced by evapotranspiration. It uses a simplified representation of downward water flow whereby water moves from the top soil layer downward by sequentially filling each layer to "field capacity" before draining to the layer below. Water is removed from the "root zone" by evapotranspiration, which is represented using an empirical model based on reference evapotranspiration, transpiration coefficients, and moisture content in the root zone. Water is redistributed as surface runoff when the soil cannot accept all the available water at the surface. Precipitation is stochastically simulated on a daily timestep based on observed weather records.

This report also documents the use of the model for predicting the range and patterns of net infiltration at the Yucca Mountain site for the next 10,000 years. *Future Climate Analysis* (BSC 2004 [DIRS 170002], Section 7.1) forecasts three distinct climates during the next 10,000 years at Yucca Mountain. The present-day climate is predicted to persist for the next 400 to 600 years, followed by a warmer and much wetter monsoon climate lasting from 900 to 1,400 years. Following the monsoon climate, a cooler and wetter glacial-transition climate is expected. The work in this report provides an estimate of the net infiltration up to 10,000 years into the future for the Yucca Mountain Site.

Additional provisions in 10 CFR 63.341 [DIRS 176544] require the U.S. Department of Energy (DOE) to assess the peak dose that would occur after 10,000 years. The U.S. Nuclear Regulatory Commission (NRC) released proposed rules (70 FR 53313 [DIRS 178394]) that DOE represent the effects of climate change after 10,000 years by assuming that deep percolation rates vary between 13 to 64 mm/yr. Predictions of peak dose after 10,000 years are expected to utilize the deep percolation rates as proposed by the NRC.

The specific purpose of the model documented in this report is to provide a spatial representation, including epistemic and aleatory uncertainty, of the predicted mean annual net infiltration at the Yucca Mountain site during each climate. The resulting maps of mean annual net infiltration provide input directly to the updated versions of the following model reports:

- *UZ Flow Models and Submodels* (BSC 2004 [DIRS 169861])
- *Calibrated Properties Model* (BSC 2004 [DIRS 169857]).

Information from this model report indirectly feeds total system performance assessment (TSPA) through its connection with the identified downstream products. This model is not intended to be a direct input to TSPA.

Daily precipitation provides water for potential infiltration. The infiltration model simulates processes occurring in and on the soil, including return of water vapor to the atmosphere by evaporation and plant transpiration (evapotranspiration), flow along the ground surface (runoff/run-on), and infiltration into the bedrock below the soil.

This complete revision of the infiltration model report is developed in accordance with *Technical Work Plan for: Infiltration Model Assessment, Revision, and Analyses of Downstream Impacts* (BSC 2006 [DIRS 177492], Section 1.1.4). The purpose of the revision is to increase confidence in the results by improving the traceability, transparency, and reproducibility of the model development, the selection of inputs for calculations, and the determination of net infiltration maps and fluxes. To those ends, this revision includes the following changes:

- A Mathcad calculation, MASSIF (Mass Accounting System for Soil Infiltration and Flow), replaces the INFIL software (INFIL VV2.0, STN: 10307-2.0-00 [DIRS 139422]; INFIL VVA_2.a1. 2001, STN: 10253-A_2.a1-00 [DIRS 147608]) used in the previous revision of this report (BSC 2004 [DIRS 170007]), while the underlying conceptual models for MASSIF and INFIL remains similar. The reasons for replacing the INFIL software and completely revising the previous revision of this report are explained in a DOE report (DOE 2007 [DIRS 180680], Sections 5.2 and 5.3).

- This revision includes an uncertainty analysis, replacing and expanding work included in *Analysis of Infiltration Uncertainty* (BSC 2003 [DIRS 165991]).

- Instead of taking input directly from multi-decade precipitation records, those records provide the basis for the development of stochastic parameters. Precipitation inputs are selected from 1,000-year stochastic simulations, assuring that the full range of annual precipitation uncertainty is considered, including years with heavy precipitation. Ten representative years are selected from the 1,000-year simulations for each climate state.

- An evapotranspiration submodel, based on guidelines published by the Food and Agriculture Organization (FAO) of the United Nations in Irrigation and Drainage Paper 56 (FAO-56), replaces the submodel that was used in INFIL. The guidelines are based on a combination FAO Penman-Monteith model (Allen et al. 1998 [DIRS 157311], Preface).

- All previous inputs to the infiltration calculations have been revised or requalified.

1.2 LIMITATIONS

This section presents a list of limitations associated with the net infiltration model estimates presented in this report. These limitations arise from a number of sources, including limited knowledge of the system, simplifications invoked to represent the system, and general uncertainties.

The estimates of mean annual net infiltration at the soil–bedrock interface are made without consideration of how the properties of the rock at deeper locations vary with depth. Instead of net infiltration, some authors call this quantity “deep drainage” or “potential recharge.” *UZ Flow Models and Submodels* (BSC 2004 [DIRS 169861]) describes the method for calculating replenishment of the aquifer from the surface, “recharge,” taking into consideration the potential recharge as well as the complex, three-dimensional hydrogeologic structure and properties of the fractured bedrock and other considerations.

One consideration is the possibility that a significant fraction of the water that enters bedrock is lost to evaporation in the Tiva Canyon welded tuff (TCw). Such a water loss has been suggested by researchers looking at the stable oxygen isotopic chemistry of secondary calcite deposited in the TCw (Whelan et al. 2002 [DIRS 160442], pp. 743 to 744; Figure 8). This study suggests that evaporation losses from the unsaturated zone (UZ) may extend to the top of the Paintbrush nonwelded unit (PTn), which means that evaporative losses from the UZ may extend as deep as 100 m below the surface (Whelan et al. 2002 [DIRS 160442], Figure 8). The net infiltration model domain described in this report extends only from the surface to the soil–bedrock interface, and the net infiltration flux includes all water that moves downward across this interface. The current UZ flow model (BSC 2004 [DIRS 169861]) does not explicity allow water to evaporate from the UZ domain. Therefore, evaporation from the TCw is not explicitly captured by either of these models. However, the resulting UZ flow fields predicted by the UZ flow model (BSC 2004 [DIRS 169861]) are weighted by comparing UZ model results to thermal and chemical data observed in the UZ domain (deeper than the net infiltration modeling domain). These datasets generally indicate that percolation rates below the TCw are lower than the net infiltration predicted above the TCw. Thus, the UZ model assigns higher weights to the lower range of the net infiltration distribution and therefore may indirectly account for water loss in the TCw.

The model documented in this report is valid only for the Yucca Mountain site and for the climates specified in *Future Climate Analysis* (BSC 2004 [DIRS 170002], Section 7.1). For each climate, the model produces maps of average annual infiltration as a function of location, with no time dependence. These output maps cover the variability and range of uncertainty in average annual net infiltration over the modeling domain.

Infiltration predictions are limited by the uncertainty in future weather patterns. Although a substantial body of literature supports the use of stochastic precipitation models, there are no records to support extrapolation of historical weather records from the last few decades to 1,000 years. Each available and relatively complete precipitation record, whether from the Yucca Mountain site, from a nearby weather station, or from a site representative of a future climate, covers no more than about 60 years. The methods used to represent future climate conditions for this model are described in Section 6.5.1 and Appendix F.

Infiltration predictions are also limited by uncertainties in the hydrologic properties of the soil and upper zone of the fractured bedrock that covers the 125-km^2 infiltration modeling domain. These uncertainties arise primarily from several sources. The first is the use of a pedotransfer function to estimate soil hydrologic properties from measured grain size distributions. This work is documented and the resulting soil properties are qualified for use in *Data Analysis for Infiltration Modeling: Development of Soil Units and Associated Hydraulic Parameter Values* (BSC 2006 [DIRS 176335]). The pedotransfer approach introduces uncertainty due to the fact that the Hanford soil property database represents soils in a location and depositional environment that is different from Yucca Mountain (Hanford, WA). Another source of uncertainty is in the saturated conductivity of the bedrock at the soil–bedrock interface. This parameter set is based on work documented in *Data Analysis for Infiltration Modeling: Bedrock Saturated Hydraulic Conductivity Calculation* (BSC 2006 [DIRS 176355]). The saturated conductivity values and uncertainty are based on measurements of fracture apertures, fracture densities, saturated conductivities of bedrock matrix and fracture filling material, and a model of

conductivity based on the combination of these measurements. For each bedrock type, the lower end of the conductivity uncertainty range assumes completely filled fractures, and the upper end of the conductivity uncertainty range assumes a small open fracture component in each of the filled fractures. When multiple bedrock types are included in the uncertainty analysis, the extent of fracture filling can vary independantly between rock types (see Sections 6.5.2.5 and 6.5.2.6). However, a limitation of this approach is that heterogeneity within a bedrock type is not represented. Because this approach is based on indirect measurements of saturated conductivity, there is a potential for significant model uncertainty in the results of the conductivity estimates.

Uncertainty in the soil depth representing the zone of shallow soils is significant. The upscaled value of soil depth for the shallow soil depth class varies by a factor of 5 (see Section 6.5.2.4). Such variation is the result of the fact that very few qualified measurements of soil depth were available upon which to base a model of soil depth across the site. As shallow soil depth is shown to be the most significant physical parameter influencing mean net infiltration, the uncertainty in this parameter represents an important limitation on the accuracy of the mean net infiltration over the site.

Despite the intent of estimating the spatial distribution of mean annual net infiltration across the model domain, the accuracy of net infiltration estimates at any one location is limited by uncertainties in soil, bedrock, and vegetation properties at that location. As described briefly above, there are few direct measurements of soil and rock properties at Yucca Mountain. In order to run the model, it was necessary to define these properties for every 30 × 30-m grid cell in the infiltration modeling domain. The approach taken was to upscale and group the few available measurements and estimates for properties. This approach assumes that small scale variations in soil and rock properties are not as significant as variations that occur between different soil and rock types. This assumption is valid as long as small scale spatial variations in net infiltration are not important for downstream users. An example of this limitation is the answer to the question of whether net infiltration at Yucca Mountain is focused beneath stream channels. The results of the uncertainty analysis described in Section 6.5.7 indicate that little to no net infiltration occurs beneath stream channels where soil is especially thick. However, in Sections 7.1.3.1 and 7.1.3.2, it is shown that this particular result is very sensitive to the spatial distribution of soil conductivity. Since there is very little direct information about such a spatial distribution, there is considerable and significant uncertainty in the spatial distribution of net infiltration results. Furthermore, because soil and bedrock properties are represented as uniform over a spatial area assumed to define a given soil or rock type, the actual spatial variability of net infiltration is likely underestimated by the model. In addition, other processes that might effect the spatial distribution of net infiltration on a local scale (e.g., interflow) are assumed to be insignificant and are not included in the model (Section 5).

Finally, it should be stressed that the approach used to estimate water flow and storage within the rootzone is a simplification of the actual physical processes that control flow in this environment. The use of the “field capacity” concept acts as a flow switch allowing downward water flow at a rate equal to the saturated hydraulic conductivity when the average water content in a layer equals or exceeds “field capacity,” and allowing no flow to occur when average water content in a layer is less than “field capacity.” In reality, water will flow within the vadose zone in response to gradients in total soil-water potential, which is the sum of various components such

as elevation, matric, pressure, temperature, and osmotic potentials. This approximation is discussed more fully in Sections 5 and 6.4.

1.3 SCOPE OF THIS DOCUMENT

Sections 2 through 5 of this document address topics including quality assurance (QA), software, qualified inputs, and other prerequisites to a detailed discussion of model development and implementation, which is discussed in Section 6. Section 2 identifies the overall QA requirements and methods that were applied during model development and calculations. Section 3 identifies both qualified and exempt software used in the technical effort. Lists of qualified direct inputs are the primary content of Section 4. Section 5 documents assumptions used in the absence of direct confirming data or evidence.

The principal technical discussions are in Section 6. That discussion includes the conceptual model, the mathematical model, and the implementation as a Mathcad calculation (MASSIF), in Sections 6.1 through 6.4. Sections 6.5 through 6.7 discuss the development of site-specific climate inputs, a site-specific geospatial database, sensitivity studies, the treatment of uncertainty, and the results of calculations for the three climates.

Section 7 addresses validation of the model. The technical work plan (TWP) (BSC 2006 [DIRS 177492], Section 2.2.1) specifies the validation activities and validation criteria for this model.

The conclusions of this report appear in Section 8. They include a list of technical data items that are output from this product.

In order to improve the readability of this report, many technical details are included in appendices at the end of the report. More detailed technical information is available from the Technical Data Management System (TDMS), using data tracking numbers (DTNs) provided throughout this report.

Work documented in this report addresses the open Key Technical Issue (KTI): USFIC 3.01, *Monte Carlo approach for estimating net infiltration* (BSC 2004 [DIRS 180945], Appendix D). That KTI documented concerns that high net infiltration values in the statistical distribution of net infiltration estimates were not being adequately represented by the outputs of the previous analysis. The present model analysis is a complete revision to the previous estimates and does explicitly include representation of the upper end of the net infiltration uncertainty distribution. This work does not specifically evaluate impacts to closed KTIs supported by previous models of net infiltration.

1.4 DEVIATIONS FROM THE TECHNICAL WORK PLAN

One deviation from the TWP (BSC 2006 [DIRS 177492]) relates to the use of neutron logging data from 99 boreholes in the vicinity of Yucca Mountain. The TWP (BSC 2006 [DIRS 177492], Section 2.2.1.5) states the following:

> The neutron log data will be used for post-model validation by comparing the infiltration values (averaged over areas of similar infiltration characteristics such as similar soil type or thickness) to the area averaged values from MASSIF. The range of uncertainty of the infiltration values must overlap to allow validation to be accepted.

After examining the neutron data and reviewing the methods used to estimate net infiltration flux at each neutron borehole, this comparison was determined to be of limited use for the model development and validation and therefore was not used. See Section 7.2.1.1.3 for a discussion of the neutron logging data.

Another minor deviation from the TWP relates to the use of the soil lysimeter data from the Nevada Test Site (NTS). The TWP states that these data "are available in support of this post-model validation activity." In fact, the lysimeter data are used for confidence building during model development (Section 7.1.2.1) and not for post-model validation.

2. QUALITY ASSURANCE

Planning and preparation of this report was initiated under the Bechtel SAIC Company (BSC) Quality Assurance (QA) Program. Therefore, forms and associated documentation prepared prior to October 2, 2006, the date this work transitioned to the Lead Laboratory, were completed in accordance with BSC procedures as identified in Section 4.1 of the TWP (BSC 2006 [DIRS 177492]. Forms and associated documentation completed on or after October 2, 2006, were prepared in accordance with Lead Laboratory procedures.

Development of this model report and the supporting modeling activities are subject to the Yucca Mountain Project QA program, as indicated in the TWP (BSC 2006 [DIRS 177492], Section 8.1). Approved QA procedures (BSC 2006 [DIRS 177492], Section 4.1) have been used to conduct and document the activities described in this model report. The TWP also identifies the methods used to control the electronic management of data (BSC 2006 [DIRS 177492], Section 8.4). The modeling activities and associated calculations herein were conducted and documented following SCI-PRO-006, *Models*.

This model report provides simulation results for infiltration into the UZ under present and potential future climates. The UZ (including soil and rock above the water table) is part of natural barriers that are classified in *Q-List* (BSC 2005 [DIRS 175539]) as "Safety Category" because it is important to waste isolation. The report contributes to the process models used to support performance assessment; the conclusions do not directly impact engineered features important to preclosure safety.

INTENTIONALLY LEFT BLANK

3. USE OF SOFTWARE

A list of controlled and baselined software items used in this report is provided in Table 3-1. Each software item is used within the range for which it was qualified. All software used for the work documented in this report was selected because it was appropriate for the intended use. No limitations on the use of selected software or on the use of outputs from selected software were identified for this work. The use of the software items was consistent with its intended use and within the documented qualified validation ranges for the software. No software item was used prior to qualification to develop any qualified technical data outputs. Section 4 discusses the inputs used in this model for all software. Mathcad V. 13.1, Microsoft (MS) Excel 2003, Excel 2000, MS Access™ 2003, MS Internet Explorer v.6.0.2800, and Surfer 8 are commercial-off-the-shelf (COTS) software items that have been determined exempt in accordance with Section 2.0 of IM-PRO-003, *Software Management*. HYDRUS 1-D (Šimùnek et al. 2005 [DIRS 178140]) is unqualified software and was used solely for the purpose of model corroboration. The use of HYDRUS-1D for model corroboration is documented in Section 7.2.2 and Appendix K. This model corroboration activity provides indirect support for model validation, which is considered an unqualified activity. HYDRUS 2-D (Šimùnek 1999 [DIRS 178228]) is discussed in section 6.2.4.1, but is not used in the analysis. INFIL VVA_2.a1 [DIRS 147608] and INFIL VV2.0.2001 [DIRS 139422] are discussed in the report as historical references only and were not used in the analysis.

Table 3-1. Qualified Software Used in This Report

Software Name	Version	Software Tracking Number (STN)	Platform/Operating System	DIRS
LHS	2.51	10205-2.51-01	DEC AlphaServer ES45 Model 2/ Open VMS 8.2	178784
ArcGIS Desktop	9.1	11205-9.1-00	PC/Windows XP	176015
ENVI+IDL	4.2	11204-4.2-00	PC/Windows XP	178783
MVIEW	4.0	10072-4.0-00	PC/Windows 2000	173438

3.1 LHS V. 2.51

The Latin Hypercube Sampling (LHS) software, Version 2.51 (LHS V. 2.51 [DIRS 178784], STN: 10205-2.51-01), baselined October 03, 2006, uses the Open VMS 8.2 operating environment for quality-affecting work supporting the infiltration model. The LHS software: (1) performs Latin hypercube sampling; (2) generates the distribution for each parameter to be sampled: NORMAL, LOGNORMAL, UNIFORM, LOGUNIFORM, or USER-DEFINED distributions (cumulative, continuous, and discrete); (3) generates a correlation matrix; and (4) detects invalid input data sets.

3.2 ARCGIS DESKTOP V. 9.1

The ArcGIS Desktop software, Version 9.1 (ArcGIS Desktop V. 9.1 [DIRS 176015], STN: 11205-9.1-00), baselined in December 12, 2005, uses the Personal Computer (PC) MS Windows XP operating environment for quality-affecting work supporting the infiltration model. The ArcGIS Desktop software item integrates a collection of software files for developing a complete Geographic Information System (GIS) for the infiltration model. The

software item extends the shape file, geodatabase, and coverage model with support from advanced geometry (three-dimensional coordinates and true curves), complex networks and relationships among feature classes, planar topology, and other object-oriented features within the MS Windows XP operating environment.

3.3 ENVI+IDL V. 4.2

The ENVI+IDL software, Version 4.2 (ENVI+IDL V. 4.2 [DIRS 178783], STN: 11204-4.2-00), baselined December 5, 2005, uses the PC MS Windows XP operating environment for quality affecting work supporting the infiltration model. The ENVI+IDL software: (1) conducts Radiometric Corrections to the Region of Interest (ROI) data; (2) accepts image formats including but not limited to flat LANDSAT, QUICKBIRD and U.S. Geological Survey (USGS) digital elevation model maps; (3) conducts land cover characterization calculations based on data in the ROI; (4) conducts geometric corrections to the ROI data such that the precision of the calculated geographic locations are on the order of the precision of the input data pixels; and (5) accepts generic image formats including but not limited to ASCII, BMP, HDF and JPEG.

3.4 MVIEW V. 4.0

The MVIEW software, Version 4.0 (MVIEW V. 4.0 [DIRS173438], STN: 10072-4.0-00), baselined on July 1, 2005, for the PC MS Windows 2000 operating environment, is a stand-alone executable program that was used to perform sentivity analyses on net infiltration model outputs. Specifically, it was used for stepwise regression analysis and the calculation of partial correlation coefficients and standaradized regression coefficients. This work is described in Appendix H.

3.5 EXEMPT SOFTWARE ITEMS

The following COTS software is considered exempt under Section 2.0 of IM-PRO-003.

Standard spreadsheet and database software (MS Excel 2003 and MS Access 2003) were used for calculations supporting the development of the stochastic weather input files, generating visualization plots of data, and other miscellaneous standard calculations included this report. These software items are controlled as part of MS Office 2003 Professional SP-2 (STN: 610236-2003-00).

The plotting program Surfer 8.02 (STN: 610469-8.02-00) was used to generate visualization maps of net infiltration. The use of Surfer 8 is exempt from qualification under Section 2.0 of IM-PRO-003 because it is used solely for visual display or graphical representation of data. Maps of net infiltration results were generated using Surfer 8.02 and can be spot-checked by the reviewers. Grid cell results were imported into the Surfer 8.02 software and gridded using a Nearest-Neighbor algorithm, which employed the same grid-cell size of 30 × 30 m as the original data. The only data conversion performed by the software was to mask or blank out regions outside of the domain, since the gridding produces a domain that is a bounding box of the imported data. This was done using standard features of the Surfer 8 software.

Mathcad V. 13.1 (STN: 611161-13.1-00) is a COTS controlled software item determined to be exempt in accordance with Section 2.0 of IM-PRO-003. This exemption was reinforced by the conclusions of an Office of Quality Assurance surveillance (OQA-SI-06-015), which determined

that QARD Revision 18 had no impact on the exempt status of MASSIF as long as the procedural requirements of the modeling procedure were met (DOE 2006 [DIRS 179958]). Incremental checking of MASSIF documented in Output DTN: MO0703MASSIFIM.001 satisfied the checking verification requirement needed to meet these procedural requirements. The net infiltration model (MASSIF) was developed and implemented using standard functions included with Mathcad. MASSIF is a hydrologic mass-balance accounting calculation that accounts for the partitioning of water that falls as precipitation to runoff, evapotranspiration (ET), soil moisture storage, and net infiltration, through the automated solution of a series of standard equations which are amenable to verification by hand calculations.

Mathcad allows the infiltration model calculations to be automated, which allows that same set of calculations to be repeated as often as necessary to cover the domain of interest. The results of the MASSIF calculation are not dependent upon the software program used. The calculation was implemented in Mathcad because Mathcad calculational functions are easily recognizable and formatted consistent with their presentation in standard textbooks and hence, are innately traceable and transparent. The TWP (BSC 2006 [DIRS 177492]) describes how the net infiltration model, MASSIF, is verified by comparing each calculation against independent hand calculations performed by an independent checker/reviewer.

INTENTIONALLY LEFT BLANK.

4. INPUTS

4.1 DIRECT INPUT

All direct data inputs used in the development and application of the net infiltration model, MASSIF, to estimate net infiltration for Present Day and potential future climates are listed in Table 4-1. These data consist of topographic, geologic, vegetation, and climate parameters and properties that are appropriate to and required for the development and application of the water-balance approach to watershed modeling that is the basis for the net infiltration model. The data referenced in Table 4-1 contain information necessary to construct and implement the mathematical model as a Mathcad calculation. The data are fully appropriate for the site-scale infiltration model. All non-qualified direct inputs are qualified for their intended use in Appendix A.

Two direct input DTNs discussed below have been used for different purposes in Sections 6 (Model Discussion) and 7 (Model Validation). While the procedure SCI-PRO-006 Rev 02 indicates in Attachment 2 that data used to develop a model cannot be used to validate a model, it is argued here that the different uses of the same data are acceptable.

In the first case, weather observations from ten weather stations representing Present Day climate from DTN SN0608WEATHER1.005 [DIRS 177912] were used in Section 6 and Appendix F to develop stochastic model parameters used to simulate long-term weather for the site. These derived parameters were used as inputs to a stochastic precipitation simulation, which produced weather input files to the MASSIF model in Section 6. Note that the actual historical weather observations were not used as model input to MASSIF in Section 6, but rather to parameterize the general weather patterns and characteristics for a stochastic simulation that was used to generate a set of simulated weather years used as input to the calculations documented in Section 6.5. In contrast, in Section 7, certain local weather observations from specific stations were used as MASSIF model inputs to simulate net infiltration, evapotranspiration and runoff at specific locations and for specific historical periods in order to match measurements of net infiltration, evapotranspiration, and runoff made at these locations during those same periods. Because weather measurements are unique in time and space, it is unreasonable and impractical to separate their use in model development and model validation.

In the second case, a set of qualified borehole locations (DTN: MO9906GPS98410.000 [DIRS 109059]) were used in Section 6 and Appendix E to georeference satellite imagery so that the imagery could be used to characterize the vegetation response as a function of time and space. In contrast, in Section 7, neutron logging measurements made in the same boreholes were compared with the results of the MASSIF model. In order to identify the MASSIF model grid cells in which the boreholes lie, it was appropriate to use the set of qualified borehole locations for this identification.

Table 4-1. Direct Input Data

Input Data Type	Input Data Description	Location in This Model Report	Source
Conversion Factors	Conversion factor from watts to joules	Appendix D	IEEE/ASTM SI 10-1997 [DIRS 151762]
Shuttle radar topography	Surface elevation	Appendix B; Output DTNs: SN0608DRAINDYM.001, SN0608NDVIQBIM.001	DTN: SN0601SRTMDTED.001 [DIRS 177242]
LandSat images	Satellite imagery	Output DTNs: SN0608NDVIAUXD.001, SN0608NDVILSTM.001	DTN: SN0601ALANDSAT.001 [DIRS 177239]
Digital aerial orthorectified photographs	Aerial photography	Appendix E, Output DTN: SN0608NDVIAUXD.001	DTN: SN0601DOQQYM98.001 [DIRS 177240]
Quickbird images	Satellite imagery	Appendix E, Output DTN: SN0608NDVIQBIM.001	DTN: SN0601QBSAT802.001 [DIRS 177241]
Survey of field locations	Ground control point coordinates	Appendix E, Output DTN: SN0608NDVIAUXD.001	DTN: MO0512COV05112.000 [DIRS 177249]
	Borehole coordinates		DTN: MO9906GPS98410.000 [DIRS 109059]
	Ecological study plot coordinates	Appendix D; Section 6.5.3	DTN: MO9901ESPYMNYE.000 [DIRS 177247]
Soil maps	Soil depth class and type boundaries	Sections 6.5.2.2, 6.5.2.4, 6.5.2.5, Appendix B; Output DTNs: SN0606T0502206.011, SN0701SPALAYER.002	DTN: MO0608SPASDFIM.006 [DIRS 178082]
Bedrock map	Bedrock boundaries	Sections 6.5.2.2, 6.5.2.4, Appendix B; Output DTNs: SN0606T0502206.011, SN0701SPALAYER.002	DTN: MO0603SPAGRIDD.003 [DIRS 177121], file *IHU_map_file2.txt*
UZ model boundary and repository footprint	Identification of grid cells inside and outside boundaries	Appendix B; Output DTN: SN0612FTPRNUZB.002	DTN: LB0208HYDSTRAT.001 [DIRS 174491]
Soil properties	Permanent wilting point, moisture content, water holding capacity, saturated hydraulic conductivity	Section 6.5.2.3	DTN: MO0605SEPALTRN.000 [DIRS 178089]
	Terrain albedo	Table 6.5.4.1-4, Appendix A	Brutsaert 1982 [DIRS 176615], p. 136, Table 6.4
	Evaporation layer depth	Table 6.5.4.2-4, Appendix A	Allen et al. 2005 [DIRS 176009], p. 4
		Table 6.5.4.2-4	Allen et al. 1998 [DIRS 157311], p. 144
	Minimum transpiration coefficient	Table 6.5.4.2-2	Allen et al. 1998 [DIRS 157311], pp. 207 and 209
	Soil moisture depletion coefficient	Table 6.5.4.2-3	Allen et al. 1998 [DIRS 157311], p. 162
	Readily evaporable water	Table 6.5.4.2-5	Allen et al. 1998 [DIRS 157311], p. 144, Table 19
	Soil depth measurements	Section 6.5.2.4.1	DTN: GS011208312212.004 [DIRS 176317]

Table 4-1. Direct Input Data (Continued)

Input Data Type	Input Data Description	Location in This Model Report	Source
Bedrock saturated hydraulic conductivity	Saturated hydraulic conductivity	Section 6.5.2.5	DTN: MO0605SPABEDRK.005 [DIRS 177122]
Precipitation/climate	Atmospheric pressure, dew point, precipitation quantity, precipitation rate, relative humidity, solar flux, temperature, wind direction, wind speed, and/or wind vector magnitude	Appendix D, Section D3.2.4; Output DTNs: MO0602SPAWEATH.000, MO0602SPAPRECP.000	DTN: MO0206SEPQ1998.001 [DIRS 166731]
			DTN: MO0209SEPQ2000.001 [DIRS 166730]
			DTN: MO0305SEP01MET.002 [DIRS 166164]
			DTN: MO0305SEP02MET.002 [DIRS 166163]
			DTN: MO0312SEPQ1997.001 [DIRS 167116]
		Appendix D, Section D3.2.4; Output DTN: MO0607SEPTOTAL.003	DTN: MO0312SEPQ1993.001 [DIRS 176092] (Data was evaluated and determined to be appropriate prior to use)
			DTN: MO0606SEPRECIP.001 [DIRS 177136] (Data was evaluated and determined to be appropriate prior to use)
		Output DTN: SN0610T0502206.031	DTN: MO0605SEPHOURL.000 [DIRS 177237]
		Appendix D; Output DTN: MO0605SPADAYWA.000	DTN: MO0605SPASPOKA.000 [DIRS 177135]
		Appendix F; Output DTN: SN0609T0502206.023	DTN: SN0601PRECPTMP.002 [DIRS 176122]
		Appendix F; Output DTNs: SN0609T0502206.023, SN0608T0502206.019	DTN: SN0603DWEATHER.002 [DIRS 177917]
	Atmospheric pressure, dew point, precipitation quantity, relative humidity, temperature, and/or wind speed	Appendix F; Output DTNs: SN0609T0502206.023, SN0610T0502206.030, SN0608T0502206.019, SN0610T0502206.031	DTN: SN0608WEATHER1.005 [DIRS 177912]
	Stations representing future climate	Appendix F; Section 6.5.1.1, Table 6.5.1.1-1	DTN GS000308315121.003 [DIRS 151139]
	Psychrometric constant	Section 6.5.3.6.1	Allen et al 1998 [DIRS 157311], p. 214, Table 2.2
	Temperature lapse rate	Appendix F; Section 6.5.1	Maidment 1993 [DIRS 125317], p. 3.3
	Maximum daily precipitation amount	Appendix F; Section 6.5.1	Maidment 1993 [DIRS 125317], p. 3.36, Table 3.10.2
	Snowmelt coefficient	Section 6.5.1, Table 6.5.1.7-1, Appendix F	Maidment 1993 [DIRS 125317], p. 7.24
	Sublimation coefficient	Section 6.5.1, Table 6.5.1.7-1, Appendix A	Hood et al. 1999 [DIRS 177996], p. 1794
	Solar constant	Table 6.5.4.1-5	Allen et al. 1998 [DIRS 157311], p. 48
		Table 6.5.4.1-5, Appendix A	Dewitte et al. 2004 [DIRS 178528], p. 214

Table 4-1. Direct Input Data (Continued)

Input Data Type	Input Data Description	Location in This Model Report	Source
Precipitation/climate (continued)	Turbidity coefficient	Table 6.5.4.1-6, Appendix A	Allen et al. 2005 [DIRS 176207], Appendix D, p. D-8
	Dew point offset	Table 6.5.4.1-2, Appendix A	Allen et al. 2005 [DIRS 176207], Appendix D, p. D-29
			Temesgen et al. 1999 [DIRS 178312], pp. 29 to 30, Table 4
Vegetative coverage	Ground cover	Appendix D, Section D3.2.2, Tables D-6 through D-14; Output DTNs: MO0606SPAVEGAS.001, SN0608NDVIANAL.001	DTN: MO9907GCESPYMN.000 [DIRS 157659]
	Growth stage lengths	Appendices A, D, Section D3.2.1, Tables D-2 and/or D-3	Rundel and Gibson 1996 [DIRS 103614], Figure 4.13, p. 106
			Newman 1992 [DIRS 174673], p. 3
			Smith et al. 1995 [DIRS 103628], pp. 342, 349, Figure 2
			Hamerlynck et al. 2000 [DIRS 177022], p. 602, Figure 6
			Hamerlynck et al. 2002 [DIRS 177128], p. 103, Figure 7
			Hamerlynck et al. 2002 [DIRS 177046], p. 774
			Hulbert 1955 [DIRS 177129], p. 1
	Mean plant height, mean maximum plant height	Section 6.5.3.3, Table 6.5.3.3-1, Appendices A, D, Section D3.2.1, Table D-5	Hulbert 1955 [DIRS 177129], Table 6, p. 186
			Newman 1992 [DIRS 174673], p. 2
			Rundel and Gibson 1996 [DIRS 103614], Tables 4.1 and 4.2
	Stomatal resistance	Appendices A, D, Section D3.2.3, Table D-16	Huxman et al. 1999 [DIRS 177133], pp. 770 and 774
			Huxman and Smith 2001 [DIRS 177132], p. 197
			Hamerlynck et al. 2002 [DIRS 177128], p. 101
	Soil moisture depletion coefficient adjustment	Section 6.4.4.2	Allen et al. 1998 [DIRS 157311], p. 162
	Elevation of Crater Flat used to develop stomatal resistance inputs	Section D3.2.3	Smith et al. 1995 [DIRS 103628], p. 340
	Stomatal resistance	Appendices A, D, Section D3.2.3, Table D-16	Naumburg et al. 2003 [DIRS 177143], p. 280, Figure 3
			Hamerlynck et al. 2000 [DIRS 177130], p. 188
			Hamerlynck et al. 2004 [DIRS 176045], p. 213

Table 4-1. Direct Input Data (Continued)

Input Data Type	Input Data Description	Location in This Model Report	Source
Vegetative coverage (continued)	Stomatal resistance (continued)		Hamerlynck et al. 2000 [DIRS 177022], p. 602
			Pataki et al. 2000 [DIRS 177161], p. 893
			Smith et al. 1995 [DIRS 103628], pp. 343 and 344
	Atmospheric pressure	Appendices A, D, Table D-17	Allen et al. 1998 [DIRS 157311], pp. 213 to 214, Table 2.1
	Rooting depths	Section 6.5.3.2, Tables 6.5.3.2-1 and/or 6.5.3.2-2, Appendix A	Canadell et al. 1996 [DIRS 177626], pp. 583 to 595, Appendix 1
			Hansen and Ostler 2003 [DIRS 177619], p. 85, Table 7-1
			Jackson et al. 2002 [DIRS 177171], p. 624, Table 1
			Rundel and Gibson 1996 [DIRS 103614], p. 99, Figure 4-10
			Rundel and Nobel 1991 [DIRS 128001], pp. 355 to 357
			Schenk and Jackson 2002 [DIRS 177638], p. 491, Figure 9
			Yoder and Nowak 1999 [DIRS 177167], p. 91, Figure 6
			Harris 1967 [DIRS 177630], p.97, Figure 6
			Hulbert 1955 [DIRS 177129], p. 191
			Link et al. 1990 [DIRS 177142], p. 512
			Rickard 1985 [DIRS 177635], p.170
			Foxx et al. 1984 [DIRS 177628], p. 6, Table 3
			Richards and Caldwell 1987 [DIRS 177927], pp. 486 to 489
			Sturges and Trlica 1978 [DIRS 177928], pp. 1282 to1285
			Ryel et al. 2003 [DIRS 177632], p. 760
			Seyfried et al. 2005 [DIRS 178060], pp. 282 to 283
			Leffler et al. 2004 [DIRS 177926], p. 10, Figure 1
			Zlatnik 1999 [DIRS 177639], p. 7
			Anderson 2002 [DIRS 177625]

Table 4-1. Direct Input Data (Continued)

Input Data Type	Input Data Description	Location in This Model Report	Source
Vegetative coverage (continued)	Mean plant height	Section 6.5.3.3, Table 6.5.3.3-2, Appendix A	USDA 2002 [DIRS 178073]
			Schultz and McAdoo 2002 [DIRS 178065], p. 2
			Tirmenstein 1999 [DIRS 177641]
			Tirmenstein 1999 [DIRS 177642]
			Utah State University 2002 [DIRS 177646], p. 2
			Utah State University 2002 [DIRS 177644], p. 2
			Utah State University 2002 [DIRS 177647] , p. 1
			Utah State University 2002 [DIRS 177648], p. 2
			Utah State University 2002 [DIRS 177649], p. 2
			Utah State University 2002 [DIRS 177650], p. 2
			Utah State University 2004 [DIRS 177643], p. 1
			Weber et al. 1993 [DIRS 177931], pp. 355 to 357
			Zlatnik 1999 [DIRS 177639], p. 7
			Stewart and Hull 1949 [DIRS 177146], pp. 58 to 59

4.2 CRITERIA

The general requirements to be satisfied by the TSPA are stated in 10 CFR Part 63 [DIRS 176544]. The acceptance criteria that will be used by the NRC to determine whether the technical requirements have been met are identified in *Yucca Mountain Review Plan*, *Final Report* (YMRP) (NRC 2003 [DIRS 163274]).

The acceptance criteria identified in Section 2.2.1.3.5.3 of the YMRP (NRC 2003 [DIRS 163274]) that are applicable to this report are included below. How these components are addressed is summarized in Section 8.3 of this report.

A*cceptance Criteria from Section 2.2.1.3.5.3, Climate and Infiltration.*

Acceptance Criterion 1: ***System Description and Model Integration Are Adequate.***

(1) The total system performance assessment adequately incorporates, or bounds, important design features, physical phenomena, and couplings, and uses consistent and appropriate assumptions throughout the climate and net infiltration abstraction process.

(2) The aspects of geology, hydrology, geochemistry, physical phenomena, and couplings, that may affect climate and net infiltration, are adequately considered. Conditions and assumptions in the abstraction of climate and net infiltration are readily identified and consistent with the body of data presented in the description.

(3) The abstraction of climate and net infiltration uses assumptions, technical bases, data, and models that are appropriate and consistent with other related U.S. Department of Energy abstractions. For example, the assumptions used for climate and net infiltration are consistent with the abstractions of flow paths in the unsaturated zone (UZ) and flow paths in the saturated zone (SZ) (Sections 2.2.1.3.6 and 2.2.1.3.8 of the Yucca Mountain Review Plan, respectively). The descriptions and technical bases provide transparent and traceable support for the abstraction of climate and net infiltration.

(4) Sufficient data and technical bases to assess the degree to which FEPs have been included for this abstraction are provided.

(5) Adequate spatial and temporal variability of model parameters and boundary conditions are employed to model the different parts of the system.

(6) Average parameter estimates are used in process-level models over time and space scales that are appropriate for the model discretization.

(7) Projections of future climate change are based on evaluation of paleoclimate information over the past 500,000 years. For example, numerical climate models, if used for projection of future climate, are calibrated based on such paleoclimate data.

(8) Guidance in NUREG–1297 and NUREG–1298 (Altman et al. 1988 [DIRS 103597]; 1988 [DIRS 103750]), or other acceptable approaches for peer reviews and data qualification, is followed.

Acceptance Criterion 2: ***Data Are Sufficient for Model Justification.***

(1) Climatological and hydrological values used in the license application (e.g., time of onset of climate change, mean annual temperature, mean annual precipitation, mean annual net infiltration, etc.) are adequately justified. Adequate descriptions of how the data were used, interpreted, and appropriately synthesized into the parameters are provided.

(2) Estimates of present-day net infiltration using mathematical models at appropriate time and space scales are reasonably verified with site-specific climatic, surface, and subsurface information.

(3) The effects of fracture properties, fracture distributions, matrix properties, heterogeneities, time-varying boundary conditions, evapotranspiration, depth of soil cover, and surface-water run off and run-on are considered, such that net infiltration is not underestimated.

(4) Sensitivity or uncertainty analyses are performed to assess data sufficiency and determine the possible need for additional data.

(5) Accepted and well-documented procedures are used to construct and calibrate numerical models.

(6) Reasonably complete process-level conceptual and mathematical models are used in this model report. In particular: (a) mathematical models provided are consistent with conceptual models and site characteristics; and (b) the robustness of results from different mathematical models is compared.

(7) This Criterion was listed in the TWP, but is not included in present report because expert elicitation was not used to support model development.

Acceptance Criterion 3: ***Data Uncertainty Is Characterized and Propagated through the Model Abstraction.***

(1) Models use parameter values, assumed ranges, probability distributions, and bounding assumptions that are technically defensible, reasonably account for uncertainties and variabilities, and do not result in an under-representation of the risk estimate.

(2) The technical bases for the parameter values used in this abstraction are provided.

(3) Possible statistical correlations are established between parameters in this abstraction. An adequate technical basis or bounding argument is provided for neglected correlations.

(4) The hydrologic effects of future climate change that may alter the rates and patterns of present-day net infiltration into the UZ are addressed. Such effects may include changes in soil depths, fracture-fill material, and types of vegetation.

Acceptance Criterion 4***: Model Uncertainty Is Characterized and Propagated through the Model Abstraction.***

(1) Alternate modeling approaches of FEPs, consistent with available data and current scientific understanding, are investigated. The results and limitation are appropriately considered in the abstraction.

(2) The bounds of uncertainty created by process-level models are considered in this abstraction.

(3) Consideration of conceptual model uncertainty is consistent with available site characterization data, laboratory experiments, field measurements, natural analogue information and process-level modeling studies; and the treatment of conceptual model uncertainty does not result in an under-representation of the risk estimate.

Acceptance Criterion 5: ***Model Abstraction Output Is Supported by Objective Comparisons.***

(1) This Criterion was listed in the TWP, but is not included in present report because the output from this model is not a direct TSPA abstraction.

(2) Abstractions of process-level models may conservatively bound process-level predictions.

(3) Comparisons are provided of output of abstracted models of climate and net infiltration with output of sensitivity studies, detailed process-level models, natural analogs, and empirical observations, as appropriate.

Acceptance Criteria from Section 2.2.1.1.3

(3) Technical Basis for Barrier Capability is Adequately Presented.

4.3 CODES, STANDARDS, AND REGULATIONS

No codes, standards, or regulations, other than those identified above in Section 4.2, were used in this model report.

INTENTIONALLY LEFT BLANK

5. ASSUMPTIONS

In procedure SCI-PRO-006, an assumption is defined as:

> A statement or proposition that is taken to be true or representative in the absence of direct confirming data or evidence, or those estimations, approximations, limitations, simplifications, and/or decisions made during model development (such as when expanding the range of variables to achieve conservatism).

The assumptions included in this section are only those which are made in the absence of direct or confirming data. In Section 6, there are many "modeling decisions" that were made that might be thought of as assumptions. These are listed in Table 5-1 at the end of this section.

5.1 CERTAIN COMPONENTS OF THE WATER BALANCE MODEL CAN BE NEGLECTED FOR MODELING NET INFILTRATION AT YUCCA MOUNTAIN

The water balance equation used in this model of net infiltration includes the most important terms in the water balance and neglects terms that are reasonably assumed to be negligible. The model includes precipitation (rain and snow), evapotranspiration (ET), net infiltration, snowmelt, sublimation of snow, run-on, and runoff. The terms that are assumed to be negligible and are thus not represented in the model include: interception, interflow, storage of water on surface (either in puddles or in stream channels), subsurface vapor flow, and dew deposition.

- Interception is the process whereby a fraction of the total precipitation is stored on and eventually evaporated from the surface of plants without reaching the ground. In densely vegetated regions interception is a significant process; however, in arid regions with sparse vegetation, this process is assumed to be negligible.

- Interflow (sometimes called "storm seepage") is lateral flow of liquid water in the unsaturated zone that can occur during and following precipitation events. This flow is driven by a lateral head gradient component, which is typically the result of a sloping land surface. Such flows are neglected in the current model for the following reasons. First, most of the model domain is characterized by relatively low slopes. For example, the median slope for the model domain is approximately 10 degrees from horizontal and 90% of the domain has a slope less than 25 degrees. The lower the slope the less the lateral head gradient. Second, bulk bedrock conductivity values tend to be significantly higher than the conductivities in the overlying soil and, therefore, once water reaches the soil–bedrock interface, it would tend to enter bedrock instead of flowing laterally along the interface. Soil layering (anisotropic conductivity), if present, might increase the likelihood of interflow. However, steep slopes tend to be associated with shallow soils, where soil layering is unlikely to be important. Even if significant interflow does occur in certain areas, it is not likely to flow over several grid cells because of the shallow soils and high bedrock conductivity. Observations also support this assumption. For example, if significant interflow were occurring at the site, one would expect that stream flows would continue for several days following large precipitation events, seeps would form at the toes of slopes, and mass wasting would occur when thin soils on steep slopes became saturated. None of these indicators of significant interflow characterize the site.

- Storage of water on the surface can occur in the form of puddles and/or as stream channel storage. Small ephemeral puddles do form on areas of bare bedrock after precipitation events, but only about 0.3% of the domain consists of bare bedrock (431 cells out of 139,092 cells; see Table 6.5.2.4-1). Stream flows do not tend to persist significantly beyond the precipitation period as discussed in the validation section (Section 7.1.3). For these reasons, surface water storage is assumed negligible and is excluded from the water balance.

- Subsurface vapor flow is driven by a gradient in matric potential in the subsurface. Releatively significant gradients in matric potential have been measured in semiarid regions with deep soil profiles (Walvoord et al. 2002 [DIRS 178108]; Scanlon et al. 2003 [DIRS 178109]). The presence of these gradients indicates upward vapor flow (Walvoord 2002 [DIRS 178108]); however, the fluxes inferred are of very low magnitude compared with the fluxes associated with episodic liquid water infiltration events that characterize shallow soil regions. Results of the simplified water mass balance approach described in this report suggest that little to no net infiltration occurs beneath thick soils and, therefore, including subsurface vapor flow in deep soil areas would not significantly change these results. In contrast, most of the net infiltration occurs beneath shallow soils, and little is known about the relative magnitude of subsurface vapor flow in these regions. For this reason, this process is assumed to be negligible and is excluded from the water balance.

- Deposition of water as dew is not considered in the modeling. It is assumed that this deposition mechanism is small relative to precipitation and therefore any contribution to net infiltration will be negligible. Dew deposition may be an important source of water to native vegetation, especially during especially dry periods, but its effect on net infiltration is not considered to be important.

- The approach used to estimate water flow and storage within the root zone is a simplification of the actual physical processes that control flow in this environment. The use of the "field capacity" concept acts as a flow switch allowing downward water flow at a rate equal to the saturated hydraulic conductivity when the average water content in a layer equals or exceeds "field capacity" and allowing no flow to occur when average water content in a layer is less than field capacity. In reality, water will flow within the vadose zone in response to gradients in total soil-water potential, which is the sum of various components such as elevation, matric, pressure, temperature, and osmotic potentials. The approach used here assumes that these components can be adequately represented with a unit head gradient when field capacity is equaled or exceeded and with a head gradient of zero when water content is less than field capacity. For this application, the value of field capacity is defined as the water content range between values of suction pressure equal to −0.33 and −0.1 bars. As explained in Sections 6.2.2 and 6.5.2.3, this range of values is considered an approximation for the uncertainty in this property. Osmotic potential is usually a very minor contributor to the total potential unless pore-water concentration gradients are very high, which is not supported by observations at Yucca Mountain.

5.2 FAO-56 METHODS FOR DEVELOPING BASAL TRANSPIRATION COEFFICIENTS ARE APPROPRIATE FOR DESERT ENVIRONMENT

FAO-56 is an internationally recognized set of guidelines for estimating evapotranspiration. The guidelines were developed primarily for agricultural applications but also include guidance for applying the methods to natural, non-agricultural areas.

FAO-56 methods for developing basal transpiration coefficient (K_{cb}) profiles for natural vegetation (Allen et al. 1998 [DIRS 157311], pp. 187 to 193) are applicable to desert vegetation and appropriate and defensible for developing K_{cb} profiles for vegetation at Yucca Mountain (see Section 6.4.4 for description of FAO-56 methods and use of K_{cb}s in the MASSIF model).

This assumption is needed to support use of FAO-56 methods that were originally developed for agricultural crops. While methods for natural vegetation are included in FAO-56, they have not yet been widely used for desert vegetation. The FAO-56 methods for developing K_{cb}s (Allen et al. 1998 [DIRS 157311], pp. 187 to 193) are described, justified for use, and implemented in Appendix D.

Methods provided in FAO-56 for calculating K_{cb} (Allen et al. 1998 [DIRS 157311], pp. 187 to 193) from effective ground cover are appropriate for desert vegetation. The use of effective ground cover measured on reference area plots at Yucca Mountain (Section 6.5.3.6 and Appendix D) directly accounts for the sparse vegetation typical of the Yucca Mountain area. It also allows for weighting (by cover) of vegetation types (e.g., annuals and perennials) within associations. The FAO-56 methods provide for corrections in wind speed, minimum relative humidity, plant height, and stomatal resistance that differ between the FAO-56 standards for agricultural crops and the desert vegetation and climate of Yucca Mountain. Partitioning evaporation and transpiration and applying corrections for stomatal control in the FAO-56 methods are appropriate measures for the Yucca Mountain environment.

5.3 ASSUMPTIONS RELATED TO SIMULATING YUCCA MOUNTAIN VEGETATION USING LANDSAT TM DATA

In Yucca Mountain's arid climate, it is assumed that vegetation responds directly (and linearly) to the total annual precipitation and that the annual vegetation response is linearly related to the basal transpiration coefficient (K_{cb}) and, thus, evapotranspiration. This assumption is supported by correlations between precipitation and vegetation indices (NDVI) in semiarid environments (Scanlon et al. 2005 [DIRS 175977], pp. 6036 to 6037). It is also assumed that the vegetation response measured by NDVI over a single wet year (1998) can be scaled in magnitude to represent the vegetation response for other years (Section 6.5.3). This assumption implies that the timing and relative shape of the vegetation response with time can be represented by the response measured during a single year. The vegetation response for different years is simulated by multiplying the response for 1998 by a precipitation factor based on the difference in annual precipitation from the annual precipitation measured in 1998. This assumption is a necessary simplification because it would be a very significant undertaking to model the dynamic vegetation response to actual daily weather patterns, and such effort is not warranted for the intended purpose of the model. Data from two additional years (dry and moderate precipitation) were used to test the appropriateness of this assumption (Appendix E, Section E-7). The test

indicated that this assumption generally appears valid for predicting the vegetation during the wettest period of the year when net infiltration is most likely to occur. It is not as accurate in predicting the timing and magnitude of the tails of the vegetation response. However, the tails represent times when ET is not as important, and therefore the errors from year to year likely cancel each other out, depending on the weather patterns. It is possible that during the monsoon climate, this assumption may introduce a bias since the period of the year with significant precipitation moves later in the year (late summer). The current assumption will predict vegetation tailing off during this period rather than the vegetation responding to the late season precipitation. The net result of this bias is likely to be an overprediction of net infiltration for this climate, since transpiration may be underestimated during the period of maximum precipitation. Other implications of this assumption are that it ignores the potential effects to vegetation of fire, disease, pests, and other specific environmental factors that may change the vegetation response in the future.

5.4 PHYSICAL PROPERTIES ARE ASSUMED TO REMAIN CONSTANT

It is assumed in this model that the physical properties of the soil, bedrock, and water will remain constant over the time periods being considered in the model (1 day to 10,000 years).

- Over time periods significantly exceeding 10,000 years, it is likely that soil erosion and deposition processes will affect soil depth patterns over the site, but it is assumed that for the next 10,000 years soil depth will remain constant.

- It is assumed that soil formation processes that can significantly change soil properties (conductivity, porosity, field capacity, etc.) will not alter soil properties in the next 10,000 years.

- It is assumed that bedrock conductivity, which is controlled by the nature and properties of the material (caliche) that fills fractures near the soil bedrock interface, will not significantly change in the next 10,000 years.

It is assumed the fluid properties (viscosity and density) can adequately be represented as being constant. In reality, temperature variations result in variations in viscosity and density that contribute to variations in the hydraulic conductivity. For example, the increase in the viscosity of water from 30ºC to 10ºC is about 64% (CRC 2006 [DIRS 178081], p. 6-2), which results in a similar associated decrease in hydraulic conductivity. This temperature range was chosen as an example and is not representative of temperature changes expected within the root zone. The density of water also can influence the hydraulic conductivity. Water density changes as a function of temperature and dissolved concentrations of solutes. The density of water changes only slightly (<1%) in the temperature range between 30ºC and 10ºC (CRC 2006 [DIRS 178081] p. 6-2). The change in density due to dissolved constituents will also be very small since the total dissolved concentration of pore waters collected at the site is relatively low. These examples illustrate that water properties can affect hydraulic conductivity; however, the uncertainty in the hydraulic conductivity of the soil based on other factors is much larger than the potential influence of thermal changes to viscosity and density. Moreover, the sensitivity of net infiltration to soil conductivity has been shown to be low (Sections 6.7 and 7.1.4), and thus any thermal effect on conductivity can be neglected.

5.5 MISCELLANEOUS ASSUMPTIONS AND APPROXIMATIONS

This section lists an assortment of miscellaneous assumptions and approximations that were made using professional judgment in the process of developing the MASSIF model and applying it to Yucca Mountain (Table 5-1). The purpose of this list is to disclose explicitly all these assumptions in one place in the report and point interested readers to the relavant sections of the report where these assumptions are explained and justified. Many of the assumptions listed here were made because there was insufficient direct data with which to represent the process in question. In this case, a decision had to be made as to how to model the process. In these cases, professional judgement, informed by the YMRP acceptance criteria, guided the development of the assumption. There is the possibility that when additional field data is collected or reanalyzed, some of these assumptions may prove to be unsupported by data, which may result in a change to net infiltration predictions. The aim is that assumptions will not bias the net infiltration results, but in certain cases this was not possible. For example, the assumption that no water is removed from bedrock by evapotranspiration does bias the results towards overestimating net infiltration; however, reliable and quantitative information on how much water is removed from bedrock at the site was not available, and therefore a simplifying assumption was necessary given the explicit criteria stating that net infiltration not be underestimated (e.g., Criterion 2.3). Other items listed in Table 5-1 are considered approximations of the actual process. In these cases, it is not the intent of this report to argue that the approximation is what actually occurs in nature; rather, the intent is that the approximation is an adequate representation of the process considering the intended purpose of the model.

Table 5-1. Miscellaneous Assumptions and Their Locations in the Report

Misc. Assumption Number	Description of Assumption	Location in Report (Section)
1	Precipitation is assumed to occur at the same time in all parts of the domain. The frequency of precipitation is calculated for a reference elevation of 1,524 m and is applied to all cells of the domain. This assumption was necessary because there is insufficient data to predict the spatial distribution of precipitation for each event.	6.4.1.1, 6.5.1.3
2	Precipitation is assumed to fall as snow on days when the average daily temperature is below 0°C. Average daily temperature is assumed to be the arithmetic mean of the minimum and maximum daily temperature. This assumption is necessary because a daily time step is used in the modeling.	6.4.1.2
3	The duration during which snowmelt is available at the surface is assumed to be 12 hours on a day with no precipitation. If precipitation does occur, the duration that snowmelt is available at the surface is equal to the duration of the precipitation event on that day. The duration that run-on is available at the surface is assumed to be equal to the duration of the precipitation event.	6.4.2, 6.4.3
4	It is assumed that only one precipitation event can occur during a day. Observed multiple precipitation events during a day are combined into a single event that lasts for the sum of the duration of the multiple events and produces the combined precipitation. It is also assumed that precipitation events do not extend past midnight. For example, if it began to rain at noon on day 1 and continued to rain for 24 hours, this “event” would be represented in the model as two precipitation events (an 11-hour event on day 1 and a 13-hour event on day 2).	6.5.1.7, 6.4.3
5	Evaporation is assumed to cease when the water content of the soil reaches one half the wilting point for the soil.	6.4.4

Table 5-1. Miscellaneous Assumptions and their Locations in the Report (Continued)

Misc. Assumption Number	Description of Assumption	Location in Report
6	It is assumed that maximum rooting depth is uniform over the whole domain. Actual rooting depth is limited by the soil depth because it is also assumed that nearly all of the water that is evapotranspired comes from the soil layer in which active roots are present. This assumption means that it is valid to neglect any evapotranspiration from the bedrock immediately below the soil. It is recognized that roots do sometimes extend into bedrock along fractures; however, no locally relevant studies or data were identified which could be used to quantify the relative amount of water these roots might remove compared with roots in the soil.	6.5.3.2
7	Average daily wind speed is estimated from monthly mean wind speed data from weather stations located within the modeling domain. It is assumed that these daily wind speed estimates are adequate for representing wind speed during future climates over the next 10,000 years.	6.4.5.2
8	It is assumed that for the purpose of estimating incoming solar radiation that each grid cell has a uniform slope (flat surface) and that features that can shade parts of the surface are not important for estimating incoming solar radiation.	6.4.5.2
9	The Hargreaves adjustment coefficient calculated from weather data for years 1998, 2001, and 2002 is assumed to be representative of atmospheric conditions for the next 10,000 years.	6.4.5.2
10	It is assumed that the turbidity coefficient over the next 10,000 years will vary between 0.5 and 1.1. Conditions outside this range are not expected to occur.	6.5.4.1
11	Initial water content used for net infiltration calculation is set to a uniform and constant level for each soil type. It is assumed that this approach adequately represents the conditions in the soil at the beginning of the water year. Real saturations may differ spatially, but there is no basis upon which to set an appropriate initial condition for each grid cell separately.	6.5.4.2
12	For the purpose of using satellite imagery to estimate vegetation responses, it is necessary to assume that the air mass over the Yucca Mountain region is homogeneous everywhere in the satellite image.	E1.1
13	It is assumed that the timing of the vegetation response during the wet water year of 1998 is representative of the timing of the vegetation response during all other years. This assumption was tested for water year 2001 and shown to be generally valid. If the timing of the response in 1998 is close to the mean timing response for all years, then the assumption is still valid since the errors on any given year will tend to be canceled. However, if the timing of 1998 is biased in one direction, this assumption could result in a biased estimate of evapotranspiration. Given the uncertainties in parameters used to calculate evapotranspiration, the impact of such a bias is assumed to be relatively small.	E1.1
14	It is assumed that the linear relationship derived between NDVI and K_{cb} measurements for a few representative years is applicable for future climates expected over the next 10,000 years.	E1.1
15	It is assumed that the vegetation measured at environmental study plots during dry, moderate, and wet years is comparable and similar to vegetation in those same plots during different dry, moderate, and wet years. In order to make these comparisons, an effort was made to scale vegetation linearly with annual precipitation before comparing.	D2.2

Table 5-1. Miscellaneous Assumptions and their Locations in the Report (Continued)

Misc. Assumption Number	Description of Assumption	Location in Report
16	It is assumed that all subsurface flow can be represented by Darcy's Law and that all vertical flow in the soil and into the bedrock is driven by a unit gradient. It is also assumed that there is no conductivity limitation to water entering the surface (evaporation) layer. A conductivity limitation does exist for water flowing from the evaporation layer to the lower root zone. This assumption was made for the following reasons. The processes of interception and surface storage are not explicitly represented in the MASSIF model; however, these processes will act to store some initial amount of precipitation that is not available for runoff. In addition, the typically dry conditions in the surface layer of the soil will result in capillary suction that in effect reduces any limitation due to soil conductivity for this region and that draws in water faster than the saturated conductivity of the soil during the initial wetting period. Since the thickness of the evaporation layer is considered to be uncertain and is sampled in LHS, the effect of this assumption varies with the sampled thickness.	6.4.2
17	It is assumed that conditions affecting evaporation on east (E) and west (W) slopes represent an approximate average of the conditions that would exist on N and S slopes. Thus, vegetation on E and W slopes will be interpolated as a temporal average of N and S slopes.	E3.1
18	It is assumed that vegetation response on flat and gentle slopes (<5°) can be represented as averages between N and S slopes (and therefore, in this simple interpolation, equivalent to E and W slopes). Vegetation responses for all intermediate slopes and azimuths can be represented by weighted averaging between the endmember conditions for N and S slopes.	E3.1
19	It is assumed that any run-on generated in the northern part of Yucca Wash, which has been artificially cut off during watershed delineation, will not significantly affect estimates of net infiltration for that drainage.	6.5.2
20	It is assumed that the maximum daily precipitation possible at Yucca Mountain during the next 10,000 years is equal to or less than the largest observed rainfall in the USA during a 24-hour period over a 26-km^2 area (983 mm; Maidment 1993 [DIRS 125317], p. 3.36, Table 3.10.2).	6.5.1.7

INTENTIONALLY LEFT BLANK

6. MODEL DEVELOPMENT

Section 6 describes and discusses the model used to predict net infiltration at Yucca Mountain. Section 6.1 provides a listing of the features, events and processes (FEPs) addressed by the report.

Section 6.2 includes a description of the processes that are involved in and related to net infiltration. These processes are described in terms of the near-surface water (mass) balance, and include net precipitation, surface water run-on/runoff, change in water storage in the active zone, evaporation, and transpiration. A discussion related to modeling these processes is given, followed by a presentation of criteria for selecting models and model approaches for estimating net infiltration at Yucca Mountain. A brief discussion of existing models and why they were not used for this application is given.

In Section 6.3, the model developed to estimate net infiltration at Yucca Mountain is summarized, the rationale for its development is given, and some of its key features are described. This model, referred to as MASSIF (Mass Accounting System for Soil Infiltration and Flow) is based on a mass balance equation that is solved for each computational cell for each day of the simulation.

The mathematical basis for the MASSIF model is described in Section 6.4. The mathematical representations of the key water balance components are presented in this section, including those for precipitation (Section 6.4.1), water transport and storage (Section 6.4.2), surface runoff and run-on (Section 6.4.3), evapotranspiration (Section 6.4.4), and reference evapotranspiration (Section 6.4.5).

Analyses of Yucca Mountain net infiltration for three pre-10,000-year future climates using MASSIF are described in Section 6.5. Climatic inputs for anticipated climate episodes are described in Section 6.5.1 and include the amount of precipitation, the minimum and maximum temperatures, and the average wind speed. Geologic inputs such as spatial distributions for soil types, soil depth classes and bedrock types, and geologic data used to define watersheds and other site characteristics are given in Section 6.5.2. Vegetation parameters are presented in Section 6.5.3. This section includes a discussion of potential vegetation for different climates, rooting depth, plant height, transpiration coefficients, and vegetation coverages for different climates. A discussion of how Landsat images are used to estimate transpiration coefficients for future climates using predicted precipitation is included. Additional parameters related to describing vegetation are given in Section 6.5.4.

The criteria for considering parameter uncertainty in the calculation of net infiltration are given in Section 6.5.5. Section 6.5 also includes a discussion of the calculation procedures, including a description of the post-processing of results (Section 6.5.6). Finally, results of net infiltration calculations are provided in Section 6.5.7 for each of the three future climates considered.

Section 6.6 contains a discussion of the infiltration prediction uncertainties.

Sensitivity analyses of net infiltration at Yucca Mountain are given in Section 6.7. For each climate considered, a sensitivity study was conducted to identify those parameters whose uncertainty might significantly influence the uncertainty in average net infiltration. Parameters

considered included both generic model parameters and the input parameters that are specific to the Yucca Mountain site. Bases for exclusion of parameters from sensitivity studies are given.

This model is not intended to be a direct input to TSPA. Rather, it is intended to provide boundary conditions for the unsaturated zone (UZ) modeling, which in turn provides direct feeds to TSPA.

6.1 FEATURES, EVENTS, PROCESSES

Table 6.1-1 contains a list of 13 FEPs taken from the FEP List (DTN: MO0508SEPFEPLA.002 [DIRS 175064]). The selected FEPs are those that are associated with the subject matter discussed in the present report. The cross-reference for each FEP to the relevant section(s) of this report is also given in Table 6.1-1.

Table 6.1-1. FEPs Addressed in This Model Report

FEP Number	FEP Name	Relevant Sections
1.2.02.01.0A	Fractures	6.5.2
1.3.01.00.0A	Climate change	6.5.1, Appendix F
1.4.01.01.0A	Climate modification increases recharge	6.5.1, Appendix F
2.2.03.01.0A	Stratigraphy	6.5.2
2.2.03.02.0A	Rock properties of host rock and other units	6.5.2
2.2.07.01.0A	Locally saturated flow at bedrock/ alluvium contact	5, 6.2, 6.3, 6.4
2.2.07.02.0A	Unsaturated groundwater flow in the Geosphere	6.2, 6.3, 6.4
2.3.01.00.0A	Topography and morphology	6.5.2, Appendix B
2.3.11.01.0A	Precipitation	6.5.1, Appendix F
2.3.11.02.0A	Surface runoff and flooding	6.2, 6.3, 6.4
2.3.11.03.0A	Infiltration and recharge	Entire

6.2 INFILTRATION PROCESSES

This section includes a description of the processes that are involved in and related to net infiltration. These processes are described in terms of the near-surface water balance. Next a discussion related to modeling these processes is given, followed by a presentation of criteria for selecting models and model approaches for estimating mean annual net infiltration at Yucca Mountain. Finally, a brief discussion of existing models and why they were not used for this application is given.

6.2.1 Processes Controlling Net Infiltration

Near surface hydrologic processes are generally described in the context of the hydrologic cycle, which describes the pathways and reservoirs through which water moves near and on the surface of the earth. The hydrologic reservoirs consist of the atmosphere, biomass, soil, surface water (streams, lakes, puddles, etc.), snow, pore water in the bedrock overlying the water table, and

groundwater. Water moves between these reservoirs via a set of natural processes, including precipitation, infiltration, soil water movement and retention (e.g., drainage and interflow), evaporation, transpiration, run-off, and net infiltration (see Figure 6.2.1-1).

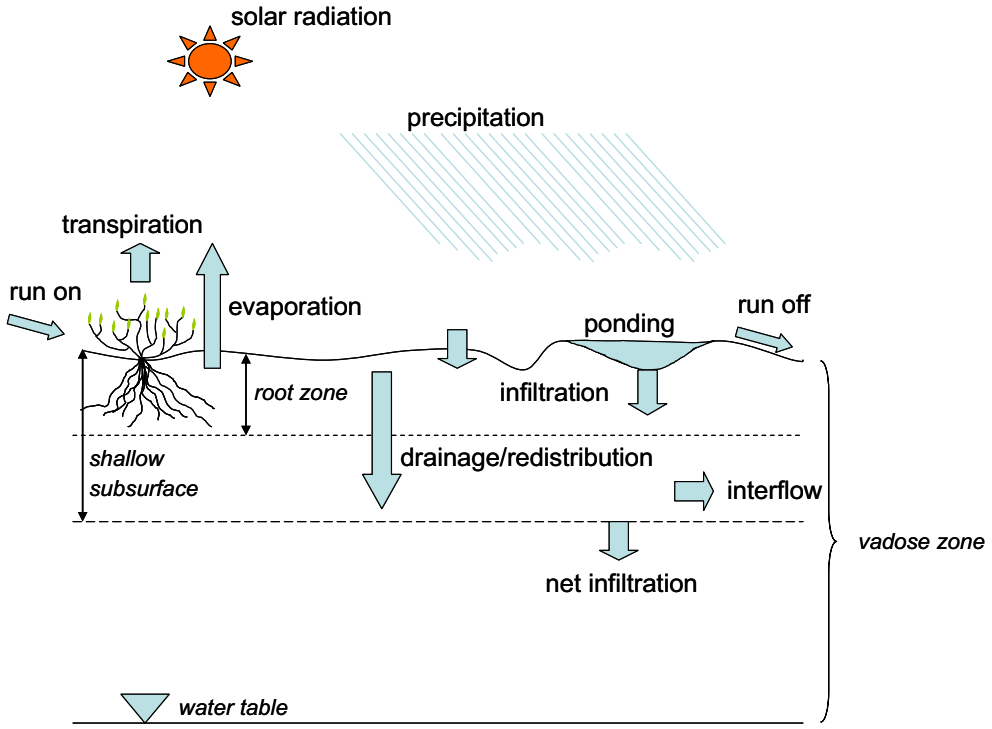

NOTE: Figure not to scale.

Figure 6.2.1-1. Processes Controlling Net Infiltration

The term "infiltration" refers to the volume flux of water through the soil–atmosphere interface, while the term "net infiltration" refers to the volume flux of water to below the shallow zone where most evaporation and transpiration occurs. In this report, "mean annual net infiltration" refers to the temporally averaged net infiltration at a given location, and "spatially averaged net infiltration" refers to the average of mean net infiltration over a specific area, such as the 125 km^2 infiltration modeling domain used for representing the region around Yucca Mountain.

The depth to which evaporation and transpiration are significant processes is often referred to as the active zone to reflect the dynamic nature of the processes in this zone. The active zone often coincides with the root zone or may extend beyond it. The amount of water in the active zone varies substantially over time; below this depth the water content changes are attenuated. In general, when thin soils predominate, the active zone is confined to the soil layer on top of the rock, and net infiltration is defined as the amount of water that moves from the surface layer of soil into the underlying rock. Others have used such terms as "recharge," "drainage," and "deep percolation" to describe net infiltration. These terms imply that water moving below the active zone will eventually recharge phreatic aquifers at depth. While this may occur in humid environments, in arid and semiarid environments with very deep vadose zones, all water moving below the active zone may not recharge the aquifer since lateral and upward flow within the deep vadose zone can occur (Scanlon et al. 1997 [DIRS 142228], p. 463).

In arid and semiarid regions such as the desert basins of the southwestern United States, the processes controlling net infiltration are highly variable in both time and space, and the dominant mechanisms may vary throughout the basin. Net recharge to underlying groundwater in desert basins is often considered to be the sum of several distinct dominant processes occurring in different regions of the basin. Important regions include mountain block, mountain front, and ephemeral stream channels and interdrainage areas of the basin floor.

Mountain block regions are characterized by very thin soils covering fractured bedrock. Areas with thin soils have less total water storage capacity and therefore have a greater potential for high net infiltration as compared with deeper soil regions. Precipitation tends to be higher here than in other regions but is highly variable in time and space. The source of precipitation (i.e., snow melt versus convective storms) can be important. Runoff may be very large in areas of high relief or other areas during storms. Evapotranspiration is often limited because vegetation is sparse. Difficulties in studying infiltration in this region (i.e., installing and maintaining gauging stations or other instrumentation) mean that very little quantitative information is available on mountain block net infiltration.

Soils in the mountain front region are typically thicker than that of mountain blocks, and relief is not as high. As with mountain block regions, the type of precipitation can be important. Runoff can also be important, and net infiltration in the mountain front region is very often focused beneath losing streams. Vegetation is also often focused around these streams, so evapotranspiration can be important.

Infiltration processes on basin floors have been studied more thoroughly than mountain block or mountain front regions. Basin floors typically receive less precipitation than surrounding mountains; however, they make up the majority of land surface and so may receive the majority of rain that falls within the basin. In contrast with mountain block and mountain front regions, basin floors are often characterized by deep vadose zones, although in the case of Yucca Mountain, the vadose zone is thinner under the basin floor than under the mountain. In general, limited infiltrability of soils, intense convective storms, and high evapotranspiration rates tend to limit net recharge in interdrainage areas of the basin floor. Ephemeral channels and surface water bodies, however, are often the locus of focused net infiltration.

A common approach for conceptualizing net infiltration (I) is by means of a near-surface water balance equation:

$$I = P + RO - \Delta W - E - T \qquad \text{(Eq. 6.2.1-1)}$$

where

P is net precipitation
RO is surface water run-on/runoff
ΔW is the change in water storage in the active zone
E is evaporation
T is transpiration.

Net precipitation is the supply of water to the soil surface in the form of rain and snowmelt, minus evaporation of liquid water stored on the surface and sublimation of snowpack. Infiltration across the soil atmosphere boundary is the sum of the net precipitation and run-on minus runoff.

Key processes of the near-surface water balance that affect net infiltration are described subsequently.

Net precipitation

In the general case, for net infiltration to occur at a location, water must be delivered to the ground surface as net precipitation and/or run-on (surface flow). Run-on is water that has moved on the surface from adjacent areas. Precipitation may be in the form of liquid water (rain) or a solid (snow), which later melts to supply liquid water to the soil surface. Precipitation can be described by the type (e.g., rain or snow), the amount (typically in depth units, e.g., mm) and duration of precipitation event. The intensity is the average precipitation rate (amount divided by duration). Snow has the added characteristic of water depth equivalent, averaging 10% water by volume. Some precipitation is temporarily stored on the surface and returned to the atmosphere before it infiltrates or runs off, including evaporation of water intercepted by vegetation and/or accumulated in surface depressions and sublimation of snowpack. Evaporation of surface water and sublimation of snowpack will depend principally upon climatic conditions.

Subsurface water movement and retention

Water movement in near-surface soil can be described by a flux law of the form:

$$\text{Flux} = \text{gradient} * \text{conductivity}$$

The applicable gradient for this flux law is that of the soil water potential. The soil water potential is most often comprises two principal terms: the gravitation potential and the pressure potential. For unsaturated systems, the pressure potential is a negative quantity and is often referred to as matric potential or by its positive-termed value, suction potential. The gradient attributable to gravity always acts downward, whereas the matric potential gradient can be in any direction. Consequently, the net soil water potential gradient and the resulting water movement can be in any direction (e.g., upward, downward, or laterally); the net soil water potential can also be zero corresponding to equilibrium conditions and no water movement. The hydraulic conductivity is the property that describes the ability of the soil to transmit liquid water and decreases nonlinearly with decreasing water content in an unsaturated soil, as capillary forces become relatively more important.

Infiltration

Water delivered to the soil surface from rain, snowmelt or run-on from adjacent areas will infiltrate the soil at a rate that depends on soil properties, transient soil water content, and water potential conditions. The infiltration rate is defined as the volume flux of water (mm^3/mm^2-yr) flowing into the soil profile per unit area of soil surface. The infiltration rate (or flux) resulting from water at atmospheric pressure being made freely available at the soil surface is referred to as the soil's infiltrability (Hillel 2004 [DIRS 178856], p. 260). Infiltrability varies with time and

is a function of the initial wetness and water potential, as well as soil texture, soil structure, and the layering of the soil profile. The rate of infiltration relative to the rate at which water is supplied to the surface will determine the amount that accumulates and/or runs off: water applied to the soil surface at a rate that exceeds the infiltrability of the soil will pond at the surface and/or run off; water applied to the soil surface at a rate less than the infiltrability will all infiltrate into the soil.

In general, infiltrability is highest in the early stages of infiltration and decreases with time, eventually approaching a constant rate. The decrease in infiltrability with time is usually due to the decrease in water potential gradients in the soil profile as infiltration proceeds. In some cases, however, the decreasing infiltrability may be caused by deterioration of the soil structure, formation of a surface crust, small particles migrating into and blocking soil pores, or entrapment of air bubbles.

Water movement after infiltration

When the natural processes that supply water to the soil surface (rain, snowmelt, run-on) stop operating and free water on the surface disappears, the infiltration process ceases. Depending on net soil water potential gradient, water in the soil can move downward, upward, remain stationary (retained), or move laterally (interflow).

Interflow can occur as a result of vertical heterogeneity in soil conductivity (e.g., vertical layering), conductivity differences along the soil–bedrock interface, and as a result of a lateral head gradient (e.g., from a sloping land surface).

Often after substantial infiltration, water will continue to move downward under unsaturated conditions, increasing the wetness of successively deeper layers. This type of flow is often referred to as redistribution. The relatively dry deeper soil draws water from the upper soil that has been wetted, redistributing water between the zones. The relative size of the two zones is a function of the initial wetting depth. Redistribution is a dynamic process that depends upon the relative dryness of the lower zone, the initial wetting depth, and the time-varying hydraulic properties of the conducting soil. The initial redistribution rate can be very high when driven by steep matric potential gradients (i.e., if the initial wetting depth is small and the underlying layer is very dry). When matric potential gradients are small (for example when the initial wetting depth is large and the lower zone is relatively wet), the initial redistribution rate is lower.

Whatever the initial rate, soil moisture redistribution will tend to decrease with time because the water potential gradient decreases and the hydraulic conductivity of the wetter layer decreases with decreasing moisture content. Often, water movement within a soil profile will slow sufficiently after an infiltration event to such an extent that the amount of water in the soil profile remains nearly constant, at least temporarily. Early observations of this tendency led to the concept of field capacity. It was noted that the rate of water content change during redistribution decreases with time and often becomes negligible after a few days. The water content at which internal drainage becomes negligible is taken as the definition of field capacity of a soil (Hillel 2004 [DIRS 178856], p. 310).

Upward soil water movement will occur when the net soil water potential gradient is upward. This situation can arise when the near-surface soil dries in response to evapotranspiration and the resulting upward matric potential gradient overcomes the gradient due to gravity. Upward soil water movement is limited to a large extent by the very low hydraulic conductivity of relatively dry soils. Some upward water movement may be in the form of water vapor movement.

Soil water retention

The amount of water in a soil layer or profile within the active zone will change with time in response to water that enters or leaves the system from downward or upward water movement and/or evapotranspiration. The amount of soil water retained is a function of its moisture characteristic curve, which is the relationship between the soil water potential and the water content. Moisture characteristic curves are different for soils of different characteristics (e.g., texture); two adjacent soil layers at equilibrium (i.e., same water potential) have different water contents if their moisture characteristic curves are different. Moisture characteristic curves are also hysteretic as the amount of soil water retained depends on whether the soil is being wetted or dried.

Surface Water Runoff

Whenever the water delivery rate (precipitation + run-on) exceeds the soil's infiltrability, water accumulates on the soil surface. This free water is often referred to as surface water excess. Some water can be stored on vegetation surfaces as well. Because the soil surface is not flat and smooth, the surface water excess collects in depressions, forming puddles (ponding). If ponding exceeds the surface water storage capacity of the depressions, surface runoff commences.

Runoff comprises a wide variety of flow patterns. At one extreme is thin, sheet-like runoff called overland flow. Overland flow is often the primary type of surface runoff from small natural areas or areas having little topographic relief. As runoff accelerates and gains in erosive power, it eventually forms channels. Further erosion can deepen these channels, and individual channels may eventually converge, forming dendritic networks characteristic of stream flow.

Evapotranspiration

Water within the soil profile can be removed from the soil profile by direct evaporation or through extraction and transpiration by plants. Direct evaporation is the dominant mechanism of water transfer from the soil to the atmosphere when the soil surface is bare, while transpiration may dominate for vegetated soil surfaces. However, since the processes of evaporation and transpiration are often difficult to discern separately, they are commonly lumped into a single process called evapotranspiration (ET). Evapotranspiration is dependent on a variety of biotic and abiotic factors including vegetation characteristics (e.g., root density), climatic conditions (e.g., solar radiation), and soil properties (e.g., hydraulic conductivity function).

Direct evaporation from the soil occurs when three conditions persist: (1) presence of a sustained supply of thermal energy to change water from liquid to gas phase (latent heat); (2) presence of a water vapor pressure gradient at the soil–atmosphere surface; and (3) presence of a continuous supply of water from or through the soil.

Transpiration, loss of water from the plant to the atmosphere, is largely a passive response to the atmospheric environment. Terrestrial plant growth requires CO_2 for photosynthesis, which diffuses through open stomata on plant leaf surfaces to intercellular spaces inside the leaf. Concurrently, water vapor diffuses out of the leaf, from wet cell membranes through stomatal pores to the much dryer atmosphere (transpiration). Some of the water extracted from the soil by plant roots is used in photosynthesis and other essential metabolic processes. However, 95% to 99% of the water that passes through a plant is lost to the atmosphere through transpiration (Nobel 1983 [DIRS 160500], p. 506). Transpiration requires energy to convert water within the vegetation to water vapor, and also requires a water vapor gradient between the vegetation and the atmosphere. The supply of water for transpiration is dependent on the water uptake from the soil and transport within the vegetation. As the adjacent soil dries, water uptake by the vegetation slows. As the rate of water uptake decreases, the vegetation becomes water stressed and eventually will be unable to extract any water from the soil. The amount of water in the soil at this point is referred to as the wilting point and depends on both soil and vegetation characteristics.

6.2.2 Modeling Processes Controlling Net Infiltration

A model to estimate net infiltration must account for the terms of the water balance described by Equation 6.2.1-1. Each of these terms is by itself a complex physical process that can be approximated with simplified representations or models. There are usually a number of models to choose from for each process, including empirical models and physical models of varying detail. In this section, the choices of modeling approaches will be introduced.

The physical processes involved in net infiltration are interdependent. Therefore, the estimate of one term affects the estimate of another and, consequently, affects the estimate of net infiltration. For example, runoff is often calculated as a function of the amount of water stored in the near-surface soil; the drier the soil, the less runoff occurs. As more water enters the soil surface, there is more opportunity for net infiltration.

Net infiltration models are most often implemented within computer programs that combine models of the relevant physical processes. There are many computer programs that can be used to calculate net infiltration along with other water balance components (e.g., Ravi and Williams 1998 [DIRS 178131]). These programs were often developed for specific applications (e.g., contaminant transport, agriculture) and with varying requirements for predictive accuracies. Consequently, existing computer programs can incorporate significantly different models and approaches for estimating water balance components.

Modeling the Components of the Near Surface Water Balance

This section examines various conceptual models used to represent the components of the water balance equation. These components include net precipitation, water movement in the soil profile, evapotranspiration, and runoff.

Net precipitation

A net infiltration model requires precipitation as an input, specifically, the amount, the type, and the duration of the precipitation. The precipitation input can be directly from records of meteorological data or can be derived from empirical models to represent a particular climate, including future climates. Most precipitation data and estimates provide daily total amounts. Daily amounts can be applied over a portion of a day to reproduce observations regarding precipitation intensity, which can vary as a function of season. Whether precipitation falls as rain or snow is a function of the temperature of the atmosphere through which it falls. Observations of snowfall and air temperature have shown that when air temperature is below 0°C, nearly 100% of precipitation falls as snow (Maidment 1993 [DIRS 125317], p. 7.2). Once snow has accumulated on the ground it can either sublimate or melt. Results of studies aimed at measuring sublimation in the field arrive at a wide range of values (1% to 80% of snow loss for the season), depending upon site location and methods used to measure sublimation (Hood et al. 1999 [DIRS 177996]). Snowmelt is commonly predicted from either an energy balance model or from an empirical temperature index approach. The energy balance approach requires extensive climatic data and parameters describing the snowpack characteristics. Snowmelt calculated from the temperature index method is calculated as proportional to the difference between the air temperature and the melting point of snow (0°C).

Soil water movement

The model for water movement within the near-surface soils is an important component of a net infiltration model. The amount and location of water within the soil profile as a function of time will be determined largely from the representation of this process. One common approach for modeling water movement and storage in unsaturated soil is based on the concept of "field capacity." Field capacity for a given soil layer is the amount of water that the soil can hold without significant gravity drainage occurring. Once the saturation of the soil layer exceeds the field capacity of the soil layer, excess water moves downward to the next soil layer. Field capacity is often described as the water content when gravity drainage from the soil becomes negligible. Because this definition is imprecise, field capacity is usually defined at a prescribed value of matric potential consistent with the hydraulic conductivity of the soil becoming very small. The most common value of matric potential associated with field capacity values is −1/3 bar, which is about −340 cm of matric potential head, although the water content at −0.1 bar is also considered representative, especially for coarse soils. Estimates of water movement within a soil profile can be made with the field capacity as the single material parameter for each layer or unit. The field capacity approach implies only gravity-driven (downward) advective water movement. Matric potential gradients, which will affect downward water movement and can result in upward water movement in some cases, are not accounted for with this approach.

A more physically based approach for estimating unsaturated water movement is by means of Richards' equation, which is a differential equation that describes transient flow in an unsaturated porous medium. Richards' equation must be solved numerically for essentially all realistic conditions. With this approach, water movement is driven by gradients in net soil water potential, so matric potential gradients as well as that from gravity are included. The rate of water movement is proportional to the hydraulic conductivity of a soil, which is a varying function of the amount of water in the soil. This approach utilizes the soil water characteristic

curve, which describes the amount of water a soil holds at all matric potentials, not just the single value assigned at "field capacity." This approach requires more parameters, such as the hydraulic conductivity function and the soil water characteristic curve of each soil layer or unit, than the field capacity approach.

Evapotranspiration

Evaporation and transpiration are processes by which water is removed from a soil. These processes are often combined together and referred to as evapotranspiration (ET), in part because it can be difficult to decouple water loss from these two processes. Estimates of ET are usually proportional to the climatic conditions that describe the atmosphere's demand for water (e.g., solar radiation, temperature, wind speed, relative humidity). Potential evapotranspiration (PET) and reference evapotranspiration (ET_0) are two terms that are commonly used to characterize the climatic conditions and usually represent an upper bound of the amount of ET that can occur. Often, actual ET is less than PET or ET_0, especially in drier climates, because soil moisture limits evaporation, transpiration, or both.

Evapotranspiration can be estimated as a combined term with no attempt to distinguish between evaporation and transpiration. However, because they are separate processes, many models estimate evaporation and transpiration separately. Evaporation can be estimated by different approaches. One common empirical approach is to estimate evaporation as a function of the near-surface water content of the soil, taking into account the observation that below some critical water content the evaporation rate decreases as the surface soil dries. This approach can also be implemented in terms of time by expressing the evaporation rate as a function of time after wetting. Alternatively, mechanistic models of evaporation can be implemented. Such a model often employs a boundary layer at the soil surface through which heat and moisture are exchanged with the atmosphere. Once the immediate soil surface layer dries, diffusive vapor movement occurs from within the soil profile. This type of model must be incorporated into a water movement model that allows for suction-driven flow in addition to water vapor diffusion.

Similar to evaporation, there are a wide range of models for estimating transpiration. There are models that incorporate elements of the plant physiology including water movement within individual roots. However, the most common transpiration models are largely empirical. One distinguishing characteristic of transpiration models is the location from which water is extracted from the soil profile. Lumped models extract moisture from the root zone uniformly with depth. Other models impose an assumed distribution of water extraction from the root zone, which can be proportional to a root density distribution that changes with depth. Some models employ root zones that change as vegetation matures.

Transpiration rates depend on the status of the vegetation with respect to its seasonal growth and development. A common modeling approach to capture this behavior is to use crop or transpiration coefficients, which describe the time-varying ability of the vegetation to extract moisture over the course of its growing season. A related approach is to estimate transpiration rates as a function of the amount of vegetation as measured or estimated from the fractional cover (fraction of soil surface covered by vegetation) or leaf area index (leaf surface area per unit soil surface beneath it).

Transpiration models often relate transpiration rate to the water content of the surrounding soils. Below some water content known as the wilting point, vegetation cannot extract sufficient moisture to sustain itself from the surrounding soils, and transpiration ceases. The wilting point is usually defined as water content at a value of suction head at which the vegetation will fail; thus, the value of suction depends on the vegetation and ranges from 15 bars for many common agricultural crops to greater than 60 bars for desert-adapted vegetation.

Another challenge for representing transpiration is defining the vegetation present at a study site as a function of location, time during the growing season, and under different annual conditions (e.g., drought). Depending on the scale of the site, either on-site vegetation characterization is performed or, if the site is large, satellite multispectral remote sensing (e.g., LANDSAT) data is typically used to measure the quantity and distribution of vegetation via the determination of a vegetation index (e.g., Normalized Difference Vegetation Index). When satellite data is used to characterize vegetation, it is typically calibrated with direct measurements made on the ground (e.g., Leaf Area Index).

Runoff

Runoff can be estimated a number of ways. One approach is to estimate runoff as the difference between precipitation and the surface infiltration. The infiltration into the surface soil in response to a specific precipitation event can be estimated using a model of subsurface water movement. A simple approach is to estimate runoff from a water balance of the near-surface soils; infiltration in excess of that required to fill the porosity of the near-surface soils will be runoff. Under some limited conditions, analytical infiltration models (e.g., the Green-Ampt model as discussed by Maidment 1993 [DIRS 125317], pp. 5.32 to 5.39) can also be used to estimate the surface infiltration and hence runoff.

A common alternative modeling approach is to estimate runoff as a function of surface condition and precipitation data. There are models of this type that estimate runoff in response to specific storms, daily precipitation, or on a seasonal or annual basis. Factors that can be used to describe the surface condition include the amount of moisture in the soil, the type of soil, and the extent to which the surface is vegetated and/or developed. Models of this type often utilize the "curve number" approach where runoff is estimated as a function of a single empirical term (the curve number) which is related to the soil and vegetative cover properties in the watershed that are tabulated in handbooks. Most runoff models include "abstraction," which is storage of precipitation in surface depressions and on vegetation.

6.2.3 Criteria for Selection of Net Infiltration Model Components

As described previously, there are a wide variety of models and model components that could be used for the net infiltration modeling, varying in terms of their conceptual basis and numerical implementation. Criteria for evaluating models and model components for net infiltration modeling at Yucca Mountain are given below.

1. The model and model components should be consistent with the overall project purpose.

The purpose of the net infiltration model is to produce estimates of annual net infiltration for the Yucca Mountain site over long periods of time subjected to different future climate scenarios. It

is not the purpose of the model to describe the detailed spatial and temporal character of water movement in the subsurface, describe the details of water consumption by plants or of transport of water vapor in the surface soils, or determine peak surface water flow rates and sediment transport during runoff events.

2. Model component complexity should be consistent with available input data.

The choice of a modeling approach should be consistent with the nature and quality of the data available. In general, as model complexity and detail increase, the requirements for input parameters increase as well. Because few direct and qualified measurements of soil properties exist for the Yucca Mountain site, it is appropriate to represent the ability of the soil to hold and transmit water with a simple model such as one based on the concept of field capacity rather than a more mechanistic model such as one based on Richards' equation. Since the modeling domain is so large and varied, the choice of a simple runoff model linked to the water balance model at each cell is justified over a more complicated runoff model. The availability of high quality satellite data which can be used to estimate the spatial and temporal variability of vegetation justifies the use of a more sophisticated model of evapotranspiration.

3. Model components must be consistent with other model components.

The model components of the water balance terms are interdependent both in a conceptual and computational sense and must be formulated and implemented in a consistent manner. For example, the amount of evapotranspiration is expected to depend on the subsurface water content. Downward water movement will depend on the amount of water removed from the soil by evapotranspiration. Thus, the water movement model and evapotranspiration must be integrated.

4. The model should be computationally efficient.

The computations will involve modeling a very large spatial extent over long periods of time. The model domain covers approximately 125 km^2, and estimates of net infiltration are required for many thousands of years. Further, numerous simulations will be required to assess parameter sensitivities and different climate scenarios. In order to perform all of the necessary computations in a reasonable amount of time, the model should be computationally efficient.

5. The model should be accessible and open.

To increase credibility and facilitate review of the calculations, the net infiltration model should be in as accessible a format as possible. Details of the calculations, including inputs, should be readily available to any interested party. In addition, the computations should be able to be independently reproduced.

6. The model and model components should demonstrate reasonable predictive capability.

The model and model components should be demonstrated to have the ability to reasonably predict or estimate the quantities of interest by comparing to measured data, results of other calculations, and/or other estimates.

6.2.4 Alternative Models Considered

There were a number of models that were considered to provide estimates of net infiltration at Yucca Mountain. The models can be grouped based on how they consider subsurface water movement, either with Richards' equation or with a water balance approach that uses field capacity. Within each of these groups are many specific models. One representative model is described below for each group in order to provide a representative description of the capabilities and limitations of existing models considered for estimating net infiltration at Yucca Mountain. These models are HYDRUS-1D and HELP, respectively.

6.2.4.1 Richards' Equation Approach: HYDRUS-1D Program

Summary of HYDRUS-1D

HYDRUS-1D (Šimůnek et al. 2005 [DIRS 178140]) is a software package for simulating water, heat, and solute movement in one-dimensional variably saturated media. There is also a HYDRUS-2D (Šimůnek et al. 1999 [DIRS 178228]) code, which is a two-dimensional version of the software.

The HYDRUS-1D program numerically solves the Richards' equation for variably saturated water flow and convection-dispersion type equations for heat and solute transport. The software has been used in many studies in support of agricultural projects, landfill design projects, and other studies where detailed predictions of soil moisture and storage, infiltration and evapotranspiration rates, and distribution of dissolved compounds and heat are required. It has also been used in near-surface water balance modeling to evaluate land–atmosphere interactions, deep drainage, and groundwater recharge.

HYDRUS-1D was compared to codes with similar capabilities. The benchmarking analyses presented by Chen et al. (2002 [DIRS 178132]) and Scanlon et al. (2002 [DIRS 177213]) suggested that all the codes considered provided similar results. HYDRUS-1D and HYDRUS-2D, along with the other four codes, were selected out of 248 fate and transport codes in an evaluation by MDH Engineered Solutions Corp. (2003 [DIRS 178204], Section 5.1, p. 20) and were considered as the best in their category.

HYDRUS-1D incorporates a modified Richards' equation in the following form:

$$\frac{\partial \theta}{\partial t} = \frac{\partial}{\partial x}\left[K\left(\frac{\partial h}{\partial x} + 1 \right) \right] - S \qquad \text{(Eq. 6.2.4.1-1)}$$

where

h is the water pressure head [L]
θ is the volumetric water content [L^3L^{-3}]
t is time [T]
x is the spatial coordinate [L] (positive upward)
S is the sink term [$L^3L^{-3}T^{-1}$]
K is the unsaturated hydraulic conductivity function [LT^{-1}] given by

$$K(h,x) = K_s(x)K_r(h,x) \quad \text{(Eq. 6.2.4.1-2)}$$

where K_r is the relative hydraulic conductivity [dimensionless] and K_s the saturated hydraulic conductivity [LT^{-1}]. The unsaturated soil hydraulic properties, $\theta(h)$ and $K(h)$, in Equation 6.2.4.1-1 are in general highly nonlinear functions of the pressure head. HYDRUS permits the use of five different analytical models for the hydraulic properties.

Equation 6.2.4.1-1 assumes that the air phase plays an insignificant role in the liquid flow process and that water flow due to thermal gradients can be neglected.

The equation incorporates a sink term to account for water uptake by plant roots. The sink term, S, is defined using the form proposed by Feddes et al. (1974 [DIRS 178173]):

$$S(h) = \alpha(h)S_p \quad \text{(Eq. 6.2.4.1-3)}$$

where the root-water uptake water stress response function $\alpha(h)$ is a prescribed dimensionless function of the soil water pressure head ($0 \le \alpha(h) \le 1$), and S_p the potential water uptake rate [T^{-1}].

When the potential water uptake rate is nonuniformly distributed over the root zone, S_p becomes

$$S_p = b(x)T_p \quad \text{(Eq. 6.2.4.1-4)}$$

where $b(x)$ is the normalized water uptake distribution [L^{-1}] and T_p is the potential transpiration [L/T]. This function describes the spatial variation of the potential extraction term, S_p, over the root zone and is obtained by normalizing any arbitrarily measured or prescribed root distribution function.

The flow region may be composed of nonuniform soils. The water flow part of the model can deal with prescribed head and flux boundaries and boundaries controlled by atmospheric conditions, as well as free drainage boundary conditions. The governing flow and transport equations are solved numerically using Galerkin-type linear finite element schemes.

Evaluation of HYDRUS for estimating infiltration at Yucca Mountain

There are several reasons that HYDRUS-1D was not used for estimating net infiltration at Yucca Mountain. The first is that HYDRUS-1D is a one-dimensional model and therefore unable to simulate water movement along the surface as runoff between cells. While this limitation could

have been overcome by either linking together adjacent models or examining other versions of the HYDRUS codes that include two- and three-dimensional implemtations, other models and methods were easier to implement. The second reason this code was not used was because the previous model used by the project was a mass-balance model and the available data sets describing soil properties were more compatible with a mass balance, field capacity approach. Appropriate properties could have been estimated and developed for a Richards' equation approach, but this was not pursued. Finally, the strength of a Richards' equation approach is that it can simulate the spatial and temporal details of unsaturated water movement in soil. This ability, however, requires substantial and detailed information about the soil structure and variability of properties such as moisture characteristic curves and hydraulic conductivity functions. At the Yucca Mountain site, the available soil property dataset was limited in the number of samples and the types of measurements made. For these reasons, it was decided to implement a mass balance modeling approach based on the field capacity concept instead of a more physically based approach using the Richards' equation.

6.2.4.2 Water Balance Model Incorporating Field Capacity Approach: Hydrologic Evaluation of Landfill Performance (HELP) Model Computer Program

Summary of HELP

Hydrologic Evaluation of Landfill Performance (HELP) (Schroeder et al. 1994 [DIRS 178136]) is the software package that incorporates a quasi-two-dimensional water balance model to simulate water movement in the unsaturated zone. The code was developed by the U.S. Army Engineer Waterways Experiment Station (WES) for the U.S. Environmental Protection Agency (EPA) Risk Reduction Engineering Laboratory. The primary purpose of the model was to assist in the comparison of landfill design alternatives as judged by their water balances.

The HELP program was tested extensively using both field and laboratory data (Schroeder et al. 1994 [DIRS 178136]). HELP simulation results were compared to field data for 20 landfill cells from seven sites (Schroeder and Peyton 1987 [DIRS 178857]). The lateral drainage component of HELP was tested against experimental results from two large-scale physical models of landfill liner/drain systems (Schroeder and Peyton 1987 [DIRS 178754]). The model is widely used in the USA and internationally (Dho et al. 2002 [DIRS 178133]).

The inputs to the HELP model are daily climatologic data, soil characteristics, and design specifications. The climatologic data include daily precipitation, mean daily temperature, and total global solar radiation and may be either provided by the user or generated stochastically. It also includes growing season, average annual wind speed, average quarterly relative humidity, normal mean monthly temperature, maximum leaf area index, evaporative zone depth and latitude.

The soil data include porosity, field capacity, wilting point, saturated hydraulic conductivity, and Soil Conservation Service runoff curve number for antecedent moisture condition II. The model contains default soil characteristics for 42 material types for use when measurements or site-specific estimates are not available. The layers in the landfill are typed by the hydraulic function that they perform. Four types of layers are available: vertical percolation layers, lateral drainage layers, barrier soil liners, and geomembrane liners.

HELP calculates water balance on a daily basis as follows. Snowfall and rainfall are added to the surface snow storage, if present, and then snowmelt plus excess storage of rainfall is computed. The total outflow from the snow cover is then treated as rainfall in the absence of a snow cover for the purpose of computing runoff. A rainfall-runoff relationship is used to determine the runoff. Surface evaporation is then computed. Surface evaporation is not allowed to exceed the sum of surface snow storage and intercepted rainfall. Interception is computed only for rainfall, not for outflow from the snow cover. The snowmelt and rainfall that does not run off or evaporate is assumed to infiltrate into the landfill. Computed infiltration in excess of the storage and drainage capacity of the soil is routed back to the surface and is added to the runoff or held as surface storage.

The rainfall-runoff process is modeled using the Soil Conservation Service curve-number method (Maidment 1993 [DIRS 125317], pp. 9.21 to 9.26). Potential evapotranspiration is modeled by an energy-based Penman method. The program uses an albedo of 0.23 for soils and vegetation and 0.60 for snow. The vegetation data is generated by a vegetative growth model. Vertical drainage is assumed to be driven by gravity alone and is limited only by the saturated hydraulic conductivity and available storage of lower segments. If unrestricted, the vertical drainage rate out of a segment is assumed to equal the unsaturated hydraulic conductivity of the segment corresponding to its moisture content, provided that moisture content is greater than the field capacity or the soil suction of the segment is less than the suction of the segment directly below.

Evaluation of HELP for estimating net infiltration at Yucca Mountain

HELP was not used to estimate net infiltration at the Yucca Mountain site primarily because it was developed for a different type of application, and consequently it is not consistent with the overall purpose of estimating net infiltration at Yucca Mountain for thousands of years under different climate conditions. To be used for this type of application, HELP would require substantial modifications.

Most water balance models that incorporate field capacity were developed for specific applications rather than as general purpose models. In the case of HELP, it was developed to evaluate landfill systems. Many of the features and capabilities of HELP, such as lateral flow in drainage layer and geomembrane layers, are not applicable for estimating net infiltration at Yucca Mountain. Other features, such as modeling entire slopes as a single element, are not consistent with the terrain of Yucca Mountain. Some of the features not explicitly included in HELP relevant to the Yucca Mountain site include: permitting run-on from adjacent locations; saturation of thin soil layers; ET that is a function of slope, azimuth, and elevation; and specifying bedrock as a lower boundary.

6.3 DESCRIPTION OF THE CONCEPTUAL MODEL – MASS ACCOUNTING SYSTEM FOR SOIL INFILTRATION AND FLOW (MASSIF)

The model developed to estimate net infiltration at Yucca Mountain is referred to as MASSIF (Mass Accounting System for Soil Infiltration and Flow). In this section, MASSIF is summarized, the rationale for its development is given, and some of its key features are summarized.

6.3.1 Summary of MASSIF

MASSIF estimates net infiltration at the Yucca Mountain site based on a daily water balance calculation of the near-surface soils. The MASSIF model defines net infiltration as the water that passes out of the soil layer into the underlying bedrock. The water balance includes net precipitation as input, water storage and movement within the soil including evapotranspiration, and water moving from the soil into the underlying bedrock.

The model domain is composed of a number of cells with equal surface area that extend from the surface to the contact with the underlying bedrock. The description of each cell includes the cell depth as defined by the soil layer depth; soil type and associated properties; cell elevation, azimuth and slope; and vegetation-related characteristics. Each cell is composed of one to three soil layers, depending on the soil depth. The topmost layer is relatively thin and is divided into two sections (nodes) representing the bare surface fraction and the fraction of the surface covered with vegetation (canopy fraction). The top layer is designated as the evaporation zone. The second layer extends from the bottom of the first layer to the bottom of the root zone or to the soil–bedrock interface in the case that the maximum rooting depth is greater than the soil depth. Layers 1 and 2 comprise the evapotranspiration zone. The third layer extends from the bottom of the root zone (Layer 2) to the soil–bedrock interface. When soil depth is less than maximum rooting depth, Layer 3 is not represented (thickness is set to zero).

Daily climatic data are input to the model, including precipitation and maximum and minimum air temperature. Precipitation and mean temperature are adjusted for cell elevation. Snow, snowmelt, and sublimation are included in the model.

Subsurface water movement within the model is one-dimensional; that is, there is no subsurface water movement between adjacent cells. The model allows rain and snowmelt to run off the top of one cell onto an adjacent cell that is at a lower elevation. Runoff can occur if the net precipitation exceeds the ability of the thin surface soil layer to store and transmit water to underlying soils. Runoff will also occur if the entire cell from the bedrock to the surface saturates. In the case of runoff, water is diverted to the surface of the next downstream cell.

Subsurface water movement is estimated by means of a daily water balance approach for each cell. Subsurface water movement within the model is one-dimensional; that is, there is no subsurface water movement between adjacent cells. Downward water movement from layer to layer within a cell is based on the field capacity concept. Field capacity of the soil represents the amount of water that is held by the layer after gravity drainage. Water in excess of the field capacity will be available to move downward to a lower layer. Water is removed from the root zone based on a daily calculation of evapotranspiration (ET) for each cell. The ET calculation is derived from the "dual crop" version of the FAO-56 method, which produces separate estimates of evaporation and transpiration depending upon the fraction of the surface covered by vegetation. ET is calculated proportional to a reference ET, which accounts for the atmospheric demand for water based on daily climatic conditions at each cell. The FAO-56 methods provide for corrections in wind speed, minimum relative humidity, plant height, and stomatal resistance that differ between the FAO-56 standards for agricultural crops and the desert vegetation and climate of Yucca Mountain. These adjustments were implemented in the model.

Water above field capacity in the bottom-most soil layer can enter the underlying bedrock layer, limited by the effective saturated hydraulic conductivity of the bedrock. Any water that moves into the bedrock layer is net infiltration for that cell and passes out of the bottom of the model.

6.3.2 Rationale for Key Components of MASSIF Model

The representations of subsurface water movement and evapotranspiration are key components of MASSIF. Subsubsurface water movement is modeled with a water balance that uses the field capacity approach and ET is calculated with the FAO-56 method that represents the root zone as a lumped entity.

The rationale for using these modeling approaches is discussed below in the context of the model component selection criteria given in Section 6.2.3.

1. Model components should be consistent with the overall project purpose.

The purpose of the net infiltration model is to produce estimates of annual net infiltration for the Yucca Mountain site over long periods of time. The net infiltration model is not being developed to describe the detailed spatial and temporal character of other water balance components, such as the details of water consumption by plants or of transport of water vapor in the surface soils. This purpose is reflected in the model components of MASSIF: a field capacity approach using estimates of the amount of water that drains from a soil layer but does not explicitly model water movement within the soil layer; and the FAO-56 method that estimates daily ET values over a lumped root zone but does not explicitly model ET details such as water uptake by individual roots or transport of water within the plant.

2. Model component complexity should be consistent with available input data.

The amount and type of available input data for the net infiltration model are necessarily limited due to the large spatial coverage of the model and the relatively few directly measured data. These limitations preclude the expectation of accurate predictions at specific locations. The need to estimate many of the inputs results in net infiltration values that are representative and consistent with the characteristics and properties of locations at Yucca Mountain rather than being considered site-specific predictions.

Data required as input to model subsurface water movement include soil thickness above bedrock, soil types and layering, and corresponding soil hydraulic properties. Most of these data are not measured directly for the vast majority of the Yucca Mountain domain and must be estimated from a few measurements, including soil thickness and soil properties. There are few available measurements of soil hydraulic properties, and very little information on subsurface soil characteristics such as layering. A significant advantage of using a field capacity approach is that it requires a very limited amount of input pertaining to hydraulic properties. Further, although not directly available for the Yucca Mountain soils, the field capacity values required as input can be reasonably estimated from other information that may be available, such as soil textural characteristics.

The lack of measured, site-specific input data indicates that there can be little merit in attempting to precisely model subsurface water movement at discrete locations within the domain and that an approach more complicated than one that uses field capacity is not warranted. With the limitations of the inputs, it is not apparent whether estimates of net infiltration would be more accurate with a model that implemented a water balance using the field capacity approach or a more complicated Richards' equation approach.

The detailed data required to explicitly model transpiration from vegetation associated with a particular cell are largely unknown. These unknowns include the number and distribution of specific plants and seasonally dependent plant surface characteristics such as leaf area index and height or root length and density. Further, extrapolating these data in response to future climate changes would be extremely difficult.

The FAO-56 method is consistent with the limited availability of detailed data regarding ET at Yucca Mountain. This method to estimate ET has been developed to allow for its use when there is limited direct information regarding vegetation characteristics. The FAO-56 method does not model individual plants but instead provides a typical response of vegetation types based on transpiration coefficients that involve day of the year, location, annual precipitation, and daily water status of the soil. Transpiration is assumed to remove water from the entire lumped root zone and does not specify a distribution of subsurface water extraction.

Despite the limitations on available field data, the methods incorporated into the MASSIF model provide an integrated tool that can be used to estimate net infiltration and evaluate uncertainty in net infiltration arising from parameter uncertainty. In addition, MASSIF is ideally suited for evaluating and ranking input parameter sensitivities. For these reasons the MASSIF conceptual model is considered adequate for its intended use.

3. Model components should be consistent with the complexity and uncertainties of other aspects of the net infiltration model.

Uncertainty in net infiltration estimates may come from sources other than the models for subsurface water movement and ET. An important example is the need for daily precipitation as a principal input for calculations of the daily water balance, subsequent runoff, soil water movement, and ET. The precipitation input relies on estimates of possible future climates that are by their nature associated with substantial uncertainty. For this reason, precipitation input is represented by a stochastically generated set of precipitation years that include rare and possibly important extremes.

4. Model components must be consistent with other model components.

Because they are both directly related to the water balance, the water movement model must be integrated with the model for ET. This is important with respect to net infiltration because a very large fraction of surface infiltration is expected to be consumed as ET. The FAO-56 method uses the field capacity concept to account for water in the near-surface and root zone, consistent with the use of the field capacity approach in the subsurface water movement model.

5. Model components should be computationally efficient.

Both the field capacity approach and the FAO-56 method are computationally straightforward and do not require iterative numerical solutions.

6. The model should be accessible and open.

MASSIF was developed using Mathcad, a widely available commercial software package that allows the combination of formatted text, figures, and mathematical calculations in the same document. The benefit of this approach over using compiled code is that the documentation of the calculation exists side-by-side with the actual calculation routines, inputs, and results. The use of Mathcad was practical largely because MASSIF utilizes a daily water balance using a field capacity approach, rather than another more involved approach to water movement that would require sophisticated and computationally intense numerical solution methods. All equations, inputs, assumed values, and constants are explicitly shown in the MASSIF Mathcad files, allowing independent verification and use of the model by those other than the model developers.

7. The model should demonstrate reasonable predictive capability.

The validation of MASSIF is discussed in Chapter 7.

6.3.3 Description of Key MASSIF Elements

Climatic input to model

Daily climatic data input to the model includes precipitation and minimum and maximum air temperature. These values are adjusted for the elevation of a particular cell. Precipitation is in the form of snow if the average air temperature is below 0°C. Snow is allowed to sublimate during snowfall rather than as part of the snowpack. When the average temperature is above 0°C, snowpack melts at a temperature-dependent rate. Rain and snowmelt are input to the top of each cell.

Initial runoff

The initial runoff from a cell is calculated based on the ability of the surface soil layer to store and transmit water to a lower layer. Net precipitation (rain, snowmelt, and run-on from an adjacent cell) are applied to the surface soil layer. If water content is in excess of the saturated water content of the soil after water redistribution (described below), this excess is diverted as runoff and is available to the next downstream grid cell.

Subsurface water movement

Subsurface water movement is modeled within each grid cell as a one-dimensional (vertical) water balance. The top boundary of each cell is the atmosphere/land surface contact and the bottom boundary is the underlying bedrock. The model of the soil between these boundaries depends on the soil depth at a cell location, the rooting depth of the vegetation, and the evaporation depth. The evaporation depth is the relatively shallow depth in which the soil is

dried directly by evaporation. The rooting depth is the assumed extent of the root system and defines the depth from which evapotranspiration will occur.

The soil is divided into one to three layers, depending on the soil depth for the cell (Figure 6.3.3-1):

The surface layer (Layer 1) is set to the evaporation depth unless the soil depth is less than this, in which case, the surface layer is set to the soil depth. The surface layer is divided into two nodes to differentiate between surface soil that is within the vegetation canopy and bare soil outside the canopy.

If the soil depth is greater than the evaporation depth, then a second soil layer is represented (Layer 2). If the soil depth is less than the rooting depth, the second layer extends from the surface layer to the bottom of the soil profile. If soil depth is greater than the maximum rooting depth, then the second layer extends to the maximum rooting depth.

If the soil depth is greater than the rooting depth, then a third soil layer is represented and extends from the maximum rooting depth to the bottom of the soil profile.

The bedrock interface is located beneath the bottom-most soil layer.

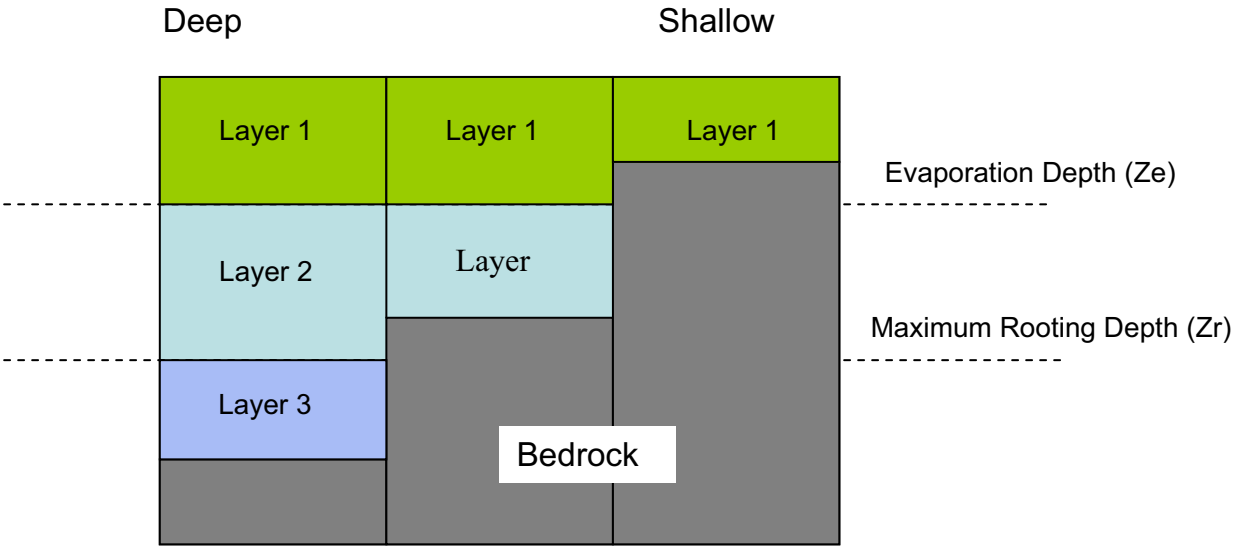

Figure 6.3.3-1. Schematic Figure Showing How Soil Layers Are Assigned for Different Soil Depth Scenarios

There are two principal computational steps that are calculated on a daily basis: water movement within the soil profile followed by water removal due to evapotranspiration.

a. Water movement

Surface infiltration is applied to the vegetated and bare soil nodes of the surface layer in proportion to their areal fraction. The total amount of water within each node is compared to the field capacity. Water in excess of the field capacity is allowed to move to the second layer,

which describes the balance of the root zone. The process is repeated, and water in excess of field capacity in the second layer is passed into the third soil layer which describes the region below the root zone. Finally, water in excess of field capacity in the third layer is passed into the underlying fractured rock, where it becomes net infiltration.

Flow limits are implemented between soil layers and between the soil and the rock. The amount of water that can pass between layers is calculated from Darcy's law assuming a unit gradient (gravity flow) and the effective saturated hydraulic conductivity value for the soil and for the bedrock. When one or more of these flow limits is reached, the overlying soil node can accumulate water in excess of field capacity and up to the soil saturated water content. When the soil saturated water content has been reached in the surface layer, excess water supplied to the soil is manifested as runoff.

The bare-soil and vegetated nodes that comprise the surface layer can have different water contents preceding a precipitation or run-on event. It is conceptually possible that one of them might reach the saturation limit while the other remains below. The physical distance between the bare-soil and canopy regions is on the order of the plant size, while the area of a "cell" is 30 m × 30 m. This means that excess water (runoff) from one of the surface nodes should first be supplied to the other surface node describing the surface layer before it is added to the runoff from the cell.

b. Evapotranspiration

Water is removed from the surface layer and Layer 2 based on a daily calculation of ET for each cell. The ET calculation is derived from the dual crop version of the FAO-56 method, which produces separate estimates of evaporation and transpiration. Evaporation is assumed to occur over the exposed and wetted fraction of the surface layer, which is the portion of the soil surface that is exposed to evaporative energy. Transpiration occurs from the "root zone," which comprises the surface layer and the underlying Layer 2.

The first step in estimating ET is to calculate the reference ET (ET_0), which is ET from a hypothetical crop of well-watered grass. ET_0 is the principal means by which the FAO-56 method accounts for the effect of daily climate on ET. For each cell, ET_0 is calculated based on the location of the cell with respect to the sun, cell elevation, daily temperatures and wind speed.

Total transpiration from the root zone is calculated by multiplying ET_0 times a transpiration coefficient for each cell. The transpiration coefficient accounts for the difference between the characteristics associated with a cell's specific vegetation to those assumed for the ET_0 calculation. The transpiration coefficient is a function of the day of the year to reflect the development stage of the vegetation. In the case where there is no vegetation or during dormant periods, the transpiration coefficient can be nonzero to allow for a relatively small amount of "diffuse evaporation" from Layer 2, which accounts for the slow process of water being drawn up from the second layer and evaporated.

A basal transpiration coefficient function, which reflects ideal climatic and soil water conditions, is first assigned to a cell based on the vegetation community anticipated for the year given the annual precipitation as well as the cell's azimuth and slope. The basal transpiration coefficient is

adjusted for daily climatic conditions and is reduced to account for soil water stress if the water content of the root zone is below a value that results in reduced transpiration for a particular vegetation type. When the root zone water content is reduced all the way down to the wilting point, plants are assumed to be unable to extract water from the soil and the transpiration coefficient is set to a minimal value. This minimum value represents conditions when evaporation and transpiration rates are at their minimum and water loss is primarily diffusive. This minimum value is a function of soil properties. The total transpiration is partitioned between the surface layer and Layer 2 based on the relative amounts of water in these layers.

Evaporation is assumed to occur only from the portion of the surface layer that is directly exposed to solar radiation, that is, the bare soil fraction. Evaporation is calculated by multiplying ET_0 times an evaporation coefficient for each cell. When the soil surface is wet, evaporation is limited by the energy available to the exposed surface, and the evaporation coefficient is determined from energy-related factors. As the soil surface dries below a critical water content, the evaporation coefficient is reduced, reflecting the influence of subsurface moisture diffusion (see Section 6.4 and Appendix G).

Surface water routing

The model first considers the highest elevation cell within a watershed, calculates the water balance for that cell, and then progresses to the cell with the next highest elevation. In this way, runoff from a cell can be included as run-on to an adjacent cell. All of the runoff is added to the neighboring adjacent cell with the lowest elevation.

6.4 MATHEMATICAL DESCRIPTION OF THE MODEL

This section of the report describes the mathematical foundations of the MASSIF model. It presents the equations used and introduces the input parameters required to run the model. The justification for parameter values and distributions for the calculation of net infiltration at Yucca Mountain are provided in later sections and appendices. As much as possible, only pointers to these sections of the report are provided in this section.

The objective of the MASSIF model is to calculate net infiltration for each cell of a grid representing a watershed bounded by surface water divides. The limitations and input requirements of the model are described in Appendix G along with a detailed description of the model algorithm. In this section, the mathematical basis for the model is discussed in terms of the applicable physics. The basis of the model is the following water (volume) balance equation for the soil that is solved for each computational cell for each day of the simulation:

$$R_{off} = P_{rain} + R_{on} + SM - \Delta\theta - ET - NI \qquad \text{(Eq. 6.4-1)}$$

where

R_{off} is runoff,
P_{rain} is precipitation as rain,
R_{on} is run-on,
SM is snowmelt,

$\Delta\theta$ is the change in water storage in the soil,
ET is evapotranspiration, and
NI is net infiltration.

Additionally, a water (volume) balance equation for the snowpack of each cell is solved for each day of the simulation:

$$\Delta SP = P_{snow} - SUB - SM \qquad \text{(Eq. 6.4-2)}$$

where

ΔSP is the change in the water storage of the snowpack
P_{snow} is precipitation as snow,
SUB is the sublimation,
SM is snowmelt.

Figure 6.4-1 illustrates that the soil and snowpack form the two water reservoirs represented in the water balance. Snowmelt (SM in Figure 6.4-1) is the only pathway for P_{snow} to reach the soil. Water movement in the model is considered to be vertical below the surface. The only water transport between cells is via runoff (R_{off}) from one cell, which is added to a downstream cell as run-on (R_{on}). In the sections below are descriptions of how each of these quantities is represented in the model.

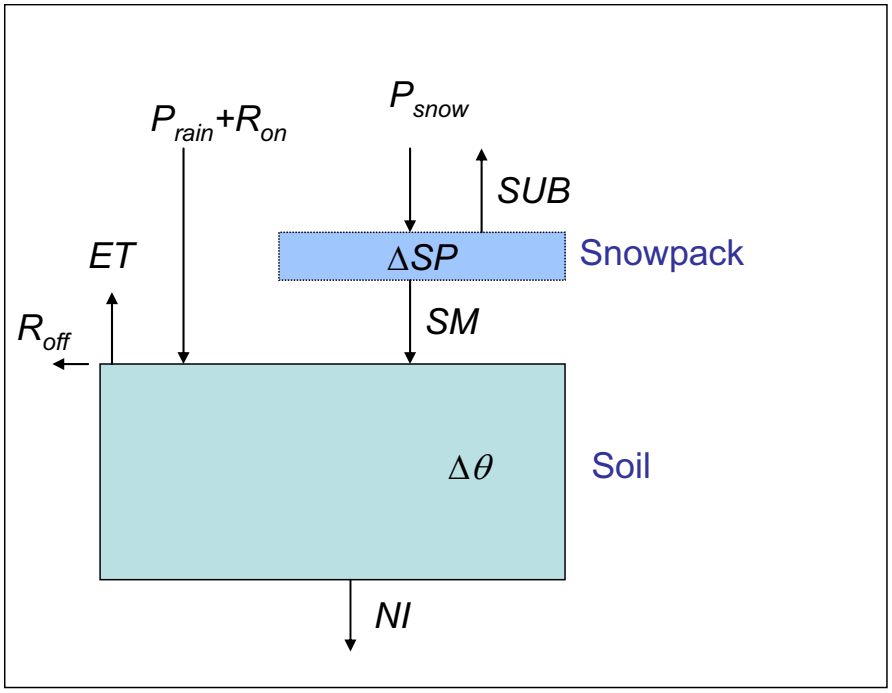

Figure 6.4-1. Schematic Showing the Water Reservoirs and Fluxes Included in the Water Balance

6.4.1 Precipitation (P)

6.4.1.1 Adjusting Precipitation for Elevation

Daily values of total precipitation ($P_{rain} + P_{snow}$) at a reference elevation are input to the model. Precipitation on a given day is either in the form of rain or snow depending on the air temperature where it falls. Studies of regional precipitation have shown that total annual precipitation for a given a site is typically correlated with elevation (e.g., Daly et al. 2002 [DIRS 177096], p. 102; Phillips et al. 1992 [DIRS 177091], p. 120). In addition, other factors such as local rain shadows caused by nearby mountains can also be important factors influencing the total amount of precipitation (Phillips et al. 1992 [DIRS 177091], p. 120). In the MASSIF model, elevation is the only factor considered for adjusting precipitation by location. Daily precipitation adjusted for elevation is given by:

$$P = P_{ref}\left(1 + (elev - elev_{ref})\, C_{Precipcor}\right) \qquad \text{(Eq. 6.4.1.1-1)}$$

where

P is the precipitation (mm) adjusted to an elevation, $elev$ (m),

P_{ref} is the precipitation (mm) at the reference elevation, $elev_{ref}$ (m), and

$C_{Precipcor}$ is the precipitation lapse rate (fractional change in precipitation at the reference elevation / m of elevation change).

The development of the precipitation lapse rate for the Yucca Mountain net infiltration calculation is discussed in detail in Appendix F, Section F2.1.

One limitation of this approach is that it is assumed that when precipitation occurs at the reference elevation, it occurs everywhere in the domain (Section 5). A more complicated model might allow precipitation to occur in parts of the domain while other parts of the domain remain dry. Such sophistication was deemed unnecessary for the current development.

6.4.1.2 Precipitation Type as a Function of Temperature

Precipitation is assumed to be snowfall (P_{snow}) whenever the average daily temperature at a cell location is equal to or less than 0°C. Inputs to the model are maximum and minimum daily air temperatures at the reference elevation. Average daily temperature at the reference elevation is calculated in the model as the mean of the minimum and maximum temperatures. These temperatures are then corrected for elevation from the reference elevation for each grid cell in the geospatial database. The elevation correction decreases temperature linearly with increasing elevation at a rate referred to as the temperature lapse rate. The temperature correction equation used in MASSIF is given in Section 6.4.5.3 and Appendix G. The development of the temperature lapse rate for the Yucca Mountain net infiltration calculation is discussed in detail in Section 6.5.1 and Appendix C.

6.4.1.3 Duration of Daily Precipitation Events

Precipitation can occur over a range of durations from brief and intense thunderstorms to prolonged storms that last the entire day. For the purposes of modeling the water transport in the soil, the period of time that water is available at the surface of the soil may be important. The MASSIF model requires as input an effective duration in hours for each day of precipitation (*duration*). The development of the precipitation durations for the Yucca Mountain net infiltration calculation is discussed in detail in Section 6.5.1 and Appendix F.

6.4.1.4 Fate of Snowpack

Snowpack will melt on days when the average air temperature at a cell location is above 0°C. The snow melts at a rate proportional to the average daily air temperature (T_{avg}) at a cell (Maidment 1993 [DIRS 125317], p. 7.24):

$$SM = C_{snowmelt} * T_{avg} \quad \text{(Eq. 6.4.1.4-1)}$$

where SM is the daily snow melt (mm of water) and $C_{snowmelt}$ is a constant (mm/°C). If it rains on a day when there is snowmelt, the rain and snowmelt are combined and applied as input to the top soil surface over the effective precipitation duration for that day. On days without precipitation, snowmelt is applied over a 12-hour duration. Rain is input to the top soil surface on the day of precipitation regardless of whether there is snow accumulated on the surface from prior snow events. These constraints simplify a complex process that is affected by the pattern of precipitation and temperature during the day. Such details are important for models designed for forcasting but are not considered important for the MASSIF model, which is aimed at making long-term predictions for large areas. Some portion of snow will sublimate; the total annual sublimation can be described as a percentage of the total annual amount of snow (Hood et al. 1999 [DIRS 177996]). In MASSIF, daily sublimation (SUB, mm) was calculated as a fixed percentage ($C_{sublime}$) of the precipitation (P_{snow}, mm) on days that it snows.

$$SUB = P_{snow} * (C_{sublime}) \quad \text{(Eq. 6.4.1.4-2)}$$

This approach ensures that the cumulative annual sublimation will be the desired percentage of the annual snow but does not necessarily accurately reproduce daily sublimation rates. However, this limitation is not considered to be important for the intended purpose of the MASSIF model, which is to estimate mean annual net infiltration as a function of location. The development of $C_{snowmelt}$ and $C_{sublime}$ for the Yucca Mountain net infiltration calculation is discussed in Section 6.5.1.

6.4.2 Mathematical Representation of Water Transport and Storage

As explained in Section 6.3, rather than employing a Richards' equation approach to solve for subsurface water movement, a simpler "field capacity" approach is adopted. In this approach the soil at a given location is divided into a series of layers and nodes (Figure 6.4.2-1). In this context, layers refer to vertical soil horizons and nodes refer to distinct volumes of soil considered in the water mass balance. The model accommodates up to three layers and four nodes. The top or surface layer is divided into two nodes and the bottom two layers are each

represented by a single node. A daily water balance is performed on each node in each cell of the watershed.

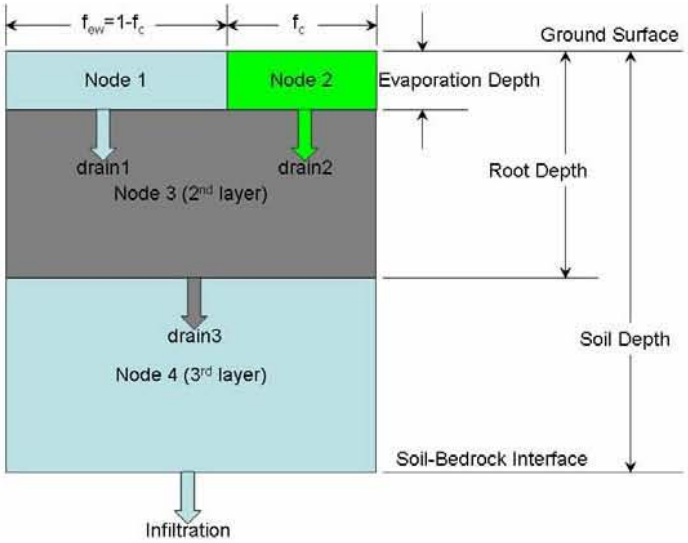

Source: Output DTN: SN0701T0502206.037.

NOTE: f_c is the fraction of the surface covered by the vegetation canopy and f_{ew} is the fraction of the surface that is exposed and wetted.

Figure 6.4.2-1. Schematic Showing the Vertical Soil Layers and Computational Nodes Present in a Single Model Cell

In each of the soil nodes, the amount of water is accounted for by the "*Water level*." *Water level* is the equivalent height of water in the layer per unit area and is measured in length units (e.g., cm). *Water level* is related to the average volumetric water content (θ) in a layer as:

$$Water\ level = \theta * node\ thickness \quad \text{(Eq. 6.4.2-1)}$$

Typically, the amount of water that can be stored in a layer is defined by the field capacity of the layer. The integrated field capacity (*FC,* mm) for a particular node is the product of the intrinsic field capacity (θ_{FC}, m^3/m^3) and the node thickness:

$$FC = \theta_{FC} * node\ thickness \quad \text{(Eq. 6.4.2-2)}$$

Drainage or downward daily water movement (*Drain*, mm) from a soil node to the next lower node is assumed to occur when the water level exceeds the field capacity for that node. Layers 2 and 3 (Nodes 3 and 4) can accept water at a maximum rate defined by the saturated hydraulic conductivity (K_{sat_soil}, mm/yr) and the precipitation duration. This rate, the soil conductivity infiltration limit ($Limit_{soil}$, mm), is given by:

$$Limit_{soil} = K_{sat\_soil} * duration \quad \text{(Eq. 6.4.2-3)}$$

The *duration* (hr) is the amount of time during the day during which precipitation occurs. If there is only snowmelt on a day, a 12-hour duration is assumed. The basis for this simplifying assumption is that snowmelt would be most likely to occur during the day when temperatures

tend to be higher and cease at night, when it is colder. K_{sat_soil} is the saturated conductivity of the soil. The amount of water that moves downward (*Drain*, mm) is:

$$Drain = MIN(Limit_{soil}, Water\ level - FC) \quad \text{(Eq. 6.4.2-4)}$$

The water level of the layer is reduced by this amount and the water level of the underlying layer is increased by this amount, thereby passing water to a lower layer. The development of θ_{FC} and K_{sat_soil} for the Yucca Mountain net infiltration calculation is discussed in Section 6.5.2.

The shading of the vegetative canopy retards evaporation under the canopy. As a result, the surface layer of soil under the canopy frequently has higher water content than the adjacent exposed soil. To reflect this, the surface layer is divided into two nodes. Node 1 (the "evaporation node") models the bare soil; Node 2 (the "canopy node") models the canopy region. The water levels in these two nodes are calculated separately.

During a precipitation event, one of the two surface nodes in a cell may exceed field capacity before the other. For instance, the canopy node (Node 2) may reach field capacity before the adjacent bare soil node (Node 1). The distance between the two nodes (Node 1 and Node 2) reflects the physical dimensions of the individual plant canopies and the inter-plant spacings. This distance is expected to be much smaller than the cell dimension (30 m). Therefore, in the MASSIF model, surplus water from Node 2 is supplied to Node 1 before it is supplied as runoff to the downstream cell. Conversely, surplus water from Node 1 is supplied to Node 2 before it is supplied as runoff to the downstream cell. Water will drain from the 1st to the 2nd layer only after the water levels of both Node 1 and Node 2 exceed field capacity.

It should be noted that there is no soil conductivity limitation imposed on the surface layer, which can accept all the water that it can hold regardless of the precipitation rate. The effect of this assumption is that a certain amount of water can be delivered to the surface before any runoff can result. As long as the thickness of the surface layer is relatively small, the effect of this assumption on infiltration will be small. See Section 5 for a more detailed discussion of this assumption. The development of a parameter representing the thickness of the surface layer (*Ze*) for the Yucca Mountain net infiltration calculation is discussed in Section 6.5.4.

Net infiltration or drainage from the bottom-most soil layer is calculated and is compared to the maximum amount of water the bedrock can accept. This maximum amount of water accepted by the rock ($Limit_{rock}$) is calculated from Darcy's law for saturated flow where a unit gradient is assumed (gravity flow).

$$Limit_{rock} = K_{sat\_rock} * duration \quad \text{(Eq. 6.4.2-5)}$$

K_{sat_rock} (mm/hr) is the saturated hydraulic conductivity of the rock. Thus, the amount of water that moves from Node 4 into the underlying bedrock (daily net infiltration, mm) is calculated as:

$$NetInfiltration = MIN(Limit_{rock}, Water\ level_4 - FC_4) \quad \text{(Eq. 6.4.2-6)}$$

The bedrock may not be able to accept all of the excess water from the bottom-most soil layer. In this case, the soil layer (Node 4) is permitted to exceed field capacity to accommodate the water that cannot move into the bedrock layer. If there is sufficient excess water to exceed the

porosity of the layer, then the excess water above full saturation is distributed to the next layer above (Layer 2, Node 3). If Layer 2 saturates, water is passed to Nodes 1 and 2 in proportion to the amount that was originally drained from them. The development of K_{sat_rock} for the Yucca Mountain net infiltration calculation is discussed in Section 6.5.2.

On days with precipitation events with durations less than 24 hours, the water redistribution calculation is conducted twice. First, the calculation is conducted for the duration equal to the precipitation event duration. It is during this calculation that water is added to the top of the cell. In the second calculation, if there is water in excess of field capacity in the bottom layer, it has the opportunity to enter the bedrock during the remainder of the day at a rate limited by the rock hydraulic conductivity. During this calculation, the duration is the difference between a full day and the precipitation event duration.

6.4.3 Surface Runoff and Run-on (Roff and Ron)

Runoff from a cell can result from the water redistribution calculation when either (1) the entire soil profile becomes saturated or, (2) the first layer becomes saturated due to the soil conductivity infiltration limit. In either case, the water in excess of saturation will produce runoff from the cell. This runoff is then added to the next downstream cell, which is identified in the input to the model (see Appendix B for an example). For this reason, the calculation for a watershed is conducted for cells in order of decreasing elevation. The run-on duration is assumed to be the precipitation duration (Section 5.6). The runoff events measured at the Yucca Mountain site (Section 7.1.3) rarely extend beyond days with precipitation. Furthermore, the runoff data is expressed as daily amounts and the duration of the events is not available and therefore this assumption was necessary.

6.4.4 Mathematical Representation of Evapotranspiration

The FAO-56 method (Allen et al. 1998 [DIRS 157311]) was adapted for use in calculating evapotranspiration (ET) (see Appendicies C, D, E, and Section 6.5.3). Water is removed from the root zone via ET as illustrated in Figure 6.4.4-1. There are five discrete components of ET in the model: (1) bare soil evaporation, which occurs only in the fraction exposed and wetted (f_{ew}) portion of surface layer; (2) transpiration from the f_{ew} portion of the surface layer; (3) transpiration from the canopy (f_c) portion of the surface layer; (4) transpiration from Layer 2; and (5) diffusive evaporation from Layer 2 (not shown on figure).

The “root-zone” thickness is considered to be constant over the entire domain. It represents the the depth to which water can be extracted by ET. Spatial variations in ET are determined by the amount of vegetation at a given location.

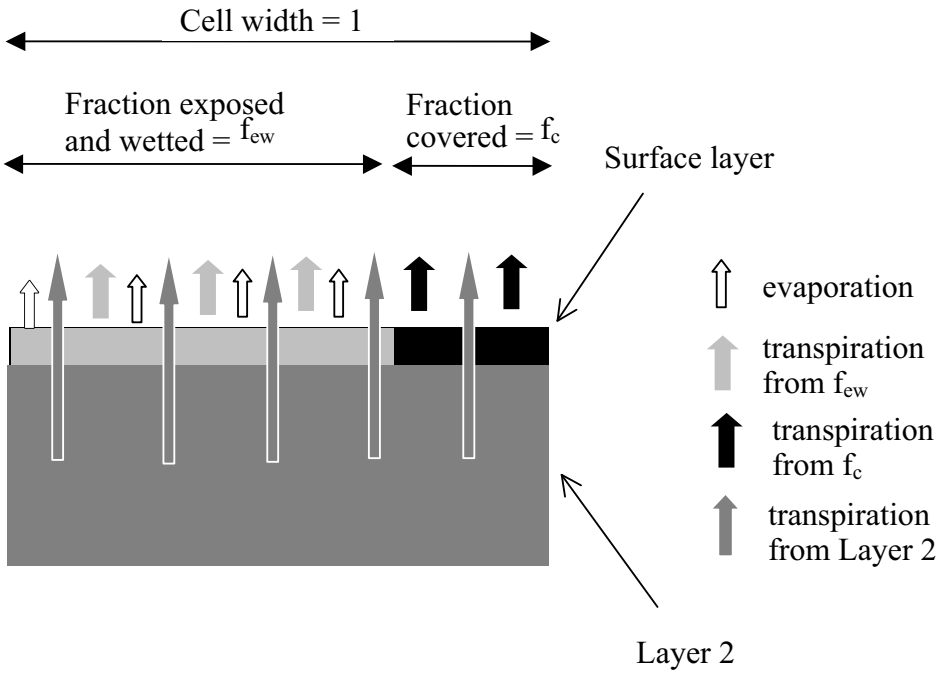

Source: Derived from conceptual model presented in Allen et al. 1998 [DIRS 157311], pp. 135 to 158.

NOTE: A diffusive evaporation component is part of the transpiration from Layer 2.

Figure 6.4.4-1. Evaporation and Transpiration from the f_{ew} and f_c Portions of the Root Zone

The ET calculations are made after the daily water redistribution calculation described above. The ET calculation follows the dual crop FAO-56 method, where *ET* (mm) is proportional to the reference ET (ET_0, mm), and explicitly accounts for soil evaporation and transpiration separately (Allen et al. 1998 [DIRS 157311], Equation 80).

$$ET = (K_e + K_s K_{cb}) * ET_0 \quad \text{(Eq. 6.4.4-1)}$$

where

K_e is the soil evaporation coefficient (dimensionless),
K_{cb} is the basal transpiration coefficient (dimensionless), and
K_s is a water stress coefficient (dimensionless).

The ET_0 calculation depends only on cell-specific, climatic conditions. The development of the parameters used in this calculation for the Yucca Mountain site is described in Appendix C and Section 6.5.4. The mathematical model for the calculation of ET_0 is described below in Section 6.4.5.

6.4.4.1 Basal Transpiration, Soil Evaporation Coefficients, and Canopy Coefficient

The basal transpiration coefficient (K_{cb}, dimensionless) depends on the amount and type of vegetation present within a cell and on the time of year. The value of K_{cb} is near zero when the plants are absent or dormant at the beginning and end of the growing season. K_{cb} reaches its peak near the middle of the growing season. For agricultural crops, FAO-56 provides look-up tables for determining K_{cb}. For native vegetation, FAO-56 provides methods for estimating K_{cb} based on specific plant characteristics (e.g., stomatal conductance) and fractional cover data, which can be either measured directly or estimated from satellite data. For the purpose of describing the mathematical foundation of the MASSIF model, K_{cb} is treated as an input to the calculation of ET. In the discussion below, it is assumed that values of K_{cb} for each day of the calculation are known in order to apply the MASSIF model. The development of K_{cb} values for the Yucca Mountain net infiltration calculation required developing a site-specific methodology, which is discussed as part of the analysis in Section 6.5.3, Appendix D, and Appendix E.

The basal transpiration coefficient is constrained to be between a minimum and maximum value. The maximum basal transpiration coefficient ($K_{c\,max}$) represents an upper limit of the evaporation and transpiration that can occur on a given day based on available energy. $K_{c\,max}$ (dimensionless) ranges between 1.05 and 1.30 and is calculated using Equation 72 from FAO-56 (Allen et al. 1998 [DIRS 157311]):

$$K_{c\max} = \max\left(\left\{1.2 + \left[0.04\left(u_2 - 2\right) - 0.004\left(RH_{\min} - 45\right)\right]\left(\frac{h_{plant}}{3}\right)^{0.3}\right\}, \left\{K_{cb} + 0.05\right\}\right) \quad \text{(Eq. 6.4.4.1-1)}$$

where u_2 (m/s) is the average daily wind speed at 2 m, RH_{min} is the minimum daily relative humidity, and h_{plant} is the characteristic plant height (m).

The minimum basal transpiration coefficient represents dry soil with no vegetation cover ($K_{c\,min}$, dimensionless). $K_{c\,min}$ may be greater than zero to account for evaporation occurring from Layer 2 (Node 3) and beneath the vegetation canopy (Node 2), as these evaporative losses are not explicitly included in the calculation of evaporation from the evaporative node (Node 1). The development of $K_{c\,min}$ for the Yucca Mountain net infiltration calculation is discussed in Section 6.5.4.

The soil evaporation coefficient (K_e) is found from Equation 71 of FAO-56 (Allen et al. 1998 [DIRS 157311]):

$$K_e = K_r * (K_{c\,max} - K_{cb}) <= f_{ew} * K_{c\,max} \quad \text{(Eq. 6.4.4.1-2)}$$

where K_r is a soil evaporation reduction coefficient described in the next section.

Vegetative cover varies seasonally. In the spring, the vegetative cover coefficient (f_c) increases as the plants grow. Later in the year, as the ground dries out and transpiration drops due to water stress, the vegetative cover coefficient declines. The correlation recommended in FAO-56 (Allen et al. 1998 [DIRS 157311], Equation 76) is used to model the time variation of the canopy coefficient:

$$f_c = \left(\frac{K_{cb} - K_{c\min}}{K_{c\max} - K_{c\min}} \right)^{\left(1+0.5h_{plant}\right)} \quad \text{(Eq. 6.4.4.1-3)}$$

To avoid numerical problems, f_c is constrained to be greater than 10^{-4} (Appendix G, Section G4.2.3.1, Step 9), which ensures that f_{ew} is always less than 1.

6.4.4.2 Depletions and Water Stress Coefficients

The amount of soil water in the root zone affects the daily ET. In the FAO-56 method, the amount of water in a soil layer is described in terms of depletion. *Depletion* (mm) is related to the *water level* parameter:

$$Depletion = FC - water\ level \quad \text{(Eq. 6.4.4.2-1)}$$

Depletions are calculated for the evaporation node of the surface layer, for the canopy node of the surface layer, and for the entire root zone. The approach used for these calculations is based on the approach outlined in the FAO-56 method, but is somewhat different in that depletions are calculated after the redistribution of water in the two surface nodes. The depletion for the evaporation and canopy nodes is calculated from the field capacities and water levels in these nodes. Depletion of the root zone is calculated from the field capacities and water levels in the surface layer and Layer 2 using area-weighted values for the evaporative (Node 1) and canopy (Node 2) nodes.

The total amount of water available for evaporation (*TEW*, mm) is calculated from Equation 73 of FAO-56 (Allen et al. 1998 [DIRS 157311]):

$$TEW = (\theta_{FC} - 0.5 * \theta_{WP}) * Z_e \quad \text{(Eq. 6.4.4.2-2)}$$

where θ_{WP} is the permanent wilting point (m^3/m^3), below which vegetation cannot extract moisture from the soil, and Z_e is the surface layer thickness (m). Z_e is dependent on soil texture and length of drying periods common to the model area. The equation for *TEW* implies that water will not be evaporated at water contents less than ½ θ_{WP}. This assumption is based on recommendations from FAO-56. The development of θ_{WP} and Z_e for the Yucca Mountain net infiltration calculation is discussed in Sections 6.5.2 and 6.5.4, respectively.

The evaporation rate depends on the amount of water in the evaporation node (Node 1). When the soil surface is wet, the maximum rate of evaporation is controlled by the amount of available energy at the soil surface (Allen et al. 1998 [DIRS 157311], p. 145). Readily evaporable water (*REW*) is the maximum depth of water that can be evaporated from the upper soil layer prior to the onset of hydraulic limitations that reduce the rate of water supply below that of energy

demands. When the depth of evaporation exceeds *REW*, there is a reduction of the evaporation rate. The development of *REW* for the Yucca Mountain net infiltration calculation is discussed in Section 6.5.4.

$$K_r = (TEW - D_e) / (TEW - REW) \quad \text{(Eq. 6.4.4.2-3)}$$

where D_e is the depletion of the evaporative node (Node 1). K_r is constrained to be between 0 and 1.

Depletion of the root zone is calculated from the field capacities and water levels in the surface layer and Layer 2, using area-weighted values for the evaporative and canopy nodes. Two additional parameters are used to describe the water status in the root zone, the total available water (*TAW*) and the readily available water (*RAW*). *TAW* (mm) is the amount of water available for ET in the root zone, and is calculated from Equation 82 of FAO-56 (Allen et al. 1998 [DIRS 157311]):

$$TAW = (\theta_{FC} - \theta_{WP}) * Z_r \quad \text{(Eq. 6.4.4.2-4)}$$

where Z_r is the root zone thickness (mm) (assumed to be greater than zero). The development of Z_r for the Yucca Mountain net infiltration calculation is discussed in Section 6.5.3. *RAW* (mm) is the limit of the water in the root zone below which the transpiration rate is affected. It is calculated as a function of *TAW* (Allen et al. 1998 [DIRS 157311], Equation 83):

$$RAW = p * TAW \quad \text{(Eq. 6.4.4.2-5)}$$

where p (dimensionless) is the fraction of *TAW* that vegetation can remove without suffering stress and is constrained to be between 0 and 1. Characteristics of the vegetation as well as the climate and soil type determine the value of p (Allen et al. 1998 [DIRS 157311], p. 162). The development of p for the Yucca Mountain net infiltration calculation is discussed in Section 6.5.4.

An adjustment of p as a function of daily ET is recommended in FAO-56 (Allen et al. 1998 [DIRS 157311], p. 162):

$$p_{adj} = \max(0.1,\min(p+0.04(5-ET),0.8)) \quad \text{(Eq. 6.4.4.2-6)}$$

In the MASSIF model the adjusted p (p_{adj}) is used in place of p in Equation 6.4.4.2-5.

The impact of water stress in the root zone on transpiration is reflected in the transpiration stress coefficient. The transpiration stress coefficient is calculated from Equation 84 of FAO-56 (Allen et al. 1998 [DIRS 157311]):

$$K_s = (TAW - D_r) / (TAW - RAW) \quad \text{(Eq. 6.4.4.2-7)}$$

where D_r (mm) is the root zone depletion. K_s is 1 when D_r is less than *RAW* and is 0 when D_r is greater than *TAW*.

Transpiration from the evaporation node (Node 1) is calculated as a portion of the total calculated transpiration and is based on the amount of water in the surface layer compared to the amount of water in the entire root zone. This fractional partitioning coefficient (K_{tie}) (Allen et al. 2005 [DIRS 176009], Equation 27) is:

$$K_{tie} = [(1 - D_e/TEW)/(1 - D_r/TAW)]*(Ze/Zr)^{0.6} \quad \text{(Eq. 6.4.4.2-8)}$$

Unlike the current model, the FAO-56 procedure does not explicitly keep track of the water content of the surface layer under the vegetation canopy (Node 2). Therefore, the fractional partitioning coefficient for the canopy region (K_{tic}) is calculated in a manner similar to K_{tie}:

$$K_{tic} = [(1 - D_c/TEW)/(1 - D_r/TAW)]*(Ze/Zr)^{0.6} \quad \text{(Eq. 6.4.4.2-9)}$$

where D_c (mm) is the depletion of the canopy node.

6.4.4.3 ET Calculation

The ET is calculated as the sum of the evaporative losses from the evaporative node portion of the surface layer and transpiration from the root zone. Daily evaporation (E, mm) is calculated as:

$$E = K_e * ET_0 \quad \text{(Eq. 6.4.4.3-1)}$$

The daily evaporation calculated by Equation 6.4.4.3-1 applies to the entire surface area of a cell. In reality, the evaporation only takes place in the bare soil portion of the cell (Node 1). Hence, the depth of water evaporated from the fraction of evaporative node is E / f_{ew}. E is constrained so that TEW is not exceeded.

Daily transpiration (T, mm) from the root zone is calculated as:

$$T = K_s * K_{cb} * ET_0 \quad \text{(Eq. 6.4.4.3-2)}$$

The total daily transpiration is partitioned between the surface layer nodes (Nodes 1 and 2) and Layer 2 (Node 3). The daily transpiration from the evaporative node (T_e) is:

$$T_e = K_{tie} * T \quad \text{(Eq. 6.4.4.3-3)}$$

For the canopy node, the daily transpiration (T_c) is:

$$T_c = K_{tic} * T \quad \text{(Eq. 6.4.4.3-4)}$$

The daily transpiration from Layer 2 (Node 3) is:

$$T2 = T - T_e * f_{ew} - T_c * f_c \quad \text{(Eq. 6.4.4.3-5)}$$

Transpiration is limited so that the water level of any of the nodes does not go below the wilting point.

After the ET calculation, the water levels in each node are updated. For the evaporative node (Node 1) and canopy node (Node 2), the changes in the water level due to ET is ($-E/f_{ew} - T_e$) and ($-T_c$), respectively. The change in the water level of Layer 2 is ($-T2$).

6.4.5 Mathematical Representation of Reference Evapotranspiration on Flat and Sloped Surfaces

The evapotranspiration rate from a reference surface, not short of water, is called the reference crop evapotranspiration or reference evapotranspiration and is denoted as ET_0 (Allen et al. 2005 [DIRS 176207], p. 2).

The concept of the reference evapotranspiration was introduced to study the evaporative demand of the atmosphere independent of vegetation type, phenological development, and management practices. As water is abundantly available at the reference evapotranspiring surface, soil factors do not affect ET. Relating ET to a specific surface provides a reference to which ET from other surfaces can be compared. This approach obviates the need to define a separate ET level for each type of vegetation and stage of growth. ET_0 values measured or calculated at different locations or in different seasons are comparable as they refer to the ET from the same reference surface.

For convenience and reproducibility, the reference surface has recently been standardized by the American Society of Civil Engineers (ASCE) as a hypothetical vegetated surface having specific characteristics (Allen et al. 2005 [DIRS 176207]). The reference evapotranspiration (ET_0) is defined as the ET rate from a uniform surface of dense, actively growing vegetation having an assumed height of 0.12 m and having a surface resistance of 70 s m^{-1} (for 24-hour calculation time-steps) and an albedo of 0.23, closely resembling the evaporation of an extensive surface of green, cool season grass of uniform height, not short of soil water (Allen et al. 1998 [DIRS 157311], p. 24).

The only factors affecting ET_0 are climatic parameters. Consequently, ET_0 is a climatic parameter and can be computed from weather data. ET_0 expresses the evaporating power of the atmosphere at a specific location and time of the year and does not consider the local vegetation characteristics, soil factors, or precipitation amounts. Even though there are many methods for calculating ET_0 cited in the literature, the FAO Penman-Monteith method is recommended as the standard method for determining ET_0 (Allen et al. 1998 [DIRS 157311], pp. 7 and 65; Irmak et al. 2005 [DIRS 176861] p. 1,064; Droogers and Allen 2002 [DIRS 176786], p. 33). The method has been selected because it closely approximates grass ET_0 at the location evaluated, is physically based, and explicitly incorporates both physiological and aerodynamic parameters (Allen et al. 1998 [DIRS 157311], p. 7). Moreover, procedures have been developed for estimating missing climatic parameters when the FAO Penman-Monteith equation is used.

The FAO Penman-Monteith method to estimate ET_0 was derived from the original Penman-Monteith equation (Jensen et al. 1990 [DIRS 160001], p. 93) and associated equations for aerodynamic and surface resistance for 24-hour calculation time-steps (Allen et al. 1998 [DIRS 157311], pp. 24 and 65):

$$ET_0 = \frac{0.408\Delta(R_n - G) + \gamma \frac{900}{T+273} u_2 (e_s - e_a)}{\Delta + \gamma(1 + 0.34 u_2)} \quad \text{(Eq. 6.4.5-1)}$$

where

ET_0 is the reference evapotranspiration [mm d^{-1}]
R_n is the net radiation at the crop surface [MJ m^{-2} d^{-1}]
G is the soil heat flux density [MJ m^{-2} d^{-1}]
T is the mean daily air temperature at 2 m height [°C]
u_2 is the wind speed at 2 m height [m s^{-1}]
e_s is the saturation vapor pressure [kPa]
e_a is the actual vapor pressure [kPa]
e_s-e_a is the saturation vapor pressure deficit [kPa]
Δ is the slope of the vapor pressure curve [kPa $°C^{-1}$]
γ is the psychrometric constant [kPa $°C^{-1}$].

The reference evapotranspiration, ET_0, provides a standard to which (1) evapotranspiration during different periods of the year or in other regions can be compared, and (2) evapotranspiration from specific vegetation types and surfaces can be related via some form of a 'crop coefficient.'

The FAO Penman-Monteith equation is a reasonable, simple representation of the physical and physiological factors governing the evapotranspiration process. By using the FAO Penman-Monteith definition for ET_0, one may calculate crop (or vegetation cover) coefficients (K_c) at research sites by relating the measured crop (or vegetation cover) evapotranspiration (ET) with the calculated ET_0, i.e., $K_c = ET/ET_0$. In the crop coefficient approach, differences in the vegetation canopy and aerodynamic resistance relative to the hypothetical reference crop are accounted for within the crop coefficient. Thus, the K_c factor serves as an aggregation of the physical and physiological differences between vegetation covers and surface wetness conditions and the reference definition (Allen et al. 1998 [DIRS 157311], p. 25). The net radiation in the ET_0 calculation (Equation 6.4.5-1) is defined for the reference (full cover clipped grass) surface. Differences in albedo, temperature, etc., that impact R_n for specific vegetation cover are incorporated into the K_c.

6.4.5.1 Data Required for Daily Calculation of ET0

Equation 6.4.5-1 is applied daily to compute reference evapotranspiration for each grid cell to account for influences of elevation, slope, and azimuth at each cell. Although calculation of ET_0 on an hourly time-step can provide a slightly more accurate calculation (Allen et al. 1998 [DIRS 157311], p. 74) provided high quality hourly weather data are available, calculation of ET_0 with the FAO Penman-Monteith equation using 24-hour time steps in most conditions can

provide accurate results (Allen et al. 1998 [DIRS 157311], p. 72; Allen et al. 2006 [DIRS 176785], pp. 2 to 3). The MASSIF model accepts data only in daily time-steps. The data for appropriate use of the FAO Penman Monteith equation consist of:

a) Meteorological data

- Air temperature: daily maximum (T_{max}) and minimum (T_{min}) air temperatures
- Air humidity: mean daily actual vapor pressure (e_a) derived from psychrometric, dew-point temperature or relative humidity data
- Wind speed: daily average over 24 hours for wind speed measured at or adjusted to 2-m height (u_2)
- Radiation: net radiation (R_n) measured or computed from solar and longwave radiation or from the recorded duration of sunshine.

To ensure the integrity of computations, the weather measurements should be made at 2 m (or translated to that height) above an extensive surface of green grass, fully shading the ground and not short of water (Allen et al. 1998 [DIRS 157311], p. 25).

b) Location information

- Altitude above sea level (m)
- Latitude (degrees north or south).

These data are used to adjust air temperature from the reference weather station for the average atmospheric pressure (function of site elevation) and to compute exoatmospheric radiation (R_a).

6.4.5.2 Use of the FAO Penman-Monteith Equation with a Limited Set of Weather Data

Modeling reference evapotranspiration over a study area requires an extensive dataset that reflects the anticipated variation in meteorological parameters over the range of grid cell elevation, slope, and exposure to the sun for all times of the year.

When a complete dataset of weather parameters is not available, the FAO Penman-Monteith equation can be applied using a minimum set of critical inputs. Daily maximum and minimum air temperature data are the minimum data requirements necessary to apply the FAO Penman-Monteith method (Allen et al. 1998 [DIRS 157311], p. 64; 2005 [DIRS 176207], p. E-1). The estimation of other weather variables can be based on minimum and maximum air temperature or on average values (for wind speed). Keying solar radiation and vapor pressure (via dew-point temperature) on daily air temperature extremes helps to preserve the strong correlation among these variables (Allen 1997 [DIRS 176568], p. 56; 1998 [DIRS 157311], p. 60; 2005 [DIRS 176207], pp. E-4 and E-5).

The use of an alternative ET_0 procedure requiring only limited meteorological parameters (for example, the Priestley-Taylor, Blaney-Criddle or Hargreaves ET equations) is not recommended by FAO-56 (Allen et al. 1998 [DIRS 157311], p. 58). The FAO Penman-Monteith method is

recommended as the sole standard method for the computation of ET_0 from meteorological data even for the cases when only a limited dataset is available (Allen et al. 1998 [DIRS 157311], p. 58; 2005 [DIRS 176207], p. E-1). Procedures used for estimating missing climatic data (solar radiation, vapor pressure, and wind speed) for the Yucca Mountain calculation of net infiltration are outlined in Appendix C. Differences between ET_0 estimated by the FAO Penman-Monteith equation with, on one hand, a limited data set and, on the other hand, a full data set, are expected to be small, especially when averaged over periods of 5 days or longer (Allen et al. 1998 [DIRS 157311], p. 60).

Next a discussion of the methods used to estimate weather parameters from air temperature is presented. These methods were used for the Yucca Mountain calculation of net infiltration and are described in Appendix C.

Solar Radiation Data Derived from Air Temperature Differences

The degree of cloud cover in a location is related to the difference between the daily maximum and minimum air temperature. Clear-sky conditions result in high temperatures during the day (T_{max}) because the atmosphere is transparent to the incoming solar radiation and in low temperatures during the night (T_{min}) because less outgoing long-wave radiation is absorbed by the atmosphere and retransmitted back to the surface. On the other hand, in overcast conditions, T_{max} is relatively lower because a significant part of incoming solar radiation never reaches the earth's surface and is instead absorbed or reflected to space by clouds. Similarly, $T_{\min}$ will be relatively higher, as cloud cover acts as a blanket and decreases the net outgoing long-wave radiation from the surface. Therefore, the difference between the maximum and minimum air temperature ($T_{max} - T_{min}$) is highly correlated with daily relative solar radiation and can be used as an indicator of the fraction of exoatmospheric radiation that reaches the earth's surface. This principle is the basis of the recommended FAO-56 equation when developing estimates of solar radiation using only air temperature data (Allen et al. 1998 [DIRS 157311], p. 60). The equation is the following:

$$R_s = K_{Rs}\ R_a \sqrt{\left(T_{\max} - T_{\min}\right)} \qquad \text{(Eq. 6.4.5.2-1)}$$

where

R_a is the exoatmospheric solar radiation [MJ m^{-2} d^{-1}] (R_a is the solar radiation at the earth's surface if there were no atmosphere)
T_{max} is the maximum air temperature [°C]
T_{min} is the minimum air temperature [°C]
K_{Rs} is the Hargreaves adjustment coefficient [$°C^{-0.5}$] (Hargreaves and Allen 2003 [DIRS 176787], p. 55; Allen et al. 1998 [DIRS 157311], p. 60).

The development of K_{Rs} and related parameters for the Yucca Mountain net infiltration calculation is discussed in Appendix C and Section 6.5.4.

Solar radiation estimated from Equation 6.4.5.2-1 represents the solar radiation associated with T_{max} and T_{min} measured and assuming that the surface is horizontal. Additional computations are applied to consider the effect of slope and orientation, as well as differences in elevation.

Humidity Data

Where humidity data are lacking or are of questionable quality, an estimate of actual vapor pressure (e_a) can be made assuming that dew-point temperature (T_{dew}) is near the daily minimum air temperature (T_c). This estimation implicitly assumes that near sunrise, when the air temperature is near T_{min}, the air may be nearly saturated with water vapor and relative humidity may be nearly 100%. The relationship $T_{dew} \approx T_{min}$ holds for locations where the vegetation cover in the vicinity of the station is well watered. However, particularly for arid regions, the air might not saturate when its temperature is at its minimum due to dryness of the air mass. Hence, T_{min} will generally exceed T_{dew} by some amount. In these situations, T_{dew} is better approximated by subtracting a fixed temperature offset (K_o) from T_{min}, depending on the aridity of the region and local environment (Allen et al. 1998 [DIRS 157311], pp. 58 to 59; 2005 [DIRS 176207], p. E-2), so that:

$$T_{dew} = T_{\min} - K_o \qquad \text{(Eq. 6.4.5.2-2)}$$

where K_o is the average offset between T_{dew} and T_{min}. The development of K_o for the Yucca Mountain net infiltration calculation is discussed in Appendix C and Section 6.5.4.

Wind Speed

Daily wind speed is required as input for the calculation of ET_0. The development of daily wind speed estimates for the Yucca Mountain net infiltration calculation is discussed in Appendices C and F, and Section 6.5.1.

6.4.5.3 Effect of Surface Elevation, Orientation, and Slope on ET_0

Inclination and exposure of the surface to the sun impact several components of the surface energy balance and consequently ET_0 calculated by the FAO Penman-Monteith equation. In addition, substantial variation in surface elevation within a study area requires modification of some parameters. The next section provides a description of how input weather parameters for the FAO Penman-Monteith ET_0 equation are adjusted for elevation, slope, and orientation of a given grid cell.

Solar Radiation

The amount of solar radiation received by a given surface is controlled by the geometry of the surface, atmospheric transmittance, and the relative location of the sun. The local geometry is controlled by surface slope, azimuth, and elevation.

Most solar radiation (R_s) information is calculated at weather stations located in flat, nearly horizontal locations, so that estimation of R_s on sloped surfaces must be generally based on models. Equation 6.4.5.2-1 is applied to estimate solar radiation incident to a horizontal surface. For inclined surfaces, the total (global) radiation reaching the surface is modeled as a sum of three components: direct (beam) radiation, which is the solar radiation that is not absorbed or scattered by the atmosphere and that reaches the surface directly from the sun; diffuse radiation, which originates from the solar beam but is scattered toward the surface; and finally, a diffuse

radiation component incident on the subject surface due to reflection from ground surfaces in view of the subject surface.

Appendix C describes the procedure used for the MASSIF model to estimate solar radiation for an inclined surface based on solar radiation measured or estimated over a horizontal surface. The procedure for inclined surfaces assumes an extensive surface having uniform slope at each point of calculation, so that effects of protruding surrounding terrain on blocking the sun or reflecting radiation are not considered. This simplification of terrain substantially speeds computational time for application of the procedure to the relatively large study area composed of a large number of grid cells and allows the use of a purely analytical solution. The simplification of terrain form provides sufficiently accurate results and is congruent with the discretization of slopes and azimuths on the mountain, where slope is discretized into 6 general classes and azimuth into 12 general classes (Appendix C).

Elevation also affects the amount of radiation that reaches a surface due to atmospheric attenuation. In general, for a clear sky day, the solar radiation increases with altitude due to the smaller air mass.

Air Temperature

Atmospheric pressure decreases with increasing altitude. Consequently, rising parcels of air tend to cool by adiabatic expansion; similarly, falling parcels tend to warm up due to adiabatic compression. The net effect of this is a vertical decrease in temperature with increase in elevation following the adiabatic lapse rate. The rate at which air cools (or warms) depends on the moisture status of the air. If the air is unsaturated, the rate of temperature change is about 1°C/100 meters and is called the *dry adiabatic lapse rate* (Rosenberg et al. 1983 [DIRS 177526], p. 118). If the air is saturated, the rate of temperature change is smaller due to latent heat of vaporization of condensing water vapor and is called the *saturated adiabatic rate*. The saturated adiabatic lapse rate applies to rising air when the relative humidity has reached 100% and condensation of water vapor is taking place.

It is recognized that in addition to elevation, local topography can modify the relationship between elevation and temperature. These effects are governed largely by the relationship between slope orientation, received solar radiation, and surface heating. In the northern hemisphere, north-facing slopes receive less radiation than south-facing slopes and are typically cooler (Lookingbill and Urban 2003 [DIRS 176789], p. 142).

Additional topographic effects result from the influence of terrain on mountain winds and the generation of local airflows. As a result, mountain valleys, middle-hill slopes, and ridges can have different temperature regimes (Lookingbill and Urban 2003 [DIRS 176789], p. 142).

Because of uncertainties in estimating secondary topographic effects on temperature, the vertical lapse method is the most common approach for the estimation of air temperature changes based on mean elevation differences, particularly in areas with mountainous or complex terrain; this is the approach used in the MASSIF model. This method adjusts for the mean observed decrease in temperature with increase in elevation. Lapse models are most often applied to monthly averages or daily extremes (Bolstad et al. 1998 [DIRS 176784], p. 162). The lapse rate approach

ignores local effects associated with differences in aspect and relative slope position. A common approach to representing the lapse rate is by a linear equation such as:

$$T_{lapse} = T_{ref} - \frac{LR}{1{,}000}\left(z_{cell} - z_{ref}\right) \qquad \text{(Eq. 6.4.5.3-1)}$$

where

T_{lapse} is the elevation-adjusted daily air temperature for a given grid cell with elevation z_{cell} [°C]
z_{cell} is the elevation of the grid cell [m]
T_{ref} is the daily air temperature at the reference weather station [°C]
z_{ref} is the elevation of the reference weather station [m], and
LR is the temperature lapse rate in °C per 1,000 m.

This equation is used to represent the lapse rate in the MASSIF model. The development of the temperature lapse rate parameters (LR and z_{ref}) for the Yucca Mountain net infiltration calculation is discussed in Appendices C and F, and Section 6.5.1.

Vapor Pressure

The saturation vapor pressure decreases with a decreasing air temperature. Given a relatively constant amount of moisture in the air, represented by the actual vapor pressure, the ratio between actual and saturated vapor pressure (i.e., relative humidity) increases with any decrease in temperature. Because air temperature decreases with elevation, saturation vapor pressure will also decrease with elevation for a given air mass. Because actual vapor pressure is relatively constant for a given air mass over a region, the relative humidity of the air will increase with altitude up to a point where saturation is reached. At this point, actual vapor pressure will be limited to the mean saturation vapor pressure, with increasing condensation of part of the air moisture with any additional increase in attitude.

The actual vapor pressure (e_a) in the FAO Penman-Monteith equation (Equation 6.4.5-1) is computed from the daily lapse-corrected temperatures. The saturation limit to the vapor pressure is computed using the lapse-corrected estimated dew temperature (Equation 6.4.5.2-2). Details of the calculation of vapor pressure are given in Appendix C.

Wind Speed

Wind speed is affected by the topographical features of a given area, especially in mountainous terrain. However, simulation and modeling of wind speed as a function of surface topography is difficult for even highly instrumented terrain. Generally wind speed is extrapolated from area weather stations with adequate accuracy for estimating ET (Allen et al. 2005 [DIRS 176207], pp. E-6 to E-7). The MASSIF model does not adjust wind speed to account for elevation, slope, or aspect.

6.5 ANALYSIS OF YUCCA MOUNTAIN NET INFILTRATION

This section addresses the use of the model for the analysis of net infiltration at the Yucca Mountain site during anticipated future climates, beginning with descriptions of the methods used to prepare inputs. Sections 6.5.1, 6.5.2, 6.5.3, and 6.5.4, respectively, discuss the development of parameters representing the anticipated weather, the site geology, the anticipated vegetation, and miscellaneous parameters. Section 6.5.5 discusses parameter screening decisions for the uncertainty analysis. Sections 6.5.6 through 6.5.7 cover the calculation procedures and the results of the calculations.

It should be noted that in the development of uncertainty distributions for all input parameters to the model, there was a need to define "nominal" values for each of the parameters. Such nominal values are defined in each section along with their uncertainty distribution. The nominal values were chosen to be representative and a number of different approaches were taken depending on the underlying parameter distribution. For many parameters a mean or median value was selected; however, for others, other values were selected and are justified for use in the particular section of the report or appendix. Nominal values are used in the calculation of net infiltration uncertainty when the uncertainty of the given parameter was less than the threshold used to identify parameters to be varied in the uncertainty analysis.

6.5.1 Weather Parameters for Anticipated Climate Episodes

Calculation of net infiltration requires an input file containing precipitation, temperature extremes, and mean wind speed on a daily basis. The MASSIF model varies precipitation and temperature with elevation and accepts input for an elevation of 1,524 m (5,000 ft), corresponding to the top of Yucca Mountain. It also requires a linear fit to hours of precipitation as a function of total precipitation for the day.

Appendix F details the development of weather input files for calculation of net infiltration at Yucca Mountain. This section provides background information about anticipated climates at Yucca Mountain and summarizes Appendix F.

6.5.1.1 Climate Episodes

Future Climate Analysis (BSC 2004 [DIRS 170002) estimated climatic variables for the next 10,000 years by forecasting the timing and nature of climate change at Yucca Mountain. That analysis assumed that climate is cyclical, so past climates provide insight into potential future climates, and further assumed that a relation exists between the characteristics of past climates and the sequence of those climates in the 400,000-year earth-orbital cycle (BSC 2004 [DIRS 170002], Section 5). Each cycle, consisting of 400,000-year periods and four approximately 100,000-year subcycles, is a series of glacial and interglacial couplets. Radiometric and isotopic analyses of calcite deposits at Devils Hole corroborate that past climate is cyclical and linked to earth-orbital forcing functions (BSC 2004 [DIRS 170002], Sections 6.3 and 6.4). *Future Climate Analysis* uses the microfossil record from cores drilled at Owens Lake, California, to reconstruct a climate history for the last long orbital cycle, calibrated to an elevation equivalent to the top of Yucca Mountain (BSC 2004 [DIRS 170002], Section 6.5).

Based on these paleoclimate records and the cyclical nature of climate, *Future Climate Analysis* provides climate estimates for the next 10,000 years.

Nevertheless, forecasting long-term future climates is highly speculative and rarely attempted (BSC 2004 [DIRS 170002], Section 1). The uncertainty in such forecasts is aleatoric. That is, it arises from natural randomness and cannot be reduced through further testing and data collection; it can only be characterized. This analysis of net infiltration places emphasis on capturing the full range of the aleatoric uncertainty.

Future Climate Analysis (BSC 2004 [DIRS 170002], Section 6.6, Table 6-1) predicts three climate episodes during the next 10,000 years at Yucca Mountain. The Present-Day climate is part of the interglacial climatic interval, reflective of a warm and arid climatic condition. The Present-Day climate is predicted to persist for another 400 to 600 years. Following the Present-Day climate will be a warmer and wetter monsoonal climatic condition. The Monsoon climate will persist for approximately 900 to 1,400 years. Between the Monsoon climate and the next glacial climate interval is a transition period labeled the Glacial Transition climate. The Glacial Transition climate will be cooler and wetter than the relatively brief monsoonal period, persisting for the remainder of the 10,000-year regulatory period (BSC 2004 [DIRS 170002], Section 7).

There is variability within each climate state (Present-Day, Monsoon, and Glacial Transition) akin to the larger earth-orbital climatic cycle but of shorter frequency and smaller amplitudes. The seasonal cycles are related to the earth's orbit and the tropical and polar air masses. For all three future climates, temperature and precipitation variability in the western region of the conterminous United States is dominated by the interplay, expansion, and contraction of tropical and polar air masses, driven seasonally by the earth's solar orbit. The northern edge of the tropical air masses, the Subtropical Highs, are characterized by hot, dry, high-pressure and descending air. The southern edge of the polar air masses, called the Polar Lows, are typically low-pressure, consist of rising air that creates cool, wet, high precipitation and low evaporation climate (BSC 2004 [DIRS 170002], Section 6.2). A "mixing zone" exists between the tropical and polar air masses. This mixing zone in the northern hemisphere is called the westerlies. As the westerlies pass over large water bodies, moisture is picked up. When the moisture-laden westerlies cross over from water to land masses, moisture is released. In the western United States, the westerlies coming from the Pacific Ocean provide moisture to the western half of the United States. The Yucca Mountain region lies within a major rain shadow created and sustained by the Sierra Nevada Mountains and the Transverse Range. Consequently, as the westerlies move eastward from the Pacific Ocean inland, moisture-laden air is released west of the Yucca Mountain region. It is the interplay between these large air masses, which affect the expansion and contraction of the rain shadow, coupled with regional topology that dominates the annual cyclical weather in the Yucca Mountain region.

DTN: GS000308315121.003 [DIRS 151139] lists representative meteorological stations for each of the three anticipated climate episodes. These are reproduced in Table 6.5.1.1-1. Section 6.5.1.2 below explains how the precipitation and temperature record at a meteorological station is represented by a set of 24 parameters. For each of the three anticipated climate episodes, Sections 6.5.1.3 through 6.5.1.5 describe the development of nominal values and uncertainty ranges for the weather parameters, including twelve more parameters for wind speed. A MASSIF calculation requires an input weather file containing daily precipitation, temperature

extremes, and wind speed. Section 6.5.1.6 describes the development of the weather input file using specific values for each of the 36 precipitation, temperature, and wind speed parameters. Section 6.5.1.7 discusses additional weather parameters, those that are not included in the weather input file.

Table 6.5.1.1-1. Meteorological Stations Selected to Represent Future Climate States at Yucca Mountain

Climate State	Duration	Representative Meteorological Stations	Locations of Meteorological Stations	
Present-Day	400 to 600 years	Site and regional meteorological stations	Yucca Mountain region	
Monsoon	900 to 1,400 years	Average Upper Bound: Nogales, Arizona Hobbs, New Mexico	North Latitude 31° 21’ 32° 42’	West Longitude 110° 55’ 103° 08’
		Average Lower Bound: Site and regional meteorological stations	Yucca Mountain region	
Glacial Transition	8,000 to 8,700 years	Average Upper Bound: Spokane, Washington Rosalia, Washington St. John, Washington	North Latitude 47° 38’ 47° 14’ 47° 06’	West Longitude 117° 32’ 117° 22’ 117° 35’
		Average Lower Bound: Beowawe, Nevada Delta, Utah	North Latitude 40° 35’ 25” 39° 20’ 22”	West Longitude 116° 28’ 29” 112° 35’ 45”

Source: DTN: PGS000308315.003 [DIRS 151139].

6.5.1.2 Parameterization of Precipitation and Temperature Records

Existing weather records cover less than 100 years. Because the probability distribution for precipitation is very skewed, there is no *a priori* assurance that a sample of so few years for a given climate will adequately represent average infiltration over hundreds or thousands of years. In order to capture the full range of uncertainty, the performance assessment must assure that rare precipitation events have been considered. Therefore, rather than use the meteorological records directly as input, this analysis characterizes each record in terms of periodic functions and additional parameters. Periodic functions summarize the records of precipitation, temperature, and wind speed at a meteorological station. This approach assures that the climate inputs are appropriate and adequate for predicting average infiltration.

Two of the periodic functions represent the succession of wet and/or dry days as a first-order Markov process and are therefore stochastic (see Appendix F, Section F1.1.1). Two other stochastic, periodic functions represent the variation in daily precipitation as a lognormal distribution. Each function, either of the two for precipitation or either of the two Markov probabilities, varies with the day of the year. Specifically, the precipitation record is represented by the following four functions, each of which depends on the day of the year, *d*, for *d* between 1 and 365:

$p_{00}(d)$: the probability that day d is dry, given that day $d-1$ is dry

$p_{10}(d)$: the probability that day d is dry, given that day $d-1$ is wet

$\lambda(d)$: mean of the lognormal precipitation distribution, given that day d is wet

$m(d)$: mean of the natural logarithm of the amount of precipitation, given that day d is wet.

For each of the four stochastic precipitation functions, a two-term Fourier series represents its variation with *d*. For example:

$$p_{00}(d) = a_{00} + b_{00}\sin(\theta_{00} + 2\pi d/365) \qquad \text{(Eq. 6.5.1.2-1)}$$

Therefore, there are twelve parameters that represent the precipitation record for a meteorological station: a_{00}, b_{00}, θ_{00}, a_{10}, b_{10}, θ_{10}, a_{λ}, b_{λ}, θ_{λ}, a_m, b_m, and θ_m. Appendix F describes the method used to calculate this set of precipitation parameters from a meteorological record and reports the results for each relevant meteorological station.

The value of a periodic precipitation function reaches its maximum when the sine function is 1.0. For example, the maximum value for $p_{00}(d)$ occurs when

$$d = d_{\max 00} = Mar1 + 365\left(\frac{1}{4} - \frac{\theta_{00}}{2\pi}\right) = May31 - 58\theta_{00} \qquad \text{(Eq. 6.5.1.2-2)}$$

The periodic functions that summarize the temperature record for a meteorological station are not stochastic. Rather, they represent the average minimum and maximum temperatures for each day of the year. Because wet days tend to have smaller differences between the minimum and maximum, wet days and dry days have separate representations, resulting in a total of four periodic temperature functions: $T_{md}(d)$, $T_{Md}(d)$, $T_{mw}(d)$, and $T_{Mw}(d)$. Each of these periodic temperature functions is also represented by a two-term Fourier series. For example,

$$T_{md}(d) = \gamma_{md} + \alpha_{md}\sin[2\pi(\beta_{md} + d)/365] \qquad \text{(Eq. 6.5.1.2-3)}$$

Therefore, there are twelve more parameters that represent the temperature record for a meteorological station: α_{md}, β_{md}, γ_{md}, α_{Md}, β_{Md}, γ_{Md}, α_{mw}, β_{mw}, γ_{mw}, α_{Mw}, β_{Mw}, and γ_{Mw}, where subscripts denote minimum (*m*) or maximum (*M*) temperature on wet (*w*) or dry (*d*) days. Appendix F describes the method used to calculate this set of temperature parameters from a meteorological record and reports the results for each relevant meteorological station.

6.5.1.3 Weather-File Parameters for the Remainder of the Present-Day Climate

The present-day-like climate interval is an interval of time when summers are warm to hot. Snowpack at high elevation is typically low to moderate because the polar front does not remain fixed at a southerly position during the winter and so does not set up a storm wave train that moves Pacific moisture over the Sierra Nevada Mountains. The wettest years, which represent the upper-bound moisture regimes during Present-Day climate, will typically be years when Pacific air flow focuses Pacific moisture toward southern Nevada, such as the El Nino climates that have been common during the last couple of decades. Dry years, which represent the lower-bound moisture regimes during Present-Day climate, will be those years with minimal winter precipitation, typically years when the polar front remains largely north of the region and summer precipitation is dominated by subtropical high activity but not to the degree necessary to a monsoon-type climate (BSC 2004 [DIRS 170002], pp. 6-46 to 6-47).

Tables F-1 and F-2 provide the results of parameterization of precipitation records for ten local and regional meteorological stations. These include five Yucca Mountain stations, four Nevada Test Site (NTS) stations, and one National Climatic Data Center (NCDC) station, Amargosa Farms.

The NCDC normal precipitation provides corroboration for the Fourier coefficients for Amargosa Farms (NOAA 2002 [DIRS 178676], pp. 3, 12). The NCDC normal precipitation for 1971 through 2000 is 100 mm, where missing data have been replaced using a weighting function derived from other station data and data from neighboring stations, and the peak precipitation months are February and March.

Table F-3 shows that the mean annual precipitation (MAP) calculated for Amargosa Springs from the zero-order Fourier coefficients (Equation F-42) is 119 mm, using the 26 years for which the records are complete, 1968, 1969, 1979-2000, 2002, and 2003. The phases of −1.17 radians and −2.61 radians for the Markov probabilities (Table F-4) correspond to maximum wet-day probabilities in February through April, using Equation 6.5.1.2-2. The phase of +2.34 radians for the precipitation amount (Table F-5) corresponds to peak storm size in January.

Tables F-7 and F-8 contain the results of parameterization of temperature records at four Yucca Mountain meteorological stations.

Appendix F also describes the use of temperature and precipitation lapse rates to adjust each station's parameters to an elevation equivalent to the top of Yucca Mountain (5,000 ft or 1,524 m). *Handbook of Hydrology* (Maidment 1993 [DIRS 125317], p. 3.3) provides a dry adiabatic temperature lapse rate of 0.01°C/m, with an implied uncertainty of ±0.005°C/m. In reality, a simple relationship does not exist to relate temperature and elevation at a given site. Rather, there are many complex factors which control local temperatures (e.g., ground conditions, wind patterns, slope and azimuth, etc.). It is assumed in this analysis that the use of the dry adiabatic temperature lapse rate is a reasonable approximation to the local terrestrial temperature lapse rate in areas such as Yucca Mountain, where terrain is not steep and conditions are generally windy enough to cause airflow over (rather than around) the terrain and dry enough that condensation is insignificant (Smith 2004 [DIRS 179904] pp. 193 to 222). It is shown in Section 7.1.4 that this assumption does not introduce a significant bias in estimates of net infiltration, and therefore this simplification is adequate for its intended use. This value has two applications:

1. In the development of Present-Day climate weather inputs, to adjust the zero-order temperature parameters to 1,524 m.

2. In the MASSIF model, for all climates, to adjust the input temperatures from an elevation of 1,524 m to the elevation of each cell, regardless of climate.

Appendix F uses the parameters for the ten stations to develop a lapse rate for each zero-order precipitation parameter of the Present-Day climate. These lapse rates provide the basis for adjustment of the zero-order parameters to 1,524 m. That is, both the frequencies of wet days and the wet-day precipitation amounts include adjustment for elevation.

Using an approximation (Equation F-42), the appendix estimates the MAP for each of the ten stations. These values lead to a lapse rate for MAP of 6.3 ± 0.7%/100 m (Table F-3). The MASSIF model uses this lapse rate to adjust input precipitation from an elevation of 1,524 m to the elevation of each cell. In effect, the model makes the assumption that the lower frequency of precipitation at lower elevations may be adequately represented by having the same wet days as at 1,524 m, but providing an extra reduction in the amount of precipitation.

For each selected station, Table F-6 lists the probability of a wet day and the MAP, calculated in accordance with the following formulas (Appendix F, Equations F-41 and F-42):

- Mean probability that a day is wet: $\frac{1-a_{00}}{1-a_{00}+a_{10}}$
- MAP: $365\frac{1-a_{00}}{1-a_{00}+a_{10}}a_{\lambda}$.

The adjusted values for MAP for each station range from 170 to 250 mm.

The potential range of MAP is corroborated by other data. For example, Thompson et al. (1999 [DIRS 109462]) interpolated Present-Day climate estimates to an elevation of 1,524 m. On the basis of U.S. Weather Service "normal" values, based on three decades of records, without detailed coverage near Yucca Mountain, the estimated MAP was 125 mm. However, a baseline derived from 10 years of NTS data yielded an estimated MAP of 189 mm (Thompson et al. 1999 [DIRS 109462], Table 4). Neither of these estimates used measurements taken at the Yucca Mountain site; however, both values are within the range of the combined parameter uncertainties.

Also, the National Oceanic and Atmospheric Administration (NOAA) provides historic climatic data by divisions, with Yucca Mountain located on the boundary between Nevada Division 3 to the north and Nevada Division 4 on the south. Thompson et al. (1999 [DIRS 109462]) found that one-year precipitation totals in Division 3, generally at higher elevation, ranged from about 75 mm to one value as high as 360 mm for the period of record (about 100 years). Division 4 areas, which are at lower elevation, had a range of one-year precipitation from less than 50 mm to one value as high as 325 mm for the period of record (Thompson et al. 1999 [DIRS 109462], p. 30, Figure 16). The range of MAP from the combined parameter uncertainties is well within the range of these one-year extremes.

The wind speed at two meters above ground is summarized for a meteorological station as an average for each month of the year. Therefore, there are twelve wind-speed parameters, $u_2(m)$, for m from 1 to 12. Appendix F, Section F3.1, describes the method used to calculate a monthly wind speed averaged over four Yucca Mountain meteorological stations.

Table F-22 lists the nominal value and uncertainty for each parameter of the weather input file for the Present-Day climate. The approximate uncertainty distribution for each zero-order precipitation parameter is a uniform distribution. The extremes of the distribution are the minimum and the maximum values among those obtained by analysis of the ten stations, extended by one standard error. These values also appear in Tables F-4 and F-5. The nominal value is the mid-point between these extremes.

For each of the eight first-order precipitation parameters, the nominal value is the mean of the values for the ten meteorological stations. The approximate uncertainty distribution is usually a normal distribution, established by the mean and standard deviation for the 10 stations. The one exception is $b_{10,1}$, which is only two standard deviations above zero, so that a uniform distribution, defined by the extreme values from the 10 stations, is a more representative distribution of this non-negative parameter. The values for the phase parameters are consistent with peak precipitation in the winter.

All of the temperature parameters have uncertainty distributions that are uniform, with a range determined by the minimum and maximum values for the four sites, as given in Tables F-8 through F-10. Each nominal value is at the center of its range. For determining temperature parameters, fewer weather stations were deemed necessary than for determining precipitation parameters because temperature is less directly related to net infiltration than precipitation and because the factors that effect temperature, such as ground conditions (color, vegetation) at sites far from Yucca Mountain may not be representative of conditions at Yucca Mountain. The wind speed averages have normal distributions, based on the mean and standard error calculated in Output DTN: SN0610T0502206.030.

The amount of runoff from a precipitation event is influenced by the intensity of the precipitation. The daily totals do not indicate the duration of an event within a day. Therefore, the duration of precipitation is one of the climate parameters required for simulating infiltration.

6.5.1.4 Weather-File Parameters for the Monsoon Climate

According to *Future Climate Analysis*, the monsoon climate is characterized in the Owens Lake record by species that imply a monsoon sufficient to generate diluting surface flow in the Owens River. An upper-bound value for the monsoon climate must have MAP higher than the values near Owens Lake (up to 270 mm) and mean annual temperature (MAT) as high or higher than Owens Lake today. *Future Climate Analysis* selected the stations at Hobbs, New Mexico, and Nogales, Arizona, with MAP levels of 418 mm and 414 mm, respectively, but noted that the MAP at these sites may not be high enough to generate the appropriate lake in the Owens Basin. An expansion of the summer rain regime to the Owens Basin region also would have expanded well north of Yucca Mountain. Because Yucca Mountain would be more centrally located within such a summer rain regime, it may experience upper-bound levels of MAP that are higher than those identified from the analogue meteorological stations (BSC 2004 [DIRS 170002], pp. 6-47 to 6-50).

Future Climate Analysis concludes that the conditions at Yucca Mountain today are representative of the dry lower bound for the monsoon climate. As for seasonal variation, climate during this period would vary from episodes of intense summer rain to present-day-like climates with relatively more winter and less summer precipitation (BSC 2004 [DIRS 170002], p. 6-50).

Tables F-12 and F-13 provide the results of parameterization of precipitation records for the Hobbs and Nogales meteorological stations. The NCDC precipitation normals provide corroboration for the Fourier coefficients for these stations. For each NCDC precipitation normal, missing data have been replaced using a weighting function derived from other station data and data from neighboring stations.

The NCDC normal precipitation for 1971-2000 at Hobbs is 461 mm, and the peak precipitation months are July and August (NOAA 2002 [DIRS 178675], pp. 3 and 15). The coefficients for Hobbs in Tables F-12 and F-13 are based on 38 years for which the records are complete, 1952, 1954, 1955, 1957, 1959 to 1967, 1969 to 1980, 1982, 1983, 1985 to 1990, 1992 to 1994, 1996, and 1998 (Output DTN: SN0609T0502206.023, *Monsoon/Precipitation Fourier Analyzer V2.3 Hobbs*, worksheet: "Input"). Applying Equation F-42 to the coefficients yields a MAP of 406 mm. The phases of +2.25 and +1.35 for the Markov probabilities (Table F-12) correspond to maximum wet-day probabilities in July through September. The phase of −1.09 for the precipitation amount (Table F-13) corresponds to peak storm size in July and August.

The NCDC normal precipitation for 1971 to 2000 at Nogales is 483 mm, and the peak precipitation months are July through September (NOAA 2002 [DIRS 178674], pp. 3 and 16). The coefficients for Nogales in Tables F-12 and F-13 are based on 29 years for which the records are complete, 1948, 1951, 1953 to 1958, 1960, 1962 to 1965, and 1967 to 1982 (Output DTN: SN0609T0502206.023, *Monsoon/Precipitation Fourier Analyzer V2.3 Nogales*, worksheet: "Input"). Applying Equation F-42 to the coefficients yields a MAP of 421 mm. The phases of +1.74 and +2.30 for the Markov probabilities (Table F-12) correspond to maximum wet-day probabilities in July and August. The phase of −2.01 for the precipitation amount (Table F-13) corresponds to peak storm size in September.

Equation F-42, which includes only the zero-order parameters, tends to underestimate MAP for stations experiencing a monsoon climate. That is because the first-order coefficients are relatively large and the seasonal variations in the Markov parameters are correlated with the seasonal variation in storm size.

The zero-order precipitation parameters in Tables F-12 and F-13 indicate that Hobbs has bigger storms, but Nogales has more storms. Combining the "wetter" value of each parameter would yield a MAP of 516 mm. This level of precipitation exceeds the NCDC normals and might have been enough to generate the appropriate lake in the Owens Basin during the previous cycle.

Tables F-14 and F-15 contain the results of parameterization of temperature records at the Hobbs and Nogales meteorological stations. Because Hobbs and Nogales were chosen for their values of MAP and their temperatures, without consideration of their elevation, they each represent conditions at the reference Yucca Mountain elevation of 5,000 ft (1,524 m) and need no adjustment for elevation.

It is assumed that the wind speed approximated for the Present-Day climate is an adequate approximation for the wind speed expected during the Monsoon climate.

Table F-23 lists the nominal value and uncertainty for each parameter. For the zero-order precipitation terms, the estimated uncertainty distribution is a uniform distribution. To assure that the extremes capture the full range of uncertainty, they are the minimum and maximum of all values from the analyses of Present-Day and upper-bound Monsoon sites.

As forecast in *Future Climate Analysis*, the monsoon climate is a climate where winter precipitation exists but does not dominate MAP. Climate during this period would vary from episodes of intense summer rain to present-day-like climates with relatively more winter and less summer precipitation (BSC 2004 [DIRS 170002], p. 6-50). Therefore, although the magnitude of the first-order precipitation term is uncertain, the phase of the first-order term must be that of the summer-precipitation upper-bound stations, not the winter-precipitation Yucca Mountain stations.

A monsoon climate has strong seasonal variation, which makes the first-order terms more important than for other climates. The amplitudes for the first-order terms differ greatly between the two upper-bound stations. Nogales has the greater seasonal variation in the probability that a day is wet. Hobbs has the greater variation in the average precipitation on wet days. Tables F-12 and F-13 show that some first-order magnitudes for the two stations differ by more than a factor of two, with standard deviations larger than the standard deviations in the corresponding zero-order terms.

Because *Future Climate Analysis* (BSC 2004 [DIRS 170002], p. 6-49) describes these stations as "the best choices available," it is not clear that the two values for a first-order amplitude, as different as they are, actually capture the full range of uncertainty. An alternate interpretation is that these stations are just two samples of potential upper-bound stations. In this interpretation, the potential upper-bound stations have a distribution for each parameter that may be approximated as a normal distribution, with the average and standard deviation for the two stations providing estimates for the mean and variance of the distribution. A range from one standard deviation below the lower value to one standard deviation above the upper value captures about 90% of this hypothetical distribution.

However, the magnitude of a first-order term is subject to constraints. The magnitude of a first-order term must be less than the magnitude of the zero-order term, because neither a Markov probability nor an average precipitation can be less than zero. Also, the first-order term may not cause a Markov probability to exceed 1.0. Therefore, an approximate uncertainty distribution for the magnitude of a first-order term for the upper-bound monsoon climate is a uniform distribution from one standard deviation below the lower value to one standard deviation above the upper value, subject to constraints.

The uncertainty distribution for the phase of each first-order precipitation term is a uniform distribution. The extreme values are the values for the two upper-bound stations.

Because the first-order terms for the lower-bound stations are completely out of phase with the upper-bound terms, they may be represented by negative values of the b parameters (b_{00}, b_{10}, b_{λ}, b_{m}). In Table F-23, the complete range for the amplitude of a first-order term may range from the largest value for the Present-Day climate, plus one standard deviation, but taken as negative, to the larger of the values from the upper-bound stations, plus one standard deviation, taken as positive.

All of the temperature parameters have uncertainty distributions that are uniform, with a range determined by the minimum and maximum values for the four sites, as given in Tables F-8 through F-10. Each nominal value is at the center of its range.

6.5.1.5 Weather-File Parameters for the Glacial Transition Climate

Judged from the Owens Lake record, the change to the glacial transition climate was large and fast, shifting from a strong monsoon system dominated by summer precipitation to a winter regime with sufficient effective moisture to sustain a fresh and spilling Owens Lake. Therefore, the polar front must be resident in the region during much of the winter, lowering the MAT. The genesis of greater snowpack with a resident polar mass must also lower temperature and increase MAP at Yucca Mountain, but the cooler climate never becomes very cold with high effective moisture as was true of the last two full-glacial periods. The climate during the glacial transition period was typically a cool, usually wet winter season with warm (but not hot) to cool summers that were usually dry relative to the present-day summers. The MAT should be no colder and preferably warmer than 8°C. The MAP should be higher than the 309 mm recorded near Owens Lake, because even the high historic discharge levels of that year would not be sufficient to fill and spill the lake as implied by the microfossil record. The three selected stations in eastern Washington—Rosalia, St. John, and Spokane—fit all of the criteria for the upper-bound glacial transition climate (BSC 2004 [DIRS 170002], pp. 6-50 to 6-52).

However, there are indications that there were also episodes during this climate period that were relatively warm and dry, thus demonstrating some degree of climate variability. The stations representing the lower bound should have a higher temperature, but lower than that for the Owens Lake Basin today. They may have MAP values that are similar to or even lower than present-day Owens Lake Basin, but dominated by winter precipitation. The set of meteorological data for Delta, Utah, fits all of these criteria. The site at Beowawe, Nevada, was added as a lower-bound station to avoid using a single site and because its data met most of the requirements (BSC 2004 [DIRS 170002], pp. 6-50 to 6-53).

The NCDC precipitation normal provides corroboration for the Fourier coefficients for these stations (NOAA 2002 [DIRS 178673] pp. 3 and 15; 2002 [DIRS 178677], pp. 3 and 15; and 2002 [DIRS 178676], pp. 3 and 15). For the NCDC precipitation normal, missing data have been replaced using a weighting function derived from other station data and data from neighboring stations. For each station, Table 6.5.1.5-1 provides the fraction of days that are wet and the MAP, calculated in accordance with Equations F-41 and F-42. Shown for corroboration are the normal MAPs and wettest months for these stations, as reported by the NCDC.

Table 6.5.1.5-1. Wet Day Fraction and Mean Annual Precipitation Implied by Adjusted Parameters

Meteorological Station	Wet Day Fraction	Implied MAP (mm)	Years Used for Fourier Analysis (Mar. 1 to Feb. 28)	NCDC Normal MAP for 1971 to 2000 (mm)	NCDC Wettest Month(s)
Beowawe	17%	241	10 years: 1983, 1986 to 1989, 1993 to 1995,1999,2001	225	May
Delta	18%	207	29 years: 1972, 1973. 1975, 1976, 1978 to 1981, 1983 to 2003	214	May, Oct.
Rosalia	30%	455	28 years: 1953, 1956, 1958 to 1960, 1963 to 1971, 1973, 1975 to 1978, 1980 to 1983, 1985 to 1988, 1993	467	Dec.
Spokane	31%	419	52 years: 1948 to 1952, 1954 to 1994, 1998 to 2003	423	Nov. to Dec.
St. John	27%	431	22 years: 1964 to 1969, 1972 to 1981, 1987, 1989 to 1991, 1994, 2001	436	Dec.

Source: Fourier analysis years from Output DTN: SN060 9T0502206.023; 1971 to 2000 MAPs and wettest months from NOAA 2002 [DIRS 178673], p. 15; 2002 [DIRS 178677], p. 15; and 2002 [DIRS 178676], p. 12.

For the upper-bound stations, the phase parameters correspond to peak storm frequency in December through February, but peak storm magnitude in May through June. The lower-bound station parameters reflect peak frequency in the winter, but peak magnitude in June through August. The difference in wettest months arises because the upper-bound stations have larger seasonal variation in frequency, while the lower-bound stations have larger seasonal variation in magnitude.

Tables F-20 and F-21 contain the results of parameterization of temperature records at the five meteorological stations representing the glacial transition climate. Because these stations were chosen for their values of MAP and their temperatures, without consideration of their elevation, they each represent conditions at the reference Yucca Mountain elevation of 5,000 ft (1,524 m) and need no adjustment for elevation.

It is assumed that the wind speed approximated for the Present-Day climate is an adequate approximation for the wind speed expected during the Glacial Transition climate.

Table F-24 lists the nominal value and uncertainty for each parameter. Most of the uncertainty distributions for precipitation and temperature parameters are uniform with the ranges determined in Section F2.3 extended by one standard error where applicable, and the nominal values are the means of the distributions. The exceptions are the phase coefficients for precipitation. The table assigns a normal distribution to the phase coefficients for the Markov probabilities using the weighted average and standard deviation from Table F-18. In the case of the phase coefficients for the amount of precipitation of a wet day (Table F-19), however, the weighted standard deviations are so large that no nominal value seemed justified. These last two phase coefficients are considered as completely uncertain, so that any value is possible.

6.5.1.6 Generation of MASSIF Weather-File Input from Climate Parameters

One of the inputs to MASSIF is a weather file with data for each day. Each day's data set consists of the amount of precipitation, the minimum and maximum temperatures, and the average wind speed at two meters above the ground.

For a given set of weather parameters, a stochastic algorithm develops a 1,000-year sample of daily precipitation by sampling from a lognormal distribution. For wet days, the amount of precipitation, P, is determined from a random number $R \in (0,1)$ and the cumulative probability distribution; that is:

$$\int_0^{P(y,d)} \frac{e^{-[\ln x - m(d)]^2/2[s(d)]^2}}{xs(d)\sqrt{2\pi}} dx = R \qquad \text{(Eq. 6.5.1.6-1)}$$

where $s(d) = \sqrt{2[\ln \lambda(d) - m(d)]}$.

The domain for Yucca Mountain infiltration covers approximately 50 square miles. An infiltration calculation produces a map of daily infiltration through each of 143,000 pieces of land, averaged over a sample of years.

Therefore, it is not practical to calculate daily infiltration through each area for 1,000 years. This difficulty is addressed by taking a sample of the simulated years, including several years with high precipitation. Each sample year is weighted by its relative probability in calculating the map of average annual infiltration. This approach assures that the effects of extreme events are recognized, but given appropriate weight in the analysis.

Input to the infiltration model is a subsample of the 1,000-year sample. From the full sample sorted by total precipitation for the year, the subsample includes 1,000-year, 300-year, 100-year, 30-year, and 10-year events, with a few additional years to represent the drier portion of the probability distribution. Each year in the subsample carries a weight proportional to probability; for example, the 1,000-year event has a weight of 0.001. Appendix F contains the details of the procedures.

Daily temperature extremes and mean wind speeds are added to the weather input file as described in Appendix F.

6.5.1.7 Other Climate Parameters

Maximum Daily Precipitation

The lognormal fit to wet-day precipitation amount does not fit the probability of extreme events very well. Although the assigned probability for extremely heavy precipitation is very small, it appears to be higher than the data. Therefore, MASSIF accepts an input that limits the total precipitation for one day. The value chosen is the largest observed rainfall in the USA during a 24-hour period over a 26-km^2 area, 983 mm (Maidment 1993 [DIRS 125317], p. 3.36, Table 3.10.2).

Snowmelt Coefficient

MASSIF employs a temperature-index snowmelt equation from *Handbook of Hydrology* (Maidment 1993 [DIRS 125317], p. 7.24) for calculating daily snowmelt for days with snow accumulation. Table 7.3.7 in that source (Maidment 1993 [DIRS 125317], p. 7.24) provides temperature-index expressions for calculating daily snowmelt for various regions of North America. The closest site to Yucca Mountain is Sierra Nevada, California. This site has latitude similar to that of Yucca Mountain and is therefore the most appropriate site to use in this table. The general form of the temperature-index snowmelt equation is:

$$M = SM * T \qquad \text{(Eq. 6.5.1.7-1)}$$

where SM is the snowmelt coefficient in mm/day/°C (for days with mean daily air temperature greater than 0°C), M is snowmelt in mm/day and T is daily mean air temperature (°C). The snowmelt coefficients for the Sierra Nevada, California, are 1.78 and 1.92 for April and May, respectively (Maidment 1993 [DIRS 125317], p. 7.24).

There is large inherent uncertainty in this parameter. Maidment (1993 [DIRS 125317], Table 7.3.7, p. 7.24) reports values for the snowmelt coefficient (*SM*) ranging from 0.58 (for the Boreal forest) to 5.7 (for Southern Ontario). It appears that the greater the amount of forest cover, the lower the value of *SM*, which suggests that more snowmelt is slowed by the presence of tree shade. A mean value of 2 was selected for the MASSIF model, which is slightly higher than the Sierra Nevada values. A range of 1 to 3 (with a uniform distribution) is assumed to represent snowmelt conditions at Yucca Mountain during the Glacial Transition climate. This value was used for all climates because there is not significant snow during the Present-Day and Monsoon climates.

Sublimation Coefficient

Estimates of sublimation (or ablation) of snowpack vary widely. Hood et al. (1999 [DIRS 177996], p. 1,782) discuss a 1975 study in which sublimation was responsible for 80% of the ablation of fresh snow and 60% of the ablation of older snow during springtime conditions in the White Mountains of California. Hood et al. (1999 [DIRS 177996], p. 1,782) also discuss a 1959 study in which sublimation was only 2% to 3% of total ablation over the snow season at the Central Sierra Snow Laboratory in California.

Hood et al. (1999 [DIRS 177996], p. 1782) also discuss more recent studies (e.g., Kattelmann and Elder 1991 [DIRS 177998]) that estimated sublimation from snow to be 18% of total precipitation over two water years for Emerald Lake Basin in the Sierra Nevada, and Berg (1986 [DIRS 177995]), who reported sublimation losses from blowing show to be between 30% to 51% of precipitation for the two year period 1973 to 1975. Hood et al. (1999 [DIRS 177996], p. 1794) report sublimation from their own study to be 15%.

Based on the annual sublimation data reported by Hood et al. (1999 [DIRS 177996], p. 1794), a nominal value of 10% was selected for Yucca Mountain. This value is lower than those estimated for the Sierra Nevada; however, this is justified because the snow pack is expected to persist for shorter periods of time at Yucca Mountain in the future than it does in the Sierra

Nevada in the present climate. To incorporate uncertainty, a range of 0% to 20% (with a uniform distribution) is considered to represent annual snow sublimation amounts at Yucca Mountain during the Glacial Transition climate. This range is corroborated by the other studies discussed above. This value was used for all climates because there is not expected to be significant snow during the Present-Day and Monsoon climates.

The sublimation coefficient is multiplied by daily precipitation for days when the mean daily air temperature is less than 0°C, and that amount is removed from the precipitation total in the form of snow sublimation. The effect of this calculation is to partition 10% of daily precipitation on days when the mean daily temperature is less than 0°C into sublimation and thereby remove this water from the water balance.

Table 6.5.1.7.1 summarizes the snow parameters.

Table 6.5.1.7-1. Nominal Values and Uncertainties for Snow Parameters

Parameter Name	Parameter Symbol	Nominal Value	Uncertainty Range	Uncertainty Distribution
Snowmelt (SM)	$C_{snowmelt}$	2.0	1.0 to 3.0	Uniform
Sublimation (SUB)	$C_{sublime}$	0.1	0.0 to 0.2	Uniform

Source: Snowmelt coefficient estimates from Maidment 1993 [DIRS 125317], p. 7.24. Sublimation estimates from Hood et al. 1999 [DIRS 177996], p. 1794

Precipitation Duration

The precipitation duration is a highly variable parameter in the desert environments, so that the selection of the parameter values to be used in the MASSIF calculations needs a special justification. For each climate, this analysis develops a function that relates the precipitation duration to the amount of rain that falls on a given day. Because of limited data availability, only data from certain weather stations representing each climate were analyzed. Four sets of analyses were done to characterize precipitation duration parameters for each climate. Output DTN: SN0610T0502206.031 contains MathCAD applications in which the analyses are performed.

Table 6.5.1.7-2 lists the weather stations used for the four precipitation duration analyses.

Table 6.5.1.7-2. Weather Stations Used for Precipitation Duration Analyses

Precipitation Duration Analysis	Weather Stations	Source DTN
Present-Day	BSC Stations 1, 2, 3, 6	SN0608WEATHER1.005 [DIRS 177912]
Monsoon (upper)	Hobbs, NM, and Nogales, AZ	MO0605SEPHOURL.000 [DIRS 177237]
Glacial Transition (lower)	Delta, UT	MO0605SEPHOURL.000 [DIRS 177237]
Glacial Transition (upper)	Spokane, WA	MO0605SEPHOURL.000 [DIRS 177237]

For each analysis listed in Table 6.5.1.7-2, the daily precipitation **amount (*Amt*)** and the **number of hourly intervals (*Int*)** in which precipitation was measured at each of the weather stations were calculated for every day of the year. Days with zero precipitation (number of hourly

intervals equals zero) were filtered out. The remaining dataset was plotted (Figures 6.5.1.7-1 to 6.5.1.7-4) and fit to a linear model:

$$Int = a + b * Amt \qquad \text{(Eq. 6.5.1.7-2)}$$

where a is the y-intercept and b is the slope.

The standard error on b was estimated as:

$$SE_b = \frac{\sqrt{mean\left\{\left[\frac{Int_i - a}{Amt_i} - b\right]^2\right\}}}{\sqrt{n}} \qquad \text{(Eq. 6.5.1.7-3)}$$

where n is the number of data, and i is the data index from 1 to n.

For the MASSIF calculation, which uses a daily time step, an assumption is made that daily precipitation occurs as a single event rather than multiple shorter events separated by dry periods during the day. Given this assumption and for a given precipitation day, the number of hourly intervals is, on average, equal to one hour greater than the actual precipitation duration for that day. This is because for a given precipitation event the actual start and end times within the hourly intervals that bound these start and end times are equally likely to occur during the first half of the intervals as the last half of the interval. For example, given it rains for 0.5 hr, there is a 0.5 probability that the rain event occurred in one hourly interval and a 0.5 probability that it occurred in two hourly intervals. The mean number of intervals is 1.5, which is one hour more than the actual duration of the rainfall. This one hour offset can be shown to apply for any given duration event. Table 6.5.1.7-3 lists the results of the linear regressions as the slope and intercept-1. The intercept-1 represents the minimum precipitation duration considered in the model. Table 6.5.1.7-4 lists the nominal values and distributions for these parameters for each climate.

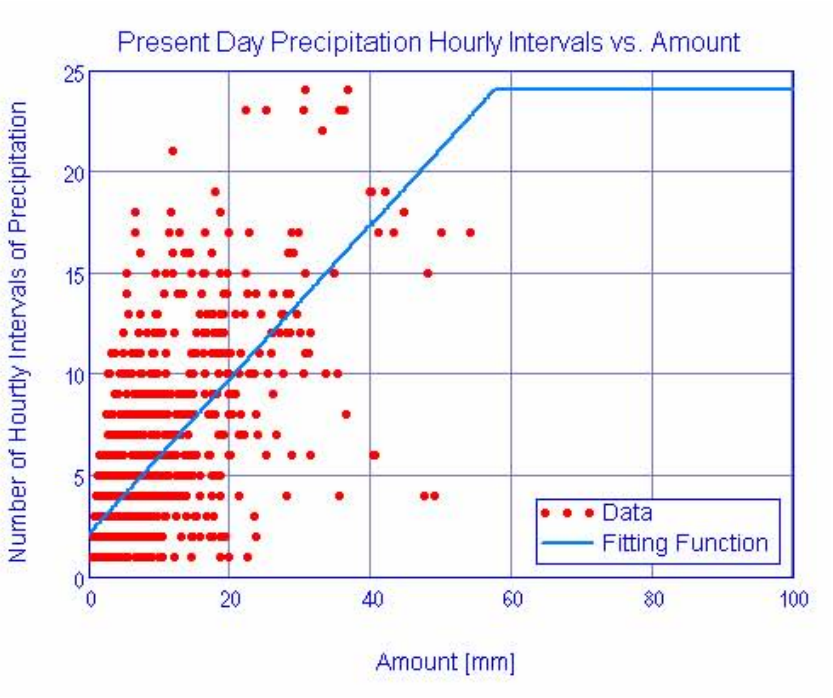

Source: Output DTN: SN0610T0502206.031.

Figure 6.5.1.7-1. Number of Hourly Intervals of Precipitation Plotted against the Daily Amount of Precipitation for the Present Weather Stations BSC1, BSC2, BSC3, and BSC6

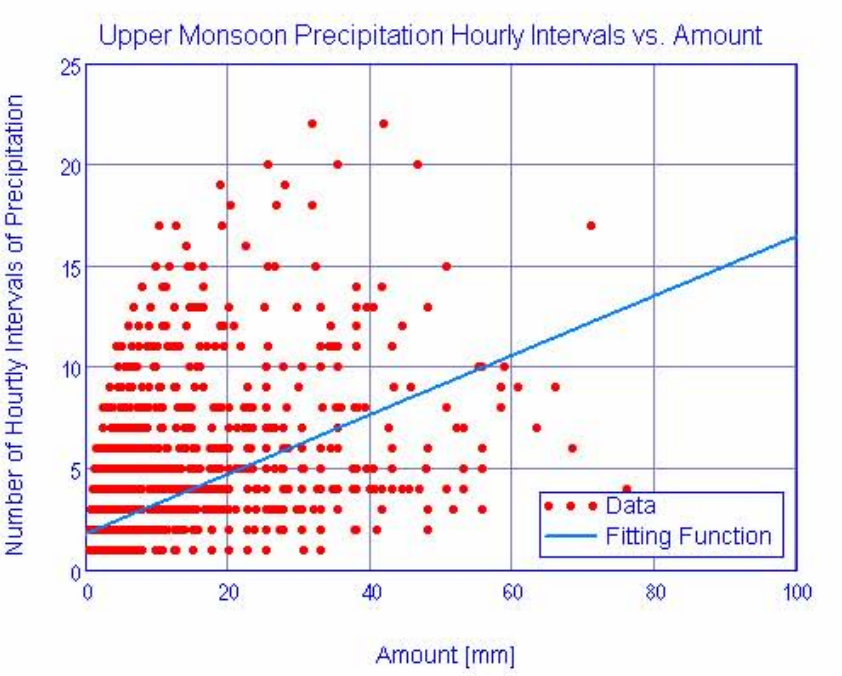

Source: Output DTN: SN0610T0502206.031.

Figure 6.5.1.7-2. Number of Hourly Intervals of Precipitation Plotted against the Daily Amount of Precipitation for the Upper Monsoon Weather Stations of Hobbs, NM, and Nogales, AZ

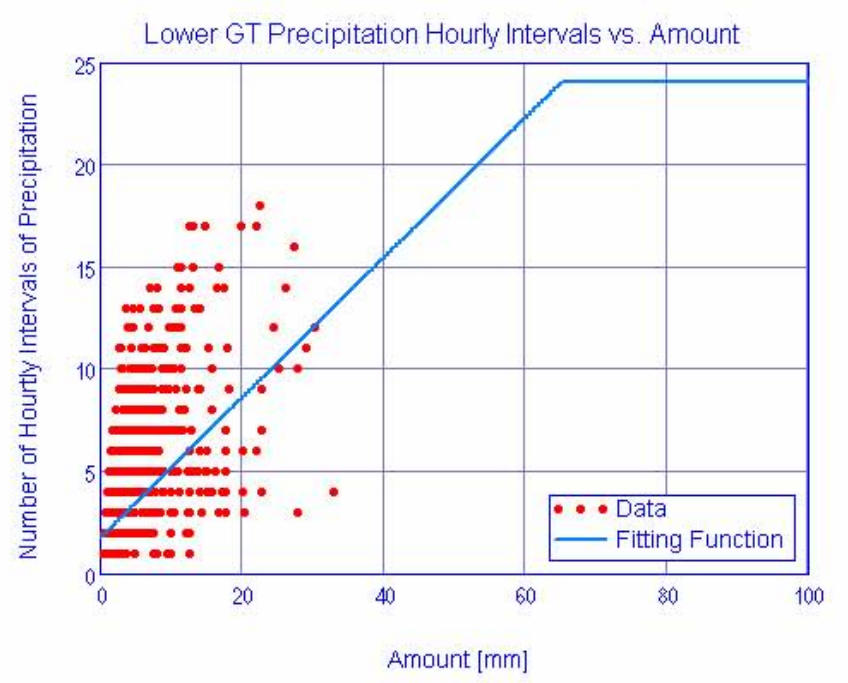

Source: Output DTN: SN0610T0502206.031.

Figure 6.5.1.7-3. Number of Hourly Intervals of Precipitation Plotted against the Daily Amount of Precipitation for the Lower Glacial Transition Weather Station of Delta, UT

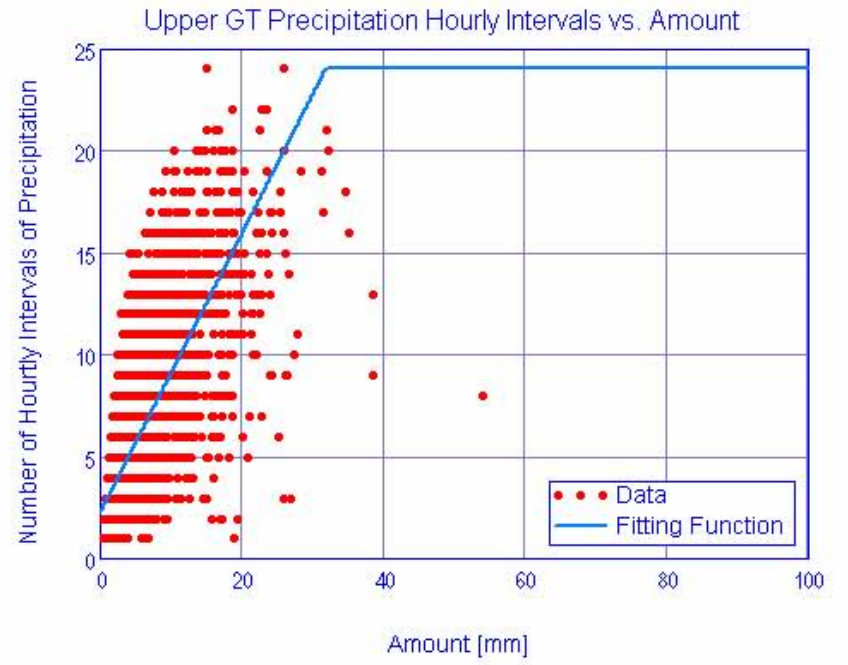

Source: Output DTN: SN0610T0502206.031.

Figure 6.5.1.7-4. Number of Hourly Intervals of Precipitation Plotted against the Daily Amount of Precipitation for the Upper Glacial Transition Weather Station of Spokane, WA

Table 6.5.1.7-3. Precipitation Duration Linear Regression Results

Precipitation Duration Analysis	Slope	Std Err on Slope	Minimum Precipitation Duration (Intercept-1)
Present-Day	0.38	0.05	1.07
Monsoon (upper)	0.15	0.01	0.76
Glacial Transition (lower)	0.34	0.02	0.70
Glacial Transition (upper)	0.68	0.03	1.22

Source: Output DTN: SN0610T0502206.031, *Precipitation Duration Parameter Values and Distributions.xls*.

Table 6.5.1.7-4. Precipitation Duration Parameter for Each Climate

Climate	Nominal Slope	Distribution (Slope)	Std Err on Slope	Minimum Precipitation Duration (Intercept-1)
Present-Day	0.38	Normal (mean = 0.38, SD = 0.05)	0.05	1.07
Monsoon	0.28 [a]	Uniform (0.14 – 0.43) [d]	0.08 [c]	0.91
Glacial Transition	0.52 [b]	Uniform (0.32 – 0.71) [d]	0.11 [c]	0.96

Source: Output DTN: SN0610T0502206.031, *Precipitation Duration Parameter Values and Distributions.xls.*

[a] Mean of Present-Day and Monsoon upper slope values (mean of values presented in Table 6.5.1.7-3 is 0.27 due to rounding in that table).

[b] Mean of Glacial Transition lower and upper slope values (mean of values presented in Table 6.5.1.7-3 is 0.51 due to rounding in that table).

[c] Standard deviation calculated using square root of Equation I-9.

[d] Upper and lower ends of uniform distribution are extended by one standard error.

6.5.2 Geologic and Geographic Inputs

Geologic inputs to MASSIF include parameters for Yucca Mountain soils and bedrock, and spatial distributions for soil types, soil depth classes, and bedrock types over the modeling domain. Geographic inputs include data used to define cell coordinates, elevations, slope, azimuth, watershed delineations, and other site characteristics. This section presents a summary of the methods used to determine each of the geologic and geographic inputs and presents the nominal values and uncertainty ranges for all the geospatial parameters. Geographic inputs are described in Section 6.5.2.1. Soil classification is presented in Section 6.5.2.2 followed by soil properties and soil depth in Sections 6.5.2.3 and 6.5.2.4, respectively. Bedrock classification and bedrock properties are presented in Sections 6.5.2.5 and 6.5.2.6, respectively.

The geologic and geographic parameters used by MASSIF were organized into a ‘geospatial’ database. Development of the geospatial database is presented in Appendix B. The database is used to identify spatially varying parameters for each cell within the modeling domain. The database includes the following:

- Cell ID
- UTM Easting (m)
- UTM Northing (m)
- Latitude (deg)

- Longitude (deg)
- Elevation (m)
- Downstream Cell ID – identifies the cell ID for the cell adjacent to and downstream of each cell, or specifies that there are no downstream cells
- Slope (deg)
- Azimuth (deg)
- Soil Depth Zone
- Soil Type
- Bedrock Type
- Potential Vegetative Response.

For the calculations described in this report, geospatial parameters are handled in two different ways. The values of some parameters are specified in the geospatial database such that they vary independently from cell to cell. Examples of parameters that very from cell to cell include elevation and potential vegetation response (PVR). For the remaining geospatial parameters, such as bedrock hydraulic conductivity or soil properties, the geospatial database contains an index that identifies groups of grid cells representing regions where particular properties are assigned uniform values. The value of the parameter is defined to be uniform over all locations with the same index. The following geospatial parameters are assigned to such grid cell groups or regions:

- Soil depth class (5 classes)
  - Soil depth
- Soil type (8 types)
  - Saturated hydraulic conductivity (K_{sat_soil})
  - Saturated water content (θ_s)
  - Field Capacity (θ_{FC})
  - Permanent Wilting Point (θ_{WP})
  - Water Holding Capacity (calculated from θ_{FC} and θ_{WP})
- Bedrock type (38 types)
  - Saturated hydraulic conductivity (K_{sat_rock}).

Geospatial parameters represent the effective properties of 30 × 30-m grid cells, or in the case of parameters assigned to grid cell groups, these parameters represent the effective properties of much larger regions of the modeling domain. For this reason, the probability distributions of the effective or "upscaled" values of geospatial parameters will vary from the underlying spatial distributions of these parameters, which are derived from individual measurements made on a smaller scale. The region boundaries for each of the parameters were established independently of the estimation of spatial distributions of properties. Therefore, the spatial distributions are interpreted as applying to the entire region within the given boundaries, regardless of the original rationale for setting the boundaries.

Uncertainty in geologic inputs is reported with the nominal values in Sections 6.5.2.2 through 6.5.2.6. For the purpose of this infiltration analysis, uncertainty in parameters is propagated through the calculation if the parameter of interest meets the criteria established for the uncertainty analysis described in Appendix I.

6.5.2.1 Geographic Inputs

Geographic inputs to MASSIF generally include data that describe the physical location and layout of each cell. Material properties associated with the soil, bedrock, or vegetation characteristics of each cell are treated separately in Sections 6.5.2.2 through 6.5.2.6 of this report. Geographic inputs include:

- UTM Easting (m)
- UTM Northing (m)
- Latitude (deg)
- Longitude (deg)
- Elevation (m)
- Downstream Cell ID – identifies the cell ID for the cell adjacent to and downstream of each cell, or specifies that there are no downstream cells
- Slope (deg)
- Azimuth (deg).

The geographic inputs were organized into a Geographic Information System (GIS) developed for the MASSIF model and described in Appendix B. The spatial inputs elevation, azimuth, and slope are used for calculations of runoff and temperature and precipitation adjustments for elevation, and are important for developing other parameters relating to evapotranspiration.

The Shuttle Radar Topography Mission (SRTM) data were selected as the best source for topography data for infiltration modeling based on criteria described in Appendix B. The SRTM data were obtained from the U.S. Geological Survey (USGS) Earth Resources Observation and Science (EROS) Data Center (DTN: SN0601SRTMDTED.001 [DIRS 177242]).

The MASSIF infiltration model domain includes the area that drains Yucca Mountain above the proposed repository waste emplacement area. Eleven separate drainages (or watersheds) were delineated; three larger basins drain the east face of the ridge and eight smaller basins drain the west face. The largest drainage in the north part of the domain (Yucca Wash) has been artificially cut off on its northern edge because of a lack of detailed information about soil and bedrock properties in this region. The implication of this cutoff is an assumption that any run-on from the parts of the drainage that are not included can be neglected for the purpose of estimating net infiltration inside this drainage. The delineation of watershed boundaries is presented in Appendix B.

The watersheds were delimited using elevation and slope to define surface water flow direction to a single outlet. The boundaries of the eleven watersheds also delineated the overall infiltration model boundary within the larger project boundary. Figure 6.5.2.1-1 shows the watershed boundaries, which lie within the larger project boundary area. The larger rectangular project boundary encompasses 226.34 km^2. The infiltration model boundary, composed of the combination of these eleven watersheds, encompasses 120.61 km^2. The eleven watersheds make up the individual model components that are used to calculate net infiltration. The individual watersheds are highlighted in Figure 6.5.2.1-2. The region identified as the "repository waste emplacement area" in Figure 6.5.2.1-2 (and Figure 6.5.2.1-1) refers to the area where infiltration results are expected to be passed on to downstream users of the infiltration data. This area is larger than the "repository footprint," which is also shown in Figure 6.5.2.1-1, and smaller than the entire infiltration modeling domain. The repository waste emplacement area is hereafter also referred to as the unsaturated zone (UZ) grid region or UZ model domain because it corresponds to the expected modeling boundaries to be used in the UZ model, downstream of this report (BSC 2004 [DIRS 169861]; BSC 2004 [DIRS 169857]). The UZ grid region is of particular interest in the present analysis because areas outside this region, though important to the infiltration model, are not expected to be used in downstream models (such as the UZ model). For this reason, grid cells within the UZ grid are given special consideration in terms of identifying which parameters to include in a model of net infiltration uncertainty for Yucca Mountain. The number of cells in each region is shown in Table 6.5.2.1-1.

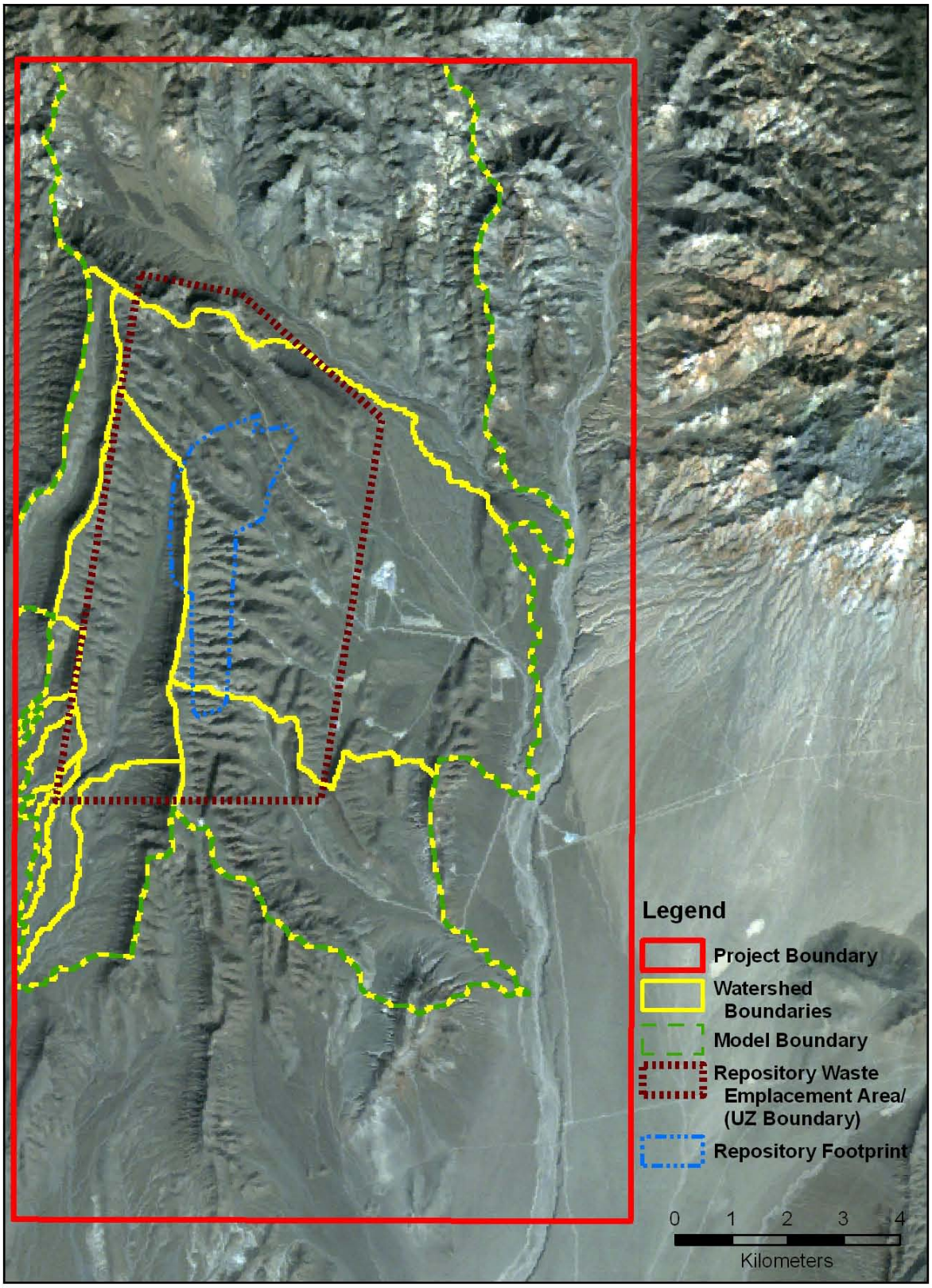

Source: Output DTNs: SN0608DRAINDYM.001, SN0612FTPRNUZB.002, and SN0608NDVILSTM.001.

Figure 6.5.2.1-1. Infiltration Modeling Boundaries

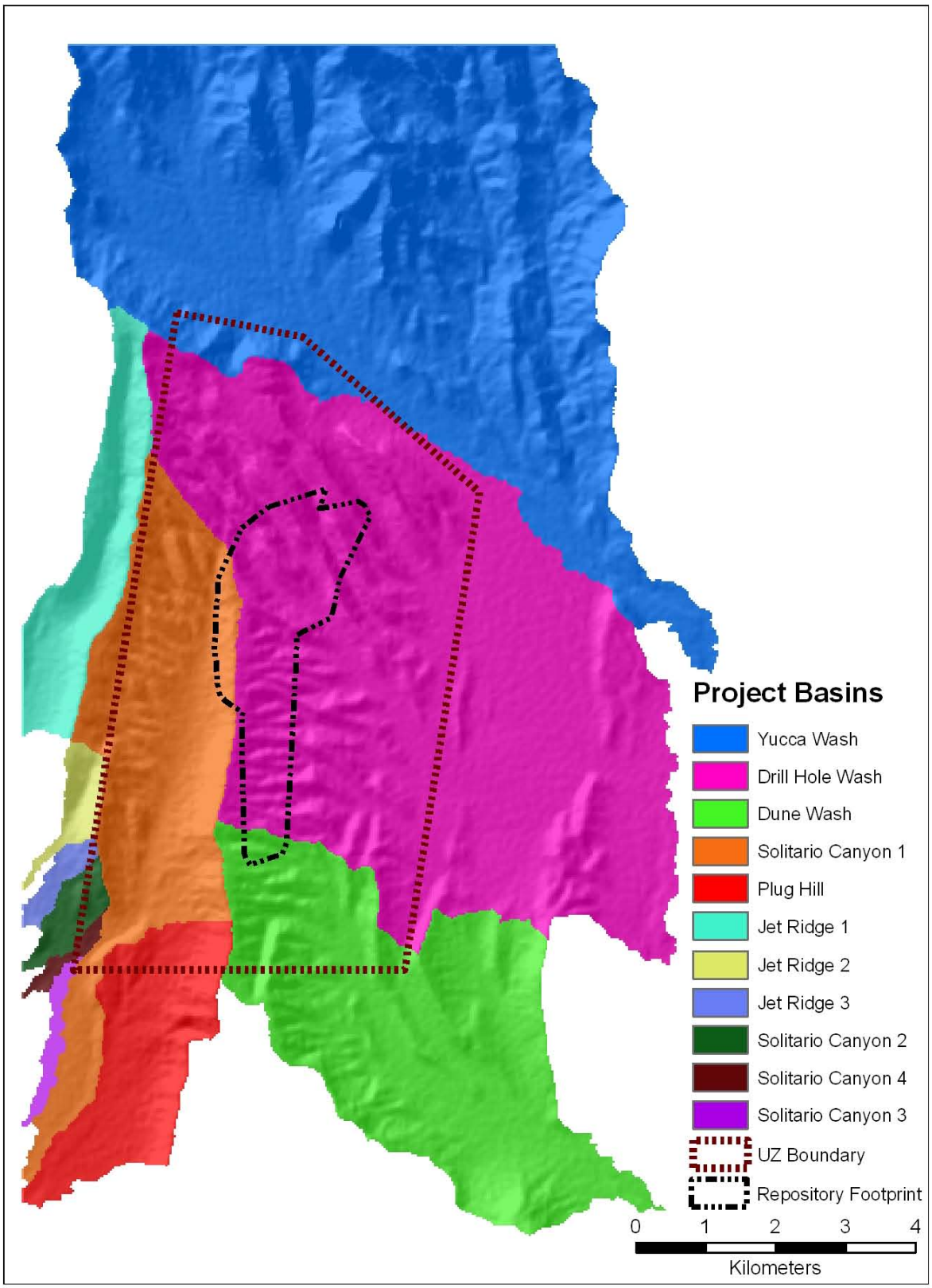

Source: Output DTNs: SN0701SPALAYER.002 and SN0612FTPRNUZB.002.

Figure 6.5.2.1-2. Yucca Mountain Watersheds (Basins)

Table 6.5.2.1-1. Number of Grid Cells within Various Boundaries in the Yucca Mountain Region

Boundary	Total Number of Cells
Project Boundary[a]	253,597
Infiltration Model Boundary (defined by eleven watersheds)[b]	139,092
Repository Waste Emplacement Area (UZ grid region)[c]	44,204
Repository Footprint [c]	6,322

[a] Output DTN SN0608ASSEMBLY.001.
[b] Output DTN SN0608DRAINDYM.001.
[c] LB0208HYDSTRAT.001 [DIRS 174491].

NOTE: Boundaries presented in this table correspond to the boundaries shown in Figure 6.5.2.1-1.

As described in Appendix B, a three-stage watershed delineation process was required to generate the fewest number of watersheds that would completely cover the Repository Waste Emplacement Area. Each watershed is a separate component of the MASSIF model, so fewer drainages result in fewer processing steps. However, the size of the drainages was dictated by two factors: the topography of the region and the UZ model domain. The surface area of each watershed varied widely, a result of the three nearly identical delineation stages needed to generate the eleven drainage basins that cover Yucca Mountain: three large, three moderate, and five small basins. During each stage, a specific threshold variable was set that would determine the size of the resulting drainages. Thus, each stage was responsible for generating either the large, medium, or small drainage basins. Variable basin sizes were necessary because the MASSIF model needed to trace potential infiltration from all locations directly over the UZ model domain down the mountain slopes to each basin pour point (the bottom-most part of the basin).

Elevation data from SRTM required processing for use in the geospatial database, as the SRTM cell size and map coordinate projections did not correspond to those needed for the infiltration model. Once cell size and projection were revised, the elevation data could then serve as the base data layer from which multiple derivative data layers could be created. These additional layers provided information, such as slope and aspect, which are required by the MASSIF infiltration model.

The raw form of the SRTM data layer was processed using Research Systems, Inc. (RSI) Environment for Visualizing Images (ENVI; ENVI + IDL, Version 4.2: STN: 11204-4.2-00) image processing software. The SRTM data were divided as a subset within the project boundary, converted to 30-m pixels and re-projected to accommodate the requirements of the MASSIF model. Elevations across the modeling domain are presented in Figure 6.5.2.1-3.

The elevation data were also used to create additional layers within the GIS including the slope and azimuth over the model area. The surface slope of each grid cell was calculated using the *slope* function in ArcGIS, which uses the elevations at eight neighboring cells. Slope was defined from 0° (horizontal) to 90° (vertical). Slopes over the infiltration modeling domain ranged between 0° and 49° (rounded to the nearest degree). A map of slopes over the modeling area is presented in Figure 6.5.2.1-4.

The azimuth layer was created using the *azimuth* function in ArcGIS, which estimates the compass direction of a vector normal to the surface of each grid cell. This parameter is used for

calculations involving the direction of incoming solar radiation. Azimuths were defined between 0° and 360° (rounded to the nearest degree). East is at 90°, South is at 180°, and West is at 270°. A map of azimuths over the modeling area is presented in Figure 6.5.2.1-5.

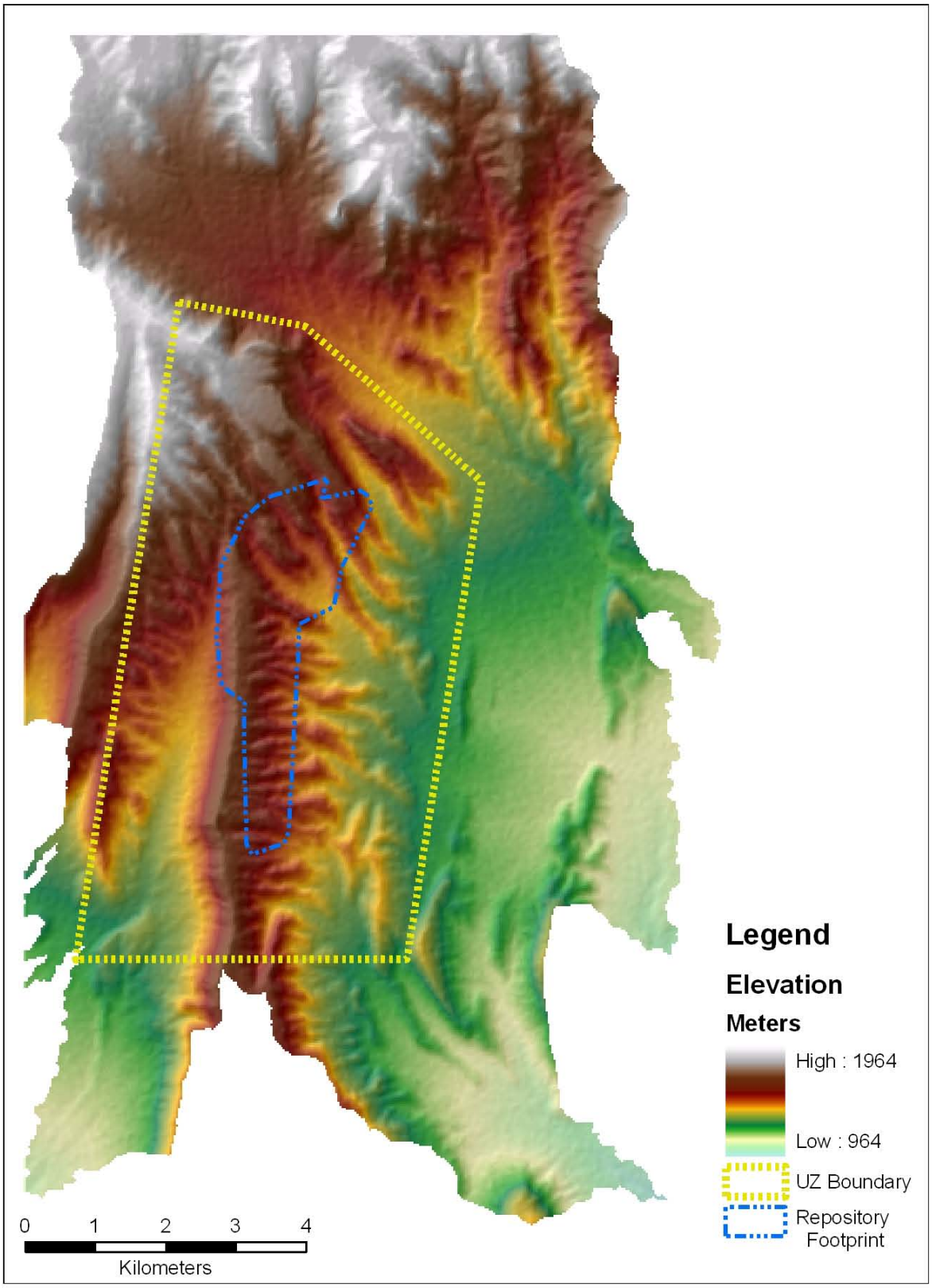

Source: Output DTNs: SN0701SPALAYER.002 and SN0612FTPRNUZB.002.

Figure 6.5.2.1-3. Elevation over the Model Area

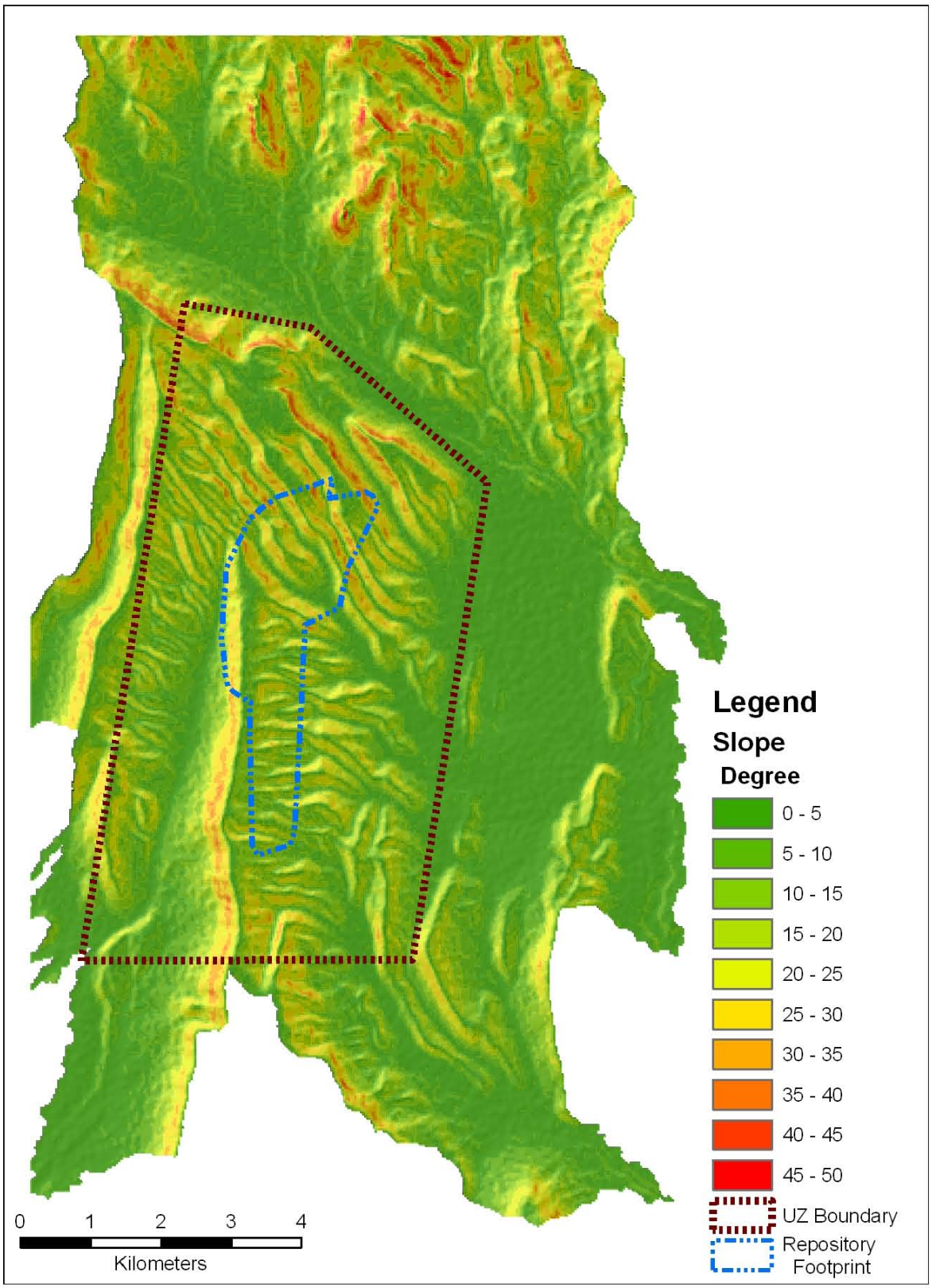

Source: Output DTNs: SN0701SPALAYER.002 and SN0612FTPRNUZB.002.

Figure 6.5.2.1-4. Slope over the Model Area

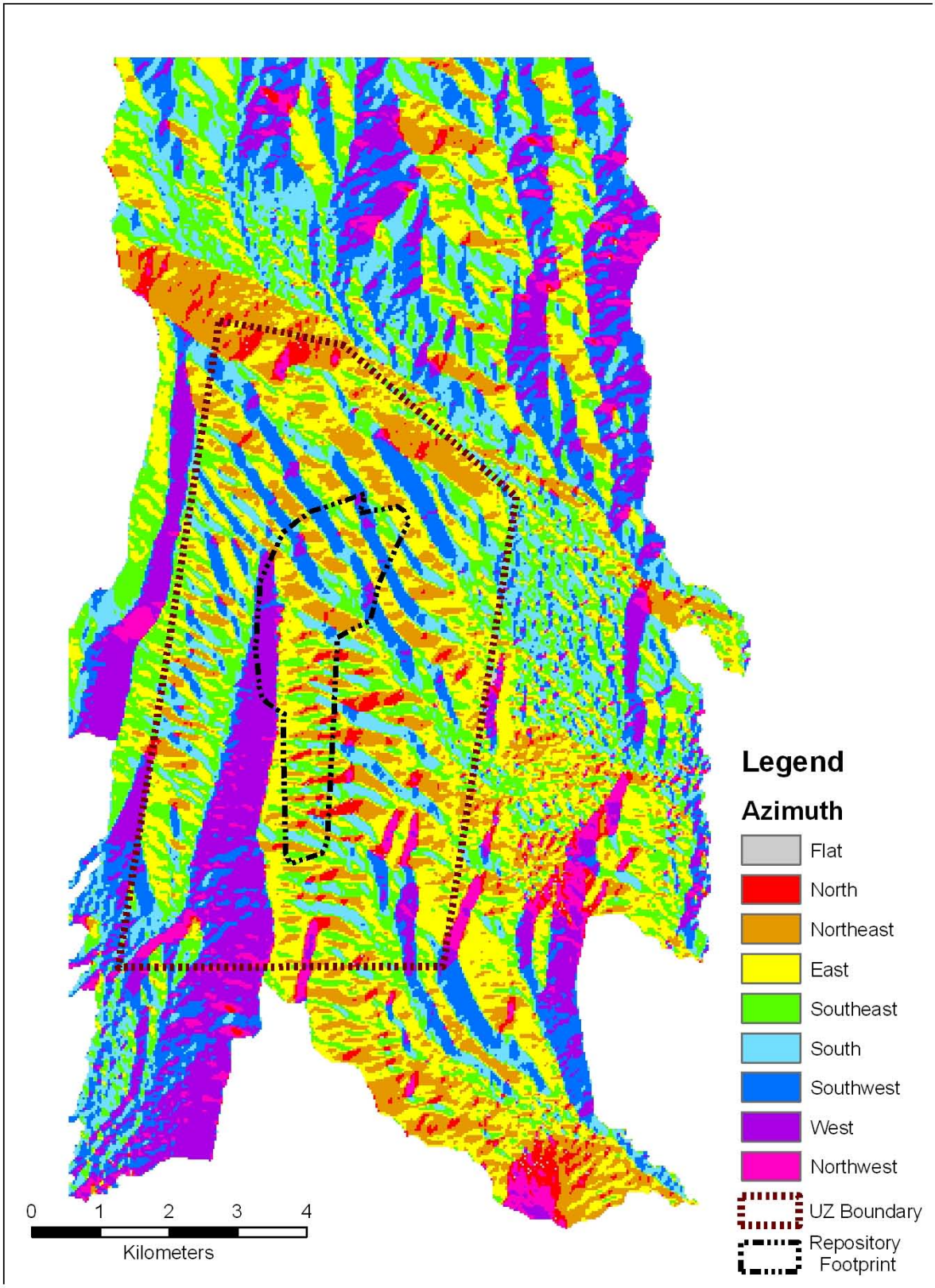

Source: Output DTNs: SN0701SPALAYER.002 and SN0612FTPRNUZB.002.

Figure 6.5.2.1-5. Azimuths for Model Area

Uncertainties in geographic inputs may arise from uncertainties in the underlying SRTM data, as well as processes used to calculate parameters from that data (i.e., slope and azimuth calculations, watershed delineation). To minimize errors caused by transforming grids between coordinate systems and projections, the grid cell locations and elevations for the infiltration modeling domain were based on the locations of the SRTM grid cells. Uncertainties in the SRTM data were analyzed by Rodriguez et al. (2005 [DIRS 177738]) and are discussed in Appendix B. The absolute geolocation error for SRTM data in North America is 12.6 m for a 90% confidence interval. The absolute elevation error for SRTM data in North America is 7 m for a 90% confidence interval.

6.5.2.2 Soil Classification

Yucca Mountain soil classifications and associated hydraulic properties are developed in *Data Analysis for Infiltration Modeling: Development of Soil Units and Associated Hydraulic Parameter Values* (BSC 2006 [DIRS 176335], Section 6.3). That report documents the development of site-specific soil units, hydraulic parameter values for soil units, and associated statistics and uncertainties for Yucca Mountain soils. Soil classifications and mapping based on analyses performed by the USGS in 1996 were evaluated for technical adequacy for use in infiltration modeling. The initial USGS soil classifications were developed from a map of surficial deposits that characterized soil types based primarily on extent of soil development, geomorphic character, and topographic position. These features provide relative ages of deposits (BSC 2006 [DIRS 176335], Section 6.2.1). The original 40 map units were combined into 10 soil units. The group of 10 soil units, referred to as the "base-case" units, is based on depositional character and relative age. The analysis (BSC 2006 [DIRS 176335], Section 6.2.3) concludes that the soil classifications developed by the USGS are appropriate for use in infiltration modeling.

The USGS classifications were also corroborated based on two other soil surveys that were completed for portions of the Yucca Mountain infiltration model area. In a 1989 soil survey, the distribution of four soil units was shown for Yucca Mountain (Resource Concepts 1989 [DIRS 103450], Figure 2). In 2004, a soil survey for the southwestern portion of Nye County was published (USDA 2004 [DIRS 173916]). The Busted Butte quadrangle of the 2004 survey (USDA 2004 [DIRS 173916]) covers the southwest portion of Yucca Mountain, which is administered by the Bureau of Land Management. The 2004 soil survey did not map the two-thirds of the Yucca Mountain infiltration model area that is administered by Nellis Air Force Base or the area that has been set aside for the Nevada Test Site. The mapping of soil units in the 1989 and 2004 soil surveys were compared with the USGS mapping of soil units (BSC 2006 [DIRS 176335], Section 6.2.4). The approach used by these two alternative soil surveys is equivalent to that used by the USGS in that the soils are identified by USDA taxonomic nomenclature and are subdivided by characteristics such as depth to bedrock, the presence or lack thereof of a duripan with depth, or observable pedogenic products. Overall, the 1989 soil survey (Resources Concepts 1989 [DIRS 103450]) and the 2004 soil survey (USDA 2004 [DIRS 173916]) corroborate the Yucca Mountain soil mapping used for input to an infiltration model with regard to approach and definition of units.

Table 6.5.2.2-1 shows the 10 soil classifications that represent the base case evaluated in *Data Analysis for Infiltration Modeling: Development of Soil Units and Associated Hydraulic Parameter Values* (BSC 2006 [DIRS 176335], Section 6.2). These soil types are described in detail that report (BSC 2006 [DIRS 176335], Section 6.2.3.2) based on their taxonomic classifications.

Table 6.5.2.2-1. Base Case Soil Units

Soil Unit	Type of Deposit [a]	Soil Taxonomic Name[a]	Number of 30 × 30-m Cells [b]	Map Area (%) [b]
1	Fluvial	Typic Argidurids	19,900	7.8
2	Fluvial	Typic Haplocalcids	44,065	17.4
3	Fluvial	Typic Haplocambids	33,115	13.1
4	Fluvial	Typic Torriorthents	4,630	1.8
5	Colluvium	Lithic Haplocambids	116,813	46.1
6	Eolian	Typic Torripsamments	12,205	4.8
7	Colluvium	Lithic Hapla	3,154	1.2
8	Bedrock	Rock	795	0.3
9	Colluvium	Typic Calciargids	16,441	6.5
10	Disturbed	Disturbed Ground	2,479	1.0

[a] BSC 2006 [DIRS 176335], Table 6-2.
[b] BSC 2006 [DIRS 176335], Table 6-3, based on a region surrounding the infiltration domain with 253,597 cells.

The distribution of soil types over the infiltration model domain is shown in Figure 6.5.2.2-1. It should be noted that Soil Unit 8 is used to describe regions of bare bedrock and thus does not have any soil properties associated with it. Similarly, Soil Unit 10, which represents only 1% of the map area, is used to identify regions of disturbed soil such as roads and parking areas. For the purpose of modeling infiltration, cells with Soil Unit 10 were replaced with the soil unit surrounding each of these grid cells. Soil Unit 10 is replaced throughout the domain because areas with disturbed soil are not expected to exist on Yucca Mountain over the time scale of interest in this analysis (10,000 years). Nearby soils best represent the soil characteristics of regions that have been disturbed.

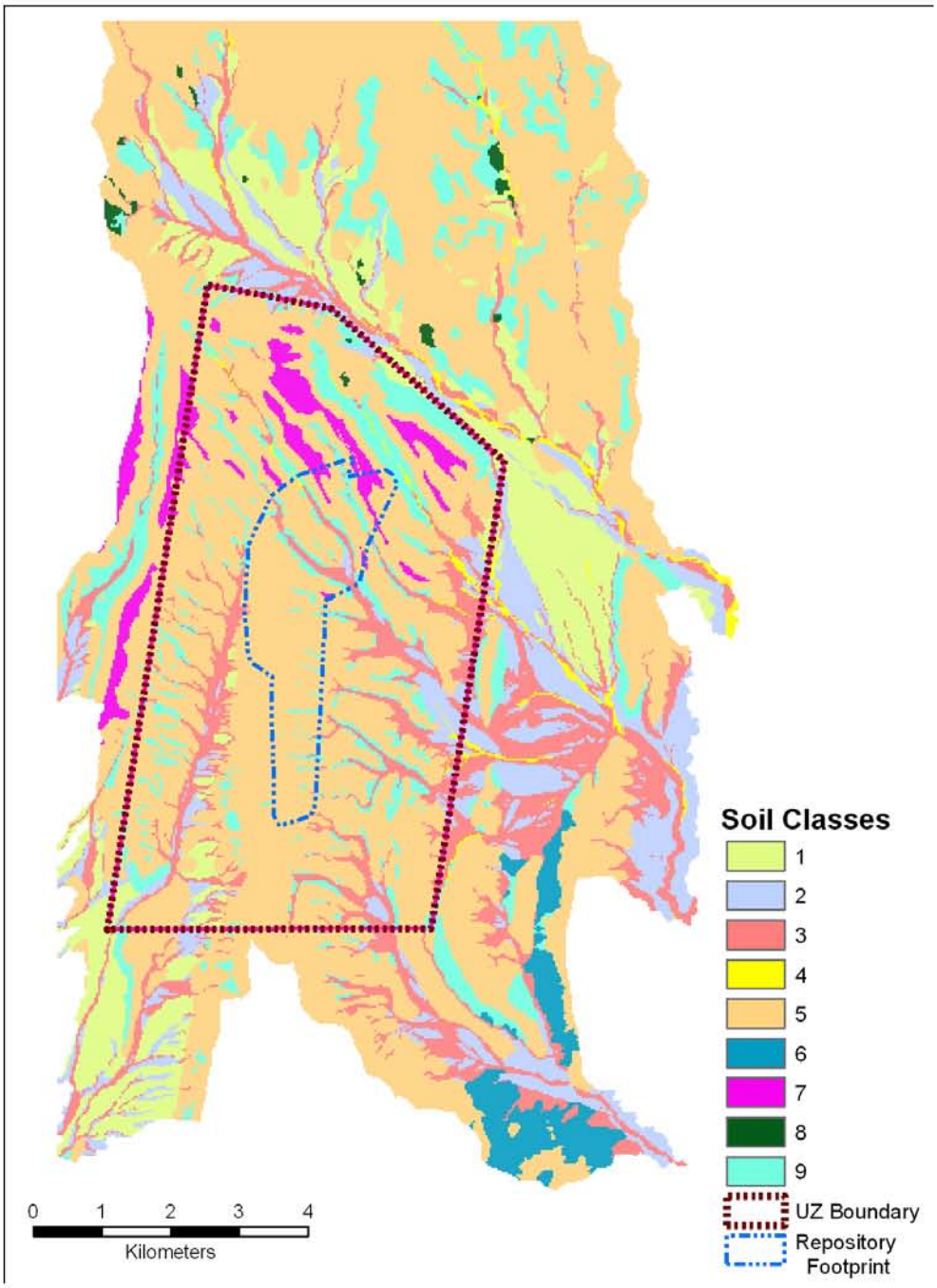

Source: Output DTNs: SN0701SPALAYER.002 and SN0612FTPRNUZB.002.

Figure 6.5.2.2-1. Map Showing Distribution of Soil Types Over the Infiltration Domain

An alternative soil classification system is presented in *Data Analysis for Infiltration Modeling: Development of Soil Units and Associated Hydraulic Parameter Values* (BSC (2006 [DIRS 176335], Section 6.2.5). The alternative soil grouping consists of four soil groups, which are combinations of the eight base case soil units. The four alternative soil groups are: Soil Group 1, Soil Group 2/6, Soil Group 3/4, and Soil Group 5/7/9. The alternative grouping was developed because several of the base case soil units had similar properties but a very limited

number of samples upon which to base the hydrologic properties for each unit. By combining soil units into fewer groups, based on depositional character (e.g., combining the 8 base case soil units into 4 groups), the sample size for each group was increased, thus providing a better basis for performing statistical analysis on the data sets without loss of relevant information or the characterization of uncertainty. Several of the base case soil units had such sparse data that it was not possible to characterize the spatial variability and uncertainty in the hydrologic properties. Figure 6.5.2.2-2 shows the distribution of the alternative soil groups over the infiltration modeling area.

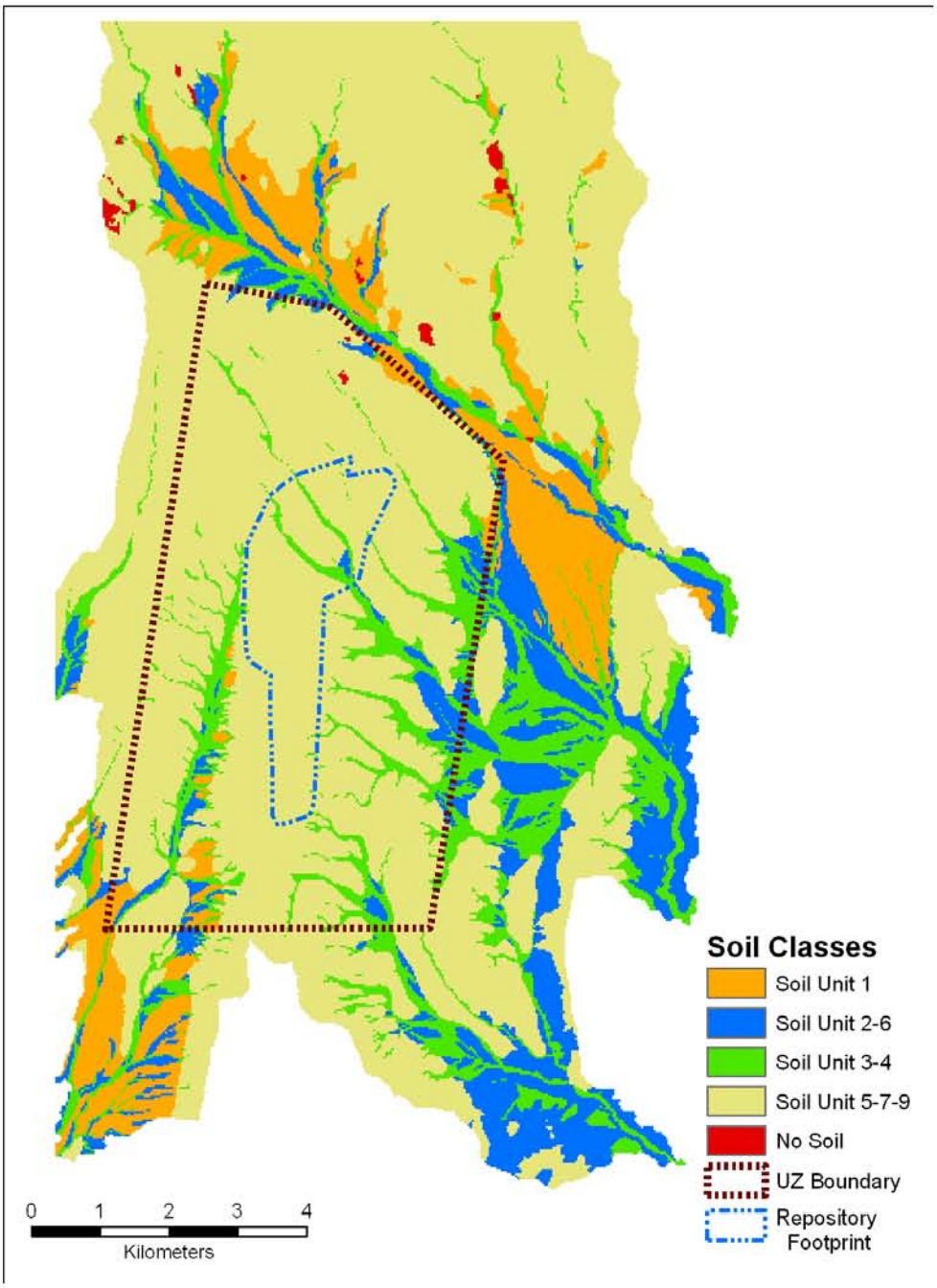

Source: Output DTNs: SN0701SPALAYER.002 and SN0612FTPRNUZB.002.

Figure 6.5.2.2-2. Map Showing Distribution of Alternative Soil Groupings over the Infiltration Domain

This infiltration analysis uses properties derived for the alternative soil grouping; however, the original base case soil unit identifiers are maintained. The base case soil units are the inputs provided in the geospatial database (see Appendix B). In order to use the properties derived for the alternative soil grouping, the appropriate properties are applied to the base case soil units (i.e., Soil Units 2 and 6 have the same properties). Table 6.5.2.2-2 shows how much of the UZ grid and total model domain each soil unit occupies.

Table 6.5.2.2-2. Soil Type Cell Counts for the UZ Grid and Infiltration Model Domain

Soil Unit	Total Cells (UZ Grid)	Percent (UZ Grid)	Total Cells	Percent (Total)
1	972	2	13,860	10
2	1,654	4	12,114	9
3	5,024	11	16,514	12
4	269	1	1,346	1
5	29,359	66	75,591	54
6	0	0	3,103	2
7	1,878	4	3,050	2
8	22	0	431	0
9	5,026	11	13,083	9
Total Cells	**44,204**		**139,092**	

Source: These values were obtained using database applications with input from DTNs: MO0608SPASDFIM.006 [DIRS 178082] (soil type and depth code for each cell) and MO0603SPAGRIDD.003 [DIRS 177121].

6.5.2.3 Soil Properties

Data Analysis for Infiltration Modeling: Development of Soil Units and Associated Hydraulic Parameter Values (BSC 2006 [DIRS 176335], Section 6.3) provides an analysis of soil properties using empirical data including grain-size distribution and fraction of rock fragments derived from laboratory analysis of soil samples collected from Yucca Mountain. Representative hydraulic parameter values of each of the soil units are developed by matching the texture of samples from Yucca Mountain soil units to similar soil textures in an analogous site (Hanford, WA) database (BSC 2006 [DIRS 176335], Section 6.1). The approach (BSC 2006 [DIRS 176335], Section 6.3) is nonparametric and is beneficial when the form of the relationship between the inputs and outputs is not known in advance, such as is the case with soil hydraulic properties.

Yucca Mountain soil samples were divided into 10 "base-case" units, and their respective hydraulic properties were determined based on a pedotransfer function approach. The soil samples were then further grouped into one of four groups that provided larger sample sizes for statistical analysis. The following hydraulic properties were determined for each of the soil groups:

- Saturated hydraulic conductivity (K_{sat_soil}).
- Field capacity (θ_{FC}), defined as the moisture content (m^3/m^3) at –0.33 bar and –0.10 bar. The range between the θ_{FC} at –0.33 bar and –0.10 bar, as well as the standard error, establishes the uncertainty range for this parameter as discussed below.
- Permanent wilting point (θ_{WP}), which is defined as the moisture content (m^3/m^3) at –60 bar.
- Saturated moisture content (θ_s) (m^3/m^3).

- Water holding capacity (θ_{HC}), which is defined as difference between the θ_{FC} and θ_{WP} (for alternative soil groups only) (m^3/m^3).

The parameters θ_{FC}, θ_{WP}, and θ_s were determined from the moisture retention curves (MRCs) provided in the analogous database from Hanford, WA. The MRCs were developed by fitting the van Genuchten soil-moisture retention model to the laboratory data, adjusted for gravel content if necessary. θ_{FC} and θ_{WP} are determined from these MRCs by scaling the appropriate moisture content from the MRC at selected matric potentials (BSC 2006 [DIRS 176335], Section 6.3).

Field capacity has been defined as the soil moisture content at which internal drainage ceases based on observations that the rate of flow and water-content changes decrease with time after a precipitation or irrigation event (Hillel 1980 [DIRS 100583], p. 67). This definition, however, was recognized as imprecise and not an intrinsic soil property independent of the way it is measured (Hillel 1980 [DIRS 100583], p. 68). This concept is most tenable on coarse-textured soils in which internal drainage is initially most rapid but soon slows down owing to the relatively steep decrease of hydraulic conductivity with increased matric potential (Hillel 1980 [DIRS 100583], p. 68). Although matric potentials of −0.33 bar or −0.10 bar have both been used to correlate measurements of soil moisture storage in the field, neither criterion applies universally to all soils and all conditions (BSC 2006 [DIRS 176335], Section 6.3). Therefore, both definitions of field capacity (−0.33 bar and −0.10 bar) have been used to estimate the range of uncertainty in this parameter as described below.

For the inputs to this infiltration model, the θ_{FC} values based on both matric potentials of –0.33 bar and –0.10 bar are used to capture the uncertainty inherent with the field capacity concept. This approach is based on using θ_{WP} and θ_{HC} as infiltration model inputs, from which θ_{FC} is calculated during model execution. The range of θ_{HC} samples incorporates both definitions of θ_{FC}. The minimum θ_{HC} value is the θ_{FC} at –0.33 bars minus the θ_{WP} minus the standard error in θ_{FC}; the upper θ_{HC} value is the θ_{FC} at –0.10 minus the θ_{WP} plus the standard error of θ_{FC}. This approach for determining the range of θ_{HC} values captures the uncertainty in the definition of θ_{FC} as well as the uncertainty in the data, as expressed by the standard error (BSC 2006 [DIRS 176335], Section 6.3). Figure 6.5.2.3-1 shows schematically the process of determining the uncertainty range in θ_{FC}. Once a range of uncertainty is established, a uniform distribution is used to select values over the range, with the nominal value taken as the midpoint of the range.

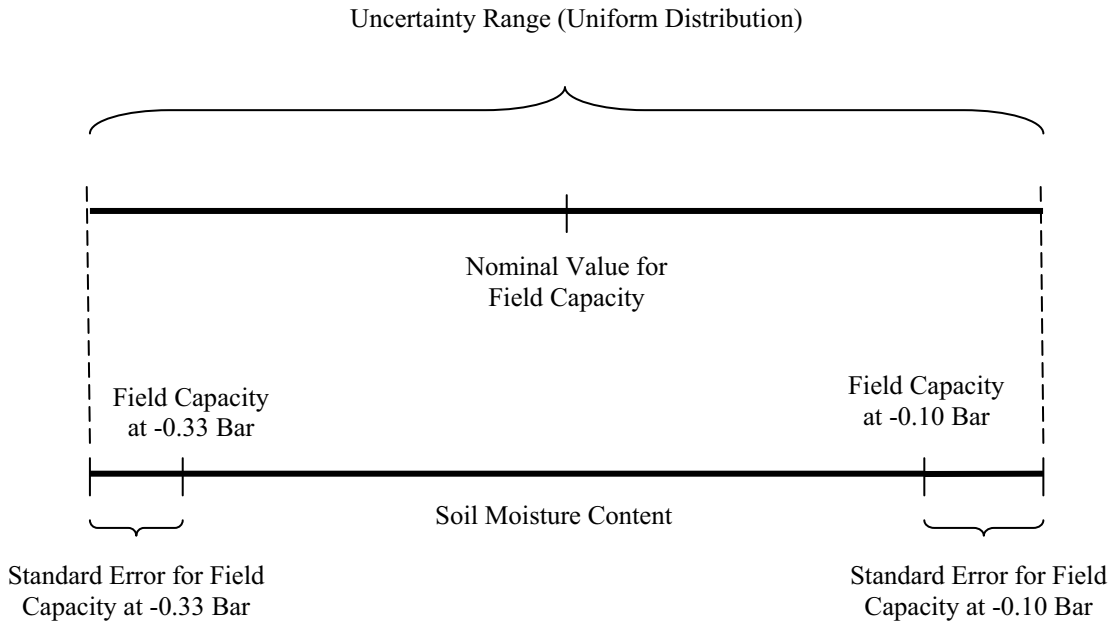

Source: Values defining the uncertainty distribution for each soil group are found in DTN: MO0605SEPALTRN.000 [DIRS 178089], *SoilUnit1FC1-10and1-3Bar_5-30-06.xls*, *SoilUnit2-6FC1-10and1-3Bar_5-30-06.xls*, *SoilUnit3-4FC1-10and1-3Bar_5-30-06.xls*, and *SoilUnit5-7-9 FC1-10and1-3Bar_5-30-06.xls*, worksheet: "HydraulicPropandStatistics."

Figure 6.5.2.3-1. Method for Determining Uncertainty Range in θ_{FC} (or θ_{HC})

The θ_{WP} is the soil moisture content below which plants are unable to withdraw soil moisture and is taken to correspond to −60 bar soil matric potential (BSC 2006 [DIRS 176335], Section 5.5). This matric potential is consistent with the lower limits of soil moisture extraction determined for several Mojave Desert shrubs that can survive soil water potentials as low −50 to −100 bars (BSC 2006 [DIRS 176335], Section 6.3). Like θ_{FC}, the definition of θ_{WP} is imprecise and therefore subject to additional variability and uncertainty as a result of the chosen definition or approach. However, because the permanent wilting point (θ_{WP}) represents the moisture content at the driest region of a soil's MRC, its values do not vary significantly from one definition to another, especially in dry desert soils. Because the θ_{HC} is defined as the difference between θ_{FC} and θ_{WP}, the uncertainty range established in the θ_{HC} captures the entire range of uncertainty of θ_{WP} as well.

Values for each of the soil parameters are given in Tables 6.5.2.3-1 and 6.5.2.3-2. Uncertainty ranges for K_{sat_soil}, θ_s, and θ_{WP} are based on a normal distribution defined with the mean and standard error as reported in DTN: MO0605SEPALTRN.000 [DIRS 178089]. Uncertainty ranges for θ_{FC} and θ_{HC} are based on the ranges described above (see Figure 6.5.2.3-1). The treatment of uncertainties, including the screening of parameters to be propagated in the uncertainty analysis for this report, is discussed in Appendix I.

Table 6.5.2.3-1. Nominal Values and Standard Error for K_{sat}, θ_s, and θ_{WP}

Saturated Hydraulic Conductivity (K_{sat_soil})				
Soil Group	**Mean Ln (K_{sat_soil}), (cm/sec)**	**Standard Error (Ln)**	**Nominal Value (cm/s)[a]**	**Nominal Value (m/s)**
1	−9.436	0.196	7.98×10^{-5}	7.98×10^{-7}
2/6	−9.105	0.175	1.11×10^{-4}	1.11×10^{-6}
3/4	−9.571	0.137	6.97×10^{-5}	6.97×10^{-7}
5/7/9	−9.593	0.079	6.82×10^{-5}	6.82×10^{-7}
Saturated Water Content (θ_s)				
Soil Group	**Mean θ_s (m^3/m^3)**	**Standard Error (m^3/m^3)**	**Nominal Value (m^3/m^3)[b]**	
1	0.23	1.31×10^{-2}	0.23	
2/6	0.21	1.18×10^{-2}	0.21	
3/4	0.16	6.69×10^{-3}	0.16	
5/7/9	0.23	7.61×10^{-3}	0.23	
Permanent Wilting Point (θ_{WP})				
Soil Group	**Mean θ_{WP} (m^3/m^3)**	**Standard Error (m^3/m^3)**	**Nominal Value (m^3/m^3)[b]**	
1	0.040	0.003	0.040	
2/6	0.037	0.003	0.037	
3/4	0.024	0.001	0.024	
5/7/9	0.039	0.002	0.039	

Source: DTN: MO0605SEPALTRN.000 [DIRS 178089], *SoilUnit1FC1-10and1-3Bar_5-30-06.xls,* S*oilUnit2-6FC1-10and1-3Bar_5-30-06.xls*, *SoilUnit3-4FC1-10and1-3Bar_5-30-06.xls*, and *SoilUnit5-7-9 FC1-10and1-3Bar_5-30-06.xls*, worksheet: "HydraulicPropandStatistics."

[a] Nominal values of saturated hydraulic conductivity are equal to exp(ln(K_{sat_soil})) for each soil group.
[b] Nominal values of θ_s and θ_{WP} are equal to mean values of θ_s and θ_{WP} for each soil group.

Table 6.5.2.3-2. Nominal Values and Standard Error for θ_{FC}, and θ_{HC}

Soil Field Capacity (θ_{FC})					
Soil Group	Mean θ_{FC} [a] (−0.10 bar) (m^3/m^3)	Standard Error (m^3/m^3)	Mean θ_{FC} [b] (−0.33 bar) (m^3/m^3)	Standard Error (m^3/m^3)	Nominal Value (m^3/m^3)
1	0.183	0.012	0.125	0.011	0.155
2/6	0.177	0.012	0.123	0.010	0.151
3/4	0.123	0.006	0.075	0.004	0.100
5/7/9	0.208	0.007	0.134	0.005	0.172
Soil Water Holding Capacity (θ_{HC})					
Soil Group	Mean θ_{HC} (−0.10 bar θ_{FC}) (m^3/m^3)	Standard Error (m^3/m^3)	Mean θ_{HC} (−0.33 bar θ_{FC}) (m^3/m^3)	Standard Error (m^3/m^3)	Nominal Value (m^3/m^3)
1	0.143	0.010	0.085	0.009	0.115
2/6	0.140	0.010	0.086	0.008	0.114
3/4	0.098	0.005	0.051	0.003	0.076
5/7/9	0.169	0.005	0.095	0.004	0.133

Source: DTN: MO0605SEPALTRN.000 [DIRS 178089], *SoilUnit1FC1-10and1-3Bar_5-30-06.xls*, *SoilUnit2-6FC1-10and1-3Bar_5-30-06.xls*, *SoilUnit3-4FC1-10and1-3Bar_5-30-06.xls*, and *SoilUnit5-7-9 FC1-10and1-3Bar_5-30-06.xls*, worksheet: "HydraulicPropandStatistics."

[a] Field capacity defined as moisture content at a pressure of −0.10 bar.
[b] Field capacity defined as moisture content at a pressure of −0.33 bar.

6.5.2.4 Soil Depth

Data Analysis for Infiltration Modeling: Technical Evaluation of Previous Soil Depth Estimation Methods and Development of Alternate Parameter Values (BSC 2006 [DIRS 178819], Section 6.2) evaluates soil depths at Yucca Mountain based on an approach that uses qualified data from boreholes, field surficial deposits mapping, and the geologic framework model (GFM) (BSC 2004 [DIRS 170029], Figure 6-10). The evaluation divides the infiltration model area into five soil depth classes. Each soil depth class region is associated with a spatial distribution of soil depth and recommendations on the treatment of soil depth for infiltration modeling. Due to the limited number of qualified measurements of soil depth within each soil depth class, it was decided that an upscaled, effective uniform value of soil depth would be used for each net infiltration realization.

A map of the soil depth classes over the infiltration model domain is given in Figure 6.5.2.4-1. The percentage of the infiltration domain as well as the percentage of the UZ model domain occupied by each soil depth class is given in Table 6.5.2.4-1.

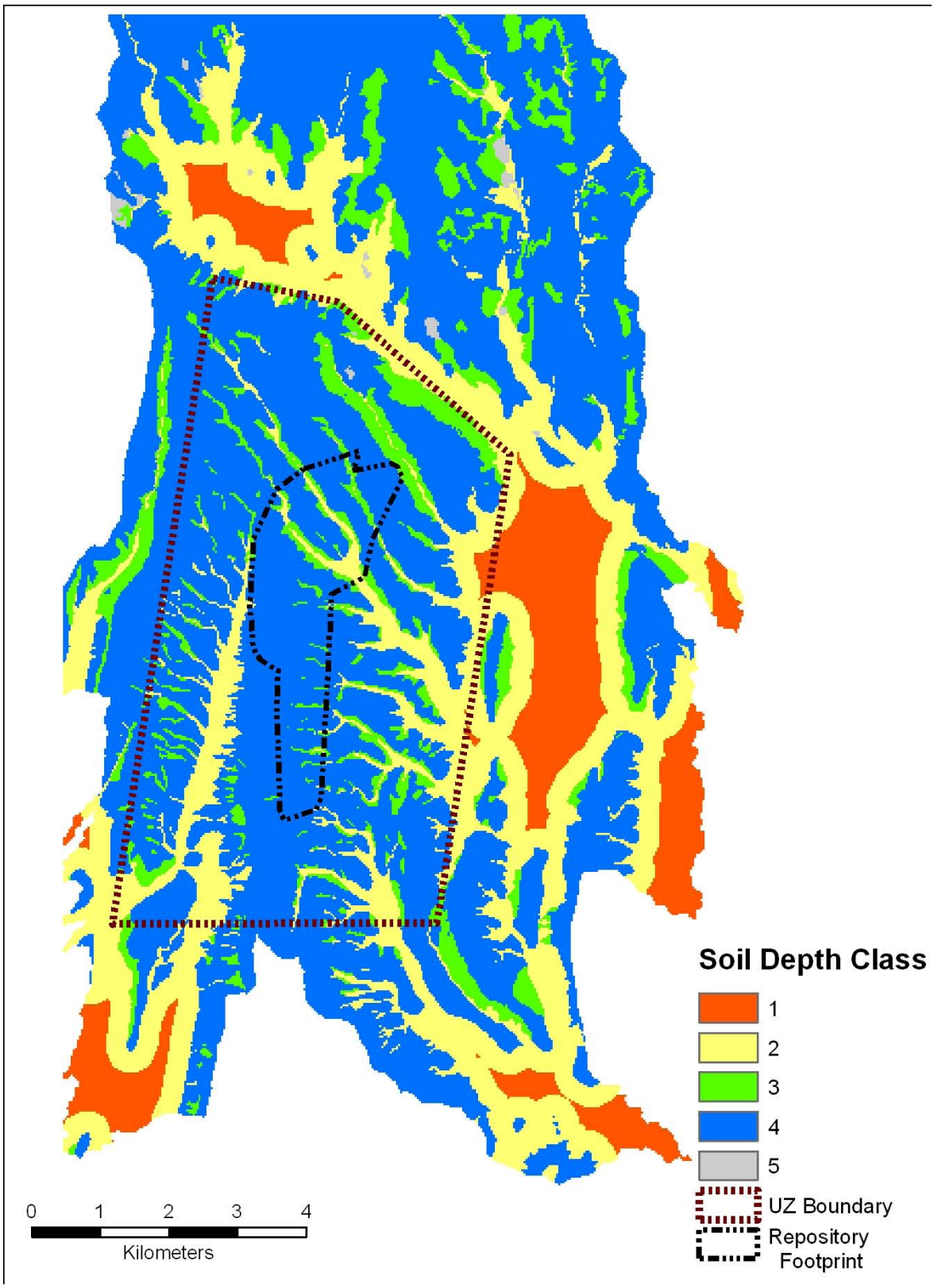

Source: Output DTNs: SN0701SPALAYER.002 and SN0612FTPRNUZB.002.

Figure 6.5.2.4-1. Map Showing Distribution of Soil Depth Classes over the Infiltration Domain

Table 6.5.2.4-1. Soil Depth Class Cell Counts for the UZ Grid and Infiltration Model Domain

Soil Depth Class	UZ Grid Total Cells	Percent (UZ Grid)	Total Cells	Percent (Total)
1	159	0	12,343	9
2	7,687	17	34,479	25
3	5,057	11	13,116	9
4	31,279	71	78,723	57
5	22	0	431	0
Total cells	**44,204**		**139,092**	

Source: These values were obtained using database applications with input from DTNS: MO0608SPASDFIM.006 [DIRS 178082] (soil type and depth code for each cell) and MO0603SPAGRIDD.003 [DIRS 177121].

Soil depth spatial distributions were developed in *Data Analysis for Infiltration Modeling: Technical Evaluation of Previous Soil Depth Estimation Methods and Development of Alternate Parameter Values* (BSC 2006 [DIRS 178819], Section 6.2.2). A discussion is presented in that report to provide recommendations on the spatial distribution of soil depth for each of the soil depth classes, and estimates of the population mean along with confidence intervals. A summary of the recommended soil depth spatial distributions for each depth class is presented in Table 6.5.2.4-2.

Table 6.5.2.4-2. Summary of Recommended Distributions for Soil Depth

Soil Depth Class Designator	1	2	3	4	5
Soil Depth Class	**Very Deep Soils**	**Moderately Deep Soils**	**Intermediate Depth Soils**	**Shallow Soils**	**Exposed Bedrock**
Sample Distribution Type	Uniform	Left-Truncated Normal (truncated at 0.5 m)	Lognormal	Lognormal	Single Value
Sample Mean	N/A	16.47 (m)	3.26 (m)	0.45 (m)	N/A
Sample Mean of the Natural Logarithm	N/A	N/A	0.61 (LN m) (1.84 m)	−1.29 (LN m) (0.27 m)	N/A
Sample Standard Deviation	N/A	14.61 (m)	4.71 (m)	0.67 (m)	N/A
Sample Standard Deviation of the Natural Logarithm	—	—	1.07 (LN m)	0.88 (LN m)	
Sample Standard Error	N/A	1.84	1.22	0.11	N/A
Sample Median (also Estimated Population Median)	95 m	12.19 (m)	2.07 (m)	0.25 (m)	N/A
Sample Minimum Value (m)	40 (m)	0.5	N/A	N/A	0
Sample Maximum Value (m)	150 (m)	64	N/A	N/A	0
Number of Data Points	4	63	15	35	N/A

Table 6.5.2.4-2. Summary of Recommended Distributions for Soil Depth (Continued)

Soil Depth Class Designator	1	2	3	4	5
Soil Depth Class	Very Deep Soils	Moderately Deep Soils	Intermediate Depth Soils	Shallow Soils	Exposed Bedrock
Estimated Population Mean	95 (m)	16.47 (m)	3.25 (m)	0.40 (m)	0
Confidence Interval for Population Mean at 80% Limit	—	14.09 to 18.86 (m)	2.21 to 5.73 (m)	0.33 to 0.52 (m)	N/A
Confidence Interval for Population Mean at 90% Limit	—	13.40 to 19.54 (m)	2.00 to 7.11 (m)	0.31 to 0.57 (m)	N/A
Confidence Interval for Population Median at 80% Limit	N/A	N/A	1.27 to 2.67 (m)	0.23 to 0.33 (m)	N/A
Confidence Interval for Population Median at 90% Limit	N/A	N/A	1.13 to 2.99 (m)	0.21 to 0.35 (m)	NA

Source: DTN: MO0608SPASDFIM.006 [DIRS 178082], *Summary of Recommended Distributions.doc*.

LN = natural logarithm; N/A = not applicable.

The soil depth class spatial distributions discussed in *Data Analysis for Infiltration Modeling: Technical Evaluation of Previous Soil Depth Estimation Methods and Development of Alternate Parameter Values* (BSC 2006 [DIRS 178819], Section 6.2) and displayed in Table 6.5.2.4-2 are subject to several types of uncertainty. Sources of uncertainty include (BSC 2006 [DIRS 178819], Section 6.2.2):

- Natural variability in soil depth that occurs at all scales in the infiltration modeling domain.
- Measurement errors made when determining soil depths at sampling localities.
- Uncertainty resulting from the difficulty in determining the soil–bedrock interface, especially in a borehole. This interface may be difficult to define when it is characterized by rubble or broken and fractured bedrock.
- Uncertainty in the statistical estimation of population parameters derived from a sample consisting of only a few observations from the population.

A summary of the characteristics of each depth class, including recommended distributions for the effective uniform soil depth to be used in the infiltration modeling, which are based on an analysis of the uncertainty in the parameters, is provided in *Data Analysis for Infiltration Modeling: Technical Evaluation of Previous Soil Depth Estimation Methods and Development of Alternate Parameter Values* (BSC 2006 [DIRS 178819], Section 6.2.3) and quoted below for all soil depth classes except Soil Depth Class 4, which is treated in more detail in the next section. The distributions used to represent the effective soil depth for these classes in this analysis are listed in Table 6.5.2.4-3.

Effective Soil Depth for Soil Depth Class 1 ($depth_{soil(1)}$)

This depth class represents very thick soils, described by a uniform distribution with lower and upper bound values of 40 and 150 m, respectively. Because this class represents depths much deeper than the rooting depth (below which water is not removed by the infiltration model), using a representative value equal to the mean for the class of 95 m is appropriate. Because soil depths in this class are large and infiltration is expected to be small, the specific value chosen within this range is unlikely to cause a significant change to predicted infiltration.

Effective Soil Depth for Soil Depth Class 2 ($depth_{soil(2)}$)

This depth class represents moderately deep soils that range in depth from 0.5 m to about 50 m. This class is intended to include the value where soil depth is sufficient to limit infiltration of water to the soil–bedrock contact, except in some channels, because the soils have sufficient storage capacity to retain precipitation in the root zone where it is subject to evapotranspiration. It is expected that infiltration in the Soil Depth Class 2 areas is most likely to occur where soil thickness is small. Consequently, the appropriate bulk parameter value will lie closer to the small soil thickness portion of the distribution, rather than near the large soil thickness values.

Effective Soil Depth for Soil Depth Class 3 ($depth_{soil(3)}$)

This depth class represents areas of thicker foot-slope soils that occur intermittently in the area. The data are represented by a lognormal distribution with an estimated population mean soil depth of 3.25 m and a sample median of 2.07 m, which is also the estimated population median; only one value is larger than 5.18 m (BSC 2006 [DIRS 178819], Figure 6-15 and Table 6-7). As seen in Figure 6.5.3.4-1, Depth Class 3 is most often found between soils of Depth Class 2 (moderately deep) and Depth Class 4 (shallow), acting as a transition from deeper to shallower soils. The depth in Soil Depth Class 3 will be small where it contacts Soil Depth Class 4 but increases where it contacts deeper depth classes, primarily Soil Depth Class 2. The majority of infiltration through Soil Depth Class 3 will occur where the depth is small. The appropriate effective uniform depth for Soil Depth Class 3 is a value that allows for the same total infiltration, through all of Soil Depth Class 3, as occurs through the spatially variable material that exists in nature. Estimating a uniform value for this depth class is especially challenging. There are very few measurements for this depth class (15 measurements, four of which indicate that there is no soil). Many of these measurements may represent disturbed regions where drilling pads were constructed and, thus, may not represent actual soil depth. Although it is common to choose the median of a lognormal distribution as a measure of central tendency, the potential underestimate previously noted suggests that the sample mean is a better measure of central tendency in this case. The 90% confidence interval about the mean ranges from 2 m to 7 m, where the lower bound of this range is approximately the median.

Effective Soil Depth for Soil Depth Class 5 ($depth_{soil(5)}$)

This class represents exposed bedrock in the area that does not have soil cover. Therefore, all cells in this class should be assigned a zero soil depth value.

Table 6.5.2.4-3 summarizes recommended distributions for all five soil depth classes.

Table 6.5.2.4-3. Summary of Recommended Distributions for Effective Soil Depths ($depth_{soil}$)

Soil Depth Class	Lower bound Soil Depth (m)	Upper Bound Soil Depth (m)	Nominal Value Soil Depth (m)	Distribution	Comments
1	N/A	N/A	95	Constant	Estimated population mean
2	N/A	N/A	16.47	Constant	Estimated population mean
3	N/A	N/A	3.26	Constant	Sample mean
4	0.1	0.5	0.25	Uniform	See Section 6.5.2.4.1
5	N/A	N/A	0	Constant	—

6.5.2.4.1 Effective Soil Depth Distribution for Soil Depth Class 4

Estimating the distribution of effective soil depth for this soil depth class is especially important because of the significant sensitivity of net infiltration to shallow soil depth and the large relative proportion of the modeling domain covered by this soil depth class. These two reasons prompted a more detailed analysis of shallow soil depth uncertainty than provided in *Data Analysis for Infiltration Modeling: Technical Evaluation of Previous Soil Depth Estimation Methods and Development of Alternate Parameter Values* (BSC 2006 [DIRS 178819], Section 6.2.2).

One upscaled value of soil depth is used to represent the spatial variability in Soil Depth Class 4 for each realization. The estimation of uncertainty in this upscaled depth is calculated from a two-steps process. The first step consists of determining a spatial distribution for Soil Depth Class 4. The second step is to determine which statistic in this distribution is an adequate upscaled soil depth (in the sense that it will lead to a reasonable estimate of spatially averaged infiltration).

Estimation of the Spatial Distribution of Soil Depth

In *Data Analysis for Infiltration Modeling: Technical Evaluation of Previous Soil Depth Estimation Methods and Development of Alternate Parameter Values* (BSC 2006 [DIRS 178819], Section 6.2.2), the spatial distribution of soil depth is represented by a lognormal distribution, estimated using probability plot fitting. This depth class is described by 35 individual measurements over an area of approximately 71 km^2. That report (BSC 2006 [DIRS 178819], Section 6.2.2) assigned each observation a distinct quantile value, even when duplicate values of soil depth were measured at different locations. Duplicate soil depth values should reflect the same quantile. Therefore, in this analysis the distribution fitting has been redone (although the probability plot fitting described below leads to nearly the same result). Two methods are applied for estimating parameters that define the lognormal distribution from the 35 observations: probability plotting and least-squares fitting. The updated fitting of these 35 observations is made in Output DTN: SN0612T0502206.039.

The first method of estimating the underlying lognormal distribution is based on a probability plot where the vertical axis represents the ordered values, while the horizontal axis represents the standard normal order distances (description of Normal Probability Plot can be found in NIST online statistical handbook at http://www.itl.nist.gov/div898/handbook/eda/section3/*normprpl.htm*). If the distribution is close to normal, then the points are linearly distributed on

the plot. The mean and standard deviation of the distribution corresponds to the Y-intercept and slope of a linear regression model, respectively.

The resulting probability plot is shown in Figure 6.5.2.4-2. The estimates for the mean and standard deviation are −1.295 and 0.93, respectively.

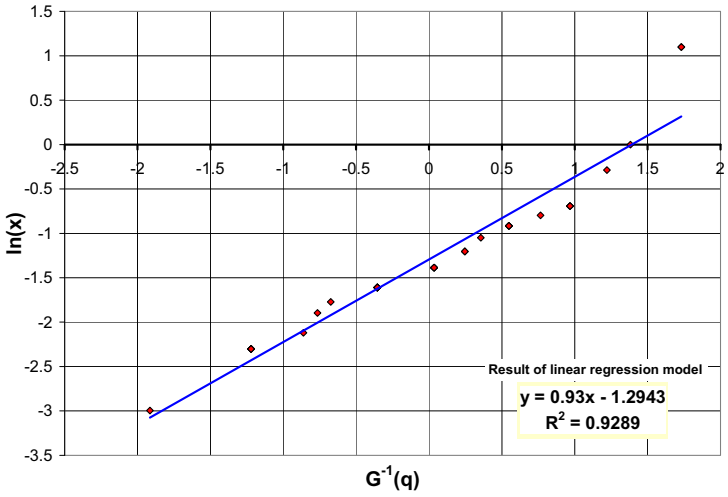

Source: Output DTN: SN0612T0502206.039, *LN_fitting_upper_bound_V2.0_12_2006.xls*. Data from DTN: GS011208312212.004 [DIRS 176317], Table S02086_001.

NOTE: Only 15 observations are displayed, as duplicates are assigned with an average quantile value.

Figure 6.5.2.4-2. Normal Probability Plot for 35 Observations of Soil Depth in Soil Depth Class 4 Region

The second method consists in fitting a lognormal distribution, such that the sum of the squared differences between the quantiles of the observed values and the quantiles of such values in the lognormal distribution is minimized.

The cumulative distribution functions (CDFs) of both lognormal fitted distributions compared with observed values are displayed in Figure 6.5.2.4-3, showing good agreement between the data and both fitting methods.

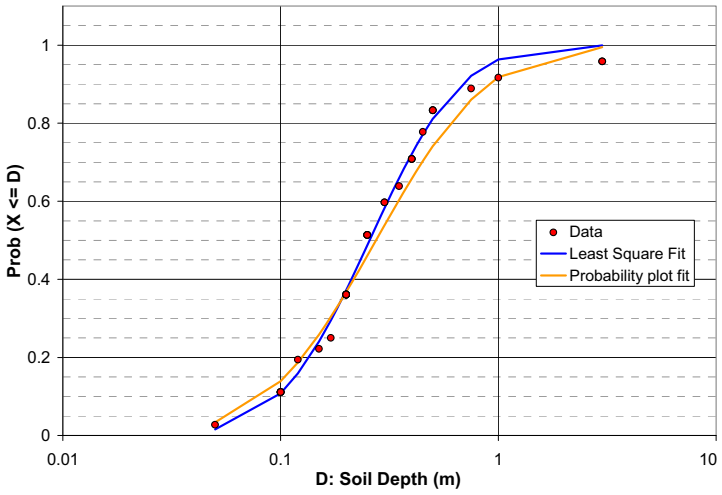

Source: Output DTN: SN0612T0502206.039, *LN_fitting_upper_bound_V2.0_12_2006.xls*. Data from DTN: GS011208312212.004 [DIRS 176317], Table S02086_001.

Figure 6.5.2.4-3. CDFs for 35 Observations (red plots), Least-square Fitted Lognormal Distribution (blue line), and Probability Plot Fitter Lognormal Distribution (orange line) in Log-scale for Soil Depth (X-axis)

However, it is unclear how well the 35 observations represent the actual spatial distribution of this soil depth class. There may be a bias toward deeper soils since none of the 35 observations include soil depth of 0 m, while observations of patches of bare rock have been made in the area covering Soil Depth Class 4 during field trips to the site. Moreover, the specific locations of observations are not documented, and it is likely that these locations were not randomly selected.

For this reason, a second source of information was used to create a second spatial distribution of shallow soil depth (Sanchez 2006 [DIRS 176569], pp. 62 to 68). This scientific notebook contains observations made by Alex Sanchez in several places at Yucca Mountain. The exact position of the observations is not known, although most of the observations are for shallow soil and should correspond to regions of Soil Depth Class 4. The observations from the scientific notebook are listed below:

Observations:

Page 62: (NRG-3 pad) Soil Depth from 0.3 to 0.5 m
Page 63: (Close up view NRG-3 pad) captured above – not considered
Page 64: (bleach bone ridge) half of the image is covered with rock (0 m) – the remaining part is with soil from 0.1 to 0.3 m
Page 65: (bleach bone ridge) same measurement as p. 3 – not considered
Page 66: (Above SD-9 pad) Soil Depth from 0 to 0.09 m
Page 67: (Yucca Crest) Soil range from 0 to 0.3 m
Page 67: (bleach bone ridge) consistent with p. 3 – not considered
Page 68: (tonsil ridge top) no soil – 0 m
Page 68: (tonsil ridge side-slope) thin soil 0.1 m
Page 68: (tonsil ridge foot-slope) up to 3 m – range from 0.1 to 3 m.

Out of these ten observations, three were not considered (as indicated above) as they concerned already included regions. One observation was split in two (p. 64) because two different patterns are seen in the photograph (one with soil and one with no soil). As a result, the new distribution was defined with eight ranges. Each range has been weighted equally (a weight of 1/8). The resulting ranges are listed in Table 6.5.2.4-4.

Table 6.5.2.4-4. Summary of Soil Depth Ranges Defined Based on Alex Sanchez Observations

Reference	Location Description	Minimum (m)	Maximum (m)	Weight	Page
A	NRG-3 pad	0.3	0.5	0.125	62
(not considered)	NRG-3 pad (closeup)	—	0.3	—	63
B	Bleach Bone Ridge (no soil)	0	—	0.125	64
C	Bleach Bone Ridge (soil)	0.1	0.3	0.125	64
(not considered)	Bleach Bone Ridge	0.1	0.3	—	65
D	SD-9 pad	0	0.09	0.125	66
E	Yucca Crest (natural)	0	0.3	0.125	67
(not considered)	Bleach Bone Ridge	0.2	0.2	—	67
F	Tonsil Ridge (Top)	0	0	0.125	68
G	Tonsil Ridge (Side)	0.1	0.1	0.125	68
H	Tonsil Ridge (Foot)	0.1	3	0.125	68

Source: Output DTN: SN0612T0502206.039, *Lower_Bound_distribution_V4.0_12_05_2006.xls*. Data from Sanchez 2006 [DIRS 176569].

All but one interval (Reference H in Table 6.5.2.4-4) were represented with a uniform distribution. The soil depth range for the Tonsil Ridge Foot (Reference H) is significantly larger than for the other observations. Therefore, it seems reasonable to increase the likelihood of values closer to the lower bound (i.e., 0.1 m), and a loguniform distribution was used instead of a uniform distribution. This approach is consistent with what was observed in the previous set of data (BSC 2006 [DIRS 178819]), for which two values are equal to 3.0 m, but no observations have been made between 1.0 and 3.0 m.

Two of the ranges included a component of bare rock (no soil) and result in lower bound values of zero (for which logarithm is not defined). In order to be able to work with log-transformed data, the distribution is defined starting with the 0.25 quantile (as a quarter of the distribution is equal to 0), and the remaining observations are associated with an equal weight of 1/6. This is consistent with the previously defined weight, as a weight of 1/6 for 3/4 of the distribution corresponds to a total weight of 1/8.

To represent the piecewise distribution, a series of two random numbers was generated; the first was used to randomly select one of the six predefined bins, and the second was used to sample a soil depth from within the selected bin. This bootstrapping approach was repeated 1,000 times to create a distribution. The resulting distribution is displayed in Figure 6.5.2.4-4.

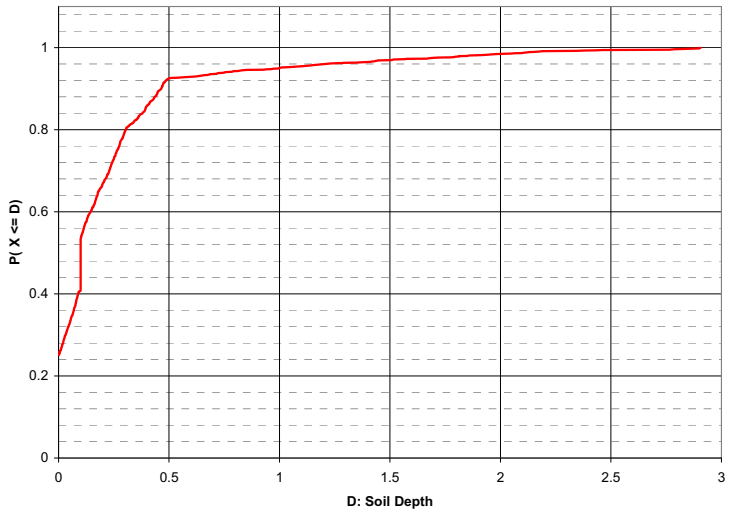

Source: Output DTN: SN0612T0502206.039, *Lower_Bound_distribution_V4.0_12_05_2006.xls*. Data from Sanchez 2006 [DIRS 176569].

Figure 6.5.2.4-4. CDF of Estimated Distribution Constructed with Eight Intervals Estimated from Alex Sanchez Notebook

The two fitting methods described above (probability plotting and least squares) were applied to the soil depth ranges obtained from the scientific notebook. However, because 25% of the distribution is equal to 0 m and a lognormal distribution is not defined for values of zero, each of these fitting methods had to be modified. Two approaches were considered for modifying the fitting methods:

- In the first approach, it is assumed that the information available is known only for values greater than zero and that nonzero values represent only 75% of the distribution. This assumption allows calculation of the arithmetic and geometric means of the fitted lognormal distributions directly, but it does not necessarily result in a good fit.

- In the second approach, it is assumed that the distribution is bimodal. Like the first approach, the fitting is done with nonzero values; however, they are considered to represent the whole distribution. The final estimates of the arithmetic and geometric means are corrected to include 25% of zero values. This approach leads to a better fit but makes the estimation of the geometric mean more difficult.

The normal probability plot is displayed in Figure 6.5.2.4-5, for both approaches. Not considering the first quarter of the distribution (first approach) leads to an asymmetry in the plot on the left (as the X-axis goes from about −0.6 to 3.2). The fit is linear except near the edges. If nonzero values are assumed to represent the whole distribution (second approach; right frame), the fit is better even near the edges.

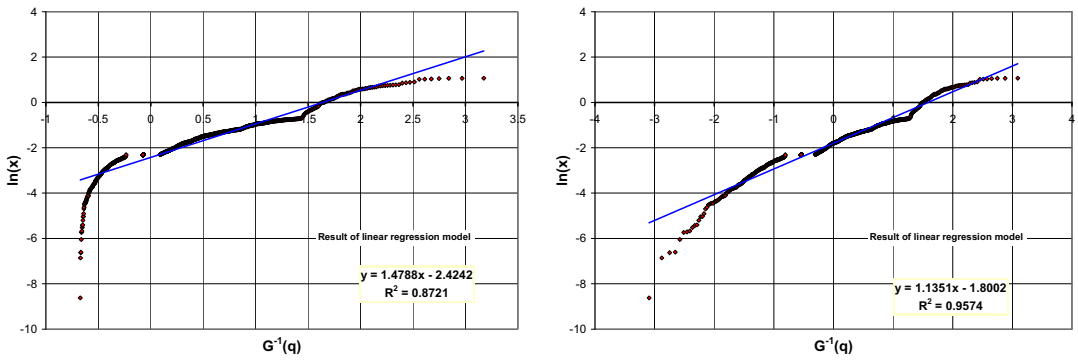

Source: Plots are produced in Output DTN: SN0612T0502206.039, *LN_fitting_lower_bound_V2.0_12_01_2006.xls*. The plot on the left is generated by setting the cell C2 on sheet "Calculations" to a value of 0.25. The plot on the right is generated when this cell is set to a value of zero. Data is from Sanchez 2006 [DIRS 176569].

NOTE: In the left frame, the non-zero values are considered to represent 3/4 of the distribution. In the right frame, the non-zero values represent the whole distribution.

Figure 6.5.2.4-5. Probability Plot for Estimated Distribution Based on Alex Sanchez Notebook

A least square fitting approach (based on quantile values) has been applied to generate a second distribution using both approaches (Figure 6.5.2.4-6).

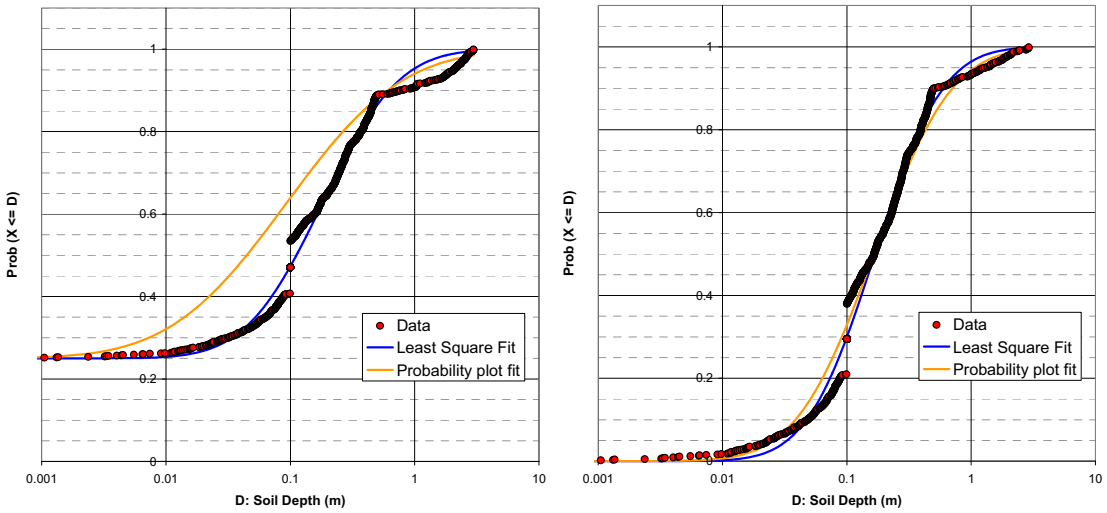

Source: Plots are produced in Output DTN: SN0612T0502206.039, *LN_fitting_lower_bound_V2.0_12_01_2006.xls*. The plot on the left is generated by setting the cell C2 on sheet "Calculations" to a value of 0.25. The plot on the right is generated when this cell is set to a value of zero. Data is from Sanchez 2006 [DIRS 176569].

NOTE: In the left frame, the non-zero values are considered to represent 3/4 of the distribution. In the right frame, the non-zero values represent the whole distribution.

Figure 6.5.2.4-6. CDFs for Estimated Distribution (red plots), Least-Square Fitted Lognormal Distribution (blue line), and Probability Plot Fitter Lognormal Distribution (orange line)

Regardless of the approach, the least-square fitting method results in a good fit for low values of soil depth (0 to 50 cm) but cannot capture the distribution behavior for deeper soils.

The probability plot fitting method does not fit the distribution for shallow soil using the first approach, but the fit for deeper soil is better. The second approach results in a reasonably good fit for shallow soil and better fit for deeper soil than the least square method.

Estimation of Upscaled Distribution of Soil Depth for Soil Depth Class 4

Because of nonlinearities between soil depth and average net infiltration, it is difficult to determine which statistic would best represent an effective uniform value of soil depth that would lead to an accurate estimate of spatially averaged net infiltration.

In hydrologic modeling, flow parameters such as permeability (typically represented with a lognormal spatial distribution) are generally upscaled to the geometric mean, and storage parameters such as porosity (typically represented with a normal spatial distribution) are typically upscaled to the arithmetic mean. Soil depth follows a lognormal spatial distribution but is a storage-type parameter. Therefore, it is hypothesized that the upscaled value should lie between the geometric and arithmetic means.

Both arithmetic and geometric means have been estimated for the fitted lognormal distributions as well as their standard errors (where standard error for geometric mean is based on the standard deviation of log-transformed data). A confidence interval has been estimated by adding or subtracting one standard error to the quantity of interest. The results are displayed below for geometric mean (Table 6.5.2.4-5) and arithmetic mean (Table 6.5.2.4-6). Confidence intervals are rounded to the first significant digit because an examination of the underlying observations seems to suggest that soil depths were generally measured or estimated to the nearest 5 cm, especially for deeper soils. Furthermore, because it can be difficult to identify the exact location of the soil–bedrock interface, it is assumed that the accuracy of the observations is only good to about 5 cm and certainly not to as little as 1 cm. For the first distribution (i.e., based on 35 observations) and for the second distribution using the first approach (i.e., considering non-zero values represents 75% of the distribution), the calculation of arithmetic and geometric means is straightforward. For the second approach on the second data set (scientific notebook), the estimate of both means has to be corrected to incorporate the second part of the bimodal distribution with values of zero soil depth.

Table 6.5.2.4-5. Estimation of Geometric Mean and Confidence Interval (by adding or subtracting one standard error)

	Estimation (log space)	Standard Error (log space)	Lower Bound (linear space)	Upper Bound (linear space)
First distribution a – Probability plot fitting	−1.2943189	0.157199	0.2	0.3
First distribution – Least Square fitting	−1.3625023	0.128382	0.2	0.3
Second distribution (1st approach) – Probability plot fitting	−2.3836264	0.053545	**0.1**	**0.1**
Second distribution (1st approach) – Least Square fitting	−1.7109852	0.035243	0.2	0.2
Second distribution – (2nd approach) – Probability plot fitting	−1.80019	0.035895	**0.1**[a]	**0.1**[a]
Second distribution – (2nd approach) – Least Square fitting	−1.78324	0.031237	**0.1**[a]	**0.1**[a]

[a] Lower and upper confidence bounds (CB) are first estimated in log scale using mean and standard deviation, and then corrected using the formula 0.75*CB+0.25*ln(0.01) – results are then calculated using an exponential function.

Table 6.5.2.4-6. Estimation of Arithmetic Mean and Confidence Bounds (by adding or subtracting one standard error)

	Estimation	Standard Error	Lower Bound	Upper Bound
First distribution – Probability plot fitting	0.4223722	0.08371	0.3	**0.5**
First distribution – Least Square fitting	0.3416151	0.051012	0.3	0.4
Second distribution (1st approach) – Probability plot fitting	0.3867008	0.0498	0.3	0.4
Second distribution (1st approach) – Least Square fitting	0.3362301	0.016686	0.3	0.4
Second distribution – (2nd approach) – Probability plot fitting	0.314756	0.016133	0.2[a]	0.2[a]
Second distribution – (2nd approach) – Least Square fitting	0.273798	0.011132	0.2[a]	0.2[a]

[a] Lower and upper confidence bounds (CB) are first estimated using mean and standard deviation and then corrected using the formula 0.75*CB+0.25*0.

The correction is applied directly on the lower and upper confidence bounds, as it is not possible to estimate directly the updated standard deviation.

The estimate of arithmetic mean is done by simply summing, for each bound, 75% of the previous value, to 25% of a value of 0.

The estimate of geometric mean is more difficult. Indeed, if any of the values of the distribution are equal to zero, the geometric mean is equal to zero. Thus, the inclusion of zero values will lead to a useless estimate. One solution to this problem is to associate a very small (constant) value to represent the fraction of the spatial distribution with zero soil depth. Of course, as the geometric mean is equivalent to an arithmetic mean calculated on log-transformed data, taking a value too small will lead again to a very low value of the geometric mean. Therefore, it was assumed that the presence of 1 cm of soil is essentially equivalent to there being no soil in regards to the resulting net infiltration. The geometric mean was then estimated using log-

transformed data, estimating the mean and its confidence bounds, summing 75% of these bounds with 25% of the logarithm of 0.01 m (approximately −4.6), and exponentiating the results to convert to a linear scale. Higher values of soil, from 2 to 9 cm, have been tested to represent the fraction of bare rock and to estimate the sensitivity of confidence bounds to the selected values. With a 10-cm accuracy, all values lead to the same confidence interval.

The minimum value estimate is equal to 0.1 m (bounds for geometric mean using probability plot fitting method on second data set using first approach and geometric mean on second data set using second approach). The maximum is equal to 0.5 m (upper bound of arithmetic mean using probability-plot fitting method on first dataset). Because there is no reason to favor any of these values (or any intermediate value), it has been decided to consider a uniform distribution between 0.1 m and 0.5 m to represent uncertainty in the upscaled quantity used to represent effective uniform value of Soil Depth Class 4.

6.5.2.5 Bedrock Classification

An infiltration hydrogeologic unit (IHU) system was developed consisting of bedrock types (IHUs) that have differing hydrogeologic properties with special emphasis on hydraulic conductivity (BSC 2006 [DIRS 176355], Section 6.2). The IHUs are defined on the basis of lithostratigraphic contacts in boreholes (BSC 2004 [DIRS 170029]). The correlation of lithostratigraphic units and IHUs enables the extrapolation of the IHUs to exposures at the ground surface where most of the correlated lithostratigraphic units have been documented on the following geologic maps:

- Preliminary Geologic Map of Yucca Mountain, Nye County, Nevada, with Geologic Sections (Scott and Bonk 1984 [DIRS 104181])
- Bedrock Geologic Map of the Central Block Area, Yucca Mountain, Nye County, Nevada (Day et al. 1998 [DIRS 101557])
- Digital Geologic Map of the Nevada Test Site and Vicinity, Nye, Lincoln and Clark Counties, Nevada, and Inyo County, California, Revision 4; Digital Aeromagnetic Map of the Nevada Test Site and Vicinity, Nye, Lincoln, and Clark Counties, Nevada, and Inyo County, California; and Digital Isostatic Gravity Map of the Nevada Test Site and Vicinity, Nye, Lincoln, and Clark Counties, Nevada, and Inyo County, California (Slate et al. 2000 [DIRS 150228]).

For map units that do not have any correlative IHUs, proxy IHUs have been proposed that are based on similarities in lithostratigraphic characteristics. These correlations of IHUs to lithostratigraphic units to map units are the basis for the new bedrock hydraulic conductivity map (Figure 6.5.2.5-1).

The infiltration model uses an input file containing 253,597 records of data with each record corresponding to a 30 × 30-m grid cell in the model area. The model area includes the entire Busted Butte 7.5 min quadrangle and the southern half of the Topopah Spring NW 7.5 min quadrangle. Because bedrock hydrologic properties are assigned on the basis of lithology, bedrock geologic units were assigned to each grid cell. This was accomplished with a digital

manipulation of existing geologic mapping data covering the area (BSC 2006 [DIRS 176355], Section 6.2.2).

In DTN: MO0603SPAGRIDD.003 [DIRS 177121] (*IHU_map_file2.txt*), each comma delimited record includes fields representing x- and y-coordinates for the center of the associated 30 × 30-m cell. The lithologic mapping unit corresponding to the center-cell coordinates was determined from the source polygon coverages using both ARCINFO and EarthVision (BSC 2006 [DIRS 176355], Section 6.2). The source files use a number code to designate stratigraphic units in the digital coverage files. The stratigraphic unit identified is shown at the point at the center of the cell in the "Geology" field of DTN: MO0603SPAGRIDD.003 [DIRS 177121].

The use of the center point of a grid cell to determine lithology can result in a generalization of the bedrock geology from that shown on the source maps. Cells that contain contacts between two or more units have been generalized to the unit found at the center of the cell. This means that thin units may occasionally be under- or over-represented in the file or that contacts may be displaced by up to 15 m. Given that the infiltration model contains over 250,000 cells, this level of generalization is considered acceptable for the purposes of the infiltration model when the natural variation within each lithologic unit and the uncertainties regarding the properties assigned to each unit are considered.

The three source maps (DTNs: GS971208314221.003 [DIRS 107128], *cb6k.ps*; MO0003COV00095.000 [DIRS 146848], *scotbons.e00*; and MO0603GSCGEOMP.000 [DIRS 176585], *ofr-99-0554-e00.tar*) each show significant areas covered by deep Quaternary alluvium (BSC 2006 [DIRS 176355], Figures 6-3, 6-4, and 6-5). Since the infiltration model needs the bedrock types underlying this alluvium to calculate infiltration into the bedrock from any water that percolates through the alluvium and reaches the bedrock contact, the GFM (DTN: MO0012MWDGFM02.002 [DIRS 153777]) was queried, and all cells within the GFM range that were classified as alluvial type were identified according to their underlying bedrock type (BSC 2006 [DIRS 176355], Section 6.2.2). Areas on the north, east, and south edges of the model area are not covered by the GFM and are still shown as alluvium (IHUs 490 and 491) in Figure 6.5.2.5-1. For infiltration modeling, the bedrock conductivity report (BSC 2006 [DIRS 176355], Section 7) recommends that the saturated hydraulic conductivity value for IHU 405 be used as the bedrock saturated hydraulic conductivity value for those areas mapped as IHUs 490 and 491 in DTN: MO0603SPAGRIDD.003 [DIRS 177121].

Table 6.5.2.5-1 shows the bedrock cell counts for each bedrock type in the UZ grid as well as the infiltration model domain. Note that the infiltration calculation model domain (containing 139,092 cells) is smaller than the region mention above (containing 253,597 cells) because the infiltration model uses watersheds within that domain as its boundaries. As can be seen in Table 6.5.2.5-1, bedrock types 405 and 406 are the most prominent in the UZ modeling domain, each occupying more than 15% of the total area.

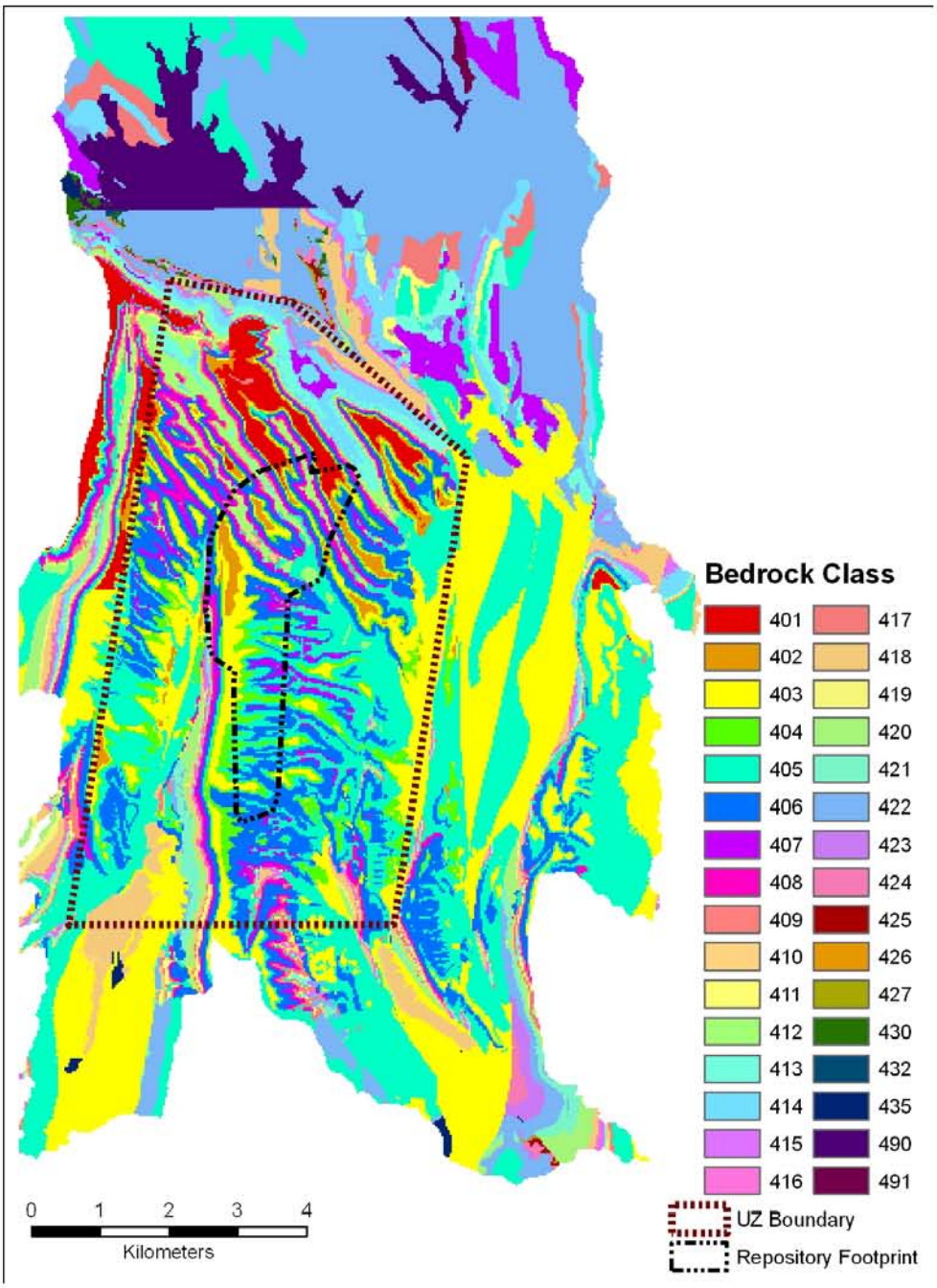

Source: DTN: MO0603SPAGRIDD.003 [DIRS 177121].

Output DTNs: SN0701SPALAYER.002 and SN0612FTPRNUZB.002.

Figure 6.5.2.5-1. Distribution of Infiltration Hydrogeologic Units across the Model Area

Table 6.5.2.5-1. Bedrock Cell Counts for the UZ Grid and Infiltration Model Domain

Bedrock IHU	UZ Grid Total Cells	Percent (UZ Grid)	Total Cells	Percent (Total)
401	1,757	4	2,974	2
402	1,482	3	1,651	1
403	6,317	14	24,672	18
404	3,589	8	3,921	3
405	9,980	23	30,953	22
406	8,617	19	11,819	8
407	2,658	6	5,701	4
408	1,607	4	2,562	2
409	771	2	1,827	1
410	149	0	483	0
411	147	0	1,058	1
412	1,765	4	2,620	2
413	1,037	2	2,608	2
414	1,304	3	3,974	3
415	289	1	1,106	1
416	47	0	373	0
417	174	0	2,222	2
418	1,256	3	4,702	3
419	41	0	296	0
420	454	1	1,742	1
421	379	1	1,044	1
422	362	1	24,427	18
423	11	0	483	0
424	11	0	432	0
425	0	0	124	0
426	0	0	20	0
427	0	0	85	0
428	0	0	0	0
429	0	0	0	0
430	0	0	234	0
431	0	0	0	0
432	0	0	30	0
433	0	0	0	0
434	0	0	0	0
435	0	0	257	0
436	0	0	0	0
437	0	0	0	0
438	0	0	0	0
490	0	0	4,513	3
491	0	0	179	0
Total cells	**44,204**		**139,092**	

Source: DTN: MO0603SPAGRIDD.003 [DIRS 177121].

6.5.2.6 Bedrock Saturated Conductivity

Saturated hydraulic conductivity (K_{sat}) data were developed for each of 38 rock types, or IHUs (Section 6.5.2.5) that form the bedrock at Yucca Mountain. Bulk hydraulic conductivity (K_{bulk}) is calculated for a composite porous medium consisting of matrix and fractures filled with permeable caliche.

In the conceptual model, bedrock hydraulic conductivity is the last resistance to flow before water enters the UZ model. As conceptualized, the bedrock has no thickness in the infiltration model; it only acts as a skin, limiting the portion of the flux reaching the bedrock that is allowed to infiltrate into the UZ model. The spatial distributions of the matrix and the filled-fracture K_{sat} are each described as lognormal, characterized by a median and standard deviation of the logarithm.

For each bedrock geologic unit, the approach used to calculate the mean and the variance of the bulk bedrock saturated hydraulic conductivity is as follows:

- The bedrock is modeled as consisting of matrix rock and fractures filled, at least at the soil–bedrock interface, with caliche
- Each of these materials is characterized by its median and standard deviation of $\log_{10} K_{sat}$ (BSC 2006 [DIRS 176355], Sections 6.4.3 and 6.4.4)
- The fraction of the soil–bedrock interface occupied by fractures, termed the fracture volume fraction, is characterized by a beta distribution (BSC 2006 [DIRS 176355], Section 6.3)
- The bedrock hydraulic conductivity is calculated by combining these data and by propagating the uncertainty (BSC 2006 [DIRS 176355], Section 6.4.5 and Appendix B). Uncertainties related to bedrock hydraulic conductivity are further discussed in Appendix I.

Conceptually, flow in the matrix and filled-fracture material is through parallel flow paths as represented by Equation 6.5.2.6-1. K_{bulk} for the composite porous medium of matrix and fractures filled with permeable caliche is, therefore, calculated as the arithmetic mean of the two K_{sat} values weighted by volume fraction (BSC 2006 [DIRS 176355], Equation 6-4):

$$K_{bulk} = f_{vf} K_{ff} + (1 - f_{vf}) K_m \qquad \text{(Eq. 6.5.2.6-1)}$$

where

f_{vf} is the fracture volume fraction,
K_{ff} is the K_{sat} of the fracture-filling material,
K_m is the K_{sat} of the matrix material, and
K_{bulk} is the K_{sat} of the composite bedrock.

K_{bulk} is the sum of two terms, of which the first is the product of a lognormal and a beta distribution. This multiplication does not lead to any classical distribution. Moreover, the addition of the two resulting distributions is difficult to estimate analytically because they are not independent, because of f_{vf}. Therefore, a Monte Carlo approach was used to estimate the shape of the resulting distribution: 30,000 values were sampled from the distribution of each input variable of f_{vf}, K_{ff}, and K_m, from which K_{bulk} is estimated (BSC 2006 [DIRS 176355], Section 6.4.5.1).

The resulting Monte Carlo distribution of K_{bulk} values, representing the spatial variability, is close to a lognormal distribution in shape for most of the 38 infiltration units. The distribution of bedrock saturated hydraulic conductivity over the infiltration model based on the consideration of filled fractures is shown in Figure 6.5.2.6-1, depicting the distribution of IHUs (Figure 6.5.2.5-1) with colors for various IHUs representing their respective saturated hydraulic conductivities. For most of the model area, bedrock saturated hydraulic conductivity based on the consideration of filled fractures is 2.4×10^{-7} m/s or less.

Field observations (Sanchez 2006 [DIRS 176569], pp. 26 to 61) indicate that caliche infilling of fractures and other voids is pervasive in many areas, but in others, particularly where soil cover is thin (because soil is the source of the caliche), it is spotty, does not completely fill fractures, or is absent. Also, additional field observations (Sweetkind et al. 1995 [DIRS 106959], p. 48, Figure 2, and Appendix 2; 1995 [DIRS 106958], pp. 12 and 34) show that in general at least some proportion of fractures are not completely filled (BSC 2006 [DIRS 176355], Section 6.4.5.4). Comparison of the infiltration rate measured in the Alcove 1 infiltration test with the mean bulk bedrock K_{sat} for IHU 404 (BSC 2006 [DIRS 176355], Section 6.4.5.3) also suggests that the fractures at that location are not completely filled. In view of these observations, the bulk bedrock saturated hydraulic conductivity calculated for filled fractures must be regarded as a lower bound of bulk bedrock saturated hydraulic conductivity. The upper bound of bulk bedrock saturated hydraulic conductivity must be set by some estimate of the percent of fractures containing an additional hydraulic aperture.

The relationship that was used to estimate the effect of open fractures on permeability is (Freeze and Cherry 1979 [DIRS 101173], Equation 2.87):

$$k = (Nb^3)/12 \qquad \text{(Eq. 6.5.2.6-2)}$$

where k is permeability, N is the fracture density, and b is the hydraulic aperture. The relationship between permeability and hydraulic conductivity (K_{sat}) is (Freeze and Cherry 1979 [DIRS 101173], Equation 2.28):

$$K_{sat} = kg\rho/\mu \qquad \text{(Eq. 6.5.2.6-3)}$$

where g is the acceleration due to gravity, and ρ and μ are the density and dynamic viscosity of water, respectively. Equations 6.5.2.6-1, 6.5.2.6-2, and 6.5.2.6-3 are used in calculations done in DTN: MO0605SPABEDRK.005 [DIRS 177122] (*Fracture_lengths2 v2.xls*). Resulting bulk K_{sat} values from some of these calculations are shown in Figure 6.5.2.6-2. Few data are available to quantify either the proportion of fractures that are unfilled or the hydraulic aperture to characterize them. Reasonable values may be inferred from the sources identified in *Data*

Analysis for Infiltration Modeling: Bedrock Saturated Hydraulic Conductivity Calculation (BSC 2006 [DIRS 176355], Section 6.4.5.4.2), including the Alcove 1 infiltration test (DTN: MO0605SPAFABRP.004 [DIRS 180539]), and analysis of fracture air-permeability data and fracture frequency data described in *Data Analysis for Infiltration Modeling: Bedrock Saturated Hydraulic Conductivity Calculation* (BSC 2006 [DIRS 176355]). Figure 6.5.2.6-2 shows a comparison of bedrock saturated hydraulic conductivities calculated using 100-µm and 200-µm aperture fractures for 10%, 50%, and 100% of fractures, and saturated hydraulic conductivities for completely filled fractures, and completely open fractures (data from air permeability measurements). Error bars are included for the plots of completely filled versus completely open fractures. In addition, the inferred saturated hydraulic conductivity from the Alcove 1 test (DTN: MO0605SPAFABRP.004 [DIRS 180539]) is included in this figure. Note that the Alcove 1 data point is approximately halfway between the filled fracture, and the 200-µm aperture fracture saturated hydraulic conductivities. Based on these values, the upper bound of bulk bedrock K_{sat} has been calculated based on the consideration of an additional 200-µm hydraulic aperture with all fractures. For the purpose of stochastic simulation, the distribution of bulk bedrock K_{sat} between these bounds is taken as loguniform. The upper and lower bounds, and the means and variances calculated from the bounds, are summarized in Table 6.5.2.6-1.

The range of K_{sat} values represented by the upper and lower bounds in Table 6.5.2.6-1 are used to establish uncertainty ranges for each of the bedrock types based on a loguniform distribution. The treatment of uncertainties, including the screening of parameters to be propagated in the uncertainty analysis for this report, is discussed in Appendix I.

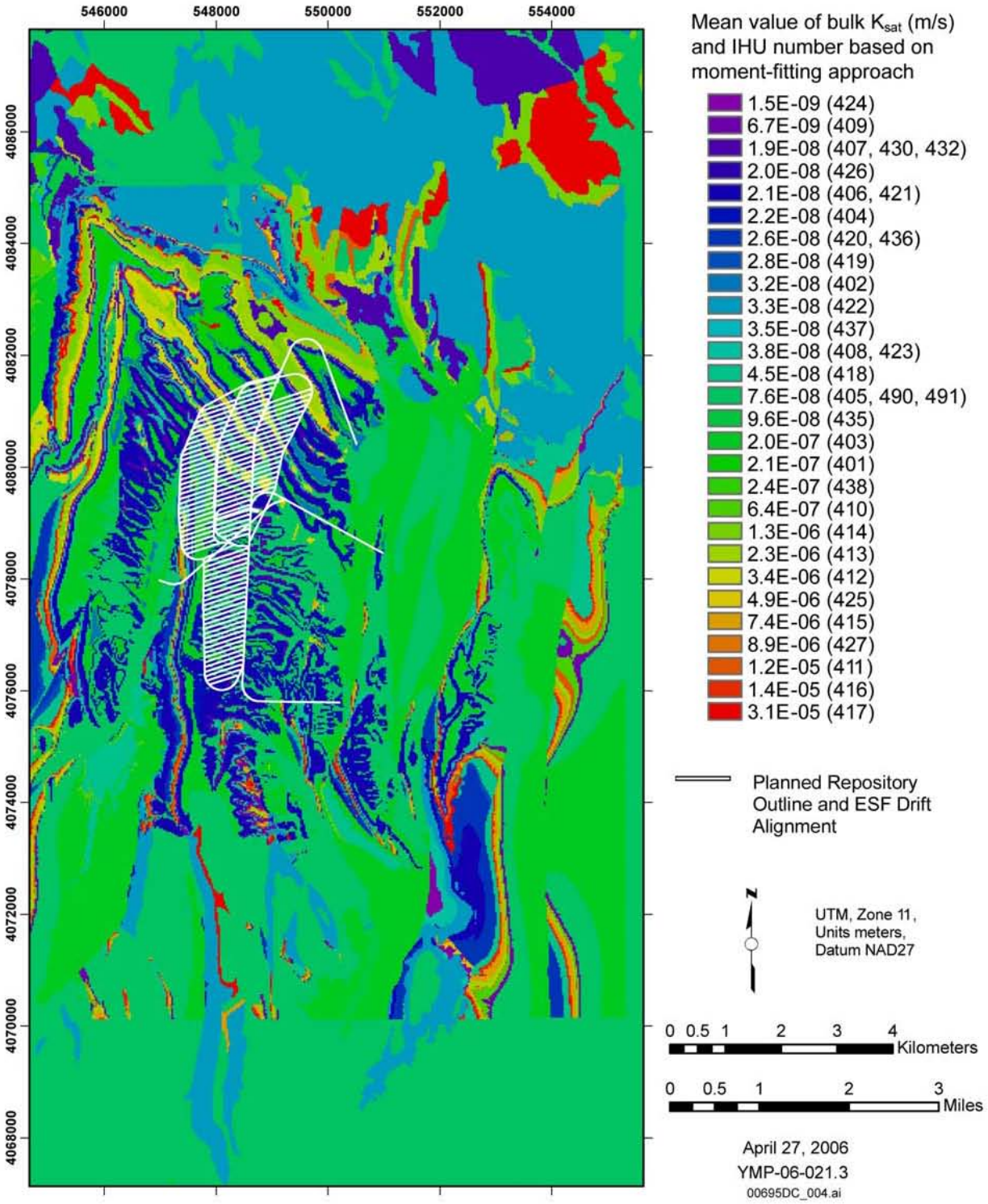

Source: BSC 2006 [DIRS 176355], Figure 6-11.

NOTE: Infiltration hydrogeologic unit (IHU) numbers are provided in parentheses in the map legend.

Figure 6.5.2.6-1. Distribution of Saturated Hydraulic Co nductivity over the Model Area Based on the Consideration of Filled Fractures

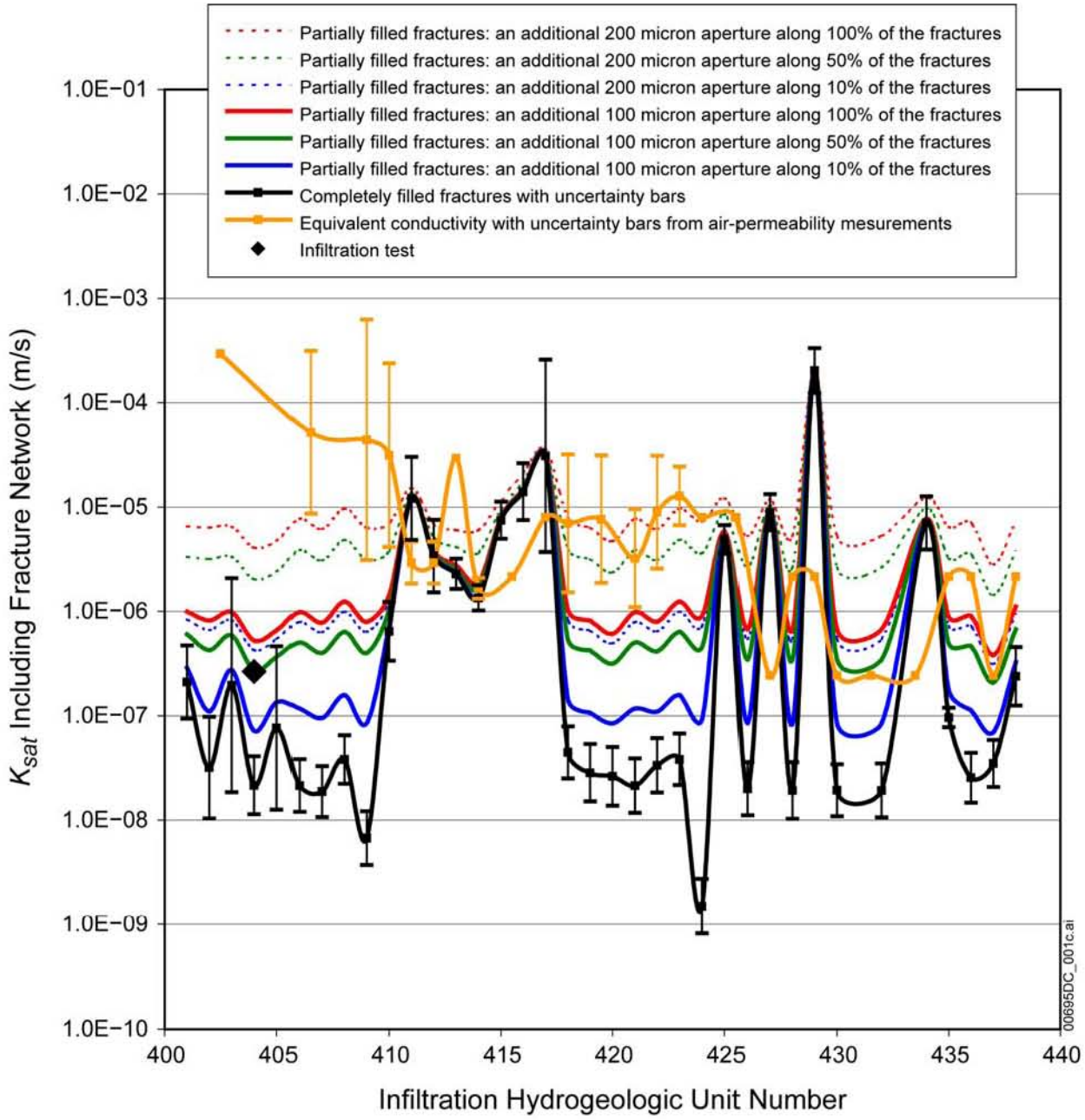

Source: DTN: MO0605SPABEDRK.005 [DIRS 177122], *Fracture_lengths2 v2.xls*, worksheet: "Comparison to Filled Fractures."

NOTES: While data are presented as cont inuous functions to improve visual depiction, the data are not continuous between IHUs. Filled-fracture data are the mean of K_{bulk} (DTN: MO0605SPABEDRK.005 [DIRS 177122]). For some IHUs, for example IHUs 411 through 417, the bedrock matrix material is sufficiently permeable without any unfilled fractures, so there is no significant increase in saturated hydraulic conductivity.

IHU = infiltration hydrogeologic unit.

Figure 6.5.2.6-2. Variation of Bulk Saturated Hydraulic Conductivity, K_{sat}, as a Function of Various Partially Filled Fracture Networks, with Comparison to the Alcove 1 Infiltration Test

Table 6.5.2.6-1. Bulk Bedrock K_{sat}

IHU		Upper Bound [a]	Lower Bound [b]	Mean [c]	Variance [c]
Number	Symbol	(m/s)	(m/s)	(m/s)	(m^2/s^2)
401	hcr4	6.5×10^{-6}	2.1×10^{-7}	1.8×10^{-6}	2.8×10^{-12}
402	hcr3	6.3×10^{-6}	3.2×10^{-8}	1.2×10^{-6}	2.4×10^{-12}
403	hcr2	6.5×10^{-6}	2.0×10^{-7}	1.8×10^{-6}	2.8×10^{-12}
404	hcr1	4.1×10^{-6}	2.2×10^{-8}	7.7×10^{-7}	9.9×10^{-13}
405	**hcul**	$\mathbf{4.8 \times 10^{-6}}$	$\mathbf{7.6 \times 10^{-8}}$	$\mathbf{1.1 \times 10^{-6}}$	$\mathbf{1.5} \times 10^{-12}$
406	**hcmn**	$\mathbf{7.7 \times 10^{-6}}$	$\mathbf{2.1 \times 10^{-8}}$	$\mathbf{1.3 \times 10^{-6}}$	$\mathbf{3.4 \times 10^{-12}}$
407	hcll	6.1×10^{-6}	1.9×10^{-8}	1.1×10^{-6}	2.1×10^{-12}
408	hcln	9.6×10^{-6}	3.8×10^{-8}	1.7×10^{-6}	5.4×10^{-12}
409	hcv2	6.3×10^{-6}	6.7×10^{-9}	9.2×10^{-7}	2.1×10^{-12}
410	hcv1	7.0×10^{-6}	6.4×10^{-7}	2.7×10^{-6}	3.0×10^{-12}
411	hbt4	1.5×10^{-5}	1.2×10^{-5}	1.4×10^{-5}	7.9×10^{-13}
412	hym	6.9×10^{-6}	3.4×10^{-6}	4.9×10^{-6}	1.0×10^{-12}
413	hbt3	6.0×10^{-6}	2.3×10^{-6}	3.9×10^{-6}	1.1×10^{-12}
414	hpc	6.0×10^{-6}	1.3×10^{-6}	3.1×10^{-6}	1.7×10^{-12}
415	hbt2	1.2×10^{-5}	7.4×10^{-6}	9.4×10^{-6}	1.4×10^{-12}
416	htrv3	2.1×10^{-5}	1.4×10^{-5}	1.7×10^{-5}	4.2×10^{-12}
417	htrv1	3.6×10^{-5}	3.1×10^{-5}	3.3×10^{-5}	2.1×10^{-12}
418	htrn	7.9×10^{-6}	4.5×10^{-8}	1.5×10^{-6}	3.8×10^{-12}
419	htrl	6.3×10^{-6}	2.8×10^{-8}	1.2×10^{-6}	2.3×10^{-12}
420	htul	4.7×10^{-6}	2.6×10^{-8}	9.0×10^{-7}	1.3×10^{-12}
421	htmn	7.7×10^{-6}	2.1×10^{-8}	1.3×10^{-6}	3.4×10^{-12}
422	htll	6.2×10^{-6}	3.3×10^{-8}	1.2×10^{-6}	2.3×10^{-12}
423	htln	9.6×10^{-6}	3.8×10^{-8}	1.7×10^{-6}	5.4×10^{-12}
424	htpv3	7.3×10^{-6}	1.5×10^{-9}	8.5×10^{-7}	2.4×10^{-12}
425	htv2v	1.2×10^{-5}	4.9×10^{-6}	8.0×10^{-6}	4.3×10^{-12}
426	htv2z	5.3×10^{-6}	2.0×10^{-8}	9.4×10^{-7}	1.6×10^{-12}
427	htv1v	1.2×10^{-5}	8.9×10^{-6}	1.0×10^{-5}	6.5×10^{-13}
428	htv1z	5.3×10^{-6}	1.9×10^{-8}	9.4×10^{-7}	1.6×10^{-12}
429	hacv	2.0×10^{-4}	2.0×10^{-4}	2.0×10^{-4}	5.2×10^{-13}
430	hacz	5.3×10^{-6}	1.9×10^{-8}	9.4×10^{-7}	1.6×10^{-12}
431	habtv	—	—	—	—
432	habtz	5.3×10^{-6}	1.9×10^{-8}	9.4×10^{-7}	1.6×10^{-12}
433	hpuvv	—	—	—	—
434	hpuvz	1.2×10^{-5}	7.0×10^{-6}	9.4×10^{-6}	2.3×10^{-12}
435	hpuc	6.4×10^{-6}	9.6×10^{-8}	1.5×10^{-6}	2.6×10^{-12}

Table 6.5.2.6-1. Bulk Bedrock K_{sat} (Continued)

IHU		Upper Bound [a]	Lower Bound [b]	Mean [c]	Variance [c]
Number	Symbol	(m/s)	(m/s)	(m/s)	(m^2/s^2)
436	hpmlc	7.0×10^{-6}	2.6×10^{-8}	1.2×10^{-6}	2.8×10^{-12}
437	hpbvz	2.8×10^{-6}	3.5×10^{-8}	6.4×10^{-7}	5.1×10^{-13}
438	hbucm	7.2×10^{-6}	2.4×10^{-7}	2.1×10^{-6}	3.5×10^{-12}

Source: DTN: MO0605SPABEDRK.005 [DIRS 177122], *Fracture_lengths2 v2.xls*, worksheet: "upper and lower bounds."

[a] Upper-bound K_{sat} is the sum of K_{sat} with all fractures filled and K_{sat} of 100% unfilled fractures with hydraulic aperture 200 μm.

[b] Lower-bound K_{sat} is the K_{sat} with all fractures filled (DTN: MO0605SPABEDRK.005 [DIRS 177122], moment-fitting mean value).

[c] Mean and variance are calculated based on the upper and lower bounds (BSC 2006 [DIRS 176355], Section 6.4.5.5, Equations 6-7 and 6-8).

NOTES: IHUs 405 and 406 (bolded) cover more than 15% of the UZ modeling domain and are included in the uncertainty analysis described in Sections 6.5.5 to 6.5.7.

IHUs 490 and 491 are assigned the same conductivity as IHU 405 as recommended in BSC 2006 [DIRS 176355], Section 7.

IHU = infiltration hydrogeologic unit.

6.5.3 Vegetation Parameters

This section describes the development of model input parameters used to describe the characteristics of the vegetation that is expected to be present at Yucca Mountain during the three future climates being considered. Parameters include maximum rooting depth (Z_r), plant height (h_{plant}), basal transpiration coefficients (K_{cb}), normalized difference vegetation index (NDVI) corrected for the Yucca Mountain environment (NDVI'), and the slope and intercept of the least squares regression between K_{cb} and NDVI'.

- Section 6.5.3.1 discusses the types of vegetation that are likely to be present during the Monsoon and Glacial Transition climates. Vegetation for the Present-Day climate is described in Section D2.2. This information is needed in order to estimate ranges for vegetation parameters.

- Section 6.5.3.2 describes the development of the parameter distributions for maximum rooting depth.

- Section 6.5.3.3 describes the development of the parameter distributions for plant height.

- Section 6.5.3.4 presents an overview of how estimates of transpiration coefficients are made in the model.

- Section 6.5.4.5 discusses inputs developed from satellite data that are used to estimate the effects of spatial and temporal factors on the vegetation response within the model domain.

- Section 6.5.3.6 discusses inputs developed from ground measurements of vegetation response at a set of ecological study plots at the Yucca Mountain site.

- Section 6.5.3.7 explains how satellite data and data collected on the ground are used together to determine transpiration coefficients.

6.5.3.1 Potential Vegetation for Monsoon and Glacial Transition Climates

To develop distributions for plant height and rooting depth for Monsoon and Glacial Transition climates it was necessary to consider what taxa might reasonably be expected to occur at Yucca Mountain. The species composition of future vegetation communities at Yucca Mountain is a complex issue. It is recognized that multiple possibilities for vegetation assemblages exist and outcomes are dependent on several factors including climate, disturbance, and species-specific ability to adapt or migrate. The potential for certain plant taxa to occur was evaluated by considering several factors including predicted future-climate rainfall and temperature patterns, natural vegetation associated with the climate at analogue meteorological station locations, historical vegetation change in response to climate change, species tolerance ranges and requirements, and current species composition of plant communities at Yucca Mountain. It is important to note that edaphic factors and topography at Yucca Mountain differ from those of natural vegetation stands associated with analogue meteorological station locations. Therefore, species were not selected as potential components of future vegetation simply on the basis that they are likely to occur in natural vegetation stands associated with the analogue meteorological stations.

6.5.3.1.1 Monsoon Climate and Vegetation at Analogue Sites

The Monsoon climate state is predicted to last around 900 to 1,400 years, with temperature and precipitation patterns in the lower bound similar to current conditions at Yucca Mountain (BSC 2004 [DIRS 170002], pp. 6-44 to 6-45, Table 6-1). Temperature and precipitation patterns during the upper bound Monsoon climate are predicted to be similar to those in Hobbs, New Mexico, and Nogales, Arizona (BSC 2004 [DIRS 170002], pp. 6-44 to 6-45, Table 6-1). The main difference between the Present-Day climate and upper-bound Monsoon climate that would affect species composition of plant communities at Yucca Mountain is a substantial increase in summer precipitation. Average monthly minimum and maximum air temperatures are predicted to be slightly lower for the upper-bound Monsoon climate state compared to the Present-Day climate (Table 6.5.3.1-1).

Table 6.5.3.1-1. Monthly Temperature and Precipitation for Upper-Bound Monsoon (Nogales, Arizona, and Hobbs, New Mexico) and Present-Day (Desert Rock) Climates

	Nogales, Arizona[a] (1971 to 2000)				Hobbs, New Mexico[b] (1914 to 2001)				Desert Rock, Nevada[b,c] (1984 to 2000)			
	Temperature[d] (°C)			Pcp[e] (mm)	Temperature[d] (°C)			Pcp[e] (mm)	Temperature[d] (°C)			Pcp[e] (mm)
Month	Mean	Max	Min		Mean[f]	Max	Min		Mean	Max	Min	
Jan.	7.5	17.7	−2.7	33.3	—	13.6	−2.3	11.4	6.6	12.7	0.4	23.6
Feb.	9.2	19.5	−1.2	27.7	—	16.6	0.0	11.2	9.1	15.5	2.7	22.1
March	11.5	21.8	1.1	25.4	—	20.5	2.9	13.0	12.1	19.1	5.1	15.0
April	14.7	25.7	3.6	12.4	—	25.3	7.8	20.3	16.3	23.8	8.7	8.9
May	18.7	30.1	7.3	8.1	—	29.7	12.9	52.8	20.8	28.5	13.2	7.1
June	23.9	35.4	12.4	13.7	—	33.7	17.4	48.0	25.9	34.1	17.8	1.8
July	26.1	34. 6	17.5	108.5	—	34.3	19.2	53.8	29.0	36.8	21.2	18.3
August	25.3	33.4	17.2	107.7	—	33.3	18.6	60.7	28.4	36.1	20.8	16.0
Sept.	22.8	32.3	13.2	42.7	—	29.9	15.2	66.8	23.9	31.8	16.1	8.4
Oct.	17.1	27.8	6.4	46.7	—	25.1	9.1	39.9	17.9	25.6	10.2	9.1
Nov.	11.2	22.0	0.3	19.8	—	18.4	2.6	14.7	10.1	16.9	3.2	11.2
Dec.	7.8	18.1	−2.4	37.3	—	14.4	−1.4	14.2	6.2	12.7	−0.2	14.2

[a] Western Regional Climate Center 2003 [DIRS 162307].
[b] Western Regional Climate Center 2002 [DIRS 165987].
[c] Desert Rock, located in Mercury, Nevada, is used here to represent climate at Yucca Mountain.
[d] Temperature was converted from °F to °C (°C = [°F−32]/1.8).
[e] Precipitation was converted from inches to millimeters (mm = inches × 20.54).
[f] Mean temperature was not available for Hobbs, New Mexico.

Using the monthly climate summaries for Nogales and Hobbs (Table 6.5.3.1-1), approximately 66% to 80% of total annual precipitation (average = 460 mm) falls between May and October when average monthly maximum temperatures range from 25°C to 34°C. Average minimum winter temperatures (November to February) range from −2.3°C to 2.8°C. These climate conditions support both high Sonoran (Nogales) and northern Chihuahuan (Hobbs) desert vegetation.

Much of the Sonoran Desert is subtropical and typically supports a diverse mix of trees, shrubs, and cacti represented by the genera *Cercidium* (paloverde), *Olneya* (desert ironweed), *Prosopis* (mesquite), *Larrea* (creosotebush), *Carnegiea* (saguaro), and *Lophocereus* (senita cactus), with distinct winter and summer floras (Smith et al. 1997 [DIRS 103636], p. 23). This diversity is due to a variety of factors including a mixture of soil types in the region, virtual absence of frost, and a bimodal pattern of yearly rainfall. However, low elevation bajadas and valley floors dominated by *Larrea – Ambrosia* desert scrub are typical of northern and western regions with vegetation similar to that found at Yucca Mountain. Nogales lies near the mid-eastern boundary of the Sonoran Desert.

Much of the Chihuahuan desert region has calcareous soils derived from limestone beds. Vegetation is often dominated by grasses and frost-tolerant plants such as yuccas and agaves. Grasslands generally dominate valley basins (Smith et al. 1997 [DIRS 103636], p. 24). Upper bajadas with deep soils are often dominated by desert scrub or arborescent woodland (Smith et al. 1997 [DIRS 103636], p. 24). Important perennial grass genera in the Chihuahuan Desert include *Bouteloua* (grama), *Erioneuron* (woollygrass), *Muhlenbergia* (muhly), *Scleropogon* (burrograss), *Pleuraphis* (galleta grass), and *Sporobolis* (dropseed). Desert scrub vegetation in northern reaches of the Chihuahuan Desert is dominated by *Larrea* and *Prosopis* with *Flourensia* (tarbush), *Ephedra* (jointfir), and *Yucca* as co-dominants. Hobbs, New Mexico, is near the northeastern boundaries of the Chihuahuan desert.

6.5.3.1.2 Glacial Transition Climate and Historical Vegetation Change

The Glacial Transition climate state is predicted to follow the Monsoon climate and last about 8,700 years. This climate state is characterized by cool wet winters and warm dry summers, with precipitation and temperature patterns similar to those in eastern Washington (BSC 2004 [DIRS 170002], pp. 6-44 to 6-45, Table 6-1). Data from analogue climate stations at St. John, Rosalia, and Spokane, Washington, indicate that total annual precipitation at Yucca Mountain during the Glacial Transition climate state will be about 460 mm, with about 60% falling between November and March (Table 6.5.3.1-2). Average minimum temperatures are below freezing during this time period. Cold desert shrub and shrub steppe vegetation typical of that found in the Great Basin extends into the eastern Washington area (Smith et al. 1997 [DIRS 103636], p. 6) where the analogue climate stations are located.

Table 6.5.3.1-2. Monthly Temperature and Precipitation for the Glacial Transition Climate

	Rosalia, Washington [a] (1948 to 2000)				Spokane, Washington [a] (1889 to 2000)			
	Temperature[b] (°C)			Pcp[c] (mm)	Temperature[b] (°C)			Pcp[c] (mm)
Month	Mean	Max	Min		Mean	Max	Min	
January	−2.1	1.3	−5.6	57.4	−2.7	0.5	−5.9	50.5
February	0.8	4.7	−3.1	41.4	0.1	3.9	−3.8	39.9
March	3.8	8.8	−1.1	40.1	4.1	9.0	−0.8	35.1
April	7.7	13.9	1.5	34.5	8.6	14.6	2.5	28.2
May	11.7	18.6	4.9	39.4	12.9	19.4	6.5	35.3
June	15.2	22.4	7.9	34.8	16.7	23.4	10.1	30.7
July	18.9	27.7	10.2	16.3	21.0	28.8	13.2	14.2
August	18.9	27.8	10.1	18.0	20.3	28.1	12.5	15.7
September	14.6	22.9	6.2	21.3	15.2	22.4	8.1	20.6
October	8.6	15.7	1.6	35.1	9.1	15.1	3.1	30.0
November	2.5	6.6	−1.7	56.6	2.4	6.0	−1.2	53.3
December	−1.2	2.1	−4.6	60.5	−1.4	1.5	−4.3	55.6

[a] Western Regional Climate Center 2002 [DIRS 165987].
[b] Temperature was converted from °F to °C (°C = [°F−32]/1.8).
[c] Precipitation was converted from inches to millimeters (mm = inches × 20.54).

Paleobotanical evidence from fossilized plant material preserved in packrat (*Neotoma* spp.) middens and fossil pollen preserved in lake and cave deposits have been used to reconstruct historical climate and floral composition of the four major deserts of western North America (Smith et al. 1997 [DIRS 103636], pp. 25 to 27). Packrat middens provide the primary source of evidence for historical vegetation in the Mojave Desert. The flora of the Mojave Desert during the late Wisconsin (21,000 to 11,000 years before present (B.P.)), early Holocene (11,000 to 8,000 years B.P.), and middle Holocene (8,000 to 4,000 years B.P.) are relevant to this analysis.

During the period 23,000 to 11,000 years B.P, juniper-dominated pygmy conifer woodlands (north of 36°N latitude) existed at lower elevations that are currently occupied by desert scrub vegetation (Smith et al. 1997 [DIRS 103636], p. 26). Desert taxa persisted in these woodlands as components of under-stories and south slopes. It was estimated that these woodlands were prevalent at elevations ranging from 600 m to 1,200 m below current distributions. Currently on the Nevada Test Site, open pygmy conifer woodlands occur at elevations above 1,830 m throughout the central and northwestern mountains and mesas (Wills and Ostler 2001 [DIRS 177624], p. 35). These woodlands are dominated by *Pinus monophylla* at higher elevations and *Juniperus osteosperma* at lower elevations (e.g., northwestern part of Pahute Mesa). *Artemisia* spp. are co-dominants in both woodlands (Wills and Ostler 2001 [DIRS 177624], p. 35). Thus, during this period, these woodlands would have existed at elevations starting at 630 to 1,230 m on the Nevada Test Site, well within the elevations of the infiltration model domain for Yucca Mountain.

During the terminal Wisconsin and early Holocene (12,000 to 8,000 years B.P.), summer precipitation increased in most of the Sonoran and Chihuahuan deserts due to monsoonal moisture patterns (Smith et al. 1997 [DIRS 103636], p. 27). However, this moisture did not reach the Mojave and western Sonoran Deserts, which had begun conversion to desert shrublands. During this time period coniferous woodlands still dominated most of the Sonoran and Chihuahuan deserts. *Larrea - Ambrosia* desert scrub of the Mojave and western Sonoran Deserts was in place by the middle Holocene (8,000 years B.P.). Elevational and geographic changes in species distributions have occurred over the past 8,000 years in response to climatic variation, but there has been little change in general floristic composition in the Mojave since the middle Holocene (Smith et al. 1997 [DIRS 103636], p. 28).

6.5.3.1.3 Potential Vegetation for Future Climate States at Yucca Mountain

During the Holocene, entire plant communities did not migrate intact to new ranges. Instead, different taxa responded individualistically to changes in climate, and plant communities were reshuffled based on differences in species' ability to reestablish themselves (Tausch et al. 1993 [DIRS 177620], pp. 442 to 443). Several factors affect migration and establishment of species into new areas not previously colonized, including:

(1) The ability to arrive in the new habitat. Long-haul dispersal mechanisms include dispersal by water, wind, birds, large mammals, and humans.

(2) The extent to which habitat conditions at the new site meet germination, establishment, growth, and reproduction requirements of the arriving species.

(3) The extent to which climatic change favors the new species over established species with respect to tolerance ranges and ability to compete for nutrients.

(4) The extent to which the new species tolerates or exploits disturbance patterns of the new site or affects changes in disturbance patterns (e.g., fire frequency).

Based on these requirements, several of the taxa that are common to the Sonoran and Chihuahuan Deserts would be unlikely candidates for colonization at Yucca Mountain during the Monsoon climate state. For example, assuming propagules arrived at Yucca Mountain either through migration or human introduction, establishment of taxa such as *Carnegiea* and *Lophocereus*, which are extremely susceptible to freezing temperatures, may be limited by average minimum air temperatures during winter months that are predicted for the Yucca Mountain Monsoon climate. Species such as *Flourensia cernua* grow in limestone or calcareous soils that are clay loams or gravelly clay, unlike those found at Yucca Mountain. *Cercidium* and *Prosopis* sp. are facultative riparian species in parts of their ranges but also occur in upland communities where precipitation is sufficient or where roots can tap into the water table. It is not likely that monsoon conditions predicted for Yucca Mountain would support establishment of *Cercidium*- or *Prosopis*-dominated communities.

Taxa that currently exist at Yucca Mountain and that are also found within the climatic regions of the analogue meteorological stations are likely to persist and in some cases perhaps expand their distributions. These include shrubs (e.g., *Larrea*, *Ambrosia*, and *Ephedra*), yuccas, cacti (e.g., *Echinocereus*), and grasses (e.g., *Muhlenbergia* and *Pleuraphis*). The Monsoon climate could support an increase in abundance of summer active grasses such as *Pleuraphis jamesii* and in species with relatively high temperature and moisture requirements for germination such as *L. tridentata*. While establishment of new species at Yucca Mountain during the Monsoon climate state cannot be ruled out, it is assumed instead that the abundance of grasses would increase, distinct winter/summer floras might develop with increases in abundance of existing winter/summer species, and shrub species such as *L. tridentata* and *A. dumosa* might increase in abundance. These changes would likely result in increased leaf area index over current climate values, proportional to the increase in precipitation, but overall physiognomy would be similar to current climate.

The predicted time period for the glacial transition climate state (8,700 years) is long enough that changes in vegetation at Yucca Mountain would be likely to occur. Changes in species composition, community types, and distribution ranges will likely be dynamic throughout the glacial transition period, influenced by disturbance type and frequency in addition to climate changes. Paleobotanical studies provide evidence to suggest that habitat conditions at elevations similar to those at Yucca Mountain likely supported open pygmy conifer woodlands during the last glacial transition state with pinyon dominant at higher elevations (> 1,800 m) and juniper at lower elevations. Pinyon-juniper woodlands exhibit widespread ecological amplitude and occupy steep mountain slope habitats to alluvial fans and steppes in the Great Basin. Recent range expansion into alluvial fan and steppe habitats has been attributed to fire suppression and overgrazing during the last 100 to 150 years (West 1999 [DIRS 178536], p. 21). This community type occurs across a wide range of surface soils from stony, cobbly, and gravelly sandy loams to clay loams with soil depths ranging from less than 0.5 m to greater than 1.5 m (Roundy and Vernon 1999 [DIRS 178534], p. 174), and average precipitation ranging from

280 mm per year (e.g., Pahute Mesa on the Nevada Test Site; Hansen and Ostler 2003 [DIRS 177619], p. 80) to around 400 mm (e.g., pinyon-juniper zone at the Spring Mountains, S. Nevada; Lei 1999 [DIRS 178535], p. 64). The soils at Yucca Mountain and predicted temperatures and precipitation for the glacial transition climate would support open juniper woodlands similar to those found on Pahute Mesa. Great Basin species that are currently present at Yucca Mountain that could increase in abundance under the glacial transition climate state include *Artemisia tridentata*, *Ephedra nevadensis*, *Krascheninnikovia lanata*, *Ericameria* spp., and *Chrysothamnus viscidiflorus*. Increased precipitation would support an increase in perennial grasses that are present at the mountain. These include *Achnatherum hymenoides*, *Poa* spp., *Achnatherum speciosum*, and *Elymus elymoides*. As with the Monsoon climate, these changes would likely result in increased leaf area index over current climate values, proportional to the increase in precipitation predicted for the glacial transition climate.

An alternative projection of vegetation under the glacial transition climate state is a system dominated by *Bromus tectorum*, an exotic annual grass (see Section D-5). Conversions of vast expanses of shrub steppe from communities dominated by perennial grasses and shrubs to communities dominated by *B. tectorum* have been documented throughout the Great Basin and Columbia Plateau, including the Spokane, Washington, area (e.g., Mack 1981 [DIRS 177164]). Shifts in dominance of native perennial shrubs to exotic annual grasses under glacial transition conditions have the potential to change net infiltration at Yucca Mountain. Increased net infiltration has been correlated with the presence of brome and other grass monocultures in Canada (van der Kamp et al. 2003 [DIRS 176050]). This correlation has been attributed to increases in macroporosity and permeability due to a high density of stalks and root holes that characterize grass monocultures (Bodhinayake and Si 2004 [DIRS 176211]). The shallow extent of brome grass roots may also allow excess water to infiltrate beyond the root zone and thus escape loss by evapotranspiration. Currently, two bromegrass species (*B. tectorum* and *B. madritensis* spp. *rubens*) are present at Yucca Mountain and dominate the annual flora (see Appendix D). Therefore, during the glacial transition climate, the possibility of a bromegrass monoculture at Yucca Mountain is considered for the infiltration model. Specifically, this possible future state is considered by including representative low values in the distribution range of maximum rooting depth for the glacial transition climate.

6.5.3.2 Maximum Rooting Depth

Mean maximum effective rooting depth (Z_r) is needed for water balance calculations for the root zone (Section 6.4). It is used in the calculation of water content in the root zone and root zone water depletion (Allen et al. 1998 [DIRS 157311], p. 170, Equation 85). It defines the depth to which water can be removed from the soil system, assuming that the soil depth equals or exceeds that depth. Mean maximum effective rooting depth distributions and nominal values for the different climate states are developed in this section. Based on potential composition of vegetation in future climates (Section 6.5.3.1), one distribution for Z_r was developed for the Present-Day and Monsoon climates, and a separate distribution was developed for the Glacial Transition climate.

Mean Maximum Effective Rooting Depth for Present-Day and Monsoon Climate States—The vegetation at Yucca Mountain consists mainly of deep-rooted perennial species (e.g., *Ericameria teretifolia, Larrea tridentata, Ephedra nevadensis*), shallow rooted perennials (e.g., Cactaceae and other families of CAM succulents), and shallow rooted winter/summer annuals (e.g., *Bromus madritensis* ssp. *rubens*). Great Basin desert species, such as *E. teretifolia,* tend to have deeper root systems and greater root-to-shoot ratios than Mojave Desert species such as *L. tridentata* (Smith et al. 1997 [DIRS 103636], p. 65). Root systems in general tend to exhibit a high degree of morphological plasticity and are influenced by both genetic and ecological determinants. Factors that can limit deep root growth in arid environments include decreasing nutrient concentration and microbial activity with depth, increasing soil compaction, lack of oxygen, presence of cemented hardpan, soil depth, and inter- or intra-specific competition for nutrients or space (Hansen and Ostler 2003 [DIRS 177619], pp. 22 to 28). Deep root growth is likely realized by plants at Yucca Mountain that are growing in areas where soil accumulates, such as washes, intermountain valleys, and lowlands. Also, roots can penetrate bedrock fractures where soil is present to extract stored water, but this process is assumed to be negligible compared with the amount of water that roots can extract from the soil layer, and therefore it is not included in the MASSIF model (see Section 5). A review of applicable literature was conducted to establish ranges of rooting depths for common plant species at Yucca Mountain. The information from the literature review was used to develop a nominal value and appropriate distribution of rooting depths for use in the MASSIF model.

Literature Review—Shallow rooted annual and perennial plant species are important contributors to total plant water use in the Yucca Mountain system. However, the MASSIF model, which is based on the FAO-56 method of modeling evapotranspiration, does not distinguish among depths for water extraction by roots. Therefore, the literature review focused primarily on deep-rooted perennial species in order to encompass the entire range of rooting depths. Most of the literature search focused on rooting depth studies that were conducted on the Nevada Test Site (NTS) or within the Mojave Desert. This was done to minimize uncertainty associated with generalizing findings from other areas that are based on different species, ecotypes, soils, or climate that might not be applicable to Yucca Mountain. Three studies conducted in arid to semi-arid habitats outside of the Mojave Desert were included to ensure that an appropriate range of variation was considered in development of mean maximum rooting depths. This was necessary because most of the studies that were conducted on the NTS and within the Mojave Desert limited evaluation of rooting depths to about 2 m and therefore did not provide information below that depth. The three studies conducted outside the Mojave Desert show potential for deeper rooting than 2 m and provide a measure of variation not accounted for in the Mojave Desert studies.

Brome grasses (*Bromus rubens* and *B. tectorum*) are generally the dominant annuals on Ecological Study Plots (ESPs) at Yucca Mountain (see Tables D-6 through D-14, and Section D5) and can form dense stands in wet years. These grasses generally have shallower root systems than most perennial shrub species. To account for the potential for brome monocultures to form at Yucca Mountain, rooting depths for these grasses were included in the literature search. No information was found for brome rooting depths in the Mojave Desert; therefore, studies from the Great Basin Desert were used for this grass.

Rooting depths and rooting morphologies for dominant plant species growing in Rock Valley on the NTS were described by Rundel and Gibson (1996 [DIRS 103614], pp. 98 to 99). Root systems were excavated from a wash area with relatively deep sediments. In general, shrub species had roots to depths of about 1 to 2 m. Scaled drawings of root systems showed roots for *L. tridentata*, *A. dumosa*, *E. nevadensis*, and *L. andersonii* to depths of about 1.5, 1.3, 1.5, and 2.0 m, respectively (Rundel and Gibson 1996 [DIRS 103614], p. 99, Figure 4-10). These four species are common at Yucca Mountain and are often dominant or primary species in vegetation associations in the area (Section D2.2). Rundel and Nobel (1991 [DIRS 128001], pp. 355 to 357) described the architecture of root systems for several desert plant species and provide community rooting profiles for shrub species in three Mojave Desert locations (California, Mid Hills, and Granite Mountains). The rooting profiles were determined from excavations of root systems and were provided for the following species that are important at Yucca Mountain: *Ericameria cooperi* (synonymous with *Haplopappus cooperi*), roots to 1.4 m; *Ericameria teretifolia* (synonymous with *Chrysothamnus teretifolius*), roots to 1.8 m; *Hymenoclea salsola*, roots to 2 m; *Eriogonum fasciculatum*, roots to 0.9 m; *Menodora spinescens*, roots to 1.2 m; and *Salazaria mexicana*, roots to 0.80 m.

Using measurements of soil water content beneath shrubs, Yoder and Nowak (1999 [DIRS 177167], p. 91, Figure 6) showed that deep roots of *L. tridentata*, *A. dumosa*, and *E. nevadensis* extracted soil water uniformly to depths of 1.2, 1.8, and 2.0 m, respectively (depths rounded to nearest tenth of a meter). The study was conducted over a three-year time period on eight study sites at the NTS. Volumetric soil water content was measured with a neutron probe at 0.2 m depth increments to the depth of the access tubes (about 2 m) (Yoder and Nowak 1999 [DIRS 177167], pp. 82 to 83). The authors suggested that the soil moisture extraction patterns indicated that even though rooting densities decrease significantly with depth, deep roots are important for soil water uptake and may contribute to long-term survival of desert plants (Yoder and Nowak 1999 [DIRS 177167], pp. 93 to 94).

Hansen and Ostler (2003 [DIRS 177619], pp. 49 to 65) estimated rooting depth for several native shrub species on the NTS. Rooting depth estimates were made using a conversion factor established from correlations between plant height and maximum root depth. The conversion factor was established in previous NTS studies (Hansen and Ostler 2003 [DIRS 177619], p. 43). Rooting depths were estimated as part of an effort to reduce uncertainties in performance assessment models that were developed for the Area 5 Radioactive Waste Management Site (RWMS) and the Area 3 RWMS. The vegetation in Area 5 and surrounding landscape was classified as a Larrea–Ambrosia association (Hansen and Ostler 2003 [DIRS 177619], p. 17). Because of the high amount of human-caused disturbance in Area 3 and the immediate vicinity, three plots at various distances were selected to represent vegetation (Hansen and Ostler 2003 [DIRS 177619], pp. 18 to 19). One of the plots was located in a Grayia–Lycium association, one in a Larrea–Grayia–Lycium association, and one in an Atriplex–Krascheninnikovia association. Vegetation characteristics were collected for *L. tridentata, Acamptopappus shockleyi, A. dumosa, H. salsola, Atriplex confertifolia, A. canescens, E. nevadensis, L. andersonii, Krascheninnikovia lanata, Grayia spinosa, Artemisia spinescens, Chrysothamnus viscidiflorus, Menedora spinescens,* and *Krameria erecta* (Hansen and Ostler 2003 [DIRS 177619], pp. 49, 52, 55, 58, 62, and 65). These species also commonly occur at Yucca Mountain. The ranges of estimated maximum rooting depths based on above-ground information collected for these species were

0.96 to 1.15 m for Area 5 and 0.72 to 1.8 m for Area 3 (Hansen and Ostler 2003 [DIRS 177619], p.85, Table 7-1).

In a review of maximum rooting depths of species found in eleven major terrestrial biomes, Canadell et al. (1996 [DIRS 177626]) compiled information from direct observations of roots in road cuts, mine shafts, open-cut mines, and trenches. For deserts, they included a rooting depth of 2.0 m for *C. viscidiflorus* growing at a study site in Idaho (Canadell et al. 1996 [DIRS 177626], p. 588, Appendix 1). Soils for this area were classified as aeolian sandy loam (Canadell et al. 1996 [DIRS 177626], p. 588, Appendix 1), similar to those in a subset of vegetation associations found at Yucca Mountain (CRWMS M&O 1998 [DIRS 104589], pp. 5, 9, and 10). While climatic conditions vary between the Idaho site and Yucca Mountain, both are considered arid to semi-arid environments, and genetic potential for reaching maximum rooting depths to 2 m was demonstrated for *C. viscidiflorus*.

Schenk and Jackson (2002 [DIRS 177638], p. 481 to 482) collected more than 1,300 records on rooting depths for individual plants from literature sources for a variety of arid to semi-arid ecosystems and for several vegetation growth forms. They found that maximum rooting depths of shrubs in xeric environments receiving 125 to 250 mm of precipitation were about 5 m (Schenk and Jackson 2002 [DIRS 177638], p. 491, Figure 9). In a study on woody plant invasions of grasslands, Jackson et al. (2002 [DIRS 177171], p. 624, Table 1) showed that desert plants at a study site in Jornada, New Mexico (mean annual precipitation = 230 mm) extracted nutrients from depths of at least 3 m.

Rooting depths for *B. tectorum* ranged from about 0.5 m to 2.0 m (Harris 1967 [DIRS 177630], p. 97, Figure 6; Hulbert 1955 [DIRS 177129], pp. 190 to 195; Link et al. 1990 [DIRS 177142], p. 512; Rickard 1985 [DIRS 177635], p. 170; Foxx et al. 1984 [DIRS 177628], p. 6, Table 3). Hulbert (1955 [DIRS 177129], pp. 190 to 195) studied root systems of bromegrasses using pit excavations, lithium chloride tracers, and soil moisture depletion. He found that the depth of *B. tectorum* roots ranged from about 0.75 to 2.0 m. Foxx et al. (1984 [DIRS 177628], p. 5, Table 3) reported a range of 0.3 to 1.10 m for *B. tectorum* rooting depths and Harris (1967 [DIRS 177630], p. 97, Figure 6) excavated roots of *B. tectorum* to depths of 1.1 m. In brome dominated communities in eastern Washington, Rickard (1985 [DIRS 177635], p. 170) reported that roots were inefficient at extracting soil moisture from below about 0.5 m. This result was similar to those reported by Link et al. (1990 [DIRS 177142], p. 512) with *B. tectorum* roots in natural stands to depths of 0.45 m.

Parameter Development—Based on the literature search, mean maximum rooting depths for desert shrubs was 1.6 m and ranged from 0.5 m to 5.0 m (Table 6.5.3.2-1). In general, root density decreases exponentially with depth. However, studies showed that Mojave desert shrubs used all the water available down to about 2 m (Yoder and Nowak 1999 [DIRS 177167], p. 91, Figure 6) and desert plants extracted nutrients from depths of 3 m (Jackson et al. 2002 [DIRS 177171], p. 624, Table 1), suggesting the potential importance of roots to deep water removal from the soil system at Yucca Mountain. In the MASSIF model, the depths of shallow soils on rocky slopes and the crest at Yucca Mountain control rooting depth (i.e., actual rooting depths are the lesser of maximum rooting depth and soil depth). However, soil depths for alluvium at Yucca Mountain (mean = 16.4 m for Soil Depth Class 2 and minimum = 40 m for Soil Depth Class 1; see Section 6.5.2, Table 6.5.2.4-4) exceed the genetic potential for rooting

depths of desert shrubs. The MASSIF model does not account for spatial variability in rooting depth. For each model run, one maximum rooting depth is selected for the entire model domain. Therefore, to avoid assignment of an extreme rooting depth to the entire model domain, the distribution ranges (for all climate states) were defined by means and standard deviations.

For Present-Day and Monsoon climate states, a nominal value of 1.6 m is used for maximum rooting depth (mean of values in Table 6.5.3.2-1). A uniform distribution with lower and upper bounds of 0.6 m and 2.6 m, respectively (the nominal value ±1 standard deviation, Table 6.5.3.2-1), is used for model uncertainty and sensitivity studies.

Table 6.5.3.2-1. Rooting Depths for Present-Day and Monsoon Climates

Reference	Vegetation and Associated Rooting Depths
Canadell et al. 1996 [DIRS 177626], p. 588, Appendix 1	*Chrysothamnus viscidiflorus* = 2.0 m
Hansen and Ostler 2003 [DIRS 177619], p. 85, Table 7-1	Area 5 RWMS[a] = 1.2 m Area 3 RWMS = 1.8 m
Jackson et al. 2002 [DIRS 177171], p. 624, Table 1	Desert shrubs = 3 m
Rundel and Gibson 1996 [DIRS 103614], p. 99, Figure 4-10	*Ambrosia dumosa* = 1.3 m *Ephedra nevadensis* = 1.5 m *Larrea tridentata* = 1.5 m *Lycium andersonii* = 2.0 m
Rundel and Nobel 1991 [DIRS 128001], pp. 355 to 357	*Ericameria cooperi* = 1.4 m *Ericameria teretifolia* = 1.8 m *Eriogonum fasciculatum* = 0.9 m *Hymenoclea salsola* = 2 m *Menodora spinescens* = 1.2 m *Salazaria mexicana* = 0. 80 m
Schenk and Jackson 2002 [DIRS 177638], p. 491, Figure 9	Maximum for xeric shrubs = 5.0 m
Yoder and Nowak 1999 [DIRS 177167], p. 91, Figure 6	*Larrea tridentata* = 1.2 m *Ambrosia dumosa* = 1.8 m *Ephedra nevadensis* = 2.0 m
Harris 1967 [DIRS 177630], p.97, Figure 6	*Bromus tectorum* (cheatgrass) = 1.1 m
Hulbert 1955 [DIRS 177129], p.191	*Bromus tectorum* = 2.0 m
Link et al. 1990 [DIRS 177142], p. 512	*Bromus tectorum* = 0.5 m
Rickard 1985 [DIRS 177635], p.170	*Bromus tectorum* = 0.5 m
Foxx et al. 1984 [DIRS 177628], p. 6, Table 3	*Bromus tectorum* = 1.1 m
	Mean = 1.6 m
	Standard Deviation = 0.95
	Range = 0.5 to 5.0 m
Recommended Distribution Parameters: Nominal Value = 1.6 m; Range = Uniform from 0.6 to 2.6 m	

[a] The maximum of the reported range was used.

Mean Maximum Rooting Depth for the Glacial Transition Climate State—Precipitation and temperatures predicted for the glacial transition climate state could support open juniper woodland/sagebrush vegetation assemblages (Section 6.5.3.1). This is based on historical biogeography of the Mojave Desert and tolerance ranges for common plants in Great Basin juniper woodland/sagebrush vegetation assemblages (see Section 6.5.3.1). Common Great Basin species that are currently present at Yucca Mountain, or within a reasonable migration distance,

were selected to represent future climate vegetation for establishing mean maximum rooting depth (Table 6.5.3.2-2).

Literature Review—Foxx et al. (1984 [DIRS 177628]) obtained means and ranges of rooting depths for several Great Basin species from an extensive bibliographic study that contained 1034 different rooting citations. Common Great Basin grasses that are currently present at Yucca Mountain and likely to occur under glacial transition climate conditions included *Achnatherum hymenoides* (previous nomenclature: *Oryzopsis hymenoides*), *Poa* spp., *Stipa comata,* and *Bromus tectorum* (Foxx et al. 1984 [DIRS 177628], p. 5, Table 3). (See the Present-Day and Monsoon climates section above for review of *B. tectorum* rooting depths.) *Achnatherum hymenoides*, *Poa* spp. and *S. comata* were reported to have relatively deep rooting depths with ranges of 0.45 to 1.22 m, 0.35 to 2.13 m, and 0.63 to 1.68 m, respectively (Table 6.5.3.2-2). The upper limit of these ranges, rounded to nearest tenth, was used to represent maximum rooting depths for these grasses (Table 6.5.3.2-2). Foxx et al. (1984 [DIRS 177628]) also included rooting depths for two common Great Basin shrubs (*Ericameria nauseosa* [previous nomenclature: *Crysothamnus nauseosus*] and *Artemesia tridentata*), and two trees (*Juniperus monosperma* and *Pinus edulis*) that are likely to occur in an open juniper woodland. Mean rooting depths reported for these species were used instead of the upper limit of the ranges. This was necessary because the reported upper limits were extremes that were much deeper than any other reports for these species and therefore not very likely to occur. The mean rooting depths for *E. nauseosa* and *A. tridentata* were 2.9 and 2.5 m, respectively (Table 6.5.3.2-2). The mean rooting depth for both *J. monosperma* and *P. edulis* was 6.4 m (Table 6.5.3.2-2). In a review of the botanical characteristics of *Juniperus osteosperma*, Zlatnik (1999 [DIRS 177639], p. 7) reported a rooting depth of 4.5 m (Table 6.5.3.2-2). In a review of the botanical characteristics of *P. edulis*, Anderson (2002 [DIRS 177625], p. 5) reported a rooting depth of 6.0 m (Table 6.5.3.2-2). The reviews by Zlatnik (1999 [DIRS 177639]) and Anderson (2002 [DIRS 177625]) were parts of the USDA Forest Service sponsored database: Fire Effects Information System (FEIS). The FEIS database contains comprehensive literature reviews of several hundred plant species that are thoroughly documented with complete bibliographies.

In a review of maximum rooting depths by Canadell et al. (1996 [DIRS 177626], p. 588, Appendix 1), which is described in the previous section, rooting depths were included for *A. tridentata* growing at study sites in Colorado and Idaho. The maximum rooting depths reported for this species were 1.8 and 2.3 m (Table 6.5.3.2-2). In a study on water transport between soil layers at a site in Utah, Richards and Caldwell (1987 [DIRS 177927], p. 488) determined that roots of *A. tridentata* occurred to depths of about 2 m. In another study of water transport through soils by roots of *A. tridentata*, Ryel et al. (2002 [DIRS 177632], p. 760) reported roots to 3.4 m. Sturges and Trlica (1978 [DIRS 177928]) excavated roots of *A. tridentata* from different positions on a north facing hillside at a study site in south central Wyoming. They found that *A. tridentata* roots at the lower and midslope sites extended into the 1.8 to 2.1 m sampling depth (Sturges and Trlica 1978 [DIRS 177928], p. 1,283). Roots tended to be shallower at the ridge location (1.2 to 1.5 m). The upper limits of the ranges for lower and midslope sites were used in this analysis (Table 6.5.3.2-2).

Parameter Development—A nominal value of 2.5 m is used for maximum rooting depth for the glacial transition climate state. This is the mean value of rooting depths in Table 6.5.3.2-2. A uniform distribution with a lower bound of 1.0 m and an upper bound of 4.0 m (mean ± one

standard deviation rounded to the nearest meter) is used for model uncertainty and sensitivity studies. The lower bound value of 1 m is equal to the mean of the rooting depths for the *Bromus tectorum* listed in Table 6.5.3.2-2, and therefore this distribution includes the possibility of a brome monoculture during the glacial transition climate period.

Table 6.5.3.2-2. Maximum Rooting Depth for the Glacial Transition Climate State

Reference	Plant Species	Reported Rooting Depth (m)	Rooting Depth Used in Distribution (m)[a]
Foxx et al. 1984 [DIRS 177628], p. 5, Table 3	*Achnatherum hymenoides*	0.45 to 1.22	1.2
Foxx et al. 1984 [DIRS 177628], p. 6, Table 3	*Artemisia tridentata* (big sagebrush)	2.5 [b]	2.5
Richards and Caldwell 1987 [DIRS 177927], p. 488	*Artemisia tridentata*	2.0	2.0
Sturges and Trlica 1978 DIRS 177928], p. 1,283	*Artemisia tridentata*	1.8 to 2.1	2.1
Canadell et al. 1996 [DIRS 177626], p. 588, Appendix 1	*Artemisia tridentata*	1.8 2.3	1.8 2.3
Ryel et al. 2003 [DIRS 177632], p.760	*Artemisia tridentata*	3.4	3.4
Seyfried et al. 2005 [DIRS 178060], pp. 282 to 283	*Artemisia tridentata*	1.7	1.7
Harris 1967 [DIRS 177630], p. 97, Figure 6	*Bromus tectorum* (cheatgrass)	1.1	1.1
Hulbert 1955 [DIRS 177129], p. 191	*Bromus tectorum*	1.0 to 2.0	2.0
Link et al. 1990 [DIRS 177142], p. 512	*Bromus tectorum*	0.45	0.5 (rounded)
Rickard 1985 [DIRS 177635], p. 170	*Bromus tectorum*	0.5	0.5
Foxx et al. 1984 [DIRS 177628], p. 5, Table 3	*Bromus tectorum*	0.30 to 1.10	1.1
Canadell et al. 1996 [DIRS 177626], p. 588 Appendix 1	*Chrysothamnus viscidiflorus* (green rabbitbrush)	2.0	2.0
Foxx et al. 1984 [DIRS 177628], p. 6, Table 3	*Ericameria nauseosa* [b]	2.9 [b]	2.9
Leffler et al. 2004 [DIRS 177926], p. 10, Figure 1	*Ericameria nauseosa* [b]	1.3	1.3
Foxx et al. 1984 [DIRS 177628], p. 6, Table 3, p. 18	*Juniperus monosperma* (utah juniper)	6.4 [b]	6.4
Zlatnik 1999 [DIRS 177639], p. 7	*Juniperus osteosperma*	4.5	4.5
Foxx et al. 1984 [DIRS 177628], p. 6, Table 3, p. 18	*Pinus edulis* (pinyon pine)	6.4	6.4
Anderson 2002 [DIRS 177625], p. 5	*Pinus edulis* (pinyon pine)	6.0	6.0
Foxx et al. 1984 [DIRS 177628], p. 5, Table 3	*Poa* spp.	0.35 to 2.13	2.1
Foxx et al. 1984 [DIRS 177628], p. 5, Table 3	*Stipa comata*	0.63 to 1.68	1.7
		Mean	2.5
		Standard Deviation	1.8
		Range	0.50 to 6.4
Recommended Distribution Parameters: **Nominal Value = 2.5 m; Distribution = Uniform from 0.7 to 4.3 m.**			

[a] Maximum of range.
[b] Mean rooting depth.

6.5.3.3 Plant Height

Mean plant height (h_{plant}) is used in Equation 76 from FAO-56 (Allen et al. 1998 [DIRS 157311], p. 149) to calculate the fraction of soil surface that is covered by vegetation (f_c). The f_c is one of the parameters used to calculate the evaporation component ($K_e \times ET_0$) in the soil water balance model (see Section 6.4). Mean plant height distributions and nominal values for the different climate states are developed in this section. Based on potential composition of vegetation in future climates (Section 6.5.3.1), one distribution for plant height was developed for the Present-Day and Monsoon climates, and a separate distribution was developed for the glacial transition climate.

Mean Plant Height for Present-Day and Monsoon Climate States—Several years of intensive ecological studies were conducted in Rock Valley and other areas of the Nevada Test Site under the International Biological Program (IBP) Desert Biome Program and were continued through research funded by the U.S. Department of Energy (DOE) and the University of California, Los Angeles. Rundel and Gibson (1996 [DIRS 103614]) describe these studies and the ecological communities and processes at Rock Valley and other locations on the NTS. Several characteristics of vegetation associations were studied including woody plant height.

Mean shrub heights for a variety of vegetation associations in Mojave, transition, and Great Basin desert locations reported by Rundel and Gibson (1996 [DIRS 103614], p. 89, Table 4.2) were used to develop mean plant heights for Present-Day and Monsoon climate states (Table 6.5.3.3-1). Shrub heights were collected from 68 permanent plots that were established on the NTS in 1963. Data reported from four of the associations (*Artemisia tridentata*-pinyon-juniper*, Artemisia nova,* and two *Artemisia nova*-pinyon-juniper) were not used in calculation of mean plant height because those associations do not occur on Yucca Mountain. This resulted in mean plant height values from 25 Mojave Desert sites, 24 transition desert sites, and six Great Basin Desert sites (Rundel and Gibson 1996 [DIRS 103614], p. 89, Table 4.2).

Table 6.5.3.3-1. Mean Plant Height for Present-Day and Monsoon Climates

Vegetation Association	Mean Plant Height (m)
Larrea–Ambrosia	0.34
Larrea–Lycium–Grayia	0.51
Larrea–Grayia–Lycium	0.47
Larrea–Atriplex	0.27
Larrea–Psorothamnus	0.41
Menodora–Ephedra	0.25
Larrea–Grayia–Lycium	0.47
Grayia–Lycium	0.38
Coleogyne	0.39
Coleogyne–Larrea–Grayia–Lycium	0.46
Coleogyne–Grayia–Lycium	0.39
Larrea–Atriplex–Coleogyne	0.35
Coleogyne–Grayia–Artemisia	0.47
Larrea–Lycium shockleyi–Atriplex	0.22
Lycium shockleyi–Atriplex	0.25

Table 6.5.3.3-1. Mean Plant Height for Present Day and Monsoon Climates (Continued)

Vegetation Association	Mean Plant Height (m)
Lycium pallidum–Grayia	0.59
Atriplex confertifolia	0.29
Atriplex–Kochia	0.21
Atriplex–Ceretoides	0.3
Atriplex canescens (lower elevation)	0.36
Atriplex canescens (higher elevation)	0.44
Artemisia tridentata	0.58
Mean	0.38
Standard Deviation	0.11
Range	0.21 to 0.59
Recommended Distribution Parameters: **Nominal Value = 0.40 m; Distribution = Uniform from 0.20 to 0.60 m**	

Source: Rundel and Gibson 1996 [DIRS 103614], p. 89, Table 4.2.

A nominal value of 0.4 m, based on the mean of values in Table 6.5.3.3-1 (rounded to the nearest tenth of meter), is recommended as the nominal value for average plant height for Present-Day and Monsoon climates. A uniform distribution with a lower bound of 0.2 m and an upper bound of 0.6 m is recommended for model sensitivity studies. The upper and lower bounds were determined from the range of average heights (rounded to the nearest tenth of a meter) in Table 6.5.3.3-1.

Mean Plant Height for the Glacial Transition Climate State—Precipitation and temperatures predicted for the glacial transition climate state could support open juniper woodland/sagebrush vegetation assemblages (Section 6.5.3.1). This is based on historical biogeography of the Mojave Desert and tolerance ranges for common plants in Great Basin juniper woodland/sagebrush vegetation assemblages (see Section 6.5.3.1). Common Great Basin species that are currently present at Yucca Mountain, or within a reasonable migration distance, were selected to represent future climate vegetation for establishing mean plant height (Table 6.5.3.2-2).

No single comprehensive source for plant height was available for common Great Basin Desert vegetation associations, and only one peer reviewed article reporting plant height was located in the literature search. Therefore, United States Department of Agriculture (USDA) divisions and university extensions that provided fact sheets on Great Basin plant species in Nevada and Utah were used (Table 6.5.3.3-2). Where a range of height values were reported for a species, the midpoint of the range was used to develop the nominal value and distribution limits (Table 6.5.3.3-2).

Junipers and/or pinyon pines rarely make up more than 10% to 15% cover in open woodlands. To account for this, a weighted mean and weighted range were calculated from the data in Table 6.5.3.3-2 using a weighting factor of 0.10 for juniper and pinyon heights, and 0.90 for the remaining vegetation. This resulted in a mean plant height of 1.3 m with a range of 0.64 to 1.8 m (Table 6.5.3.3-2). A uniform distribution with a nominal value of 1.3 m, a lower bound of 0.64 m, and an upper bound of 1.8 m is recommended for use in the MASSIF model.

Table 6.5.3.3-2. Plant Height for the Glacial Transition Climate State

Reference	Plant Species	Reported Height (m)	Height Used in Distribution (m)[a]
USDA 2002 [DIRS 178073], p. 2[b]	*Artemisia tridentata* (big sagebrush)	0.6 to 1.2	0.9
Schultz and McAdoo 2002 [DIRS 178065], p. 2	*Artemisia tridentata* (big sagebrush)	0.9 to 1.2	1.1
Tirmenstein 1999 [DIRS 177641], p. 1	*Artemisia tridentata* (big sagebrush)	0.9 to 3.0[c]	2.0
Tirmenstein 1999 [DIRS 177642], p.1	*Ericameria nauseosa* [d] (rubber rabbitbrush	0.3 to 2.3	1.3
Utah State University, Cooperative Extension 2002 [DIRS 177644], p. 2	*Ericameria nauseosa* (rubber rabbitbrush	0.3 to 2.3	1.3
Weber et al. 1993 [DIRS 177931], p. 1	*Ericameria nauseosa* (rubber rabbitbrush)	0.3 to 1.8	1.1
Zlatnik 1999 [DIRS 177639], p. 7	*Juniperus osteosperma* (Utah juniper)	3.0 to 8.0	5.5
Utah State University, Cooperative Extension 2004 [DIRS 177643], p. 1	*Juniperus osteosperma*	4.6	4.6
Utah State University, Cooperative Extension 2002 [DIRS 177646], p. 2	*Pinus monophylla* (singleleaf pinyon)	3.0 to 9.0	6.0
Stewart and Hull 1949 [DIRS 177146], pp. 58 to 59	*Bromus tectorum* (cheatgrass)	0.3 to 0.6	0.5
Utah State University, Cooperative Extension 2002 [DIRS 177647], p. 1	*Poa secunda* (Sandberg bluegrass)	0.3	0.3
Utah State University, Cooperative Extension 2002 [DIRS 177648], p. 2	*Stipa comata* (needle-and-thread grass)	0.1 to 0.3	0.2
Utah State University, Cooperative Extension 2002 [DIRS 177649], p. 2	*Achnatherum hymenoides* (Indian ricegrass)	0.3 to 0.8	0.6
Utah State University, Cooperative Extension 2002 [DIRS 177650], p. 2	*Elymus elymoides* (squirreltail)	0.2 to 0.5	0.4
Recommended Distribution Parameters: **Weighted Mean = 1.3[e]; Weighted Range = Uniform from 0.64 to 1.8 m[f]**			

[a] When ranges for heights were reported, the midpoint of the range was used to calculate distribution parameters.
[b] USDA = United States Department of Agriculture.
[c] Five m was reported as a maximum height for *A. tridentata*. However, this height is rarely reached and would not be supported by habitat conditions at Yucca Mountain. Therefore, the common range of 0.9 to 3.0 m that was reported was used here.
[d] Previous nomenclature: Chrysothamnus nauseosus.
[e] Weighted mean calculated as $(0.1 \times [5.5 + 4.6 + 6.0 / 3]) + (0.9 \times [0.9 + 1.1 + 2.0 + 1.3 + 1.3 + 1.1 + 0.5 + 0.3 + 0.2 + 0.6 + 0.4 / 11] = 1.3$ m.
[f] Lower limit = $(0.10 \times 4.6) + (0.90 \times 0.2) = 0.64$, upper limit = $(0.1 \times 6.0) + (0.90 \times 1.3) = 1.8$.

6.5.3.4 Method for Estimating Basal Transpiration Coefficients for the Infiltration Modeling Domain

The MASSIF model requires a certain set of inputs in order to calculate basal transpiration coefficients (K_{cb} values), which are necessary for calculating evapotranspiration (ET) for the model domain. The purpose of this section is to describe the methodology used to estimate K_{cb} for each model grid cell as a function of location, day of the year, and annual precipitation. This calculation is done within the MASSIF model, but the description of the calculation is given here, rather than in Section 6.4.4, because the methodology is specific to the analysis of Yucca Mountain net infiltration rather than general to any area. All model inputs for this calculation are identified in this section and described in more detail in following sections and appendices referenced herein.

Basal transpiration coefficients estimated using FAO-56 methods and the normalized difference vegetation index (NDVI) based on satellite reflectance data are commonly used to estimate ET for agricultural crops (e.g., Kustas et al. 1994 [DIRS 176757]; Seevers and Ottman 1994 [DIRS 176764]; Szilagyi et al. 1998 [DIRS 176839]; Szilagyi 2002 [DIRS 176840]). They are used here to establish a K_{cb} estimation model based on NDVI derived from satellite data for the MASSIF model domain.

Multiple satellite images taken throughout the growing season of three representative years (wet, moderate, and dry) are used to estimate vegetation vigor represented by NDVI at each 30 × 30-m grid cell in the model domain. Using precipitation records, water year (WY) 1998 (wet), WY2001 (average), and WY2000 (dry) were identified for use (Section E1.5). WY1998 and WY2000 were selected because they represented record wet and dry years and were needed to establish timing of plant responses and a baseline of minimum plant activity for the Yucca Mountain area (Section E1.5). Vegetation expression during the record wet year (WY1998) was sufficiently robust for determining an "ideal" curve for annual vegetation response. WY2001 was chosen to represent an average precipitation year at Yucca Mountain.

Chlorophyll, responsible for the green color of plants, absorbs red light while leaf tissue reflects highly in near infrared (Buschmann and Nagel 1993 [DIRS 176736]). NDVI is determined from the differences of reflected light in the red (R) and near infrared (NIR) spectra, normalized over the sum of the two:

$$NDVI = (NIR - R) / (NIR + R) \qquad \text{(Eq. 6.5.3.4-1)}$$

NDVI is an indicator of vegetation vigor often used for measurement of environmental response to landscape-scale hydrology, including global climate change (e.g., Running and Nemani 1991 [DIRS 176819]), rainfall (e.g., Wang et al. 2003 [DIRS 176761]) and ET (e.g., Kustas et al. 1994 [DIRS 176757]; Seevers and Ottman 1994 [DIRS 176764]; Szilagyi et al. 1998 [DIRS 176839]; Szilagyi 2002 [DIRS 176840]). NDVI has been established as a competent surrogate for estimation of ET (Kustas et al. 1994 [DIRS 176757]; Seevers and Ottman 1994 [DIRS 176764]; Szilagyi et al. 1998 [DIRS 176839]; Szilagyi 2002 [DIRS 176840]). It is used here to characterize timing and magnitude of vegetation response to precipitation, and to capture spatial dynamics in ET related to slope, azimuth, elevation, and soil characteristics of each of the grid cells in the infiltration modeling domain. NDVI was determined for selected days during the

growing season using satellite imagery of the infiltration model domain (Section E2). The resulting values were corrected for differing atmospheric conditions between satellite overpasses and for specific ground conditions characterizing the Yucca Mountain environment, including the presence of desert varnish on rocks, which affects the NDVI signal (Sections 6.5.3.5 and E2).

The analysis of NDVI data for Yucca Mountain focused on two phenomena. The first is that the timing of the vegetation response in a mountainous region is affected by the slope and azimuth of the land. For example, plants on south facing slopes tend to begin their growing season before plants on north facing slopes due to warmer conditions earlier in the season. The second phenomenon is that the potential for vegetation varies by location. This variation is due to a number of factors including local soil and weather conditions. NDVI data is very useful for comparing the amount of vegetation present at each of the model grid cells, because it represents a "snapshot" of each cell at the same period in time. Observations can be compared through time by comparing different images.

6.5.3.4.1 NDVI Timing as a Function of Slope and Azimuth of the Ground Surface

NDVI varies with time reflecting the amount of green biomass present during the growing season. This temporal profile varies depending on the slope and azimuth of the land. To characterize this effect, NDVI from a representative wet year (1998) was extracted from two subregions that distinguished north-facing slopes from south-facing slopes in the uplands of Yucca Mountain (Section E3). Smooth functions were fit to NDVI versus time for these two subregions giving an NDVI value for each day of the water year (October 1 through September 30). Data from north and south facing slopes were used to estimate NDVI profiles for slope and azimuth bins between these orientations. These derived data are input to the K_{cb} calculation in the form of an NDVI look-up table (Output DTN: SN0606T0502206.012, *Daily_NDVI_Estimation.xls*) embedded in the MASSIF Mathcad model. The look-up table has 365 rows representing days of the water year and 25 columns representing different slope and azimuth bins. The development of this table is described in more detail in Sections 6.5.3.5 and E3.

6.5.3.4.2 Potential Vegetation Response (PVR) and Precipitation Adjustments

The NDVI dataset was also used to define a spatial parameter called potential vegetation response (PVR) that represents each grid cell's potential for vegetation cover given sufficient annual precipitation. Cells with high PVR values support conditions that lead to vigorous vegetation, such as sufficient soil, water, and nutrient availability. Cells with low PVR values do not support much vegetation due to the lack of necessary soil, water, or nutrients. The development of PVR values for the Yucca Mountain infiltration model domain is described in Sections 6.5.3.5 and E4. The values are listed in the geospatial input files (Output DTN: SN0606T0502206.011).

WY1998 was chosen for fitting all simulation parameters, including PVR, NDVI slope/azimuth response curves, and a precipitation ratio for scaling the magnitude of the vegetation response (Section E1.5 discusses the rationale for selecting this year). To simulate the strength of the vegetation response, the response curve is scaled using the total annual precipitation. This is

accomplished by using the ratio of the annual precipitation of the year in question to the annual total WY1998 precipitation (Sections E5 and 5).

6.5.3.4.3 Basal Transpiration Coefficient (K_{cb})

NDVI data is ideal for identifying vegetation patterns over large areas, especially when it would be impossible to make a similar number of observations on the ground. However, in order to use NDVI as an indicator of K_{cb} values, it is necessary to compare NDVI data with vegetation measurements made on the ground.

As discussed in Section 6.4.4, the MASSIF model uses a dual transpiration coefficient ($K_c = K_{cb} + K_e$) in conjunction with reference evapotranspiration (ET_0) to estimate actual evapotranspiration (ET) (Allen et al. 1998 [DIRS 157311], p. 135, Equation 69). This dual transpiration coefficient consists of a basal transpiration component (K_{cb}), representing plant transpiration under non-limiting water conditions, and an evaporation component (K_e; see Section 6.4.4). This approach can be applied to natural vegetation using measured values of leaf area index (LAI, a unitless measure of leaf area per ground area) or effective ground cover (percent of ground covered by vegetation) and adjustments for stomatal control (Allen et al. 1998 [DIRS 157311], pp. 187 to 193).

Measurements of vegetation cover that were made at a set of ecological study plots (ESPs) at Yucca Mountain during a period that included three representative water years (wet, average precipitation, and dry) were used to calculate K_{cb} values using FAO-56 methods (Allen et al. 1998 [DIRS 157311], pp. 187 to 193). The resulting K_{cb} profiles (or K_{cb} curves) are time-based and relate to ground conditions at the ESPs for the three representative years. The development of these profiles (Output DTN: MO0606SPABASAL.001) is described in Section 6.5.3.6 and Appendix D.

6.5.3.4.4 Estimating K_{cb} in the MASSIF Infiltration Model

A K_{cb} represents the amount of water that could be used by a stand of vegetation if water were not limiting (Allen et al. 1998 [DIRS 157311], p. 135). It is used in the MASSIF infiltration model with K_e and ET_0 to estimate actual evapotranspiration for each of the model grid cells for each daily time step according to the following equation (Allen et al. 1998 [DIRS 157311], p. 135, Equation 69):

$$ET_{cell} = ET_o \times \left(K_s K_{cb} + K_e\right) \qquad \text{(Eq. 6.5.3.4-1)}$$

where ET_{cell} is actual ET for a model grid cell on a given day and K_s is a stress coefficient (0 to 1) that reduces ET when soil water is limiting (Section 6.4.4). During dry periods or periods when plants are not actively transpiring, ET_{cell} is dominated by evaporation. When plants are physiologically active, transpiration becomes important.

The MASSIF infiltration model predicts K_{cb} from NDVI'[1] for each grid cell for each day of the year through the following steps:

1. A "base" NDVI' ($NDVI'_{base}$) is identified from the NDVI look-up table based on the day of year (row) and the cell's specific slope and azimuth values (column). This "base" NDVI' value accounts for the variation in the timing of the vegetation response due to the slope and azimuth of the cell (Sections 6.5.3.4.1, 6.5.3.5, and E3). This base value represents NDVI' in 1998 for a cell with PVR = 1, and the slope and azimuth in the same bin as the cell of interest.

2. The base NDVI' value is adjusted for PVR developed for each grid cell ($NDVI'_{base,pvr}$) (Sections 6.5.3.4.2, 6.5.3.5, and E4). This step accounts for spatial variability of vegetation.

$$NDVI'_{base,pvr} = NDVI'_{base} \times PVR_{cell} \qquad \text{(Eq. 6.5.3.4-2)}$$

3. The base NDVI' adjusted for PVR ($NDVI'_{base,pvr}$) is adjusted for precipitation to account for variations between yearly precipitation amounts ($NDVI'_{base,pvr,ppt}$) (Sections 6.5.3.5 and E5).

$$NDVI'_{base,pvr,ppt} = NDVI'_{base,pvr} \frac{PPT_{YR}}{PPT_{1998}} \qquad \text{(Eq. 6.5.3.4-3)}$$

where PPT_{YR} is the annual precipitation for the water year of interest, which is calculated within MASSIF from the weather input file (Appendix G), and PPT_{1998} is the annual precipitation for the water year 1998 (Output DTN: SN0606T0502206.012, *NDVI'_correct_to_90,91,93.xls*, sheet: "Precip_Ratios," cell: C22).

4. $NDVI'_{base,pvr,ppt}$ values are converted to cell values of K_{cb} (Kcb_{cell}) using a linear function derived in Section 6.5.3.7 as follows:

$$Kcb_{cell} = NDVI'_{base,pvr,ppt} \times C_{Kcb2} + C_{Kcb1} \qquad \text{(Eq. 6.5.3.4-4)}$$

C_{Kcb1} is the intercept and C_{Kcb2} is the slope of the linear function relating NDVI' and K_{cb} developed in Section 6.5.3.7.

6.5.3.5 NDVI' Look-up Table and PVR Parameter Development

This section summarizes the development of the NDVI' look-up table and the values of PVR for each cell in the model domain. The discussion is a summary of Appendix E, in which the details of this development are described.

[1] NDVI' is NDVI corrected for differing atmospheric conditions between satellite overpasses and for specific ground conditions characterizing the Yucca Mountain environment, including the presence of rock varnish. This correction is described in Sections 6.5.3.5 and E2.

6.5.3.5.1 Direct Inputs

Direct inputs used to develop the NDVI' look-up table and the values of PVR are:

- Landsat TM (thematic mapper) images of the infiltration model domain (DTN: SN0601ALANDSAT.001 [DIRS 177239])
- Precipitation for WYs 1990, 1991, 1993 (Output DTN: MO0607SEPTOTAL.003), 1998, 2000, and 2001 (Output DTN: MO0602SPAPRECP.000)
- Geospatial data including input to PVR, slope and azimuth of model grid cells, ESP location coordinates, etc.

Digital Ortho Quarter Quad (DOQQ)	DTN: SN0601DOQQYM98.001 [DIRS 177240]
Shuttle Radar Topography	DTN: SN0601SRTMDTED.001 [DIRS 177242]
Ground Control Points	DTN: MO0512COV05112.000 [DIRS 177249]
	DTN: MO9906GPS98410.000 [DIRS 109059]
ESP Location Coordinates	DTN: MO9901ESPYMNYE.000 [DIRS 177247]

6.5.3.5.2 Development of NDVI' Look-up Table

Selected scenes from a 20-year archive of Landsat TM were chosen as the basis for characterizing large-scale Yucca Mountain vegetation patterns. Table 6.5.3.5-1 lists the images chosen for three representative water years (dry [2002], moderate [2001], and wet [1998]).

Table 6.5.3.5-1. Landsat TM Data Used for Characterization of Yucca Mountain Vegetation

WY1998		WY2001		WY2002	
Filename	Sensor	Filename	Sensor	Filename	Sensor
t519971102	TM5	t520001009	TM5	t720011207	TM7
t519980121	TM5	t520010129	TM5	t720020124	TM7
t519980310	TM5	t520010318	TM5	t720020225	TM7
t519980411	TM5	t520010419	TM5	t720020329	TM7
t519980427	TM5	t520010505	TM5	t720020414	TM7
t519980529	TM5	t520010606	TM5	t720020430	TM7
t519980630	TM5	t520010724	TM5	t720020516	TM7
t519980716	TM5	t520011012	TM5	t720020601	TM7
t519980817	TM5	t720001220	TM7	t720020617	TM7
		t720010326	TM7	t720020719	TM7
		t720010630	TM7	t720020804	TM7
		t720010817	TM7		
		t720011004	TM7		

Source: DTN: SN0601ALANDSAT.001 [DIRS 177239].

NOTE: Filenames list satellite, year, month, and day.

Two Landsat satellites were available for the periods of interest, TM5 and TM7 (Section E2.1). The basic processing steps are summarized as follows:

1. Reflectance data from the scenes listed in Table 6.5.3.5-1 were used to calculate NDVI from Equation 6.5.3.4-1 for each pixel of each scene. Pixel size of TM data is approximately 28 × 28 m.

2. NDVI was then corrected for atmospheric differences between scenes and the images were geocorrected using a set of ground control points (DTN: MO0512COV05112.000 [DIRS 177249]) (Sections E2.2 and E2.3). Geocorrection ensures that pixels on each image overlie each other so that differences in pixels between scenes can be identified.

3. The NDVI values were scaled to calculate $NDVI_{offset}$, which is calculated as:

$$NDVI_{offset} = NDVI - NDVI_0 \qquad \text{(Eq. 6.5.3.5-1)}$$

   where NDVI is the atmospheric and geocorrected NDVI and $NDVI_0$ is the NDVI expected in areas with no vegetation (Section E2.4).

4. A positive NDVI signal arising from desert varnish that was present on many exposed rocks in the area was subtracted to get NDVI' for time steps throughout the growing season for the three water years. NDVI' represents a clean and coherent vegetation signal from the TM data To remove the effect of rock varnish, $NDVI_{offset}$ values from the lowest vegetation period of the driest year were subtracted from the other scenes (Section E2.6):

$$NDVI'_i = NDVI_{offset-i} - NDVI_{offset-min-i} \quad \text{(Eq. 6.5.3.5-2)}$$

where *i* refers to the i^{th} pixel and *min* refers to NDVI expression during a very dry year when vegetation response would be near zero.

The effects of slope and azimuth on NDVI' values over time for WY1998 were determined by extracting NDVI' from two subregions of pixels with either north- or south-facing slopes (Section E3.2). The NDVI' values from these subregions (Section E3.2) were fit with smooth curves and extended to other subregions of slope and azimuth by geometric interpolation (Figure 6.5.3.5-1). These curves represent NDVI' values for WY1998 and are referred to as "base" NDVI'.

Base NDVI' values for each day of the water year defined for 13 unique classes of slope and azimuth were organized into a table for use as direct input to the infiltration model (Section E3, Table E-4; Output DTN: SN0606T0502206.012, *Daily_NDVI_Estimation.xls*). Each of the model grid cells was assigned a slope-azimuth class (Section E3). Based on the slope-azimuth class, the model assigns the corresponding base NDVI' for the WYDOY from Table E-4 to each grid cell.

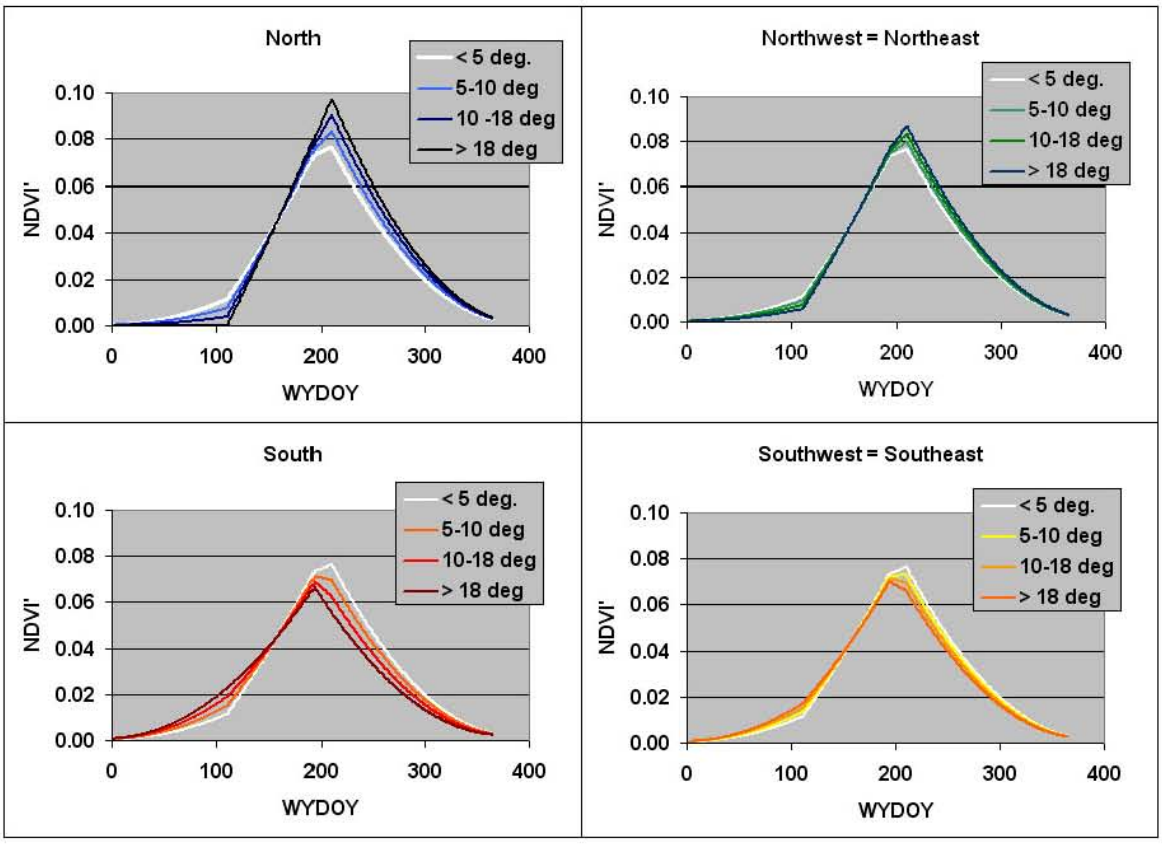

Source: Output DTN: SN0606T0502206.012, *Daily_NDVI_Estimation.xls*.

NOTE: There are 13 unique combinations of curves. The curve representing level ground (<5°) and E and W slopes is reproduced (white) in each graph.

Figure 6.5.3.5-1. Temporal Curves Developed by the Weighting Functions in Table E-4

6.5.3.5.3 Development of the Potential Vegetation Response for Each Grid Cell in the Model Domain

PVR was used to scale each model grid cell to the strength of the vegetation response for the actual conditions in that cell (Section E4) and was calculated as:

$$PVR_i = [(\text{average } NDVI_{offset})_{max} - (\text{average } NDVI_{offset})_{min}]_i / \text{average } NDVI_{1-i}$$

(Eq. 6.5.3.5-3)

where

$i = i^{th}$ model grid cell
max = wet year
min = dry year
average_{1-i} = average of grid cells, from the 1st to the i^{th}, within the area of interest.

The denominator of PVR, the average value of grid cells within the area of interest, normalized the results for a subset area overlying the proposed repository. This area was chosen as a rectangle of 12,702 grid cells (11.43 km^2) (Figure 6.5.3-2). Normalization provided scaling to permit better understanding of PVR distribution: a PVR of 1.0 represents the approximate average vegetation response overlying the repository. PVR varies from 0 (no vegetation response) to about 4 (see Section E4 for determination and verification of PVR). Figure 6.5.3.5-2 shows a map of PVR values for most of the infiltration modeling domain.

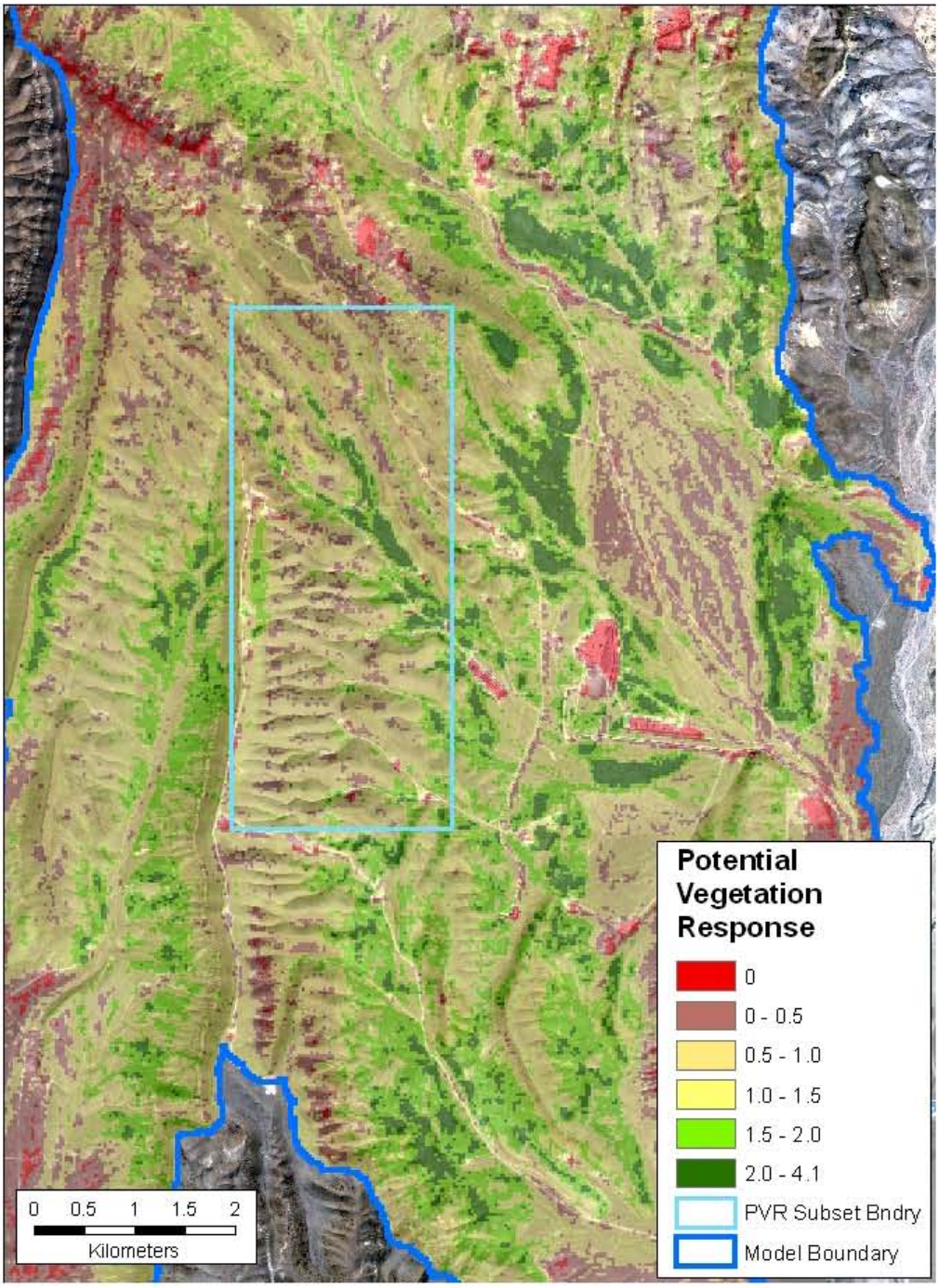

NOTE: The PVR data is one of the MASSIF Spatial Data inputs, Output DTN: SN0606T0502206.011. The other files are *PVR_subset_.evf* and *nad27_boundary_evf* in Output DTN: SN0608NDVIAUXD.001. Background is Quickbird DTN: SN0601QBSAT802.001 [DIRS 177241].

Figure 6.5.3.5-2. Map of Potential Vegetation Response for the Central Region of the Infiltration Modeling Domain

WY1998 was chosen for fitting all simulation parameters, including PVR, NDVI' look-up table, and a precipitation ratio for scaling the magnitude of the base NDVI' response. WY1998 is an ideal choice as the very high level of precipitation induced a maximal NDVI' response. This maximal response corresponds to a strong "signal" in an environment that generally has a weak vegetation signal, hence boosting the signal-to-noise ratio.

Methods are used in Appendix E to correct for non-systematic variation in NDVI parameters (Section E2.4). Analyses are performed in Appendix E to confirm the appropriateness of NDVI' processing parameters (Section E2.5) and the NDVI' algorithm (Section E7) to increase confidence in the values used in the MASSIF model. Additionally, uncertainties associated with calculation of NDVI' are addressed in Section E7.4.

6.5.3.6 Determination of K_{cb} from Ground Cover Measurements Made at Ecological Study Plots

This section provides a brief description of the calculation of K_{cb} values for a set of ecological study plots (ESPs), representing three vegetation associations, for three representative years (wet, moderate, and dry). These K_{cb} values are then used in Section 6.5.3.7 to determine appropriate parameter values to use to convert grid-cell values of NDVI' to K_{cb} values required for the calculation of evapotranspiration. Details of K_{cb} calculations and development of inputs are in Appendix D.

The FAO-56 K_{cb} profile for agricultural crops reflects transpiration under optimal growth and non-limiting water conditions. The generalized K_{cb} profile (Figure 6.5.3.6-1) includes four growth stages (Allen et al. 1998 [DIRS 157311], pp. 95 to 96): an initial growth stage (planting date to approximately 10% ground cover), a development stage (10% ground cover to effective full cover), a mid-season stage (effective full cover to start of maturity), and a late season stage (maturity to harvest or senescence). Effective full cover is defined as the time when soil shading is nearly complete (Allen et al. 1998 [DIRS 157311], p. 95). Transpiration coefficients are developed for the initial growth stage ($K_{cb\ ini}$), the mid-season stage ($K_{cb\ mid}$), and the end of the late season stage ($K_{cb\ end}$) (Figure 6.5.3.6-1). The curve is constructed by drawing straight line segments through each of the four growth stages (Figure 6.5.3.6-1).

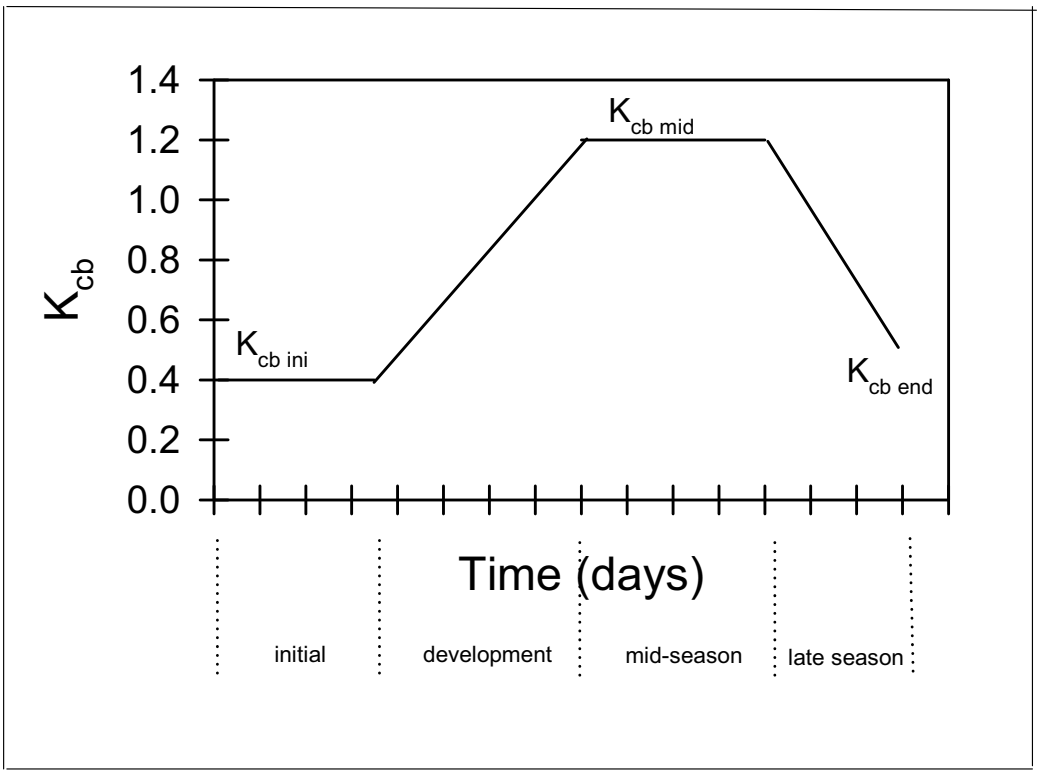

Source: Allen et al. 1998 [DIRS 157311], p. 100, Figure 26.

Figure 6.5.3.6-1. Generalized Crop Coefficient Curve

Characteristics of desert vegetation at Yucca Mountain differ from agricultural crops in several ways, including low effective ground cover that rarely exceeds 30% during peak growth periods (CRWMS M&O 1996 [DIRS 102235], p. 23), little morphological change in perennial vegetation across growth stages (e.g., little change in average maximum vegetation height and maintenance of a percentage of green canopy throughout the year), and greater degree of stomatal control resulting in lower rates of water loss compared to agricultural crops. Additionally, desert vegetation assemblages consist of a variety of plant species that have different growth stage lengths and contribute differently to total ground cover when compared to agricultural crops that are generally planted in monocultures. Climatic conditions at Yucca Mountain differ from standard FAO-56 conditions, with lower minimum relative humidity (RH_{min}) and higher wind speeds (u_2). To account for these differences, FAO-56 methods for calculating K_{cb} for natural vegetation using effective ground cover, adjustments for stomatal control over water loss, and adjustments for local RH_{min} and u_2 were used (Allen et al. 1998 [DIRS 157311], pp. 187 to 193; see Appendix D for details).

6.5.3.6.1 Vegetation Reference Areas

The flora and climate of Yucca Mountain have been described as characteristically Mojavean (Beatley 1975 [DIRS 103356]; 1976 [DIRS 102221]), with vegetation on the crest and upper slopes that is transitional to Great Basin Desert flora (Beatley 1976 [DIRS 102221]). Vegetation communities at Yucca Mountain have been characterized by a number of authors (e.g., Beatley 1976 [DIRS 102221]; O'Farrell and Collins 1984 [DIRS 102160]; CRWMS M&O 1996 [DIRS 102235]) and have often been described in terms of associations. Using a simple classification scheme, the vegetation at Yucca Mountain can generally be delineated into four associations named for dominant or co-dominant species: *Coleogyne* (COL), *Larrea-Ambrosia* (LA), *Lycium-Grayia* (LG), and *Larrea-Lycium-Grayia* (LLG) (CRWMS M&O 1996 [DIRS 102235], pp. 7 to 8, Table 2-1).

The LA, LG, and LLG vegetation associations are the most common in the infiltration model domain. The LG association is representative of the vegetation that overlies the proposed repository on the upper slopes and crest of Yucca Mountain (elevation = 1,300 to 1,600 m; DTN: MO9907SADESYYM.000 [DIRS 177169]). The LLG association is representative of the vegetation of mid-elevation intermountain valleys within the infiltration modeling domain (1,150 to 1,300 m; DTN: MO9907SADESYYM.000 [DIRS 177169]). The LA association is representative of low elevation vegetation within the infiltration modeling domain (940 to 1,150 m, DTN: MO9907SADESYYM.000 [DIRS 177169]). The LG association is considered critically important to the infiltration modeling effort because the vegetation is representative of that overlying the proposed repository where infiltration to interred waste casks could occur. Vegetation cover and plant species composition data from the LA, LG, and LLG vegetation associations were used to develop K_{cb} profiles over time using FAO-56 methods. K_{cb}s estimated for the LG association are used to develop the least-squares regression between K_{cb} and NDVI' as described in Section 6.5.3.7. K_{cb}s estimated for the LA, LLG, and LG associations are used to evaluate appropriateness of NDVI' (Sections E2 and E7) and to determine whether the magnitude of K_{cb}s is appropriate for desert vegetation (Section D7).

Parameter Inputs – Direct inputs to K_{cb} calculations were:

- Species-specific cover data and species composition from the ESPs collected in 1990, 1991, and 1993 (Output DTN: MO0606SPAVEGAS.001). Cover data (per species) were averaged over the 12 ESPs per association for each year. Total cover for annual, drought deciduous, and evergreen vegetation was determined for the LA, LG, and LLG associations and used as input to K_{cb} calculations. See Section D2.2 for description of annual, drought deciduous, and evergreen vegetation types.

- Growth stage lengths for annual, drought deciduous, and evergreen vegetation (Section D3.2.1).

- Plant height for LA, LG, and LLG associations (Section D3.2.1).

- Stomatal resistance for dominant species within annual, drought deciduous, and evergreen vegetation types (Section D3.2.3).

- Mean daily wind speed and air temperature, and minimum daily relative humidity from Yucca Mountain Meteorological Site 1 for WY1998, WY2000, and WY2001 (Output DTN: MO0602SPAWEATH.000). Minimum relative humidity (RH_{min}) and wind speed (u_2) adjustments to K_{cb}s were from the same water years as were used for NDVI' determinations. Adjustments in K_{cb}s invoked by RH_{min} and u_2 were small compared to variation in K_{cb}s among years, vegetation types, and associations (see Section D3.2.4).

- The psychrometric constant (γ) for the elevation of Yucca Mountain Meteorological Site 1 from Allen et al. (1998 [DIRS 157311], p. 214, Table 2.2).

These inputs are developed in Section D3.2.

Vegetation cover and species composition, needed for K_{cb} calculations, were measured on the ESPs during peak growth periods from 1989 to 1994 (Section D2.2). Vegetation cover at Yucca Mountain is largely dependent on precipitation; therefore, precipitation records for the ESPs from 1989 to 1994 were evaluated to determine wet, normal, and dry years that could be paired with the years that NDVI' were determined for (Section D2.2). Based on precipitation records, vegetation cover and species composition data were used from the following three years in K_{cb} calculations: WY1991 (average), an average precipitation year for the Yucca Mountain area (about 150 mm; CRWMS M&O 1996 [DIRS 102235], p. 21, Figure 4-3); WY1993 (wet), the highest precipitation year on record for the years that cover data were collected (about 240 mm; CRWMS M&O 1996 [DIRS 102235], p. 21, Figure 4-3); and WY1990 (dry), the lowest precipitation year on record for the years that cover data were collected (about 60 mm; CRWMS M&O 1996 [DIRS 102235], p. 21, Figure 4-3). For verification of NDVI processing parameters, wet, dry, and average precipitation years from the two data sets (NDVI' and K_{cb}) were paired by normalizing and scaling NDVI' using annual precipitation. For the K_{cb} − NDVI' regression, wet and average years from the two data sets were paired. The dry year was not used in the K_{cb} − NDVI' regression because the vegetation signal for 2002 was essentially zero throughout the year for the LG association (Section E7.1).

Profiles of K_{cb} versus day of year (Figure 6.5.3.6-2) were calculated from these direct inputs using equations from FAO-56 (Allen et al. 1998 [DIRS 157311], Chapter 9). These calculations are discussed in detail in Appendix D.

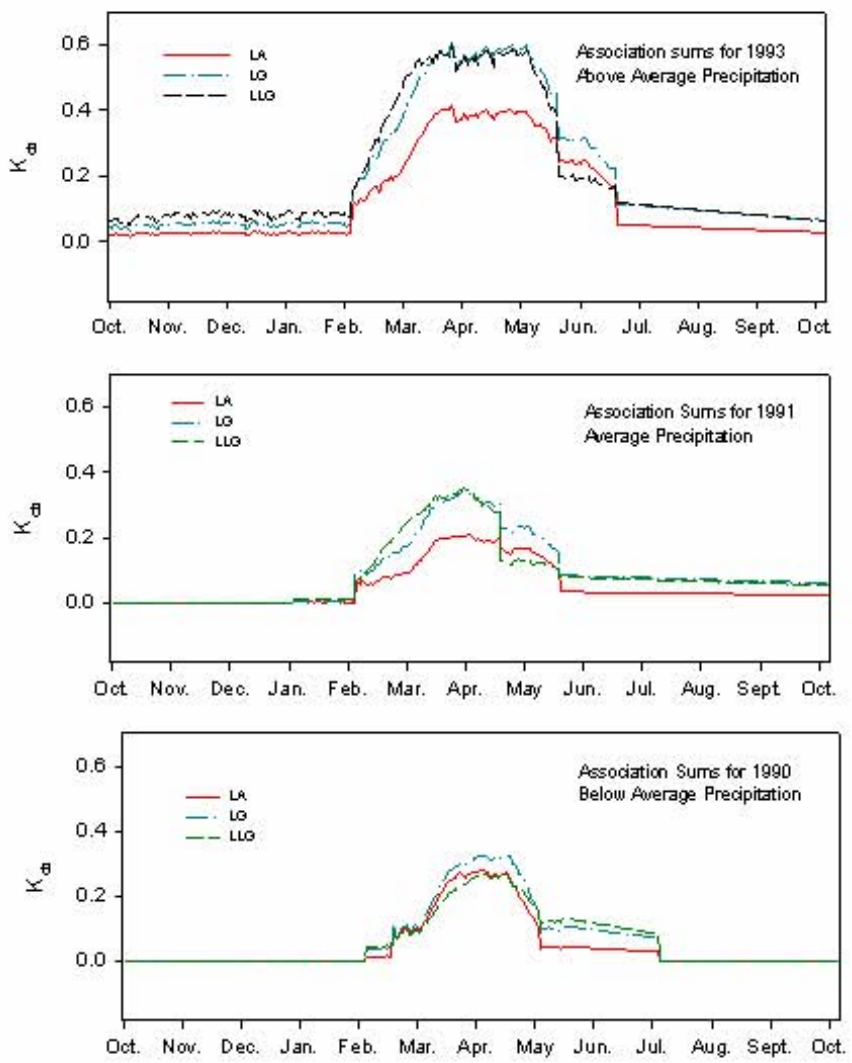

Source: Output DTN: MO0606SPABASAL.001.

Figure 6.5.3.6-2. Transpiration Coefficient (K_{cb}) Profiles for LA, LG, and LLG Vegetation Associations for Water Years 1993, 1991, and 1990

Use of separate K_{cb} − NDVI' regressions for each vegetation association would require that each model grid cell be assigned to one of the three associations. This was not feasible due to lack of detailed spatial data for vegetation associations and the potential for vegetation change through time. As an alternative to using separate K_{cb} − NDVI' regressions for each association, and for use in uncertainty analyses, upper and lower bounds for K_{cb}s were calculated for the LG association profiles for WY1991 and WY1993. Upper and lower bounds for daily K_{cb}s were determined for each profile by using high and low input values for vegetation cover, plant height, and stomatal resistance (Figure 6.5.3.6-3). The high and low values were taken from the input data sets. See Section D4 for selection of inputs and details of calculations. The uncertainty bounds for the LG association K_{cb} profiles encompassed the variation observed among associations (compare Figures 6.5.3.6-2 and 6.5.3.6-3). Therefore, the K_{cb}s with uncertainty bounds for WY1993 and WY1991 for the LG association (Figure 6.5.3.6-3) are recommended

for use in K_{cb} − NDVI regressions for the Yucca Mountain area. The upper and lower bounds of the profiles are used in Section 6.5.3.7 to calculate standard uncertainties for the LG association K_{cb} profiles.

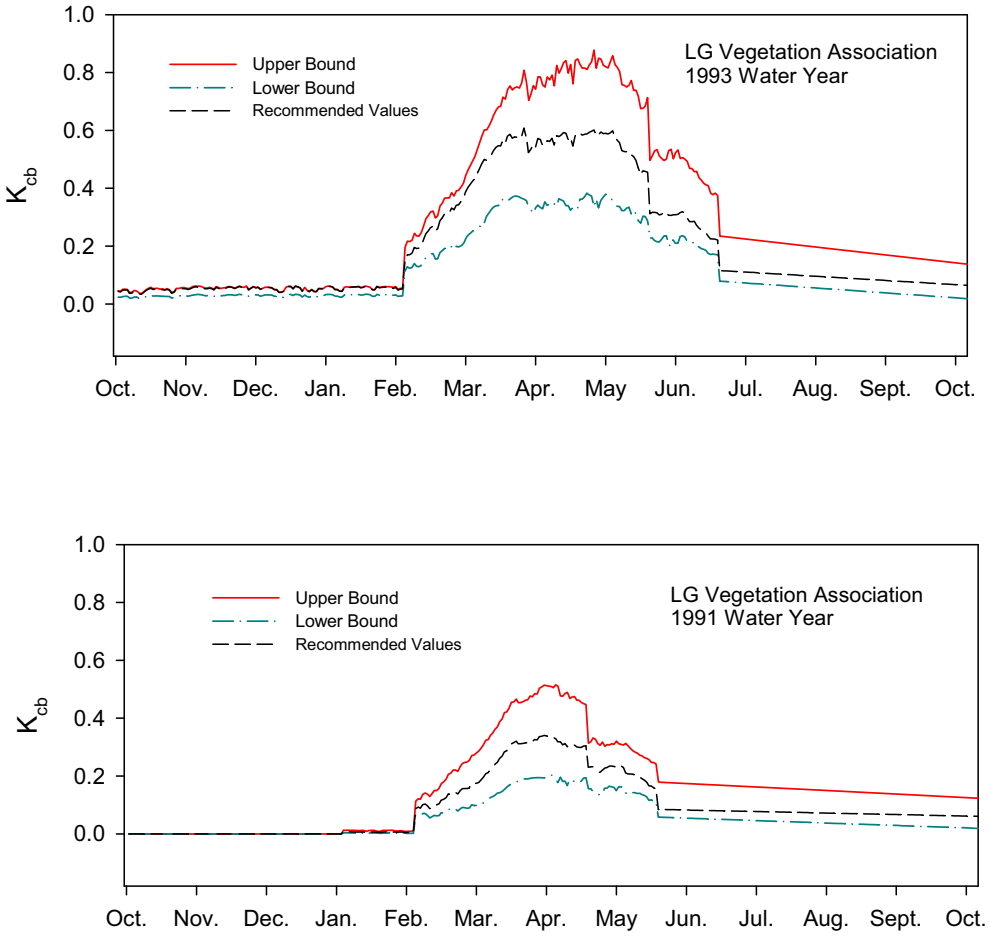

Source: Output DTN: MO0606SPABASAL.001.

NOTE: Recommended values are the same as those for the LG association for WY1993 and WY1991 in Figure 6.5.3.6-2.

Figure 6.5.3.6-3. Transpiration Coefficient Profiles for LG Vegetation Associations with Upper and Lower Bounds

6.5.3.7 Correlating K_{cb} Profiles with NDVI'

In order to implement the FAO-56 methodology for estimating evapotranspiration at Yucca Mountain, it was necessary to estimate values for basal transpiration coefficients (K_{cb}) as a function of NDVI corrected for the Yucca Mountain environment (NDVI'). NDVI is widely used by researchers to estimate green biomass, leaf area index (LAI), and patterns of productivity in both agricultural and natural ecosystems. Among other factors, transpiration coefficient values are dependent on LAI or cover of vegetation, both of which are dependent on precipitation. Several studies have demonstrated a strong linear relationship between transpiration coefficients and NDVI for agricultural crops (e.g., Duchemin et al. 2006

[DIRS 178498]; Tasumi et al. 2005 [DIRS 177653]; Bausch and Neale 1987 [DIRS 177652]; Ray and Dadhwal 2001 [DIRS 177336]). Verification analyses of the NDVI' algorithm (Sections E7.2 and E7.3) showed strong linear relationships between estimated K_{cb}s and simulated NDVI', and between average percent ground cover data collected during peak growth and simulated peak NDVI' for the ecological study plots (ESPs) at Yucca Mountain. Based on evidence that the K_{cb} − NDVI relationship is generally linear, a least-squares method was selected to fit a linear relationship to the K_{cb}s and NDVI' developed for Yucca Mountain.

The method of minimizing Chi squared (χ^2) as described by Bevington and Robinson (1992 [DIRS 147076], Chapter 6) was used to define a linear fit to the data in the form:

$$y(x) = a + bx \qquad \text{(Eq. 6.5.3.7-1)}$$

where

$y(x)$	=	estimated K_{cb}
a	=	y-intercept
b	=	slope of the regression line
x	=	NDVI' for a model grid cell

The slope and intercept parameters (a and b, respectively) are used as model input to the analysis of net infiltration. Their values and their associated uncertainties are developed in this section.

6.5.3.7.1 Use in the Infiltration Model

The slope and intercept parameters that define the linear fit between K_{cb} and NDVI' are used in the MASSIF model to predict K_{cb} from NDVI' for each model grid cell. The predicted K_{cb} is used in the calculation of evapotranspiration for each model grid cell. See Section 6.5.3.4.4 for a discussion of where and how these parameters are used in the calculation.

6.5.3.7.2 Parameter Development

Transpiration coefficient profiles (Appendix D) and NDVI' (Appendix E) developed for *Lycium-Grayia* (LG) ESPs were used in this analysis. As described in Section 6.5.3.6.1, the LG vegetation association was chosen because it best represents the type of vegetation that is present directly above the repository footprint.

Parameter Inputs—Direct inputs to the intercept and slope parameters were K_{cb}, NDVI', and water year precipitation data sets (Output DTNs: MO0606SPABASAL.001, MO0607SEPTOTAL.003, and MO0602SPAPRECP.000). Measured NDVI' data for 1998 (wet year) and 2001 (average precipitation year) were paired with the wet (1993) and average precipitation (1991) years for which K_{cb}s were estimated. The dry year (2002) was not included in the fitting analysis because the vegetation response measured by NDVI' was essentially zero throughout the year on the LG plots (Figure E-26). This minimal response was due to the exceptionally low amount of precipitation that fell that year (about 34 mm). Measured NDVI'

was scaled to 1993 and 1991 with a modified version of Equation E-8 that used the precipitation ratio for each of the two paired years:

$$NDVI'_{j1993} = NDVI'_{j1998} \times \frac{\sum WY\ 1993\ precip.}{\sum WY\ 1998\ precip.} \qquad \text{(Eq. 6.5.3.7-2)}$$

$$NDVI'_{j1991} = NDVI'_{j2001} \times \frac{\sum WY\ 1991\ precip.}{\sum WY\ 2001\ precip.} \qquad \text{(Eq. 6.5.3.7-3)}$$

where:

j = j^{th} day of the water year

Σ WY = sum of water year precipitation

Precipitation ratios were determined from the average water year precipitation for Yucca Mountain Meteorological Sites 2, 3, and 4 (Table 6.5.3.7-1). These sites were chosen because they represent a range of elevations at Yucca Mountain and variation in precipitation at those elevations.

Satellite images were chosen to establish vegetation responses throughout the water year (Section E2.1). For the LG sites, nine images were processed for 1998 and ten images were processed for 2001 (Section E2.1). The resulting NDVI' values were multiplied by the precipitation ratios to get the scaled NDVI' values used in the regression analysis (Table 6.5.3.7-2).

Table 6.5.3.7-1. Water Year Precipitation Totals, Means, and Ratios for Water Years 1991, 1993, 1998, and 2001

	Wet Years		Average Years	
Monitoring Site	1998 Pcp [a] (mm)	1993 Pcp (mm)	2001 Pcp (mm)	1991 Pcp (mm)
Site 2	369.32	261.87	186.18	91.56
Site 3	402.59	240.92	204.22	121.73
Site 4	360.93	248.67	192.28	99.05
Mean [b]	377.61	250.49	194.23	104.11
Ratio [c]	0.6633		0.5360	

Source: Output DTNs: MO0607SEPTOTAL.003 and MO0602SPAPRECP.000.

[a] Precipitation total for water year.
[b] Mean water year total for Sites 2, 3, and 4.
[c] Ratios of water year precipitation for wet years and average precipitation years.

Table 6.5.3.7-2. NDVI' Estimated for the LG Ecological Study Plots Scaled for Water Years 1993 and 1991

WY DOY[a]	Date of Satellite Image	NDVI' for WY 1998[b]	Scaled NDVI' for WY 1993[c]
33	11/2/97	0.0067	0.0044
113	1/21/98	0.0271	0.0180
161	3/10/98	0.0558	0.0370
193	4/11/98	0.0859	0.0570
209	4/27/98	0.0924	0.0613
241	5/29/98	0.0724	0.0480
273	6/30/98	0.0376	0.0249
289	7/16/98	0.0186	0.0123
321	8/17/98	0.0234	0.0155
WY DOY[a]	**Date of Satellite Image**	**NDVI' for WY 2001[b]**	**Scaled NDVI' for WY 1991[d]**
9	10/9/00	0.0168	0.0090
81	12/20/00	0.0237	0.1270
169	3/18/01	0.0472	0.0253
177	3/26/01	0.0539	0.0289
201	4/19/01	0.0773	0.0414
217	5/5/01	0.0490	0.0263
249	6/6/01	0.0277	0.0148
273	6/30/01	0.0218	0.0117
297	7/24/01	0.0202	0.0108
321	8/17/01	0.0166	0.0089

[a] WY DOY = Water year day of year.
[b] Output DTN: SN0606T0502206.012, *NDVI'_correct_to_90,91,93.xls*.
[c] NDVI' × precipitation ratio, where ratio = 0.6633 (from Table 6.5.3.7-1).
[d] NDVI' × precipitation ratio, where ratio = 0.5360 (from Table 6.5.3.7-1).

Figures 6.5.3.7-1 and 6.5.3.7-2 show the relationship between profiles of estimated K_{cb} and measured NDVI' as a function of time for the wet and average precipitation years. The uncertainties in these data are shown on the plots as upper and lower bounds for the K_{cb} profiles and as standard uncertainties (± one standard deviation) for the NDVI' values. See Appendices D and E for details about how uncertainty was estimated.

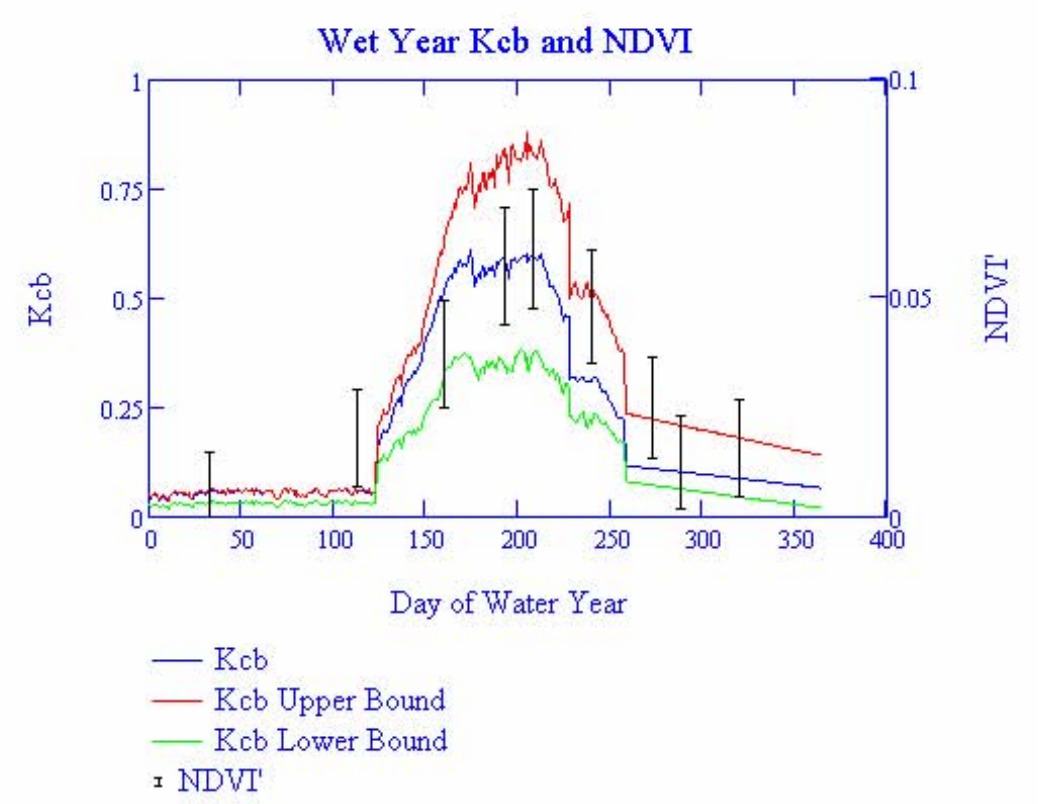

Source: Output DTNs: MO0606SPABASAL.001 and SN0606T0502206.012.

Figure 6.5.3.7-1. Comparison of Estimated K_{cb} and Precipitation-Scaled NDVI' for the LG Vegetation Association for a Wet Year

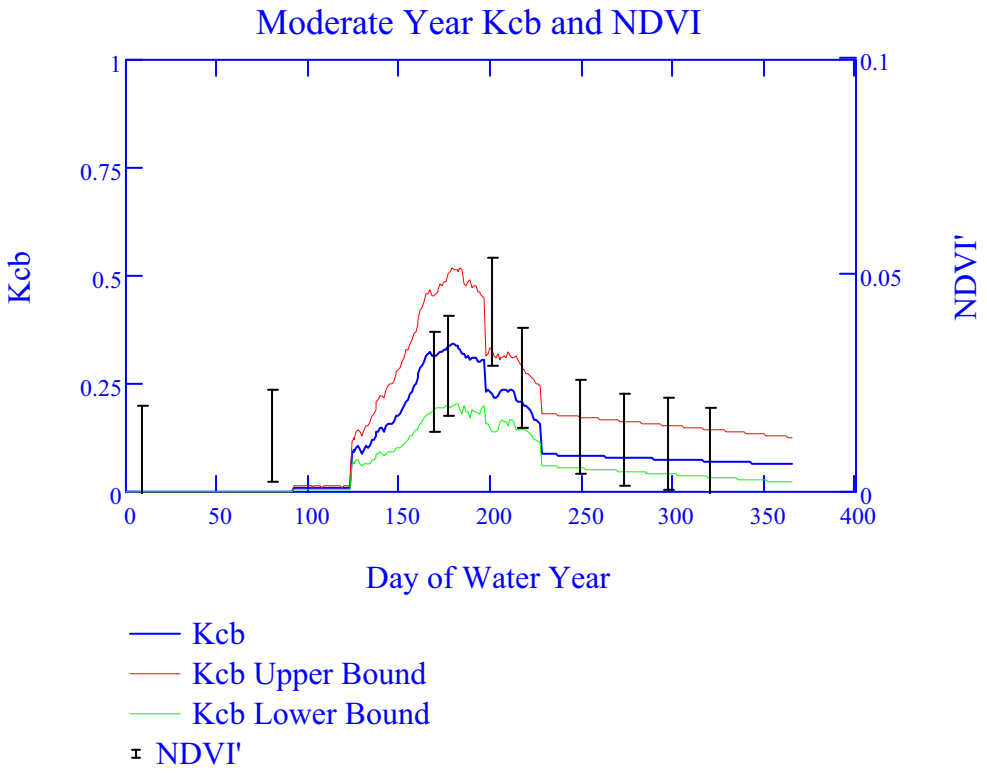

Source: Output DTNs: MO0606SPABASAL.001 and SN0606T0502206.012.

Figure 6.5.3.7-2. Comparison of Estimated K_{cb} and Precipitation Scaled NDVI' for the LG Vegetation Association for an Average Precipitation Year

Transpiration coefficients for the days that NDVI' was determined in the two water years were extracted from Output DTN: MO0606SPABASAL.001 (Table 6.5.3.7-3). These values and the corresponding NDVI' values were used in the regression analysis.

Table 6.5.3.7-3. Transpiration Coefficients (K_{cb}) with Standard Deviations for the LG Vegetation Association

WY 1993 DOY [a]	WY 1993 K_{cb}	Std Uncert [b]	WY 1991 DOY [a]	WY 1991 K_{cb}	Std Uncert [b]
33	0.0569	8.353×10^{-3}	9	0	1×10^{-3}[c]
113	0.0554	7.636×10^{-3}	81	0	1×10^{-2}[c]
161	0.5164	0.088	169	0.3112	0.077
193	0.5897	0.145	177	0.3363	0.089
209	0.5887	0.132	201	0.2238	0.055
241	0.3107	0.093	217	0.2057	0.042
273	0.1087	0.044	249	0.0811	0.034
289	0.1010	0.042	273	0.770	0.033
321	0.0855	0.039	297	0.0728	0.033
			321	0.0686	0.032

Source: Output DTN: MO0606SPABASAL.001.

[a] WY DOY = Water Year Day of Year.
[b] Standard Uncertainty for transpiration coefficients (K_{cb}).
[c] Calculated uncertainty was zero and therefore was set to 0.01 as described below and in source DTN.

Standard uncertainties for the individual K_{cb} values in Table 6.5.3.7-3 were based on a uniform distribution between the upper and lower bounds of the profile using the following equation:

$$\sigma(x) = \frac{A - B}{\sqrt{12}} \qquad \text{(Eq. 6.5.3.7-4)}$$

where:

σ = standard deviation
x = K_{cb}
A = upper bound for K_{cb}
B = lower bound for $K_{cb.}$

The derivation of Equation 6.5.3.7-4 is in Output DTN: MO0610SPALINEA.000. Under conditions when the calculated uncertainties were zero (e.g., early in the growing during the average precipitation year; Figure 6.5.3.7-2), the standard uncertainty was set to 0.01. This was done to avoid having to treat zero uncertainties as special cases in the slope and intercept formulas (Equations 6.5.3.7-6 and 6.5.3.7-7). The value of 0.01 was determined by decreasing the standard uncertainty until it had no effect on the final calculated slope value (Output DTN: MO0610SPALINEA.000).

Least Squares Regression Analysis—To determine the least squares fit between K_{cb} and NDVI' in the form of Equation 6.5.3.6-1, the method of minimizing χ^2 was used. In this case, χ^2 is defined as the sum of the weighted, squared deviations in the variable y_i (Bevington and Robinson 1992 [DIRS 147076], pp. 102 to 103, Equation 6.9):

$$\chi^2 = \sum \left[\frac{1}{\sigma_i} \left(y_i - a - b x_i \right) \right]^2 \qquad \text{(Eq. 6.5.3.7-5)}$$

where

σ_i = standard deviation of K_{cb} on the ith day
y_i = K_{cb} on the ith day
a = intercept of the least squares regression equation (Equation 6.5.3.6-5)
b = slope of the least squares regression equation (Equation 6.5.3.6-6)
x_i = NDVI' on the ith day

The following equations were used to determine values of a and b that minimize χ^2 (Bevington and Robinson 1992 [DIRS 147076], p. 104, Equation 6.12):

$$a = \frac{1}{\Delta} \left(\sum \frac{x_i^2}{\sigma_i^2} \sum \frac{y_i}{\sigma_i^2} - \sum \frac{x_i}{\sigma_i^2} \sum \frac{x^i y^i}{\sigma_i^2} \right) \qquad \text{(Eq. 6.5.3.7-6)}$$

$$b = \frac{1}{\Delta} \left(\sum \frac{1}{\sigma_i^2} \sum \frac{x_i y_i}{\sigma_i^2} - \sum \frac{x_i}{\sigma_i^2} \sum \frac{y_i}{\sigma_i^2} \right) \qquad \text{(Eq. 6.5.3.7-7)}$$

$$\Delta = \sum \frac{1}{\sigma_i^2} \sum \frac{x_i^2}{\sigma_i^2} - \left(\sum \frac{x_i}{\sigma_i^2} \right)^2 \qquad \text{(Eq. 6.5.3.7-8)}$$

where

a = intercept of the least squares regression equation
σ_i^2 = variance of K_{cb} on the ith day
y_i = K_{cb} on the ith day
b = slope of the least squares regression equation
x_i = NDVI' on the ith day.

These calculations were performed using Mathcad software and are available in Output DTN: MO0610SPALINEA.000. The resulting slope and intercept for the least squares regression equation were 9.7 and −0.05, respectively (Output DTN: MO0610SPALINEA.000). The K_{cb} and NDVI' data are plotted in Figure 6.5.3.7-3 with the fitted regression line and 95% confidence intervals. Methods for determining uncertainties in a and b are discussed below.

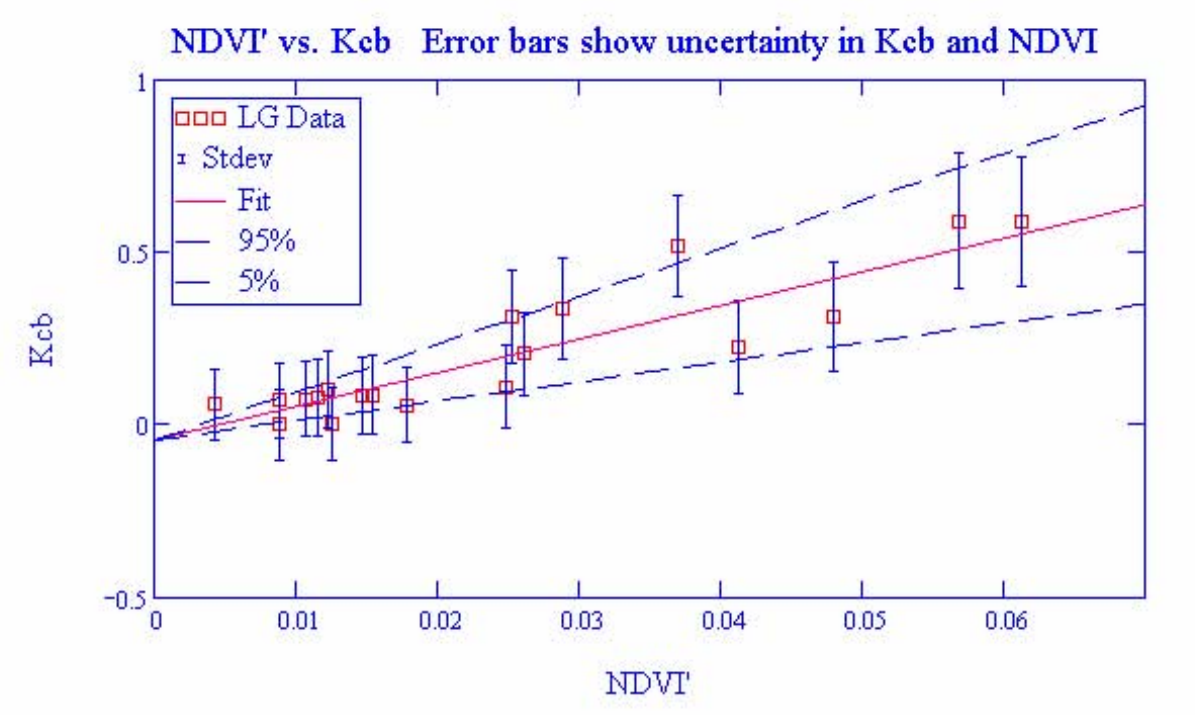

Source: Output DTN: MO0610SPALINEA.000.

Figure 6.5.3.7-3. Linear Relationship between Transpiration Coefficients (K_{cb}) and Normalized Difference Vegetation Indices Corrected for the Yucca Mountain Environment (NDVI')

Parameter Uncertainties and Distributions—Uncertainties in the intercept and slope were calculated as the variance in each parameter based on uncertainties associated with individual estimated points. The following equations were used from Bevington and Robinson (1992 [DIRS 147076], pp. 108 to 109, Equations 6.21 and 6.22):

$$\sigma_a^2 = \frac{1}{\Delta} \sum \frac{x_i^2}{\sigma_i^2} \qquad \text{(Eq. 6.5.3.7-9)}$$

$$\sigma_b^2 = \frac{1}{\Delta} \sum \frac{1}{\sigma_i^2} \qquad \text{(Eq. 6.5.3.7-10)}$$

where

σ_a^2 = variance of the intercept
σ_b^2 = variance of the slope.

The remaining variables are defined above.

Two sources of uncertainty were considered in the calculation of the variance in K_{cb}s used in Equations 6.5.3.7-6 through 6.5.3.7-10 These sources included a direct contribution due to uncertainties in K_{cb}s, and an indirect contribution from uncertainties in NDVI' to the total

uncertainty in predicted K_{cb}s. The following two functions were used from Bevington and Robinson (1992 [DIRS 147076], p. 100, Equations 6.2 and 6.3):

$$\sigma_{yI} = \sigma_x \frac{dy}{dx} \quad \text{(Eq. 6.5.3.7-11)}$$

$$\sigma_y^2 = \sigma_{yI}^2 + \sigma_{yD}^2 \quad \text{(Eq. 6.5.3.7-12)}$$

where

σ_{yI} = indirect uncertainty in K_{cb} due to uncertainties in NDVI'
σ_x = standard deviation of NDVI'
$\frac{dy}{dx}$ = slope of the function y = y(x)
σ_y^2 = combined variance of predicted K_{cb}
σ_{yD}^2 = direct uncertainty due to $K_{cb.}$

An iteration using Mathcad software was performed to determine the appropriate value of $\frac{dy}{dx}$ to use in Equation 6.5.3.7-11 (Output DTN: MO0610SPALINEA.000, *Kcb-NDVI_Regression.xmcd*). The resulting slope that was used in Equation 6.5.3.7-11 was 9.7 (Output DTN: MO0610SPALINEA.000; *Kcb-NDVI_Regression.xmcd*).

The standard deviations calculated for the slope and intercept were 2.1 and 0.05, respectively. These values were used to establish 90% confidence intervals for the least squares regression (Figure 6.5.3.7-3).

Table 6.5.3.7-4 summarizes the recommended values and distributions for the slope and intercept for the regression line for predicting K_{cb} from NDVI' in the MASSIF model. Because the magnitude of the intercept (C_{Kcb1}) is relatively small, it is appropriate to consider this parameter as a constant for the purposes of calculating net infiltration. The reasoning for this is that when K_{cb} is small, its value is controlled by the uncertainty in the value of $K_{c\ min}$ rather than C_{Kcb1}. When K_{cb} is large, its value is controlled by the value of C_{Kcb2}, which has a larger influence and uncertainty than C_{Kcb1}.

Table 6.5.3.7-4. Best-Fit Parameter Values Describing the Relationship between NDVI' and K_{cb}

Parameter Description	Symbol	Nominal Value (mean)	Standard Deviation	Distribution	Climate
Slope between NDVI' and K_{cb}	C_{Kcb2}	9.7	2.1	normal	all
Intercept for linear regression between NDVI' and K_{cb}	C_{Kcb1}	−0.05	0.05	normal	all

6.5.4 Additional Parameter Development

6.5.4.1 Input Parameters for Reference Evapotranspiration Calculations

Reference evapotranspiration (ET_0) is calculated for use in the infiltration model as a function of slope and azimuth using the standardized FAO-56 Penman-Montieth equation (Equation C-37). ET_0 is calculated for reference conditions that are defined for the grass reference crop as a vegetated, clipped, cool-season grass surface having uniform height (0.12 m), is actively growing, and completely shading the ground, with an adequate water supply (Allen et al. 1998 [DIRS 157311], p. 15). This ET_0 represents a near maximum evaporative index that occurs under conditions of high soil water availability to support ET and full vegetation cover (Allen et al. 1998 [DIRS 157311], pp. 7 and 23). The use of the ET_0 definition requires the input of weather data representing a well-watered environment. ET from native vegetation is calculated by multiplying ET_0 by a "crop" or "transpiration" coefficient. The upper limit on this coefficient is 1.2 (Allen et al. 1998 [DIRS 157311], pp. 110 (Table 12) and 189). Several input parameters that may vary with time or conditions are required for this calculation (Table 6.5.4.1-1). These input parameters are described in this section and nominal values and ranges of uncertainty are established.

Table 6.5.4.1-1. Input Parameters for Reference Evapotranspiration

Parameter	Description
$K_{0\,winter}$	Dew point offset from minimum temperature (T_{min}) for winter months
$K_{0\,rest}$	Dew point offset from T_{min} for spring, summer, and fall months
$K_{0\,winter\ start}$	Starting day of year for winter dew point
$K_{0\,winter\ end}$	Last day of year for winter dew point
K_{Rs}	Adjustment coefficient in Hargreaves' radiation formula
α_T	Terrain albedo
G_{sc}	Solar constant (MJ/m^2/min)
K_{cln}	Atmospheric turbidity coefficient

The methods in Appendix C assume that the only weather inputs to the FAO-56 Penman-Montieth equation are maximum and minimum air temperature, which are used to estimate all other needed weather parameters.

Dewpoint Offset (K_0)—Dewpoint temperature (T_{dew}) is used to calculate actual vapor pressure (e_a), which is used in Equation C-37 to calculate ET_0 (see Appendix C and Section 6.4.5.2). Allen et al. (1998 [DIRS 157311], p. 36 and Annex 6, pp. 257 to 262) recommended use of T_{dew} calculated from daily minimum temperature (T_{min}) when humidity data are not available, or when reference conditions are not met at the weather station location. Under humid, well-watered reference conditions, T_{min} is approximately equal to T_{dew} (Allen 1996 [DIRS 176485], pp. 103 to 104, Figure 7). This relationship is well established for reference ET conditions and occurs because condensation of vapor from the air and the corresponding release of latent heat prevent near-surface T_{min} from decreasing below T_{dew} (Allen 1996 [DIRS 176485], p. 103). However, under increasing aridity (i.e., in semiarid and arid climates), the difference between T_{min} and T_{dew} increases, even under reference conditions, due to dryness of the regional air mass and due to

reduced effects of evaporative cooling caused by lower ET (Allen 1996 [DIRS 176485], p. 104). Under non-reference (dry) conditions, the difference between T_{min} and T_{dew} increases even further. A dew point offset (K_o) is recommended for semiarid and arid climates to reflect the humidity levels anticipated under the standardized, well-watered reference ET conditions (Equation C-1; Allen et al. 1998 [DIRS 157311], Equation 6-6, p. 261).

The value for K_o in arid environments will vary seasonally with greater deviations between T_{min} and T_{dew} needed during warm dry months (Allen et al. 2005 [DIRS 176207], p. D-29). Evaluations of $T_{min} - T_{dew}$ have been performed for weather stations in a wide variety of locations (Jensen et al. 1997 [DIRS 177103], p. 398, Table 3; Temesgen et al. 1999 [DIRS 178312], pp. 29 to 30). Temesgen et al. (1999 [DIRS 178312], pp. 29 to 30, Table 4) reported values for $T_{min} - T_{dew}$ for six arid and three humid sites that ranged from 10°C to 18°C and 2°C to 6°C, respectively, for summer months, and from 4°C to 8°C and 1°C to 3°C, respectively, for winter months. However, the arid sites were non-reference (dry) stations with no irrigation to keep green vegetation growing in the vicinity of the weather station. The values reported for these stations are higher than those expected for a well-watered reference ET station in a desert environment. When local information on K_o is not available, a K_o range from 2°C to 4°C is suggested by Allen et al. (2005 [DIRS 176207], p. D-29).

It is important, in applying the $ET = K_c\ ET_0$ approach (where ET is actual ET and K_c is a transpiration or "crop" coefficient), that the ET_0 calculation represents the reference evapotranspiration that occurs from the standardized reference surface. This standardized reference surface, by definition, is an extensive surface of transpiring grass that conditions the atmospheric boundary layer by evaporative cooling and by the addition of water vapor. The conditioning of the boundary layer constitutes an important feedback process to the ET_0 rate and moderates it. The K_c coefficient, which represents the ratio of actual ET to ET_0, and the soil water stress reduction function, which reduces the ET value when soil water content is insufficient to support ET fully, are designed to function in concert with the standardized ET_0 value (Allen et al. 1998 [DIRS 157311], pp. 58, 91, and 161). The ET_0 calculation represents a near upper limit on ET that is experienced under full vegetation cover and adequate soil water supply. Under conditions of less than full vegetation cover or less than adequate soil water supply, the actual ET rate will be reduced below the standardized ET_0 rate, even though the actual air temperature may increase and humidity may decrease due to the reduced ET (Brutsaert 1982 [DIRS 176615], pp. 224 to 225 and Figure 10.5). Therefore, it is important that the ET_0 calculation be made using T_{dew} estimated using K_o values that represent the reference ET condition.

For the climate at Yucca Mountain, a nominal value for K_o of 2°C is used for winter months ($K_{o\ winter}$) when relative humidity levels are higher, and a nominal value of 4.5°C is used for spring through fall ($K_{o\ rest}$) (Table 6.5.4.1-2). These values are based on recommendations from Allen et al. (2005 [DIRS 176207], p. D-29). To account for uncertainty associated with both values, a range of 0°C to 10°C is used for uncertainty and sensitivity analyses (Table 6.5.4.1-2). The lower limit represents the potential for reference ET conditions to be met during humid times of the year or under future climate states (Allen et al. 2005 [DIRS 176207], p. D-29). The upper limit represents an extreme value for reference ET conditions under extremely arid climates and is based on work by Temesgen et al. (1999 [DIRS 178312], pp. 29 to 30).

Because the reference weather station is to reflect conditions for a well-watered setting, and because the Present-Day, Monsoon, and Glacial Transition climates and analogue stations all have lower annual precipitation than ET_0, these climates should all have similar relationships between T_{min} and T_{dew} under the reference setting. Therefore, the same nominal values and ranges were used for all climate states (Table 6.5.4.1-2).

Although the uncertainty range for this parameter is large (0°C to 10°C), it is shown in Section 7.1.4 that this parameter does not contribute significantly to uncertainty in net infiltration compared with other uncertain parameters.

Table 6.5.4.1-2. Nominal Values and Ranges for Dew Point Offset

Parameter	Climate States	Nominal Value	Range
$K_{o\ winter}$ [a]	All	2°C [b]	0°C to 10°C [c]
$K_{o\ rest}$ [d]	All	4.5°C	0°C to 10°C
$K_{o\ winter\ start}$ [e]	Present-Day and Monsoon	DOY 335 [f]	DOY 274 to 335
$K_{o\ winter\ end}$ [g]	Present-Day and Monsoon	DOY 90	DOY 90 to 151
$K_{o\ winter\ start}$	Glacial Transition	DOY 274	DOY 244 to 274
$K_{o\ winter\ end}$	Glacial Transition	DOY 120	DOY 120 to 151

[a] Dew point offset for winter period.
[b] Allen et al. 2005 [DIRS 176207], p. D-29.
[c] Lower limit from Allen et al. 2005 [DIRS 176207], p. D-29. Upper limit from Temesgen et al. 1999 [DIRS 178312], pp. 29 to 30, Table 4.
[d] Dew point offset for spring, summer, and fall period.
[e] Day of year that $K_{o\ winter}$ goes into effect.
[f] DOY = day of year.
[g] Day of year that $K_{o\ winter}$ ends.

Allen et al. (2005 [DIRS 176207], pp. D-29 and E-2) suggest application of $K_{o\ winter}$ during winter-like periods when relative humidity levels are higher than the rest of the year, and application of $K_{o\ rest}$ during spring, summer, and fall periods. At Yucca Mountain, higher relative humidity levels for winter months are likely to begin around the first of December and end in February or March (see temperatures in Table 6.5.3.1-1). Therefore, for Present-Day and Monsoon climates, it is recommended that use of the winter dew point begin on day of year 335 ($K_{o\ winter\ start}$) and end on day of year 90 ($K_{o\ winter\ end}$) (Table 6.5.4.1-2). To establish uncertainty ranges for $K_{o\ winter\ start}$ and $K_{o\ winter\ end}$, the winter period was extended by two months at each end. This resulted in a range for $K_{o\ winter\ start}$ from day of year 274 through 335 and for $K_{o\ winter\ end}$ from day of year 90 through 151 (Table 6.5.4.1-2).

Based on data from the Spokane and Rosalia analogue stations for the Glacial Transition climate, the winter period lasts (on average) from October to April (see temperatures in Table 6.5.3.1-2). During this time period, average minimum temperatures are near or below freezing; therefore, for the glacial transition climate, it is recommended that use of the winter dew point begin on day of year 274 (October 1) and end on day of year 120 (April 31) (Table 6.5.4.1-2). To establish uncertainty ranges for $K_{o\ winter\ start}$ and $K_{o\ winter\ end}$ the winter period was extended by one month at each end. This resulted in a range for $K_{o\ winter\ start}$ from day of year 244 through 274, and for $K_{o\ winter\ end}$ from day of year 120 through 151 (Table 6.5.4.1-2).

Adjustment Coefficient for Hargreaves' Radiation Formula (K_{Rs})—Net solar radiation is an input to the FAO-56 Penman-Monteith equation (Equation C-37). The Hargreaves radiation formula is used in Appendix C to estimate the incoming solar radiation on a horizontal surface from the difference in maximum and minimum temperatures (Equation C-13). The formula requires an empirical adjustment coefficient (K_{Rs} [$°C^{-0.5}$]). Allen (1997 [DIRS 176568]) demonstrated that four K_{Rs} values (0.16, 0.18, 0.19, and 0.20) were good estimators of solar radiation for different locations and elevation regimes in the western United States. These four K_{Rs} values were evaluated in Section C3 using solar radiation data measured near Yucca Mountain to determine which were most appropriate for estimating solar radiation for the Yucca Mountain area. The results of the analysis indicated that a K_{Rs} of 0.19 to 0.20 was the best estimator of solar radiation for Yucca Mountain (Output DTN: SN0602T0502206.005). Therefore, a nominal value for K_{Rs} of 0.19 is used in calculation of solar radiation (Table 6.5.4.1-3). Based on the analysis in Section C3, an uncertainty range of 0.15 to 0.22 is used (Table 6.5.4.1-3).

For the glacial transition climate, the range between maximum and minimum temperature could change some, with more humidity holding minimum temperatures at higher values. This could result in a slightly larger value for K_{Rs}. However, this increase would be small and probably would be compensated for by less R_s due to increased atmospheric attenuation under increased humidity and more general cloudiness. A general value of $K_{Rs} = 0.16$ is recommended by Allen et al. (2005 [DIRS 176207], pp. D-5 to D-6) for "interior regions" of the United States. This value is within the 0.15 to 0.22 uncertainty range. Because R_s for clear days should not be impacted by climate change by more than a few percent, the same nominal value and range for K_{Rs} are recommended for Present-Day, Monsoon, and Glacial Transition climates (Table 6.5.4.1-3).

Table 6.5.4.1-3. Nominal Value and Range for Hargreaves' Adjustment Coefficient

Parameter	Climate States	Nominal Value	Range
K_{Rs}[a]	All	$0.19°C^{-0.5}$	$0.15°C^{-0.5}$ to $0.22°C^{-0.5}$

Source: Output DTN: SN0602T0502206.005.

[a] Hargreaves' adjustment coefficient. Coefficient is developed in text based on analysis in Appendix C.

Terrain Albedo (α_T)—Terrain albedo is used to calculate reflected radiation from areas surrounding model grid cells (Equation C-24). Radiation reflected toward grid cells from surrounding surfaces can affect the energy balance of the grid cell and therefore impact ET_0. However, the value for α_T has only a small impact on the solar radiation estimate and ET_0 (Section C1.3).

The value of α_T is a function of soil color and moisture content, soil crusting and aging, and amount and characteristics of vegetation cover. The values suggested for α_T in areas with little vegetation range from 0.15 for dark soils to 0.35 for light soils (Brutsaert 1982 [DIRS 176615], p. 136, Table 6.4). Based on this range and the low cover of vegetation at Yucca Mountain, a nominal value of 0.22 is used for α_T (Table 6.5.4.1-4). Under the monsoon and glacial transition climates, terrain will be more vegetated and the value for albedo will tend toward 0.20 (Brutsaert 1982 [DIRS 176615], p. 136, Table 6.4). However, the estimation of solar radiation on slopes

(and subsequently ET_0) is relatively insensitive to terrain albedo (Section C1.3). Therefore, a nominal value of 0.22 is appropriate for all climate states. A uniform distribution between 0.15 to 0.35 is used for the three climate states for uncertainty and sensitivity analysis (Table 6.5.4.1-4). Values significantly higher than 0.35 (e.g., value of 0.90 represents snow covered ground (Brutsaert 1982 [DIRS 176615], p. 136, Table 6.4) is not justified because persistent snow cover is not expected in any of the future climate states.

Table 6.5.4.1-4. Nominal Value and Range for Terrain Albedo

Parameter	Climate States	Nominal Value	Range
α_T [a]	All	0.22 [b] (dimensionless)	0.15 to 0.35 [c]

[a] Terrain albedo.
[b] Brutsaert 1982 [DIRS 176615], p. 136, Table 6.4, low end of range for desert soils.
[c] Brutsaert 1982 [DIRS 176615], p. 136, Table 6.4, range for dark to light soils.

Solar Constant (G_{sc})—The solar constant (G_{sc} [MJ m^{-2} min^{-1}]) is used to calculate extraterrestrial radiation (R_a, Equation C-6). This constant has a small range. From approximately 1978 through 2004, the running yearly mean value of the solar constant (or total solar irradiance, TSI) ranged from 1,365.67 Wm^{-2} (0.0819 MJ m^{-2} min^{-1}) in 1987 to 1,367.42 Wm^{-2} (0.0820 MJ m^{-2} min^{-1}) in 2001 (Dewitte et al. 2004 [DIRS 178528], p. 214). The minimum and maximum of the readings (ignoring brief spikes of lower irradiance) appear to be 1,365 and 1,369 Wm^{-2} (0.0819 to 0.0821 MJ m^{-2} min^{-1}), respectively (Dewitte et al. 2004 [DIRS 178528], p. 212, Figure 2). Allen et al. (1998 [DIRS 157311], p. 47) recommended a value for G_{sc} of 0.0820 MJ m^{-2} min^{-1}. Therefore, a nominal value of 0.0820 MJ m^{-2} min^{-1} with an uncertainty range of 0.0819 to 0.0821 MJ m^{-2} min^{-1} is recommended for G_{sc} (Table 6.5.4.1-5). The nominal value and range are for all climate states.

Table 6.5.4.1-5. Nominal Value and Range for the Solar Constant

Parameter	Climate States	Nominal Value	Range
G_{sc} [a]	All	0.0820 (MJ m^{-2} min^{-1}) [b]	0.0819 to 0.0821 (MJ m^{-2} min^{-1}) [c]

[a] Solar constant.
[b] Allen et al. 1998 [DIRS 157311], p. 48.
[c] Dewitte et al. 2004 [DIRS 178528], p. 214. Values were converted from W m^{-2} to MJ m^{-2} min^{-1}.

Atmospheric Turbidity Coefficient (K_{cln})—The atmospheric turbidity coefficient (K_{cln} [dimensionless]) is used to calculate 24-hour transmissivity for beam radiation (Equation C-10). For clean sky conditions, K_{cln} should be set to 1.0 (Allen 1996 [DIRS 176485], pp. 97 and 99, and Allen et al. 2005 [DIRS 176207], p. D-8). For extremely turbid, dusty, or polluted air, K_{cln} should be $\leq$ 0.5 (Allen 1996 [DIRS 176485], pp. 97 and 99). Given that a K_{cln} of 0.5 is for extremely dirty air, and the air at Yucca Mountain is relatively clean, 0.5 is not likely to occur. Therefore, it is assumed that a value higher than 0.5 should be used for the lower limit of the K_{cln} distribution. As a reasonable alternative, a lower limit of 0.8 is used. Cleaner air in the future would cause the apparent value for K_{cln} to exceed 1.0. Therefore, a K_{cln} of 1.1 can be used to represent the impact of substantial reduction in aerosols in the atmosphere should this occur in the future (Liepert and Romanou 2005 [DIRS 178313], p. 623; Cohen et al. 2004 [DIRS 178314], p. 362).

A nominal value of 1.0 with an uncertainty range of 0.8 to 1.1 is used for K_{cln} (Table 6.5.4.1-6). A range of 0.8 to 1.1 is reasonable without going below what would be normally expected at Yucca Mountain. The nominal value and range apply to all climates.

Table 6.5.4.1-6. Nominal Value and Range for the Turbidity Coefficient

Parameter	Climate	Nominal Value	Range
K_{cln} [a]	All	1.0 [b]	0.8 to 1.1 [c]

[a] Turbidity coefficient.
[b] Allen et al. 2005 [DIRS 176207], p. D-8.
[c] Assumptions made in text.

6.5.4.2 Input Parameters for Soil Water Balance Calculations

The infiltration model contains a soil water balance component that considers water storage and movement within the soil column (Section 6.4.2). The water balance model is based on FAO-56 methods that require input parameters related to soil moisture evaporation and plant water use (Section 6.4.4). A subset of those parameters (Table 6.5.4.2-1) is described in this section and distributions and nominal values for use in the model are established. In addition, the initial water content used for each soil layer is discussed.

Table 6.5.4.2-1. Input Parameters for Soil Water Balance

Parameter	Description
K_{c_min}	*Minimum* transpiration coefficient (K_c) for dry surface soil (upper 0.10 to 0.15 m) with no vegetation cover
p	Soil moisture depletion coefficient. Average fraction of total available water for evapotranspiration (*TAW*) that can be depleted from the root zone before reduction in evapotranspiration (*ET*). Expressed as a fraction (0 to 1).
Z_e	Evaporation layer depth (m). Mean effective depth of soil experiencing drying by surface evaporation to near air dry water content.
REW	Readily evaporable water (mm). Depth of water that can be evaporated during Stage 1 drying before the drying rate declines below the potential evaporation rate.

Minimum Transpiration Coefficient ($K_{c\ min}$)—The minimum transpiration coefficient for a dry surface soil layer with no vegetation cover ($K_{c\ min}$, dimensionless) represents low-level, long-term diffuse evaporation when the soil surface layer is dry (at air dry). $K_{c\ min}$ is reduced to zero in the water balance calculations when the contributing soil profile is completely dry. K_{c_min} is also used during calculation of the fraction of soil surface that is covered by vegetation (f_c) in Equation 76 from Allen et al. (1998 [DIRS 157311], pp. 149 to 150). The f_c is used in the calculation of the evaporation component ($K_e \times ET_0$) in the soil water balance model. Under the arid conditions at Yucca Mountain, the upper soil layer often dries to low water content (air dry) during periods between precipitation events (CRWMS M&O 1999 [DIRS 105031], p. 14, Table 3). Under dry soil conditions and sparse rainfall, Allen et al. (1998 [DIRS 157311], pp. 207 and 209) recommended setting $K_{c\ min}$ to zero in order to provide for conditions when transpiration is equal to zero. For agricultural crops where residual soil water is common, a range for $K_{c\ min}$ of 0.15 to 0.20 was recommended by Allen et al. (1998 [DIRS 157311], pp. 149 to 150). Based on this information, a triangular distribution with 50% of the values equal to 0.0

and 50% of the values varying linearly between 0.0 and 0.2 is used. A nominal value of 0.0 is assumed (Table 6.5.4.2-2). However, a nominal value that is slightly higher than zero (perhaps the mean of the uncertainty distribution) would be appropriate for long periods with no precipitation. A value greater than zero allows for low-level diffusive evaporation from below the evaporation layer, a process consistent with observations that water content in a bare soil lysimeter near to the Yucca Mountain site continues to decrease even after long periods of no precipitation (Scanlon et al. 2005 [DIRS 175977]). The nominal value and distribution applies to all climates.

Table 6.5.4.2-2. Nominal Value and Range for the Minimum Transpiration Coefficient

Parameter	Climate	Nominal Value	Range
$K_{c\ min}$ [a]	All	0.0 [b]	0.0 to 0.2 [c]

[a] minimum transpiration coefficient for dry soil with no vegetation cover.
[b] Allen et al. 1998 [DIRS 157311], pp. 207 and 209. A slightly higher value is appropriate if long dry periods are to be simulated.
[c] Range from Allen et al. 1998 [DIRS 157311]. Lower bound from pp. 207 and 209, upper bound from pp. 149 to 150.

Soil Moisture Depletion Coefficient (p)—The soil moisture depletion coefficient (p, expressed as a fraction) is used to calculate readily available water (RAW) in the plant root zone (Section 6.4, Equation 6.4.4.2-5). It represents the average fraction of total available water (TAW) in the soil column that can be depleted from the root zone before reduction in actual ET occurs due to plant moisture stress (i.e., RAW is the depletion threshold at which water stress begins to occur). In the water balance model, p varies as a function of actual ET and is limited to ≤ 0.8 (Appendix G, Equation G-19).

For agricultural crops, p adjusted for actual ET rates is limited to $0.1 \leq p \leq 0.8$. Most crop species are relatively sensitive to water stress and have p values around 0.5 (Allen et al. 1998 [DIRS 157311], pp. 163 to 165, Table 22). Values for p that are less than 0.5 are for crops such as carrots and lettuce that have high water requirements and low stress thresholds. These crops require careful water management to give highest yields and quality. Desert plants are generally more tenacious than agricultural crops, and it is not likely that they exhibit stress thresholds as low as crops with high water requirements. Therefore, 0.5 should represent the lower limit of the range for p under Present-Day and future climates in this analysis (Table 6.5.4.2-3). Based on work by Allen et al. (1998 [DIRS 157311], p. 162), an upper limit for p of 0.8 is used. A nominal value of 0.65 (midpoint of range) is used (Table 6.5.4.2-3).

Table 6.5.4.2-3. Nominal Value and Range for the Soil Moisture Depletion Coefficient

Parameter	Climate State	Nominal Value	Range
p [a]	All	0.65[b]	0.5 to 0.8[c]

[a] Soil moisture depletion coefficient.
[b] Midpoint of range.
[c] Allen et al. 1998 [DIRS 157311], p. 162.

Evaporation Layer Depth (Z_e)—The mean effective depth of the surface soil layer that is subject to drying by evaporation to air dry (Z_e [m]) is used to calculate total evaporable water (TEW) using Equation 73 from Allen et al. (1998 [DIRS 157311], p. 144). The value is dependent on

soil texture and length of drying periods common to the model area, which implies that in reality it varies with location. However, in this analysis, a single effective value for this parameter is applied over the model domain. Allen et al. (1998 [DIRS 157311], p. 144; 2005 [DIRS 176009], pp. 10 to 12, Figure 9d, and Table 3) recommend a range between 0.10 to 0.15 m for Z_e. These references are primarily focused on agricultural soils. More generally, Allen et al. (2005 [DIRS 176009], p. 4) stated that a value for Z_e based on evaporation amounts observed over complete drying cycles for soils and conditions representative of the model area should be selected by the user. Coarse texture and long periods of drying that characterize most Yucca Mountain soils suggest it is reasonable to extend the evaporation layer depth somewhat beyond the upper bound (0.15 m) suggested by Allen et al. (1998 [DIRS 157311], p. 144). For this analysis it was decided to represent Z_e for the sandy-loam soils at Yucca Mountain with a uniform distribution between 0.1 and 0.2 m and a nominal value of 0.15 m (Table 6.5.4.2-4).

A number of studies from various locations corroborate this range. For instance, Rose (1968 [DIRS 178583]) found the soil water content in a sandy soil after four days to be near air-dry at the surface and increased to near field capacity at a depth of 0.12 to 0.15 m. Mutziger et al. (2005 [DIRS 178316]) found Z_e to range from 0.03 m for a clay loam soil to 0.16 m for a silt loam soil in comparisons against lysimeter measurements. Hunsaker et al. (2002 [DIRS 178529]) used Z_e = 0.15 m for a loam soil and Tolk and Howell (2001 [DIRS 178315]) and Howell et al. (2004 [DIRS 178317]) used Z_e = 0.10 for a fine sandy loam soil in Texas. Allen et al. (2005 [DIRS 178493], p. 21) found Z_e = 0.15 m for observed evaporation data from Imperial Valley, California, for silty clay and silty clay loam soils and Z_e = 0.35 m for Superstition sand. However, the authors argue that the high values of TEW (33 mm) and REW (20 mm) required to fit the Superstition sand data "do not seem realistic for a sand and may be some artifact of field data collection" (Allen et al. (2005 [DIRS 178493], p. 21). All these studies corroborate a range of 0.1 to 0.2 m.

Table 6.5.4.2-4. Nominal Value and Range for Evaporation Layer Depth

Parameter	Climate	Nominal Value	Range
Z_e [a]	All	0.15 m [b]	0.1 to 0.2 m [b]

[a] Evaporation layer depth.
[b] Range and nominal value are modified according to principles described by Allen et al. (2005 [DIRS 176009], p. 4), from a typical agricultural range also given by Allen et al. (1998 [DIRS 157311], p. 144).

Readily Evaporable Water (REW)—Readily evaporable water (*REW*, mm) is used to calculate the soil evaporation reduction coefficient (K_r) in Equation 74 from Allen et al. (1998 [DIRS 157311], p. 146). An energy limiting stage (Stage 1) and a falling rate stage (Stage 2) are considered in the evaporation process. In Stage 1, the soil surface is wet and the maximum rate of evaporation is controlled by the amount of available energy at the soil surface (Allen et al. 1998 [DIRS 157311], p. 145). Readily evaporable water is the maximum depth of water that can be evaporated from the upper soil layer during Stage 1, prior to the onset of hydraulic limitations that reduce the rate of water supply below that of energy demands. When the depth of evaporation exceeds *REW*, Stage 2 of the evaporation process begins (Allen et al. 1998 [DIRS 157311], p. 145).

The depth of *REW* is dependent on soil texture with values normally ranging from about 5 to 12 mm (Allen et al. 1998 [DIRS 157311], p. 145). Tolk and Howell (2001 [DIRS 178315]) and Howell et al. (2004 [DIRS 178317]) used *REW* = 10 mm for a clay loam soil and *REW* = 9 mm for a fine sandy loam soil near Amarillo, Texas, based on lysimeter observations. Mutziger et al. (2005 [DIRS 178316]) found best fit values for *REW* based on lysimeter observations to range from 2 mm for a clay loam to 13 mm for a silt loam soil. For sand to sandy loam soils such as those at Yucca Mountain, *REW* ranges from 2 to 10 mm (Allen et al. 1998 [DIRS 157311], p. 144, Table 19). Therefore, a uniform distribution with a range of 2 to 10 mm is used for *REW* (Table 6.5.4.2-5). A nominal value of 6.0 (midpoint of range) is used for *REW* (Table 6.5.4.2-5). Because *REW* is a function of soil properties, it is not expected to change under different climates. Therefore, the same distribution and nominal value are recommended for all climate states.

Table 6.5.4.2-5. Nominal Value and Range for Readily Evaporable Water

Parameter	Climate States	Nominal Value	Range
REW[a]	All	6 mm[b]	2 to 10 mm[c]

[a] Readily evaporable water.
[b] Midpoint of REW range reported by Allen et al. 1998 [DIRS 157311], p. 144, Table 19.
[c] From Allen et al. 1998 [DIRS 157311], p. 144, Table 19. Range of REW for sand, loamy sand, and sandy loam soils.

Initial Soil Water Content (IWCF)—The MASSIF calculation always starts at the beginning of the water year (October 1). At this time of year, the water content in the rooting zone (Layers 1 and 2) is expected, on average, to be closer to the wilting point than to the field capacity. Unaffected by evapotranspiration, soil below the rooting zone (Layer 3) is expected to be at field capacity.

If the soil is initially dry (i.e., near wilting point), part of the precipitation will result in a net increase in the soil water content over the course of the water year. If the soil is initially wet (i.e., near field capacity), the soil water content will likely decline over the water year. Generally, the net infiltration for a particular year will increase with increasing initial soil water content. The actual sensitivity is strongly dependent upon the timing and structure of the individual precipitation events.

When weather data is available, it is best to run MASSIF for the water year previous to the water year of interest. In so doing, the initial soil water contents for the water year of interest are a by-product of the calculation for the previous year. This, however, is not practical for the stochastically generated weather data used for predicting net infiltration for future climates at Yucca Mountain (Section 6.5.1 and Appendix F). The reason for this is that for each realization, 10 stochastically generated weather years are sampled from a set of 1,000 randomly generated years. Each of these sampled years is selected based on its annual precipitation and weighted for its probability of occurrence. Because many of the years are selected explicitly for their low probability and large annual precipitation, it is not appropriate to use soil water contents from these years as initial conditions for the analysis.

The statistical independence of the individual water years makes the initial soil water content, itself, stochastic. A net increase in soil water content is expected for some water years. Other

water years are expected to have a net decrease in soil water content. For a sufficiently large number of modeled water years for a particular climate, an appropriate value for initial water content should result in a net annual change in soil water content equal to zero, at the limit. However, to estimate an appropriate initial water content value with a high degree of accuracy would require running the model numerous times for each climate in order to adjust the initial water content until the net change approaches zero. Such effort was not considered necessary, because it can be shown that the resulting net infiltration is relatively insensitive to the value of the initial water content. Therefore, only two values of the initial water content were run as justification for an appropriate value to use.

The MASSIF calculation of mean infiltration for a particular climate involves modeling 400 water years (i.e., two replicates of 20 realizations, each containing 10 weighted water years). The weighted net change in soil water content for the 400 water years is calculated for each of two assumed initial water contents. One of the assumed initial contents results in a net increase in soil water content; the other results in a net decrease. Hence, the "correct" initial water content is bounded by the two assumed initial values. These assumed initial water contents (expressed as fractions) used in the estimating of net infiltration for the three climates considered are listed in Table 6.5.4.2-6. Comparison of the net infiltration rates calculated for each of the assumed initial values indicates the sensitivity of net infiltration to initial soil water content. The results of this comparison are included in Section 6.5.7.4. To convert initial water content fractions to actual water content (θ) apply the following:

$$\theta = IWCF(\theta_{FC} - \theta_{WP}) + \theta_{WP} \qquad \text{(Eq. 6.5.4-1)}$$

where *IWCF* is the initial water content fraction, θ_{FC} is the field capacity of the soil, and θ_{WP} is the permanent wilting point of the soil. Values for the field capacity and permanent wilting point for the Yucca Mountain soil groups are listed in Tables 6.5.2.3-2 and 6.5.2.3-1, respectively.

Table 6.5.4.2-6. Nominal Value and Range for Initial Water Content Fractions

Parameter	Climate States	Nominal Value	Upper Value
IWCF [a]	Present-Day and Glacial Transition	0[b]	0.1[c]
IWCF [a]	Monsoon	0.1[b]	0.2[c]

[a] Initial water content fraction expressed as the fractional value between wilting point and field capacity (0 = wilting point).
[b] Value used for estimating net infiltration.
[c] Value used to bound the "correct" initial water content.

6.5.5 Parameter Uncertainty Screening

This section describes the methodology used to determine which of all the uncertain input parameters listed in Appendix I and developed in the preceding sections are to be varied in the net infiltration uncertainty analysis performed for each climate state.

The first step in the uncertainty analysis is the elimination of parameters that do not have a large contribution to uncertainty in net infiltration. This step considers two properties associated with each parameter, its relative uncertainty, and its influence on the average net infiltration.

In several places, the MASSIF model uses a formula that is an approximation for a function. Such approximations have inherent uncertainties based on the form of the equation and the values of the coefficients. It is considered in this analysis that uncertainties in these approximations are small compared to uncertainties in other parameters. Therefore, the parameter uncertainty analysis does not vary any coefficients of function approximations. Appendix I, Section I1.1 identifies the coefficients that were not considered individually in the sensitivity studies but rather are included as part of model uncertainty.

Of the remaining parameters, some have different values for different climates. Others may have the same nominal values but different uncertainties. Parameters in either of these categories require a separate treatment for each climate.

Section I1.2 provides screening results for those parameters for which neither the nominal value nor its uncertainty varies appreciably for the three climates of interest. Subsequent sections of Appendix I summarize the screening for parameters specific to the Present-Day, Monsoon, and Glacial Transition climates, respectively.

The detailed analysis of parameter uncertainty excludes many parameters on the basis of low uncertainty. The criterion for low uncertainty is that the relative uncertainty is less than 15%. For most parameters, comparison with the nominal value of the parameter determines the relative uncertainty. The exceptions are:

- For the first-order term of a Fourier series for a Markov probability *a,* comparison with the smaller of *a* or 1-*a* determines the relative uncertainty
- For the first-order term of a Fourier series for a temperature minimum or maximum, comparison with the difference between the minimum and maximum determines the relative uncertainty
- The uncertainty of a second-order term of a Fourier series uses the same basis as the first-order term
- The uncertainty of a phase term in a Fourier series is relative to half of a year.

The analysis in Appendix I also excludes, on the basis of low influence, parameters that are not expected to influence more than 15% of the net infiltration. The most common exclusion arguments in such cases are:

- The parameter applies to less than 15% of the area of interest (e.g., geophysical properties)
- The parameter applies to less than 15% of the days in the analysis (e.g., monthly wind speed).

There remains the possibility of a systematic error that extends to a larger region of space or time. A systematic error in a group of parameters is an issue of model uncertainty rather than parameter uncertainty.

6.5.5.1 Sampled Parameter Values for Present-Day Climate

For the Present-Day climate, Table 6.5.5.1-1 summarizes the eleven parameters varied independently in the uncertainty analysis (the eight climate-independent parameters plus three additional parameters). Two plant parameters were varied (the mean plant height and the maximum effective rooting depth).

Table 6.5.5.1-1. Parameters Varied Independently in Uncertainty Analysis for Present-Day Climate

Parameter Symbol	Parameter Name and Description	Uncertainty Range	Uncertainty Distribution
a_m	Annual average of the natural logarithm of the amount of daily rainfall on days with precipitation (Section 6.5.1.2)	0.50 to 1.07 (ln mm)	uniform
h_{plant}	Plant height (Section 6.5.3.3)	0.2 m to 0.6 m	uniform
Z_r	Maximum rooting depth (Section 6.5.3.2)	0.6 m to 2.6 m	uniform
$depth_{soil}(4)$	Soil depth for soil depth class 4 (Section 6.5.2.4.1)	0.1 m to 0.5 m	uniform
$K_{sat\_rock}(405)$	Bulk saturated hydraulic conductivity of bedrock IHU 405 (Section 6.5.2.6)	7.6×10^{-8} m/s to 4.8×10^{-6} m/s	loguniform
$K_{sat\_rock}(406)$	Bulk saturated hydraulic conductivity of bedrock IHU 406 (Section 6.5.2.6)	2.1×10^{-8} m/s to 7.7×10^{-6} m/s	loguniform
$\theta_{HC}(5/7/9)$	Holding capacity of soil group 5/7/9 (Section 6.5.2.3)	0.09 to 0.17 (m^3/m^3)	uniform
REW	Readily evaporable water (Section 6.5.4.2)	2 to 10 mm	uniform
K_{c_min}	Minimum transpiration coefficient (K_c) (Section 6.5.4.2)	0.0 to 0.2 (unitless)	50% of values = 0.0, 50% of values vary linearly from 0.0 to 0.2 [pdf is $(0.2\text{-}K_{cmin})/0.04$]
Z_e	Evaporation layer depth (Section 6.5.4.2)	0.1 to 0.2 m	uniform
C_{Kcb2}	Slope of the NDVI' – K_{cb} function (Section 6.5.3.7)	9.7 ± 2.1 (unitless)	normal

NOTE: See Table I-2.

One weather parameter, a_m (Section 6.5.1.2), was also varied. Another weather parameter, a_λ, (Section 6.5.1.2) was not varied independently, but rather was correlated with a_m (Table 6.5.5.1-2). Although the relative uncertainty in a_λ is somewhat less than the arbitrary 15% criterion, it was included in the uncertainty analysis so that its value would remain consistent with the value of a_m.

Table 6.5.5.1-2. Parameters Correlated with Other Parameters That Varied Independently in Uncertainty Analysis for Present-Day Climate

Parameter Symbol	Parameter Name and Description	Uncertainty Range	Uncertainty Distribution
a_λ	Annual average of the mean amount of daily rainfall on days with precipitation (Section 6.5.1.2)	4.0 to 6.5 mm	uniform

NOTE: See Table I-3.

Tables 6.5.5.1-3 and 6.5.5.1-4 report two separate sets of sampled values for the parameters listed in Table 6.5.5.1-1. These are output from two separate LHS runs. Treating them as a single set risks the possibility that unintended correlations may go undetected.

Table 6.5.5.1-3. Sampled Parameter Values for Replicate 1 of Present-Day Net Infiltration Runs

Vector	a_m	h_plant	Z_r	Z_e	Sdepth4	lnRks_405	lnRks_406	HC_579	REW	Kc_min	CKcb2
unit	ln (mm/day)	m	m	m	m	ln (m/s)	ln(m/s)	m^3/m^3	n/a	mm	n/a
1	0.7581	0.4251	1.165	0.1472	0.2515	−13.47	−14.63	0.158	6.188	0	16.2
2	0.7418	0.2455	1.776	0.136	0.2883	−15.7	−12.8	0.09653	8.363	0.1755	10.21
3	0.5438	0.2623	0.872	0.159	0.2049	−14.75	−14.74	0.1276	6.934	0	12.89
4	0.5993	0.3259	1.261	0.1411	0.3894	−15.35	−16.36	0.1607	3.075	0	8.885
5	0.8359	0.5256	2.54	0.1676	0.1172	−12.67	−16.17	0.1035	5.974	0.05953	8.415
6	0.9782	0.3692	2.427	0.13	0.27	−16.26	−15.09	0.1153	3.539	0	8.19
7	0.9323	0.4083	0.6888	0.174	0.4557	−13.19	−13.53	0.1431	3.657	0.1076	6.045
8	0.8565	0.4926	2.116	0.1336	0.3451	−16.03	−12.51	0.152	6.671	0	6.331
9	1.029	0.3804	1.003	0.1078	0.1666	−15.4	−13.95	0.1487	4.581	0.0504	11.8
10	0.5624	0.5859	2.319	0.1927	0.4603	−14.28	−12.04	0.1389	5.383	0.00441	14.07
11	0.9179	0.4658	1.461	0.1876	0.4385	−14.35	−17.19	0.1202	2.773	0	9.318
12	0.8879	0.5693	0.982	0.1149	0.4161	−15.95	−16.7	0.1013	8.564	0.01971	11.46
13	0.7943	0.3504	2.07	0.1	0.328	−12.33	−13.57	0.1105	2.259	0.08441	12.36
14	1.053	0.2347	1.973	0.1833	0.2314	−12.95	−13	0.1693	9.479	0	10.43
15	1.011	0.2853	1.377	0.1989	0.3715	−13.86	−15.87	0.09083	7.343	0	10.96
16	0.6181	0.4443	1.68	0.1155	0.3051	−12.57	−15.37	0.1257	9.619	0	7.134
17	0.6674	0.3057	2.229	0.1218	0.493	−13.97	−16.82	0.1336	8.866	0.03784	7.366
18	0.6734	0.5428	1.506	0.1789	0.1434	−15.02	−17.46	0.1648	7.667	0.116	9.826
19	0.7188	0.5003	0.7734	0.1543	0.1359	−13.57	−12.36	0.1071	4.816	0	3.2
20	0.5131	0.2161	1.851	0.1609	0.1878	−14.66	−14.14	0.1357	4.275	0.02272	9.588

Source: Output DTN: SN0701T0502206.043, file: *LHS_PD_R1.OUT*.

Table 6.5.5.1-4. Sampled Parameter Values for Replicate 2 of Present-Day Net Infiltration Runs

Vector	a_m	h_plant	Z_r	Z_e	Sdepth4	lnRks_405	lnRks_406	HC_579	REW	Kc_min	CKcb2
unit	ln (mm/day)	m	m	m	m	ln (m/s)	ln(m/s)	m^3/m^3	n/a	mm	n/a
1	0.5654	0.5941	2.308	0.1237	0.381	−12.74	−15.78	0.1324	7.022	0	11.06
2	0.7297	0.4746	1.179	0.128	0.3764	−13.51	−11.85	0.1212	6.081	0.03304	9.318
3	0.7605	0.5753	2.278	0.1895	0.1741	−16.38	−13.96	0.1686	4.899	0.005494	5.31
4	0.6937	0.3278	1.662	0.1448	0.4845	−15.02	−13.5	0.1342	2.708	0.1917	8.319
5	0.5565	0.2071	1.897	0.1178	0.2575	−15.9	−14.42	0.1388	3.801	0	10.59
6	0.9578	0.5229	1.483	0.1006	0.4514	−16.16	−17.3	0.1272	8.884	0.04929	6.208
7	0.8666	0.429	0.9073	0.137	0.2097	−13.74	−14.72	0.1578	3.038	0.1424	13.54
8	0.8928	0.3409	0.8492	0.1978	0.4216	−14.36	−14.95	0.1599	8.476	0	8.862
9	0.6608	0.4175	1.989	0.1487	0.1102	−15.58	−16.95	0.09143	4.602	0.02741	11.22
10	0.6218	0.2798	1.302	0.1649	0.3126	−13.34	−15.6	0.1622	5.503	0	9.877
11	0.7144	0.3877	0.639	0.1075	0.2601	−14.9	−15.12	0.1454	7.854	0	12.42
12	0.9528	0.2539	1.01	0.1314	0.2339	−15.28	−12.43	0.1077	8.387	0	7.44
13	0.5894	0.3122	1.758	0.1575	0.1259	−12.62	−16.59	0.1149	9.991	0.07304	4.343
14	1.021	0.3608	2.447	0.113	0.2935	−12.36	−12.66	0.146	4.212	0	7.867
15	0.8056	0.5496	0.7667	0.1653	0.4018	−13.05	−17.39	0.1043	3.46	0	9.365
16	0.9094	0.4983	1.245	0.1768	0.1846	−13.98	−13.05	0.0943	2.379	0	6.962
17	0.5251	0.5132	1.502	0.1949	0.3357	−14.15	−12.16	0.1238	9.501	0.08352	12.87
18	0.8363	0.2251	2.542	0.1803	0.4721	−14.69	−16.34	0.1018	5.831	0.01402	10.18
19	1.048	0.4428	2.142	0.1729	0.3597	−15.42	−13.67	0.1118	7.234	0	15.47
20	0.9855	0.2889	2.046	0.1527	0.1593	−13.13	−15.99	0.1508	6.559	0.1059	11.67

Source: Output DTN: SN0701T0502206.043, file: *LHS_PD_R2.OUT*.

6.5.5.2 Sampled Parameter Values for Monsoon Net Infiltration Calculations

Tables 6.5.5.2-1 and 6.5.5.2-2 summarize the 19 parameters varied in the uncertainty analysis for the Monsoon climate, including the eight parameters that are climate independent. Two plant parameters were varied (the mean plant height and the maximum effective rooting depth). The slope of precipitation duration versus amount of precipitation was varied for this climate.

Four weather parameters were varied directly. Four additional weather parameters were not varied independently but rather were correlated with a_m and b_{m1} (Section 6.5.1.2). These seven weather parameters provided variation in the weather input files for model calculations.

Table 6.5.5.2-1. Parameters Varied Independently in Uncertainty Analysis for Monsoon Climate

Parameter Symbol	Parameter Name and Description	Uncertainty Range	Uncertainty Distribution
a_{00}	Annual average of the probability of no precipitation given that the previous day was dry (Section 6.5.1.2)	0.896 to 0.944 (unitless)	uniform
a_m	Annual average of the natural logarithm of the amount of daily rainfall on days with precipitation (Section 6.5.1.2)	0.5 to 1.3 (ln mm)	uniform
$b_{m,1}$	Amplitude of the annual variation in the median amount of daily rainfall on days with precipitation (Section 6.5.1.2)	−0.3 to +0.5 mm	uniform
γwet_{max}	Annual average maximum daily temperature on days with precipitation (Section 6.5.1.2)	14 C to 22 C	uniform
h_{plant}	Plant height (Section 6.5.3.3)	0.2 m to 0.6 m	uniform
Z_r	Maximum rooting depth (Section 6.5.3.2)	0.6 m to 2.6 m	uniform
Rate of duration increase with precipitation	Slope of the relationship between duration of daily precipitation and amount of daily rainfall (Section 6.5.1.7)	0.14 hr/mm to 0.43 hr/mm	uniform
$depth_{soil}(4)$	Soil depth for soil depth class 4 (Section 6.5.2.4.1)	0.1 m to 0.5 m	uniform
$K_{sat\_rock}(405)$	Bulk saturated hydraulic conductivity of bedrock IHU 405 (Section 6.5.2.6)	7.6×10^{-8} m/s to 4.8×10^{-6} m/s	loguniform
$K_{sat\_rock}(406)$	Bulk saturated hydraulic conductivity of bedrock IHU 406 (Section 6.5.2.6)	2.1×10^{-8} m/s to 7.7×10^{-6} m/s	loguniform
$\theta_{HC}(5/7/9)$	Holding capacity of soil group 5/7/9 (Section 6.5.2.3)	0.09 to 0.17 (m^3/m^3)	uniform
REW	Readily evaporable water (Section 6.5.4.2)	2 to 10 mm	uniform
K_{c_min}	Minimum transpiration coeficient (K_c) (Section 6.5.4.2)	0.0 to 0.2 (unitless)	50% of values = 0.0, 50% of values vary linearly from 0.0 to 0.2 [pdf is $(0.2-K_{cmin})/0.04$]

Table 6.5.5.2-1. Parameters Varied Independently in Uncertainty Analysis for Monsoon Climate (Continued)

Parameter Symbol	Parameter Name and Description	Uncertainty Range	Uncertainty Distribution
Z_e	Evaporation layer depth (Section 6.5.4.2)	0.1 to 0.2 m	uniform
C_{Kcb2}	Slope of the NDVI' – K_{cb} function (Section 6.5.3.7)	9.7 ± 2.1 (unitless)	normal

NOTE: See Table I-5.

The Monsoon climate is described in the future climate report (BSC 2004 [DIRS 170002]) as being something between the current desert climate (with most of the rain in winter) and a classical Monsoon climate (with most of the rain in summer). This uncertainty has been modeled by fixing the phase of the annual variation (all θ values) such that most of the rain falls in summer, and authorizing the amplitude (all b values) to vary between positive values (keeping most of the rain in summer) and negative values (switching the largest amount of rain to winter).

One of the amplitude values, b_m, is varied independently. All the other amplitudes are estimated using simple linear regression. Even though there is no correlation between annual average (a values) and amplitude (b values), the resulting weather parameters have to be checked in order to suppress any physical impossibilities:

- $b_{00,1}$ cannot be higher than $1-a_{00}$ (as it will create a probability of having a dry day larger than 1)
- b_λ cannot be higher than a_λ, as it will create a negative value for some daily amounts of rain
- (a_m-b_m) cannot be higher than $(b_\lambda-a_\lambda)$ as it will lead to a negative variance in the estimate of lognormal parameters
- a_m should not equal b_m, because this would lead to a probability of rain equaling zero one day of the year.

The first configuration is unlikely to happen. Therefore, in the event that sampling results in one vector that contains a physically impossible set of values, the entire set of sample vectors is discarded. The second configuration is more likely to happen. In order to reduce the likelihood, a very small positive correlation (0.2) has been induced between a_m and b_m in order to limit the high values of b_n associated with low values of a_m.

Tables 6.5.5.2-3 and 6.5.5.2-4 report two separate sets of sampled values for the parameters listed in Table 6.5.5.2-1. These are output from two separate LHS runs. Treating them as a single set risks the possibility that unintended correlations may go undetected.

Table 6.5.5.2-2. Parameters Correlated with Other Parameters that Varied Independently in Uncertainty Analysis for Monsoon Climate

Parameter Symbol	Parameter Name and Description	Uncertainty Range	Uncertainty Distribution
a_{λ}	Annual average of the mean amount of daily rainfall on days with precipitation (Section 6.5.1.2)	4.0 mm to 9.0 mm	uniform
$b_{00,1}$	Amplitude of the annual variation in the probability of no precipitation given that the previous day was dry (Section 6.5.1.2)	−0.03 to +0.07 (unitless)	uniform
$b_{10,1}$	Amplitude of the annual variation in the probability of no precipitation given that precipitation occurred during the previous day (Section 6.5.1.2)	−0.13 to +0.10 (unitless)	uniform
$b_{\lambda,1}$	Amplitude of the annual variation in the mean amount of daily rainfall on days with precipitation (Section 6.5.1.2)	−1.3 mm to +4.5 mm	uniform

NOTE: See Table I-6.

Table 6.5.5.2-3. LHS Sampled Parameter Values for Replicate 1 of Monsoon Net Infiltration Runs

Vector	a_00	a_m	b_m1	gTmaxwet	h_plant	Z_r	Z_e	Sdepth4	lnRks_405	lnRks_406	HC_579	REW	Kc_min	CKcb2	PDur_S
unit	n/a	ln(mm/day)	ln(mm/day)	C	m	m	m	m	ln (m/s)	ln(m/s)	m^3/m^3	n/a	mm	n/a	hr/mm
1	0.9067	1.125	0.4051	18.64	0.3054	1.824	0.1908	0.3113	−13.87	−13.3	0.1682	3.442	0.0843	7.826	0.3568
2	0.8965	0.5781	−0.2631	19.57	0.5387	1.114	0.1874	0.1264	−14.2	−16.79	0.1504	6.287	0	12.73	0.2712
3	0.9023	0.7363	0.3423	15.36	0.325	1.689	0.1118	0.4428	−14.56	−17.65	0.1429	8.985	0.1049	9.724	0.1696
4	0.9275	1.061	0.4207	21.44	0.4432	1.423	0.1602	0.1989	−16.23	−12.95	0.1306	9.243	0	8.984	0.3059
5	0.9213	0.7742	0.1524	21.94	0.2951	2.116	0.1666	0.3437	−13.92	−14.65	0.1055	9.615	0.01062	12.44	0.1886
6	0.933	0.9675	−0.03294	20.53	0.2452	2.29	0.1003	0.2006	−15.92	−14.12	0.1646	2.932	0	10.98	0.264
7	0.8996	0.9273	0.0448	17.79	0.3716	2.502	0.1415	0.1405	−13.14	−15.06	0.09422	4.91	0	6.884	0.3841
8	0.9252	1.002	0.2258	16.41	0.461	0.8874	0.171	0.1184	−15.08	−15.5	0.09803	4.457	0.006191	5.049	0.214
9	0.9229	1.178	−0.205	16.22	0.5855	2.499	0.1093	0.2328	−13.64	−13.15	0.1604	5.848	0.06511	9.505	0.1422
10	0.9156	0.6756	0.2745	21	0.3942	0.6282	0.1288	0.3785	−13.03	−15.96	0.1267	2.628	0	8.413	0.162
11	0.9102	0.581	0.2053	19.72	0.5406	1.288	0.1303	0.3815	−15.54	−11.85	0.1218	3.611	0.1635	10.18	0.4008
12	0.9391	0.8708	0.08648	17.28	0.2655	2.326	0.1975	0.3223	−12.53	−14.83	0.1108	4.374	0.03362	9.308	0.208
13	0.9118	1.225	−0.112	20.39	0.5031	1.903	0.1766	0.4864	−15.57	−17.26	0.1065	5.575	0	6.44	0.4055
14	0.9195	1.059	0.4613	14.58	0.4223	1.389	0.1588	0.2531	−13.35	−14.26	0.1226	8.454	0	11.79	0.3338
15	0.9315	0.8584	0.3102	14.88	0.4955	2.092	0.1529	0.2885	−15.18	−15.74	0.09032	2.114	0.02338	14.65	0.2873
16	0.9364	1.283	−0.1742	15.97	0.2213	0.7093	0.1351	0.1638	−14.86	−16.46	0.1403	6.561	0.1118	13.5	0.3274
17	0.913	0.6378	−0.2292	14.32	0.2024	1.564	0.1493	0.423	−16.16	−12.42	0.1351	7.142	0	5.214	0.2306
18	0.9411	0.8047	−0.06011	16.82	0.577	0.9239	0.1843	0.4775	−14.52	−13.73	0.1566	7.561	0	10.54	0.2441
19	0.9045	1.183	0.114	18.92	0.3409	1.04	0.1232	0.4081	−12.36	−12.35	0.1168	7.891	0	11.47	0.3638
20	0.9429	0.5327	0.0161	18.12	0.4199	1.746	0.1151	0.2717	−12.83	−16.91	0.1479	8.14	0.05213	7.808	0.4274

Source: Output DTN: SN0701T0502206.043, file: *LHS_MO_R1.OUT*.

Table 6.5.5.2-4. LHS Sampled Parameter Values for Replicate 2 of Monsoon Net Infiltration Runs

Vector	a_00	a_m	b_m1	gTmaxwet	h_plant	Z_r	Z_e	Sdepth4	lnRks_405	lnRks_406	HC_579	REW	Kc_min	CKcb2	PDur_S
Unit	n/a	ln(mm/day)	ln(mm/day)	C	m	m	m	m	ln (m/s)	ln(m/s)	m^3/m^3	n/a	mm	n/a	hr/mm
1	0.9227	1.273	0.01857	15.89	0.4409	1.859	0.1861	0.133	−14.78	−14.82	0.1498	6.326	0.07519	7.287	0.4036
2	0.9373	0.8946	0.4701	20.15	0.553	2.388	0.1388	0.4377	−12.74	−15.79	0.1354	4.975	0.1088	6.384	0.2138
3	0.9086	1.126	0.4439	14.19	0.2715	0.8323	0.1327	0.1795	−14.12	−17.46	0.1064	3.106	0.04746	13.31	0.1948
4	0.9346	0.5468	−0.1458	17.2	0.5617	0.7332	0.1411	0.2506	−12.53	−16.36	0.1214	4.784	0	7.781	0.3952
5	0.9031	0.8296	0.2223	18.9	0.3857	2.126	0.1736	0.4512	−13.4	−11.83	0.1103	8.644	0.1838	11.38	0.3509
6	0.9303	0.6374	0.05896	19.82	0.3568	1.233	0.1952	0.3069	−15.78	−17.32	0.1546	9.343	0.07028	9.864	0.1536
7	0.9037	1.044	0.1159	16.29	0.5336	2.272	0.1943	0.2997	−13.17	−13.68	0.1503	7.429	0	12.07	0.1989
8	0.9211	0.925	−0.1345	16.7	0.2395	2.055	0.1771	0.4068	−12.3	−15.24	0.1337	7.637	0	8.417	0.3154
9	0.9434	1.176	−0.2048	21	0.3732	1.36	0.1666	0.3408	−15.67	−12.36	0.1029	2.44	0.03615	12.71	0.2349
10	0.9397	0.5984	0.1465	17.89	0.25	0.9088	0.1451	0.2792	−13.82	−12.88	0.09914	8.287	0	11.03	0.2732
11	0.9186	1.084	−0.2737	18.42	0.4659	1.74	0.1175	0.4856	−13.66	−17.07	0.1439	7.048	0.0006832	11.79	0.2538
12	0.9166	1.008	0.3811	21.2	0.2165	1.674	0.1023	0.2064	−15.26	−15.34	0.1692	5.921	0	9.198	0.3094
13	0.9003	0.5226	−0.2312	17.51	0.3183	1.158	0.1243	0.1815	−13.96	−13.01	0.1605	4.333	0.1496	10.65	0.2949
14	0.9066	0.7207	−0.02292	14.95	0.2848	1.998	0.1522	0.3859	−16.21	−15.97	0.09321	6.706	0	4.349	0.3762
15	0.9105	0.795	0.0928	18.3	0.5842	1.454	0.1054	0.1563	−16.05	−14.28	0.1251	9.119	0	10.36	0.165
16	0.8981	1.207	0.3761	21.77	0.4923	0.6555	0.1804	0.3771	−14.35	−14.52	0.1149	3.852	0	8.936	0.3419
17	0.9324	1.26	0.3254	15.56	0.4199	1.079	0.1124	0.3267	−14.68	−13.27	0.1396	9.942	0.03252	9.452	0.3587
18	0.9271	0.6934	0.2956	20.66	0.5026	2.457	0.1615	0.2355	−14.95	−16.6	0.1291	5.459	0	16.2	0.4277
19	0.9146	0.9732	−0.06155	19.35	0.3301	2.587	0.1282	0.1006	−12.88	−13.86	0.09664	3.411	0.01259	5.306	0.1723
20	0.9293	0.7715	0.1949	14.52	0.426	1.53	0.1567	0.477	−15.4	−12.54	0.1641	2.068	0	7.876	0.2582

Source: Output DTN: SN0701T0502206.043, file: *LHS_MO_R2.OUT*.

6.5.5.3 Sampled Parameter Values for Glacial Transition Net Infiltration Calculations

A total of 17 parameters were varied for the Glacial Transition climate, as listed in Tables 6.5.5.3-1 and 6.5.5.3-2. Eight of these were climate independent. Two plant parameters were varied (the mean plant height and the maximum effective rooting depth). For this climate, the analyses varied both parameters of the precipitation duration model, but only one was varied independently, so that they could be correlated.

Table 6.5.5.3-1. Parameters Varied Independently in Uncertainty Analysis for Glacial Transition Climate

Parameter Symbol	Parameter Name and Description	Uncertainty Range	Uncertainty Distribution
a_{00}	Annual average of the probability of no precipitation given that the previous day was dry (Section 6.5.1.2)	0.78 to 0.89 (unitless)	uniform
a_m	Annual average of the natural logarithm of the amount of daily rainfall on days with precipitation (Section 6.5.1.2)	0.48 to 0.92 (ln mm)	uniform
$\theta_{\lambda,1}$	Phase of the annual variation of mean daily rainfall on days with precipitation (θ_λ in Section 6.5.1.2)	−π radians to + π radians	uniform
Rate of duration increase with precipitation	Slope of the relationship between duration of daily precipitation and amount of daily rainfall (Section 6.5.1.7)	0.32 to 0.71 hr/mm	uniform
h_{plant}	Plant height (Section 6.5.3.3)	0.6 to 1.8 m	uniform
Z_r	Maximum rooting depth (Section 6.5.3.2)	1.0 to 4.0 m	uniform
$depth_{soil}(4)$	Soil depth for soil depth class 4 (Section 6.5.2.4.1)	0.1 to 0.5 m	uniform
K_{sat_rock} *(405)*	Saturated hydraulic conductivity of bedrock IHU 405 (Section 6.5.2.6)	7.6×10^{-8} m/s to 4.8×10^{-6} m/s	loguniform
K_{sat_rock}*(406)*	Saturated hydraulic conductivity of bedrock IHU 406 (Section 6.5.2.6)	2.1×10^{-8} m/s to 7.7×10^{-6} m/s	loguniform
θ_{HC}*(5/7/9)*	Holding capacity of soil group 5/7/9 (Section 6.5.2.3)	0.09 to 0.17 (m^3/m^3)	uniform
REW	Readily evaporable water (Section 6.5.4.2)	2 to 10 mm	uniform
K_{c_min}	Minimum transpiration coefficient (K_c) (Section 6.5.4.2)	0.0 to 0.2 (unitless)	50% of values = 0.0, 50% of values vary linearly from 0.0 to 0.2 [pdf is $(0.2-K_{cmin})/0.04$]
Z_e	Evaporation layer depth (Section 6.5.4.2)	0.1 to 0.2 m	uniform
C_{Kcb2}	Slope of the NDVI' – K_{cb} function (Section 6.5.3.7)	9.7 ± 2.1 (unitless)	normal

NOTE: See Table I1.5-1.

Three weather parameters were varied directly. Two additional weather parameters were not varied independently but rather were correlated (Table 6.5.5.3-2). These five weather parameters provided variation in the weather input files for model calculations.

Tables 6.5.5.3-3 and 6.5.5.3-4 report two separate sets of sampled values for the parameters listed in Table 6.5.5.3-1. These are output from two separate LHS runs. Treating them as a single set risks the possibility that unintended correlations may go undetected.

Table 6.5.5.3-2. Parameters Correlated with Other Parameters That Varied Independently in Uncertainty Analysis for Glacial Transition Climate

Parameter Symbol	Parameter Name and Description	Uncertainty Range	Uncertainty Distribution
a_λ	*Constant term in Fourier series for λ(d)*	3.1 to 4.5 mm	uniform
$\Theta_{m,1}$	*Phase of first-order term in Fourier series for m(d)*	−π radians to + π radians	uniform
Intercept-1	Minimum precipitation duration	0.70 to 1.22 hr	uniform

NOTE: See Table I1.5-2.

Table 6.5.5.3-3. LHS Sampled Parameter Values for Replicate 1 of Glacial Transition Net Infiltration Runs

Vector unit	a_00 n/a	a_m nn(mm/day)	Theta_m Rad.	h_plant m	Z_r m	Z_e m	Sdepth4 m	lnRks_405 ln (m/s)	lnRks_406 ln(m/s)	HC_579 m^3/m^3	REW n/a	Kc_min mm	CKcb2 n/a	PDurS hr/mm
1	0.8747	0.7566	−1.623	0.8611	3.521	0.1932	0.2497	−16.38	−11.92	0.1148	4.581	0.0155	11.03	0.4411
2	0.8292	0.8827	2.278	1.42	2.554	0.1793	0.4767	−15.19	−12.55	0.1464	7.789	0.04158	8.484	0.4007
3	0.7971	0.6492	−2.833	1.487	1.419	0.1992	0.4258	−14.24	−17.22	0.1017	7.04	0.09898	8.721	0.5143
4	0.858	0.5297	−2.462	0.6196	2.869	0.1545	0.3851	−14.73	−15.18	0.1547	3.588	0	6.372	0.6802
5	0.8447	0.8589	−2.671	1.243	1.74	0.1477	0.1302	−12.86	−13.51	0.1392	3.619	0.1607	4.114	0.4314
6	0.8734	0.9179	−0.4545	1.569	3.333	0.1196	0.313	−13.96	−16	0.1111	6.643	0	9.093	0.3936
7	0.8808	0.4879	−0.7859	1.768	1.288	0.1326	0.275	−15.53	−13.79	0.1515	5.252	0	10.34	0.3647
8	0.7825	0.6082	2.97	1.199	2.999	0.1737	0.1163	−15.83	−16.42	0.1033	2.566	0	7.52	0.4645
9	0.7856	0.5563	0.263	1.043	3.683	0.123	0.4457	−13.55	−15.56	0.1642	2.859	0.06294	14.04	0.3385
10	0.8069	0.8465	−1.057	1.007	2.651	0.1137	0.1428	−13.84	−14.89	0.1245	5.005	0.02871	15.15	0.5591
11	0.864	0.5167	2.142	1.131	2.278	0.1407	0.2999	−13.37	−12.91	0.1095	7.229	0.1517	11.28	0.6545
12	0.8366	0.6785	1.592	1.702	3.814	0.1031	0.2148	−14.94	−15.73	0.1439	8.252	0.09082	5.406	0.6956
13	0.7944	0.7074	0.9706	1.549	1.105	0.1698	0.1803	−12.47	−12.28	0.1614	6.124	0	9.609	0.6191
14	0.8333	0.8214	−0.2879	0.9441	2.197	0.1556	0.222	−16.17	−17.01	0.1679	9.471	0.04516	11.98	0.6407
15	0.8088	0.724	−1.271	1.275	1.528	0.1265	0.4104	−15.68	−14.6	0.09311	5.98	0	12.25	0.598
16	0.8225	0.6255	−2.19	1.674	3.875	0.1885	0.3645	−13.21	−14.24	0.1366	8.821	0	10.45	0.5275
17	0.8894	0.7742	2.798	1.344	2.46	0.185	0.3535	−12.97	−17.45	0.1264	2.149	0	12.98	0.5525
18	0.8512	0.5774	0.3831	0.6971	1.833	0.1397	0.1702	−14.48	−16.53	0.119	9.614	0	7.98	0.3503
19	0.8131	0.8003	1.482	0.789	2.029	0.1092	0.4891	−14.96	−14.06	0.1317	4.113	0	6.983	0.5785
20	0.8525	0.6582	0.8224	0.7201	3.152	0.1629	0.3206	−12.43	−13.18	0.09419	8.679	0.002592	10.01	0.4816

Source: Output DTN: SN0701T0502206.043, file: *LHS_GT_R1.OUT*.

Table 6.5.5.3-4. LHS Sampled Parameter Values for Replicate 2 of Glacial Transition Net Infiltration Runs

Vector unit	a_00 n/a	a_m nn(mm/day)	Theta_m Rad.	h_plant m	Z_r m	Z_e m	Sdepth4 m	lnRks_405 ln (m/s)	lnRks_406 ln(m/s)	HC_579 m^3/m^3	REW n/a	Kc_min mm	CKcb2 n/a	PDurS hr/mm
1	0.8371	0.7218	−1.236	1.748	1.432	0.17	0.1171	−13.69	−12.99	0.1138	7.399	0.0509	6.478	0.6032
2	0.8595	0.8843	−2.887	0.7525	2.344	0.1115	0.2203	−15.28	−15.98	0.1386	8.307	0	12.84	0.6578
3	0.8681	0.8738	−0.8745	0.8444	2.795	0.1294	0.3214	−12.89	−12.16	0.1059	5.133	0	8.706	0.4326
4	0.7966	0.6956	0.5525	1.612	3.888	0.135	0.4615	−15.41	−11.83	0.1275	8.701	0	9.991	0.6206
5	0.8854	0.4926	1.872	1.478	3.283	0.1051	0.2466	−13.35	−13.67	0.1643	6.025	0.07518	10.88	0.5715
6	0.8161	0.5203	0.979	1.179	1.124	0.1239	0.4404	−14.42	−14.47	0.1475	3.193	0	12.01	0.6392
7	0.7927	0.7458	2.678	1.707	2.951	0.1618	0.2769	−12.62	−15.33	0.0938	6.829	0	11.42	0.5145
8	0.8225	0.7718	2.28	0.6145	3.153	0.1819	0.3755	−14.18	−12.51	0.143	3.413	0.008806	5.912	0.6903
9	0.7813	0.8071	−2.129	1.387	2.05	0.1158	0.4249	−13.97	−16.57	0.1611	4.725	0.06246	3.838	0.3543
10	0.8763	0.9106	3.06	1.109	1.519	0.1543	0.4049	−15.02	−15.74	0.1165	5.9	0.1032	9.484	0.4064
11	0.8643	0.5518	−1.415	1.039	2.437	0.1304	0.498	−12.75	−16.33	0.107	9.287	0	8.11	0.3792
12	0.8031	0.6281	−2.228	0.9849	1.774	0.1873	0.2066	−12.34	−15.1	0.1183	2.37	0.04421	12.26	0.4879
13	0.8309	0.5733	0.8117	0.9121	2.811	0.199	0.2801	−16.14	−14.05	0.1344	7.794	0	13.4	0.328
14	0.8281	0.6455	−0.2558	1.353	1.671	0.1917	0.3147	−14.89	−17.01	0.133	9.625	0.02813	10.56	0.6973
15	0.8504	0.8532	−2.696	1.674	2.516	0.1499	0.3976	−15.57	−12.9	0.1256	4.265	0.1277	14.82	0.4452
16	0.881	0.5436	−1.748	1.269	3.463	0.1762	0.3433	−15.83	−17.15	0.09403	2.694	0.0208	7.154	0.5809
17	0.8561	0.7389	−0.4868	1.209	1.233	0.1597	0.178	−14.6	−13.4	0.1549	6.542	0	7.402	0.3749
18	0.8429	0.82	2.177	1.532	3.783	0.1418	0.1952	−13.88	−17.52	0.1689	3.974	0	10.16	0.4602
19	0.7865	0.5986	1.491	0.8085	1.985	0.1003	0.1204	−16.2	−14.82	0.1011	5.334	0	9.013	0.5461
20	0.8078	0.6642	0.02717	0.6989	3.552	0.1652	0.148	−13.1	−14.37	0.1517	9.109	0.174	8.317	0.5152

Source: Output DTN: SN0701T0502206.043, file: *LHS_GT_R2.OUT*.

6.5.6 Calculation Procedure

6.5.6.1 Assembling Model Input

For each of the three future climates, two Latin Hypercube Sample (LHS) replicates were generated (Output DTN: SN0701T0502206.043). A LHS replicate is a complete structured set of Monte Carlo samples covering the entire probability range of all the sampled parameters (LHS User's Manual, STN 10205-2.51-01 [DIRS 178784]). Each replicate in this analysis consists of 20 realizations of input parameter values (Section 6.5.5). Two replicates were run to test the stability of the distribution of infiltration results. The comparison between these two replicates is discussed in Section 6.5.7.9. Tables in Section 6.5.5 list the parameters that were varied for each climate accompanied by the probability distributions from which the parameters were sampled. Some of the parameters that were varied included stochastic parameters describing precipitation that affect the generation of the weather input files (Appendix F). For each realization, a separate weather input file was generated, which used the sampled values of these parameters, representing epistemic uncertainty:

- Present-Day Weather files: Output DTN: SN0701T0502206.040
- Monsoon Weather files: Output DTN: SN0701T0502206.041
- Glacial Transition Weather files: Output DTN: SN0701T0502206.042.

In addition, each of these weather file realizations used a different set of random numbers, which resulted in differing patterns of precipitation and reflected aleatory uncertainty.

For each realization, the appropriate weather input file and parameter set was selected and the MASSIF net infiltration model was run for each of the 11 watersheds separately (Output DTN: SN0701T0502206.037).

6.5.6.2 Model Execution

MASSIF was run in a separate Mathcad file for each of the realizations. Names of these files were of the form *Present Day R1 V03.xmcd*. The first part of the name indicates the climate (Present-Day, Monsoon, Glacial Transition). The second part of the name (R1 or R2) indicates the replicate number. The third part of the name (V01 thru V20) indicates realization number. Within each of the 40 Mathcad files (20 realizations × 2 replicates), the MASSIF routine was executed for each of the 11 watersheds.

Results of each realization are stored in subdirectories named V01 thru V20, which are subdirectories of the directories "Replicate 1" and "Replicate 2." Each realization generated 55 separate ASCII output files. For each of the 11 watersheds, 5 types of files were generated:

1. File listing 10 annual values (columns 1 thru 10) and the weighted mean value (column 11) of precipitation for each cell [file name example: *Precip_WS01_PD_R1_V01.prn*]

2. File listing 10 annual values (columns 1 thru 10) and the weighted mean value (column 11) of net infiltration for each cell [file name example: *Infil_WS01_PD_R1_V01.prn*]

3. File listing 10 annual values (columns 1 thru 10) and the weighted mean value (column 11) of run-on for each cell [file name example: *Runon_WS01_PD_R1_V01.prn*]

4. File listing 10 annual values (columns 1 thru 10) and the weighted mean value (column 11) of runoff for each cell [file name example: *Runoff_WS01_PD_R1_V01.prn*]

5. File listing the annual integrated (spatially and temporally) values of (column 1) change in water storage, (column 2) change in snow level, (column 3) precipitation, (column 4) evapotranspiration, (column 5) net infiltration, (column 6) annual sublimation, and (column 7) runoff [file name example: *Watershed_WS01_PD_R1_V01.prn*].

The naming convention of the output files indicates the output variable stored and the source of the inputs. Hence, the output file name "Precip_WS01_PD_R1_V01" indicates that the file contains values of precipitation for watershed 1 (WS01) for the present day (PD) for replicate 1 (R1) and realization 1 (V01). The number of rows in each of the first 4 output types (Precip, Infil, Runon, and Runoff) is equal to the number of cells in the watershed. The cells are listed in the same sequence as in the corresponding geospatial file. The file containing integrated values (Watershed….) has 10 rows corresponding to the 10 precipitation years modeled.

The 40 Mathcad files (for each climate) in which each realization is computed were designed so that the calculation can be spot-checked at a later date by an independent reviewer. The reviewer is allowed to select a watershed (# 1 to 11) and a single precipitation year (1 to 10). MASSIF is then executed for the chosen combination. Results of the reviewer's calculation are automatically displayed along with the results that are stored in the appropriate results subdirectory. This process gives the independent reviewer the capability to verify the reproducibility of the stored results.

6.5.6.3 Post-Processing of Results

Post-processing of results for each climate consists of following a set of defined calculation steps, which are described in detail in Mathcad file *MASSIF Results Documentation.xmcd* in Output DTN: SN0701T0502206.037.

6.5.7 Results of Net Infiltration Calculations

The results of the net infiltration calculation performed for the 125 km^2 infiltration modeling domain around Yucca Mountain are presented in this section. The calculations described in this section are included in Output DTN: SN0701T0502206.037. *UZ Flow Models and Submodels* (BSC 2004 [DIRS 169861]) and *Calibrated Properties Model* (BSC 2004 [DIRS 169857]) are use preliminary set of results that were generated during the preparation of initial drafts of this report and are slightly different than the qualified output DTNs described in this section. These preliminary output DTNs are discussed in Appendix L. The output DTNs with net infiltration results for each climate that are considered qualified in this report include the following Output DTNs: SN0701T0502206.034 (Present-Day), SN0701T0502206.036 (Monsoon), and SN0701T0502206.035 (Glacial Transition).

As discussed in Sections 6.5.5 and 6.5.6, for each climate two LHS replicates of 20 realizations each were run in order to estimate the uncertainty and stability of model results. The differences between the two replicates for each climate are an indication of the additional uncertainty caused by the small sample size of 20 realizations. The results of both replicates are combined for the main uncertainty analysis.

This section is organized as follows: Sections 6.5.7.1 to 6.5.7.3 present an overview of precipitation and net infiltration results for each of the future climates considered (Present-Day, Monsoon, and Glacial Transition). These results include: (1) presentation of the precipitation variability between realizations, (2) comparisons of average values of net infiltration over various domains, and (3) a presentation of net infiltration maps representing the 10th, 30th, 50th, and 90th percentiles. Section 6.5.7.4 compares the magnitudes of the various water balance components for each climate and for runs made with an alternative set of initial soil moisture content initial conditions. Section 6.5.7.5 discusses factors that influence the temporal variability in net infiltration. Section 6.5.7.6 discusses factors that influence the spatial variability in net infiltration during the Present-Day climate. Section 6.5.7.7 illustrates daily conditions in a single grid cell in Pagany Wash in order to demonstrate some of the key features of the model. Section 6.5.7.8 summarizes the results of the uncertainty analysis.

Plots of daily precipitation and temperature used for each realization can be found in Output DTN: SN0701T0502206.037 in the individual Mathcad files in which the realizations are run.

6.5.7.1 Present-Day Simulation Results

6.5.7.1.1 Present-Day Precipitation Results

The mean annual precipitation (MAP) (at the reference elevation of 1,524 m) used for the 40 realizations representing Present-Day climate is summarized in Figure 6.5.7.1-1 and Table 6.5.7.1-1. The parameters used to represent Present-Day climate are described in Section 6.5.1 and Appendix F.

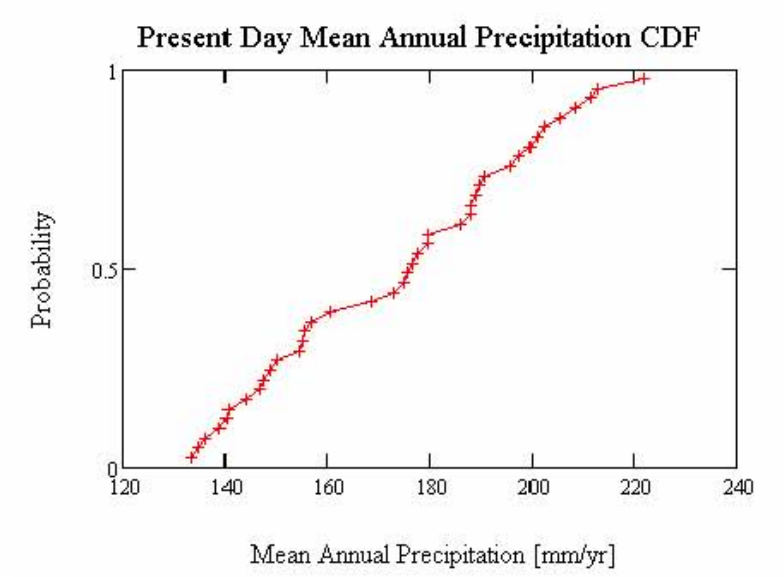

Source: Output DTN: SN0701T0502206.037, file: \Welcome to Massif\Massif\Present Day Uncertainty\Post Processing*PD_Combined_Replicates.xmcd*.

NOTE: A total of 40 realizations (2 LHS replicates) define the distribution. MAP values are for a reference elevation of 1,524 m above sea level.

Figure 6.5.7.1-1. Present-Day Mean Annual Precipitation CDF

Table 6.5.7.1-1. Mean Annual Precipitation Statistics for the 40 Realizations Used to Represent Present-Day Climate for Net Infiltration Calculations

Present-Day Precipitation	R1 (mm/yr)	R2 (mm/yr)	R1 and R2 (mm/yr)
Minimum [mm/yr]	134.9	133.6	133.6
Mean [mm/yr]	173.4	173.7	173.6
Median [mm/yr]	176.3	176.4	176.3
Maximum [mm/yr]	222.0	212.7	222.0
Standard Deviation [mm/yr]	26.2	25.3	25.4

Source: Output DTN: SN0701T0502206.037, file: \Welcome to Massif\Massif\Present Day Uncertainty\Post Processing*PD_Combined_Replicates.xmcd*.

6.5.7.1.2 Present-Day Net Infiltration Uncertainty Analysis Results

As described in Sections 6.5.5 and 6.5.6, two replicates (R1 and R2) of 20 realizations each were run for Present-Day climate mean annual net infiltration estimation. Table 6.5.7.1-2 compares mean annual net infiltration statistics for these realizations. Table 6.5.7.1-3 identifies the maps that represent the 10th, 30th, 50th, and 90th percentiles of mean annual net infiltration over the entire model domain. Figures 6.5.7.1-2 to 6.5.7.1-5 show maps of mean annual net infiltration for these four maps. Figure 6.5.7.1-6 presents a CDF of spatially averaged mean annual net infiltration over the full modeling domain for the Present-Day climate results.

Table 6.5.7.1-2. Spatially Averaged Mean Annual Net Infiltration [mm/yr] Statistics for Present-Day Simulations

Present-Day Climate	Domain	R1 (mm/yr)	R2 (mm/yr)	R1 and R2 (mm/yr)
Minimum [mm/yr]	Infiltration modeling domain (125 km^2)	2.0	3.1	2.0
	UZ modeling domain (39.8 km^2)	1.4	2.1	1.4
	Repository footprint (5.7 km^2)	1.5	1.9	1.5
Mean [mm/yr]	Infiltration modeling domain (125 km^2)	13.4	15.2	14.3
	UZ modeling domain (39.8 km^2)	14.2	16.0	15.1
	Repository footprint (5.7 km^2)	16.7	18.6	17.6
Median [mm/yr]	Infiltration modeling domain (125 km^2)	11.4	13.7	12.9
	UZ modeling domain (39.8 km^2)	12.2	12.8	12.4
	Repository footprint (5.7 km^2)	14.9	14.0	14.5
Maximum [mm/yr]	Infiltration modeling domain (125 km^2)	28.8	35.4	35.4
	UZ modeling domain (39.8 km^2)	32.6	40.9	40.9
	Repository footprint (5.7 km^2)	38.6	48.2	48.2
Standard Deviation [mm/yr]	Infiltration modeling domain (125 km^2)	8.3	9.5	8.8
	UZ modeling domain (39.8 km^2)	9.7	11.3	10.4
	Repository footprint (5.7 km^2)	11.5	13.6	12.5

Source: Output DTN: SN0701T0502206.037, file: \Welcome to Massif\Massif\Present Day Uncertainty\Post Processing*PD_Combined_Replicates.xmcd*.

Table 6.5.7.1-3. Realizations Identified for Selected Percentiles of Present-Day Spatially Averaged Mean Annual Net Infiltration

Percentile	Replicate	Realization	Net Infiltration (mm/yr)	Mean Annual Precipitation (mm/yr)
10th	R2	10	3.9	144.1
30th	R2	2	7.3	160.6
50th	R2	8	13.0	189.3
90th	R2	14	26.7	212.7

Source: Output DTN: SN0701T0502206.037, file: \Welcome to Massif\Massif\Present Day Uncertainty\Post Processing*PD_Combined_Replicates.xmcd*.

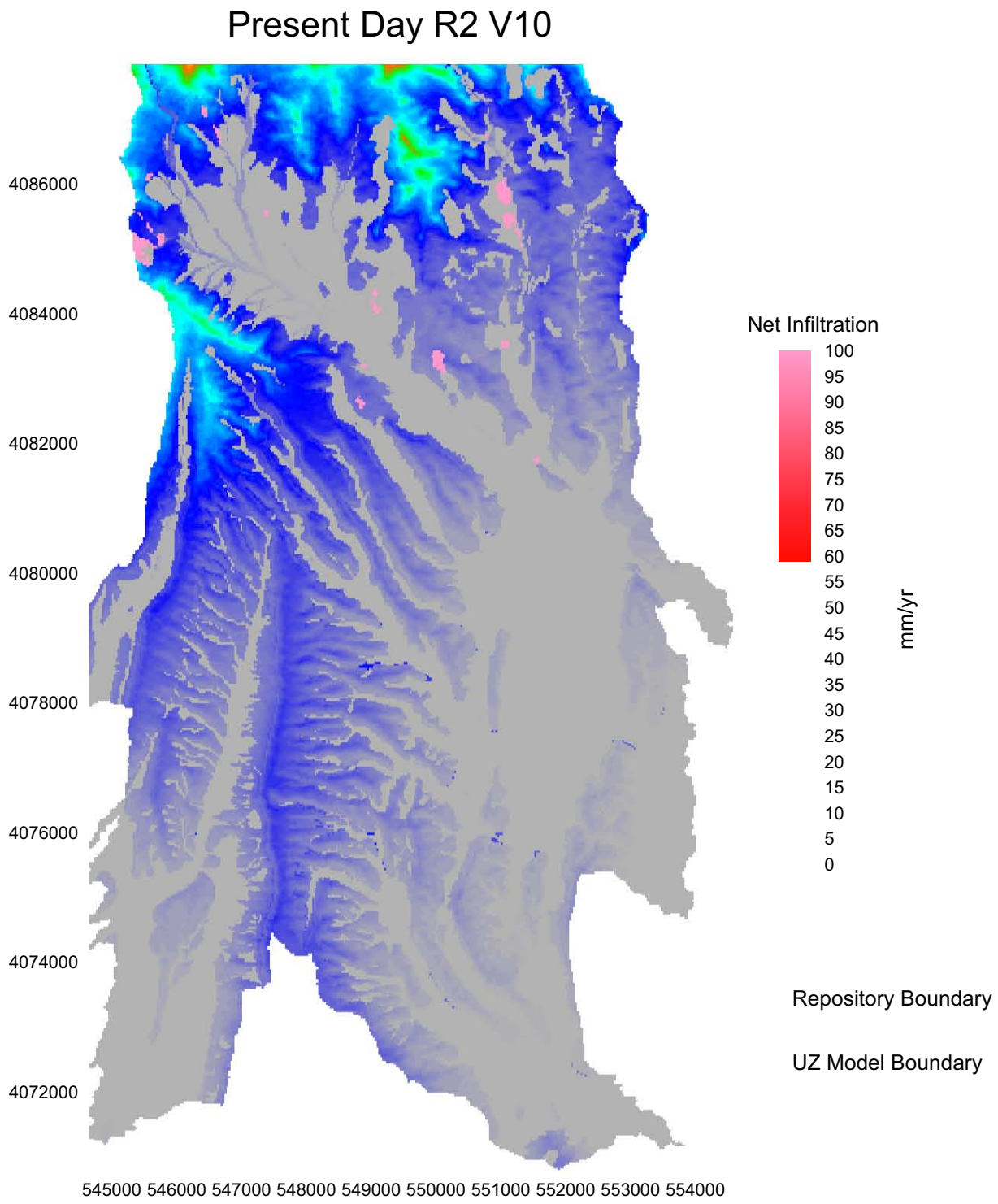

Coordinates are in meters; UTM NAD 27, Zone 11

Source: Output DTNs: SN0701T0502206.034 (Mean Annual Net Infiltration Results); SN0612FTPRNUZB.002 (UZ Model and Repository Boundaries).

Figure 6.5.7.1-2. Present-Day, 10th Percentile Mean Annual Net Infiltration Map (Replicate R2, Realization 10)

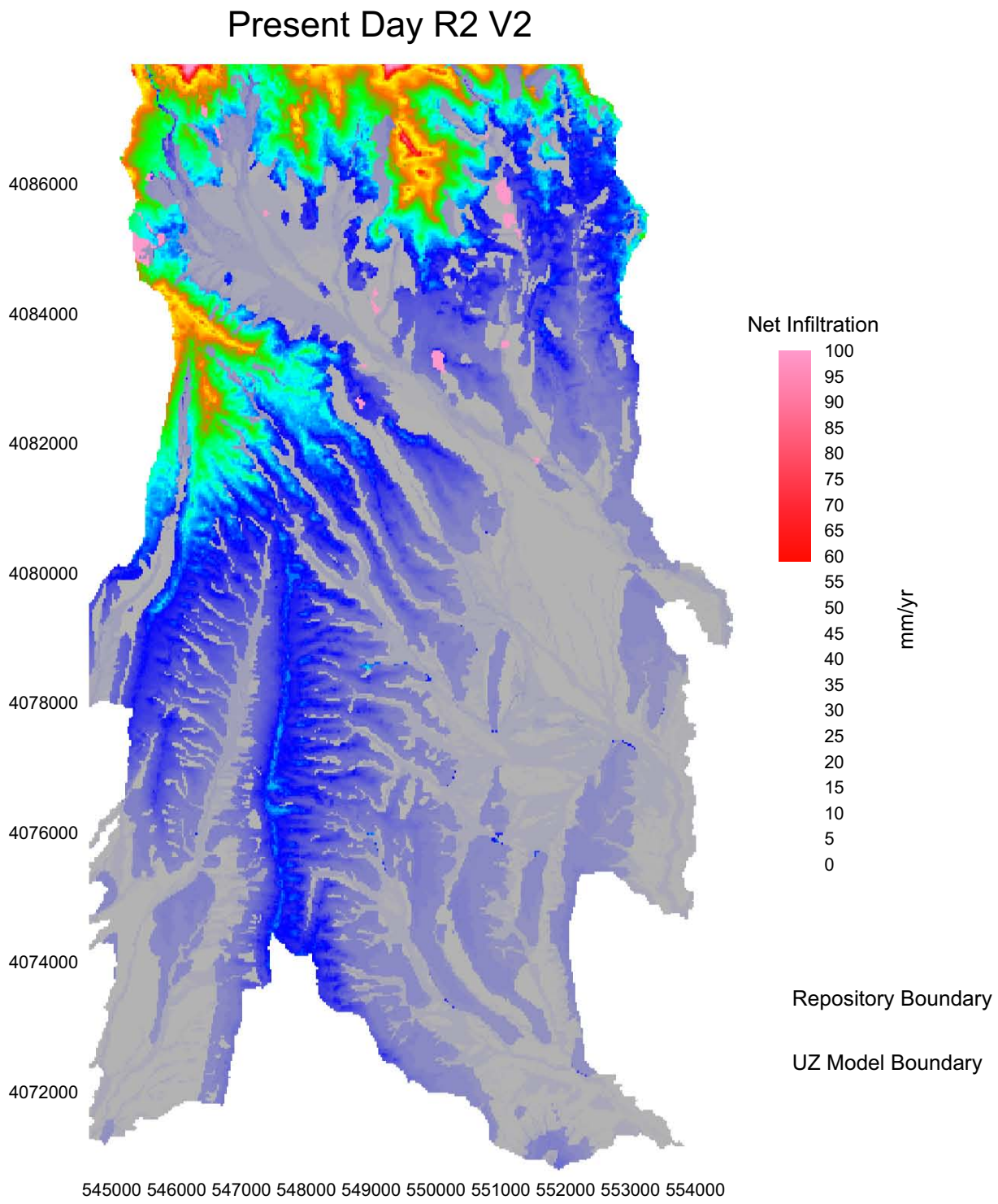

Coordinates are in meters; UTM NAD 27, Zone 11

Source: Output DTNs: SN0701T0502206.034 (Mean Annual Net Infiltration Results); SN0612FTPRNUZB.002 (UZ Model and Repository Boundaries).

Figure 6.5.7.1-3. Present-Day, 30th Percentile Mean Annual Net Infiltration Map (Replicate R2, Realization 2)

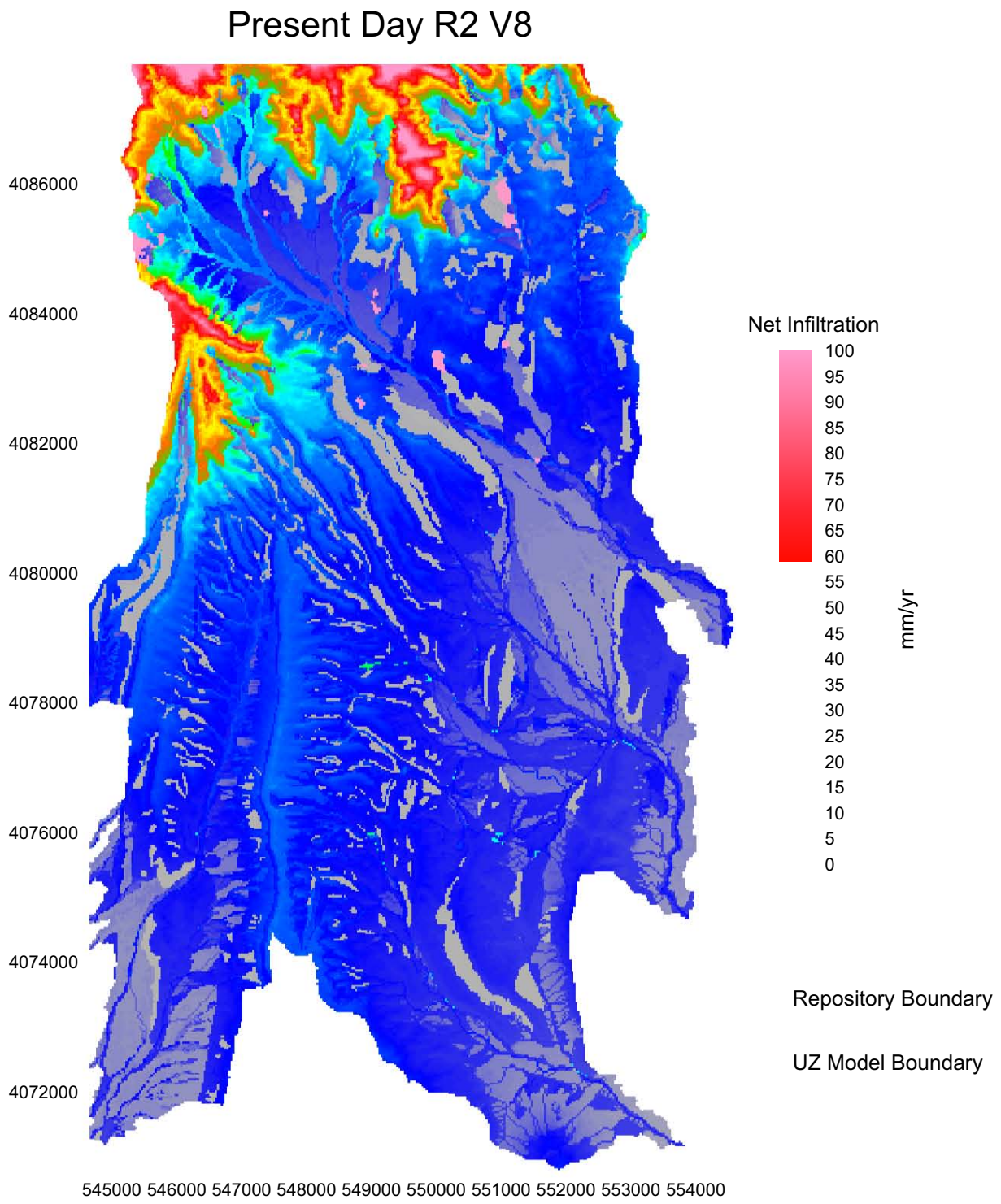

Coordinates are in meters; UTM NAD 27, Zone 11

Source: Output DTNs: SN0701T0502206.034 (Mean Annual Net Infiltration Results); SN0612FTPRNUZB.002 (UZ Model and Repository Boundaries).

Figure 6.5.7.1-4. Present-Day, 50th Percentile Mean Annual Net Infiltration Map (Replicate R2, Realization 8)

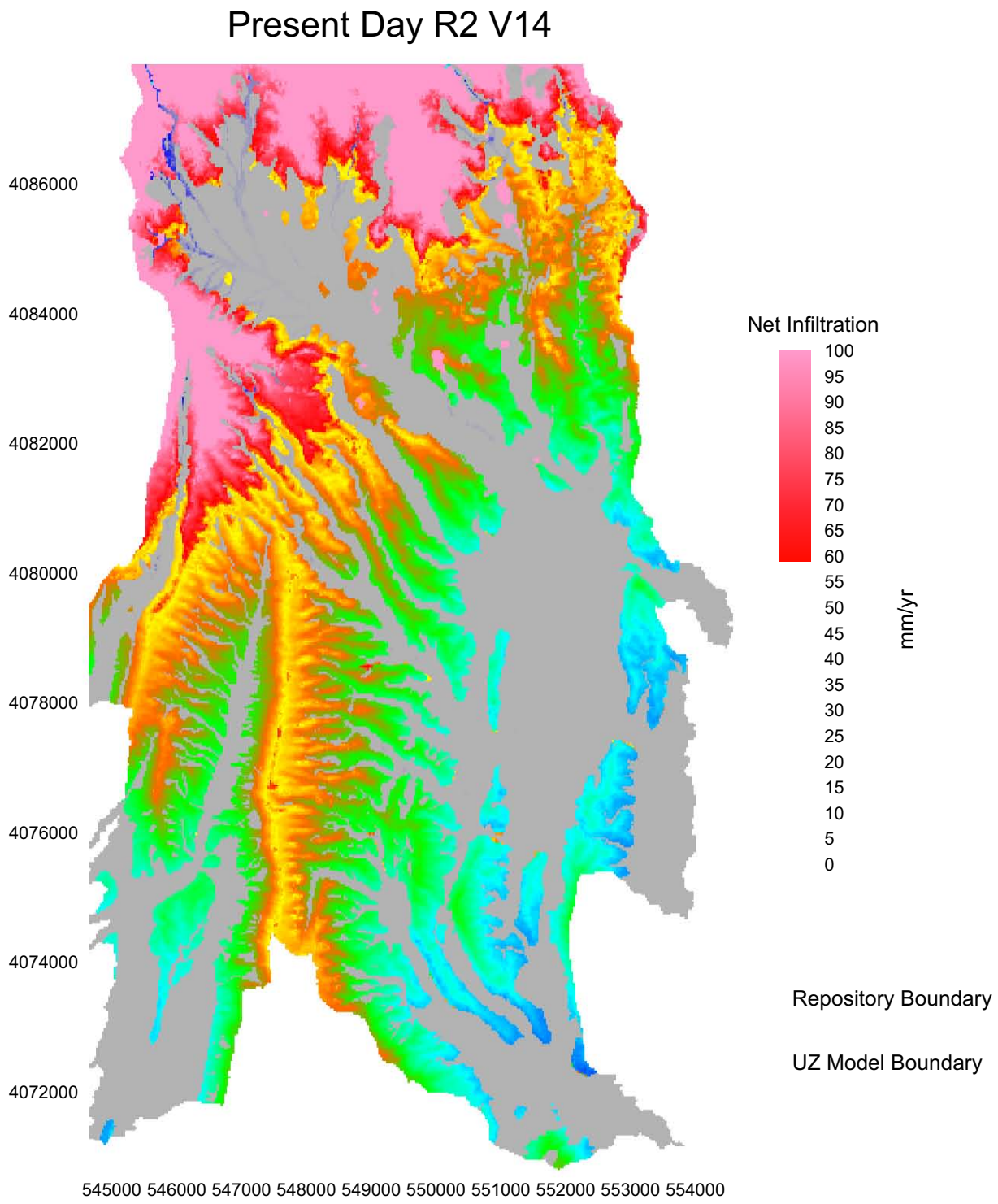

Coordinates are in meters; UTM NAD 27, Zone 11

Source: Output DTN: SN0701T0502206.034 (Mean Annual Net Infiltration Results); SN0612FTPRNUZB.002 (UZ Model and Repository Boundaries).

Figure 6.5.7.1-5. Present-Day, 90th Percentile Mean Annual Net Infiltration Map (Replicate R2, Realization 14)

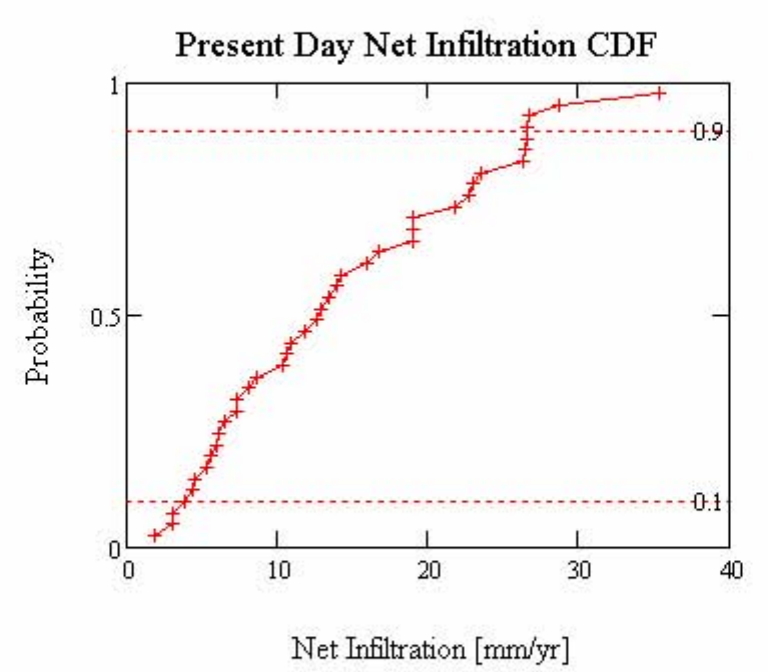

Source: Output DTN: SN0701T0502206.037, file: \Welcome to Massif\Massif\Present Day Uncertainty\Post Processing*PD_Combined_Replicates.xmcd*.

NOTE: A total of 40 realizations (2 LHS replicates) define the distribution.

Figure 6.5.7.1-6. Cumulative Distribution Function (CDF) of Present-Day Spatially Averaged Mean Annual Net Infiltration over the Infiltration Domain

6.5.7.2 Monsoon Simulation Results

6.5.7.2.1 Monsoon Precipitation Results

The mean annual precipitation (MAP) (at the reference elevation of 1,524 m) used for the 40 realizations representing Monsoon climate is summarized in Figure 6.5.7.2-1 and Table 6.5.7.2-1 below. The parameters used to represent Monsoon climate are described in Section 6.5.1 and Appendix F.

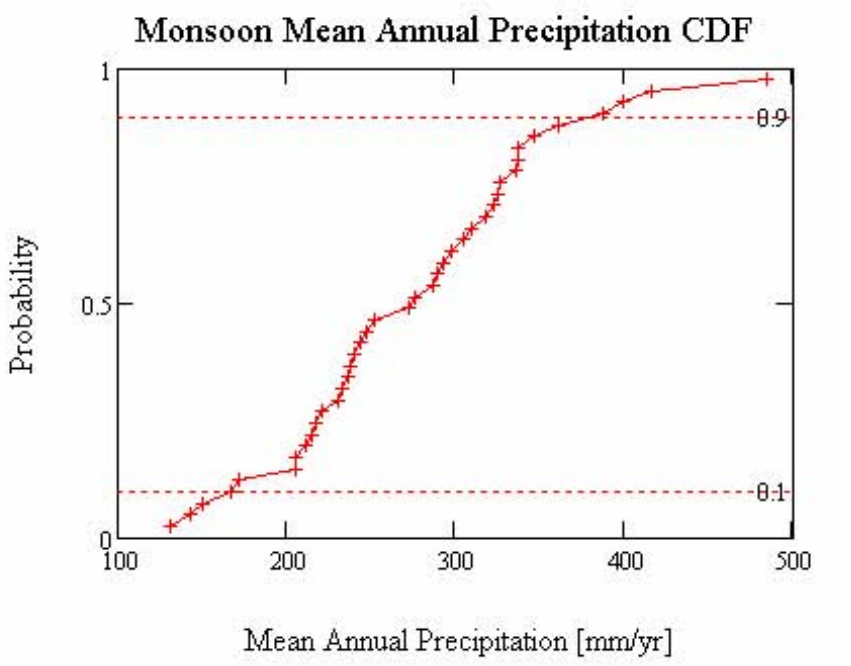

Source: Output DTN: SN0701T0502206.037, file: \Welcome to Massif\Massif\Monsoon Uncertainty\Post Processing*MO_Combined_Replicates.xmcd*.

NOTE: A total of 40 realizations (2 LHS replicates) define the distribution. MAP values are for a reference elevation of 1,524 m above sea level.

Figure 6.5.7.2-1. Monsoon Mean Annual Precipitation CDF

Table 6.5.7.2-1. Mean Annual Precipitation Statistics for the 40 Realizations used to Represent Monsoon Climate for Net Infiltration Calculations

Monsoon Precipitation	R1 (mm/yr)	R2 (mm/yr)	R1 and R2 (mm/yr)
Minimum [mm/yr]	132.1	144.0	132.1
Mean [mm/yr]	272.7	277.8	275.2
Median [mm/yr]	262.7	279.8	274.8
Maximum [mm/yr]	399.7	484.7	484.7
Standard Deviation [mm/yr]	71.9	85.5	78.0

Source: Output DTN: SN0701T0502206.037, file: \Welcome to Massif\Massif\Monsoon Uncertainty\Post Processing*MO_Combined_Replicates.xmcd*.

6.5.7.2.2 Monsoon Net Infiltration Uncertainty Analysis Results

As described in Sections 6.5.5 and 6.5.6, two replicates (R1 and R2) of 20 realizations each were run for the Monsoon climate net infiltration estimation. Table 6.5.7.2-2 compares spatially averaged mean annual net infiltration statistics for these realizations. Table 6.5.7.2-3 identifies the maps that represent the 10th, 30th, 50th, and 90th percentiles of spatially averaged mean annual net infiltration over the entire model domain. Figures 6.5.7.2-2 to 6.5.7.2-5 show maps of mean annual net infiltration for these four realizations. Figure 6.5.7.2-6 presents a CDF of spatially averaged mean annual net infiltration over the full domain for the Monsoon climate results.

Table 6.5.7.2-2. Spatially Averaged Mean Annual Net Infiltration [mm/yr] Statistics for Monsoon Simulations

Monsoon Climate	Domain	R1 (mm/yr)	R2 (mm/yr)	R1 and R2 (mm/yr)
Minimum [mm/yr]	Infiltration modeling domain (125 km^2)	3.0	2.4	2.4
	UZ modeling domain (39.8 km^2)	1.9	1.2	1.2
	Repository footprint (5.7 km^2)	2.0	1.2	1.2
Mean [mm/yr]	Infiltration modeling domain (125 km^2)	23.5	27.6	25.5
	UZ modeling domain (39.8 km^2)	25.8	30.1	28.0
	Repository footprint (5.7 km^2)	30.5	35.3	32.9
Median [mm/yr]	Infiltration modeling domain (125 km^2)	23.3	20.4	22.8
	UZ modeling domain (39.8 km^2)	25.0	22.7	24.2
	Repository footprint (5.7 km^2)	29.3	27.1	28.4
Maximum [mm/yr]	Infiltration modeling domain (125 km^2)	52.6	83.4	83.4
	UZ modeling domain (39.8 km^2)	62.2	86.2	86.2
	Repository footprint (5.7 km^2)	74.5	95.3	95.3
Standard Deviation [mm/yr]	Infiltration modeling domain (125 km^2)	14.9	21.1	18.2
	UZ modeling domain (39.8 km^2)	17.3	23.0	20.2
	Repository footprint (5.7 km^2)	20.4	26.2	23.3

Source: Output DTN: SN0701T0502206.037, file: \Welcome to Massif\Massif\Monsoon Uncertainty\Post Processing*MO_Combined_Replicates.xmcd*.

Table 6.5.7.2-3. Realizations Identified for Selected Percentiles of Monsoon Spatially Averaged Mean Annual Net Infiltration

Percentile	Replicate	Realization	Net Infiltration [mm/yr]	Mean Annual Precipitation [mm/yr]
10th	R1	17	6.3	206.5
30th	R2	10	14.4	150.7
50th	R1	2	22.9	240.8
90th	R1	7	52.6	310.2

Source: Output DTN: SN0701T0502206.037, file: \Welcome to Massif\Massif\Monsoon Uncertainty\Post Processing*MO_Combined_Replicates.xmcd*.

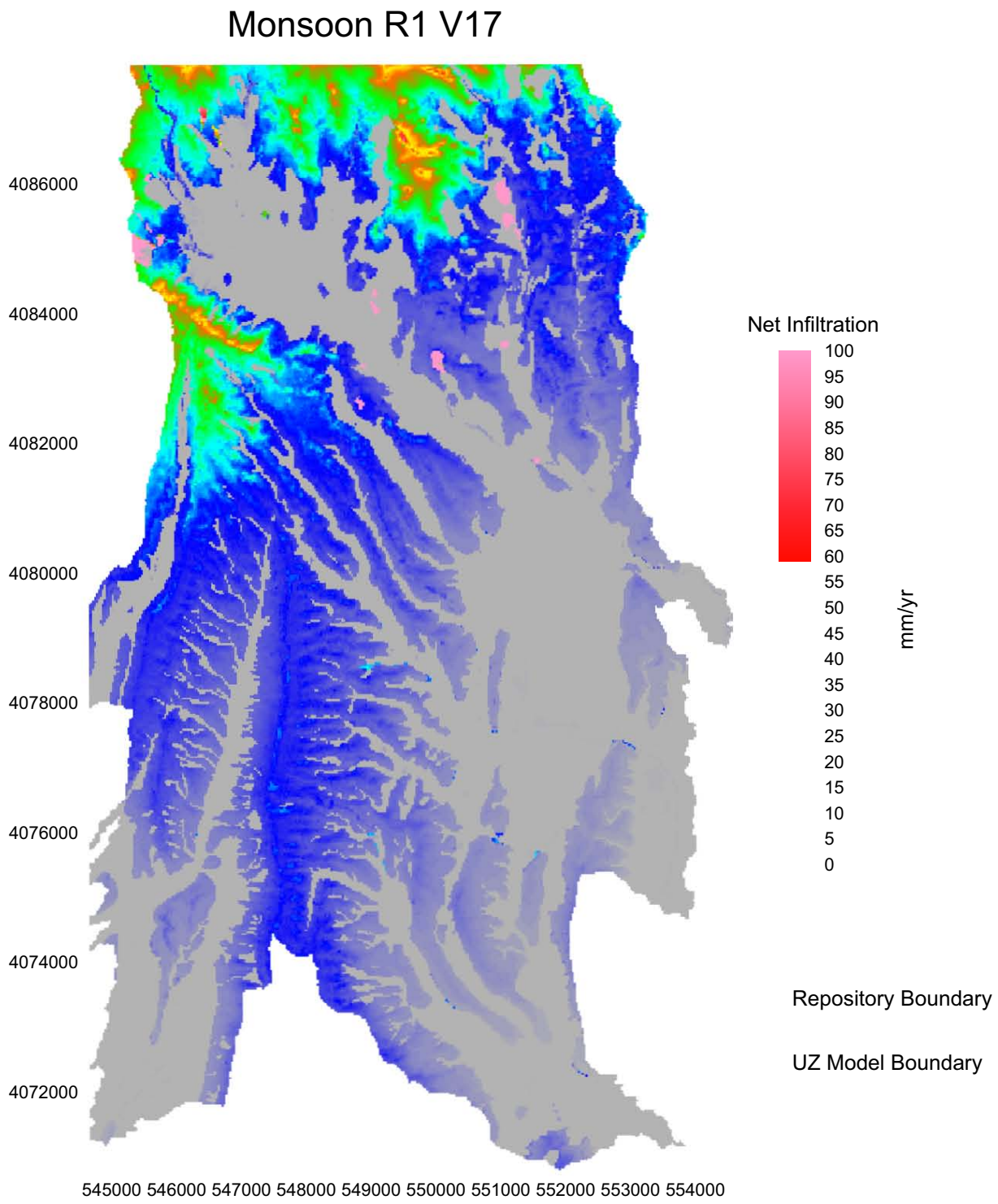

Coordinates are in meters; UTM NAD 27, Zone 11

Source: Output DTNs: SN0701T0502206.036 (Mean Annual Net Infiltration Results); SN0612FTPRNUZB.002 (UZ Model and Repository Boundaries).

Figure 6.5.7.2-2. Monsoon, 10th Percentile Mean Annual Net Infiltration Map (Replicate R1, Realization 17)

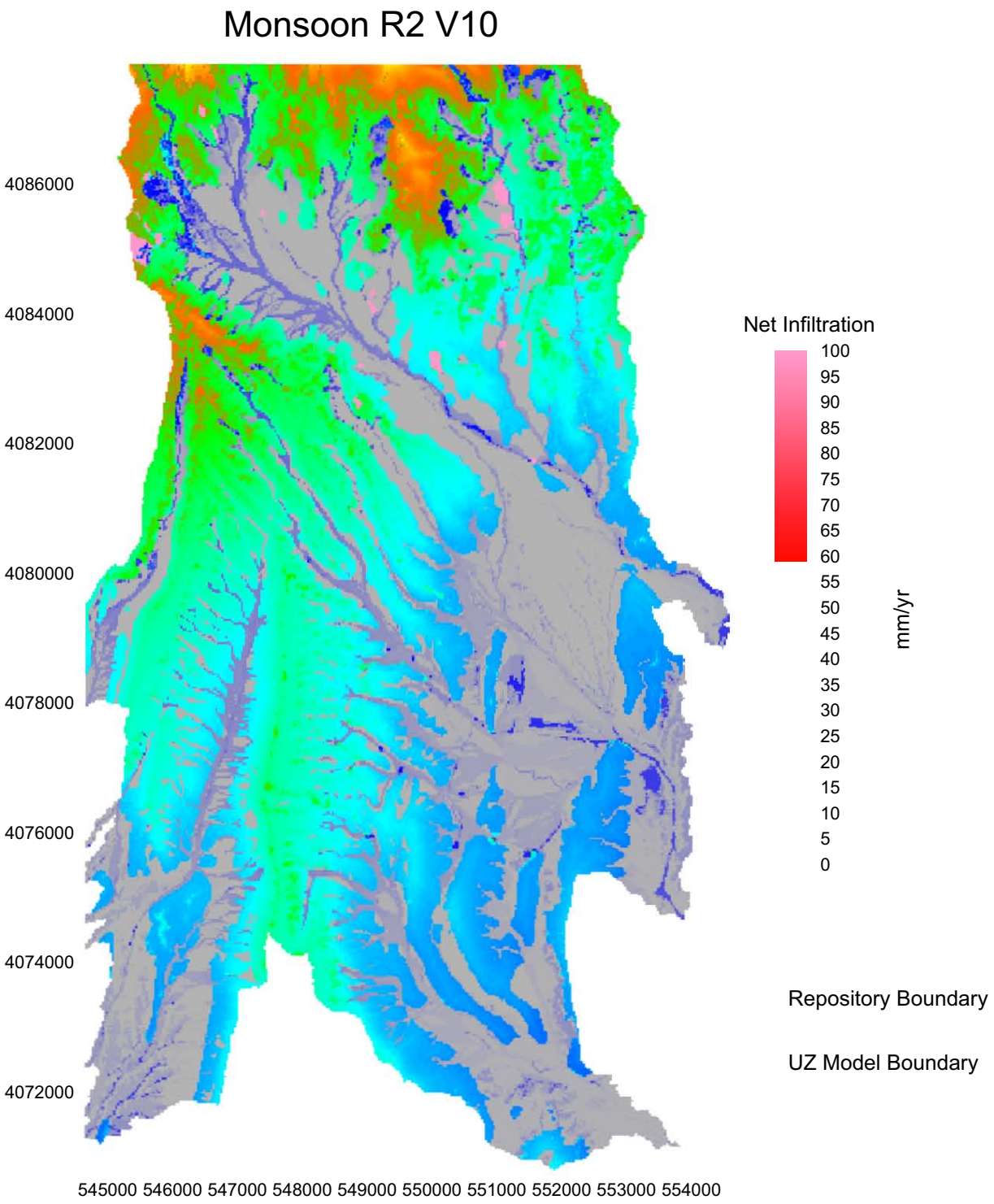

Coordinates are in meters; UTM NAD 27, Zone 11

Source: Output DTNs: SN0701T0502206.036 (Mean Annual Net Infiltration Results); SN0612FTPRNUZB.002 (UZ Model and Repository Boundaries).

Figure 6.5.7.2-3. Monsoon, 30th Percentile Mean Annual Net Infiltration Map (Replicate R2, Realization 10)

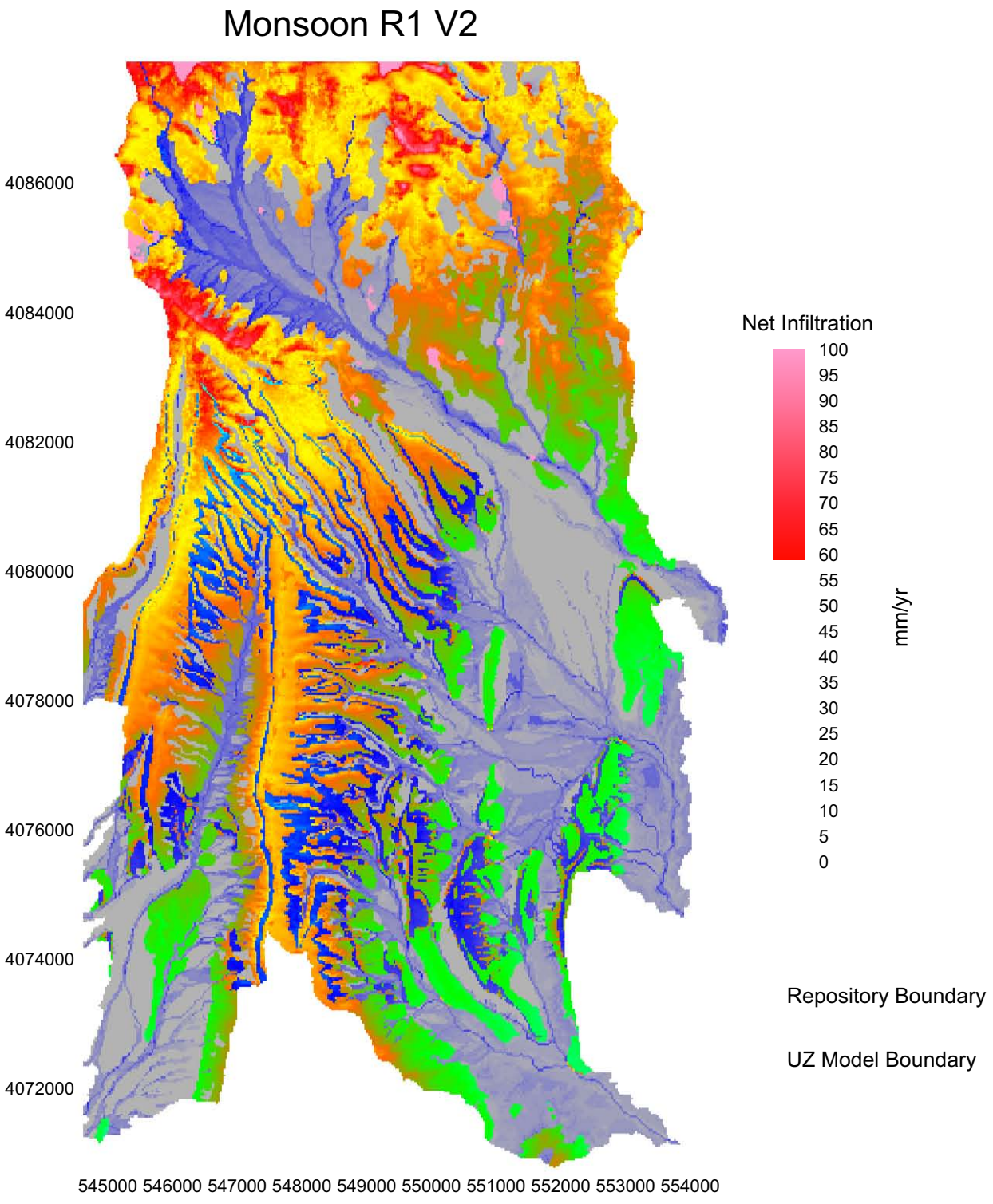

Coordinates are in meters; UTM NAD 27, Zone 11

Sourxe: Output DTNs: SN0701T0502206.036 (Net Infiltratio n Results); and SN0612FTPRNUZB.002 (UZ Model and Repository Boundaries).

Figure 6.5.7.2-4. Monsoon, 50th Percentile Net Infiltration Map (Replicate R1, Realization 2)

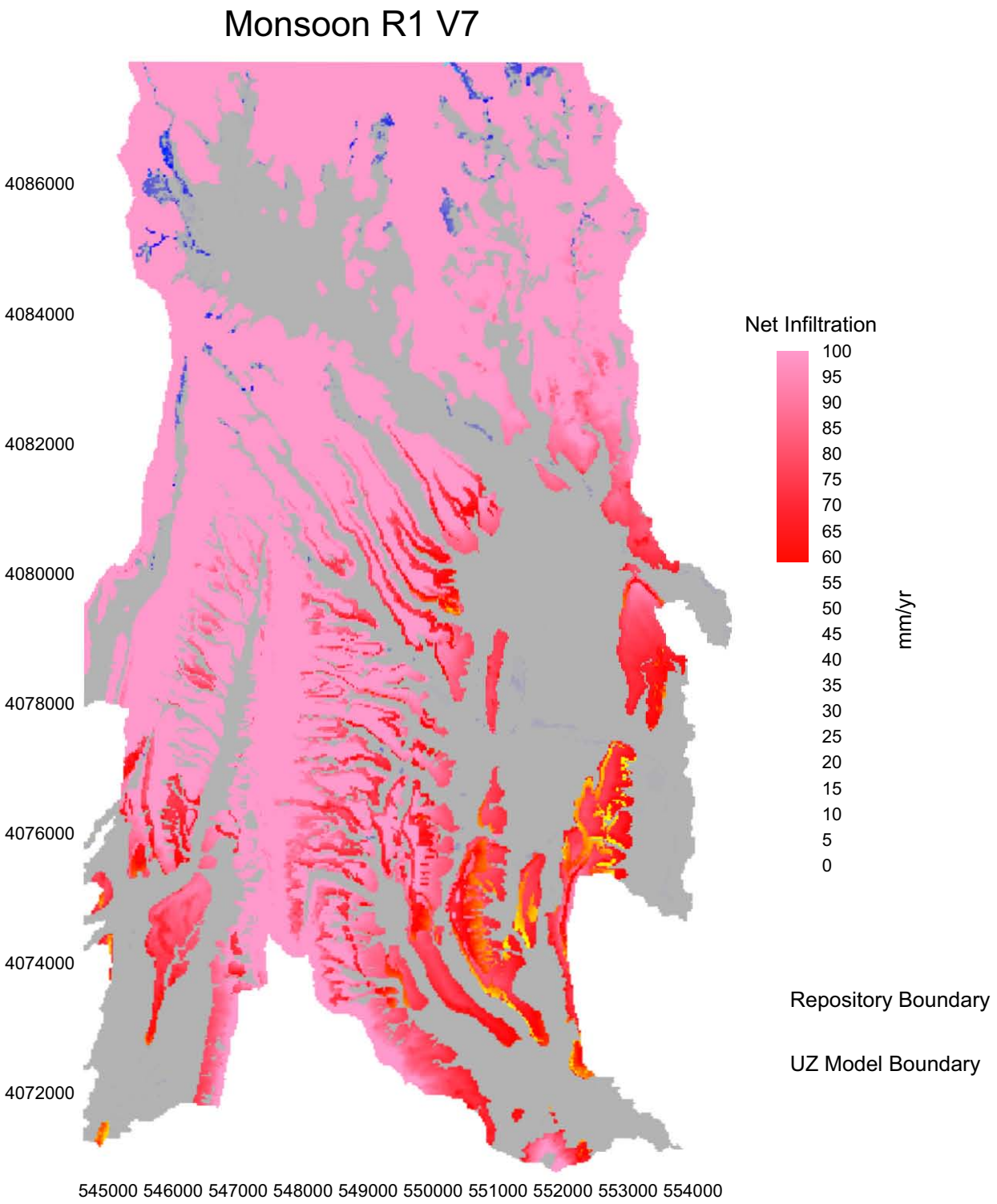

Coordinates are in meters; UTM NAD 27, Zone 11

Source: Output DTN: SN0701T0502206.036 (N et Infiltration Results); and SN0612FTPRNUZB.002 (UZ Model and Repository Boundaries).

Figure 6.5.7.2-5. Monsoon, 90th Percentile Net Infiltration Map (Replicate R1, Realization 7)

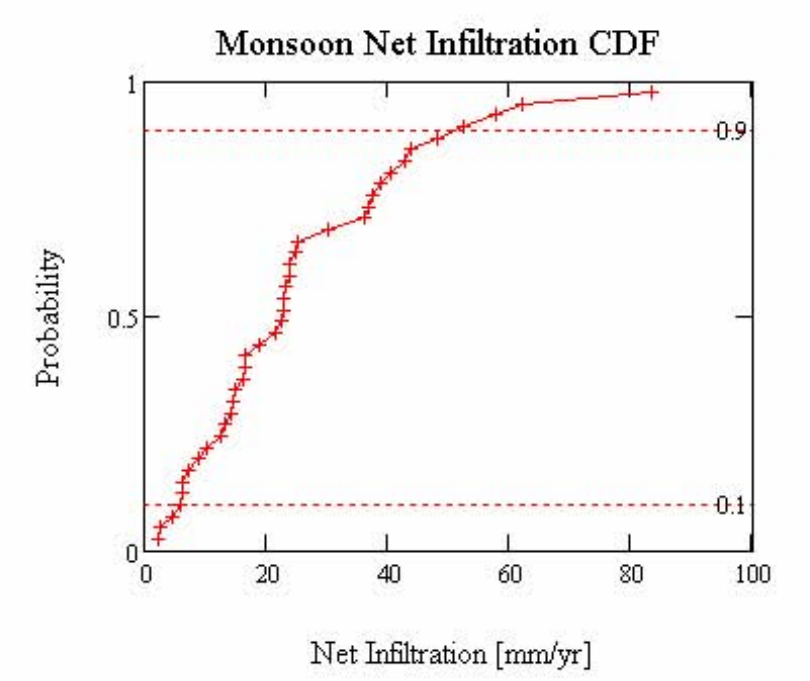

Source: Output DTN: SN0701T0502206.037, file: \Welcome to Massif\Massif\Monsoon Uncertainty\Post Processing*MO_Combined_Replicates.xmcd*.

NOTE: A total of 40 realizations (2 LHS replicates) define the distribution.

Figure 6.5.7.2-6. Cumulative Distribution Function (CDF) of Monsoon Net Infiltration Averaged over the Infiltration Domain

6.5.7.3 Glacial Transition Simulation Results

The mean annual precipitation (MAP) (at the reference elevation of 1,524 m) used for the 40 realizations representing Glacial Transition climate is summarized in Figure 6.5.7.3-1 and Table 6.5.7.3-1. The parameters used to represent Glacial Transition climate are described in Section 6.5.1 and Appendix F.

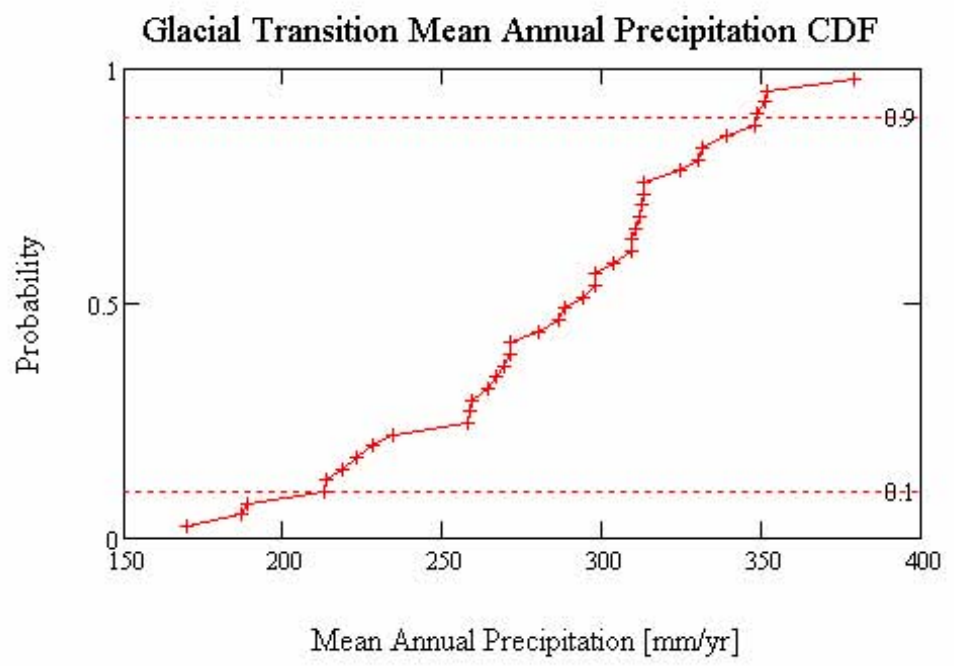

Source: Output DTN: SN0701T0502206.037, file: \Welcome to Massif\Massif\Glacial Uncertainty\Post Processing*GT_Combined_Replicates.xmcd*.

NOTE: A total of 40 realizations (2 LHS replicates) define the distribution. MAP values are for a reference elevation of 1,524 meters above sea level.

Figure 6.5.7.3-1. Glacial Transition Mean Annual Precipitation CDF

Table 6.5.7.3-1. Mean Annual Precipitation Statistics for the 40 Realizations Used to Represent Glacial Transition Climate for Net Infiltration Calculations

Glacial Transition Precipitation	R1 (mm/yr)	R2 (mm/yr)	R1 and R2 (mm/yr)
Minimum [mm/yr]	169.8	187.0	169.8
Mean [mm/yr]	282.2	284.6	283.4
Median [mm/yr]	296.5	290.3	291.5
Maximum [mm/yr]	351.9	379.3	379.3
Standard Deviation [mm/yr]	53.5	49.0	50.6

Source: Output DTN: SN0701T0502206.037, file: \Welcome to Massif\Massif\Glacial Uncertainty\Post Processing*MO_Combined_Replicates.xmcd*.

Two replicates (R1 and R2) of 20 realizations each were run for the Glacial Transition climate net infiltration estimation. Table 6.5.7.3-2 compares spatially averaged mean annual net infiltration statistics for these realizations. Table 6.5.7.3-3 identifies the maps that represent the 10th, 30th, 50th, and 90th, percentiles of spatially averaged mean annual net infiltration over the entire model domain. Figures 6.5.7.3-2 to 6.5.7.3-5 show maps of mean annual net infiltration for these percentiles. Figure 6.5.7.2-6 presents a CDF of spatially averaged mean annual net infiltration over the full domain for the Glacial Transition climate results.

Table 6.5.7.3-2. Spatially Averaged Mean Annual Net Infiltration Statistics for Glacial Transition Simulations

Glacial Transition Climate	Domain	R1 (mm/yr)	R2 (mm/yr)	R1 and R2 (mm/yr)
Minimum [mm/yr]	Infiltration modeling domain (125 km^2)	6.6	13.2	6.6
	UZ modeling domain (39.8 km^2)	4.3	8.2	4.3
	Repository footprint (5.7 km^2)	4.0	8.5	4.0
Mean [mm/yr]	Infiltration modeling domain (125 km^2)	30.8	29.2	30.0
	UZ modeling domain (39.8 km^2)	30.2	28.3	29.3
	Repository footprint (5.7 km^2)	39.9	37.5	38.7
Median [mm/yr]	Infiltration modeling domain (125 km^2)	28.5	28.1	28.5
	UZ modeling domain (39.8 km^2)	28.6	25.9	28.1
	Repository footprint (5.7 km^2)	38.6	35.9	38.6
Maximum [mm/yr]	Infiltration modeling domain (125 km^2)	64.7	56.2	64.7
	UZ modeling domain (39.8 km^2)	72.1	62.0	72.1
	Repository footprint (5.7 km^2)	97.3	81.7	97.3
Standard Deviation [mm/yr]	Infiltration modeling domain (125 km^2)	14.3	12.1	13.1
	UZ modeling domain (39.8 km^2)	16.8	14.4	15.5
	Repository footprint (5.7 km^2)	23.3	19.5	21.2

Source: Output DTN: SN0701T0502206.037, file: \Welcome to Massif\Massif\Glacial Uncertainty\Post Processing*GT_Combined_Replicates.xmcd*.

Table 6.5.7.3-3. Realizations Identified for Selected Percentile s of Glacial Transition Spatially Averaged Mean Annual Net Infiltration

Percentile	Replicate	Realization	Net Infiltration (mm/yr)	Mean Annual Precipitation (mm/yr)
10th	R2	6	13.2	271.7
30th	R2	10	22.8	264.8
50th	R1	18	28.6	223.1
90th	R2	1	47.0	286.6

Source: Output DTN: SN0701T0502206.037, file: \Welcome to Massif\Massif\Glacial Uncertainty\Post Processing*GT_Combined_Replicates.xmcd*.

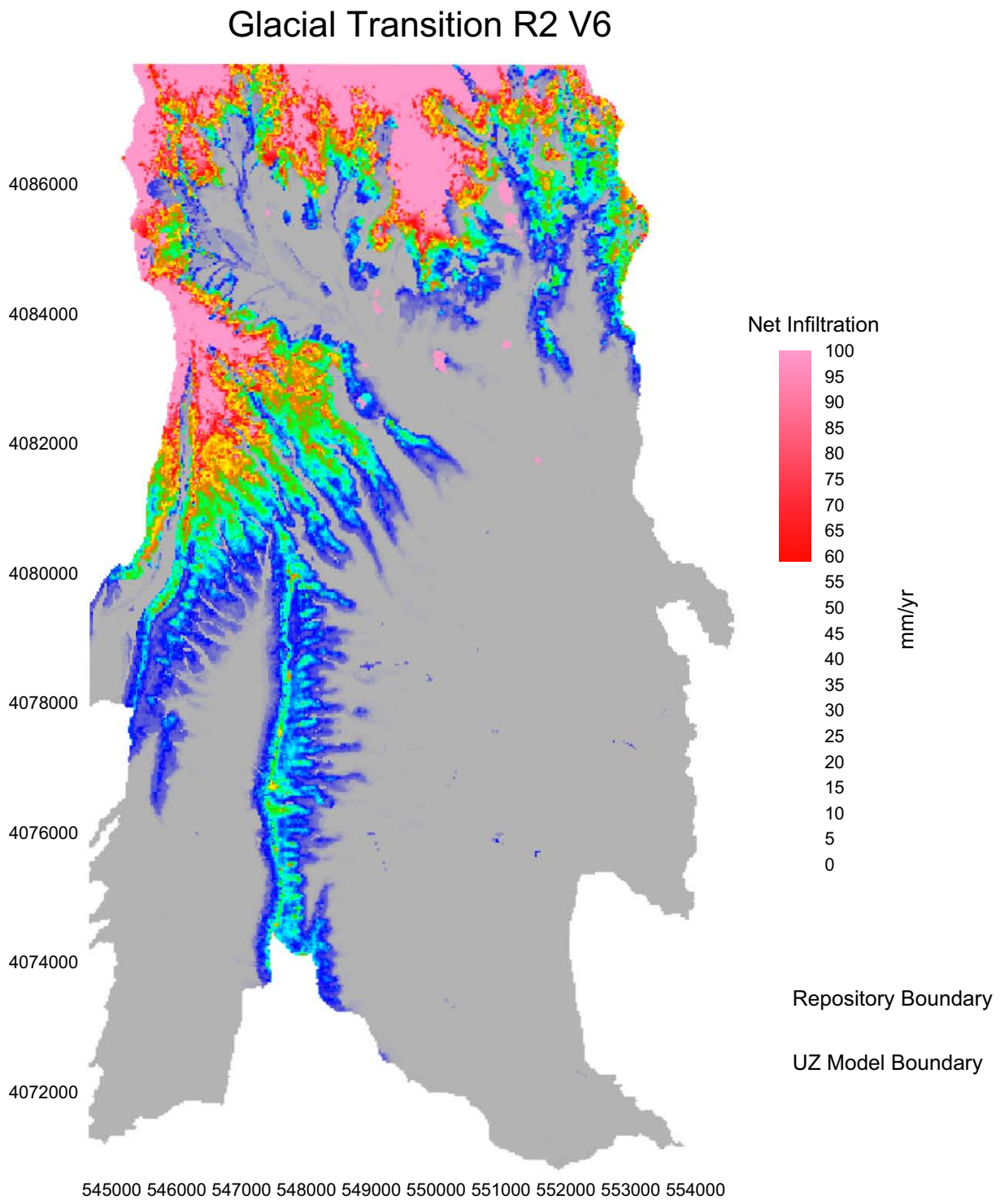

Coordinates are in meters; UTM NAD 27, Zone 11

Source: Output DTNs: SN0701T0502206.035 (Mean Annual Net Infiltration Results) and SN0612FTPRNUZB.002 UZ (Model and Repository Boundaries).

Figure 6.5.7.3-2. Glacial Transition, 10th Percentile Mean Annual Net Infiltration Map (Replicate R2, Realization 6)

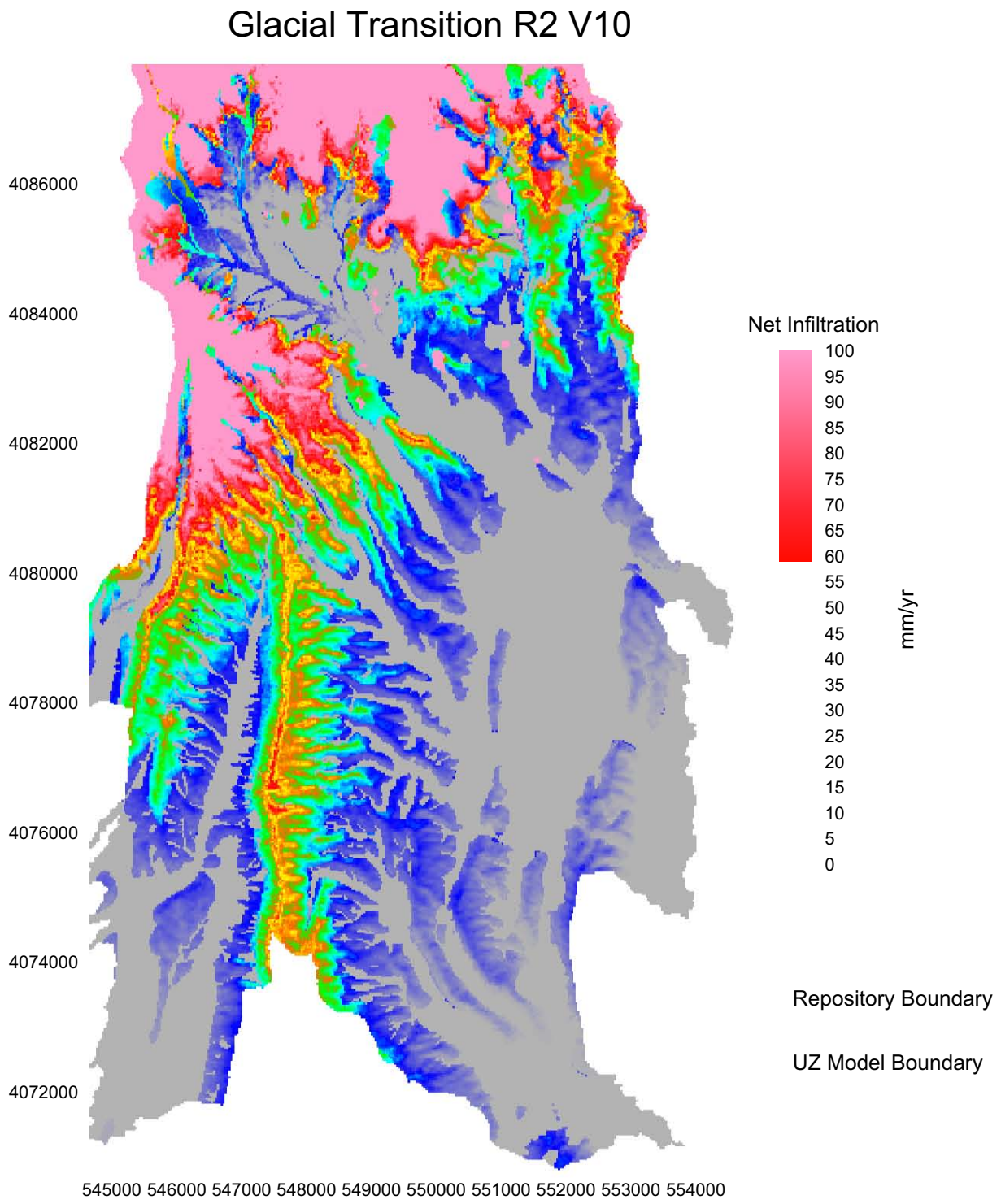

Coordinates are in meters; UTM NAD 27, Zone 11

Source: Output DTNs: SN0701T0502206.035 (Mean Annual Net Infiltration Results) and SN0612FTPRNUZB.002 UZ (Model and Repository Boundaries).

Figure 6.5.7.3-3. Glacial Transition, 30th Percentile Mean Annual Net Infiltration Map (Replicate R2, Realization 10)

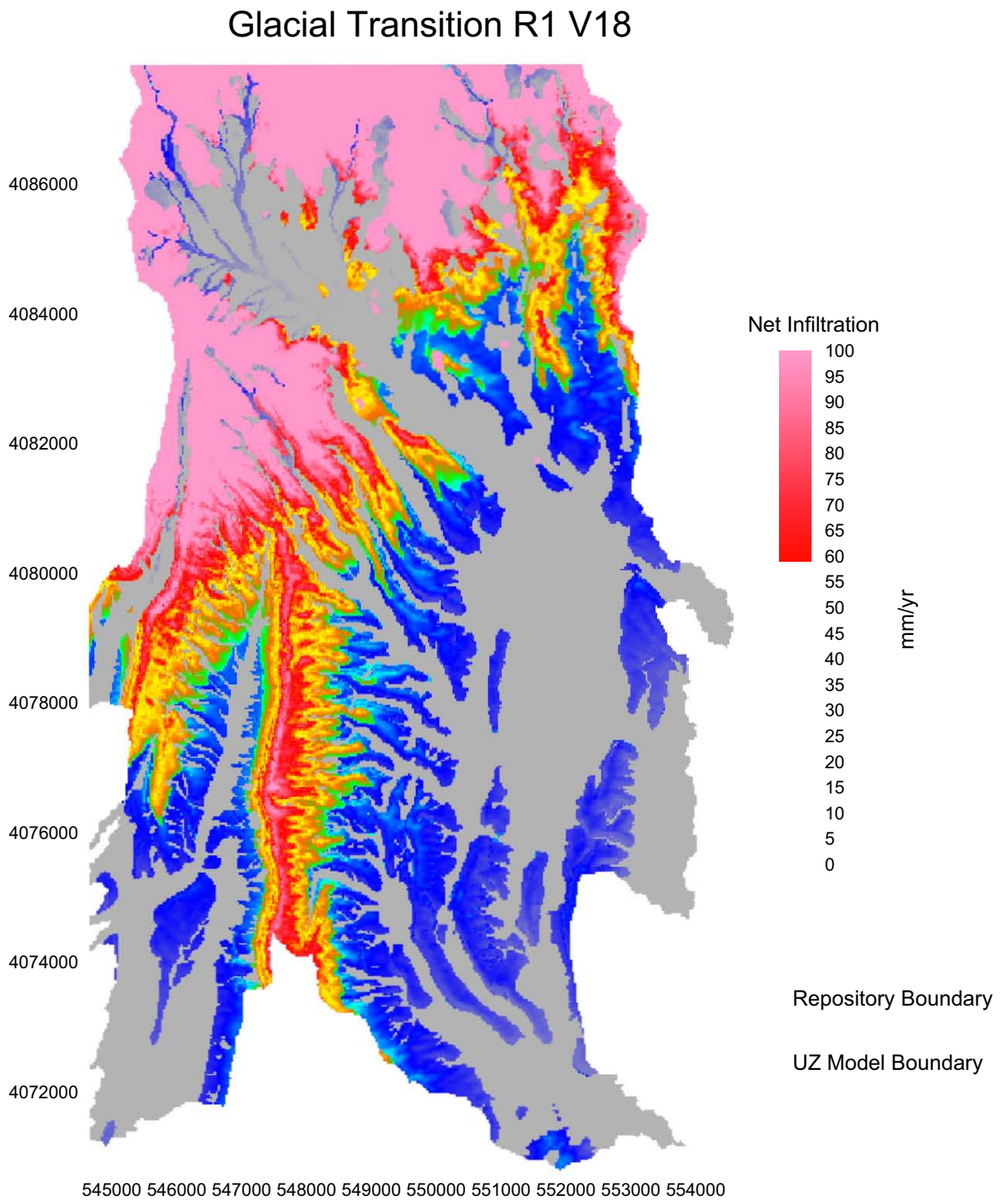

Coordinates are in meters; UTM NAD 27, Zone 11

Source: Output DTNs: SN0701T0502206.035 (Mean Annual Net Infiltration Results) and SN0612FTPRNUZB.002 UZ (Model and Repository Boundaries).

Figure 6.5.7.3-4. Glacial Transition, 50th Percentile Mean Annual Net Infiltration Map (Replicate R1, Realization 18)

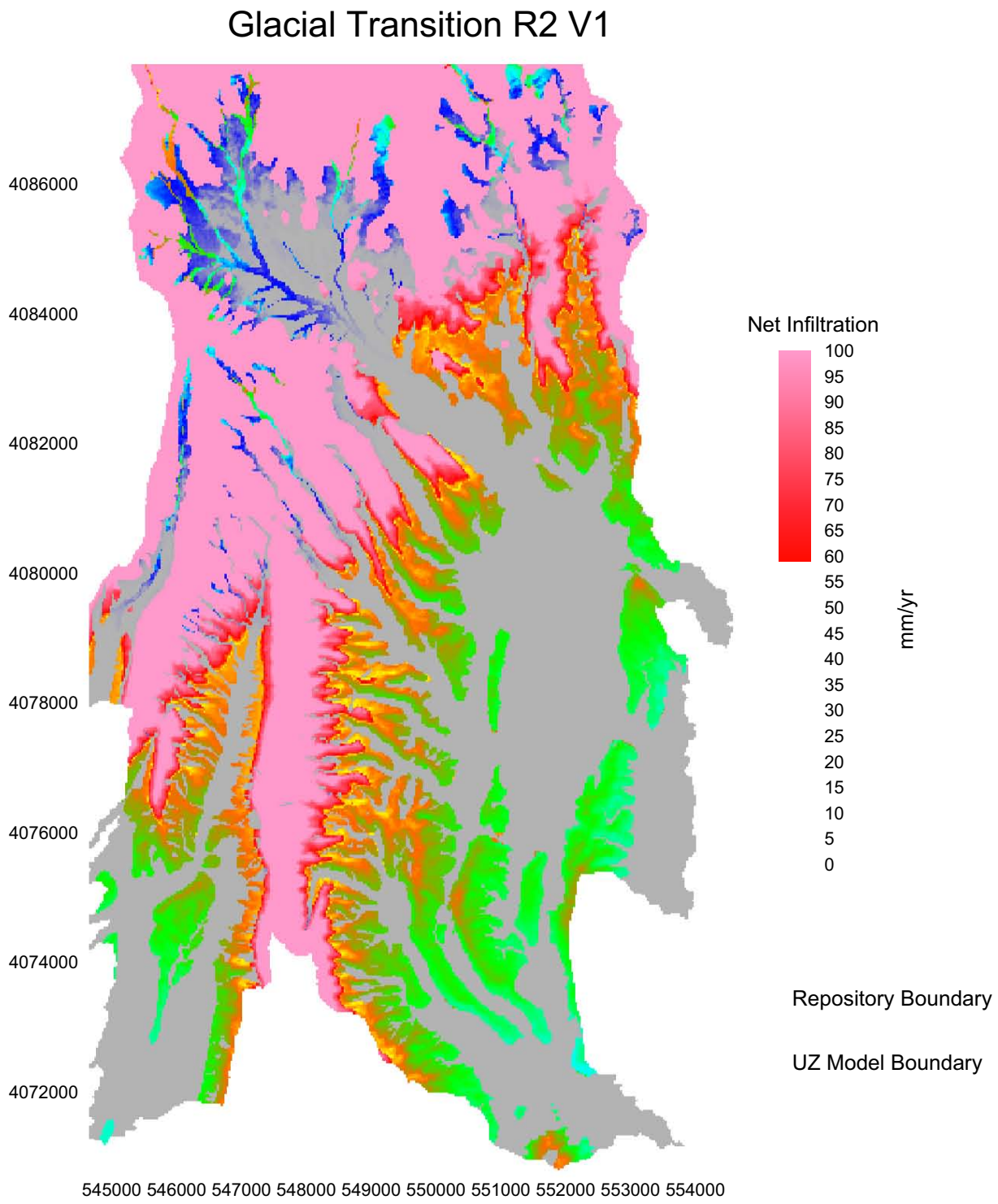

Coordinates are in meters; UTM NAD 27, Zone 11

Source: Output DTNs: SN0701T0502206.035 (Mean Annual Net Infiltration Results) and SN0612FTPRNUZB.002 UZ (Model and Repository Boundaries).

Figure 6.5.7.3-5. Glacial Transition, 90th Percentile Mean Annual Net Infiltration Map (Replicate R2, Realization 1)

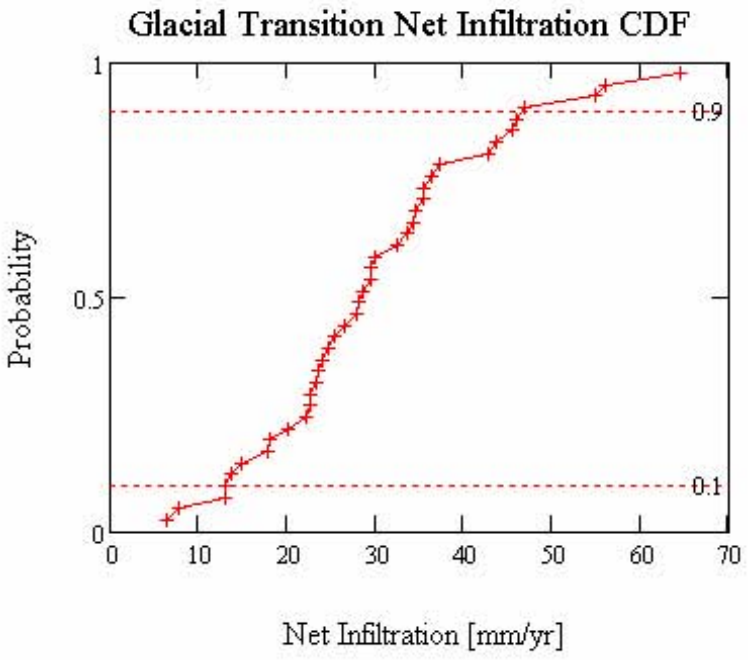

Source: Output DTN: SN0701T0502206.037, file: \Welcome to Massif\Massif\Glacial Uncertainty\Post Processing*GT_Combined_Replicates.xmcd*.

NOTE: A total of 40 realizations (2 LHS replicates) define the distribution.

Figure 6.5.7.3-6. Cumulative Distribution Function (CDF) of Glacial Transition Spatially Averaged Mean Annual Net Infiltration over the Infiltration Domain

6.5.7.4 Summary of Weighted Water Fluxes for Each Climate

For each realization, a calculation of the weighted (mean annual) amount of water that is accounted for by each of the water balance components is performed over the infiltration modeling domain for each climate (base case simulations). Because each realization consists of runs based on 10 representative years, the total water fluxes from each year are weighted by the probability of the year occurring. Thus, the weighted mean water flux represents a weighted mean water flux over the 10 representative years. All water enters the domain as precipitation and is partitioned into the various water balance components by the MASSIF model, including net infiltration (Infiltration), evapotranspiration (ET), runoff, sublimation, change in storage (Storage), and net snow pack (Snow). The mean and standard deviation of each of these weighted mean water fluxes are listed in Tables 6.5.7.4-1 to 6.5.7.4-3 for each of the three future climates, respectively. These climate means are expressed as both mm/yr and as a percentage of the mean annual precipitation. In addition, results from an alternative set of simulations (IC 1 runs) are presented in these tables. These IC1 simulations are identical to the base case simulations except that they were started with a higher soil moisture content initial condition. It is noted that the primary difference between these runs is that the IC 1 runs end up with a mean change in storage which is negative and a slightly higher net infiltration than the base case runs. This negative change in storage indicates that, on average, the IC1 runs are ending the year with lower soil moisture contents than were applied as initial conditions. The purpose of running the IC1 runs was to bracket the desired zero change in storage and demonstrate that the effect on net infiltration uncertainty is minor.

Table 6.5.7.4-1. Average and Standard Deviations of Weighted Mean Water Fluxes Fractions for the Present-Day Climate Simulations (fraction of precipitation)

Present-Day Climate	Mean (mm/yr)	SD (mm/yr)	Mean (% precip)	SD (% precip)	Mean IC1 (mm/yr)	SD IC1 (mm/yr)	Mean IC1 (% precip)	SD IC1 (% precip)
Precipitation	173.6	25.1	N/A	N/A	173.6	25.1	N/A	N/A
Infiltration	14.3	8.7	8.02%	4.50%	14.8	8.8	8.29%	4.50%
ET	151.6	20.1	87.68%	5.66%	158.9	20.5	92.02%	6.58%
Runoff	3.7	2.8	2.07%	1.56%	3.7	2.8	2.07%	1.56%
Sublimation	0.7	0.2	0.42%	0.11%	0.7	0.2	0.42%	0.11%
Storage	3.3	3.3	1.82%	1.77%	−4.6	3.9	−2.80%	2.42%
Snow	0.0	0.0	0.00%	0.00%	0.0	0.0	0.00%	0.00%

Source: Output DTN: SN0701T0502206.037, file: \Welcome to Massif\Massif\Post Processing\ *Flux Calculations All Climates.xls*.

Table 6.5.7.4-2. Average and Standard Deviation of Weighted Mean Water Fractions Fluxes for the Monsoon Climate Simulations

Monsoon Climate	Mean (mm/yr)	SD (mm/yr)	Mean (% precip)	SD (% precip)	Mean IC1 (mm/yr)	SD IC1 (mm/yr)	Mean IC1 (% precip)	SD IC1 (% precip)
Precipitation	275.2	77.0	N/A	N/A	275.2	77.0	N/A	N/A
Infiltration	25.5	17.9	8.69%	4.75%	26.1	18.0	8.89%	4.73%
ET	230.4	57.8	84.88%	8.18%	238.3	58.1	88.01%	8.93%
Runoff	15.6	12.1	5.35%	3.63%	15.6	12.1	5.36%	3.63%
Sublimation	0.1	0.2	0.04%	0.07%	0.1	0.2	0.04%	0.07%
Storage	3.6	8.6	1.04%	2.92%	−4.9	9.4	−2.29%	3.56%
Snow	0.0	0.0	0.00%	0.00%	0.0	0.0	0.00%	0.00%

Source: Output DTN: SN0701T0502206.037, file: \Welcome to Massif\Massif\Post Processing\ *Flux Calculations All Climates.xls*.

Table 6.5.7.4-3. Average and Standard Deviation of Weighted Mean Water Fractions Fluxes for the Glacial Transition Climate Simulations

Glacial Transition Climate	Mean (mm/yr)	SD (mm/yr)	Mean (% precip)	SD (% precip)	Mean IC1 (mm/yr)	SD IC1 (mm/yr)	Mean IC1 (% precip)	SD IC1 (% precip)
Precipitation	283.4	50.0	N/A	N/A	283.4	50.0	N/A	N/A
Infiltration	30.0	12.9	10.38	3.66	30.5	12.9	10.57	3.61
ET	243.7	41.7	86.16	3.90	254.6	42.2	90.15	4.46
Runoff	1.1	1.2	0.39	0.47	1.1	1.2	0.39	0.47
Sublimation	3.6	0.8	1.27	0.21	3.6	0.8	1.27	0.21
Storage	5.1	3.9	1.79	1.29	−6.4	4.7	−2.38	1.86
Snow	0.0	0.0	0.00	0.00	0.0	0.0	0.00	0.00

Source: Output DTN: SN0701T0502206.037, file: \Welcome to Massif\Massif\Post Processing*Flux Calculations All Climates.xls*.

6.5.7.5 Factors Influencing Temporal Variability in Net Infiltration

In the preceding sections, net infiltration results have been averaged over space and time for the purposes of comparing results within and between climates. A more representative model of net infiltration would include variations that occur over time. In fact, net infiltration is an episodic process. The results of these calculations shed light on the temporal nature of net infiltration at Yucca Mountain.

As described in Section 6.5.1, a long-term mean net infiltration is calculated as the weighted mean net infiltration for ten representative precipitation years, each with its associated probability of occurrence. Low probability years experience higher net infiltration but contribute only a small percentage to the long-term mean. Since the sum of the probabilities of occurrence equals 1 and the years were selected from a set of 1,000, it is possible to estimate a "recurrence interval" for each of the representative years based on its probability. The recurrence interval for a given representative year represents the average number of years that would pass before annual precipitation exceeded that predicted for the representative year. The recurrence interval is calculated as:

$$T_k = \frac{1}{1 - p_k} \qquad \text{(Eq. 6.5.7.5-1)}$$

where T_k is the recurrence interval (in years) of year k and p_k is the probability that annual precipitation on any one year will be less than the annual precipitation during year k (Maidment 1993 [DIRS 125317], p. 18.3). Thus the quantity $(1-p_k)$ represents the exceedance probability, which is the probability that annual precipitation during any one year will equal or exceed annual precipitation during year k. It is also possible to calculate the percent contribution to the long term mean net infiltration of each representative year. This is done by multiplying annual net infiltration for each year of each realization by the probability of occurrence for that year and then dividing by the long-term (weighted) mean net infiltration for each realization. Tables 6.5.7.5-1 to 6.5.7.5-3 list the exceedance probability, the mean annual net infiltration, the recurrence interval, and the fraction of contribution to long-term mean net infiltration for each of the 10 representative years (k = 1 to 10) for each of the three climates, respectively. Figures 6.5.7.5-1 to 6.5.7.5-3 plot the mean annual net infiltration and the cumulative percent contribution to the long-term mean against the recurrence interval for the three climates, respectively. The plots shows that as years with larger recurrence intervals are included, a greater percentage of the long-term mean can be estimated. The results suggest that about 80% of the long-term mean for Present-Day climate conditions is due to years with a recurrence interval of 10 years and less. The implication of these results is that net infiltration estimates based on relatively short historical weather records may tend to underestimate long-term net infiltration, however, not by more than 20%.

It is worth noting that the mean net infiltration for each representative year is not always higher for years with greater annual precipitation. For example, for the Present-Day climate, year number 1 has a lower mean net infiltration than year number 2. This occurs because factors other than total annual precipitation influence the magnitude of net infiltration. For example, annual precipitation may be very high because of an especially high amount of precipitation occurring on a single day. In such a case, runoff would tend to be higher and net infiltration

lower than if several days during the year experienced large amounts of precipitation, but the annual total was less.

Table 6.5.7.5-1. Comparison of the 10 Representative Years Used to Model Net Infiltration for the Present-Day Climate

Representative Year (k)	Probability That Precipitation Will Be Exceeded (1−p)	Mean Net Infiltration for Each Representative Year (mm/yr)	Recurrence Interval (yr)	Fraction of Contribution to Long-term Mean Infiltration
1	0.001	82.58	1,000.00	0.76
2	0.003	88.06	333.33	1.74
3	0.01	75.77	100.00	4.85
4	0.03	55.77	33.33	9.95
5	0.1	45.39	10.00	24.44
6	0.28	24.27	3.57	28.88
7	0.46	14.22	2.17	16.34
8	0.64	8.34	1.56	8.42
9	0.82	3.00	1.22	3.21
10	1	1.48	1.00	1.40

Source: Output DTN: SN0701T0502206.037, file: \Welcome to Massif\Massif\Present Day Uncertainty\Post Processing*PD_Combined_Replicates.xmcd*.

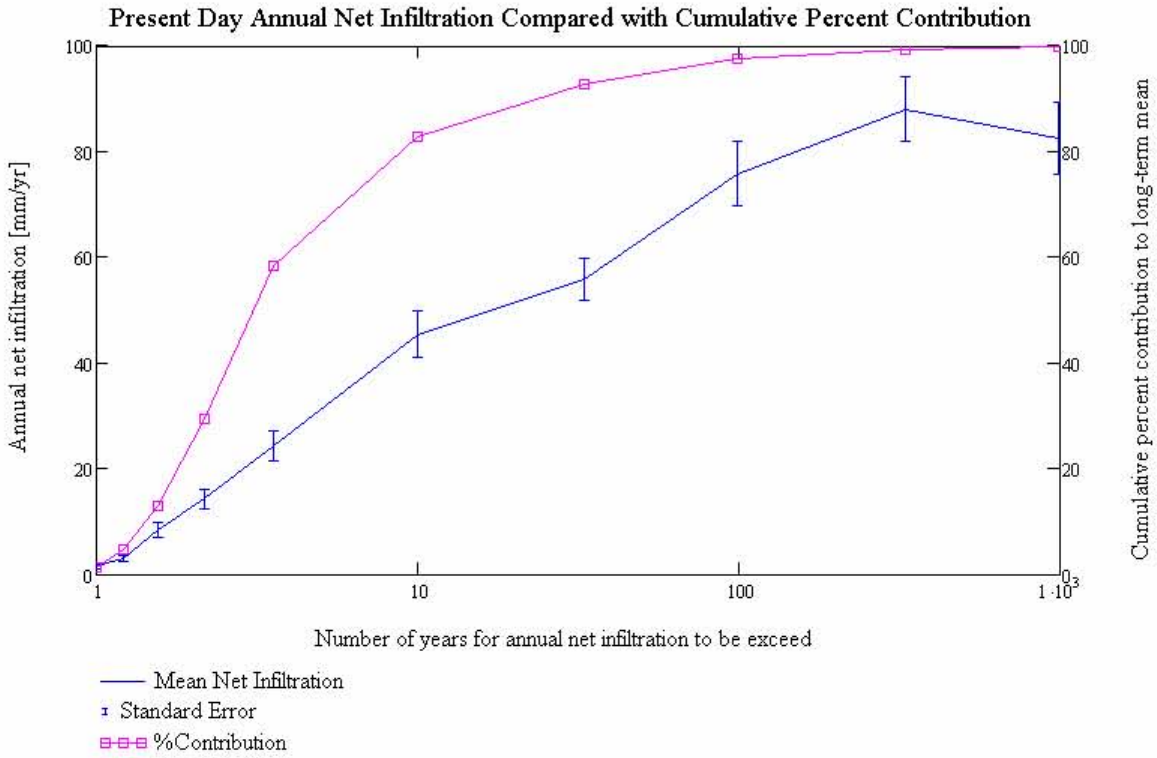

Source: Output DTN: SN0701T0502206.037, file: \Welcome to Massif\Massif\Present Day Uncertainty\Post Processing*PD_Combined_Replicates.xmcd*.

Figure 6.5.7.5-1. Annual Mean Net Infiltration and Cumulative Percent Contribution to Long-term Mean Net Infiltration as a Function of Recurrence Interval for the Present-Day Climate

Table 6.5.7.5-2. Comparison of the 10 Representative Years Used to Model Net Infiltration for the Monsoon Climate

Representative Year (k)	Probability That Precipitation Will Be Exceeded (1−p)	Mean Net Infiltration for Each Representative Year (mm/yr)	Recurrence Interval (yr)	Fraction of Contribution to Long-term Mean Infiltration
1	0.001	67.79	1,000.00	0.33
2	0.003	84.04	333.33	0.96
3	0.01	84.99	100.00	3.03
4	0.03	74.47	33.33	7.45
5	0.1	65.71	10.00	21.22
6	0.28	45.73	3.57	31.84
7	0.46	24.98	2.17	16.76
8	0.64	17.45	1.56	9.51
9	0.82	10.29	1.22	6.06
10	1	5.05	1.00	2.84

Source: Output DTN: SN0701T0502206.037, file: \Welcome to Massif\Massif\Monsoon Uncertainty\Post Processing*MOD_Combined_Replicates.xmcd*.

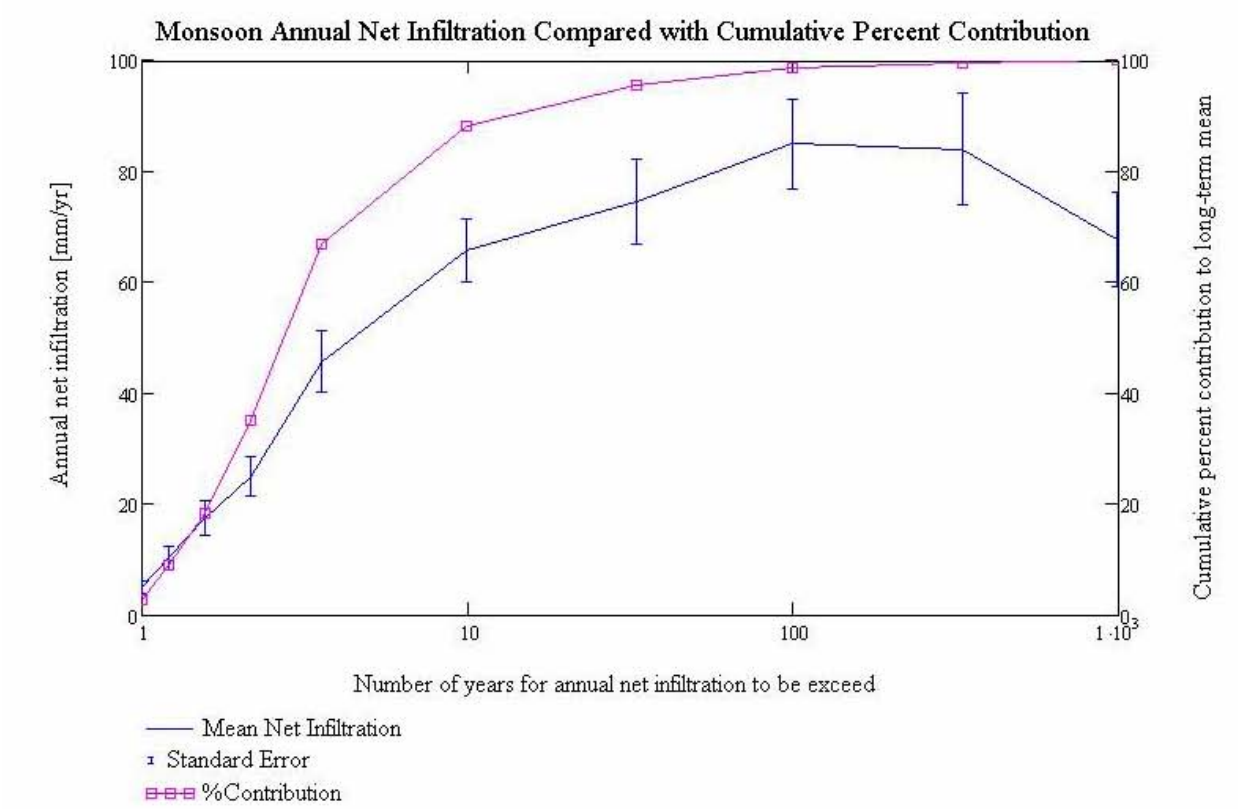

Source: Output DTN: SN0701T0502206.037, file: \Welcome to Massif\Massif\Monsoon Uncertainty\Post Processing*MO_Combined_Replicates.xmcd*.

Figure 6.5.7.5-2. Annual Mean Net Infiltration and Cumulative Percent Contribution to Long-term Mean Net Infiltration as a Function of Recurrence Interval for the Monsoon Climate

Table 6.5.7.5-3. Comparison of the 10 Representative Years Used to Model Net Infiltration for the Glacial Transition Climate

Representative Year (k)	Probability That Precipitation Will Be Exceeded (1−p)	Mean Net Infiltration for Each Representative Year (mm/yr)	Recurrence Interval (yr)	Fraction of Contribution to Long-term Mean Infiltration
1	0.001	96.45	1,000.00	0.37
2	0.003	94.04	333.33	0.69
3	0.01	78.96	100.00	2.07
4	0.03	64.75	33.33	4.76
5	0.1	53.44	10.00	12.56
6	0.28	40.90	3.57	24.85
7	0.46	32.01	2.17	19.38
8	0.64	27.07	1.56	15.45
9	0.82	20.50	1.22	11.75
10	1	13.33	1.00	8.13

Source: Output DTN: SN0701T0502206.037, file: \Welcome to Massif\Massif\Present Day Uncertainty\Post Processing*PD_Combined_Replicates.xmcd*.

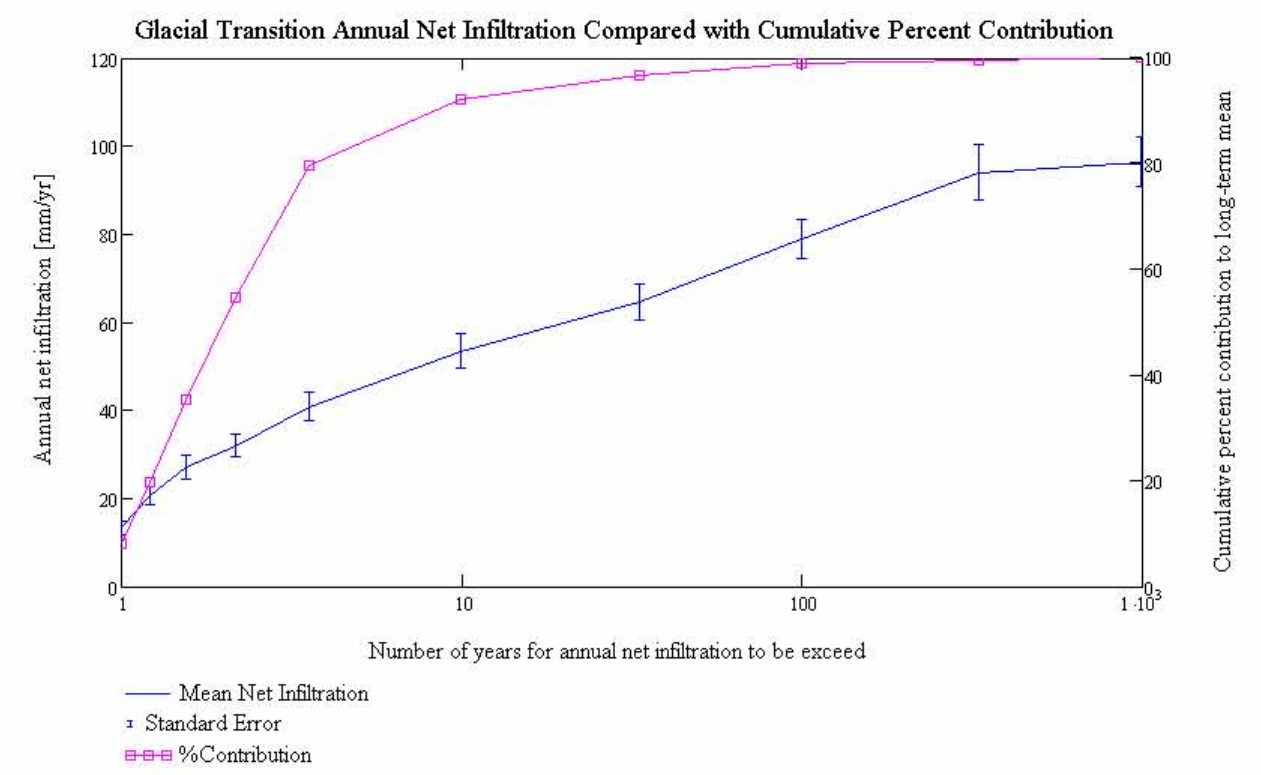

Source: Output DTN: SN0701T0502206.037, file: \Welcome to Massif\Massif\Glacial Uncertainty\Post Processing*GT_Combined_Replicates.xmcd*.

Figure 6.5.7.5-3. Annual Mean Net Infiltration and Cumulative Percent Contribution to Long-term Mean Net Infiltration as a Function of Recurrence Interval for the Glacial Transition Climate

6.5.7.6 Factors Influencing Spatial Variability in Net Infiltration

The spatial variability in net infiltration is controlled by spatial variations in the amount of precipitation, spatial heterogeneity in soil, bedrock, and vegetation properties, and lateral water distribution via runoff processes. In the MASSIF model, precipitation varies only as a function of elevation and is adjusted via a lapse correction (Section 6.4.1.1). The characterization of spatial heterogeneities of soil and bedrock properties is done by dividing the model domain into distinct soil groups, soil depth classes, and bedrock type regions inside which the given properties are assumed to be constant. The result of this approach is that the MASSIF model likely underestimates the actual spatial variability in net infiltration. The best that can be achieved with such a method is to generally characterize regional infiltration patterns. Given these limitations, the following sections illustrate which of the various property groups account for the most infiltration. The intent of this analysis is not to claim that particular property groups are necessarily significant contributors to infiltration uncertainty but rather to identify these property groups in case further study is deemed necessary. The analysis presented in this section is limited to the results of the Present-Day climate. However, since only runoff processes can divert water laterally in the model and since runoff fractions are relatively low for all climates, it is not expected that the spatial distribution of net infiltration for Monsoon and Glacial Transition climates would be all that different from that seen for the Present-Day climate.

6.5.7.6.1 Influence of Soil Depth

Soil depth is one of the most significant factors controlling local net infiltration (see Section 6.7 and Appendix H). Unfortunately, soil depth in each of the model grid cells is largely not known with any degree of accuracy (see BSC 2006 [DIRS 178819] for details). Instead, the domain has been divided into five soil depth classes where soil depth decreases with increasing class number (described in Section 6.5.2). Soil depth distributions are developed in Section 6.5.2.4 and the actual sampled soil depths for soil depth class 4 for each realization are listed in Section 6.5.5. Table 6.5.7.6-1 lists the percent of the total infiltration that occurs in each soil depth class regions for replicate R1 of the Present-Day climate net infiltration results. It is clear that areas with shallow soils (soil depth class 4) and areas with no soil (class 5) dominate the total predicted net infiltration over the full domain.

Table 6.5.7.6-1. Percent of Total Net Infiltration (and standard deviation) That Occurs in Each Soil Depth Class for Present-Day Climate Simulations (Entire Net Infiltration Modeling Domain)

Soil Depth Class	Percent of Total Infiltration [a]	Standard Deviation (%)	UZ Grid (%)	Total (%)
1	0.50	0.92	0	9
2	2.30	3.85	17	25
3	0.52	0.97	11	9
4	90.53	7.15	71	57
5	6.15	4.69	>1	>1

Source: Output DTN: SN0701T0502206.037, file: \Welcome to Massif\Massif\Present Day Uncertainty\Post Processing*PD_Combined_Replicates.xmcd*.

[a] Total infiltration is the average net infiltration over the entire 125-km^2 modeling domain over epistemic uncertainty

6.5.7.6.2 Influence of Soil Group

Soil properties also influence spatial variations in net infiltration. Table 6.5.7.6-2 lists the percent of the total infiltration that occurs in the regions a specific soil type group for the Present-Day climate simulations. Five soil type groups are used to represent spatial variations in soil properties (includes a group representing cells with bare bedrock). Soil group 5/7/9 covers approximately 65% of the infiltration domain but accounts for about 91% of the total infiltration. Areas with bare rock cover only 0.3% of the infiltration domain but account for more than 6% of the total infiltration.

Table 6.5.7.6-2. Percent of Total Net Infiltration (and standard deviation) That Occurs in Each Soil Group for Present-Day Climate Simulations (Entire Net Infiltration Modeling Domain)

Soil Group	Percent of Total Infiltration [a]	Standard Deviation (%)	UZ Grid (%)	Total (%)
1	0.48	0.94	2	10
2/6	0.66	1.27	4	11
3/4	1.78	2.65	12	13
5/7/9	90.93	6.68	81	65
Bare Rock	6.15	4.69	>1	>1

Source: Output DTN: SN0701T0502206.037, file: \Welcome to Massif\Massif\Present Day Uncertainty\Post Processing*PD_Combined_Replicates.xmcd*.

[a] Total infiltration is the average net infiltration over the entire 125-km^2 modeling domain over epistemic uncertainty.

6.5.7.6.3 Influence of Rock Type

The hydraulic conductivity of the underlying bedrock may influence the spatial variability of net infiltration. Table 6.5.7.6-3 lists the percent of the total infiltration that occurs in the regions underlain by a specific rock type for the Present-Day climate simulations. Nominal hydraulic conductivity values used for each rock type are explained in Section 6.5.2, and sampled values are listed in Section 6.5.5 for each climate-replicate combination. 30% of the total infiltration occurs in cells underlain by rock type 422, which accounts for 18% of the entire infiltration domain.

Table 6.5.7.6-3. Percent of Total Net Infiltration (and standard deviation) That Occurs in Each Rock Type for Present-Day Climate Simulations (Entire Net Infiltration Modeling Domain)

Rock Type	Percent of Total Infiltration [a]	Standard Deviation (%)	UZ Grid (%)	Total (%)
401	5.25	0.53	4	2
402	1.94	0.23	3	1
403	7.72	1.52	14	18
404	3.55	0.72	8	3
405	15.09	2.18	23	22
406	8.25	2.16	19	8
407	6.25	0.61	6	4
408	2.90	0.27	4	2
409	1.70	0.07	2	1
410	0.10	0.04	<1	<1
411	1.39	0.36	<1	1
412	2.09	0.20	4	2
413	1.40	0.08	2	2
414	2.88	0.10	3	3
415	0.55	0.07	1	1
416	0.08	0.04	<1	<1
417	2.43	0.17	<1	2
418	1.32	0.43	3	3
419	0.01	0.03	<1	<1
420	0.49	0.10	1	1
421	0.43	0.08	1	1
422	30.16	2.53	1	18
423	0.11	0.03	<1	<1
424	0.19	0.07	<1	<1
425	0.01	0.03	0	<1
426	0.01	0.03	0	<1
427	0.00	0.00	0	<1
430	1.81	1.13	0	<1
432	0.01	0.03	0	<1
435	0.20	0.02	0	<1
490	1.28	0.66	0	3
491	0.32	0.07	0	<1

Source: Output DTN: SN0701T0502206.037, file: \Welcome to Massif\Massif\Present Day Uncertainty\Post Processing*PD_Combined_Replicates.xmcd*.

[a] Total infiltration is the average net infiltration over the entire 125 km^2 modeling domain over epistemic uncertainty.

6.5.7.7 Illustration of Daily Water Balance Patterns

As an illustration of the daily behavior of the MASSIF model, a single grid cell, located in the upper part of Pagany Wash watershed, was selected for monitoring during a one-year simulation. The purpose of this illustration is to help provide a sense of the intricate calculations that are performed in the MASSIF model of net infiltration. In theory, such detailed data could be obtained for every grid cell for every simulated day. However, the number of grid cells in a watershed and computer memory resources limit the number of cells that can be monitored for a given run.

The parameter set selected was from the Present-Day Replicate 2, Realization V08, which is the 50th percentile net infiltration Present-Day simulation. The year chosen was Year 2 (probability of occurrence = 0.003) from the stochastically generated weather file for the realization. The sampled parameter values for this realization are shown in Table 6.5.5.1-4. The geospatial characteristics of this grid cell are listed in Table 6.5.7.7-1.

Table 6.5.7.7-1. Properties of the Grid Cell Selected for Illustration of Daily Water Balance Patterns

Parameter	Value
Easting [m]	548261
Northing [m]	4081803
Elevation [m]	1515
Slope [deg]	21
Azimuth [deg]	86
Soil Depth Class	4
Soil Type	5
Bedrock Type	403
PVR	0.5261

Source: Output DTN: SN0701T0502206, file: \Welcome to Massif\Massif\Present Day Uncertainty\Examples*Monitor Cell Characteristics.xls*.

There are a number of daily variables that can be monitored for a given grid cell. The figures below plot a selection of these variables for simulated year for the grid cell identified above. Figure 6.5.7.7-1 plots daily values of minimum and maximum temperatures and precipitation. The effect of precipitation on temperature in the model is evident in the plot as temperature depressions on days with rain. Such depressions result in reductions in the solar radiation and reference ET. Note that the temperature and precipitation values are lapse-corrected to the elevation of the monitored cell.

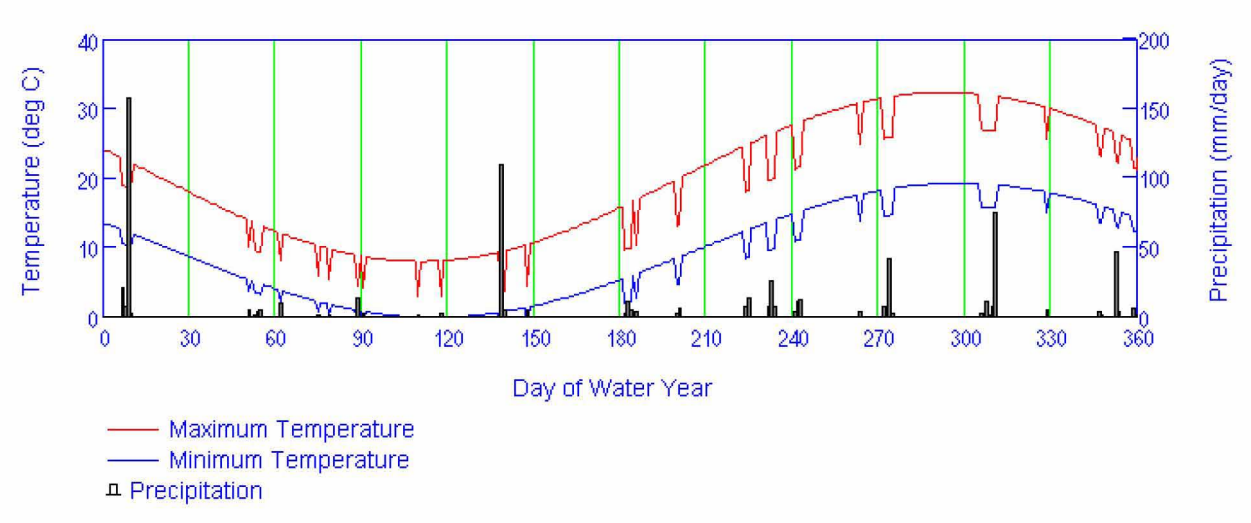

Source: Output DTN: SN0701T0502206, file: \Welcome to Massif\Massif\Present Day Uncertainty\ *Present Day R2 V08_example.xmcd*.

Figure 6.5.7.7-1. Daily Weather Inputs for the Simulated Year

Figure 6.5.7.7-2 shows how values of K_{cb} and the canopy coefficient (f_c) vary for this cell over the water year. These values are independent of the daily precipitation; however, the total annual precipitation for the water year, slope, azimuth, and PVR are used in the calculation of K_{cb} (see Section 6.5.3).

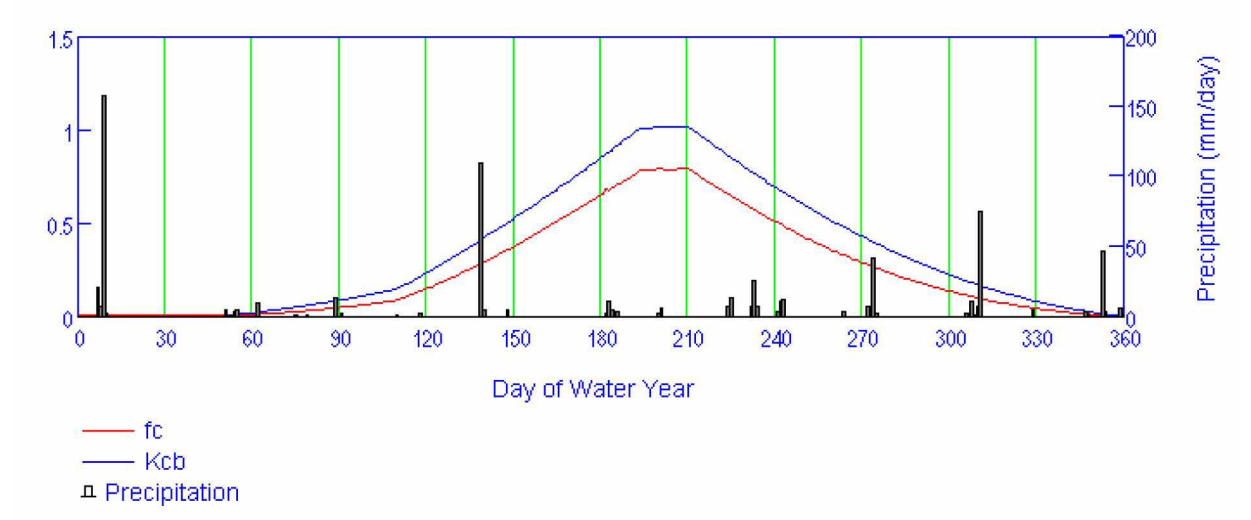

Figure 6.5.7.7-2. Daily Values of K_{cb} and Canopy Fraction (f_c) for the Simulated Year

Figure 6.5.7.7-3 shows the reference ET along with the daily water losses of evaporation and transpiration. Several features of the model are evident in these results. For example, both evaporation and transpiration are proportional to reference ET. In addition, transpiration is also proportional to K_{cb}.

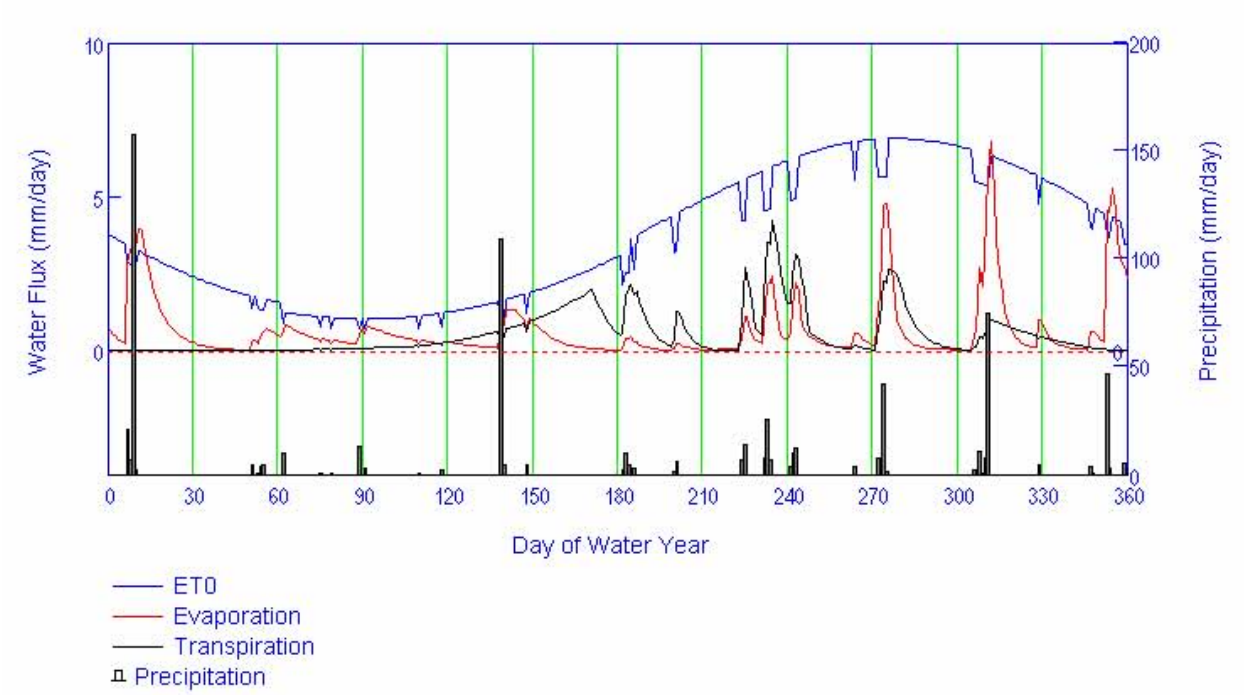

Source: Output DTN: SN0701T0502206, file: \Welcome to Massif\Massif\Present Day Uncertainty\ *Present Day R2 V08_example.xmcd.*

Figure 6.5.7.7-3. Daily Water Fluxes (Evaporation, Transpiration, and Reference ET) for the Simulated Year

Figure 6.5.7.7-3 shows the water levels in each of the four nodes in the water balance calculation. Water levels 1 and 2 are for the surface evaporation layer of thickness Z_e. Water level 3 is for layer 2 (layer below evaporation layer). In this case, layer 2 thickness is equal to soil depth minus Z_e. In this example, the thickness of node 4 is equal to zero, because soil depth is less than the maximum rooting depth. The plots illustrates that for small precipitation events, water levels can increase in the surface layer (nodes 1 and 2), while continuing to decrease in the underlying layer (for example see day 60). When precipitation is greater, enough water is added to the surface layer to exceed its field capacity and thus water levels increase in the next lower layer (for example, see day 135). Also note the difference in the rate of water level decrease between days 1 and 135 as opposed to the rate between days 135 and 200. The increased rate of water level decrease corresponds to periods of higher reference ET and vegetation vigor (K_{cb}).

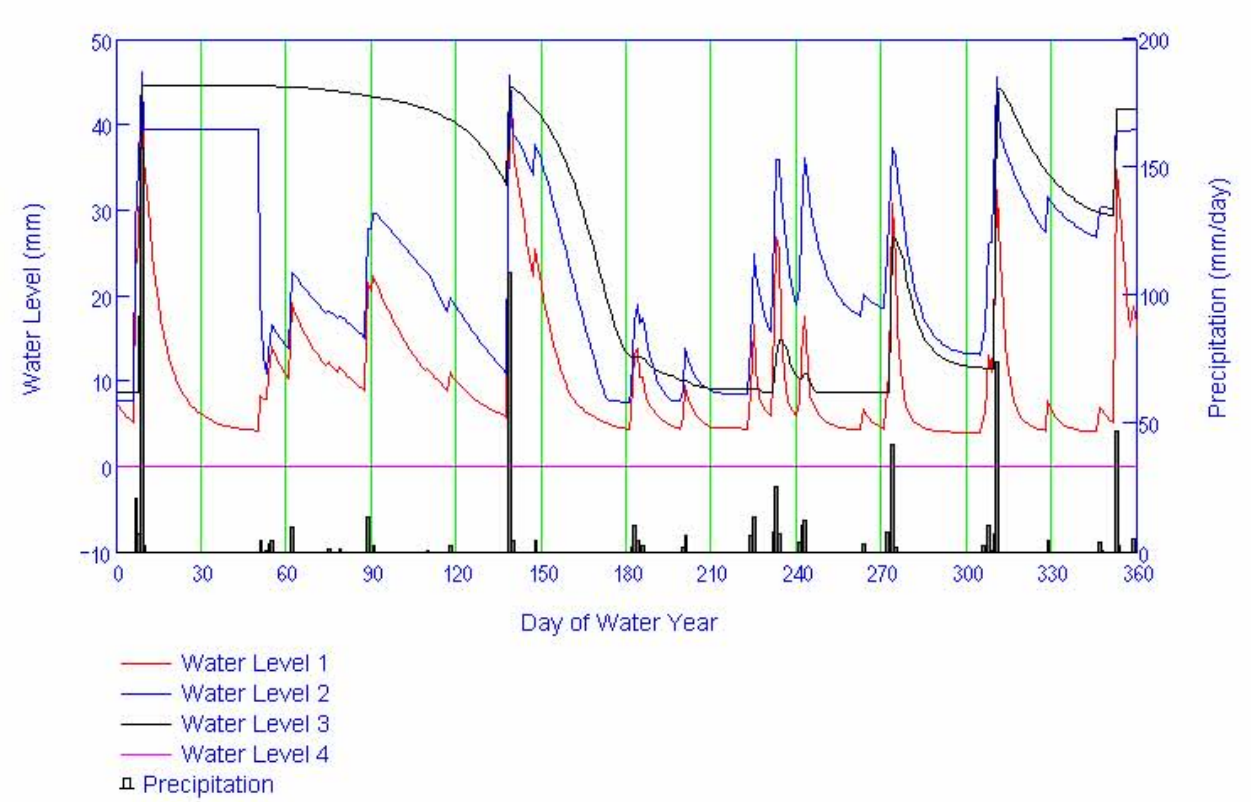

Source: Output DTN: SN0701T0502206, file: \Welcome to Massif\Massif\Present Day Uncertainty\ *Present Day R2 V08_example.xmcd*.

Figure 6.5.7.7-4. Daily Soil Water Levels for the Simulated Year

Figure 6.5.7.7-5 shows a plot of daily run-on flowing into the cell and daily runoff flowing out of the cell. In this example, such runoff events only occurred two times during the year, both during particularly large precipitation events.

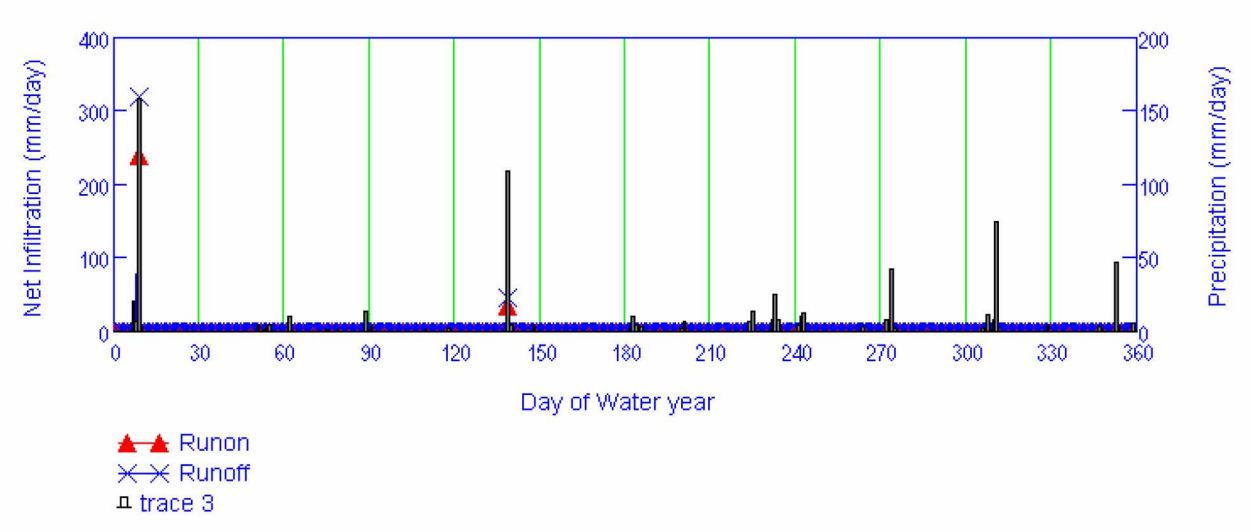

Source: Output DTN: SN0701T0502206, file: \Welcome to Massif\Massif\Present Day Uncertainty\ *Present Day R2 V08_example.xmcd*.

Figure 6.5.7.7-5. Daily Run-on and Runoff for the Simulated Year

Figure 6.5.7.7-6 shows daily net infiltration during the year. In this example, net infiltration occurred during three periods each lasting two days.

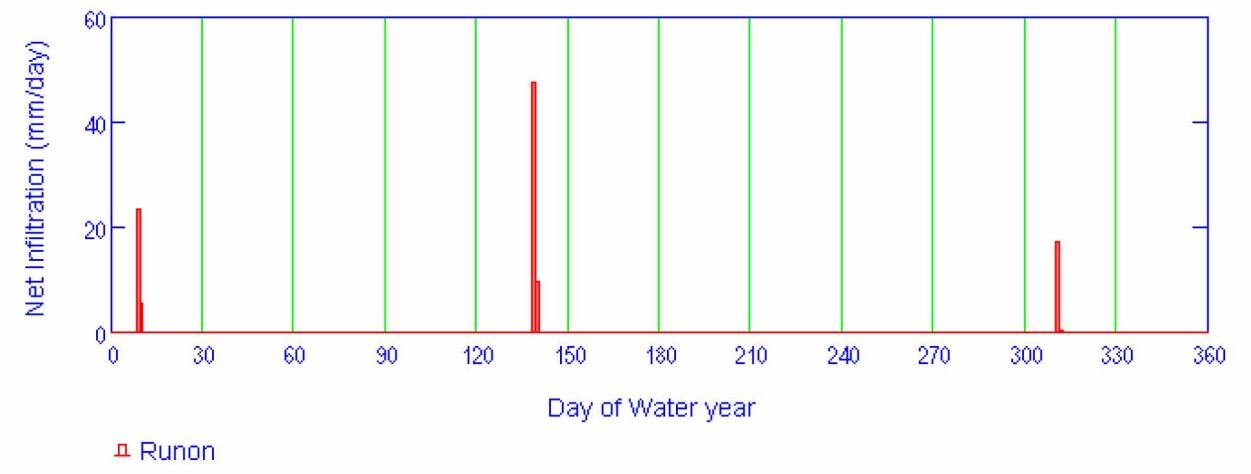

Source: Output DTN: SN0701T0502206, file: \Welcome to Massif\Massif\Present Day Uncertainty*Present Day R2 V08_example.xmcd*.

Figure 6.5.7.7-6. Daily Net Infiltration for the Simulated Year

6.5.7.8 Summary and Discussion of Net Infiltration Results for Present-Day and Future Climates

Table 6.5.7.8-1 summarizes the net infiltration statistics averaged over several spatial domains for all realizations and for all three climates. Predicted net infiltration generally is lowest for the Present-Day climate and increases in the Monsoon and Glacial Transition climates. However, net infiltration predictions for the Monsoon climate appear to be more uncertain (span a greater

range) than predictions for the Glacial Transition climate. This is the result of there being a greater amount of uncertainty in the expected precipitation in the Monsoon than for the Glacial Transition climate.

Table 6.5.7.8-1. Summary Net Infiltration Statistics for the Three Climates

	Domain	PD	MO	GT
Minimum [mm/yr]	Infiltration modeling domain (125 km^2)	2.0	2.4	6.6
	UZ modeling domain (39.8 km^2)	1.4	1.2	4.3
	Repository footprint (5.7 km^2)	1.5	1.2	4.0
Mean [mm/yr]	Infiltration modeling domain (125 km^2)	14.3	25.5	30.0
	UZ modeling domain (39.8 km^2)	15.1	28.0	29.3
	Repository footprint (5.7 km^2)	17.6	32.9	38.7
Median [mm/yr]	Infiltration modeling domain (125 km^2)	12.9	22.8	28.5
	UZ modeling domain (39.8 km^2)	12.4	24.2	28.1
	Repository footprint (5.7 km^2)	14.5	28.4	38.6
Maximum [mm/yr]	Infiltration modeling domain (125 km^2)	35.4	83.4	64.7
	UZ modeling domain (39.8 km^2)	40.9	86.2	72.1
	Repository footprint (5.7 km^2)	48.2	95.3	97.3
Standard Deviation [mm/yr]	Infiltration modeling domain (125 km^2)	8.8	18.2	13.1
	UZ modeling domain (39.8 km^2)	10.4	20.2	15.5
	Repository footprint (5.7 km^2)	12.5	23.3	21.2

Source: Output DTN: SN0701T0502206.037, file: \Welcome to Massif\Massif\Post Processing*Summary Net Infiltration All Climates.xls*.

PD = Present-Day, MO = Monsoon, GT = Glacial Transition.

One significant result of these simulations is the fact that most of the simulated net infiltration appears to occur in the regions with shallow soils rather than in the stream channels. This result raises some important questions about the predicted spatial distribution of net infiltration produced by the model. Section 7.1.3.2 presents some alternate simulations based on inferences made at Pagany Wash that result in significant infiltration in the stream channels. These alternate simulations allow soil conductivity to vary from the uncertainty distributions qualified in this report in Section 6.5.2, and therefore do not represent qualified net infiltration results. More field work would have to be performed in order to evaluate the accuracy of the spatial distribution of net infiltration in the current maps. There is greater confidence in the spatial averaged net infiltration values produced by this analysis.

6.5.7.9 Comparison of Results from Each LHS Replicate

An examination of Tables 6.5.7.1-2, 6.5.7.2-2, and 6.5.7.3-2 shows that the results from each of the two replicates run for each climate can vary considerably at the tails of the distribution but are more similar when comparing the mean and median. Because of random variation in any stochastic analysis, it is expected that there can be significant variation in the minimum and maximum values between the two replicate distributions. A more robust statistic to compare replicates is the first, second, and third quartiles (25th, 50th, 75th percentiles). The absolute differences between the two replicates for these quartiles in the infiltration modeling domain range from 0.0 (PD, 25%) to 4.8 mm (MO, 25%).

An estimate of the error on the mean net infiltration is given by the standard error on the mean (standard deviation divided by the square root of the number of samples). Standard deviations for each climate and spatial domain are listed in Tables 6.5.7.1-2, 6.5.7.2-2, and 6.5.7.3-2. The average standard errors on the mean for the infiltration modeling domain are listed in the last row of Table 6.5.7.9-1. It would not be surprising if the differences in the quartiles, closer to the tails of the distribution, were somewhat greater than the standard error on the mean. But, as is shown in Table 6.5.7.9-1, these differences are only 1.2, 0.8, and 1.3 mm greater, respectively, for the three climates (PD, MO, and GT).

The conclusion drawn from these comparisons is that there is an inherent uncertainty in the resulting net infiltration estimates made in this analysis, which is due to the small sample size. The uncertainty on the mean net infiltration over the infiltration modeling domain is estimated by the standard error on the mean, which varies from 2.0 to 4.0 mm/yr, depending on climate. This uncertainty is certainly similar to the difference between the two replicates compared at the 25th, 50th, and 75th percentiles. This result provides confidence that the results of the combined replicates are representative of the actual distribution given the uncertainty estimated by the standard error on the mean. This uncertainty would be reduced by running more LHS realizations; however, the accuracy of the model predictions will not be improved upon because this accuracy is also limited by other sources of uncertainty (e.g., model uncertainty).

Table 6.5.7.9-1. Differences in Net Infiltration Statistics between Replicates

ABS(R1-R2)	Domain	PD	MO	GT
25th Percentile [mm/yr]	Infiltration modeling domain (125 km^2)	***0.0***	***4.8***	***4.3***
	UZ modeling domain (39.8 km^2)	0.0	5.7	2.2
	Repository footprint (5.7 km^2)	0.4	6.9	1.9
50th Percentile [mm/yr]	Infiltration modeling domain (125 km^2)	***2.2***	***2.9***	***0.4***
	UZ modeling domain (39.8 km^2)	0.6	2.3	2.7
	Repository footprint (5.7 km^2)	0.9	2.2	2.7
75th Percentile [mm/yr]	Infiltration modeling domain (125 km^2)	***3.2***	***1.7***	***2.0***
	UZ modeling domain (39.8 km^2)	3.6	2.3	2.3
	Repository footprint (5.7 km^2)	4.4	2.4	3.1
Mean Standard Error on Mean	Infiltration modeling domain (125 km^2)	***2.0***	***4.0***	***3.0***

Source: Output DTN: SN0701T0502206.037, file: \Welcome to Massif\Massif\Post Processing\ *Summary Net Infiltration All Climates.xls*.

6.6 INFILTRATION PREDICTION UNCERTAINTIES

This section summarizes the results of the calculations reported in Section 6.5, including discussion of uncertainty. Section 6.6.1 analyzes the values of potential recharge (space-time averages of net infiltration) that are tabulated in Section 6.5.7. Section 6.6.2 is a discussion of the uncertainty in the calculated net infiltration at a particular location, averaged over time but not averaged over surface area. Section 6.6.3 discusses sources of model uncertainty.

Section 6.5.5 and Appendix I discuss the uncertainties in the input parameters and the screening of those uncertainties to select parameters to be varied for the uncertainty analysis. For each climate, a realization is a particular set of values for the selected parameters. Section 6.5.7 reports the results of the calculation for each realization.

A set of realizations for a particular climate provides an approximate uncertainty distribution for each calculated result. An uncertainty distribution developed from a set of realizations describes the contribution of parameter uncertainty to the uncertainty of the result. Model uncertainty also contributes to the overall uncertainty in the net infiltration estimates. Sources of model uncertainty are discussed and evaluated in Section 6.6.3.

6.6.1 Uncertainty in Potential Recharge Averaged over the UZ Model Grid

Section 6.5 reports the results of 120 calculations (2 replicates of 20 realizations for each of three climates). For each of the three climates, there are twenty calculations, called realizations, for which certain input parameters are varied in accordance with their uncertainty for that climate. This section develops summaries of the results.

Each of the sixty calculations reported in Section 6.5 provides three values for potential recharge, one for each of the following surface areas:

- Repository footprint
- Region planned for unsaturated-zone calculation (the UZ model grid)
- Entire surface treated by the MASSIF calculations.

Each value represents a space-time average over the area of interest and over the duration of the particular climate. A set of realizations for a particular climate provides three approximate uncertainty distributions, one for each of the space-time averages. This section models the uncertainty distributions of average potential recharge over the UZ model grid for each of the three climates. The UZ model grid represents the region expected to influence percolation of moisture from the surface to the vicinity of the repository.

Because the potential recharge must have positive values, a normal distribution cannot represent the uncertainty in potential recharge. Instead, this section models each uncertainty distribution as a lognormal distribution. The probability density for a lognormal distribution is (Gilbert 1987 [DIRS 163705], p. 152, Equation 12.1):

$$f(x) = \frac{1}{xS\sqrt{2\pi}} \exp\left[-\frac{1}{2S^2} (\ln x - M)^2 \right] \qquad \text{(Eq. 6.6.1-1)}$$

where M and S^2 are the true mean and variance of the random variable ln x, exp(M) is the median value of the random variable x, and M is the median value of the random variable ln x.

This section applies the W test to the logarithm of potential recharge over the UZ model grid. Testing the logarithm provides information about whether the uncertainty in potential recharge may be represented as a lognormal distribution.

This section combines both replicates for each climate and makes the approximation that the sample vectors represent random points in the parameter space. This permits the use of the W test for normality (Gilbert 1987 [DIRS 163705], Section 12.3.1). The null hypothesis for the W test is that the logarithms have a normal distribution. For a sample of size 40, the null hypothesis is rejected at the 0.02 significance level if W is less than 0.929 (Gilbert 1987 [DIRS 163705], Table A7). That is, the probability of W being less than 0.929 for a population of size 40 is less than 0.02.

If the hypothesis is not rejected, then:

- The experimental mean of ln x is an unbiased estimator of M (Gilbert 1987 [DIRS 163705], p. 27, Equation 4.3). The median value of x is exp(M).
- The experimental standard deviation of ln x is an unbiased estimator of S (ANSI/NCSL Z540-2-1997 [DIRS 157394], pp. 33, Section B.2.17, Note 1).
- The mean of x is exp(M+S^2/2) (Gilbert 1987 [DIRS 163705], p. 156, Table 12.1). (The mean of a lognormal distribution is always larger than the median.)

The following sections analyze the calculated amounts of potential recharge, averaged over the UZ model grid. To facilitate traceability, all values are rounded as shown in the tables before being used for subsequent calculations. The analyses show that the hypothesis of a lognormal distribution is not rejected for any of the three climates. Table 6.6.1-1 summarizes the parameters of the lognormal distributions. Because the uncertainty distribution is not symmetric, the table includes an uncertainty factor, defined to be exp(S). The uncertainty factor is (1) the ratio of the value "one sigma" above the median, exp(M+S), to the median and (2) the ratio of the median to the value one sigma below the median, exp(M−S).

The uncertainty in potential recharge over the UZ model grid is approximately a factor of two for the Present-Day climate or the Monsoon climate. For the Glacial Transition climate, the uncertainty factor is 1.8. Much of the uncertainty stems from uncertainty in parameters that are independent of climate. Section 6.7 discusses the relative contributions of the parameter uncertainties.

Table 6.6.1-1. Parameters of Lognormal Distributions Representing the Contributions of Parameter Uncertainty to Uncertainties in Potential Recharge, Averaged over the UZ Model Grid

Climate	M [(a)]	S [(b)]	Median (e^M) (mm/yr)	Uncertainty Factor (e^S)	Mean of Distribution exp(M+S^2/2) (mm/yr)
Present-Day	2.4	0.9	11	2	17
Monsoon	3.0	0.9	20	2	30
Glacial Transition	3.2	0.6	25	1.8	29

[(a)] Mean of ln(I_{avg}) from Tables 6.6.1.1-1, 6.6.1.2-1, and 6.6.1.3-1.
[(b)] Standard deviation of ln(I_{avg}) from Tables 6.6.1.1-1, 6.6.1.2-1, and 6.6.1.3-1.

6.6.1.1 Uncertainty in Potential Recharge over the UZ Model Grid during the Present-Day Climate

Table 6.6.1.1-1 presents the results of both replicates for the Present-Day climate, sorted by potential recharge over the UZ model grid. The table also shows the logarithms of the results, as well as the mean and standard deviation of each column.

Table 6.6.1.1-2 develops the W test for the logarithm of net infiltration. The value of W is 0.939, so that the hypothesis that the distribution is lognormal is not rejected at the 0.02 significance level. For the Present-Day climate, therefore, the uncertainty in potential recharge may be represented by a lognormal distribution. The parameters of the lognormal distribution are $M = 2.4$ and $S = 0.9$.

The median value of potential recharge is 11 mm/yr. The value of S is equivalent to an uncertainty of a factor of 2 in potential recharge over the UZ model grid. The mean value of the lognormal distribution is 17 mm/yr, close to the value of 15 mm/yr, which is the mean of the calculated values of potential recharge. The agreement between these two values corroborates that the lognormal distribution models the distribution of calculated results.

Table 6.6.1.1-1. Values of Potential Recharge over the UZ Model Grid as Calculated for the Present-Day Climate, Sorted

Replicate [a]	Vector [b]	I_{avg} (mm/yr) [c]	ln(I_{avg}) [d]		Replicate [a]	Vector [b]	I_{avg} (mm/yr) [c]	ln(I_{avg}) [d]
R1	4	1.4	0.34		R2	15	13.3	2.59
R2	4	2.1	0.74		R1	2	14.2	2.65
R1	10	2.4	0.88		R1	18	14.8	2.69
R2	10	3.4	1.22		R2	19	16.6	2.81
R2	18	3.4	1.22		R2	3	19.6	2.98
R1	7	3.7	1.31		R1	12	20.2	3.01
R2	17	3.9	1.36		R1	9	20.7	3.03
R2	1	5.4	1.69		R2	13	20.9	3.04
R1	1	5.5	1.70		R2	7	24.3	3.19
R1	17	5.5	1.70		R1	14	25.1	3.22
R1	11	5.9	1.77		R1	6	25.2	3.23
R2	2	6.0	1.79		R1	15	25.7	3.25
R1	8	6.8	1.92		R2	14	28.7	3.36
R1	20	8.3	2.12		R2	20	29.1	3.37
R2	5	8.6	2.15		R2	12	29.3	3.38
R2	6	10.3	2.33		R1	19	29.9	3.40
R2	8	10.9	2.39		R2	9	30.1	3.40
R1	3	11.4	2.43		R1	5	32.6	3.48

Table 6.6.1.1-1. Values of Potential Recharge over the UZ Model Grid as Calculated for the Present-Day Climate, Sorted (Continued)

Replicate[a]	Vector[b]	I_{avg} (mm/yr)[c]	ln(I_{avg})[d]		Replicate[a]	Vector[b]	I_{avg} (mm/yr)[c]	ln(I_{avg})[d]
R1	16	11.9	2.48		R2	16	40.9	3.71
R2	11	12.3	2.51			Mean[e]	15	2.4
R1	13	12.6	2.53		Standard Deviation[e]		10	0.9

Source: Output DTN: SN0701T0502206.037, files: \Welcome to Massif\Massif\Present Day Uncertainty\Post Processing\Intermediate Output Files*PD_Mean_Infiltration_R1.txt* and \Welcome to Massif\Massif\Present Day Uncertainty\Post Processing\Intermediate Output Files*PD_Mean_Infiltration_R2.txt*.

[a] Identifies source file in DTN.
[b] Identifies data line in source file.
[c] Rounded to nearest 0.1 mm before further calculation.
[d] Rounded to nearest 0.01.
[e] Standard deviation rounded to two significant digits if first digit is one, otherwise to one significant digit. Mean rounded consistent with standard deviation.

Table 6.6.1.1-2. W test for Lognormal Uncertainty Distribution for Potential Recharge over the UZ Model Grid during the Present-Day Climate

i [(a)]	$x_i = \ln(I_{avg})$ [(b)]	$x_i - x_{mean}$	a_i [(c)]	x_{41-i}	$a_i (x_{41-i} - x_i)$
1	0.34	−2.07	0.3964	3.71	1.336
2	0.74	−1.67	0.2737	3.48	0.750
3	0.88	−1.53	0.2368	3.40	0.597
4	1.22	−1.19	0.2098	3.40	0.457
5	1.22	−1.19	0.1878	3.38	0.406
6	1.31	−1.10	0.1691	3.37	0.348
7	1.36	−1.05	0.1526	3.36	0.305
8	1.69	−0.72	0.1376	3.25	0.215
9	1.70	−0.71	0.1237	3.23	0.189
10	1.70	−0.71	0.1108	3.22	0.168
11	1.77	−0.64	0.0986	3.19	0.140
12	1.79	−0.62	0.0870	3.04	0.109
13	1.92	−0.49	0.0759	3.03	0.084
14	2.12	−0.29	0.0651	3.01	0.058
15	2.15	−0.26	0.0546	2.98	0.045
16	2.33	−0.08	0.0444	2.81	0.021
17	2.39	−0.02	0.0343	2.69	0.010
18	2.43	0.02	0.0244	2.65	0.005
19	2.48	0.07	0.0146	2.59	0.002
20	2.51	0.10	0.0049	2.53	0.000
21	2.53	0.12		sum	5.245
22	2.59	0.18		$W=sum^2/d$	0.939
23	2.65	0.24			
24	2.69	0.28			
25	2.81	0.40			

Table 6.6.1.1-2. W test for Lognormal Uncertainty Distribution for Potential Recharge over the UZ Model Grid during the Present-Day Climate (Continued)

i [(a)]	$x_i = \ln(I_{avg})$ [(b)]	$x_i - x_{mean}$	a_i [(c)]	x_{41-i}	$a_i (x_{41-i} - x_i)$
26	2.98	0.57			
27	3.01	0.60			
28	3.03	0.62			
29	3.04	0.63			
30	3.19	0.78			
31	3.22	0.81			
32	3.23	0.82			
33	3.25	0.84			
34	3.36	0.95			
35	3.37	0.96			
36	3.38	0.97			
37	3.40	0.99			
38	3.40	0.99			
39	3.48	1.07			
40	3.71	1.30			
x_{mean}	2.41	29.3	$d=\text{sum}(x_i - x_{mean})^2$		

[(a)] Index number after sorting.
[(b)] From Table 6.6.1.1-1.
[(c)] Gilbert 1987 [DIRS 163705], Table A6.

6.6.1.2 Uncertainty in Potential Recharge over the UZ Model Grid during the Monsoon Climate

Table 6.6.1.2-1 presents the results of both replicates for the monsoon climate, sorted by potential recharge over the UZ model grid. The table also shows the logarithms of the results, as well as the mean and standard deviation of each column.

Table 6.6.1.2-2 develops the W test for the logarithm of net infiltration. The value of W is 0.930, so that the hypothesis that the distribution is lognormal is not rejected at the 0.02 significance level. For the monsoon climate, therefore, the uncertainty in potential recharge may be represented by a lognormal distribution. The parameters of the lognormal distribution are $M = 3.0$ and $S = 0.9$. The median value of potential recharge is 20 mm/yr. The value of S is equivalent to an uncertainty of a factor of 2 in potential recharge over the UZ model grid. The mean value of the lognormal distribution is 30 mm/yr, which is also the mean of the calculated values of potential recharge. The agreement between these two values corroborates that the lognormal distribution models the distribution of calculated results.

Table 6.6.1.2-1. Values of Potential Recharge over the UZ Model Grid as Calculated for the Monsoon Climate, Sorted

Replicate[a]	Vector[b]	I_{avg} (mm/yr)[c]	ln(I_{avg})[d]		Replicate[a]	Vector[b]	I_{avg} (mm/yr)[c]	ln(I_{avg})[d]
R2	20	1.2	0.18		R2	9	25.0	3.22
R1	18	1.9	0.64		R1	1	25.2	3.23
R1	20	4.6	1.53		R2	11	26.0	3.26
R1	17	5.4	1.69		R1	9	26.9	3.29
R1	3	6.5	1.87		R1	15	28.1	3.34
R2	6	6.9	1.93		R2	15	30.0	3.40
R2	4	7.6	2.03		R1	6	36.5	3.60
R1	10	9.2	2.22		R1	19	38.4	3.65
R1	11	10.6	2.36		R2	17	39.1	3.67
R1	5	13.9	2.63		R1	14	41.0	3.71
R2	14	14.6	2.68		R2	12	44.9	3.80
R2	5	15.1	2.71		R1	16	45.0	3.81
R2	10	16.0	2.77		R1	4	45.5	3.82
R1	12	17.1	2.84		R1	8	49.5	3.90
R2	18	18.1	2.90		R2	16	56.7	4.04
R2	8	18.2	2.90		R2	1	56.8	4.04
R2	13	19.3	2.96		R1	7	62.2	4.13
R2	2	22.0	3.09		R2	19	75.7	4.33
R1	13	23.3	3.15		R2	3	86.2	4.46
R2	7	23.5	3.16			Mean[e]	30	3.0
R1	2	24.9	3.21		Standard Deviation[e]		20	0.9

Source: Output DTN: SN0701T0502206.037, files: \Welcome to Massif\Massif\Monsoon Uncertainty\Post Processing\Intermediate Output Files*MO_Mean_Infiltration_R1.txt* and \Welcome to Massif\Massif\Monsoon Uncertainty\Post Processing\Intermediate Output Files*MO_Mean_Infiltration_R2.txt*.

[a] Identifies source file in DTN.
[b] Identifies data line in source file.
[c] Rounded to nearest 0.1 mm before further calculation.
[d] Rounded to nearest 0.01.
[e] Standard deviation rounded to two significant digits if first digit is one, otherwise to one significant digit. Mean rounded consistent with standard deviation.

Table 6.6.1.2-2. W Test for Lognormal Uncertainty Distribution for Potential Recharge over the UZ Model Grid during the Monsoon Climate

i [(a)]	$x_i = \ln(I_{avg})$ [(b)]	$x_i - x_{mean}$	a_i [(c)]	x_{41-i}	$a_i (x_{41-i} - x_i)$
1	0.18	−2.82	0.3964	4.46	1.697
2	0.64	−2.36	0.2737	4.33	1.010
3	1.53	−1.47	0.2368	4.13	0.616
4	1.69	−1.31	0.2098	4.04	0.493
5	1.87	−1.13	0.1878	4.04	0.408
6	1.93	−1.07	0.1691	3.90	0.333

Table 6.6.1.2-2. W Test for Lognormal Uncertainty Distribution for Potential Recharge over the UZ Model Grid during the Monsoon Climate (Continued)

i [(a)]	$x_i = \ln(I_{avg})$ [(b)]	$x_i - x_{mean}$	a_i [(c)]	x_{41-i}	$a_i (x_{41-i} - x_i)$
7	2.03	−0.97	0.1526	3.82	0.273
8	2.22	−0.78	0.1376	3.81	0.219
9	2.36	−0.64	0.1237	3.80	0.178
10	2.63	−0.37	0.1108	3.71	0.120
11	2.68	−0.32	0.0986	3.67	0.098
12	2.71	−0.29	0.0870	3.65	0.082
13	2.77	−0.23	0.0759	3.60	0.063
14	2.84	−0.16	0.0651	3.40	0.036
15	2.90	−0.10	0.0546	3.34	0.024
16	2.90	−0.10	0.0444	3.29	0.017
17	2.96	−0.04	0.0343	3.26	0.010
18	3.09	0.09	0.0244	3.23	0.003
19	3.15	0.15	0.0146	3.22	0.001
20	3.16	0.16	0.0049	3.21	0.000
21	3.21	0.21		sum	5.681
22	3.22	0.22		$W=sum^2/d$	0.930
23	3.23	0.23			
24	3.26	0.26			
25	3.29	0.29			
26	3.34	0.34			
27	3.40	0.40			
28	3.60	0.60			
29	3.65	0.65			
30	3.67	0.67			
31	3.71	0.71			
32	3.80	0.80			
33	3.81	0.81			
34	3.82	0.82			
35	3.90	0.90			
36	4.04	1.04			
37	4.04	1.04			
38	4.13	1.13			
39	4.33	1.33			
40	4.46	1.46			
x_{mean}	3.00	34.7	$d=sum(x_i - x_{mean})^2$		

(a) Index number after sorting.
(b) From Table 6.6.1.2-1.
(c) Gilbert 1987 [DIRS 163705], Table A6.

6.6.1.3 Potential Recharge over the UZ Model Grid during the Glacial Transition Climate

Table 6.6.1.3-1 presents the results of both replicates for the glacial transition climate, sorted by potential recharge over the UZ model grid. The table also shows the logarithms of the results, as well as the mean and standard deviation of each column.

Table 6.6.1.3-2 develops the W test for the logarithm of net infiltration. The value of W is 0.943, so that the hypothesis that the distribution is lognormal is not rejected at the 0.02 significance level. For the glacial transition climate, therefore, the uncertainty in potential recharge may be represented by a lognormal distribution. The parameters of the lognormal distribution are $M = 3.2$ and $S = 0.6$.

The median value of potential recharge is 25 mm/yr. The value of S is equivalent to an uncertainty of a factor of 1.8 in potential recharge over the UZ model grid. The mean value of the lognormal distribution is 29 mm/yr, which is the same as the mean of the calculated values of potential recharge. The agreement between these two values corroborates that the lognormal distribution models the distribution of calculated results.

Table 6.6.1.3-1. Values of Potential Recharge over the UZ Model Grid as Calculated for the Glacial Transition Climate, Sorted

Replicate [a]	Vector [b]	I_{avg} (mm/yr) [c]	ln(I_{avg}) [d]		Replicate [a]	Vector [b]	I_{avg} (mm/yr) [c]	ln(I_{avg}) [d]
R1	7	4.3	1.46		R1	1	28.6	3.35
R1	4	5.8	1.76		R2	12	29.1	3.37
R2	6	8.2	2.10		R1	18	29.4	3.38
R1	9	9.8	2.28		R1	10	33.1	3.50
R2	11	11.0	2.40		R2	18	33.5	3.51
R2	15	11.2	2.42		R2	20	33.5	3.51
R2	16	16.2	2.79		R1	19	33.7	3.52
R2	5	17.7	2.87		R2	8	33.7	3.52
R2	13	18.7	2.93		R2	3	34.2	3.53
R1	15	19.3	2.96		R1	14	35.3	3.56
R1	6	19.8	2.99		R1	2	37.2	3.62
R2	14	20.0	3.00		R2	2	43.8	3.78
R2	10	20.7	3.03		R1	12	46.5	3.84
R1	3	21.0	3.04		R2	7	47.2	3.85
R2	4	22.3	3.10		R1	5	49.7	3.91
R1	17	22.7	3.12		R2	1	51.8	3.95
R1	11	23.4	3.15		R1	13	57.7	4.06
R2	17	24.2	3.19		R2	19	62.0	4.13
R1	16	26.7	3.28		R1	8	72.1	4.28
R2	9	27.6	3.32			Mean [e]	29	3.2
R1	20	28.5	3.35			Standard Deviation [e]	15	0.6

Source: Output DTN: SN0701T0502206.037, files: \Welcome to Massif\Massif\Glacial Uncertainty\Post Processing\Intermediate Output Files*GT_Mean_Infiltration_R1.txt* and \Welcome to Massif\Massif\Glacial Uncertainty\Post Processing\Intermediate Output Files*GT_Mean_Infiltration_R2.txt*.

[a] Identifies source file in DTN.
[b] Identifies data line in source file.
[c] Rounded to nearest 0.1 mm before further calculation.
[d] Rounded to nearest 0.01.
[e] Standard deviation rounded to two significant digits if first digit is one, otherwise to one significant digit. Mean rounded consistent with standard deviation.

Table 6.6.1.3-2. W Test for Lognormal Uncertainty Distribution for Potential Recharge over the UZ Model Grid during the Glacial Transition Climate

i [(a)]	$x_i = \ln(I_{avg})$ [(b)]	$x_i - x_{mean}$	a_i [(c)]	x_{41-i}	$a_i (x_{41-i} - x_i)$
1	1.46	−1.76	0.3964	4.28	1.118
2	1.76	−1.46	0.2737	4.13	0.649
3	2.10	−1.12	0.2368	4.06	0.464
4	2.28	−0.94	0.2098	3.95	0.350
5	2.40	−0.82	0.1878	3.91	0.284
6	2.42	−0.80	0.1691	3.85	0.242
7	2.79	−0.43	0.1526	3.84	0.160
8	2.87	−0.35	0.1376	3.78	0.125
9	2.93	−0.29	0.1237	3.62	0.085
10	2.96	−0.26	0.1108	3.56	0.066
11	2.99	−0.23	0.0986	3.53	0.053
12	3.00	−0.22	0.0870	3.52	0.045
13	3.03	−0.19	0.0759	3.52	0.037
14	3.04	−0.18	0.0651	3.51	0.031
15	3.10	−0.12	0.0546	3.51	0.022
16	3.12	−0.10	0.0444	3.50	0.017
17	3.15	−0.07	0.0343	3.38	0.008
18	3.19	−0.03	0.0244	3.37	0.004
19	3.28	0.06	0.0146	3.35	0.001
20	3.32	0.10	0.0049	3.35	0.000
21	3.35	0.13		sum	3.761
22	3.35	0.13		$W=sum^2/d$	0.943
23	3.37	0.15			
24	3.38	0.16			
25	3.50	0.28			
26	3.51	0.29			
27	3.51	0.29			
28	3.52	0.30			
29	3.52	0.30			
30	3.53	0.31			
31	3.56	0.34			
32	3.62	0.40			
33	3.78	0.56			
34	3.84	0.62			
35	3.85	0.63			
36	3.91	0.69			
37	3.95	0.73			

Table 6.6.1.3-2. W Test for Lognormal Uncertainty Distribution for Potential Recharge over the UZ Model Grid during the Glacial Transition Climate

i [(a)]	$x_i = \ln(I_{avg})$ [(b)]	$x_i - x_{mean}$	a_i [(c)]	x_{41-i}	$a_i (x_{41-i} - x_i)$
38	4.06	0.84			
39	4.13	0.91			
40	4.28	1.06			
x_{mean}	3.22	15.0	$d=\text{sum}(x_i - x_{mean})^2$		

[(a)] Index number after sorting.
[(b)] From Table 6.6.1.1-1.
[(c)] Gilbert 1987 [DIRS 163705], Table A6.

6.6.2 Uncertainty in Local Net Infiltration

The maps resulting from the net infiltration calculations provide a value for each 30 × 30-m grid cell that represents the average over the duration of the climate. This report does not provide uncertainty estimates for each of these local values; however, at many locations the uncertainty in local conditions is much larger than the corresponding uncertainty in a spatial average.

This section provides a qualitative discussion of the uncertainty in local net infiltration. Numerical values are used, but because the analysis uses several equations that are only approximations, the results are only a rough guide to the extent of local uncertainty.

The calculations in Appendix H estimate the influence of uncertainty in input parameters on the uncertainty in a measure of infiltration. The measure of infiltration used is the average annual net infiltration over the infiltration modeling domain, as reported in Section 6.5.7. Sections H2.5, H3.6, and H4.6 conclude that the inputs whose uncertainty have the greatest impact on infiltration uncertainty are:

- Effective uniform soil depth assigned to the region defined as Soil Depth Class 4
- Precipitation parameters
- Effective uniform holding capacity assigned to Soil Group 7/8/9.

The uncertainty in precipitation is the same whether one is considering spatially averaged infiltration or local infiltration. However, the uncertainties in the other two parameters are less when taken over the entire infiltration modeling domain. This is because the averaging takes advantage of the law of large numbers: the uncertainty in the mean of an uncertainty distribution can be much less than the standard uncertainty of the distribution itself.

For example, the expected value of the throw of a single six-sided die, with sides numbered one through six, is 3.5. For a single throw, the standard uncertainty is 1.7. For the average of 100 throws, the standard uncertainty is 0.17.

This section provides a qualitative discussion of the uncertainty in calculated local net infiltration, taking Replicate 1 of the Present-Day climate as an example and considering only localities that are in Soil Depth Class 4. Further, this section considers only the effect of local uncertainty in soil depth. The analysis does not apply at any location where the soil depth is known and is approximately the same as the effective uniform depth for Soil Depth Class 4.

Let $\bar{I}_{PD}$ be the calculated annual potential recharge for the remainder of the Present-Day climate. That is, $\bar{I}_{PD}$ is the average over the infiltration modeling domain of the annual net infiltration at each location, $I_{PD}(lat, long)$, where *lat* and *long* are the latitude and longitude, respectively.

For consistency with Section 6.6.1, the analysis in this section focuses on uncertainty in the logarithm of net infiltration. The combined standard uncertainty in the logarithm of $\bar{I}_{PD}$, $u(\ln \bar{I}_{PD})$, is given by (ANSI/NCSL Z540-2-1997 [DIRS 157394], p. 19, Equation 10):

$$u^2(\ln \bar{I}_{PD}) = \sum_i \left[\frac{\partial \ln \bar{I}_{PD}}{\partial x_i} \right]^2 u^2(x_i) \qquad \text{(Eq. 6.6.2-1)}$$

where each $u(x_i)$ is the standard uncertainty of an input parameter. Equation 6.6.2-1 results from the following approximations (ANSI/NCSL Z540-2-1997 [DIRS 157394], p. 19):

- The input parameters are independent.
- The dependence of $\ln \bar{I}_{PD}$ on each input parameter, within that parameter's range of uncertainty, is linear. That is, the Taylor Series expansion about the nominal value of each parameter can be truncated after the linear term without changing the qualitative nature of the dependence.

From Section 6.6.1.1, $u(\ln \bar{I}_{PD})$ is the parameter *S* in the lognormal distribution and has a value of about 0.9, so that $u^2(\ln \bar{I}_{PD})$ is about 0.8. According to Table H-1, the regression coefficient for Soil Depth 4, R^2, is 0.33 for Replicate 1 of the Present-Day climate when aleatory uncertainty is varying. This is a low estimate; tables H-2 through H-4 provide larger coefficients for Replicate 2 or for aleatory uncertainty fixed. Therefore, the contribution from Soil Depth Class 4 is at least:

$$\left[\frac{\partial \ln \bar{I}_{PD}}{\partial x_{SD4}} \right]^2 u^2(x_{SD4}) \cong 0.33(0.9) \cong 0.3 \qquad \text{(Eq. 6.6.2-2)}$$

and the contribution to uncertainty from the other parameters is at most:

$$\sum_{i \neq SD4} \left[\frac{\partial \ln \bar{I}_{PD}}{\partial x_i} \right]^2 u^2(x_i) \cong 0.8 - 0.3 \cong 0.5, \qquad \text{(Eq. 6.6.2-3)}$$

where x_{SD4} is the effective uniform soil depth for Soil Depth Class 4.

The standard uncertainty in the effective uniform depth for Soil Depth Class 4, $u(x_{SD4})$, is about 0.12 m (Table I-2). To satisfy Equation 6.6.2-2, there must be:

$$\frac{\partial \ln \bar{I}_{PD}}{\partial x_{SD4}} \cong 5\ \mathrm{m}^{-1} \qquad \text{(Eq. 6.6.2-4)}$$

or more.

For the uncertainty in local net infiltration there is the following equation:

$$u^2(\ln I_{PD}(lat,long)) = \sum_i \left[\frac{\partial \ln I_{PD}(lat,long)}{\partial x_i}\right]^2 u^2(x_i) \qquad \text{(Eq. 6.6.2-5)}$$

Now the Taylor Series expansion is about the local value of each spatially varying parameter. Although the uncertainty distribution for a local parameter differs from the distribution for the effective uniform value, the nominal value is the same. Therefore, the Taylor Series expansion is taken about values similar to those in the previous expansion.

The approximation is made that the contribution to $u^2(\ln I_{PD}(lat,long))$ from each parameter other than Soil Depth Class 4 is the same as the contribution of that parameter to $u^2(\ln \bar{I}_{PD})$. This is clearly not true, especially for parameters that are clearly irrelevant, such as other Soil Depth classes. The justification for this approximation is that the contributions from such parameters are relatively small. Therefore,

$$u^2(\ln I_{PD}(lat,long)) \cong 0.5 + \left[\frac{\partial \ln I_{PD}(lat,long)}{\partial d(lat,long)}\right]^2 u^2(d(lat,long)), \qquad \text{(Eq. 6.6.2-6)}$$

where $d(lat,long)$ is the local soil depth.

To complete the estimation of $u^2(\ln I_{PD}(lat,long))$, this section first estimates $\frac{\partial \ln I_{PD}(lat,long)}{\partial d(lat,long)}$, then $u^2(d(lat,long))$. Note that, by definition,

$$\bar{I}_{PD} = \frac{1}{A}\iint_{lat,long} I_{PD}(lat,long)dA\,. \qquad \text{(Eq. 6.6.2-7)}$$

where A is surface area. Consequently,

$$\frac{\partial \bar{I}_{PD}}{\partial x_{SD4}} = \frac{1}{A}\iint_{lat,long} \frac{\partial I_{PD}(lat,long)}{\partial x_{SD4}}dA \qquad \text{(Eq. 6.6.2-8)}$$

$$\frac{\partial \ln \bar{I}_{PD}}{\partial x_{SD4}} = \frac{1}{A} \iint_{lat,long} \frac{I_{PD}(lat,long)}{\bar{I}_{PD}} \frac{\partial \ln I_{PD}(lat,long)}{\partial x_{SD4}} dA . \qquad \text{(Eq. 6.6.2-9)}$$

The integral on the right-hand side of Equation 6.6.2-9 involves integration over each soil depth class. Clearly, the partial derivative with respect to x_{SD4} will be much smaller within other soil depth classes than it is within Soil Depth Class 4. Also, Soil Depth Class 4 contributes over 90% of $\bar{I}_{PD}$ (Table 6.5.7.6-1), which suggests that

$$\frac{\partial \ln \bar{I}_{PD}}{\partial x_{SD4}} \cong \frac{1}{A} \iint_{(lat,long)\in SDC4} \frac{I_{PD}(lat,long)}{\bar{I}_{PD}} \frac{\partial \ln I_{PD}(lat,long)}{\partial x_{SD4}} dA . \qquad \text{(Eq. 6.6.2-10)}$$

Within Soil Depth Class 4, $I_{PD}(lat,long)$ must vary above and below $\bar{I}_{PD}$. Therefore, an intermediate estimate for $\frac{\partial \ln I_{PD}(lat,long)}{\partial x_{SD4}}$ is the value of $\frac{\partial \ln \bar{I}_{PD}}{\partial x_{SD4}}$, which is 5 m^{-1}.

Now, $\frac{\partial \ln I_{PD}(lat,long)}{\partial x_{SD4}}$ differs from $\frac{\partial \ln I_{PD}(lat,long)}{\partial d(lat,long)}$ in that the former is the change in local net infiltration as the soil depth increases in the entire region of Soil Depth Class 4, whereas the latter is the change in local net infiltration when only the local soil depth increases. The soil depth at other locations can only influence local net infiltration by adding run-on to the local precipitation at the site. However, because Table 6.5.4.7-1 indicates that runoff represents only about 2% of the precipitation, it is reasonable to estimate that, for a location within Soil Depth Class 4,

$$\frac{\partial \ln I_{PD}(lat,long)}{\partial d(lat,long)} \cong \frac{\partial \ln \bar{I}_{PD}}{\partial x_{SD4}} \cong 5 \ \text{m}^{-1}. \qquad \text{(Eq. 6.6.2-11)}$$

Table 6.5.2.4-2 indicates that the data for Soil Depth Class 4 have a standard deviation of about 0.7 m. This is an estimate of the uncertainty in local soil depth for locations within Soil Depth Class 4. Therefore, for locations within Soil Depth Class 4,

$$u^2(\ln I_{PD}(lat,long)) \cong 0.5 + [5]^2 0.7^2 \cong 13 \text{ or more}, \qquad \text{(Eq. 6.6.2-12)}$$

so that $u(\ln I_{PD}(lat,long))$ is about 4 or more, as compared with 0.9 for $u(\ln \bar{I}_{PD})$.

Recall that the standard uncertainty of 0.9 for $\ln \bar{I}_{PD}$ corresponds to an uncertainty of about a factor of two in $\bar{I}_{PD}$. The standard uncertainty of 4 for $\ln I_{PD}(lat,long)$ is equivalent to an uncertainty in $I_{PD}(lat,long)$ of a factor of fifty or more. Furthermore, the deviation of $I_{PD}(lat,long)$ from its expected value may not be in the same direction as the deviation of $\bar{I}_{PD}$ from its expected value. For example, it should not be surprising if the future measured value of $\bar{I}_{PD}$ is a factor of two higher than predicted, whereas at a particular location the measured value of $I_{PD}(lat,long)$ is a factor of twenty lower than predicted.

The preceding qualitative discussion is for the comparison of predicted and measured values of $I_{PD}(lat, long)$ for a point on the surface. In fact, MASSIF predictions of local net infiltration are not point values but averages over a 30 × 30-m grid. The effect of upscaling to 30 meters can depend strongly on the local topography. In some places, the soil depth may be nearly uniform on that distance scale and significantly different from the depth upscaled to the entire Soil Depth Class 4. In other places, the depth may vary substantially, even over this smaller distance.

If a downstream study takes as input the local net infiltration(s) from one or more calculations reported in Section 6.5, then the uncertainty analysis for that study should include an estimate of the uncertainty in local net infiltration.

6.6.3 Sources and Magnitude of Model Uncertainty

Model uncertainty represents a limitation of any model to accurately represent the physical processes being considered. Models are simplified representations of reality and, as such, introduce inherent errors in estimated quantities due to the simplifications and abstractions necessary for formulating the model. In addition to the limitations in model predictions due to model uncertainty, parameter uncertainty introduces additional uncertainty. Measurement theory provides a useful analogy to compare model and parameter uncertainties. Model uncertainty is similar to measurement accuracy, while parameter uncertainty is similar to measurement precision. Both sources of uncertainty contribute to the final uncertainty in a model prediction or measurement quantity.

In the analysis of net infiltration at Yucca Mountain, both sources of uncertainty are important and must be estimated. Most of the effort has been focused on evaluating and quantifying parameter uncertainty. As discussed in Section 6.6.1 and 6.6.2, parameter uncertainty represents approximately a factor of 2 uncertainty in the mean net infiltration averaged over the UZ model domain and a factor of approximately 6 in the uncertainty in local net infiltration predicted in areas with shallow soils. This parameter uncertainty conceivably could be reduced by additional geologic characterization work at the site (e.g., a more detailed soil depth map, a more detailed characterization of soil and rock properties).

Sources of model uncertainty in this study include: (1) the accuracy of the coupled NDVI/FAO-56 approach for estimating evapotranspiration at the site, (2) the accuracy of the layered field capacity approach for representing subsurface water flow, (3) the accuracy of the assumption that evapotranspiration from bedrock is negligible, and (4) the accuracy of the distributed runoff model used to represent surface water flow.

The uncertainty associated with the ET submodel is evaluated by comparing ET measurements using lysimeter data to simulated results using MASSIF (see Section 7.1.2). These comparisons indicate that the model performs well in the context of parameter uncertainty, especially for estimates of cumulative annual ET.

The present study was unable to explicitly test the accuracy of the field capacity approach for representing subsurface water flow against field data from the Yucca Mountain site. However, a comparison was made against HYDRUS 1-D (a comparable model that represents subsurface water flow using Richards' equation) in Section 7.2.2. This comparison demonstrates that while

the field capacity approach may not represent the transient nature of this flow accurately, it does an adequate job of representing the cumulative net infiltration over the year.

The assumption that ET from the bedrock is negligible is highly uncertain and is dependent upon knowledge of the bedrock properties and applicable physics of potential processes for water removal from bedrock overlain by soil. Certain neutron logs that extend into bedrock show that water removal does occur at certain locations (BSC 2004 [DIRS 170007], p. 6-16), however these results are not at all consistent when all the logs are examined. Therefore, the implication of this assumption is that it will tend to overestimate net infiltration model predictions, but it is not clear by how much and where these overestimates occur.

Finally, comparisons of runoff predictions with stream gauge observations (see Section 7.1.3) provide confidence that the model uncertainty related to the runoff submodel is not a significant source of uncertainty for mean net infiltration over the a large area (e.g., UZ model domain); however, this process may contribute significantly to uncertainty in local net infiltration (see Sections 7.1.3.1 and 7.1.3.2).

The challenge of estimating net infiltration model uncertainty is exacerbated by the difficulty of directly measuring net infiltration in this and similar environments. Instead, model uncertainty is usually inferred by comparing the results of the various submodels (e.g., ET, runoff, etc.) to available field data as described above. However, such comparisons do not directly evaluate the model uncertainty in net infiltration estimates. Another approach is to assume that the regional estimates of net infiltration presented in Section 7.2 are representative of net infiltration conditions expected for the UZ model domain at Yucca Mountain. If this assumption is valid, then model uncertainty could be estimated by comparing MASSIF model predictions with estimates of net infiltration and recharge from these other sites. The comparison presented in Figure 7.2.1.2-2 suggests that model uncertainty is comparable in magnitude to parameter uncertainty. However, it is not clear that the assumption that regional sites are comparable with the UZ model domain is entirely valid. The UZ model domain is characterized by uplands with very shallow soils and may host a different net infiltration regime than is more typical of the other hydrographic basins represented in Section 7.2. One indication that this assumption may not be valid is in the comparison of the net infiltration predictions with net infiltration inferred from an analysis of the 99 neutron boreholes at the Yucca Mountain site (Figure 7.2.1.1-2). This figure clearly shows that nearly all of the net infiltration estimates derived from the neutron logging analyses are higher than the values predicted by the MASSIF model. If the spatial distribution of neutron borehole locations is representative of the UZ modeling domain and the net infiltration estimates from the analysis of the neutron logs is representative of conditions away from the boreholes, this would suggest that the MASSIF model may underestimate actual net infiltration for this area by at least a factor of 2 (visually estimated from Figure 7.2.1.1-2). It is not clear, however, that either of these criteria is met, and therefore it is not clear how these data can help to estimate model uncertainty. Given these challenges, and the comparisons that have been made, it is difficult to quantify model uncertainty. Available comparisons suggest that model uncertainty may be of a comparable magnitude to parameter uncertainty. Given the complexity of modeling net infiltration over such a large and heterogeneous domain, such uncertainty is not unprecedented.

6.7 SENSITIVITY ANALYSIS

6.7.1 Introduction

A sensitivity analysis examines how uncertainty in input parameters affects the uncertainty in model results. In addition, a sensitivity analysis can identify which input parameters have the greatest influence on model predictions, so that characterization efforts and studies can be focused to reduce the uncertainty in those parameters, and thus most efficiently reduce uncertainty in the model outputs. A more detailed discussion of sensitivity analysis methods is included in Appendix H along with a detailed discussion of the results of this study for each climate.

In risk analysis, uncertainty is generally separated into two categories depending upon the source of the uncertainty. Epistemic uncertainty stems from a lack of knowledge about the system being considered. This type of uncertainty is characterized by assigning probability distributions to parameters that describe the properties of the system. Epistemic uncertainty can usually be reduced with more studies, experiments, and observations of the system. This uncertainty is also sometimes referred to as reducible or state-of-knowledge uncertainty. A second type of uncertainty is aleatory uncertainty, which refers to inherent and irreducible randomness, such as the uncertainty in weather and how much it will rain in the future. The distinguishing characteristic of aleatory uncertainty is that it is a property of the system and cannot be reduced by further study.

In the current analysis, any uncertainty associated with parameters describing the physical properties of the system is considered to be epistemic uncertainty. Moreover, the parameters characterizing mean annual precipitation (MAP) are also associated with epistemic uncertainty (there is a unique value for the average annual precipitation and associated parameters assuming analogue stations adequately represent future climates). In the modeling, the precipitation amount for a given day and the pattern of precipitation days over the year are considered as aleatory uncertainty. In order to represent the aleatory uncertainty, a Markov Chain Monte Carlo method has been used to generate a set of 1,000 possible years of daily precipitation (see Appendix F). From these 1,000 years, 10 representative years have been chosen based on annual precipitation and weighted according to their probability of occurrence. Because the parameters defining precipitation are changing in each LHS sample, so are the ten representative years. The distribution of daily precipitation within the year influences the annual infiltration. However, this influence cannot be easily quantified because it is not associated with any of the input parameters, but rather is controlled by inherent aleatory uncertainty in the system.

The sensitivity analysis summarized here includes the results of two related analyses. The first considers the results of the uncertainty analysis (see Section 6.5.7). This analysis mixes both epistemic and aleatory uncertainty. It is important to represent the effect of aleatory uncertainty, as this uncertainty is indeed present. An extension of this analysis combines the sampled precipitation parameter for each climate by only examining the effect of MAP on net infiltration for each realization. Including aleatory uncertainty in the sensitivity reduces the ability to define the influence of the physical parameters whose uncertainty can be reduced. Therefore, a second analysis was performed ("Fixed Aleatory") in which the MASSIF net infiltration model was run with LHS realizations in which only epistemic uncertainty was varied. In these fixed aleatory

analyses, for each replicate, each of the LHS realizations used the same set of ten representative years. Precipitation parameters were only changed between each climate and each replicate. Of course, in these conditions the influence of precipitation cannot be seen because it has a constant value for all realizations.

6.7.2 Summary of Results

Detailed results of the two replicates for each of the three climates are presented in Appendix H. These results are summarized here.

For all climates, the sensitivity analyses show that there are two general features that control the uncertainty in the average annual net infiltration over the modeling domain. These features include the mean annual precipitation (MAP) and the soil depth assigned to Soil Depth Class 4. These two features explain about 70% of the variance in simulated infiltration when both epistemic and aleatory uncertainty is included. MAP is not sampled directly but is the result of a stochastic simulation of representative precipitation years that relies on a set of sampled stochastic parameters, which is different for each climate.

For the Present-Day climate, a_m (annual average of the mean of the probability distribution for the natural logarithm of the amount precipitation on days with precipitation) is the only precipitation parameter that is included in the LHS sampling. For the Monsoon climate, MAP is a function of a_m, a_{00} (annual mean value of probability of a dry day given the previous day was dry), and b_m (annual amplitude of mean of the probability distribution for the natural logarithm of the amount precipitation on days with precipitation). During the Glacial Transition climate, the parameters influencing the MAP are a_m, a_{00}, and θ_m (phase of the annual variation of mean of the probability distribution for the natural logarithm of the amount precipitation on days with precipitation).

However, it is important to note that, for physical reasons, some of the precipitation parameters have been defined as linear functions of other parameters. These linear relationships are described in Appendix F.

When aleatory uncertainty is fixed, the results of the sensitivity analysis only reflect the influence of physical parameters, given a fixed precipitation record. The results of these fixed aleatory analyses are consistent for the three climates and indicate that the most important physical parameters are Soil Depth Class 4 and HC_579 (water holding capacity for soil group 5/7/9). Together the uncertainty in these parameters account for about 90% of the variance in mean net infiltration for the Present-Day and Glacial Transition climates, and about 75% of the variance for Monsoon climate. Both have a negative influence, which means that high values of these parameters leads to a reduction in net infiltration.

The influence of the other physical parameters is not clearly indicated by the analyses. Because of the small sample size of each replicate considered (20), it is probably inappropriate to draw conclusions about the influence of other physical parameters.

6.7.3 Conclusions

Mean net infiltration is primarily controlled by the uncertainty in three epistemic quantities: mean annual precipitation, soil depth of Soil Depth Class 4, and the water holding capacity of soil group 5/7/9 (HC_579).

The agreement between the two replicates for each climate and also between climates gives confidence that these results are robust.

6.8 NOMENCLATURE USED IN SECTION 6 EQUATIONS

Symbol	Description	Units	Where Used*
I	Net infiltration	L/T	Eq. 6.2.1-1
P	Net precipitation	L/T	Eq. 6.2.1-1
RO	Surface water run-on/runoff	L/T	Eq. 6.2.1-1
ΔW	Change in water storage in the active zone	L^3L^{-3}	Eq. 6.2.1-1
E	Evaporation	L/T	Eq. 6.2.1-1 (6.4.4.3-1)
T	Transpiration	L/T	Eq. 6.2.1-1 (6.4.4.3-2; 6.4.4.3-3; 6.4.4.3-4; 6.4.4.3-5)
h	Water head	L	Eq. 6.2.4.1-1
θ	Volumetric water content	L^3L^{-3}	Eq. 6.2.4.1; Eq. 6.4.2-1
t	Time	T	Eq. 6.2.4.1
x	Spatial coordinate (positive upward)	L	Eq. 6.2.4.1
S	Sink term	$L^3L^{-3}T^{-1}$	Eq. 6.2.4.1
K	Unsaturated hydraulic conductivity function	LT^{-1}	Eq. 6.2.4.1
K_r	Relative hydraulic conductivity	—	Eq. 6.2.4.1-2 (6.4.4.1-2; 6.4.4.2-3)
K_s	Saturated hydraulic conductivity	LT^{-1}	Eq. 6.2.4.1-2 (6.4.4.3-2)
α(h)	Root-water uptake water stress response function		Eq. 6.2.4.1-3
S_p	Potential water uptake rate	T−1	Eq. 6.2.4.1-3; Eq. 6.2.4.1-4
$b(x)$	Normalized water uptake distribution	L^{-1}	Eq. 6.2.4.1-4
R_{off}	Runoff	L/T	Eq. 6.4-1
P	Precipitation	L/T	Eq. 6.4-1
R_{on}	Run-on	L/T	Eq. 6.4-1
SM	Snowmelt	L/T	Eq. 6.4-1 (6.4.1.4-1)
SF	Snowfall	L/T	Eq. 6.4-1; Eq. 6.4.1.4-2
SUB	Sublimation	L/T	Eq. 6.4-1; Eq. 6.4.1.4-2)
$\Delta\theta$	Change in water storage in the soil	L^3L^{-3}	Eq. 6.4-1
ET	Evapotranspiration	L/T	Eq. 6.4-1 (6.4.4-1)
NI	Net infiltration	L/T	Eq. 6.4-1
P	Precipitation adjusted to an elevation, *elev*	L/T	Eq. 6.4.1.1-1
P_{ref}	Precipitation at the reference elevation, $elev_{ref}$	L/T	Eq. 6.4.1.1-1
$C_{Precipcor}$	Precipitation lapse rate	%change/100m	Eq. 6.4.1.1-1

Symbol	Description	Units	Where Used*
T_{avg}	Average daily air temperature	°C	Eq. 6.4.1.4-1
$C_{snowmelt}$	Snowmelt coefficient	(dimensionless)	Eq. 6.4.1.4-1
$C_{sublime}$	Sublimation coefficient	(dimensionless)	Eq. 6.4.1.4-2
Water level	Volume of water in the layer per unit area	L	Eq. 6.4.2-1 (6.4.2-4; 6.4.2-6; 6.4.4.2-1)
FC	Field capacity	L^3L^{-3}	Eq. 6.4.2-2 (6.4.2-4; 6.4.2-6; 6.4.4.21; 6.4.4.2-2; 6.4.4.2-4)
$Limit_{soil}$	Soil conductivity infiltration limit	L/T	Eq. 6.4.2-3 (6.4.2-4)
duration	Amount of time during the day during which precipitation occurs	T	Eq. 6.4.2-3 (6.4.2-5)
K_{sat_soil}	Saturated conductivity of the soil	L/T	Eq. 6.4.2-3
Drain	Amount of water that moves downward	L/T	Eq. 6.4.2-4
$Limit_{rock}$	Maximum amount of water accepted by the rock	L/T	Eq. 6.4.2-5 (6.4.2-6)
K_{sat_rock}	Saturated hydraulic conductivity of the rock	L/T	Eq. 6.4.2-5
Net infiltration	Amount of water that moves into the underlying bedrock	L/T	Eq. 6.4.2-6
K_e	Soil evaporation coefficient	(dimensionless)	Eq. 6.4.4-1 (6.4.4.1-3; 6.4.4.3-1; 6.5.3.4.1-1)
K_{cb}	Basal transpiration coefficient	(dimensionless)	Eq. 6.4.4-1 (6.4.4.1-1; 6.4.4.1-2; 6.4.4.1-3; 6.4.4.3-2; 6.5.3.4.1-1)
K_s	Water stress coefficient	(dimensionless)	Eq. 6.4.4-1 (6.4.4.2-7; 6.5.3.4.1-1)
ET_0	Reference evapotranspiration	L/T	Eq. 6.4.4-1 (6.4.4.3-1; 6.4.4.3-2; 6.4.5-1; 6.5.3.4.1-1)
u_2	Average daily wind speed at 2 m above ground	m/s	Eq. 6.4.4.1-1 (6.4.4.1-2, Eq. 6.4.5-1)
RH_{min}	Minimum daily relative humidity	(dimensionless)	Eq. 6.4.4.1-1 (6.4.4.1-2)
h_{plant}	Plant height	m	Eq. 6.4.4.1-1 (6.4.4.1-2; 6.4.4.1-3)
$K_{c\ max}$	Maximum basal transpiration coefficient	(dimensionless)	Eq. 6.4.4.1-1 (6.4.4.1-2; 6.4.4.1-3)
f_{ew}	Fraction of soil exposed and wetted	(dimensionless)	Eq. 6.4.4.1-2 (6.4.4.3-5)
f_c	Fraction of surface covered by vegetation	(dimensionless)	Eq. 6.4.4.1-3 (6.4.4.3-5)
K_{c_min}	Minimum basal transpiration coefficient	(dimensionless)	Eq. 6.4.4.1-3
TEW	Total amount of water available for evaporation	mm	Eq. 6.4.4.2-2 (6.4.4.2-3; 6.4.4.2-6; 6.4.4.2-8; 6.4.4.2-9)
θ_{FC}	Field capacity	L^3L^{-3}	Eq. 6.4.4.2-2 (6.4.4.2-4)
θ_{WP}	Wilting point below which vegetation cannot extract moisture from the soil	L^3L^{-3}	Eq. 6.4.4.2-2 (6.4.4.2-4)
Z_e	Surface layer thickness	m	Eq. 6.4.4.2-2
D_e	Depletion of the evaporative node at the end of the previous day	mm	Eq. 6.4.4.2-3 (6.4.4.2-6; 6.4.4.2-8)

Symbol	Description	Units	Where Used*
REW	Readily evaporable water = the maximum depth of water that can be evaporated from the upper soil layer prior to the onset of hydraulic limitations that reduce the rate of water supply below that of energy demands	mm	Eq. 6.4.4.2-3
TAW	Total available water = amount of water available for ET in the root zone	mm	Eq. 6.4.4.2-4 (6.4.4.2-5; 6.4.4.2-7; 6.4.4.2-8; 6.4.4.2-9)
Z_r	Root zone thickness	mm	Eq. 6.4.4.2-4
RAW	Readily available water = the limit of the water in the root zone below which the transpiration rate is affected	mm	Eq. 6.4.4.2-5 (6.4.4.2-7)
p	Fraction of *TAW* that vegetation can remove without suffering stress	(dimensionless)	Eq. 6.4.4.2-5
p_{adj}	Adjusted value of *p*	(dimensionless)	Eq. 6.4.4.2-6
D_r	Root zone depletion	mm	Eq. 6.4.4.2-7 (6.4.4.2-6; 6.4.4.2-8; 6.4.4.2-9)
K_{tie}	Fractional partitioning coefficient	(dimensionless)	Eq. 6.4.4.2-8 (6.4.4.3-3)
D_c	Depletion of the canopy node	mm	Eq. 6.4.4.2-9
K_{tic}	Fractional partitioning coefficient for the canopy region	(dimensionless)	Eq. 6.4.4.2-8 (6.4.4.3-4)
T_e	Daily transpiration from the evaporative node	L	Eq. 6.4.4.3-3 (6.4.4.3-5)
T_c	Daily transpiration from the canopy node	L	Eq. 6.4.4.3-4 (6.4.4.3-5)
$T2$	Transpiration from Layer 2	L	Eq. 6.4.4.3-5
R_n	Net radiation at the crop surface	MJ m^{-2} d^{-1}	Eq. 6.4.5-1
G	Soil heat flux density	MJ m^{-2} d^{-1}	Eq. 6.4.5-1
T	Mean daily air temperature at 2 m height	°C	Eq. 6.4.5-1 (6.5.1.7-1)
u_2	Wind speed at 2 m height	m s^{-1}	Eq. 6.4.5-1
e_s	Saturation vapor pressure	kPa	Eq. 6.4.5-1
e_a	Actual vapor pressure	kPa	Eq. 6.4.5-1
e_s-e_a	Saturation vapor pressure deficit	kPa	Eq. 6.4.5-1
Δ	Slope of the vapor pressure curve	kPa $°C^{-1}$	Eq. 6.4.5-1 (6.5.3.7-8)
γ	Psychrometric constant	kPa $°C^{-1}$	Eq. 6.4.5-1
R_s	Solar radiation on land surface	MJ m^{-2} $d^{-}1$	Eq. 6.4.5.2-1
R_a	Exoatmospheric solar radiation	MJ m^{-2} $d^{-}1$	Eq. 6.4.5.2-1
K_{Rs}	Hargreaves' adjustment coefficient	—	Eq. 6.4.5.2-1
T_{max}	Maximum air temperature	°C	Eq. 6.4.5.2-1
T_{min}	Minimum air temperature	°C	Eq. 6.4.5.2-1
T_{dew}	Dewpoint temperature	°C	Eq. 6.4.5.2-2
K_o	Average offset between T_{dew} and T_{min}	°C	Eq. 6.4.5.2-2
T_{lapse}	Elevation-adjusted daily air temperature for a given grid cell with elevation z_{cell}	°C	Eq. 6.4.5.3-1
z_{cell}	Elevation of the grid cell	m	Eq. 6.4.5.3-1
T_{ref}	Daily air temperature at the reference weather station	°C	Eq. 6.4.5.3-1
z_{ref}	Elevation of the reference weather station	m	Eq. 6.4.5.3-1
LR	Lapse rate	°C per 1,000 m	Eq. 6.4.5.3-1

Symbol	Description	Units	Where Used*
$p_{00}(d)$	Probability that day d is dry, given that day $d-1$ is dry	—	Eq. 6.5.1.2-1
a_{00}	Average annual value of $p_{00}(d)$	(dimensionless)	Eq. 6.5.1.2-1
b_{00}	Annual variability of $p_{00}(d)$	(dimensionless)	Eq. 6.5.1.2-1
θ_{00}	Phase of $p_{00}(d)$	(dimensionless)	Eq. 6.5.1.2-1
$p_{10}(d)$	Probability that day d is dry, given that day d-1 is wet	(dimensionless)	Section 6.5.1.2
$\lambda(d)$	Mean of the lognormal precipitation distribution, given that day d is wet	Ln(mm)	Section 6.5.1.2
$m(d)$	Median of the lognormal precipitation distribution, given that day d is wet	Ln(mm)	Section 6.5.1.2
$T_{md}(d)$	Temperature as a function of day of year	°C	Eq. 6.5.1.2-3
SM	Snowmelt coefficient	mm/day/°C	Eq. 6.5.1.7-1
M	Snowmelt	mm/day	Eq. 6.5.1.7-1
Int	Number of hourly intervals	(dimensionless)	Eq. 6.5.1.7-2 (6.5.1.7-3)
Amt	Amount	mm	Eq. 6.5.1.7-2 (6.5.1.7-3)
K_{bulk}	K_{sat} of the composite bedrock	m/s	Eq. 6.5.2.6-1
f_{vf}	Fracture volume fraction	(dimensionless)	Eq. 6.5.2.6-1
K_{ff}	K_{sat} of the fracture-filling material	m/s	Eq. 6.5.2.6-1
K_m	K_{sat} of the matrix material	m/s	Eq. 6.5.2.6-1
k	Permeability	m^2	Eq. 6.5.2.6-2; (6.5.2.6-3)
b	Hydraulic aperture	L	Eq. 6.5.2.6-2
K_{sat}	Saturated hydraulic conductivity	m/s	Eq. 6.5.2.6-3
ET_{cell}	Actual ET for a model grid cell on a given day	mm	Eq. 6.5.3.4.1-1
PVR	Potential vegetation response developed for each grid cell	(dimensionless)	Eq. 6.5.3.4.1-2
PPT_{YR}	Annual precipitation for the water year of interest	mm	Eq. 6.5.3.4.1-3
C_{Kcb1}	Intercept of the linear function relating NDVI' and K_{cb}	(dimensionless)	Eq. 6.5.3.4.1-4
C_{Kcb2}	Slope of the linear function relating NDVI' and K_{cb}	(dimensionless)	Eq. 6.5.3.4.1-4
T_k	Recurrence interval in years for the k^{th} representative year	yrs	Eq. 6.5.7.5-1
p_k	Probability of occurrence (weight) for year n	(dimensionless)	Eq. 6.5.7.5-1

* Defined in these equations. Equation numbers in parentheses show other equations where these terms are used but not redefined.

INTENTIONALLY LEFT BLANK

7. VALIDATION

Validation requirements for the infiltration model are specified in *Technical Work Plan for: Infiltration Model Assessment, Revision, and Analyses of Downstream Impacts* (BSC 2006 [DIRS 177492]) and SCI-PRO-006, *Models*. Planning and preparation of this report was initiated under the BSC QA Program. Therefore, forms and associated documentation prepared prior to October 2, 2006, the date this work transitioned to the Lead Laboratory, were completed in accordance with BSC procedures. Forms and associated documentation executed after October 2, 2006 were prepared in accordance with Lead Laboratory procedures.

A "Level I" validation is required for the infiltration model because the radiological dose calculated in a previous Total System Performance Assessment (TSPA) was only slightly sensitive to the net infiltration rate (BSC 2003 [DIRS 168796], Section 3.3.1). When net infiltration was increased to be more than an order of magnitude larger than in the net infiltration base case, there was little change to the mean annual dose in the nominal case, and less than a 0.01 mrem increase in the igneous-intrusion case. However, infiltration flux is important to the flow of water in the UZ above and below the repository, to seepage into the repository, and to radionuclide transport in the UZ below the repository. In recognition of this importance, a Level II validation was selected. Level II validation requires that Level I validation items 1 through 6 are satisfied, and requires documentation that demonstrates model predictions are reasonably corroborated by at least two postdevelopment model validation methods described in SCI-PRO-006, Step 6.3.2.

In accordance with the technical work plan (TWP) (BSC 2006 [DIRS 177492]), Section 7 is organized into two main sections: Section 7.1 describes validation activities associated with confidence building during model development; and Section 7.2 presents studies that address postdevelopment model validation. The model validation activities that are included in Section 7 include bullets 1, 2, and 3 from Step 6.3.2 of SCI-PRO-006. Bullet 2 is included to provide additional model corroboration and only indirectly supports model validation because the HYDRUS-1D software is unqualified and therefore cannot directly support model validation (Step 6.2.1 N of SCI-PRO-006). These validation activities are consistent with the TWP with exceptions that are documented in Section 1.4. These validation activities include:

1) *Corroboration of model results with data acquired from the laboratory, field experiments, analog studies, or other relevant observations, not previously used to develop or calibrate the model*. This activity is accomplished by comparing MASSIF results to lysimeter data from NTS and Reynolds Creek, ID; and to streamflow data and to some direct and indirect infiltration estimates from Yucca Mountain. This activity also includes the comparison of modeled precipitation to measured precipitation at Yucca Mountain and analog sites.

2) *Corroboration of model results with other model results obtained from the implementation of other independent mathematical models developed for similar or comparable intended use/purpose*. This activity is accomplished by comparing MASSIF results to HYDRUS-1D results using the same inputs and properties. This is also done in conjunction with the lysimeter data mentioned under validation activity 1.

Since HYDRUS-1D is unqualified software, this model corroboration activity only provides indirect input to model validation.

3) *Corroboration of model results with relevant information published in refereed journals or literature provided that data used to develop and calibrate a model shall not be used to validate a model*. This activity is accomplished by comparing MASSIF results to published results using other models for Nevada and other western states. Additional model corrboration activities were conducted that include an extended parameter sensitivity study, and comparison of MASSIF results to percolation flux predictions made by an expert elicitation panel on UZ flow (CRWMS M&O 1997 [DIRS 100335]).

Inputs to the model validation calculations described in this section are listed in Table 7-1. Inputs to model validation are not required to be qualified and are considered indirect inputs to this model report.

Table 7-1. Indirect Inputs to Model Validation Calculations

Input Data Description	Location in This Model Report	Source
Air temperature data from MEDA 5 for 1994-2004	Section 7.1.2.1	MO0607SEPMED94.000 [DIRS 178079]
Climate Data, Geospatial Information, and Soil Moisture and Property Data for Reynolds Creek Experimental Watershed (RCEW), Idaho	Section 7.1.2.2	SN0608T0502206.020 [DIRS 179875]
NTS lysimeter data	Section 7.1.2	Di Sanza 2006 [DIRS 178797]
RCEW lysimeter data	Section 7.1.2	Marks 2001 [DIRS 177512]
NTS lysimeter elevation, dimensions, soil properties	Section 7.1.2.1	Scanlon et al. 2005 [DIRS 175977]
Locations of the stream gauges near Yucca Mountain	Appendix B, Section 7.1.3	MO0601GSCSPINF.000 [DIRS 177236]
Surface water discharge data collected during water year 1998 from three sites near Yucca Mountain on the NTS	Section 7.1.3	MO0603SEPSTREA.000 [DIRS 179889]
Surface water discharge data collected during water year 1993 from two sites near Yucca Mountain on the NTS	Section 7.1.3	MO0605SEPSURFC.000 [DIRS 179890]
Surface water discharge data for the Yucca Mountain area, Southern Nevada, and Southern California for water year 1995	Section 7.1.3	GS960908312121.001 [DIRS 107375]
Surface water discharge data for the Yucca Mountain area, Southern Nevada, and Southern California for water year 1994	Section 7.1.3	GS941208312121.001 [DIRS 107374]
Locations of Neutron Logging Boreholes	Section 7.2.1.1.3	MO9906GPS98410.000 [DIRS109059]
Infiltration estimates made in Borehole UZ #4	Section 7.2.1.1.2	LeCain et al. 2002 [DIRS 158511]
Location of South Portal	Section 7.2.1.1.1	BSC 2003 [DIRS 165572], p. 15
Location of seepage in south ramp	Section 7.2.1.1.1	Finsterle and Seol 2006 [DIRS 177754], p. 1
Temperature data for 2003	Section 7.2.1.1.1	MO0503SEPMMD03.001 [DIRS 176097]

Table 7-1. Indirect Inputs to Model Validation Calculations (Continued)

Input Data Description	Location in This Model Report	Source
Wind speed data for 2003-2004, temperature data for 2004	Section 7.2.1.1.1	SN0607WEATHER1.005 [DIRS 177912]
Meteorological monitoring data for 2005	Section 7.2.1.1.1	MO0610METMND05.000 [DIRS 178328]
Meteorological Monitoring Data for 2004	Section 7.2.1.1.1	MO0607SEPMMD04.001 [DIRS 178311]
Storage Gauge Precipitation 2005	Section 7.2.1.1.1	MO0605SEPSGP05.000 [DIRS 178663]
Measured Soil Depth	Section 7.2.1.1	MO0004QGFMPICK.000 [DIRS 152554]
Measured Soil Depth	Section 7.2.1.1	MO0012MWDGFM02.002 [DIRS 153777]
Measured Soil Depth	Section 7.2.1.1	GS910808312212.001 [DIRS 175972]
Expert elicitation results	Section 7.2.3	CRWMS M&O 1997 [DIRS 100335], Table 3-2

The results or outputs of the model validation calculations are documented in a variety of ways. Model validation calculations using the MASSIF model are included in the folder: \Welcome to Massif\Massif\Validation Analyses, which is part of Output DTN: SN0701T0502206.037. Validation analyses related to the extended parameter sensitivity study (Section 7.1.4) is documented as part of Output DTN: SN0701T0502206.044. Other validation related analyses (e.g., analyses using HYDRUS-1D software, and comparison of precipitation records) are documented in unqualified data DTNs that are referred to as Validation Output DTNs. These DTNs are not considered to be Qualified upon completion of the AMR. In all cases, validation output DTNs are referenced in the text and figures that explain the validation calculations.

7.1 CONFIDENCE BUILDING DURING MODEL DEVELOPMENT

Confidence building during model development is described in this section for each of the primary components in the infiltration model. The primary components that contribute to the mass-balance calculation for infiltration in each cell of the model are depicted in Figure 7.1-1 and include precipitation, evapotranspiration (ET), storage, run-on, and runoff. The following sections detail the technical approach and basis for each of these components.

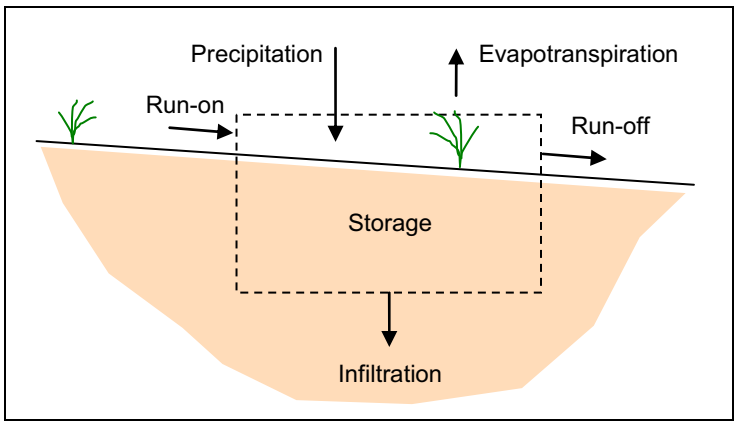

Figure 7.1-1. Control Volume for Mass-Balance Calculation of Infiltration

7.1.1 Precipitation

Existing weather records cover less than 100 years. There is no a priori assurance that a sample of so few years for a given climate will adequately represent average infiltration over hundreds or thousands of years. In order to capture the full range of uncertainty, the performance assessment must assure that rare events have been considered. Therefore, rather than use the meteorological records directly as input, this analysis used the records to characterize each record in terms of periodic functions and additional parameters. Periodic functions summarize the records of precipitation, temperature, and wind speed at a meteorological station.

Sections 7.1.1.1 and 7.1.1.2 describe the development of Fourier series parameters to simulate long-term precipitation. Sections 7.2.1.1.3, 7.2.1.1.4, and 7.2.1.1.5 compare actual precipitation data to the abstraction of precipitation data using Fourier series parameters for Present-Day, Monsoon, and Glacial Transition climates, respectively.

7.1.1.1 Comparison of Seasonal Precipitation Patterns

This section presents a comparison of monthly average precipitation measured at selected weather stations with monthly average precipitation from the 1,000-year stochastically-generated precipitation records for selected weather sites using the truncated Fourier series (one-harmonic). In addition, to provide a basis for comparison, the 1,000-year generated precipitation record for a two-harmonic truncated Fourier series is also presented. Adding another harmonic will always improve the fitting, however it also results in more parameters that need to be estimated. In addition, since each climate representation is based on weather records from several stations (rather than one) and these stations differ considerably in their precipitation seasonality, there is no meaningful way to combine parameters for the two-harmonic Fourier series such that they represent the suite of precipitation records from all stations. For this reason a single harmonic representation was used for representing precipitation patterns for each climate. Two sites for each of the three climate states predicted to occur at Yucca Mountain (Present-Day, Monsoon, and Glacial Transition climates) during the next 10,000 years are shown. The sites for the Present-Day climate are Yucca Mountain weather station Site 2 and NTS Station A12; for the Monsoon climate, Hobbs, NM and Nogales, AZ; and for the Glacial Transition climate, Spokane, WA and Delta, UT.

Figure 7.1.1.1-1(a) shows a comparison of recorded average monthly precipitation from the Yucca Mountain Site 2 weather station versus average monthly precipitation of 1,000-year generation using a one-harmonic truncated Fourier series. Figure 7.1.1.1-1(b) shows the same comparison using a two-harmonic truncated Fourier series. In this example, the two-harmonic estimate does little to improve the fit. This is because the annual precipitation pattern is characterized by a single wet and dry period rather than a two wet and dry periods during the year.

The comparison of NTS Station A12 average monthly precipitation record versus the 1,000-year generated precipitation using a one-harmonic truncated Fourier series is shown in Figure 7.1.1.1-2(a). The one-harmonic here captures the general trend of the precipitation but not as well as in the Site 2 case. The reason is that NTS Station A12 experiences a four-season trend variation that cannot be captured with only one harmonic. The two harmonic brings

significant improvement in allowing the capture of four seasons. As was the case for Site 2, the two-harmonic does a better job of more closely fitting the A12 data.

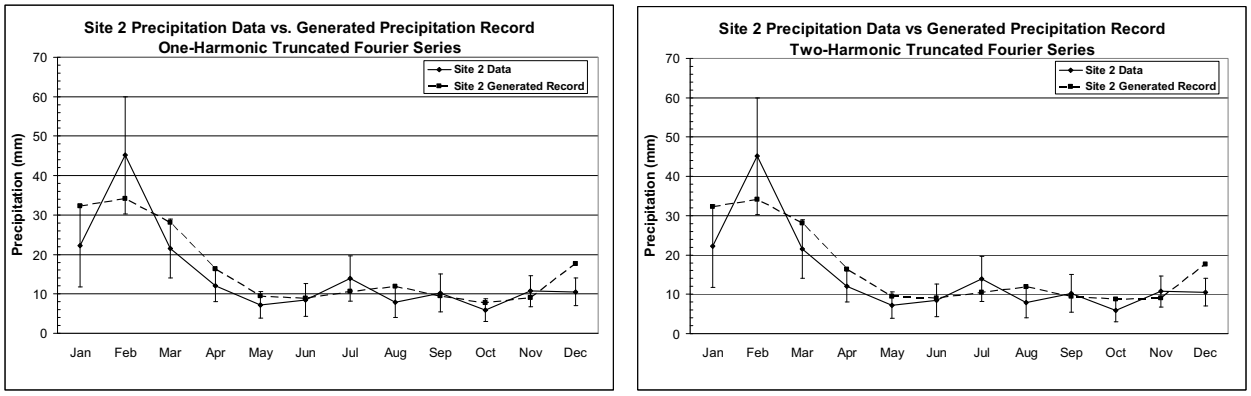

(a) (b)

Source: Validation Output DTN: SN0701T0502206.045.

Figure 7.1.1.1-1. Average Monthly Precipitation Comparison Between Observed Records and 1,000-Year Generation for Yucca Mountain Site 2: (a) Using Second Order (one-harmonic truncated) Fourier Series and (b) Using Third Order (one and two harmonics) Truncated Fourier Series

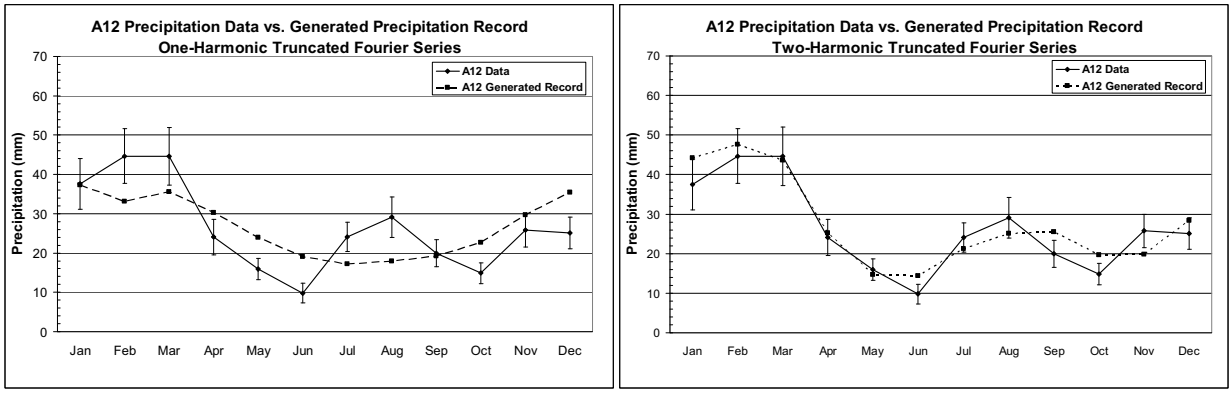

(a) (b)

Source: Validation Output DTN: SN0701T0502206.045.

Figure 7.1.1.1-2. Average Monthly Precipitation Comparison Between Observed Records and 1,000-Year Generation for Site A12: (a) Using Second Order (one-harmonic truncated) Fourier Series and (b) Using Third Order (one and two harmonics) Truncated Fourier Series

Monthly precipitation comparison for the upper-bound Monsoon analog site of Hobbs, NM is shown in Figure 7.1.1.1-3. In this case, recorded data shows a two-seasons behavior: a one-harmonic curve fits this behavior very well, as Figure 7.1.1.1-3(a) shows. Applying a two harmonic correction does not improve the fit significantly (Figure 7.1.1.1-3(b).

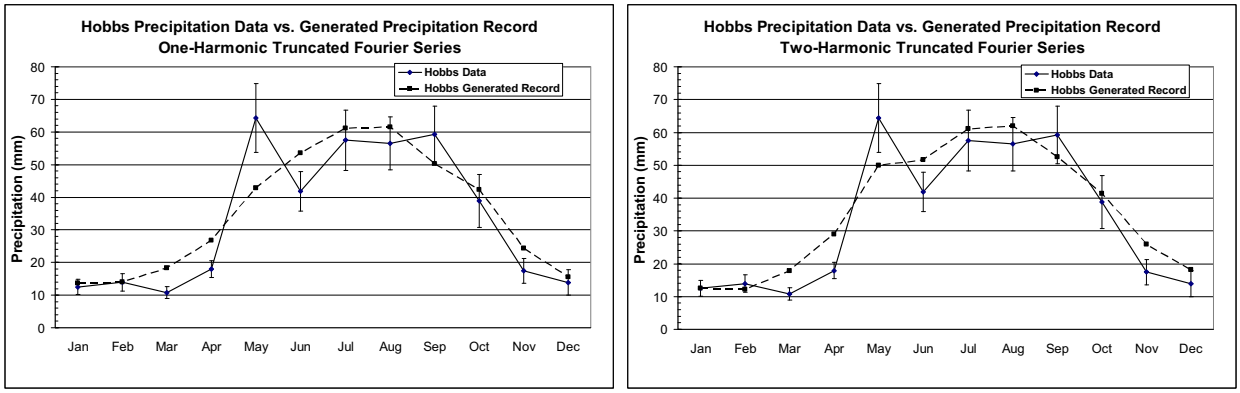

(a) (b)

Source: Validation Output DTN: SN0701T0502206.045.

Figure 7.1.1.1-3. Average Monthly Precipitation Comparison Between Observed Records and 1,000-Year Generation for Hobbs (NM): (a) Using Second Order (one-harmonic truncated) Fourier Series and (b) Using Third Order (one and two harmonics) Truncated Fourier Series

The data for the upper-bound Monsoon analog site of Nogales, AZ is shown in Figure 7.1.1.1-4. This Monsoon analog site has a more pronounced monsoon pattern that strongly spikes in July and August. The monthly average precipitation based on 1,000-year generated record using the one-harmonic truncated Fourier series does not provide a close match to the actual data. The limit is again due to the use of only one harmonic to represent a non-sinusoidal function. Adding a two-harmonic correction provides a significant improvement. It is important, however, to point out that Nogales site parameters are not directly used in our model but are first aggregated with the other representative site Hobbs, NM, which is matched quite well with a one-harmonic model.

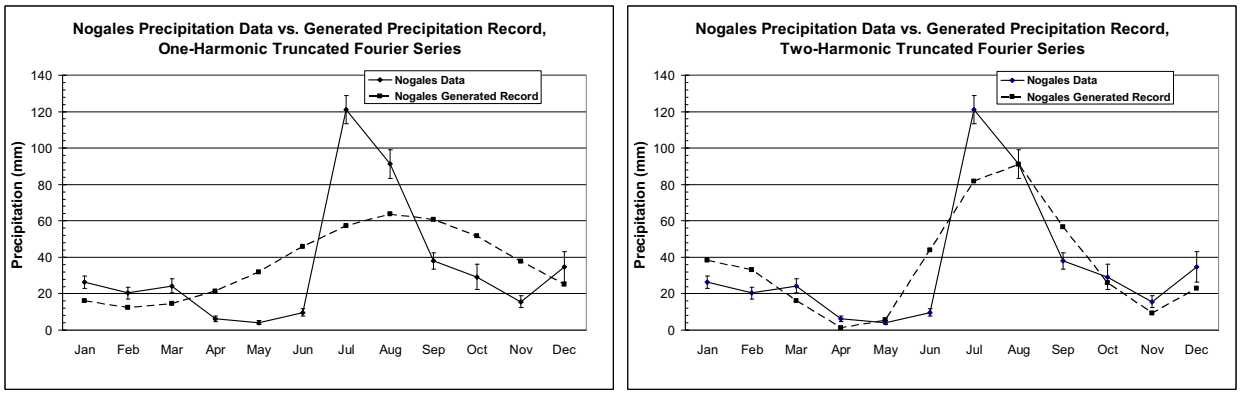

(a) (b)

Source: Validation Output DTN: SN0701T0502206.045.

Figure 7.1.1.1-4. Average Monthly Precipitation Comparison Between Observed Records and 1,000-Year Generation for Nogales (AZ): (a) Using Second Order (one-harmonic truncated) Fourier Series and (b) Using Third Order (one and two harmonics) Truncated Fourier Series

The comparison of site data for average monthly precipitation records at Spokane, WA (one of the upper-bound Glacial Transition analog site) versus the average monthly precipitation estimated from 1,000-year generated precipitation using one and two-harmonic truncated Fourier series is shown in Figure 7.1.1.1-5. The one-harmonic (a) fits the site data very well. The two-harmonic (b) correction provides a slightly improved fit.

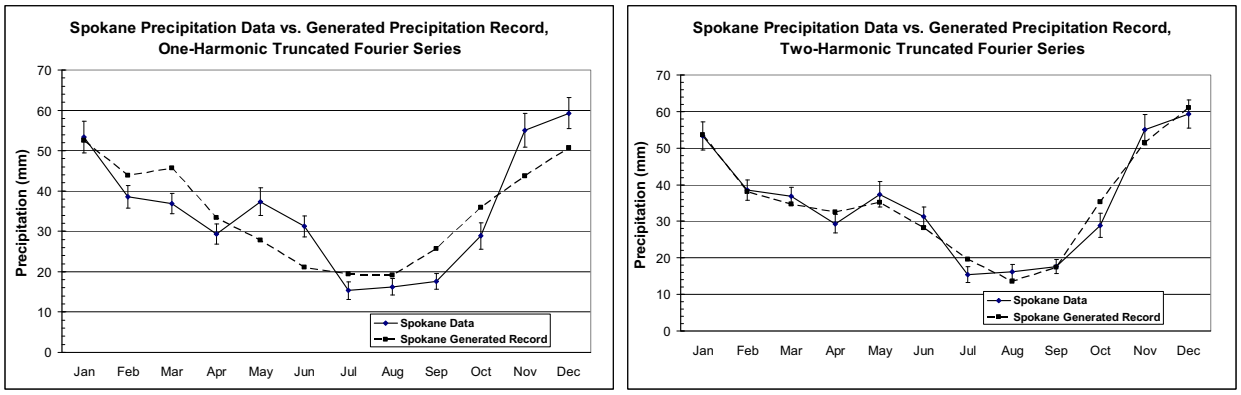

(a) (b)

Source: Validation Output DTN: SN0701T0502206.045.

Figure 7.1.1.1-5. Average Monthly Precipitation Comparison Between Observed Records and 1,000-Year Generation for Spokane (WA): (a) Using Second Order (one-harmonic truncated) Fourier Series and (b) Using Third Order (one and two harmonics) Truncated Fourier Series

The average monthly precipitation record at Delta, UT (lower-bound Glacial Transition analog site) is shown in Figure 7.1.1.1-6. Delta experiences a four-season variation with respect to precipitation, similar to the pattern at NTS Station A12 (see Figure 7.1.1.1-2). The monthly precipitation based on only one harmonic does not provide a good fit, and only a two-harmonic correction allows a good representation of monthly variation. As discussed for Nogales data, it is important to note that the parameters are aggregated with parameters fitted to other sites (e.g. Spokane), for which the one-harmonic fit is very good.

Adding another term to the Fourier series will always gives a better fit, as this additional term accounts for the residual between the Fourier series and the actual data. For half of the selected sites, precipitation records show a two-seasons variation over the year (on average), and a one-harmonic truncated Fourier series fits the data well. The second harmonic correction gives significant improvement when the selected site presents distinct four-season variations (see Figure 7.1.1.1-2 and Figure 7.1.1.1-6) or a strong gradient of differences for a period (see Figure 7.1.1.1-5).

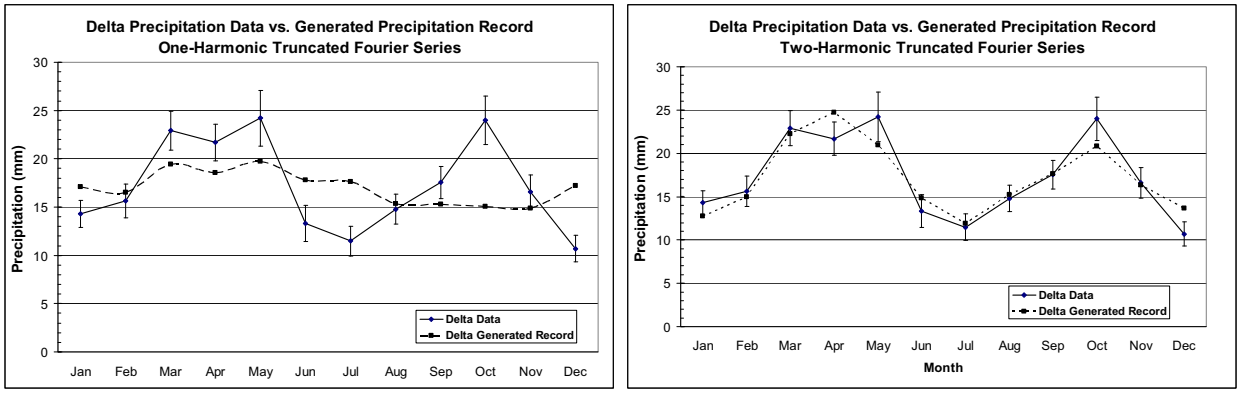

(a) (b)

Source: Validation Output DTN: SN0701T0502206.045.

Figure 7.1.1.1-6. Average Monthly Precipitation Comparison Between Observed Records and 1,000-Year Generation for Delta (UT): (a) Using Second Order (one-harmonic truncated) Fourier Series and (b) Using Third Order (one and two harmonics) Truncated Fourier Series

There is a cost of adding an additional harmonic in order to improve these fits. Four quantities are considered in our Markov Chain Monte Carlo (MCMC) model: p_{00} (probability that current day is dry knowing that previous day is dry), p_{10} (probability that current day is dry knowing that previous day is wet), λ (expected infiltration for a wet day) and m (median infiltration for a wet day). A new harmonic adds two parameters (an amplitude parameter b_i and a phase parameter θ_i) for each of the quantities, so eight new parameters are added. Several sites are used to represent the uncertainty on annual precipitation for each climate (10 for Present-Day climate, the same 10 plus 2 more for Monsoon climate, and 5 for Glacial Transition climate). The representation of uncertainty consists of aggregating each of these parameters. The value of attempting to aggregate the eight parameters representing the second harmonic is outweighed by the ambiguous and nonphysical meaning of the additional parameters. An attempt to add such complexity is considered to be unwarranted.

Moreover, each parameter has a physical meaning up to the first harmonic:

- a represents the average value of the quantity over the whole year (Appendix F, Section F1.1.2)
- b_1 represents the amplitude of (seasonal) variation of the quantity during the year
- θ_1 is the phase shift. In other words, it controls the date when the maximum value is obtained during the year.

The second harmonic parameters do not have a direct physical meaning because they represent a correction on the residual.

Therefore, it was decided to limit the representation of daily precipitation over the year with a 2nd order Fourier series (the average and one harmonic). The estimate reasonably represents the variation of daily precipitation over the year.

7.1.1.2 Comparison of Mean Annual Precipitation (MAP)

Section 7.1.1.3 to 7.1.1.5 present comparisons between the distribution of MAP measured at weather stations used to represent each climate state against distributions of MAP from the 1,000-year stochastic simulations for each climate.

Annual precipitation at Yucca Mountain for future climates is an uncertain quantity. In order to represent the possible future precipitation at the site, several representative sites have been selected for each climate. Each site has a different average annual precipitation record, representing the uncertainty.

In order to capture this uncertainty, each site has been first represented using 12 parameters. The variation of each parameter has been studied in order to determine whether this variation was significant (and should be taken into account) or not. Significant parameters were associated with a distribution and were sampled from this distribution using Latin Hypercube Sampling (a Monte Carlo technique).

Two (independent) samples of size 20 were created and used to estimate average annual precipitations. In order to verify that the distribution of average annual precipitation defined with the representative sites was captured correctly, they were compared with the distribution of average annual precipitation derived from these sites records.

Box-plots are a convenient way to represent distributions that allows easy comparison. They give a good summary of common statistics (mean, median, percentile) as well as distribution shape. The construction of a typical box-plot is shown in Figure 7.1.1.2-1.

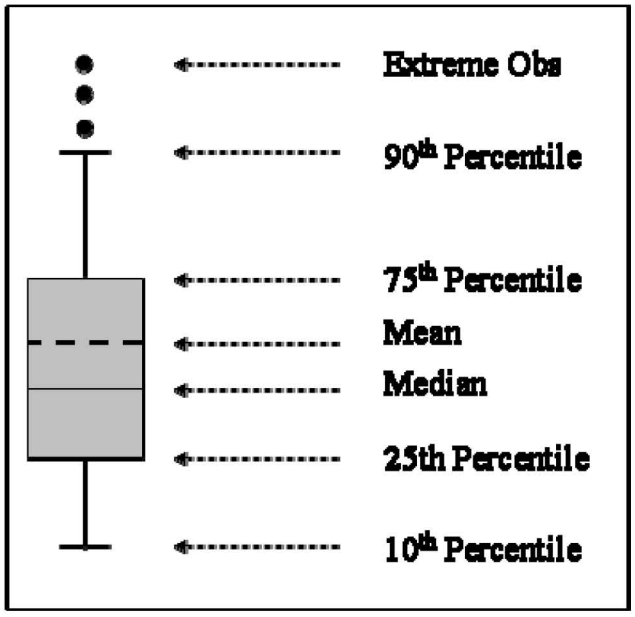

Figure 7.1.1.2-1. Theoretical Representation and Interpretation of a Box-Plot

7.1.1.3 Present-Day Precipitation Comparison

Sites used for representing Present-Day climate variations are located at different elevations. Elevation plays an important role in the amount of precipitation, and a direct comparison with raw data would not be appropriate (leftmost box-plot in Figure 7.1.1.3-1). The reference elevation applied to MASSIF is the top of Yucca Mountain (1,524 m). Parameters have first been adjusted to be more representative of average annual precipitation at the reference elevation (see second box-plot in Figure 7.1.1.3-1).

The third and fourth box-plots in Figure 7.1.1.3-1 provide a representation of annual precipitation distribution obtained with first and second set of replicate samples, respectively.

The last three box-plots of Figure 7.1.1.3-1 are similar enough to have good confidence that annual precipitation is correctly represented for Present-Day climate. Mean and median values are almost identical for all three boxes.

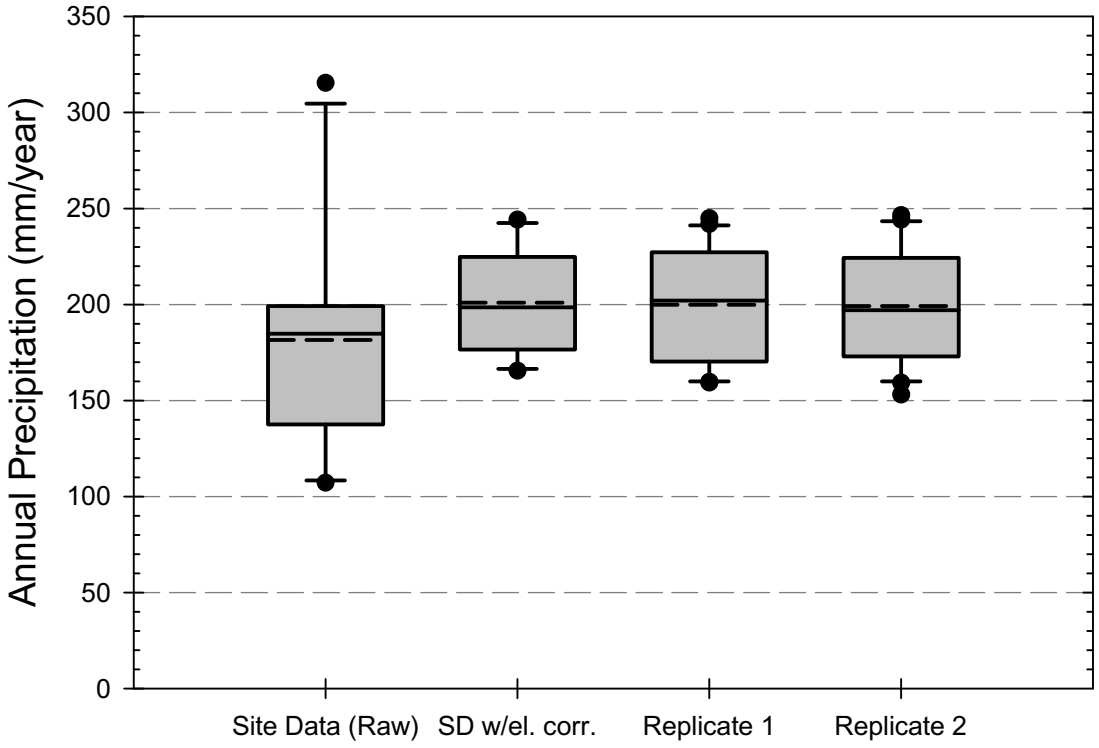

Source: Validation Output DTN: SN0701T0502206.045.

Figure 7.1.1.3-1. Box Plots Comparing Distribution of Observed Annual Precipitation from Representative Sites and Replicated Samples that Estimate Annual Precipitation for Present-Day Climate

7.1.1.4 Monsoon Precipitation Comparison

The Monsoon climate data includes the ten Present-Day climate sites as lower bounds and two sites (Hobbs, NM and Nogales, AZ) as upper bounds for annual precipitation representation. The two upper-bound sites are considered to be representative of the weather at the top of Yucca Mountain and therefore, do not need to be adjusted for elevation.

Even if their average annual precipitation is similar, the two upper-bound sites have different behavior over the year: Hobbs features a longer but less intense monsoonal period, while Nogales presents a shorter (2 months) but more intense monsoonal period (see Figures 7.1.1.1-3 and 7.1.1.1-4).

The aggregation of the two sites is thus a non-trivial issue. According to *Future Climate Analysis* (BSC 2004 [DIRS 170002]), the Hobbs and Nogales sites may underestimate annual precipitation for a monsoon climate identical to that of Owen's Lake (used as reference), so it was decided to consider the combination of parameters from Hobbs and Nogales giving the highest annual precipitation (a longer and more intense monsoonal period). This combination of parameters allows generating an average annual precipitation amount that is higher than either of the two upper bound sites.

Figure 7.1.1.4-1 presents the comparison of the range of uncertainty defined by Present-Day sites (first box) and upper-bound monsoon sites (Column 2) with the two samples of size 20 used to represent uncertainty in annual precipitation for the monsoon climate. About 75% of the data are within the range defined by the lower and upper bound of the monsoon climate representation shown in the last two boxes in Figure 7.1.1.4-1, with a mean and median around 300 mm/yr. Twenty-five percent of the data increases the range up to 580 mm/yr.

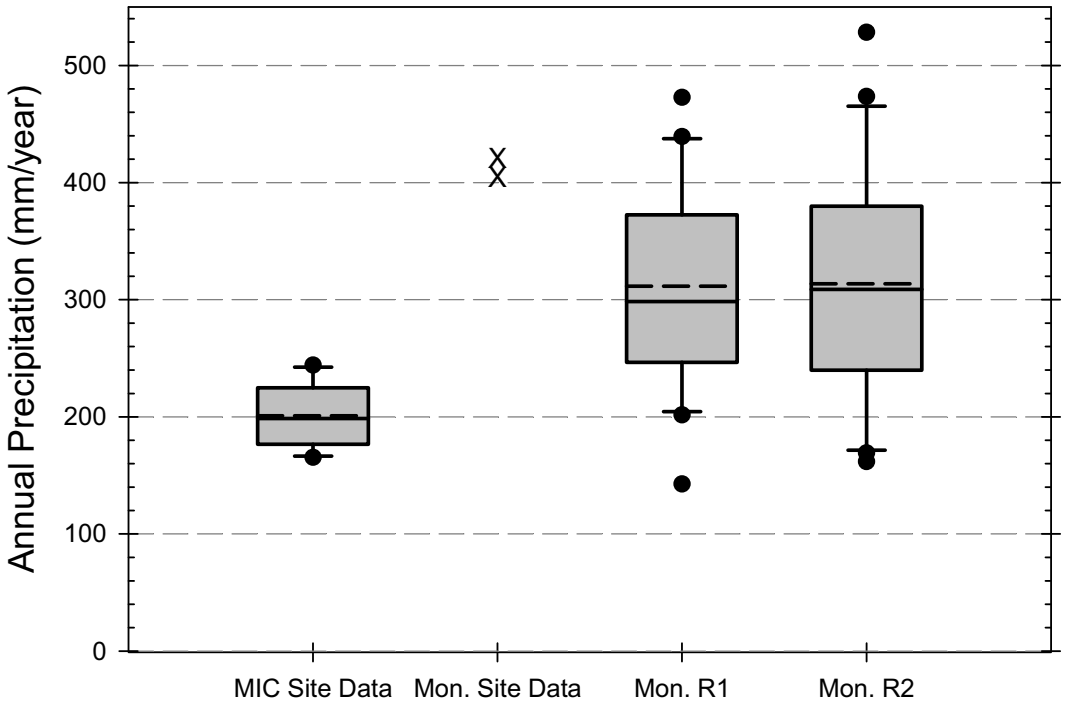

Source: Validation Output DTN: SN0701T0502206.045.

Figure 7.1.1.4-1. Box Plots Comparing Distribution of Observed Annual Precipitation from Representative Sites and Replicated Samples that Estimate Annual Precipitation for Monsoon Climate (MC). "MIC Site Data" Refers to Present-Day Climate Stations Adjusted for Elevation.

7.1.1.5 Glacial Transition Precipitation Comparison

The Glacial Transition climate data includes only two sites for lower-bound and three sites for upper-bound precipitation representations (see the five X's on the left part of Figure 7.1.1.5-1). Both sites are considered to be representative of future weather at the top of Yucca Mountain and therefore do not need to be adjusted for elevation. Distributions of mean annual precipitation based on the estimation of parameter uncertainty cover most of the range defined by the five bounding sites.

The average value for both replicates is almost identical and is close to the mid-point value of the average of the two low-bound sites annual precipitation and the three upper-bound sites annual precipitations. Therefore, this model gives a reasonable representation of uncertainty in annual precipitation for the Glacial Transition climate.

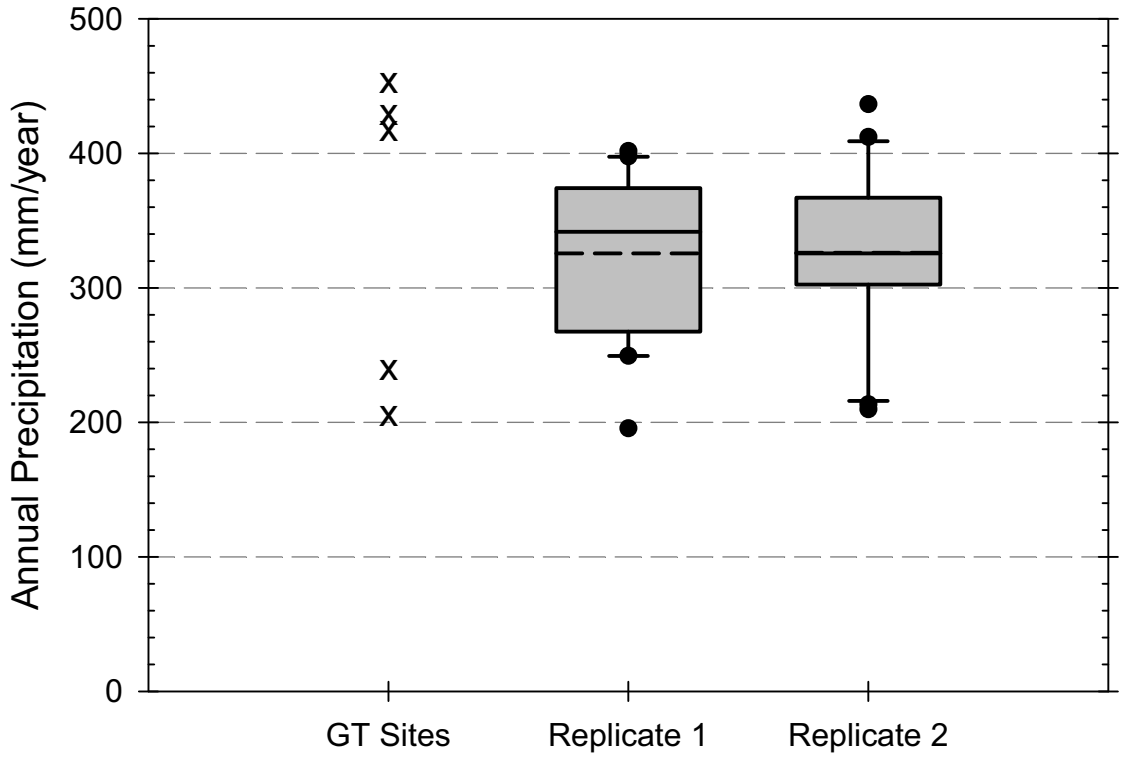

Source: Validation Output DTN: SN0701T0502206.045.

Figure 7.1.1.5-1. Plots Comparing Distribution of Observed Annual Precipitation from Representative Sites and Replicated Samples that Estimate Annual Precipitation for Glacial Transition Climate (GT).

7.1.2 Evapotranspiration and Storage

The ability of the MASSIF model to simulate daily actual ET and changes in daily soil water storage was evaluated by comparing MASSIF output to long-term observation data collected at lysimeter facilities at the NTS (Desotell et al. 2006 [DIRS 176858]), and at Reynolds Creek Experimental Watershed (RCEW) (Marks 2001 [DIRS 177512]). These lysimeter sites provide detailed water balance data that are especially valuable for evaluating model performance. The first lysimeter site is located near the Area 5 Radioactive Waste Management Site (RWMS) within the NTS and represents an analog to the present-day climate conditions at the Yucca Mountain. The second site is located within the RCEW in southwestern Idaho and represents a potential analog to the future glacial transition climate at Yucca Mountain. The climate at the RCEW is actually wetter and cooler than at Spokane, an analog site for the upper limit of the glacial transition conditions. RCEW was selected for this validation study because it represents significantly different conditions in terms of climate, soils, and vegetation from those at Yucca Mountain. Consequently, the model validation ranges can be extended as well.

The ability of MASSIF to simulate these data records provides additional model validation to establish confidence that the MASSIF mathematical model and its underlying conceptual model adequately represent with sufficient accuracy the phenomenon and processes in question as required by SCI-PRO-006. Validation includes corroboration of model results with data acquired from two analog sites, and corroboration of model results with other model results obtained from the implementation of mathematical models (the results from an alternative mathematical model incorporated using HYDRUS-1D code are discuss in Section 7.2.2). The summary of this validation activity is provided in this Section. Additional details are provided in Appendix J.

The primary purpose of weighing lysimeters is to estimate daily actual ET based on measured precipitation and observed changes in the lysimeter storage. The lysimeters are installed such that surface water run-on and runoff are removed from the water balance. Consequently, the daily water balance of such a lysimeter can be described using the following equation (Fetter 2001 [DIRS 156668], p. 31, Equation 2.1):

$$ET = P - \Delta S - D \qquad \text{(Eq. 7.1.2-1)}$$

where ET is daily actual ET, P is measured daily precipitation, ΔS is the observed daily change in the lysimeter storage (increase or decrease in storage with regard to the storage observed during the previous day), and D is the excess moisture drained from the soil. In cases when the lysimeter is sealed at the bottom, no drainage occurs, and D is equal to 0.

According to Equation 7.1.2-1, the ability to reproduce the observed changes in daily storage is equivalent to the ability to reproduce the actual daily ET in the absence of drainage. The longer the period of time over which the changes in storage are closely reproduced, the greater is the confidence in the ability of the model to adequately simulate the physical processes affecting actual ET.

The long-term observations required for good model evaluation and testing are available for both lysimeter sites. The description of the sites and the results of modeling are summarized below. The details of the modeling setup and simulations are presented in Appendix J. No drainage was observed from the NTS lysimeters. There was some small drainage from the RCEW lysimeters, but the timing and exact quantities of the drainage are not known. All files used for these simulations using MASSIF are located in \Welcome to Massif\Massif\Validation Analyses/Lysimeter within MASSIF (Output DTN: SN0701T0502206.037).

7.1.2.1 Lysimeter Simulations at the Nevada Test Site

Two weighing lysimeters were installed in Area 5 RWMS of the NTS in 1994 to conduct water balance studies. The lysimeters are located in northern Frenchman Flat (northern part of Mojave Desert). The lysimeter coordinates are: 36º 51' 9.13" (latitude) and 115º 56' 56.06" (longitude), and the lysimeter site elevation is 976 m (Scanlon et al. 2005 [DIRS 175977]).

There are a number of studies where the NTS lysimeter data were used for various water balance analyses, including calibration of flow models. The results of these studies are reported by Desotell et al. (2006 [DIRS 176858]), Scanlon et al. (2005 [DIRS 175977]), Levitt et al. (1999 [DIRS 177521]), and Levitt et al. (1996 [DIRS 163183]).

The long-term mean annual precipitation in this area reported by Desotell et al. (2006 [DIRS 176858]) is 125 mm. The mean annual precipitation calculated using the lysimeter data is 125.5 mm (Di Sanza 2006 [DIRS 178797], *NTSLysimeter.xls*), which is close to the long-term average. The mean annual temperature during the period of observation was 15.7ºC (DTN: MO0607SEPMED94.000 [DIRS 178079]). In only 1.3% of the observation time was the mean daily temperature below 0ºC. The average daily wind speed during the period of observation was 2.8 m/s (see Appendix J for details).

One lysimeter is vegetated with the creosote bush, four-wing salt bush, and annual grasses at the approximate density of the surrounding landscape (Desotell et al. 2006 [DIRS 176858]). Another lysimeter is maintained under the bare soil conditions. Each lysimeter is a 2-m by 4-m by 2-m deep steel tank filled with native alluvium at a bulk density of about 1.5 kg/m^3 (Scanlon et al. 2005 [DIRS 175977]). The alluvium was classified as a well- to poorly-graded sand with silt and gravel (Unified Soil Classification System) with approximately 70% sand, 20% gravel, and 10% fines. A schematic of one lysimeter is shown in Figure 7.1.2.1-1 (from Figure 7 in supporting information to Scanlon et al. 2005 [DIRS 175977]).

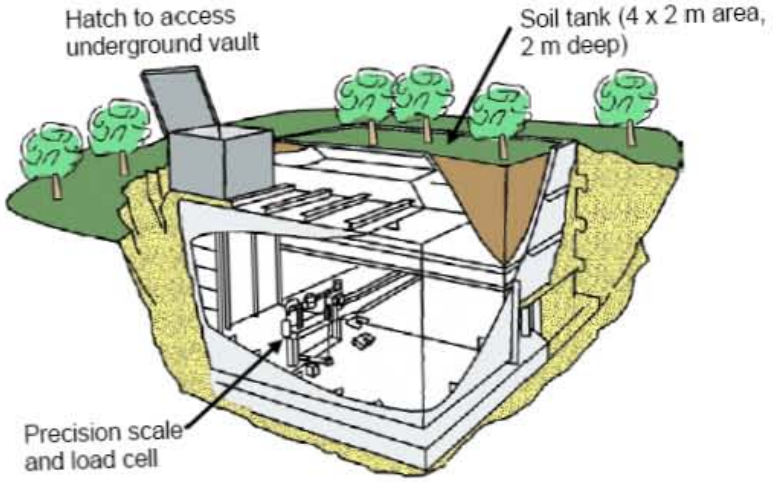

NOTE: Figure is reproduced from Figure 7 in supporting information to Scanlon et al. 2005 [DIRS 175977].

Figure 7.1.2.1-1. Schematic of one NTS Weighing Lysimeter

Eighteen core samples were collected throughout the lysimeter depth profile in 10-cm increments. The measured soil hydraulic properties are reported by Desotell et al. (2006 [DIRS 176858]) and include:

- Saturated hydraulic conductivity (geometric mean): 14 cm/hr
- Residual moisture content: 0.04 m^3/m^3
- Porosity: 0.357 m^3/m^3
- van Genuchten parameter alpha: 0.0328 cm^{-1}
- van Genuchten parameter n: 1.57.

Based on these parameters, the field capacity is 0.117 m^3/m^3 (calculated using pressure of -1/3 bar), and wilting point is 0.044 m^3/m^3 (calculated using pressure of -60 bars). Since a higher pressure may be more appropriate for the coarse grained textured soils (up to -1/10 bars) than the pressure of -1/3 bars (medium textured soils), the bare soil lysimeter storage data were analyzed during periods with heavy precipitation over a few or more consecutive days. The largest storage value was 277.3 mm. This corresponds to the moisture content of 0.139 m^3/m^3 and a pressure of -2/10 bars. This is consistent with the pressure range of -1/3 bars to -1/10 bars at which field capacity is calculated.

The lysimeter storage observations are available for the period of time from March 3, 1994 until December 31, 2004 from Di Sanza 2006 [DIRS 178797]. However, the vegetated lysimeter was irrigated for about 6 months to establish the vegetation cover and the irrigation rates are not available, and it took about 1.5 years for the transplanted vegetation to equilibrate with moisture conditions in the lysimeter box. Consequently, the period of observations for the vegetated lysimeter was considered from October 1, 1995 until December 31, 2004. The MASSIF model can be run only for a whole number of the water years. To satisfy this requirement, the bare soil lysimeter observations used began on October 1, 1994. Figure 7.1.2.1-2 shows the observation data and precipitation data for the NTS lysimeter site.

Analysis of precipitation data (see Appendix J for details) showed that 5% (bare soil lysimeter) to 10% (vegetated lysimeter) of observations have daily increases in storage that exceed daily precipitation. The maximum difference between the storage increase and precipitation was about 4 mm. Most of these observations are related to the high intensity precipitation events. Raingages are subject to under-measurement caused by (1) splash out of drops, (2) blow-by of drops due to venturi effects, and (3) evaporation of intercepted drops along the sides of the collector (Sevruk 1992 [DIRS 177480]). Consequently, some of the differences between precipitation data and lysimeter gains may have been caused by under-measurement by the precipitation gauge. The inaccuracy in precipitation measurements could be at least 4 mm. Since the ET is calculated as the difference between precipitation and storage, the 4-mm error in precipitation measurement will result in the corresponding error in the ET estimate.

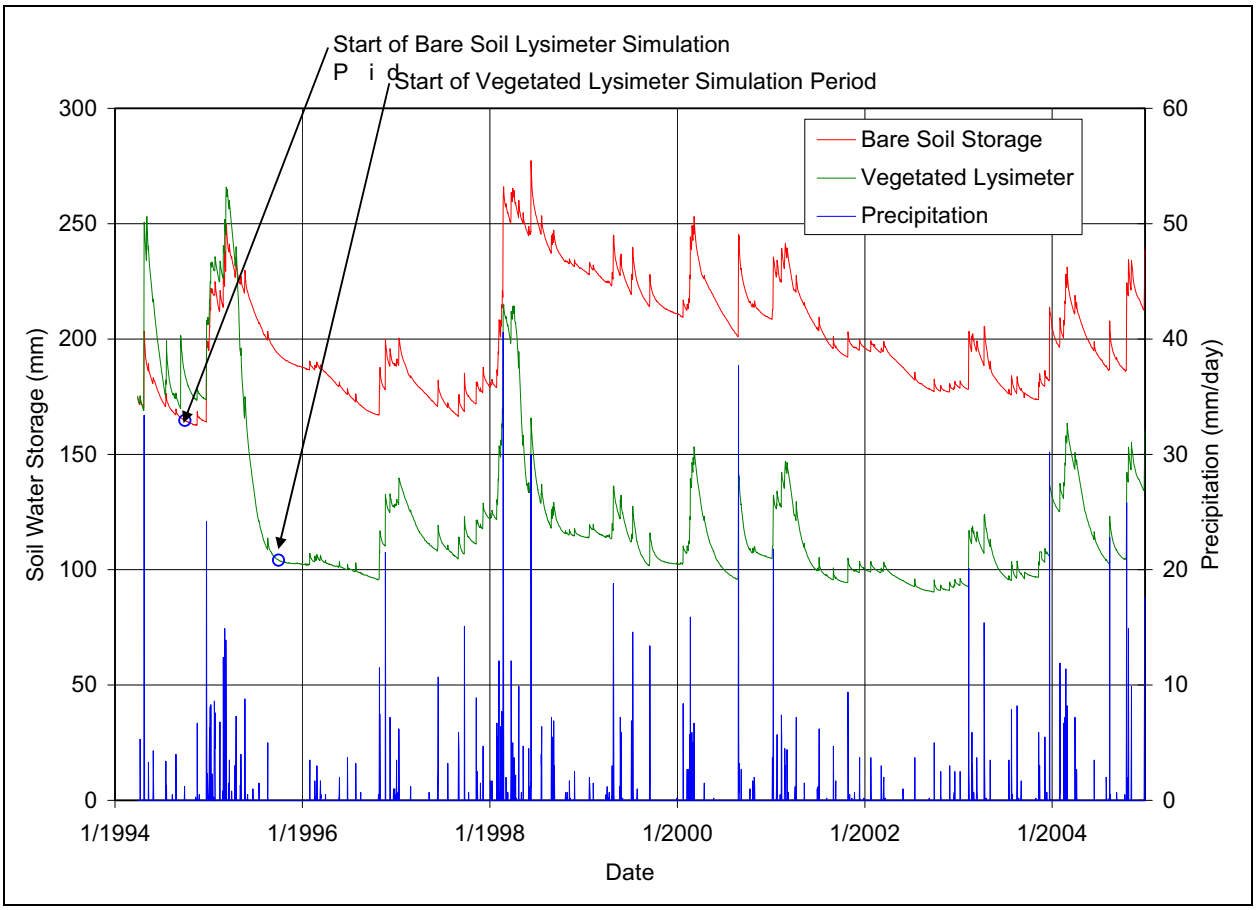

Source: Di Sanza 2006 [DIRS 178797]; compiled in Output DTN: SN0701T0502206.037, file: \Welcome to Massif\Massif\Validation Analyses\Lysimeter*NTSLysimeter.xls*.

Figure 7.1.2.1-2. Observed Daily Water Storage and Precipitation at the NTS Lysimeter Site

The MASSIF input parameters for the lysimeter simulations were defined in accordance with NTS site-specific information, when available. For certain parameters, NTS site-specific data were not available and parameter values were estimated using an inverse modeling approach described below and in Appendix J. The following MASSIF parameters cannot be specified based on the data available for the NTS lysimeter site:

- Diffusive evaporation parameter, K_{c_min}
- Canopy fraction, f_c
- C_{kcb} coefficient representing the slope of the NDVI-K_{cb} regression line (see Appendix E for details)

The values of these three parameters were estimated by minimizing the difference between the observed and calculated storages in both lysimeters. The following objective function $F1_{obj}$ was used in the conjugate gradient minimization procedure in MathCAD.

$$F1_{obj}(K_{c\_min}, f_c, C_{kcb}) = [\sum(BS^{obs}_i - BS^{cal}_i)^2 + \sum(V^{obs}_j - V^{cal}j)^2]/(N_{bs}+N_v) \quad \text{(Eq. 7.1.2.1-2)}$$

$$i=1, N_{bs} \text{ and } j=1, N_v$$

where BS^{obs}_i and BS^{cal}_i are observed and calculated bare soil lysimeter storage during the simulation day i; V^{obs}_j and $V^{cal}j$ are observed and calculated vegetated lysimeter storage during the simulation day j; N_{bs} is the number of days in the bare soil lysimeter data set; and N_v is the number of days in the vegetated lysimeter data set. As it was explained above, the bare soil lysimeter data set is from 10/01/1994 to 12/31/2004 (N_{bs}= 3745), and the vegetated lysimeter data set is from 10/01/1995 to 12/31/2004 (N_v= 3380).

In calculating bare soil lysimeter storage, the transpiration parameters p (depletion factor for computing readily available water), C_{kcb}, and f_c were set to zero to represent bare soil conditions. In calculating vegetated lysimeter storage, parameter p was set to 0.65 (see Section 6.3.3 and 6.3.4) and C_{kcb} and f_c were the objective function parameters as defined by Equation 7.1.2.1-2.

The results of the minimization are:

- $K_{c\_min} = 0.0135$
- $f_c = 0.26$
- $C_{kcb} = 2.4$
- $F1_{obj} = 137.92$ mm^2

Based on the obtained objective function value, the overall goodness of fit is 11.74 mm for both lysimeters. The estimated parameter values were used to calculate the root mean square errors for each lysimeter. The calculated mean root square errors are 11.63 mm and 11.87 mm (or about 9% of the mean annual precipitation) for the bare soil and vegetated lysimeters, respectively. Taking into account that the possible inaccuracy in storage measurements is at least 4 mm, the obtained goodness of fit is reasonable for both lysimeters. These root mean square errors are comparable to the ones reported by Desotell et al. (2006 [DIRS 176858]). The NTS lysimeters were modeled by Desotell et al. 2006 [DIRS 176858]) with UNSAT-H (Fayer 2000 [DIRS 177499]), which is a soil physics based code similar to HYDRUS-1D (see Sections 6.2.4.1, and 7.2.2) in its capability to model variably-saturated flow, except it allows for simulating vapor phase. Mean root square errors reported are 12 mm (bare soil) and 4 mm (vegetated). However, in order to obtain this fit, the potential evaporation was reduced by 50% during the winter time. No adjustment to reference ET was done in MASSIF calculations to improve the curve fitting.

The only interval with a noticeable difference between observed and calculated storages is during February through April of 1998. This corresponds to a series of large precipitation events that resulted in a significant increase in storage in both lysimeters (see Figure 7.1.2.1-2). The calculated increase in storages is about 40 mm smaller than was observed (Figure 7.1.2.1-3). The UNSAT-H curves (Desotell et al. 2006 DIRS 176858], Figures 3 and 4) also do not reproduce the observed increase.

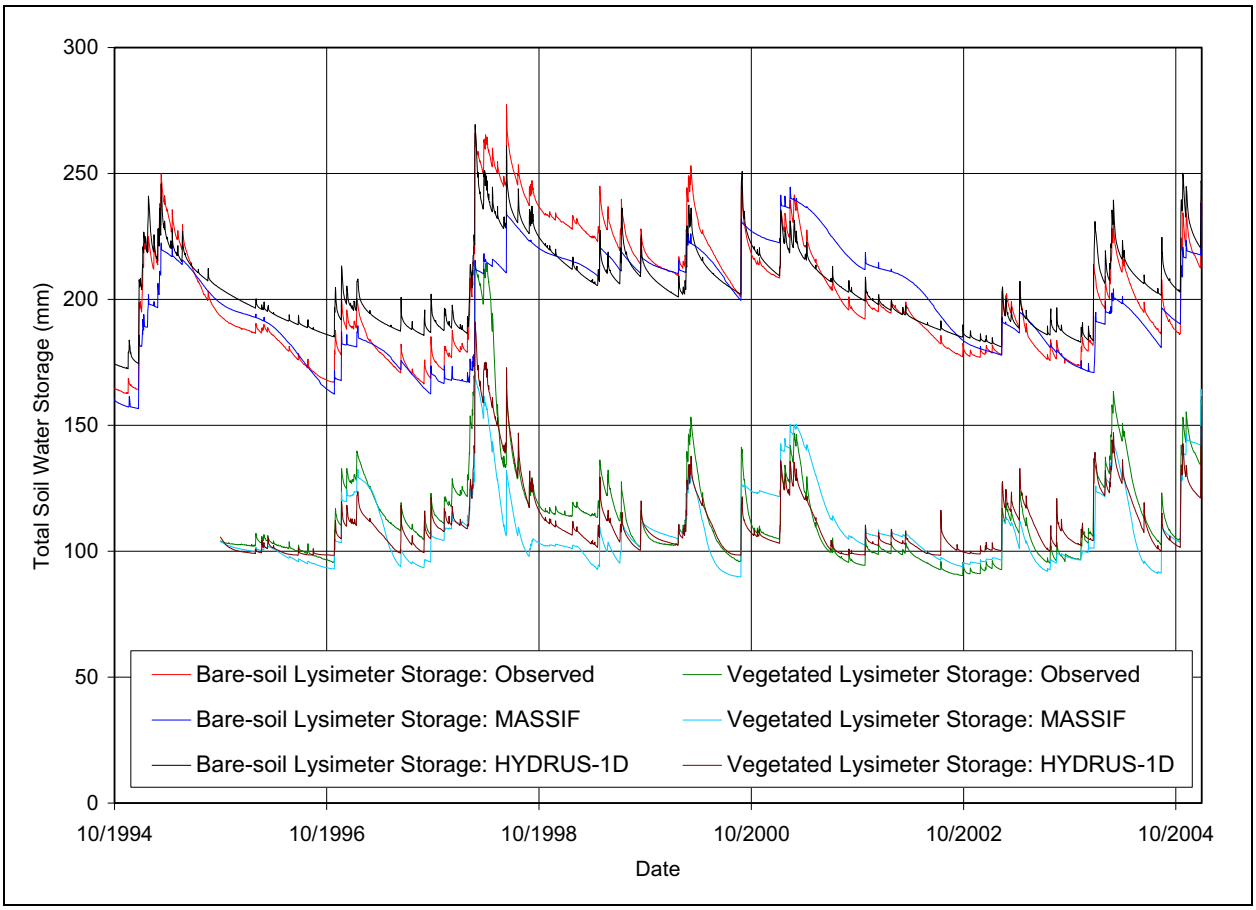

Source: Di Sanza 2006 [DIRS 178797] (lysimeter data); Validation Output DTN: SN0607T0502206.016 (Hydrus-1D data); Output DTN: SN0701T0502206.037, file: \Welcome to Massif\Massif\Validation Analyses\Lysimeter*NTSLysimeter.xls*.

Figure 7.1.2.1-3. Simulation of Soil Water Storage in the NTS Lysimeters

Some differences between the observed and calculated storages are also seen when soil water storage decreases during spring-fall periods of time. The observed storages tend to decrease more rapidly than the simulations. Desotell et al. (2006 DIRS 176858]), attributes this to the dynamic response of the plant growth that is not simulated by the model. However, the same tendency is observed in the bare soil lysimeter as well. Also, the difference between the decreasing portions of the storage curves are more pronounced in the case of the bare soil lysimeter. This may indicate evaporation at depth in the lysimeter that is a phenomenon of the lysimeter but not of the natural conditions. This can be caused by heat transfer along lysimeter walls from the surface and through lysimeter walls from the subterranean lysimeter chamber. This phenomenon is described by Howell et al. (1991 DIRS 177190]) in relation to the steel container weighing lysimeters. Other aspects of this phenomenon are given by Campbell et al. (1991 DIRS 177100]) and Kirkham et al. (1991 DIRS 177191]). However, the effects of this phenomenon cannot be bounded quantitatively in the absence of the soil profile temperature data. In contrast, it is possible that the lysimeter geometry is limiting rather than enhancing evaporation by preventing the slow upward evaporative flow of water from depths greater than the lysimeter depth.

The bare soil and vegetated lysimeter storages were also simulated with HYDRUS-1D. The same mean properties of the soil and climate data were used in the calculations (see Appendix J for details). The results of these simulations are shown in Figure 7.1.2.1-3. The mean root square errors obtained with HYDRUS-1D are 10.6 mm and 9.2 mm for bare soil and vegetated lysimeters, respectively. The same tendencies as described above in the differences between the calculated and observed storages can be noted. The mean root square errors between the storages calculated by HYDRUS-1D and MASSIF are 10.9 mm and 9.0 mm for the bare soil and vegetated lysimeters, respectively. This falls within the same range as the mean root square errors described above. The runoff and infiltration calculated by HYDRUS-1D were equal to zero (or negligibly small) during the entire period of observation in both lysimeters as well.

An important component of ET is transpiration. The transpiration in MASSIF is modeled using basal crop coefficient (K_{cb}) concept (Allen et al. 1998 [DIRS 157311]). As described in Sections 6.3.3 and 6.3.4 and Appendix E, the daily K_{cb} values are calculated from daily *NDVI'* values using the following formula (Equation 7.1.2.1-3):

$$K_{cb}=(C^{0}_{kcb}+C_{kcb} *NDVI')*P_i/P_{1998}*PVR \qquad \text{(Eq. 7.1.2.1-3)}$$

where C^{0}_{kcb} and C_{kcb} are intercept and slope of the regression line approximating the K_{cb} data plotted against the *NDVI'* data (see Appendix E); P_i is the total annual precipitation for the year in consideration; P_{1998} is the total annual precipitation in 1998 equal to 378 mm (representing the wet year); and *PVR* is the potential vegetation response. C^{0}_{kcb} and C_{kcb} were developed based on the K_{cb} and *NDVI'* values measured at the site. For the Present-Day climate nominal values for these parameters are -0.05 and 9.7, respectively (see Section 6.5.3.7). The daily *NDVI'* values used in MASSIF are tabulated for each day of the year and different combinations of the slopes and azimuths (see Appendix D for details). The base *NDVI'* values are used for the slopes less than 5º, and no azimuth correction is required for such slopes.

Regression coefficients C^{0}_{kcb} and C_{kcb} were set equal to 0 for the bare soil lysimeter. C_{kcb} was a parameter of the vegetated lysimeter in the optimization scheme described above. C^{0}_{kcb} is very small and was set to 0 for vegetated lysimeter as well. No information was available on the lysimeter site-specific *PVR* value, which is the MASSIF input parameter. The *PVR* was set equal to 1. Note that the optimization scheme estimates the value of the lumped transpiration parameter equal to C_{kcb} **PVR*. Thus, the actual values of *PVR* can be set to any arbitrary values without affecting the estimation of the lumped parameter. The estimation of this lumped parameter is achieved by adjusting $C_{kcb,}$ as a result of the manner in which the MASSIF calculation is implemented.

Shown in Figure 7.1.2.1-4 are daily K_{cb} and *NDVI'* values for the wet, average, and dry water years. These are the actual values measured at the Yucca Mountain site that include the water stress impacts caused by dry soil (see Appendix D for details on these data). The water stress impacts are maximal for the dry year and minimal for the wet year. The water years representing wet, average, and dry years are 1993, 1991, and 1990, respectively. The K_{cb} data used are for these 3 years. The *NDVI'* data (taken in 1998, 2001, and 2002) were corrected (see Appendix E) to represent the same years. The *NDVI'* data were scaled using a nominal regression slope of 9.7 (the details on how this slope was calculated are provided in Section 6.5.3.7), so they can be directly compared to the K_{cb} data.

The values based on the Yucca Mountain site-specific measurements are compared to the values calculated by MASSIF using Equation 7.1.2.1-3 above. The daily *NDVI'* values in this equation are base *NDVI'* values from the look-up table in MASSIF. P_{1998} is 378 mm. The precipitation (P_i) at the lysimeter site in 1998 (wet year), 2001 (average year), and 2002 (dry year) was 256 mm, 122 mm, and 31 mm, respectively. The *PVR* was set equal to 1, and C_{kcb} estimated from the optimization scheme is 2.4. The daily K_{cb} values calculated by MASSIF are shown in Figure 7.1.2.1-4 as "vegetated lysimeter K_{cb}" (the calculations are in the worksheet "NDVI" in *NTSLysimeter.xls* file located in folder \NTS in Validation Output DTN: SN0607T0502206.016. They are in good agreement with the *NDVI'* values measured for the LA plant association. This is the predominant association for the lower elevations and bajadas of the Yucca Mountain site (see Appendix D). LA association includes (see Appendix J) the following dominant species: *Ambrosia dumosa*, *Larrea tridentata* (creosotebush), *Menodora spinescens* (spiny menodora), and *Lycium pallidum*. The similar species are present at the vegetated lysimeter site (Scanlon et al. 2005 [DIRS 175977]).

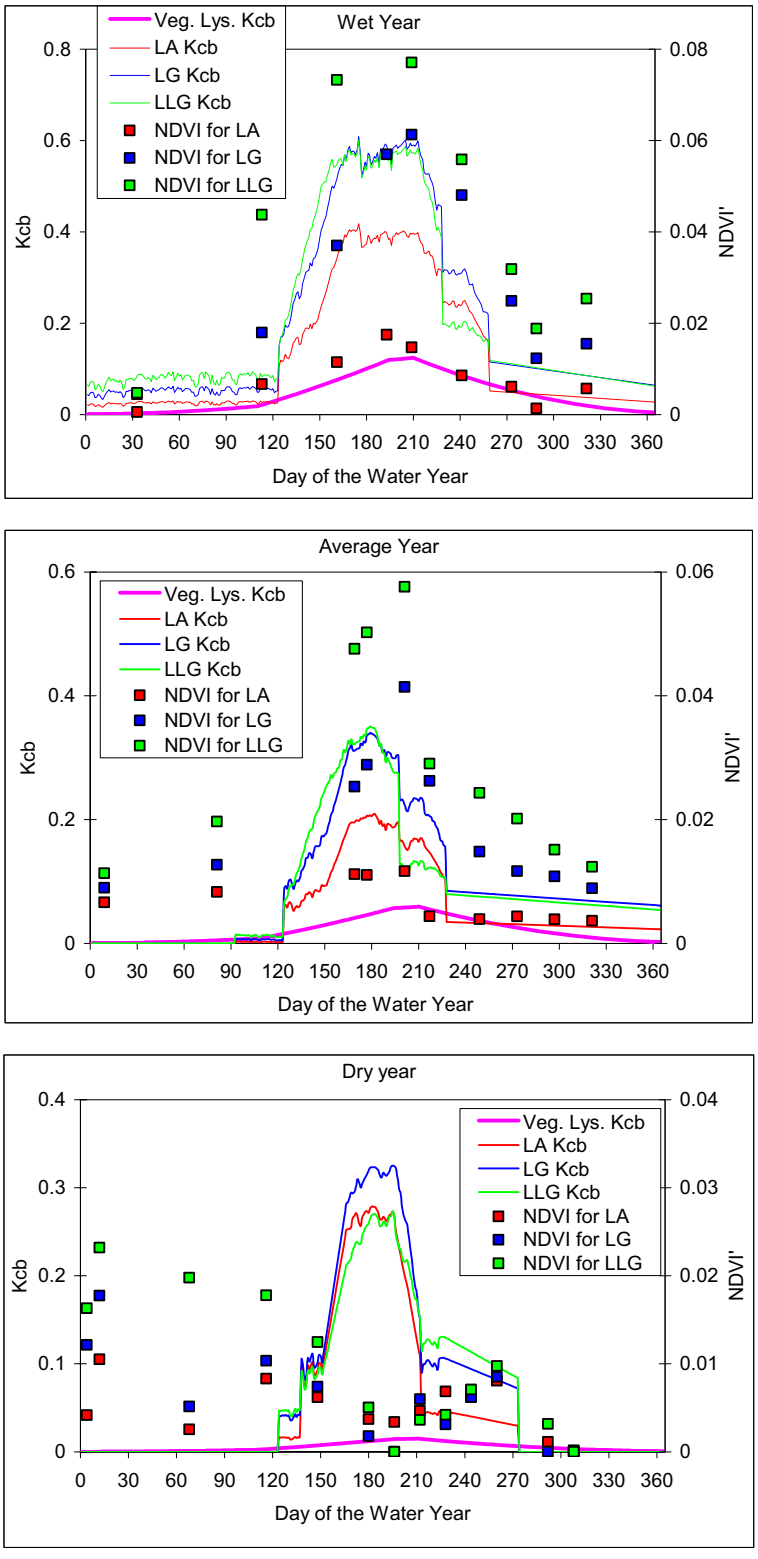

Source: Validation Output DTN: SN0607T0502206.016, file: NTS*NTSLysimeter.xls*.

Figure 7.1.2.1-4. Comparison Between the Measured K_{cb} and NDVI Values and Calculated Vegetated Lysimeter K_{cb} Values for the Different Water Years

Another parameter related to the vegetated lysimeter is the vegetation (canopy) fraction parameter f_c. It was assumed that f_c is constant for the entire period of simulation. As estimated in Appendix D, the vegetation fractions of LA association are 0.21, 0.11, and 0.15 for the wet, dry, and average years, respectively. The estimated f_c is 0.26 is close to the value for the wet year. Note that parameter K_{c_min} estimated value (0.0135) is within the ranges of K_{c_min} measured for LA association as described in Appendix D (0 for dry and average and 0.016 for the wet water years).

Summary of Lysimeter Simulations at NTS:

- The simplified water balance approach incorporated in MASSIF allows for adequate simulation of water storage and ET in both bare soil and vegetated NTS lysimeters.

- The ET parameters such as K_{cb}, K_{c_min}, and f_c estimated for the bare soil and vegetated lysimeters using MASSIF are in good agreement with the experimental data obtained for the plant association similar to the one present at the lysimeter site.

- The MASSIF results are comparable to the results obtained with physics-based models such as UNSAT-H (Desotell et al. 2006 [DIRS 176858]).

- MASSIF's ability to reproduce the lysimeter water storage over 10 years (bare soil) and 9 years (vegetated) confirms that the most important processes are represented correctly.

- The same tendencies in the differences between the observed storage and storage calculated with other models were also found using MASSIF. These tendencies are consistent with the ones described in the other studies related to the NTS lysimeters (e.g. Desotell et al. 2006 [DIRS 176858]). These differences may indicate evaporation at depth in the lysimeters that is a phenomenon of the lysimeter but not of the natural conditions.

7.1.2.2 Lysimeter Simulations at the Reynolds Creek Experimental Watershed

The RCEW data were collected by the US Department of Agriculture (USDA) Northwest Watershed Research Center (NWRC), in Boise, Idaho. The data are available from *ftp.nwrc.ars.usda.gov*. The data used in this analysis were obtained directly from USDA NWRC. The information included in the CD provided by the USDA NWRC can be found in DTN: SN0608T0502206.020 [DIRS 179875]. There are a series of articles published in the Water Resources Research Journal, vol. 37, No. 11 in November 2001 summarizing research goals and the data collection efforts at the RCEW. The series includes Seyfried et al. (2001 [DIRS 177515], 2001 [DIRS 177501], 2001 [DIRS 177505], 2001 [DIRS 177506]), Marks (2001 [DIRS 177512]), Marks et al. (2001 [DIRS 177504]), Slaughter et al. (2001 [DIRS 177354]), Pierson et al. (2001 [DIRS 177503]), Hanson et al. (2001 [DIRS 177509]), and Hanson (2001 [DIRS 177508]).

RCEW occupies 239 km^2 in the Owyhee Mountain region located in the southwestern Idaho, 80 km southwest of Boise (Hanson et al. 2001 [DIRS 177509]). Two sets of soil lysimeters were installed at RCEW. The lysimeter used in this analysis is located at the Lower Sheep Creek climate station, lysimeter LSCW. The details are presented in Appendix J.

The mean precipitation at the lysimeter site is 349 mm (Wight et al. 1986 [DIRS 177104]), and the mean annual temperature is 7.4ºC (Wight et al. 1990 [DIRS 177113]). About 21% of precipitation comes in the form of snow. These are wetter and cooler conditions than in Spokane (mean precipitation 325 mm and mean annual temperature 8.5ºC) an analog site representing the upper bound of the glacial transition climate.

The LSCW lysimeter is located at: 43º 08' 24.088" latitude, and 116º 43' 57.732" longitude, and the elevation is 1656 m (DTN: SN0608T0502206.020 [DIRS 179875]). The lysimeter diameter is 1.47 m and depth is 1.22 m. The lysimeter contains native undisturbed soil. The upper 0.1 m is loam. It is underlain by a 0.48-m-thick argillic horizon with up to 50% clay. The remaining cross section is sandy loam. The soil samples were taken at the neutron tubes 127707, 127807, and 127907 located within the lysimeter or next to it. Nine soil horizons were characterized down to the depth of 1.83 m. The soil layer is underlain by the basalt bedrock (Wight et al. 1986 [DIRS 177104]). The soil property average values weighted by the horizon thickness within the1.22 m lysimeter depth are as follows (see Appendix J for details):

- Porosity is 0.47 m^3/m^3
- Field capacity corresponds to a water content of 0.33 m^3/m^3 at the pressure of -1/3 bar
- Wilting point corresponds to a water content of 0.19 m^3/m^3 at the pressure of -15 bars (no measurements at -60 bars are available)

The vegetation at the lysimeter site is dominated by low sagebrush which grows to a height of about 0.3 m and is accompanied by perennial bunchgrasses and forbs (Seyfried et al. (2001 [DIRS 177515]). The lysimeter site contained a mature shrub along with the naturally associated plants with the slightly higher vegetation density than the surrounding landscape.

The climate data include precipitation and temperatures collected at the climate station 12 × 07 located next to the lysimeter site. The period of time from October 1, 1977 through September 30, 1984 was selected based on the availability of the soil storage data. The observation data used in this simulation are changes in water storage values during no snow season measured in the lysimeter from April 1978 through September 1984. The changes in storage were converted to the total soil water storage values using initial storage calculated for the point in time when the moisture within the profile was measured in the neutron tubes (see Appendix J for details). These data are shown in Figure 7.1.2.2-1.

The lysimeter calibration is described by Seyfried et al. (2001 [DIRS 177515]). As concluded in this publication, the lysimeter observations have the precision of $\pm$8 mm.

The MASSIF input parameters for the lysimeter simulations were defined in accordance with the site-specific information. The modeling set up is described in Appendix J. The following MASSIF parameters were estimated from the optimization scheme described below:

- Diffusive evaporation parameter, K_{c_min}
- Canopy fraction, f_c
- Coefficient representing the slope of the $NDVI'$-K_{cb} regression line, C_{kcb}
- Field capacity, θ_f.

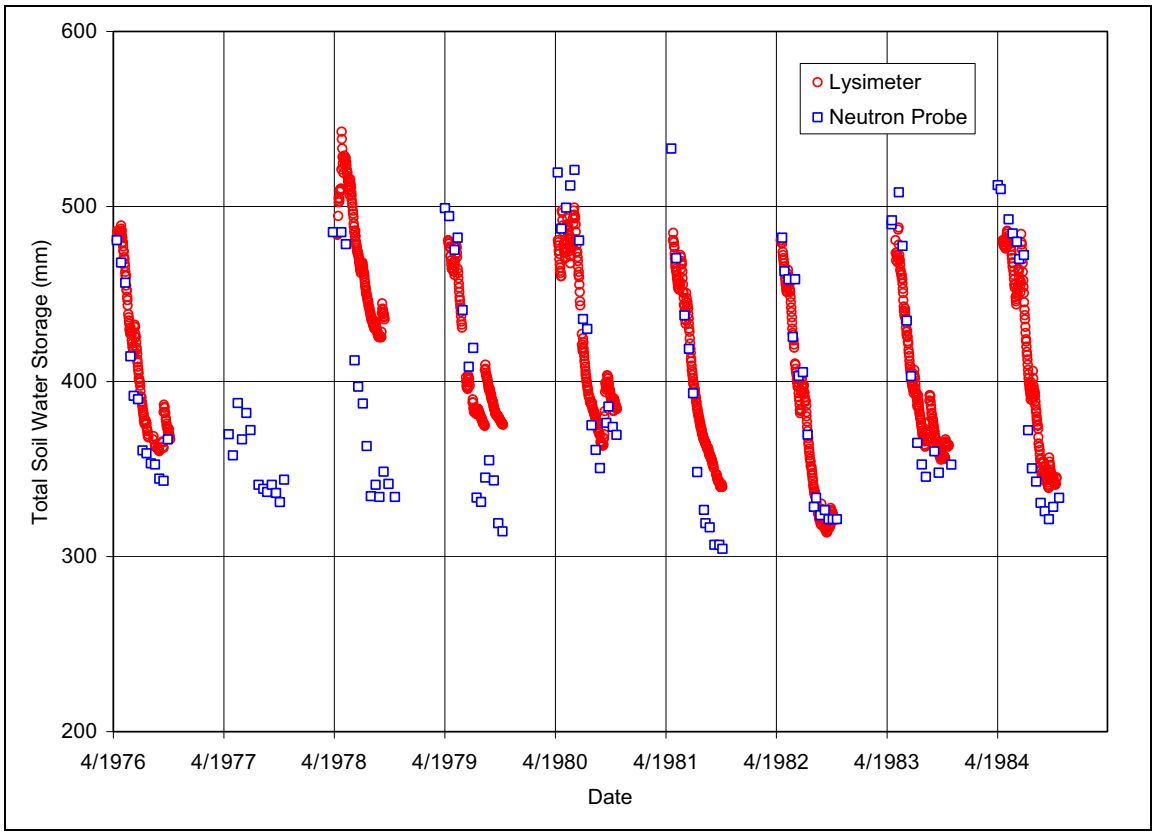

Source: Validation Output DTN: SN0607T0502206.016, *RCEWLysimeter.xls*.

Figure 7.1.2.2-1. Total Soil Water Storage Calculated Using Daily Change-in-storage from LSCW and Integrated Water Content from Neutron Probe Measurements

The values of these four parameters were estimated by minimizing the difference between the observed and calculated soil water storage. The following objective function $F3_{obj}$ was used in the conjugate gradient minimization procedure in MathCAD:

$$F3_{obj}(K_{c\_min}, f_c, C_{kcb}, \theta_f) = [\sum(S^{obs}{}_i - S^{cal}{}_i)^2]/N \qquad \text{(Eq. 7.1.2-4)}$$

where $S^{obs}{}_i$ and $S^{cal}{}_i$ are observed and calculated lysimeter storage during the simulation day i on which the observation data is available, and N is the number of observations (N=1179). Note that the lysimeter data were not recorded every day.

The results of the minimization and subsequent manual adjustment are:

- $K_{c\_min} = 0.0$
- $f_c = 0.7$
- $C_{kcb} = 13.685$
- $\theta_f = 0.415$
- $F1_{obj} = 1037.81$.

Based on the obtained objective function value, the overall goodness of fit is 32.22 mm (9.5 % of the mean annual precipitation). The goodness of fit is very similar to the one obtained for the NTS site, which is about 9% of the mean annual precipitation. Considering that the measurement precision is $\pm$8 mm, this is a reasonably good fit. The results of minimization are shown in Figure 7.1.2.2-2. The storage calculated based on the neutron probe measurements of moisture content within the soil profile is shown in Figure 7.1.2.2-2 in addition to the soil water storage measured in the lysimeter (see Appendix J for details). The storage calculated with MASSIF is well within the boundaries of the observed values.

The lysimeter site was designed to exclude run-on and runoff. The intent was also to exclude or minimize deep percolation. Very little drainage has probably occurred from the lysimeter bottom, but the timing of these small events is not known (Seyfried et al. 2001 [DIRS 177515]). Runoff and run-on calculated by MASSIF was zero. The mean annual infiltration calculated by MASSIF is 7 mm, which is 2% of the mean annual precipitation (349 mm). The actual site-specific infiltration is unknown. However, the infiltration for the rangeland in this area is considered to be around 4% (Wight et al. 1986 [DIRS 177104]). MASSIF-calculated infiltration is consistent with this estimate and the site conceptual model (little drainage). Since infiltration, if any, constitutes a very small portion of the overall water balance, it should not affect the estimates of the other water balance constituents, such as ET.

The RCEW lysimeter storage was also simulated with HYDRUS-1D. The same mean properties of the soil and climate data were used in the calculations (see Appendix J for details). The results of these simulations are shown in Figure 7.1.2.2-2. The mean root square error obtained with HYDRUS-1D is 42.3 mm (12% of the mean annual precipitation). The same tendencies as described above in the differences between the calculated and observed storages can be noted. The mean root square error between the storages calculated by HYDRUS-1D and MASSIF is 33.57 mm. The runoff calculated by HYDRUS-1D is zero during all period of observation. The mean annual infiltration is 3 mm (0.9% of precipitation), which is close to the value calculated by MASSIF.

The average monthly rates of the actual ET calculated by MASSIF for 1978 and 1979 were compared to the data presented by Wight et al. (1990 [DIRS 177113]). This is demonstrated in Figures 7.1.2.2-3 and 7.1.2.2-4. The calculated and measured ET values are in good agreement. The sum of the mean monthly ET for the six months in 1978 calculated by MASSIF and presented by Wight et al. (1990 [DIRS 177113]) are 10.05 mm and 9.84 mm, respectively. The sum of the mean monthly ET for the five months in 1979 calculated by MASSIF and presented by Wight et al. (1990 [DIRS 177113]) are 7.17 mm and 7.35 mm, respectively.

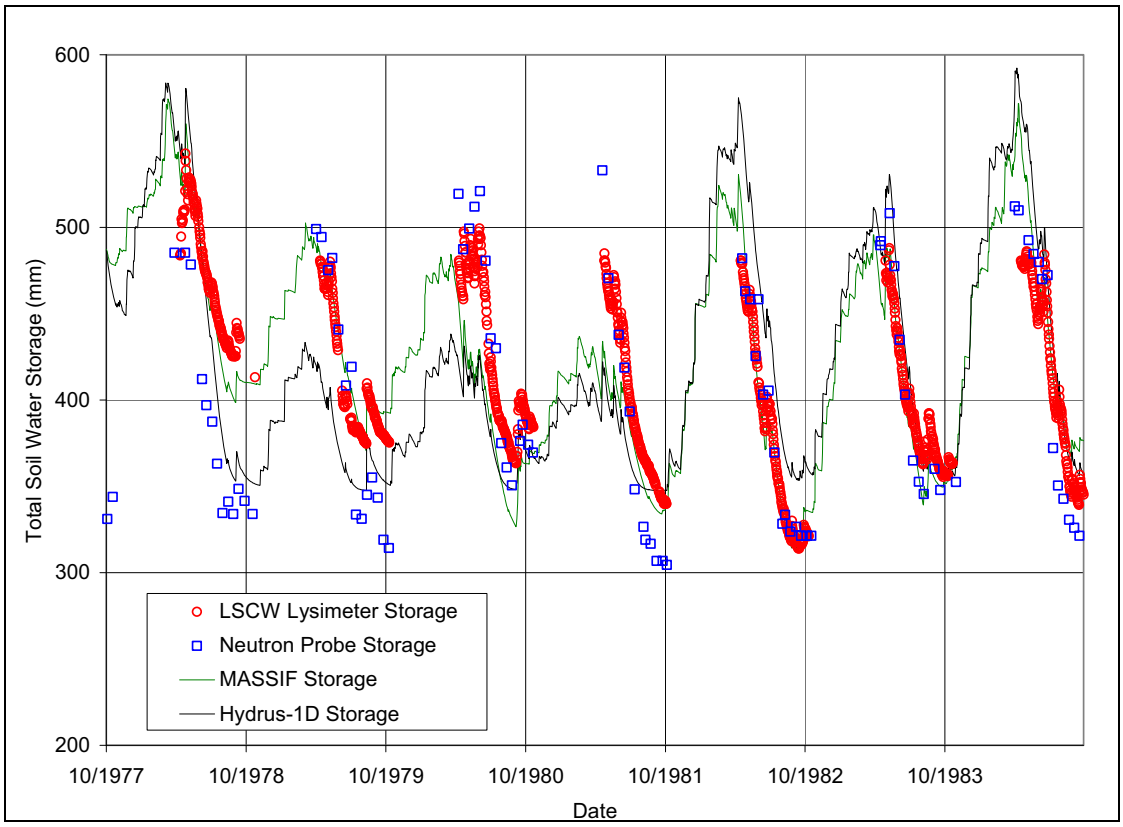

Source: DTN: SN0608T0502206.020 [DIRS 179875] (lysimeter and neutron probe data); Validation Output DTN: SN0607T0502206.016 (HYDRUS-1D data); Output DTN: SN0701T0502206.037, file: \Welcome to Massif\Massif\Validation Analyses\Lysimeter*RCEWLysimeter.xls.*

Figure 7.1.2.2-2. Simulation of Soil Water Storage in RCEW Lysimeter

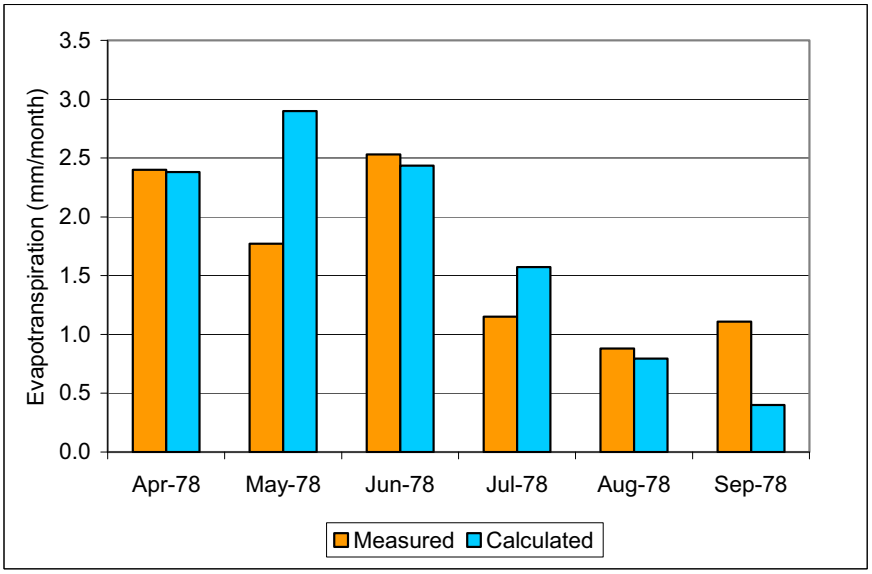

Source: Output DTN: SN0701T0502206.037.

Figure 7.1.2.2-3. 1978 Average Monthly Rates of Actual Evapotranspiration at RCEW

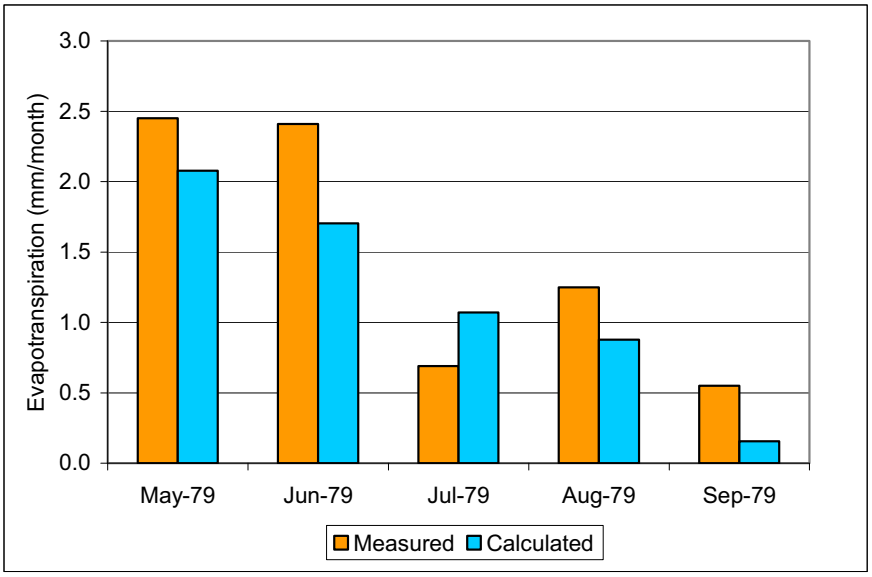

Source: Output DTN: SN0701T0502206.037.

Figure 7.1.2.2-4. 1979 Average Monthly Rates of Actual Evapotranspiration at RCEW

The field capacity estimated from the lysimeter modeling is 0.415. This falls into the range of the site-specific field capacity values of 0.28 to 0.42 obtained for the different soil horizons (see Appendix J). The maximum measured lysimeter storage was 542.7 mm. This corresponds to the field capacity of 0.44. Note that the actual soil profile is heterogeneous and the effective soil properties of the equivalent homogeneous profile are not known. The effective soil properties may be different from the weighted average values. In this case (effective field capacity is equal to the clay and clay loam field capacity), the amount of water that can be stored in the clay and clay loam layers controls the lysimeter storage.

The estimated K_{c_min} value is 0. This is consistent with the conceptual model of ET (see Section 6.3.3 and 6.3.4).

There are no daily K_{cb} data at the site. The mean K_{cb} value at the site for the growing season estimated for the site in Wight et al. (1990 [DIRS 177113]) is 0.85 (standard deviation is 0.06). The mean K_{cb} during the growing period over the seven years of observations (1978 through 1984) calculated using estimated C_{kcb} = 13.685 is 0.77. This is consistent with the estimate in Wight et al. (1990 [DIRS 177113]).

The vegetation cover f_c estimated for the site is 0.7. The estimate of the mean vegetation cover including live plants and litter at the site over the 11 years of observations provided in Wight et al. (1986 [DIRS 177104]) is 50% or 0.5.

Summary of Lysimeter Simulations at RCEW:

- The MASSIF water balance approach was capable of reproducing the changes in storage over the seven years of observations at the RCEW lysimeter site. This site is considerably different from the NTS site. The climate is wetter and cooler with 21% of

precipitation being snow, and the soils are finer with the smaller permeability and significantly higher field capacity and wilting point. The vegetation cover is twice as dense, and the plants species are different.

- The soil properties, ET parameters, and infiltration estimated using MASSIF for the RCEW lysimeter fall within the site specific ranges obtained from the literature.

- The MASSIF and HYDRUS-1D results are fairly consistent. The same tendencies in differences between the observed and calculated storages were obtained with MASSIF and HYDRUS-1D.

- The infiltration predicted by MASSIF is in good agreement with the infiltration predicted by HYDRUS-1D.

- The MASSIF ability to adequately model RCEW lysimeter site confirms that the physical processes incorporated in MASSIF are applicable to a wide range of condition. Both present-day and future climates can be thus accurately represented.

7.1.3 Run-on/Runoff

The hydrological processes of run-on and runoff are validated in the MASSIF model by comparison of measured streamflow data with MASSIF predictions of runoff (streamflow) at the discharge cells at the base of streamflow watersheds. Streamflow watersheds are sub-watersheds located within the primary eleven watersheds that encompass the Yucca Mountain infiltration model domain (see Table B-3). A streamflow watershed is defined by the location of its streamflow gauge. That is, a streamflow watershed includes all the upstream cells that can contribute runoff that eventually flows through a given streamflow gauge. Streamflow and runoff are terms that are often used interchangeably, but for this discussion, streamflow refers to the total amount of runoff within a streamflow watershed, while runoff can refer to total streamflow, or just the amount of runoff from one cell to another. Additional confidence building during model development is provided in this section by comparing streamflow data from the rare occasions during which streamflow has been recorded within the Yucca Mountain model domain, with MASSIF predictions of streamflow for those same streamflow events.

There are six streamflow gauges located within the Yucca Mountain infiltration model domain used in this analysis (see Section B5). These six gauges are part of the USGS streamflow monitoring network (Bauer et al. 1995 [DIRS 101486]). The Yucca Mountain infiltration model domain encompasses two Pagany Wash gauges, one Drill Hole Wash gauge, one Wren Wash gauge, and two Split Wash gauges.

Streamflow was recorded at some of these six gauges during storms in water years 1993, 1994, 1995, and 1998. Data collected during these four water years also include years with no streamflow, such as for water year 1994. The data record for water year 1994 is not complete for several gauges. Data with zero streamflow and incomplete records were not used, so streamflow data from water years 1995 and 1998 were used in this analysis. Streamflow data are reported as an average daily flow rate in units of cubic feet per second (cfs). These units are converted into cubic meters per day for this analysis. Table 7.1.3-1 summarizes all the available streamflow

data collected within the infiltration model domain. Total streamflow in m^3/yr are compiled in this table, and calculated by summing the average daily streamflow rate for a given water year, then converting from average daily streamflow into total annual streamflow.

The streamflow gauge locations can be found in DTN: MO0601GSCSPINF.000 [DIRS 177236]. Note that the UTM coordinates in this DTN are NAD83, while the figures in the report are NAD27. The locations of these six gauges and their associated streamflow watersheds are shown in Figure 7.1.3-1. This figure also includes the locations of all field data used for model validation (refer to Sections 7.2.1).

MASSIF calculations are performed for each of the watersheds for which runoff data was collected. Qualified runoff data exist for all of the streamflow gauges for water year 1995, and for some of the streamflow gauges for water years 1994 and 1998. All of the calculations are started at the beginning of water year 1994, and carried through to either water year 1995 or 1998, depending upon the existence of 1998 data for the particular watershed.

With the exception of soil saturated conductivity, all of the input values are the nominal values listed in Appendix I. Soil conductivities are varied by a single multiplicative factor between 0.1 and 1.2 in increments of 0.1. Hence, the first run multiplies all of the soil conductivities by 0.1, the next run multiplies all soil conductivities by 0.2, and so on. Weather data for the simulations are taken from qualified records for Yucca Mountain sites 1, 2, 3, and 6 (DTN: SN0608WEATHER1.005 [DIRS 177912]). Separate calculations are performed for each of the weather sets, and the results from the four calculations are compared. Although there are a total of seven weather stations located within the infiltration model domain (Sites 1, 2, 3, 4, 6, 7, and 8), only Sites 1, 2, 3, and 6 were used for these comparisons because they are located closest to the six streamflow watersheds.

The predicted cumulative runoff for water year 1995 at the Wren Wash streamflow gauge site is shown in Figure 7.1.3-2. The horizontal axis is the normalized soil saturated conductivity (i.e., the multiplying factor applied to the soil conductivities). Each of the colored curves is a prediction based upon a different weather station data set (YM Sites 1, 2, 3, and 6). The horizontal black line is the sum of the measured runoffs for water year 1995. The intersections of each of the prediction lines (colored lines with symbols) and the runoff measurement (solid black line) represents the best match between the MASSIF calculation and the data. For Wren Wash in water year 1995, the multipliers at the intersections are:

- YM Site 1: ~0.35
- YM site 2: ~0.36
- YM Site 3: ~0.59
- YM Site 6: ~0.60.

Table 7.1.3-1. Summary of Streamflow Gauge Data Used in this Report.

USGS Gaging Station Name	Gaging Station Name Used in this Report	USGS Station ID	Abbreviated Name	
Pagany Wash near the Prow	Upper Pagany Wash	102512531	PW8	
		Data Summary		
Water Year:	1993	1994	1995	1998
Total Streamflow (m^3/yr):	No Data	Incomplete Record	33,518	27,793
DTN:		GS941208312121.001 [DIRS 107374]	GS960908312121.001 [DIRS 107375]	MO0603SEPSTREA.000 [DIRS 179889]
Pagany Wash #1 near Well UZ-4	Lower Pagany Wash	102512533	PW9	
		Data Summary		
Water Year:	1993	1994	1995	1998
Total Streamflow (m^3/yr):	Zero	Zero	21,065	35,157
DTN:	MO0605SEPSURFC.000 [DIRS 179890]	GS941208312121.001 [DIRS 107374]	GS960908312121.001 [DIRS 107375]	MO0603SEPSTREA.000 [DIRS 179889]
Drillhole Wash above Well UZ-1	Drill Hole Wash	102512535	DW8	
		Data Summary		
Water Year:	1993	1994	1995	1998
Total Streamflow (m^3/yr):	No Data	Incomplete Record	12,233	No Data
DTN:		GS941208312121.001 [DIRS 107374]	GS960908312121.001 [DIRS 107375]	
Wren Wash	Wren Wash	1025125356	WW9	
		Data Summary		
Water Year:	1993	1994	1995	1998
Total Streamflow (m^3/yr):	No Data	Incomplete Record	10,325	No Data
DTN:		GS941208312121.001 [DIRS 107374]	GS960908312121.001 [DIRS 107375]	
Split Wash below Quac Canyon	Upper Split Wash	102512537	SW9	
		Data Summary		
Water Year:	1993	1994	1995	1998
Total Streamflow (m^3/yr):	Incomplete Record	Zero	11,254	15,413
DTN:	GS941208312121.001 [DIRS 107374]	GS941208312121.001 [DIRS 107374]	GS960908312121.001 [DIRS 107375]	MO0603SEPSTREA.000 [DIRS 179889]
Split Wash at Antler Ridge	Lower Split Wash	1025125372	SWAR	
		Data Summary		
Water Year:	1993	1994	1995	1998
Total Streamflow (m^3/yr):	Incomplete Record	Zero	Zero	No Data
DTN:	GS941208312121.001 [DIRS 107374]	GS941208312121.001 [DIRS 107374]	MO0605SEPSURFC.000 [DIRS 179890]	

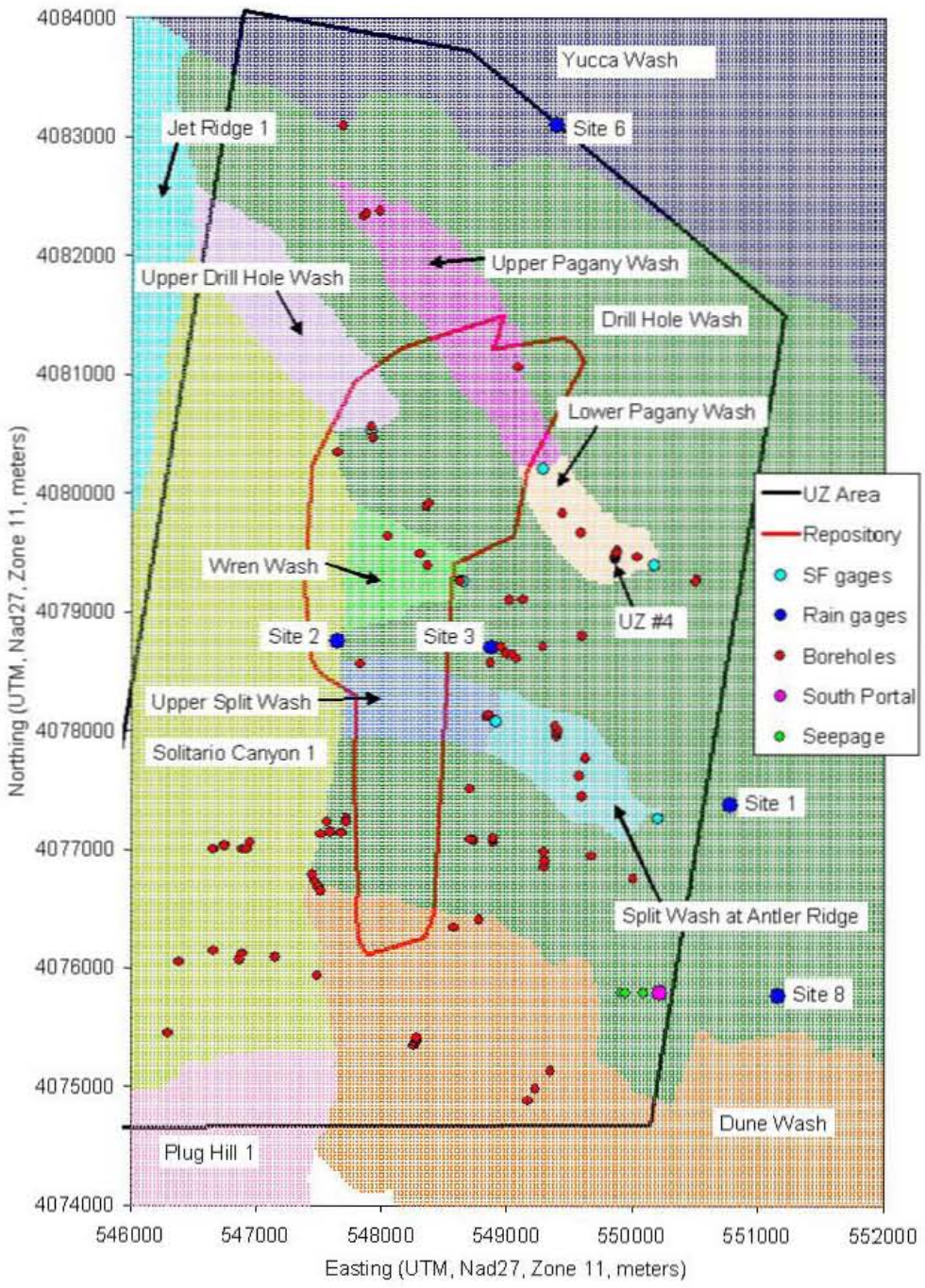

Sources: Output DTNs: SN0606T0502206.011 (Watersheds coordinates); SN0612FTPRNUZB.002 (UZ flow model and Repository areas); MO0601GSCSPINF.000 [DIRS 177236] (Locations of streamflow gauges); MO9906GPS98410.000 [DIRS 109059] (Locations of neutron logging boreholes); MO9906GPS98410.000 [DIRS 109059] (Location of UZ #4). Finsterle and Seol 2006 [DIRS 177754], p. 1 (Locations of seepage); CRWMS M&O 1997 [DIRS 100117], Table 2-1 (Locations of rain gauges); BSC 2003 [DIRS 165572], p. 15 (Location of south portal).

SF gauges = Streamflow gauges; UZ Area = UZ flow model area; Repository = Repository footprint.

Figure 7.1.3-1. Map View of Watersheds and Locations of Various Field Data

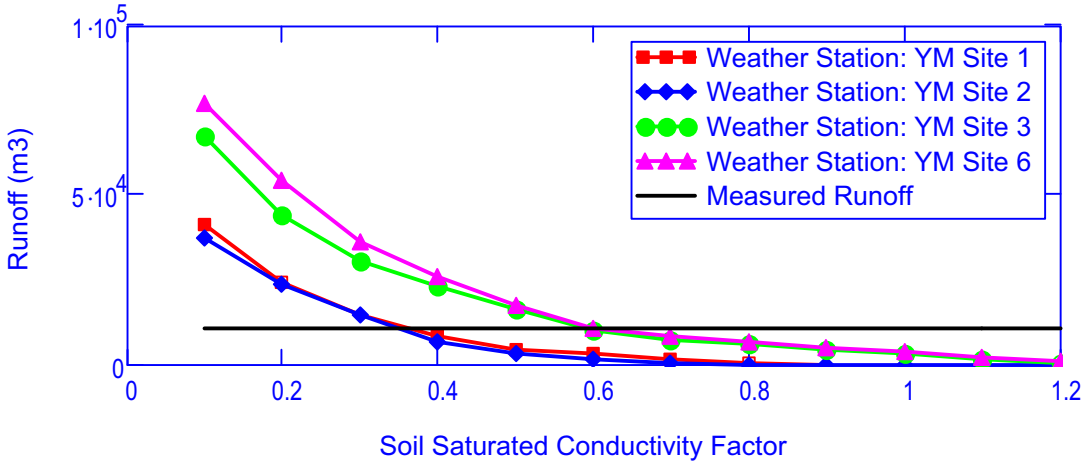

Source: Output DTN: SN0701T0502206.037, file: \Welcome to Massif\Massif\Validation Analyses\Stream Gauge Comparisons*Streamgage Plots.xmcd*.

Figure 7.1.3-2. Variation of Annual Cumulative Runoff with Soil Saturated Conductivity Factor (Wren Wash, Water Year: 1995)

While cumulative annual runoff, shown in Figure 7.1.3-2, is important, examination of the daily occurrence and amount of runoff is also important. Figure 7.1.3-3 shows calculations and measurements of daily runoff (reported as ft^3/s for a 24-hour day) for days 90 to 180 of the 1995 water year for Wren Wash. Runoff is neither calculated to occur nor measured outside of this range.

The recorded runoff is shown in the Figure 7.1.3-3 as a black arrow. Calculated runoffs are shown as vertical red and blue bars. The red and blue bars correspond to the lower and higher soil conductivity factors bounding the intercept of the measured runoff line in Figure 7.1.3-2. Hence, for weather station YM Site 1, the red bar corresponds to a soil conductivity factor of 0.3; the blue bar corresponds to a soil conductivity factor of 0.4. For YM Site 3, the red bar corresponds to a soil conductivity factor of 0.5; the blue bar corresponds to a soil conductivity factor of 0.6.

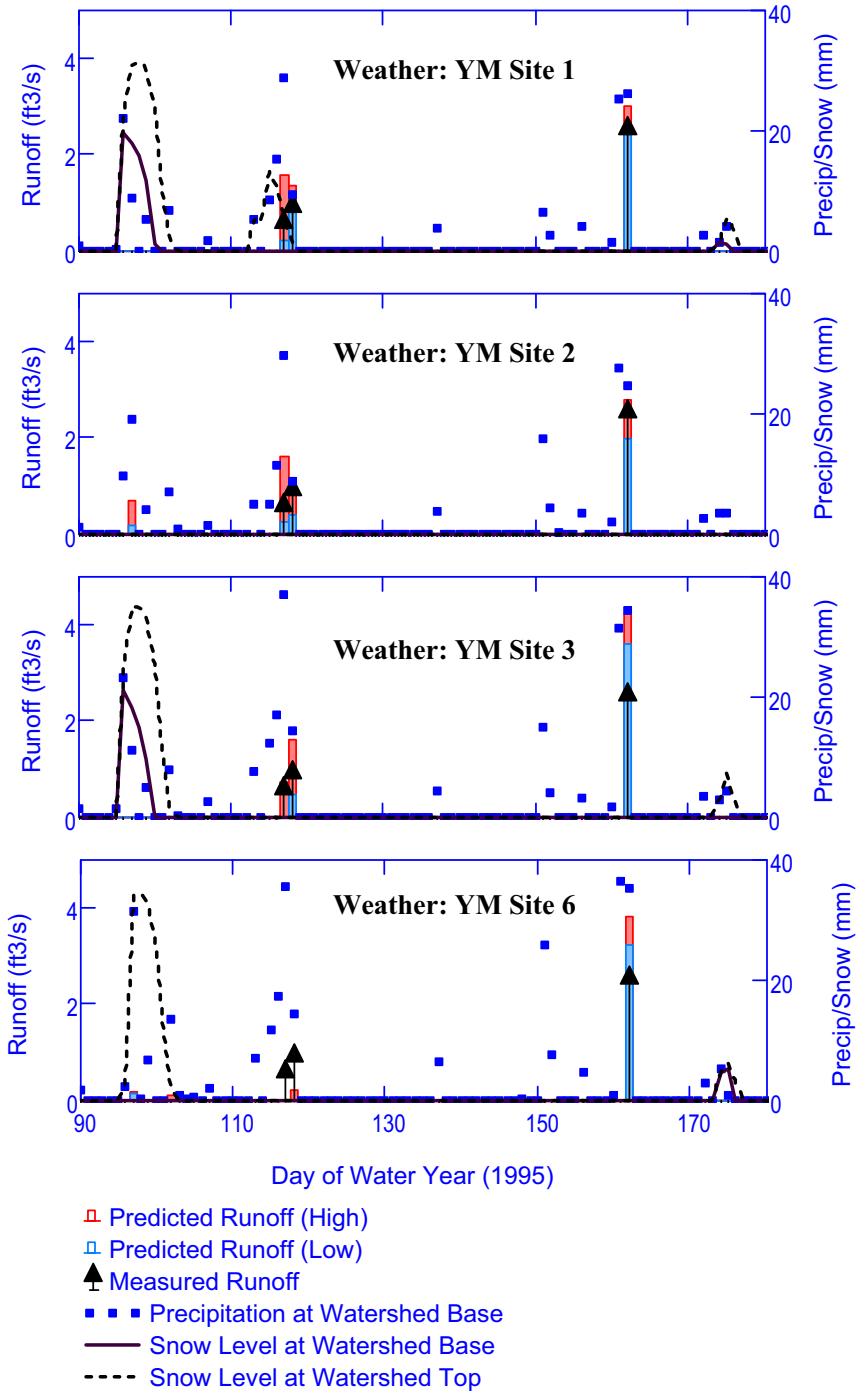

Source: Output DTN: SN0701T0502206.037, file: \Welcome to Massif\Massif\Validation Analyses\Stream Gauge Comparisons*Streamgage Plots.xmcd*.

NOTE: Daily precipitation at the base of the watersh ed is shown on the plots as blue squares. The amount of precipitation on any given day differs between weather stations. There are actually two reasons for this. The obvious reason is that precipitation amount varies with location. The less obvious reason is that each of the weather stations is located at a different elevation, and the recorded weather data must be lapse corrected to the elevation at the base of the watershed.

Figure 7.1.3-3. Predicted (Solid Bar) and Measured (Arrow) Runoff (Wren Wash, Water Year 1995)

Because the presence and/or melting of snow might affect runoff, the snow levels, in mm of water, are shown for the bottom (solid line) and top (dashed line) of the watershed. The predicted presence of snow varies with the weather data set. Use of Sites 1 and 3 produces snow at both the top and bottom of the watershed. Use of site 6 produces snow only at the top of the watershed. Use of Site 2 produces no snow at all.

This figure illustrates the fact that a comprehensive knowledge of precipitation and temperature does not exist even when measured data exists. Infiltration and runoff calculations require weather data for the entire domain. Weather station data exist for discrete locations. Geographic extrapolation of weather data has relative high levels of uncertainty. Comparison of the daily runoff plots based on each of the weather stations give some indication of the uncertainty of the runoff prediction due to uncertainty in weather data.

Given the uncertainty in soil conductivity and weather data, calculations of daily runoff are fairly good. Runoff occurs on the correct days and in roughly the "correct" amount. It is worth noting that no uncertainty estimates were recorded with the measured runoff data.

The balances of the streamflow gauge watersheds are listed below, along with the related figure numbers and figure titles. Comments on the results are inserted when characteristics of the plots deviate from the Wren Wash plots:

Upper Split Wash

Figure 7.1.3-4 Variation of Annual Cumulative Runoff with Soil Saturated Conductivity Factor (Upper Split Wash, Top: Water Year 1994, Middle: Water Year 1995, Bottom: Water Year 1998)

Figure 7.1.3-5 Predicted (Solid Bar) and Measured (Arrow) Runoff (Upper Split Wash, Water Year 1995)

Figure 7.1.3-6 Predicted (Solid Bar) and Measured (Arrow) Runoff (Upper Split Wash, Water Year 1998)

Comments: Measured runoff for water year 1994 was zero. All calculations produced zero runoff with the exception of YM Site 1 with a soil conductivity factor of 0.1

Lower Split Wash

Figure 7.1.3-7 Variation of Annual Cumulative Runoff with Normalized Saturated Conductivity of Soil (Lower Split Wash, Water Year: 1995)

Comments: Measured runoff for year 1995 was zero. Calculations using weather sites 1 and 2 produce zero or near-zero runoff for soil conductivity factors greater than or equal to 0.7. Calculations using weather sites 3 and 6 produce zero of near-zero runoff for soil conductivity factors greater than or equal to 1.1.

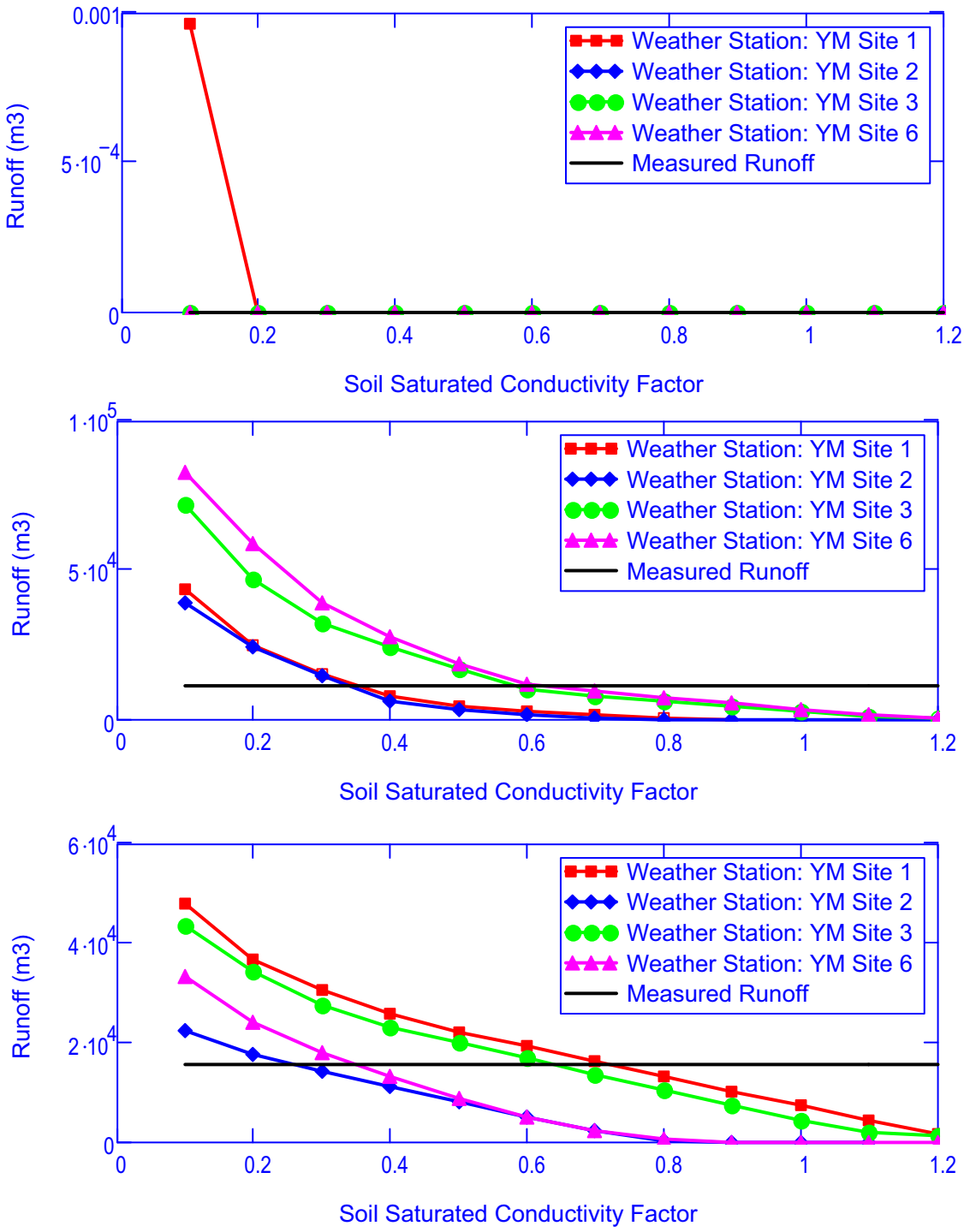

Source: Output DTN: SN0701T0502206.037, file: \Welcome to Massif\Massif\Validation Analyses\Stream Gauge Comparisons*Streamgage Plots.xmcd*.

NOTE: Upper Split Wash, Top: Water Year 1994, Middle: Water Year 1995, Bottom: Water Year 1998

Figure 7.1.3-4. Variation of Annual Cumulative Runoff with Soil Saturated Conductivity Factor

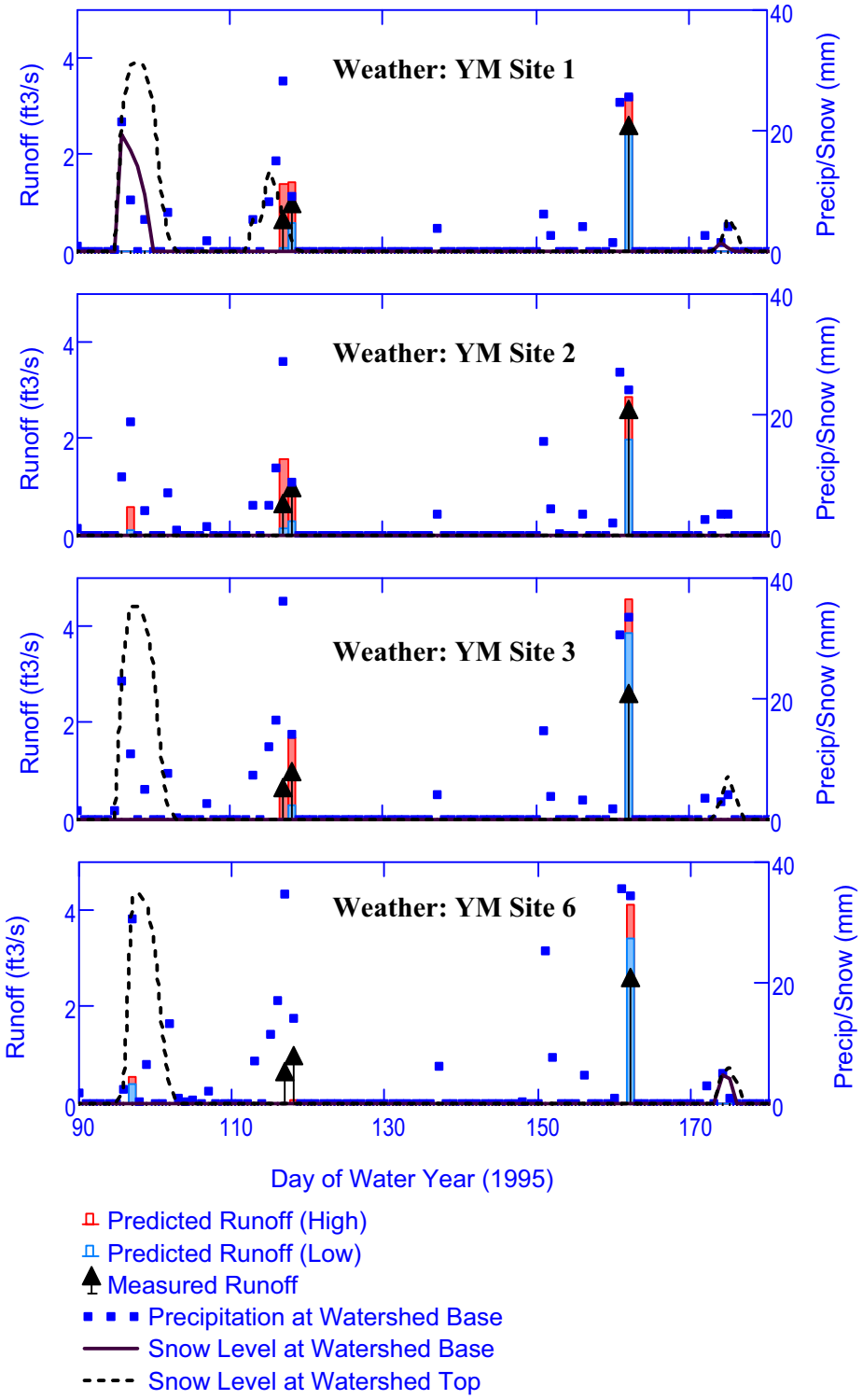

Source: Output DTN: SN0701T0502206.037, file: \Welcome to Massif\Massif\Validation Analyses\Stream Gauge Comparisons*Streamgage Plots.xmcd*.

Figure 7.1.3-5. Predicted (Solid Bar) and Measured (Arrow) Runoff (Upper Split Wash, Water Year 1995)

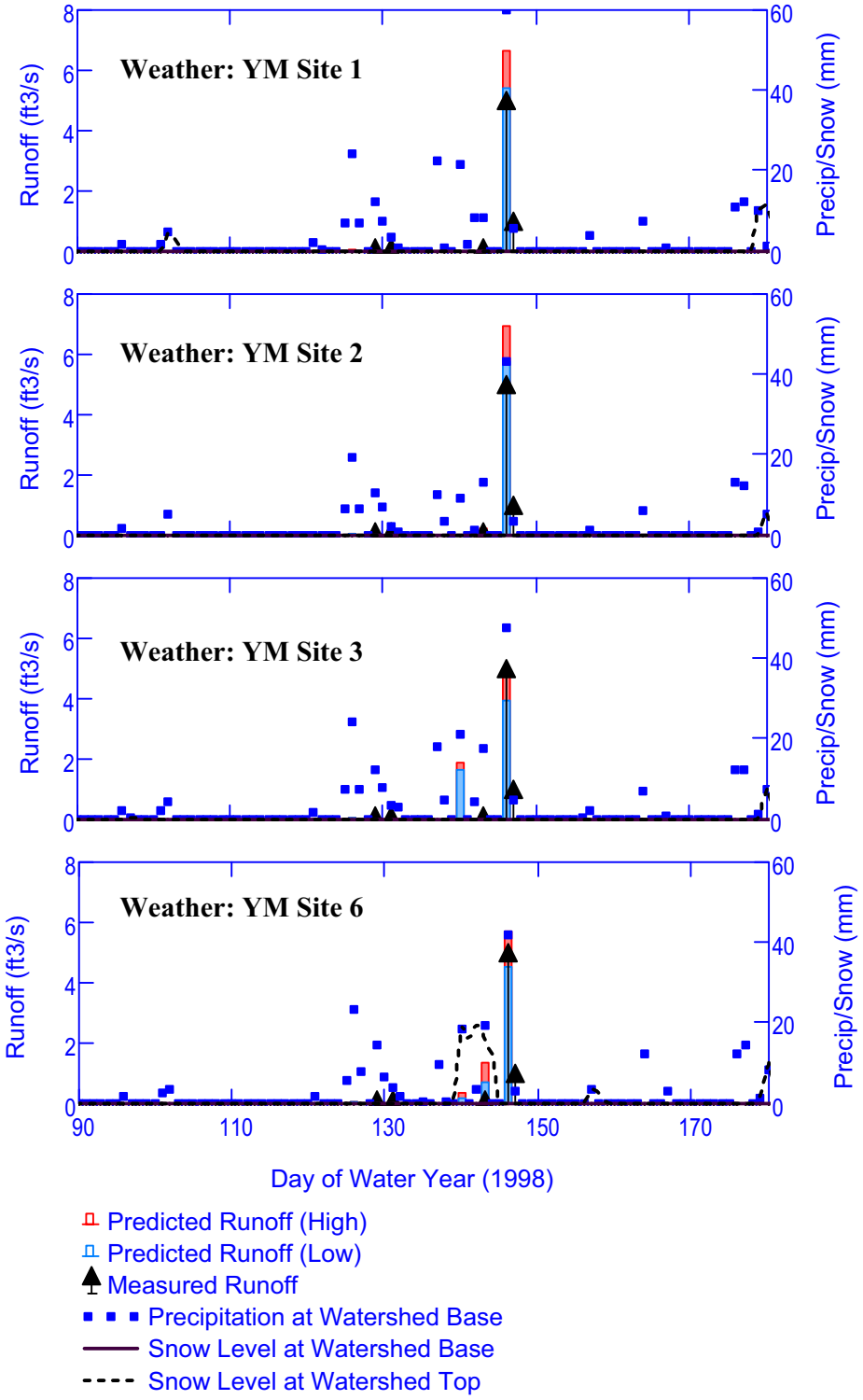

Source: Output DTN: SN0701T0502206.037, file: \Welcome to Massif\Massif\Validation Analyses\Stream Gauge Comparisons*Streamgage Plots.xmcd*.

Figure 7.1.3-6. Predicted (Solid Bar) and Measured (Arrow) Runoff (Upper Split Wash, Water Year 1998)

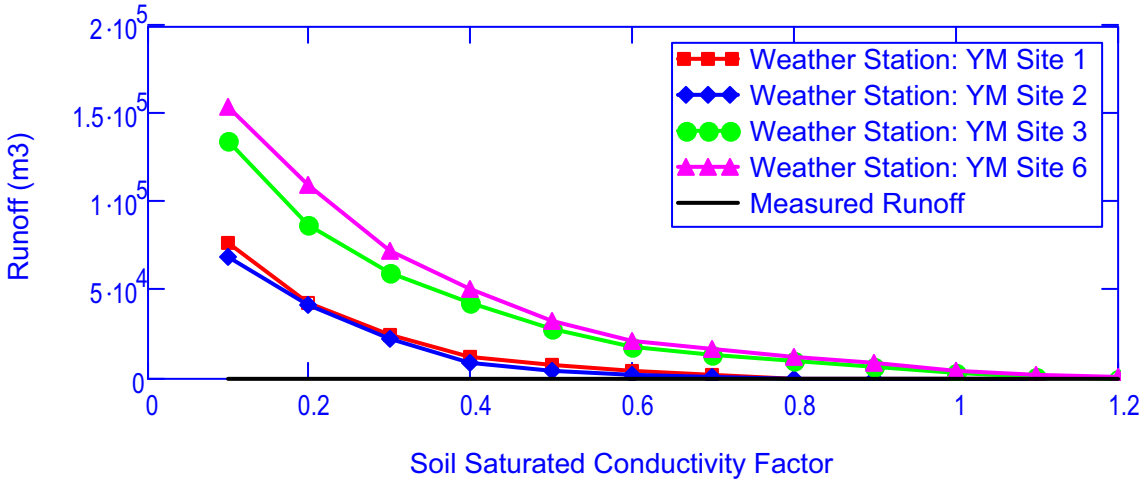

Source: Output DTN: SN0701T0502206.037, file: \Welcome to Massif\Massif\Validation Analyses\Stream Gauge Comparisons*Streamgage Plots.xmcd*.

Figure 7.1.3-7. Variation of Annual Cumulative Runoff with Normalized Saturated Conductivity of Soil (Lower Split Wash, Water Year: 1995)

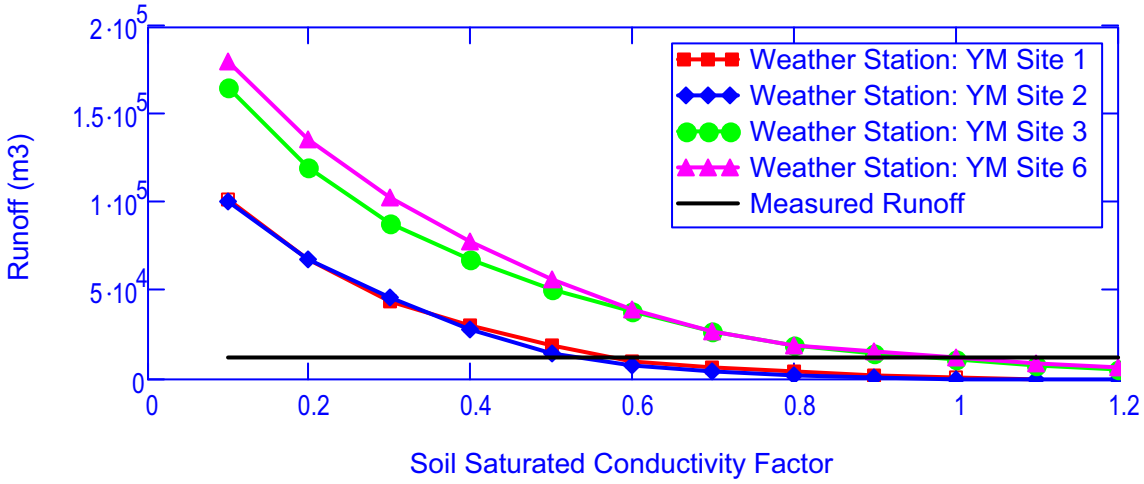

Source: Output DTN: SN0701T0502206.037, file: \Welcome to Massif\Massif\Validation Analyses\Stream Gauge Comparisons*Streamgage Plots.xmcd*.

Figure 7.1.3-8. Variation of Annual Cumulative Runoff with Soil Saturated Conductivity Factor (Drill Hole Wash, Water Year: 1995)

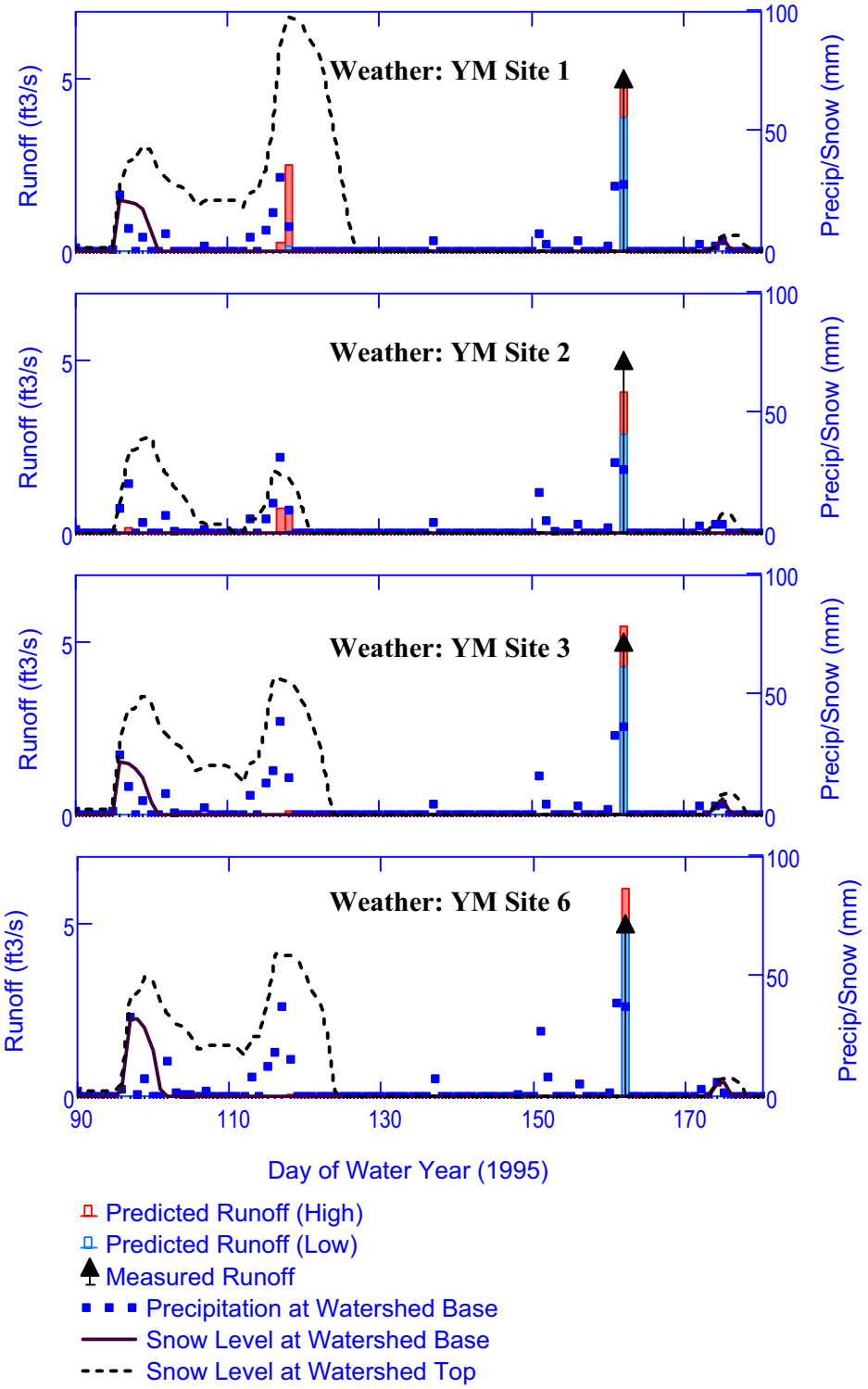

Source: Output DTN: SN0701T0502206.037, file: \Welcome to Massif\Massif\Validation Analyses\Stream Gauge Comparisons*Streamgage Plots.xmcd*.

Figure 7.1.3-9. Predicted (Solid Bar) and Measured (Arrow) Runoff (Drill Hole Wash, Water Year 1995)

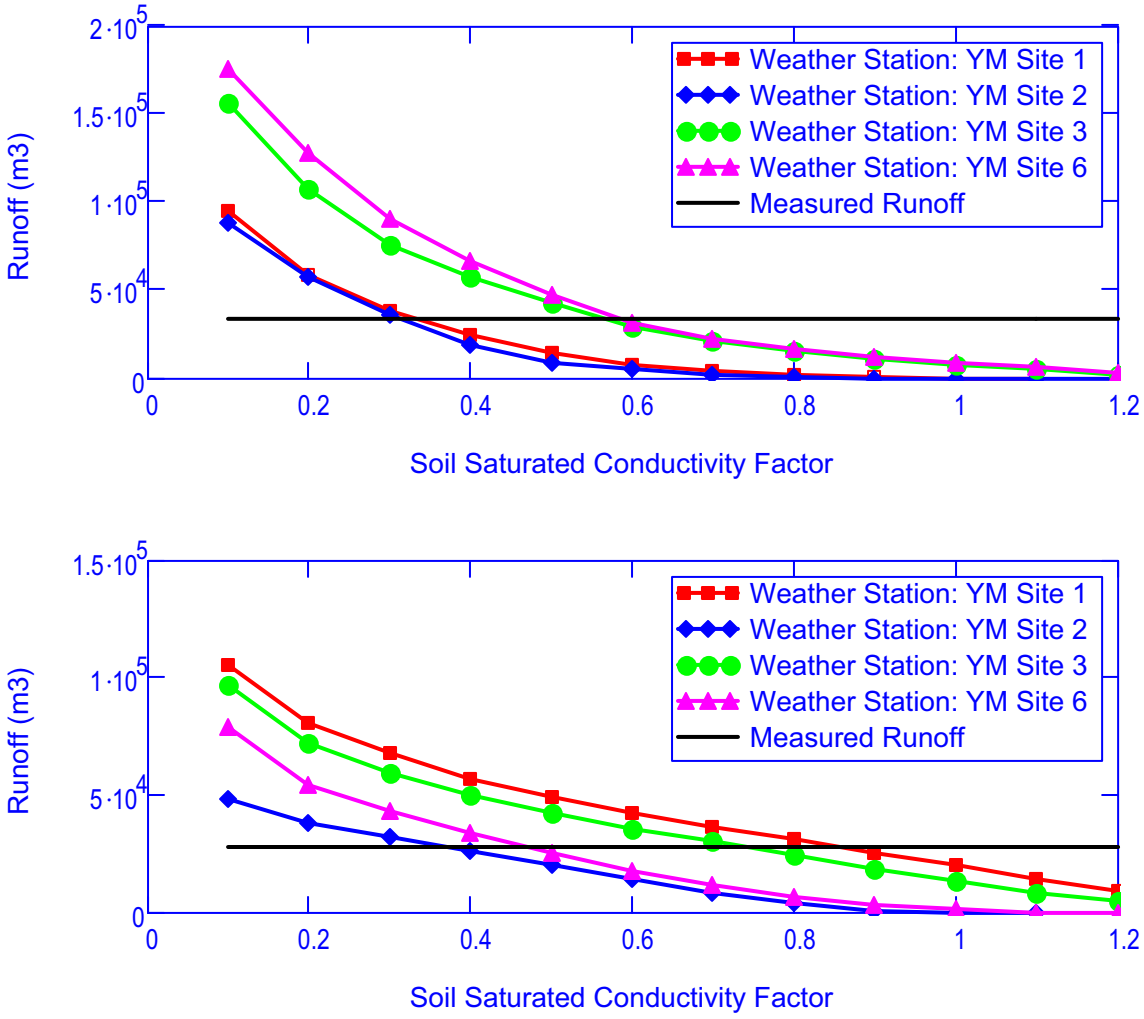

Source: Output DTN: SN0701T0502206.037, file: \Welcome to Massif\Massif\Validation Analyses\Stream Gauge Comparisons*Streamgage Plots.xmcd.*

Figure 7.1.3-10. Variation of Annual Cumulative Runoff with Soil Saturated Conductivity Factor (Upper Pagany Wash, Top: Water Year 1995, Bottom: Water Year 1998)

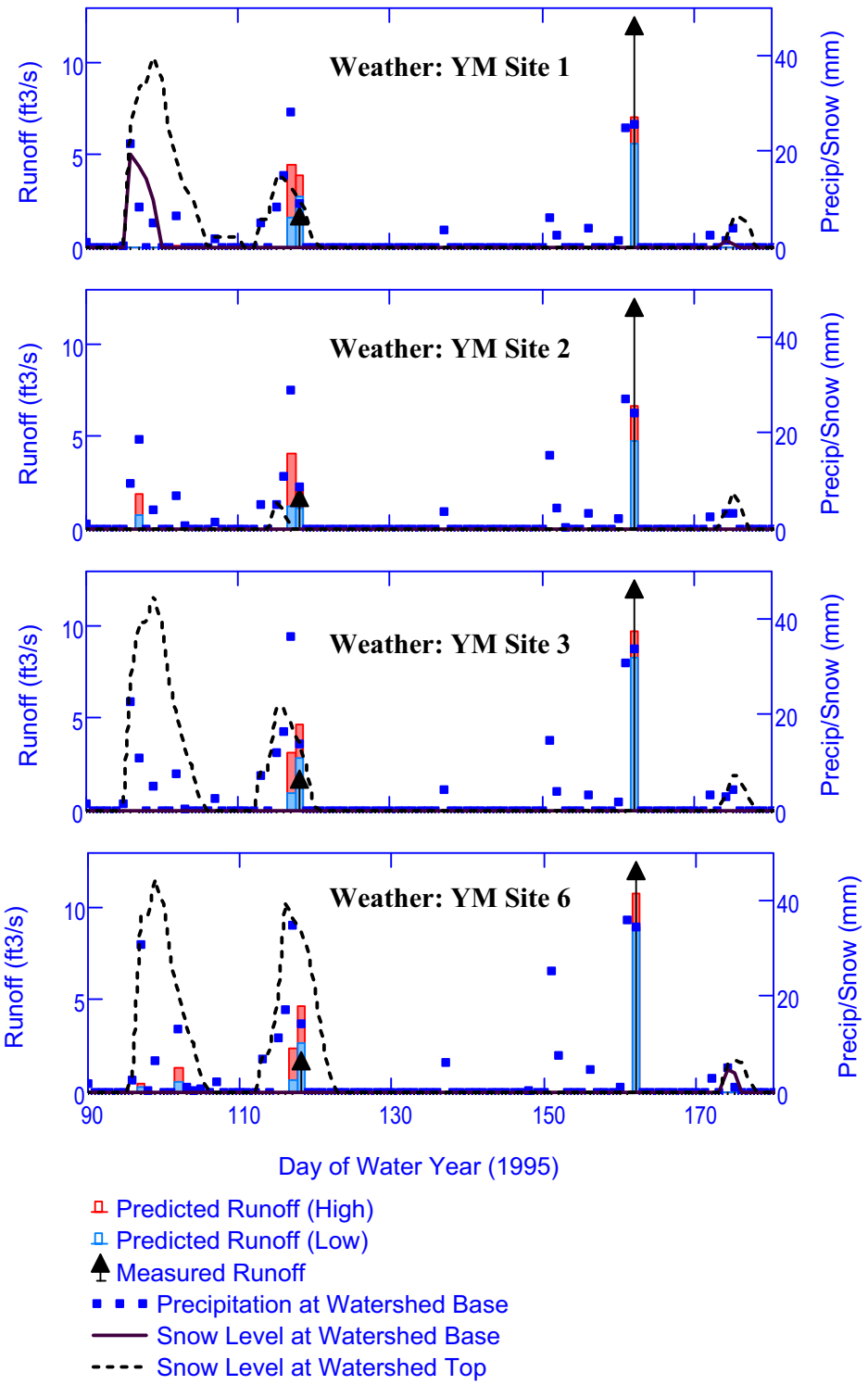

Source: Output DTN: SN0701T0502206.037, file: \Welcome to Massif\Massif\Validation Analyses\Stream Gauge Comparisons*Streamgage Plots.xmcd*.

Figure 7.1.3-11. Predicted (Solid Bar) and Measured (Arrow) Runoff (Upper Pagany Wash, Water Year 1995)

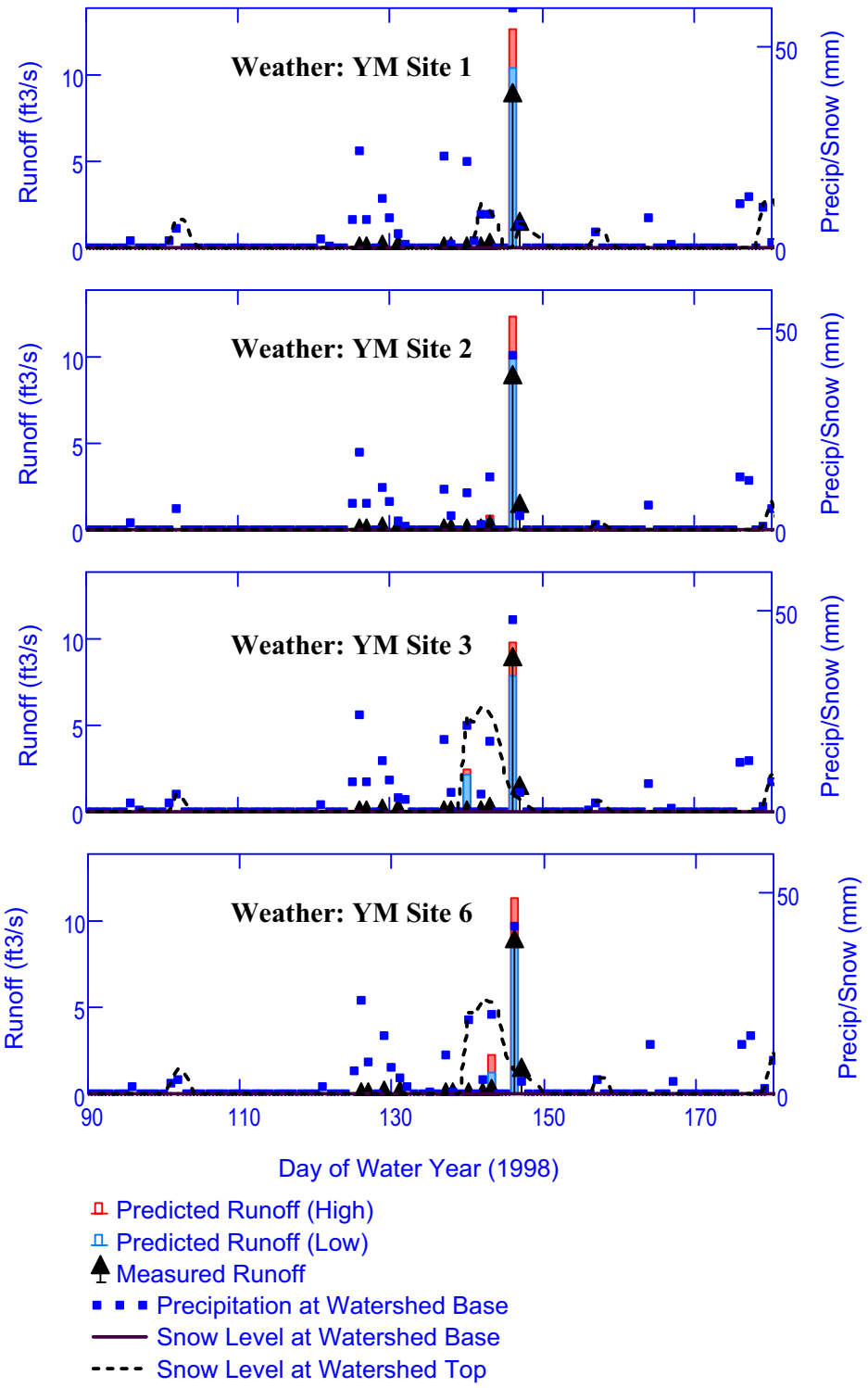

Source: Output DTN: SN0701T0502206.037, file: \Welcome to Massif\Massif\Validation Analyses\Stream Gauge Comparisons*Streamgage Plots.xmcd*.

Figure 7.1.3-12. Predicted (Solid Bar) and Measured (Arrow) Runoff (Upper Pagany Wash, Water Year 1998)

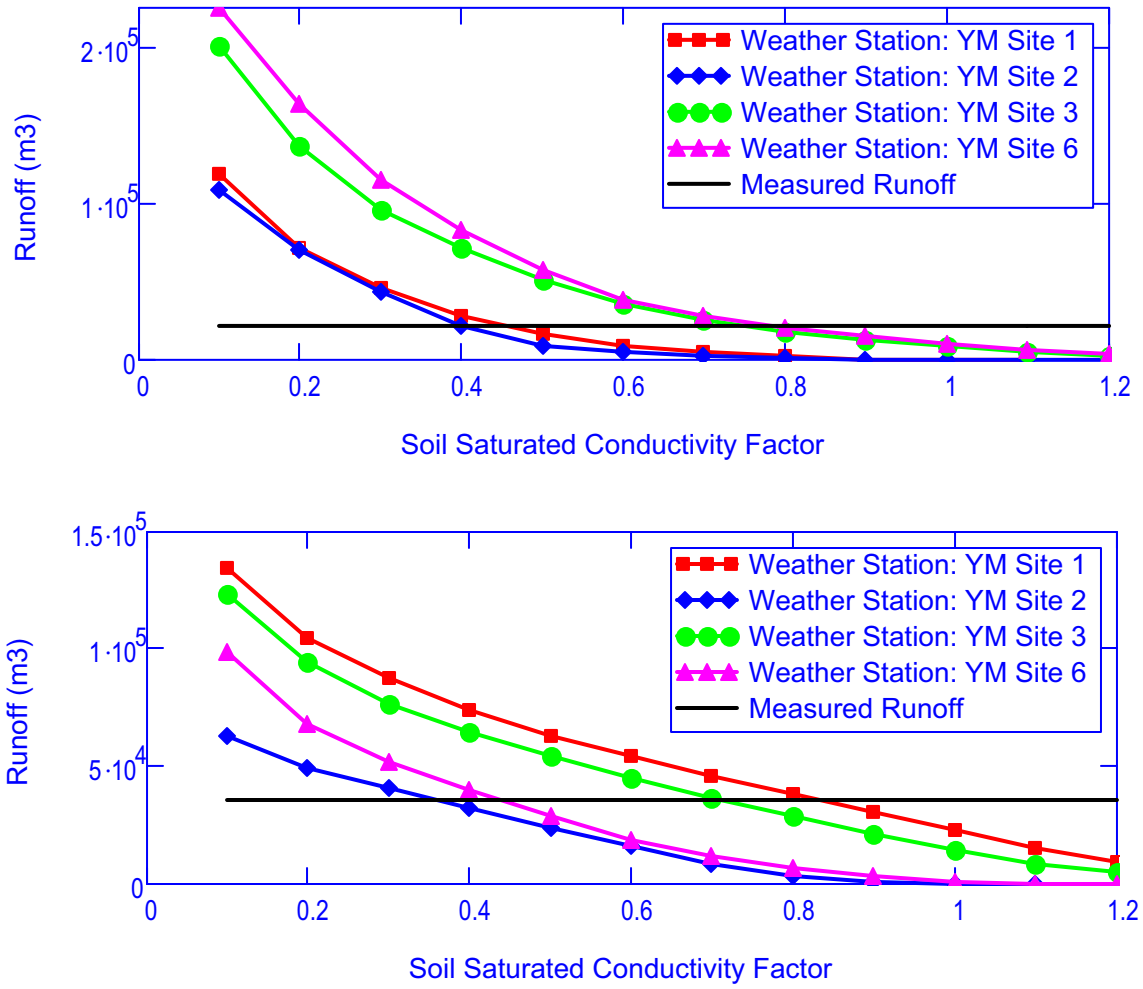

Source: Output DTN: SN0701T0502206.037, file: \Welcome to Massif\Massif\Validation Analyses\Stream Gauge Comparisons*Streamgage Plots.xmcd*.

Figure 7.1.3-13. Variation of Annual Cumulative Runoff with Soil Saturated Conductivity Factor (Lower Pagany Wash, Top: Water Year 1995, Bottom: Water Year 1998)

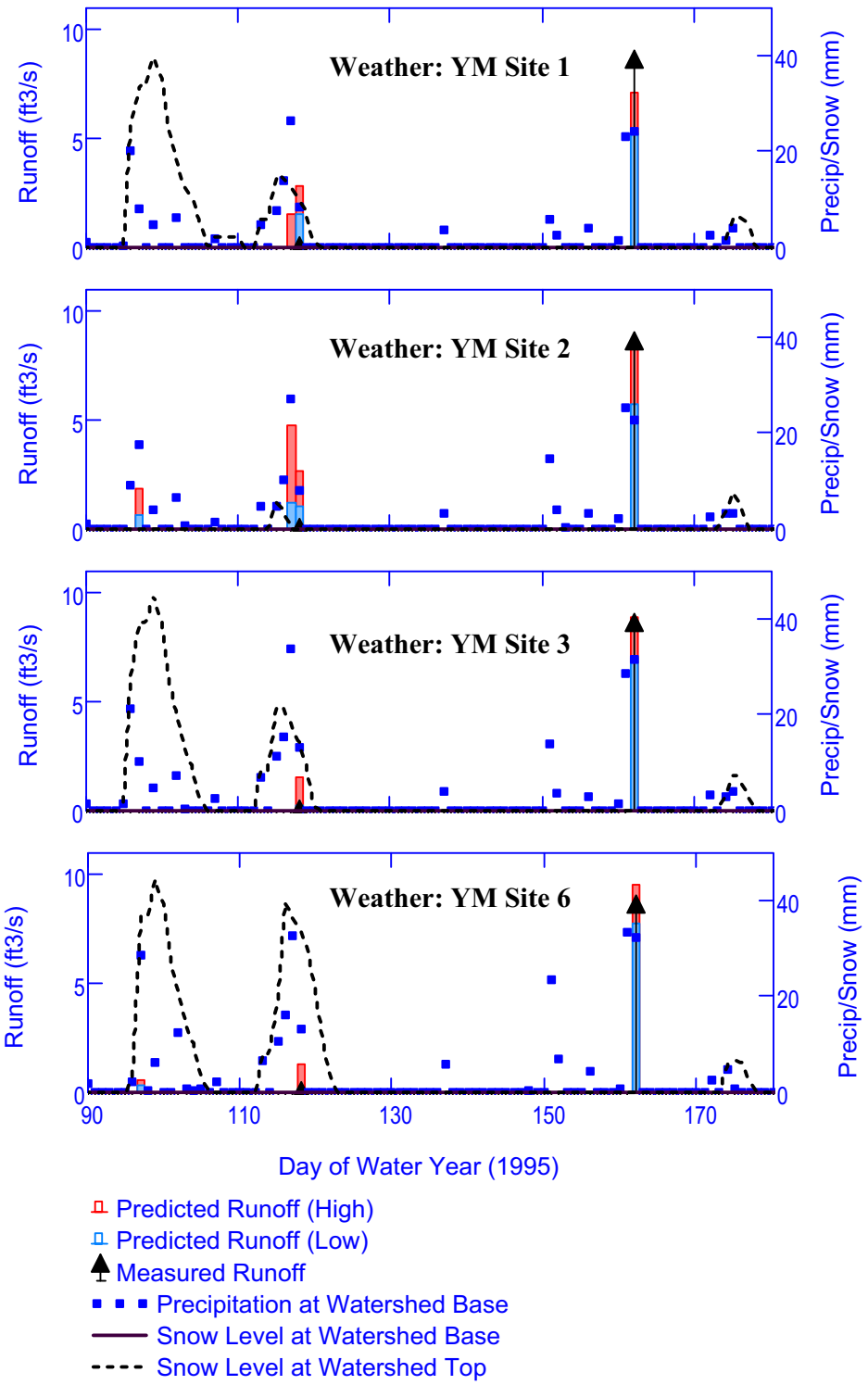

Source: Output DTN: SN0701T0502206.037, file: \Welcome to Massif\Massif\Validation Analyses\Stream Gauge Comparisons*Streamgage Plots.xmcd*.

Figure 7.1.3-14. Predicted (Solid Bar) and Measured (Arrow) Runoff (Lower Pagany Wash, Water Year 1995)

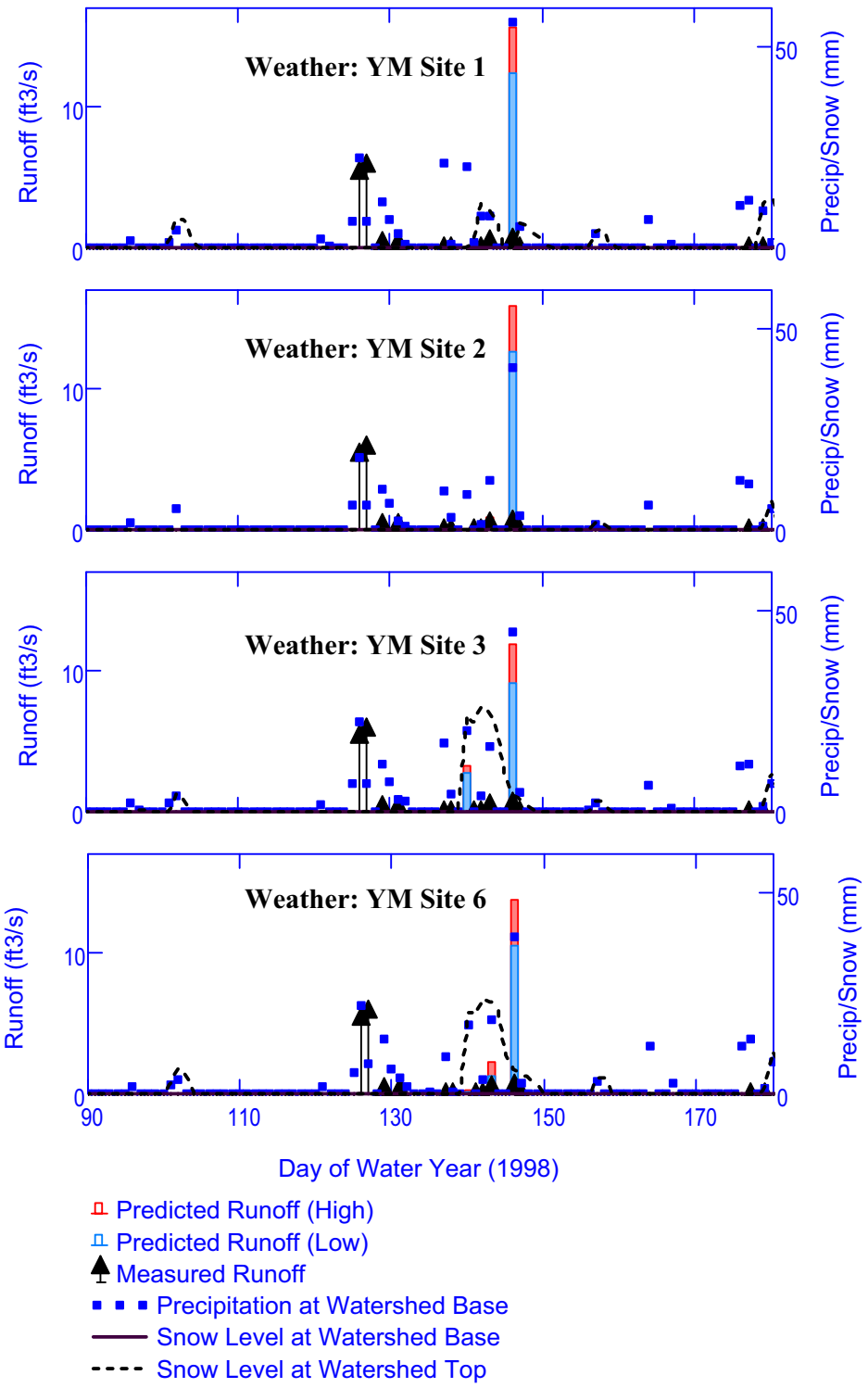

Source: Output DTN: SN0701T0502206.037, file: \Welcome to Massif\Massif\Validation Analyses\Stream Gauge Comparisons*Streamgage Plots.xmcd*.

Figure 7.1.3-15. Predicted (Solid Bar) and Measured (Arrow) Runoff (Lower Pagany Wash, Water Year 1998)

In general, MASSIF correctly predicts the timing and magnitude of runoff using the nominal parameter set with variations in the soil conductivity. Typically, the soil conductivities are reduced by multipliers of 0.3 to 0.7, which is within the range between the maximum and minimum soil conductivities for a given soil type from the Hanford soils data set (BSC 2006 [DIRS 176335], Table 6-7). Alternatively the conductivity reduction could be explained by soil structure, which can dominate water sorption in soils.

7.1.3.1 Runoff and Net Infiltration Comparison

When MASSIF is used to predict infiltration at the grid cell containing the UZ#4 borehole (LeCain et al. 2002 [DIRS 158511]) near the mouth of Lower Pagany Wash, the soil saturated conductivity must be increased by an order of magnitude to 7×10^{-6} m/s in order to match the measured infiltration (see Section 7.2.1.1.2). The rock conductivity was also increased to 10^{-3} m/s so that it had no influence on the infiltration. Soil Type 3 occupies the drainage channel in Lower Pagany Wash (Figure 7.1.3-16). Hofmann et al. (2000 [DIRS 153709]) measured the saturated hydraulic conductivity of the soil at two locations at Yucca Mountain. These locations included a measurement in Pagany Wash near borehole UE-25 UZN #14 and a measurement on a stable terrace adjacent to Fortymile Wash at borehole UE-25 UZN #85, both using a prototype-automated-infiltrometer. They found that the saturated hydraulic conductivity was 17.79 cm/hr (4.94×10^{-5} m/s) for the location in Pagany Wash and 1.78 cm/hr (4.94×10^{-6} m/s) for the terrace location (Hofmann et al. 2000 [DIRS 153709], Table 4). Both of these measurements are significantly higher than the soil conductivity used in this study. In addition, the value in Pagany Wash is an order of magnitude higher than the value on the stable terrace.

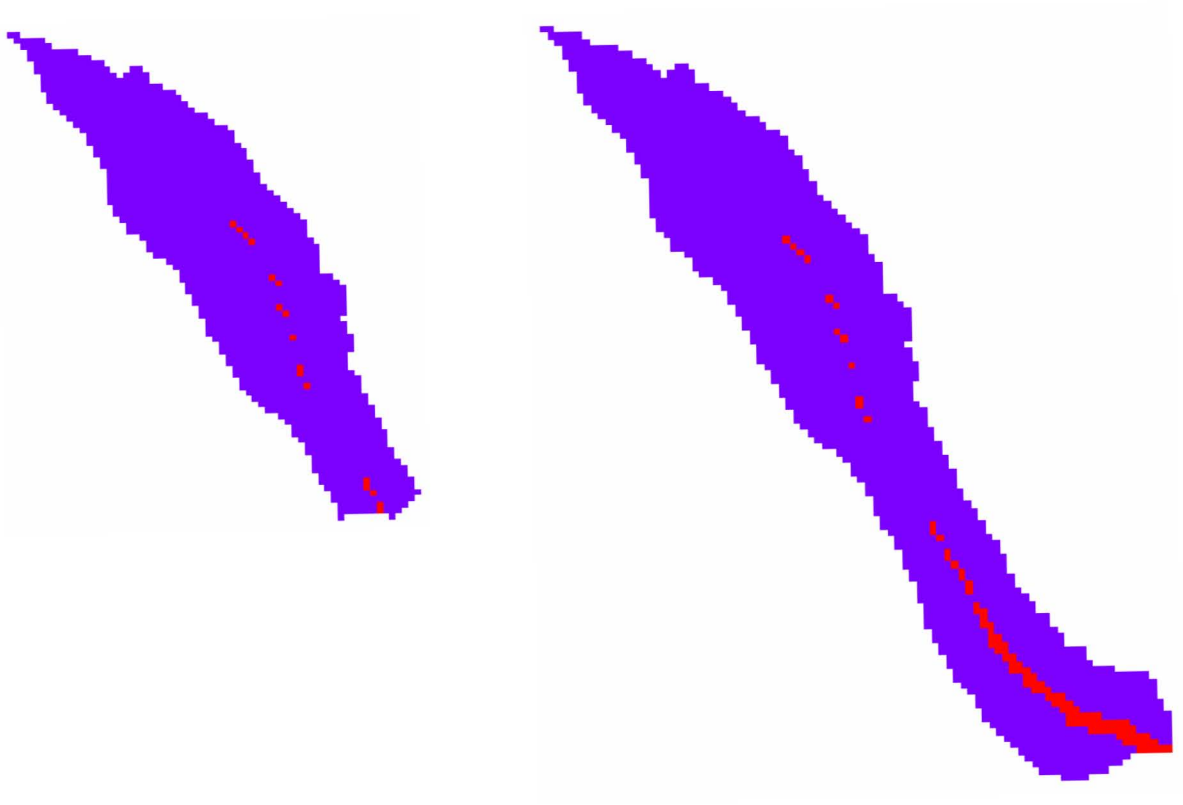

Source: Output DTNs: SN0606T0502206.011 and SN0701T0502206.037, file: \Welcome to Massif\Massif\Validation Analyses\Stream Gauge Comparisons*Streamgage Plots.xmcd*.

Figure 7.1.3-16. Locations of Soil Type 3 in Upper Pagany Wash watershed (left) and Lower Pagany Wash watershed (right) (Note: the Lower Pagany Wash watershed includes the Upper Pagany Wash watershed)

To test if this perturbation is consistent with the Pagany Wash streamflow gauge data, a variation scenario of the Pagany Wash calculations is performed with soil type 3 conductivity set to 7×10^{-6} m/s and the rock conductivities set to 1×10^{-3} m/s. The balance of the soil conductivities are varied as before using a soil saturated conductivity factor. The rest of the input parameters are set to their nominal values as in the base-case scenario described above.

For the Upper Pagany Wash, the calculated annual runoff as a function of soil conductivity factor does not change significantly for the variation scenario (compare Figure 7.1.3-17 to Figure 7.1.3-10). This is because soil type 3 occurs only sporadically in the Upper Pagany Wash (Figure 7.1.3-16). Daily runoff comparisons (Figures 7.1.3-18 and 7.1.3-19) are nearly the same as the base-case calculation (Figures 7.1.3-11 and 7.1.3-12).

For the Lower Pagany Wash, the change in the calculated annual runoff as a function of soil conductivity factor for the variation scenario (Figure 7.1.3-20) is more pronounced. The intercepts between the calculated runoffs (colored lines) and the measured runoff (solid black line) are shifted to the left when compared to the base-case calculation (Figure 7.1.3-13). This means that the conductivities of soils other than type 3 must be lower that in the base case in order to generate more run-on to the locations with soil type 3. In spite of this shift in the intercepts, the calculations of daily runoff (Figures 7.1.3-21 and 7.1.3-22) are comparable to

those for the base-case calculation of runoff (Figures 7.1.3-14 and 7.1.3-15). Both sets of soil saturated conductivities are consistent with the measured runoff data for Pagany Wash.

Despite the good agreement between the observed and predicted runoff in both of these scenarios, there is a pronounced difference in the spatial distribution of net infiltration for each of these scenarios even though the mean value of net infiltration is nearly identical between scenarios. Figures 7.1.3-23 and 7.1.3-25 show net infiltration maps for water year 1995 and 1998, respectively, for the base-case scenario (nominal soil conductivity values multiplied by the factor 0.75). Figures 7.1.3-24 and 7.1.3-26 show net infiltration maps for water year 1995 and 1998, respectively, for the variation scenario (soil type 3 conductivity set to 7×10^{-6} m/s, rock conductivities set to 10^{-3} m/s, and remaining soil conductivity values multiplied by the factor 0.55). The main difference between the scenarios is the location of the net infiltration. In the base-case scenario, net infiltration occurs primarily outside the central stream channel area and is highest in the higher portions of the watershed. In fact, there is little to no net infiltration in the upper reach of the channel and only a minor amount of infiltration in the lower reach. In the variation scenario, the net infiltration in the upper part of the basin is slightly reduced while the infiltration in the lower reach of the channel has increased greatly, especially in areas where soil type 3 is found.

This comparison between the base-case and variation simulations of Pagany Wash illustrates an important point about the inherent uncertainty in the spatial distribution of net infiltration. Soil conductivity values were not screened into the uncertainty analysis presented in Section 6.5 because the parameter uncertainty was either low or the fraction of the UZ model domain that was covered by a given soil type was below the 15% criterion (Section 6.5.2). Soil conductivity was included in the extended parameter sensitivity study (Section 7.1.4) and the uncertainty distributions for soil conductivity were even expanded in an effort to account for the need to adjust soil conductivity to match observed runoff data as described in this section. Nevertheless, soil conductivity did not result in being one of the most sensitive parameters for determining mean net infiltration. However, the present comparison suggests that there may be considerably more uncertainty as to where net infiltration is occurring than is represented by 40 realizations used to characterize infiltration uncertainty analysis in Section 6.5.7. In order to reduce this uncertainty for a given watershed more detailed information concerning the spatial distribution of soil types and properties would be required.

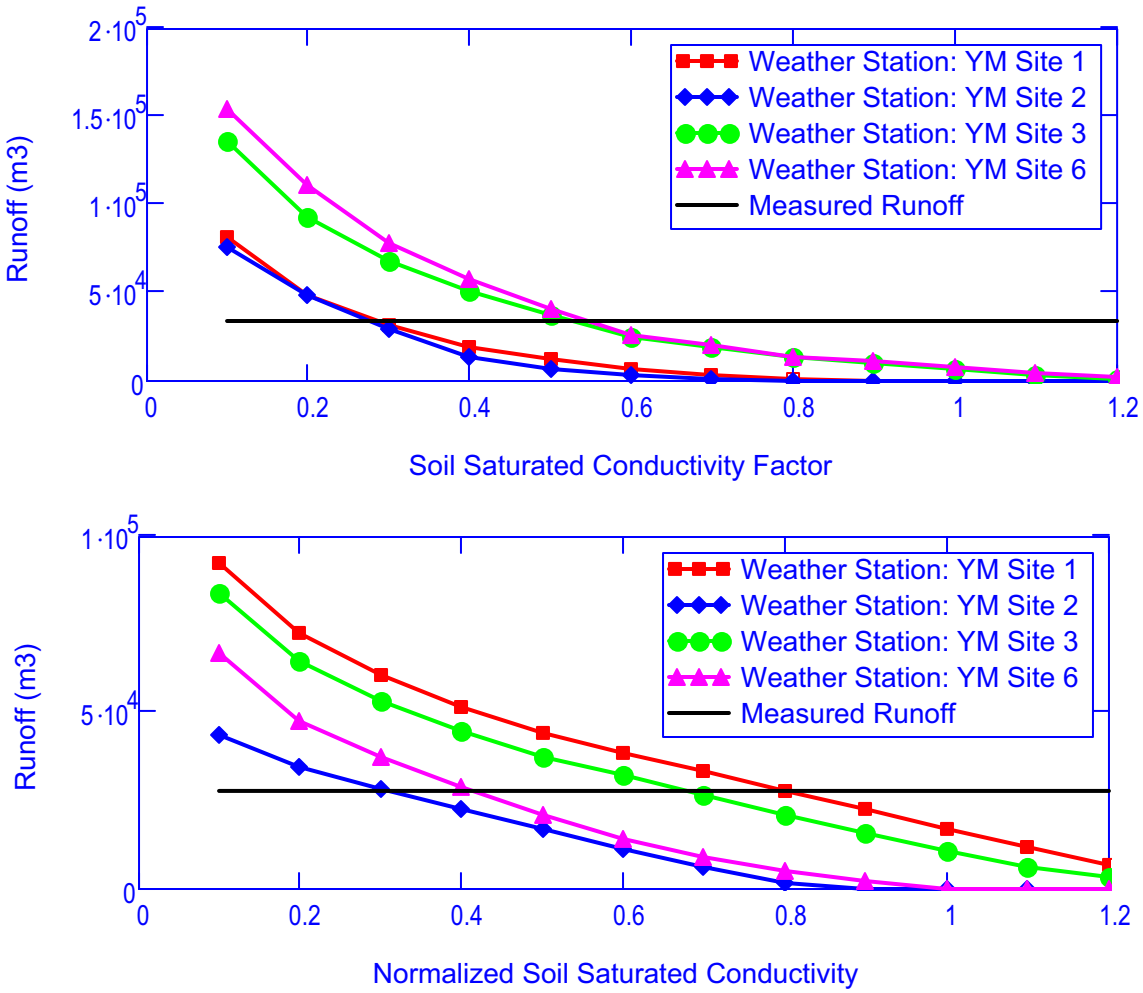

Source: Output DTN: SN0701T0502206.037, file: \Welcome to Massif\Massif\Validation Analyses\Stream Gauge Comparisons*Streamgage Plots.xmcd*.

Figure 7.1.3-17. Variation of Annual Cumulative Runoff with Soil Saturated Conductivity Factor: Soil Type 3 Conductivity Set to 7×10^{-6} m/s (Upper Pagany Wash, Top: Water Year 1995, Bottom: Water Year 1998)

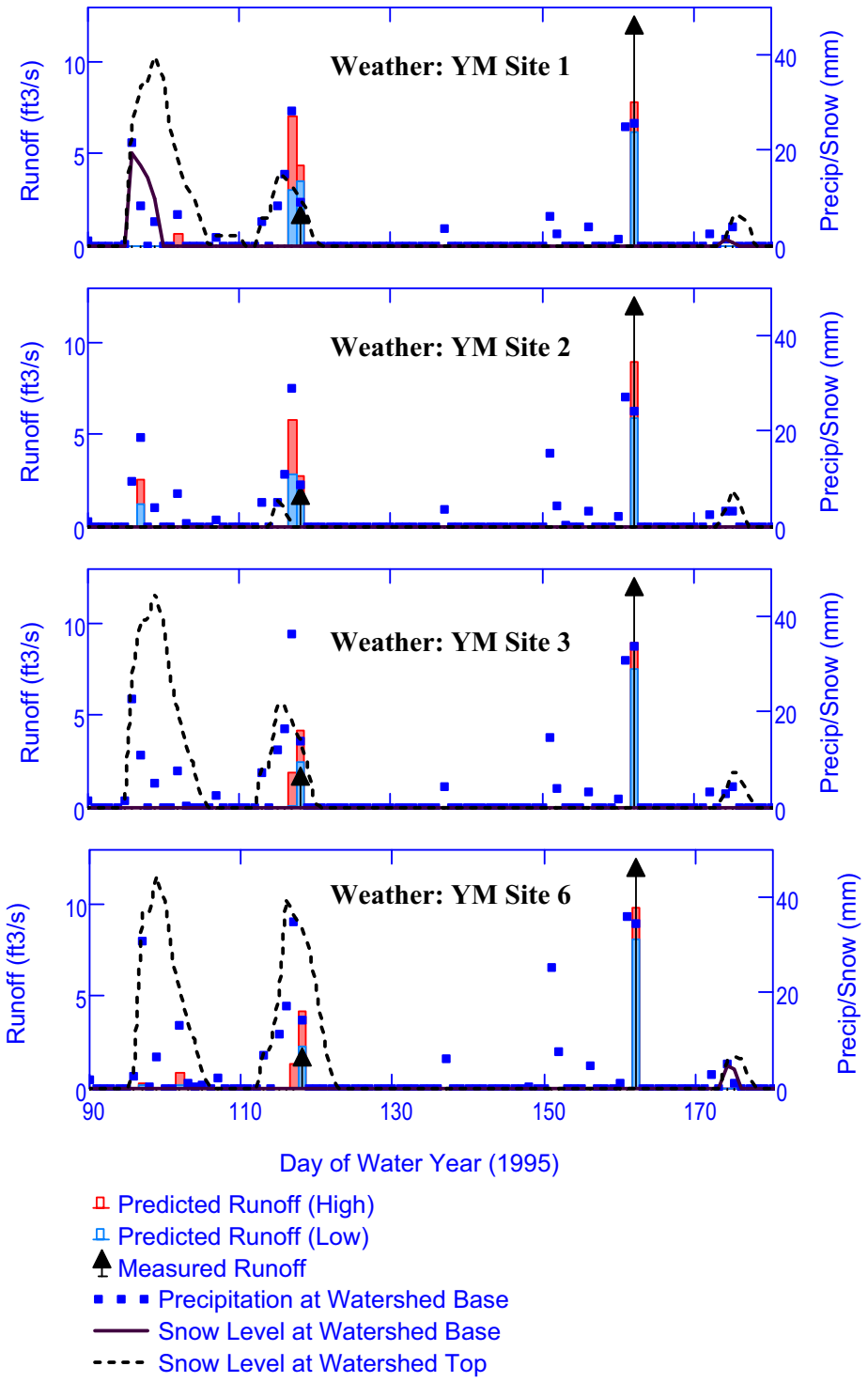

Source: Output DTN: SN0701T0502206.037, file: \Welcome to Massif\Massif\Validation Analyses\Stream Gauge Comparisons*Streamgage Plots.xmcd*.

Figure 7.1.3-18. Predicted (Solid Bar) and Measured (Arrow) Runoff: Soil Type 3 Conductivity Set to 7×10^{-6} m/s (Upper Pagany Wash, Water Year 1995)

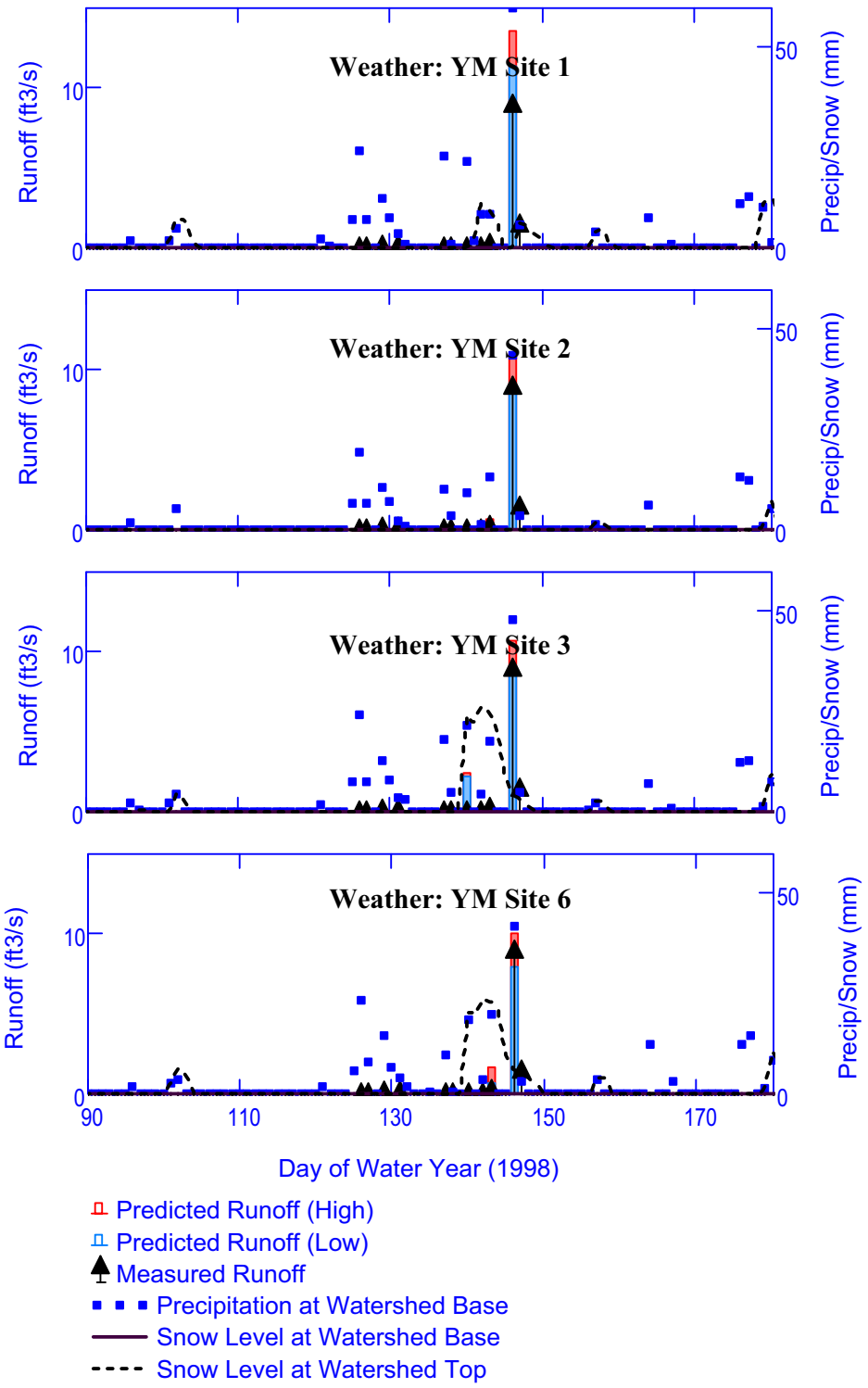

Source: Output DTN: SN0701T0502206.037, file: \Welcome to Massif\Massif\Validation Analyses\Stream Gauge Comparisons*Streamgage Plots.xmcd*.

Figure 7.1.3-19. Predicted (Solid Bar) and Measured (Arrow) Runoff: Soil Type 3 Conductivity set to 7×10^{-6} m/s (Upper Pagany Wash, Water Year 1998)

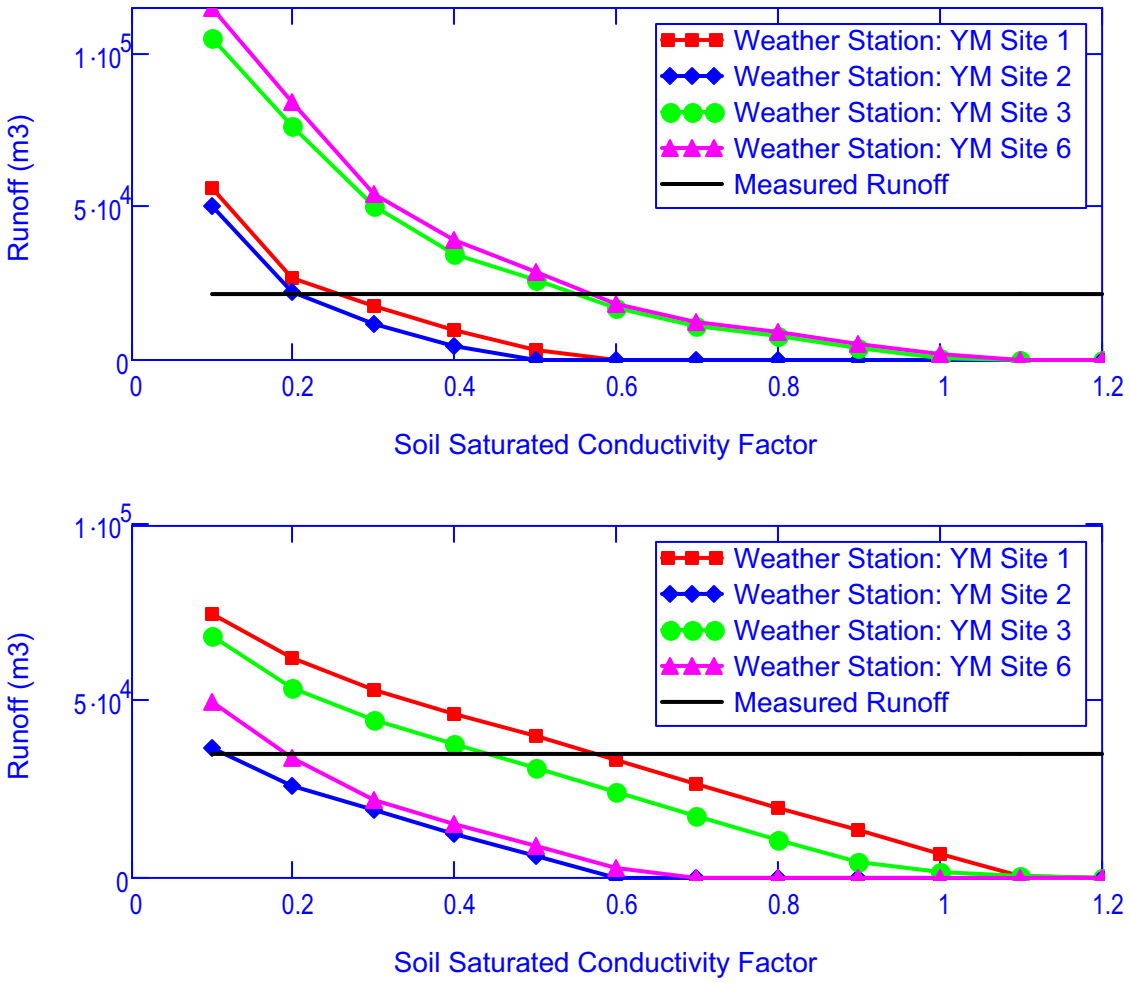

Source: Output DTN: SN0701T0502206.037, file: \Welcome to Massif\Massif\Validation Analyses\Stream Gauge Comparisons*Streamgage Plots.xmcd*.

Figure 7.1.3-20. Variation of Annual Cumulative Runoff with Soil Saturated Conductivity Factor: Soil Type 3 Conductivity Set to 7×10^{-6} m/s (Lower Pagany Wash, Top: Water Year 1995, Bottom: Water Year 1998)

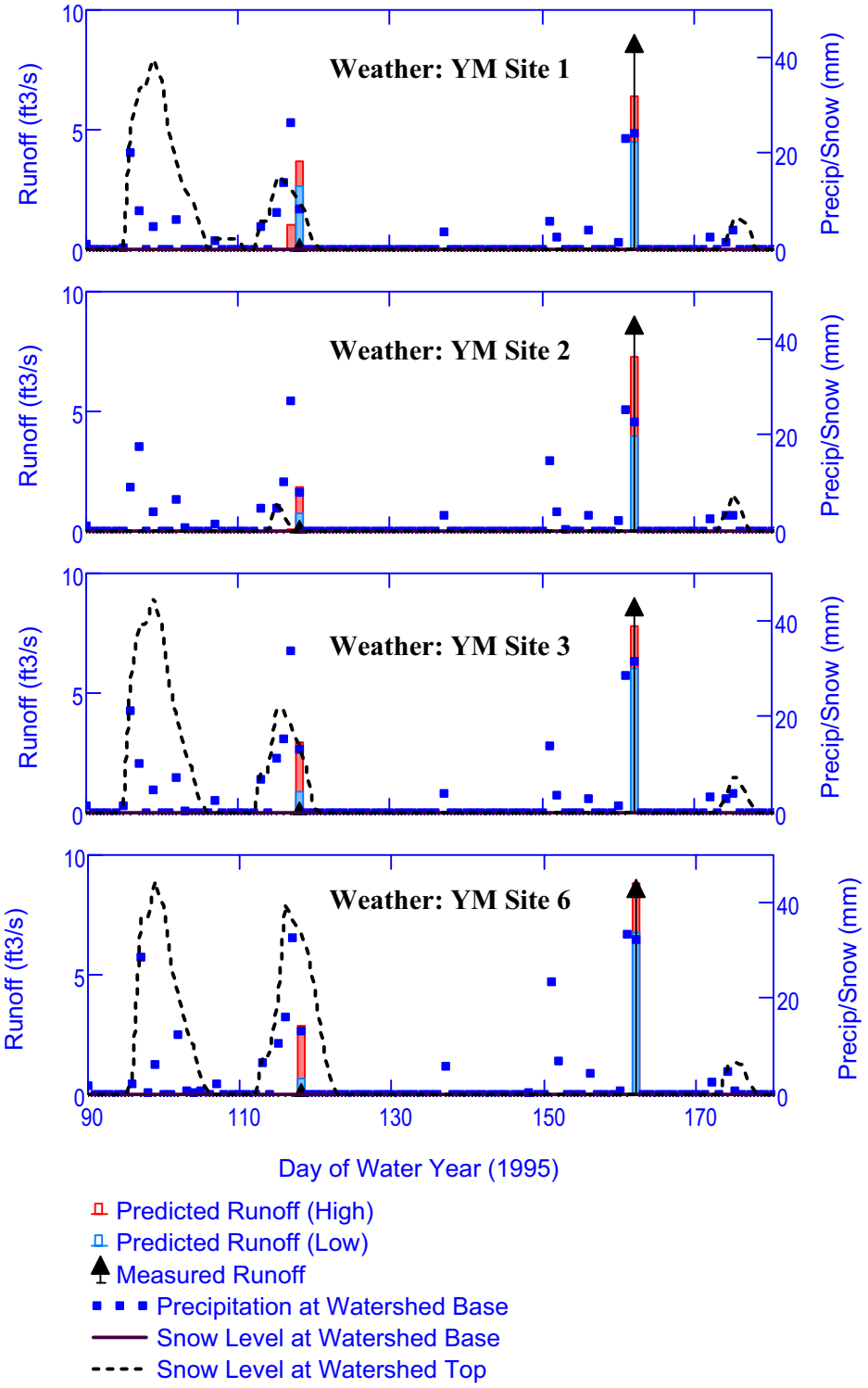

Source: Output DTN: SN0701T0502206.037, file: \Welcome to Massif\Massif\Validation Analyses\Stream Gauge Comparisons*Streamgage Plots.xmcd*.

Figure 7.1.3-21. Predicted (Solid Bar) and Measured (Arrow) Runoff: Soil Type 3 Conductivity Set to 7×10^{-6} m/s (Lower Pagany Wash, Water Year 1995)

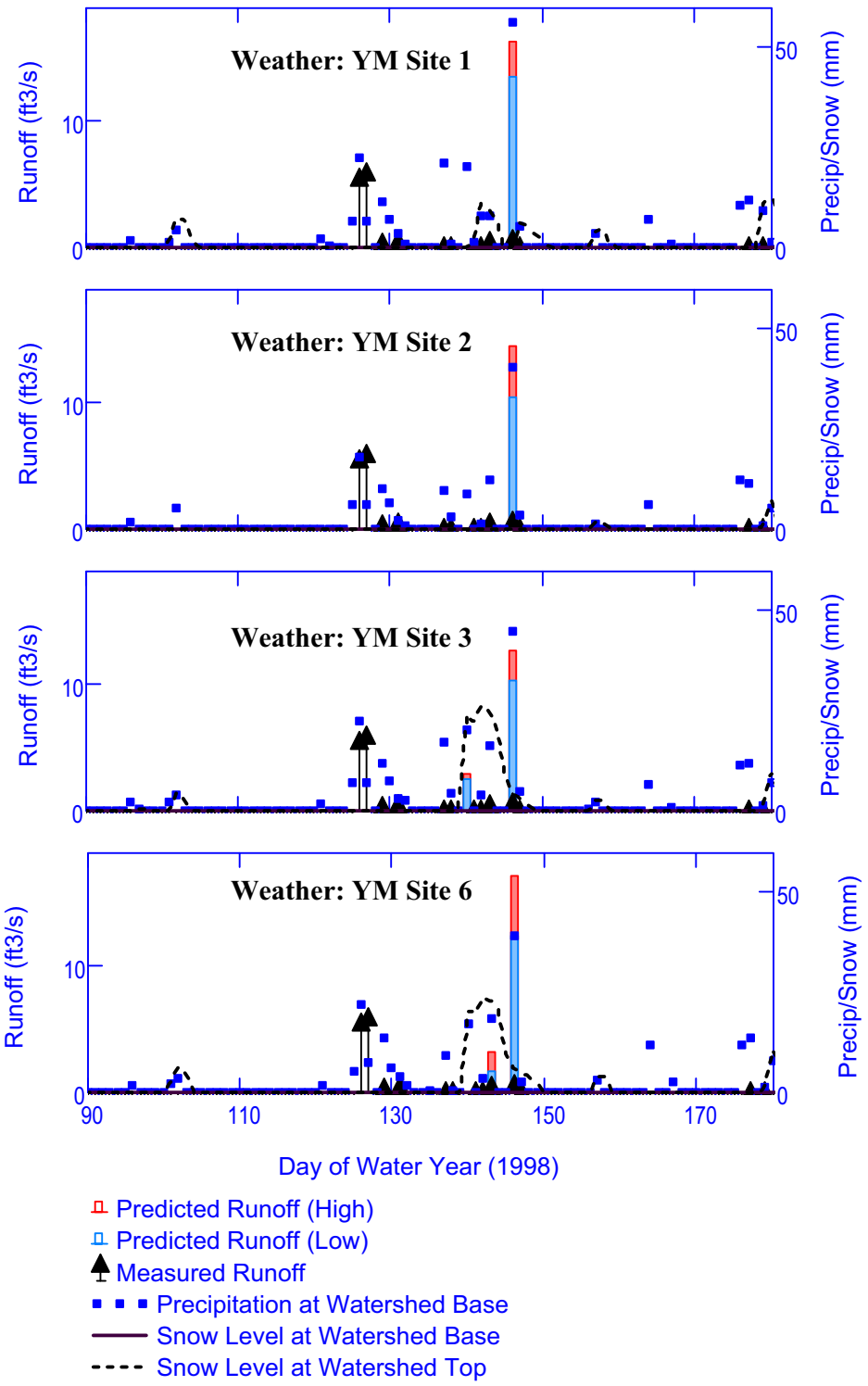

Source: Output DTN: SN0701T0502206.037, file: \Welcome to Massif\Massif\Validation Analyses\Stream Gauge Comparisons*Streamgage Plots.xmcd*.

Figure 7.1.3-22. Predicted (Solid Bar) and Measured (Arrow) Runoff: Soil Type 3 Conductivity set to 7×10^{-6} m/s (Lower Pagany Wash, Water Year 1998)

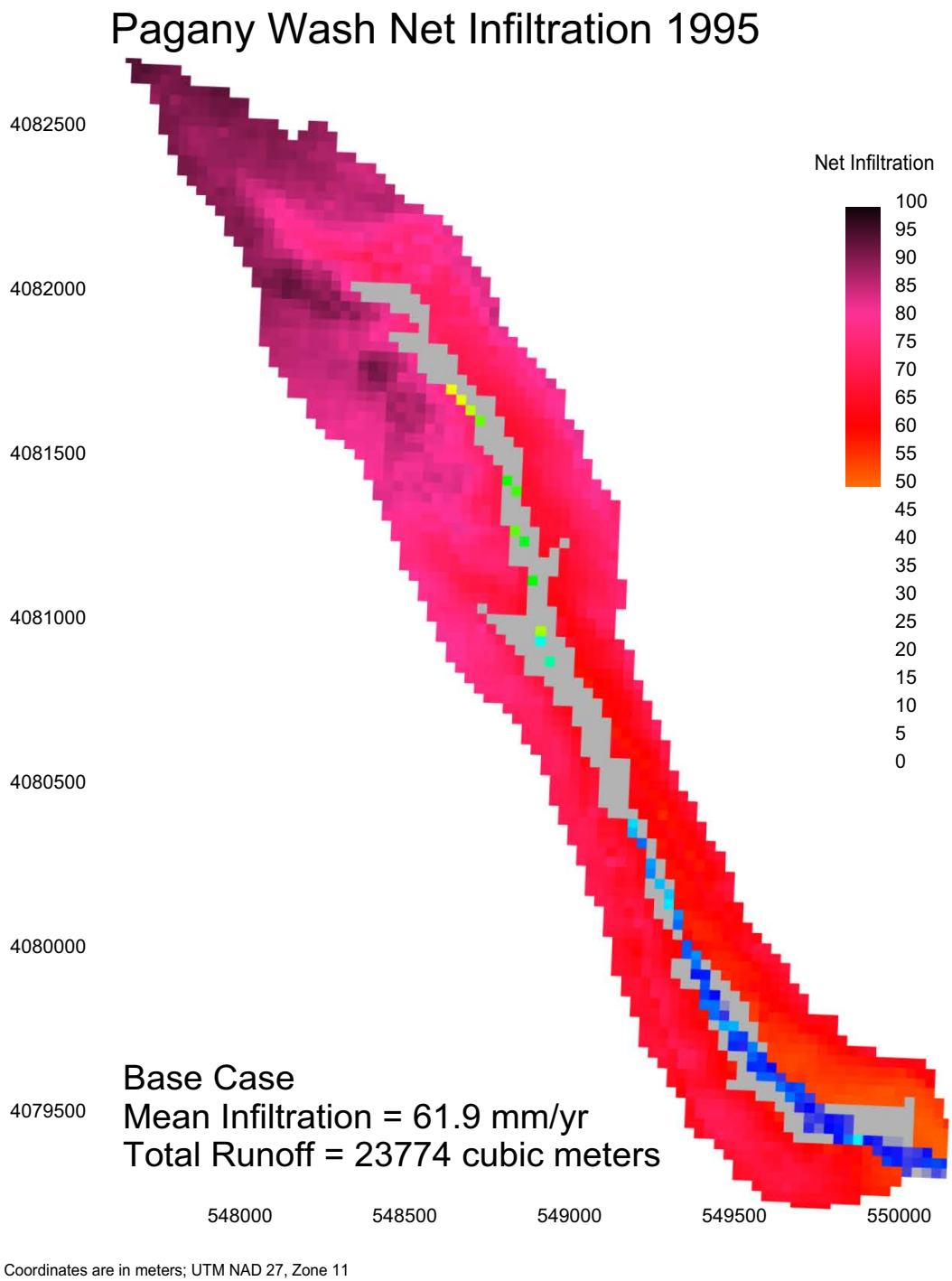

Source: Output DTN: SN0701T0502206.037, file: \Welcome to Massif\Massif\Validation Analyses\Stream Gauge Comparisons*Infiltration Study Post Processing.xmcd*.

Figure 7.1.3-23. Net Infiltration Map for the Base-case Simulation at Pagany Wash for the Water Year 1995

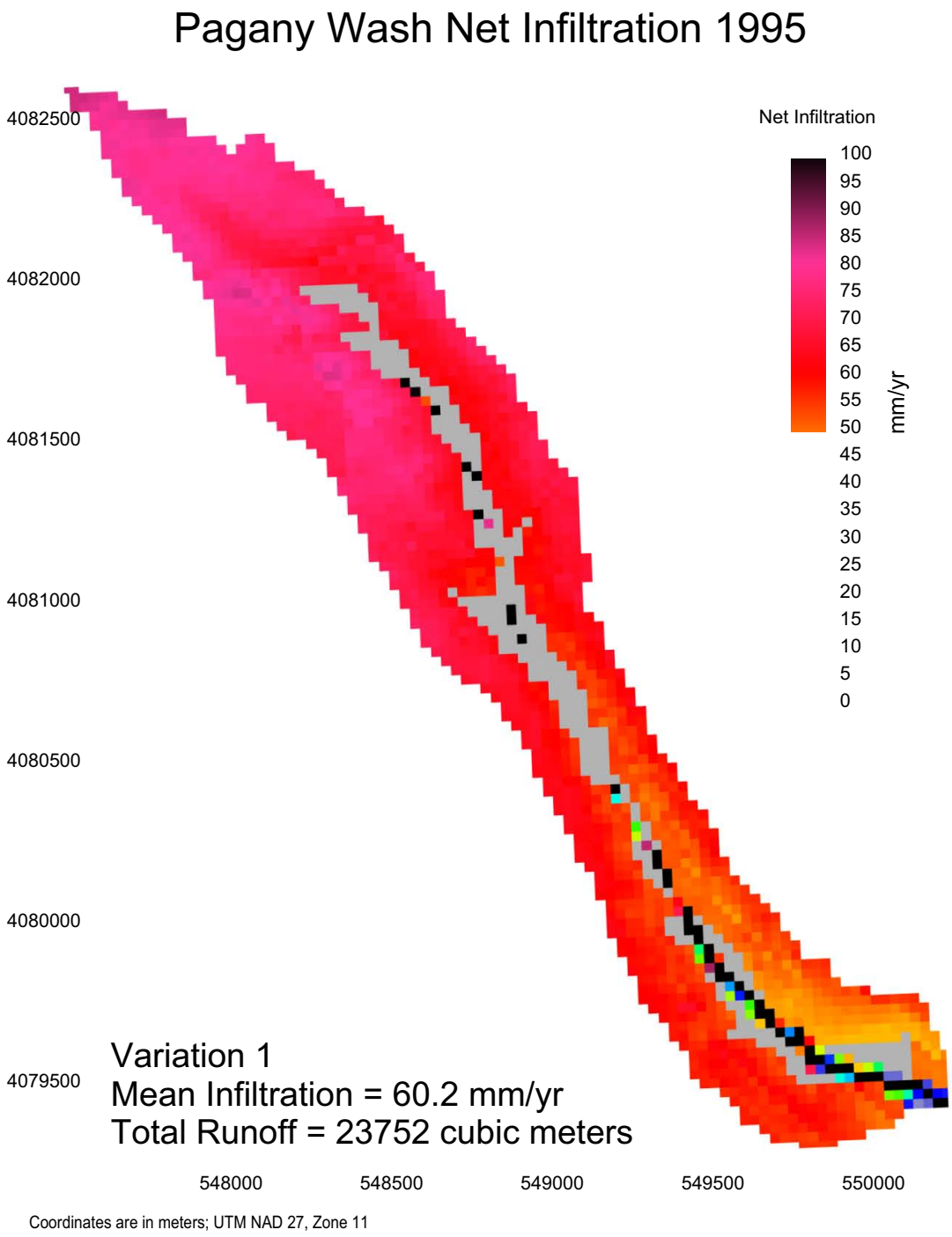

Source: Output DTN: SN0701T0502206.037, file: \Welcome to Massif\Massif\Validation Analyses\Stream Gauge Comparisons*Infiltration Study Post Processing.xmcd*.

NOTE: Upper end of the color scale is truncated such that cells that are colored black have infiltration greater than or equal to 100 mm/yr. Maximum net infiltration for this run is 463 mm/yr.

Figure 7.1.3-24. Net Infiltration Map for the Variation 1 Simulation at Pagany Wash for the Water Year1995

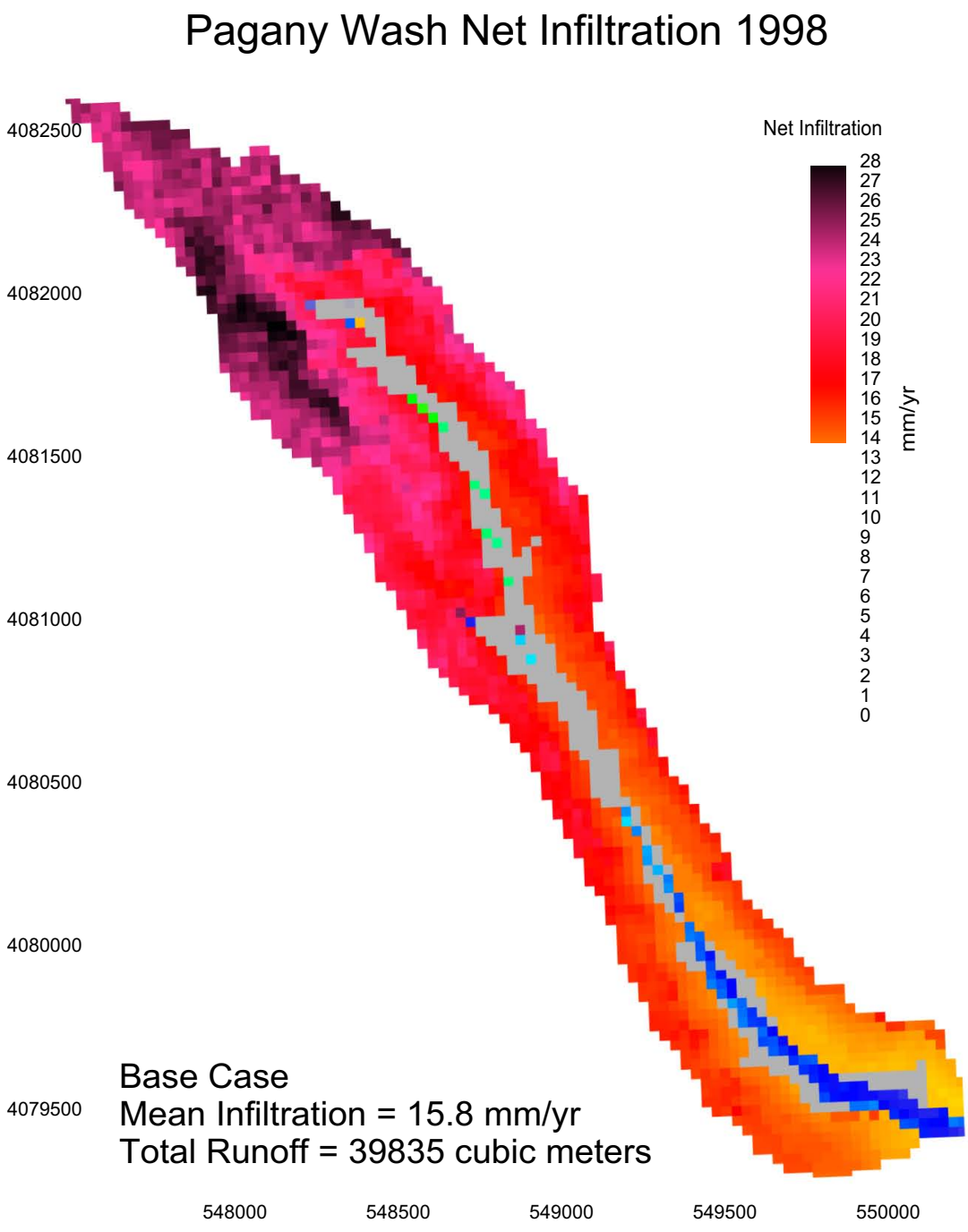

Source: Output DTN: SN0701T0502206.037, file: \Welcome to Massif\Massif\Validation Analyses\Stream Gauge Comparisons*Infiltration Study Post Processing.xmcd*.

Figure 7.1.3-25. Net Infiltration Map for the Base-case Simulation at Pagany Wash for the Water Year 1998

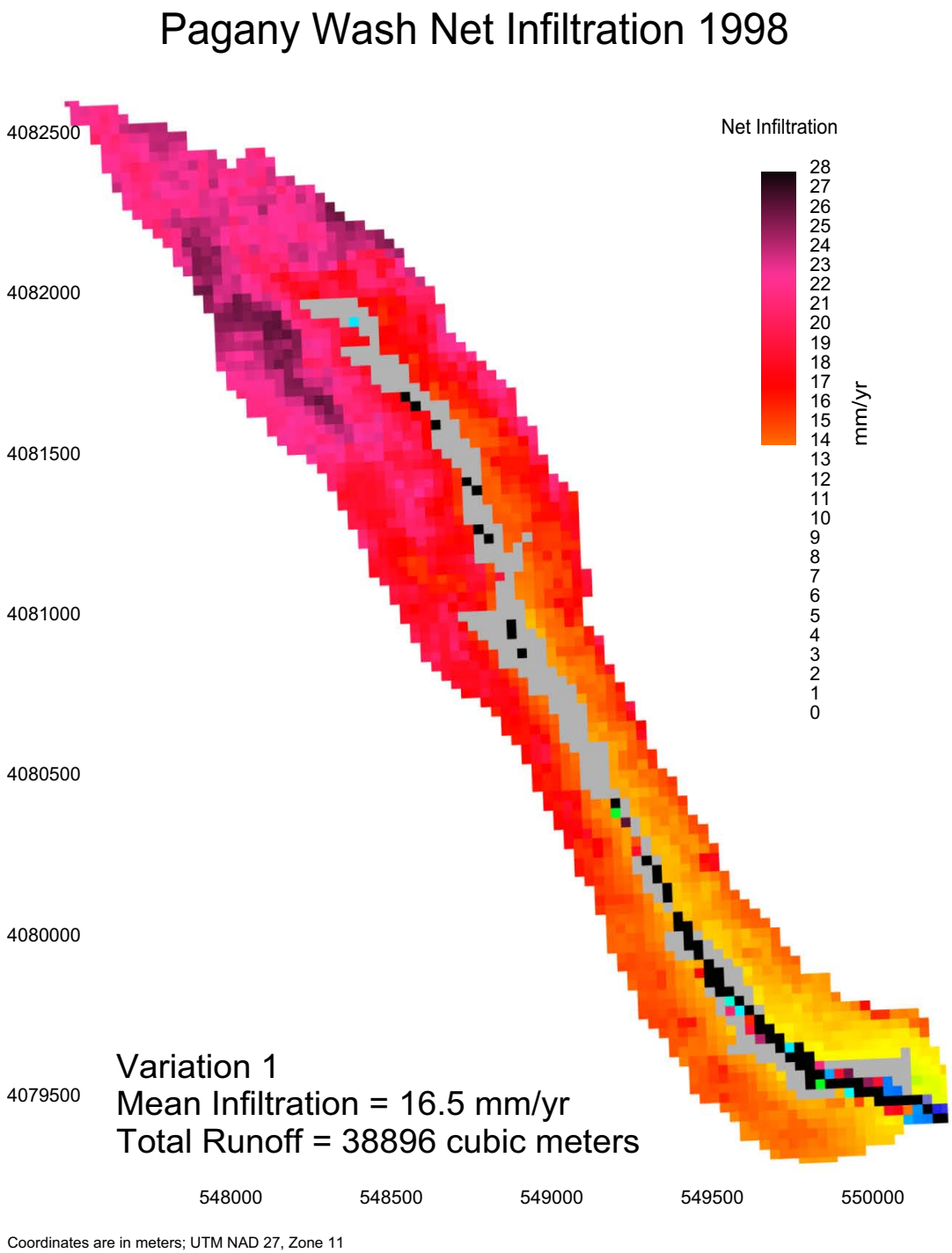

Coordinates are in meters; UTM NAD 27, Zone 11

Source: Output DTN: SN0701T0502206.037, file: \Welcome to Massif\Massif\Validation Analyses\Stream Gauge Comparisons*Infiltration Study Post Processing.xmcd*.

NOTE: Upper end of the color scale is truncated such that cells that are colored black have infiltration greater than or equal to 28 mm/yr. Maximum net infiltration for this run is 129 mm/yr.

Figure 7.1.3-26. Net Infiltration Map for the Variation 1 Simulation at Pagany Wash for the Water Year 998

7.1.3.2 Soil Conductivity Variation Illustration for Entire Net Infiltration Modeling Domain

When calculating runoff at monitored streamflow gauge sites (Section 7.1.3.2), a variation scenario was simulated for Pagany Wash watershed in which the soil conductivity of the dominant soil type representing stream channels (soil type 3) was increased by an order of magnitude while the conductivity of the other soil types was decreased by a constant factor. This scenario was investigated because of the LeCain borehole data on infiltration (Section 7.2.1.1.2). A conclusion of this scenario was to point out that the spatial distribution of soil conductivity plays an important role in determining the spatial distribution of net infiltration.

To explore the implications of the Pagany Wash study on the larger modeled domain, the four representative realizations (10th, 30th, 50th, and 90th) from the Present-Day simulations were run using an alternate soil conductivity assignment, as defined by the Pagany Wash example. Specifically, the four realizations identified in Table 6.5.7.1-3 were run with the following modifications: 1) the conductivity of soil types 3 and 4 were set to 7×10^{-6} m/s, 2) the rock conductivities were set uniformly to 10^{-3} m/s, and 3) the conductivity of the soil types other than 3 and 4 were reduced by a factor of 0.44. Soil types 3 and 4 were selected because, in general, these soil types are associated with the main stream channels (see Figure 6.5.2.2-2). These alternate runs are meant only as an example of how such differences could affect the final infiltration results. The choice of the specific soil conductivities is based on Pagany Wash simulations and data from a single high precipitation year, and this choice is probably not representative of the rest of the domain. Nevertheless, these results illustrate aspects of model sensitivity that are not explored in the sensitivity studies that look at spatial averages of net infiltration.

Figures 7.1.3.2-1 to 7.1.3.2-4 show net infiltration maps for the alternate soil conductivity realizations: 10th, 30th, 50th, 90th, respectively. These maps can be compared to Figures 6.5.7.1-2 to 6.5.7.1-5 to see how this change affects the patterns of net infiltration. One obvious difference is that the stream channels show up clearly on the infiltration maps representing the alternate soil conductivity scenario.

To quantitatively summarize these comparisons, two tables are presented below. Table 7.1.3.2-1 compares mean net infiltration over three different domains (net infiltration model domain, UZ model domain, and the repository footprint) for each realization. In addition, the runoff fraction is compared and the total weighted precipitation for each realization is listed. The tabulated results suggest that mean net infiltration over these regions and the total runoff leaving the domain are not significantly altered by this variation in soil conductivity.

Table 7.1.3.2-2 compares the percent of the total infiltration that occurs in each soil group. It is here that a significant difference can be seen from the original base-case results. In the base-case realizations, between 76% and 97% of the total net infiltration occurred in areas covered with soil types 5, 7, or 9. In the alternate soil conductivity (Variation) runs, this percentage range fell to 34% to 70%. The fraction of the total infiltration in soil types 3 and 4, increased from a range of 0.2% to 11% to a range of 20% to 55%. The lesson learned from these results is that it is impossible to determine from the available characterization data exactly where the bulk of the net infiltration occurs. Furthermore, the results suggest that the predicted mean net infiltration

over relatively large areas (e.g., UZ model domain and repository footprint) is fairly stable. It is the spatial distribution of net infiltration that is especially sensitive to the spatial distribution of soil properties.

Table 7.1.3.2-1. Comparison of Mean Net Infiltration Results of the Soil Conductivity Variation Simulations with Results of the Uncertainty Analysis

Present-Day Climate				
Percentile	10th	30th	50th	90th
Replicate	R2	R2	R2	R2
Realization	10	2	8	14
Entire Domain Infiltration (mm/yr)	3.9	7.3	13.0	26.7
Entire Domain Variation Infiltration (mm/yr)	4.1	7.7	15.9	27.2
UZ Infiltration (mm/yr)	3.4	6.0	10.9	28.7
UZ Variation Infiltration (mm/yr)	3.5	5.9	13.4	27.5
Repository Infiltration (mm/yr)	3.9	6.5	10.9	34.4
Repository Variation Infiltration (mm/yr)	3.9	4.9	9.5	28.3
Runoff Fraction (%)	0.9	1.8	3.8	1.3
Runoff Fraction Variation (%)	0.8	1.6	3.2	1.1
Mean Annual Precipitation (mm/yr)	144.1	160.6	189.3	212.7

Source: Output DTN: SN0701T0502206.037, file: \Welcome to Massif\Massif\Post Processing All Climates*PD Soil Conductivity Variation Study.xls*.

Table 7.1.3.2-2. Comparison of Percent of the Total Net Infiltration Occurring in Each Soil Group between the Soil Conductivity Variation Simulations and the Results of the Uncertainty Analysis

Present-Day Climate	Percent of Net Infiltration [%]			
Percentile	10th	30th	50th	90th
Replicate	R2	R2	R2	R2
Realization	10	2	8	14
Soil Group 1 (%)	0.2	0.7	3.5	0.0
Soil Group 1 Variation (%)	0.0	0.1	0.6	0.0
Soil Groups 2/6 (%)	0.4	1.0	5.2	0.0
Soil Groups 2/6 Variation (%)	0.0	0.1	0.7	0.0
Soil Groups 3/4 (%)	1.4	2.3	10.6	0.2
Soil Groups 3/4 Variation (%)	19.7	35.4	55.1	24.9
Soil Groups 5/7/9 (%)	85.7	88.6	76.0	97.1
Soil Groups 5/7/9 Variation (%)	66.6	54.6	34.4	69.9
Soil Group 8 (%)	12.3	7.3	4.7	2.7
Soil Group 8 Variation (%)	13.7	9.8	9.2	5.2

Source: Output DTN: SN0701T0502206.037, file: \Welcome to Massif\Massif\Post Processing All Climates*PD Soil Conductivity Variation Study.xls.*

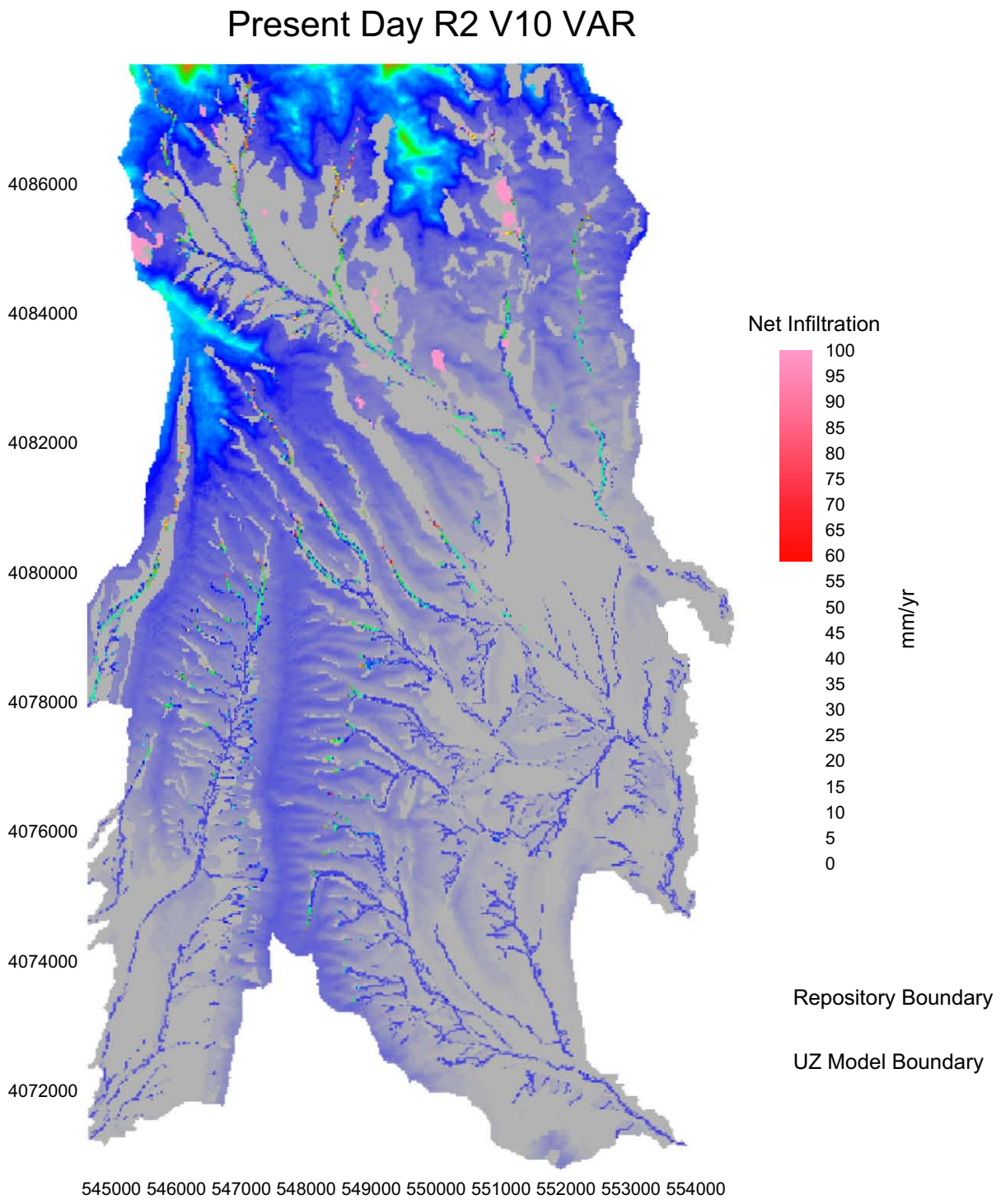

Coordinates are in meters; UTM NAD 27, Zone 11

Source: Output DTN: SN0701T0502206.037, file: \Welcome to Massif\Massif\Present Day Uncertainty\Infiltration Map Variations*Present Day R2 V10.xmcd* (net infiltration results from soil conductivity variation study); Output DTN: SN0612FTPRNUZB.002 (UZ model and repository boundaries).

Figure 7.1.3.2-1. Present-Day, 10th Percentile Net Infiltration Map (Soil Conductivity Variation) (Replicate R2, Realization 10)

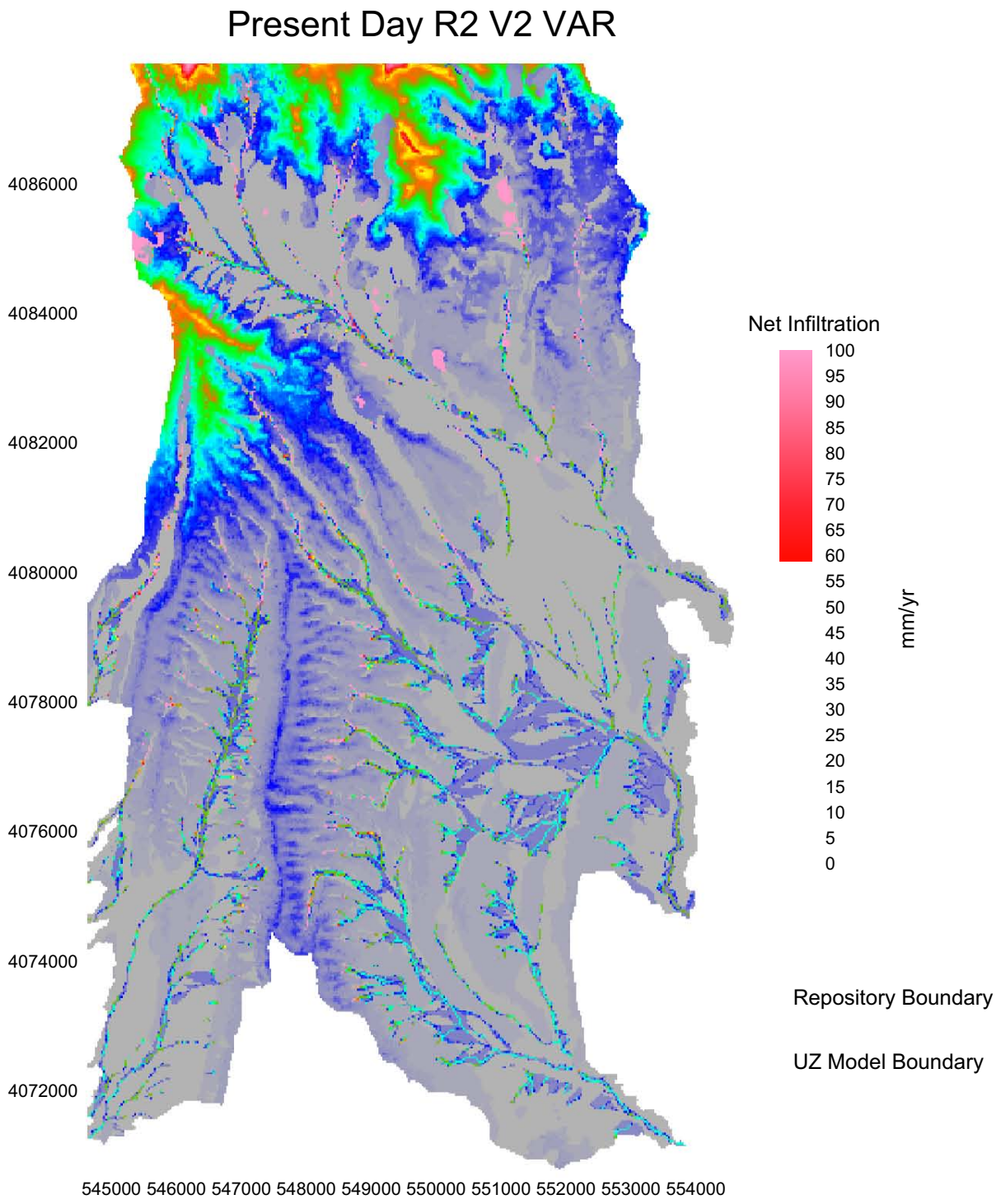

Source: Output DTN: SN0701T0502206.037, file: \Welcome to Massif\Massif\Present Day Uncertainty\Infiltration Map Variations*Present Day R2 V02.xmcd* (net infiltration results from soil conductivity variation study); Output DTN: SN0612FTPRNUZB.002 (UZ model and repository boundaries).

Figure 7.1.3.2-2. Present-Day, 30th Percentile Net Infiltration Map (Soil Conductivity Variation) (Replicate R2, Realization 2)

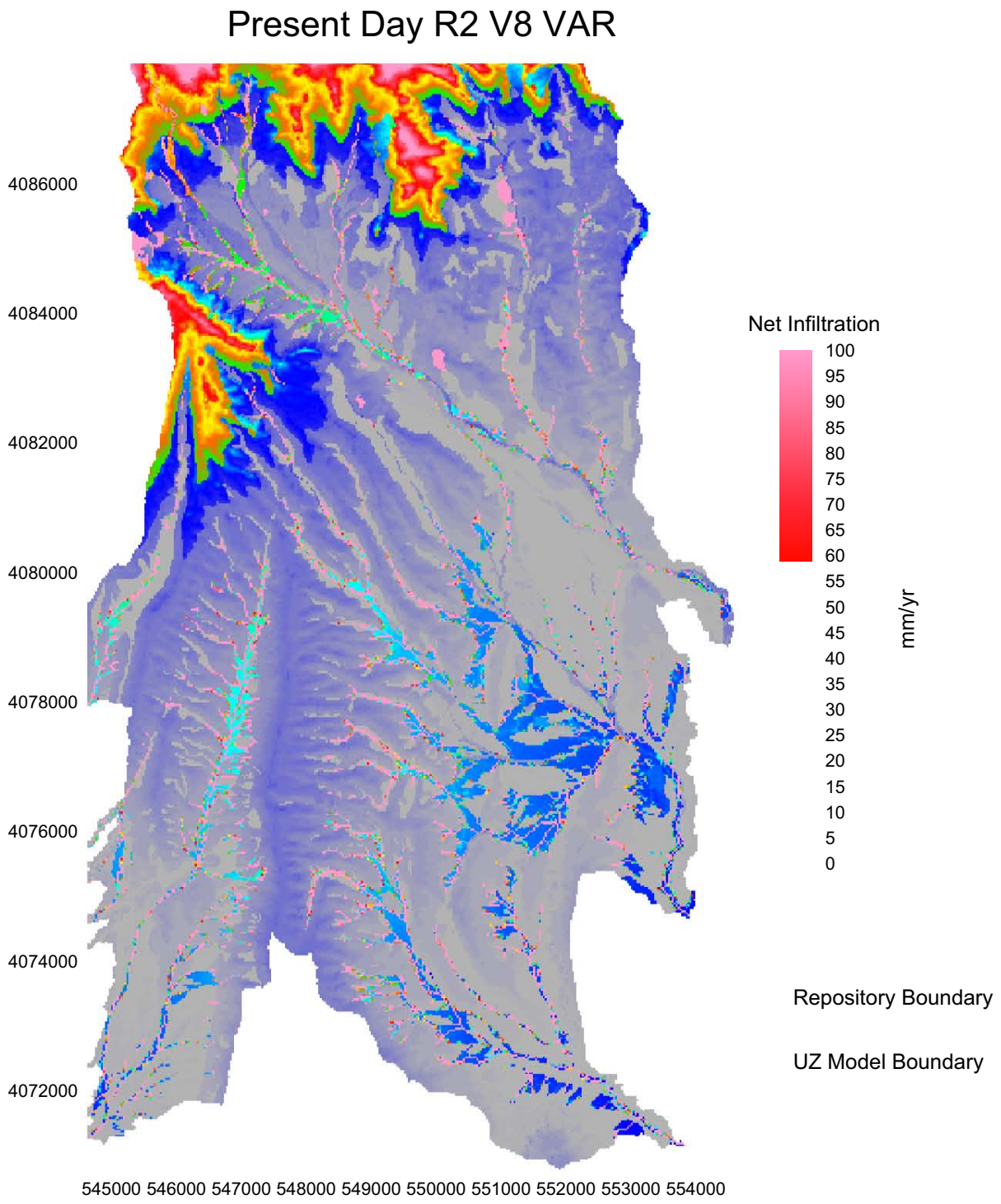

Source: Output DTN: SN0701T0502206.037, file: \Welcome to Massif\Massif\Present Day Uncertainty\Infiltration Map Variations*Present Day R2 V08.xmcd* (net infiltration results from soil conductivity variation study); Output DTN: SN0612FTPRNUZB.002 (UZ model and repository boundaries).

Figure 7.1.3.2-3. Present-Day, 50th Percentile Net Infiltration Map (Soil Conductivity Variation) (Replicate R2, Realization 8)

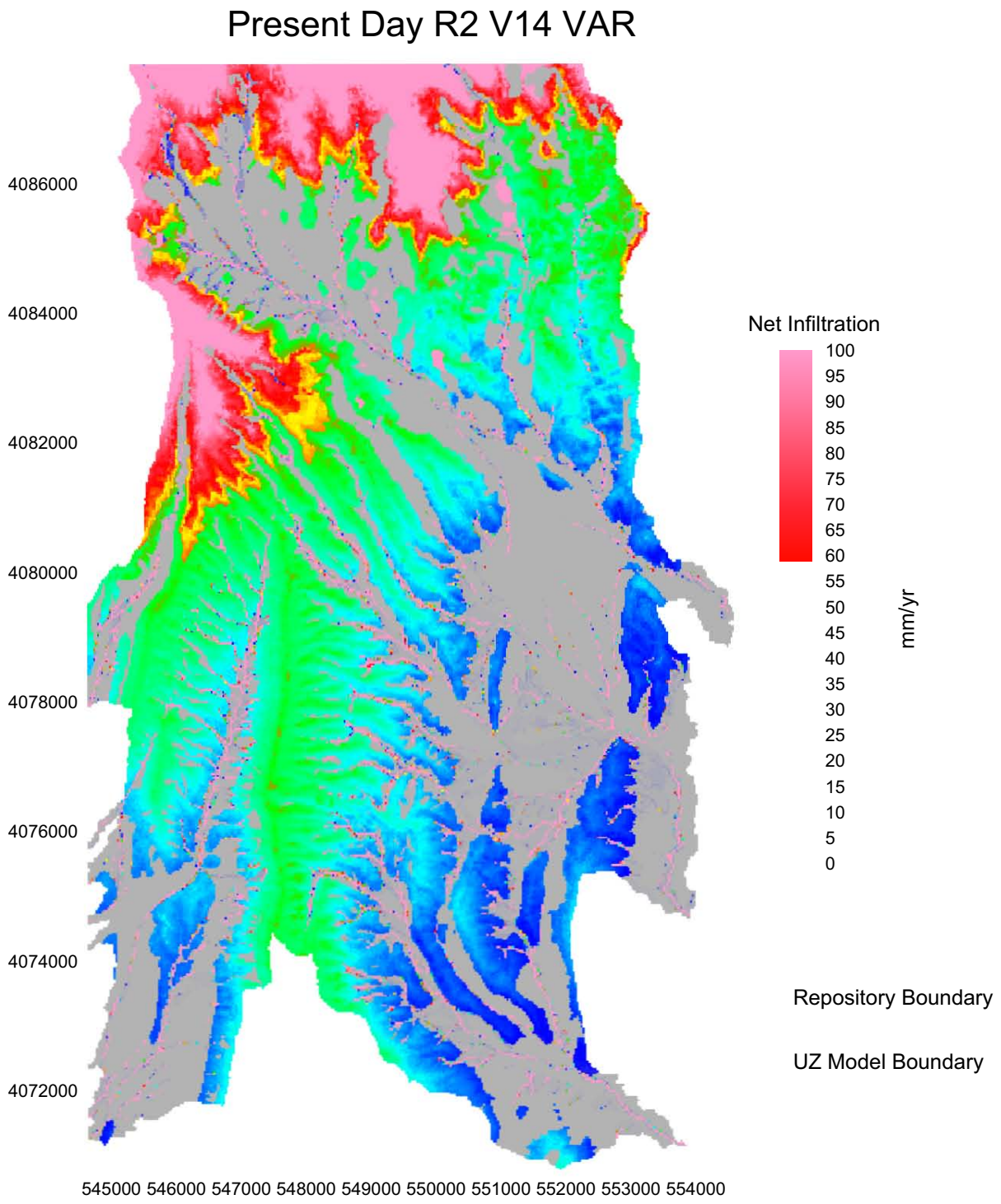

Coordinates are in meters; UTM NAD 27, Zone 11

Source: Output DTN: SN0701T0502206.037, file: \Welcome to Massif\Massif\Present Day Uncertainty\Infiltration Map Variations*Present Day R2 V14.xmcd* (net infiltration results from soil conductivity variation study); Output DTN: SN0612FTPRNUZB.002 (UZ model and repository boundaries).

Figure 7.1.3.2-4. Present-Day, 90th Percentile Net Infiltration Map (Soil Conductivity Variation) (Replicate R2, Realization 14)

7.1.4 Extended Parameter Sensitivity Study (Large LHS)

In an effort to confirm that the parameter screening criteria described in Section 6.5.5 and Appendix I did not inadvertently exclude a parameter that significantly influenced mean net infiltration, an extended parameter sensitivity study was performed. This extended study allowed 42 uncertain parameters to be varied in LHS (Output DTN: SN0701T0502206.043). A total of 200 realizations were run for the Drill Hole Wash watershed, which covers most of the repository footprint, using a single Present-Day weather input file (Output DTN: SN0701T0502206.037).

Table 7.1.4-1 lists the 42 parameter allowed to vary in this study along with their uncertainty distributions, units, and associated symbols (or descriptions) used in the report.

Table 7.1.4-1. Results of Stepwise Regression Analysis on Raw and Rank Data for Infiltration Estimate on Watershed

	LHS Name	Symbol or Description	Distribution	P1	P2	Units
1	lnRks_401	$K_{sat\_rock}(401)$	Loguniform	−15.38	−11.94	m/s
2	lnRks_402	$K_{sat\_rock}(402)$	Loguniform	−17.26	−11.97	m/s
3	lnRks_403	$K_{sat\_rock}(403)$	Loguniform	−15.42	−11.94	m/s
4	lnRks_404	$K_{sat\_rock}(404)$	Loguniform	−17.64	−12.4	m/s
5	lnRks_405	$K_{sat\_rock}(405)$	Loguniform	−16.39	−12.25	m/s
6	lnRks_406	$K_{sat\_rock}(406)$	Loguniform	−17.68	−11.77	m/s
7	lnRks_407	$K_{sat\_rock}(407)$	Loguniform	−17.78	−12.01	m/s
8	lnRks_408	$K_{sat\_rock}(408)$	Loguniform	−17.09	−11.55	m/s
9	lnRks_412	$K_{sat\_rock}(412)$	Loguniform	−12.59	−11.88	m/s
10	lnRks_414	$K_{sat\_rock}(414)$	Loguniform	−13.55	−12.02	m/s
11	lnRks_418	$K_{sat\_rock}(418)$	Loguniform	−16.92	−11.75	m/s
12	SDepth2	$depth_{soil}(2)$	Normal	10.9	22	m
13	SDepth3	$depth_{soil}(3)$	Uniform	2.1	3.2	m
14	SDepth4	$depth_{soil}(4)$	Uniform	0.1	0.5	m
15	Kc_min	K_{c_min}	Cumulative			none
16	Hc_579	$\theta_s(5/7/9)$	Uniform	9.00E-02	0.17	none
17	Hc_26	$\theta_s(2/6)$	Uniform	8.00E-02	0.15	none
18	Hc_34	$\theta_s(3/4)$	Uniform	5.00E-02	0.1	none
19	lnKs_579	$K_{sat\_soil}(5/7/9)$	Lognormal	−10.34	−8.85	cm/s
20	lnKs_26	$K_{sat\_soil}(2/6)$	Lognormal	−10.15	−8.06	cm/s
21	lnKs_34	$K_{sat\_soil}(3/4)$	Lognormal	−10.49	−8.65	cm/s
22	SWC_579	$\theta_s(5/7/9)$	Normal	0.21	0.25	none
23	SWC_26	$\theta_s(2/6)$	Normal	0.17	0.25	none
24	SWC_34	$\theta_s(3/5)$	Normal	0.14	0.18	none
25	p	p	Uniform	0.5	0.8	none
26	Z_r	Z_r	Uniform	0.6	2.6	m
27	h_plant	h_{plant}	Uniform	0.2	0.6	m
28	K0wint	$K_{o\ winter}$	Uniform	0	10	ºC

Table 7.1.4-1. Results of Stepwise Regression Analysis on Raw and Rank Data for Infiltration Estimate on Watershed (Continued)

	LHS Name	Symbol or Description	Distribution	P1	P2	Units
29	K0rest	$K_{o\ rest}$	Uniform	0	10	ºC
30	Sublim	$C_{sublime}$	Uniform	0	0.2	none
31	MAXPREC	Maximum daily precipitation	Uniform	496	983	mm
32	PREC_LR	$C_{Precipcor}$	Normal	4.1	8.5	%/100m
33	Smelt	$C_{snowmelt}$	Uniform	1	3	none
34	TEMP_LR	*LR*	Uniform	6.50E-03	1.00E-02	ºC/m
35	FDOY_DP	starting DOY for winter dew point	Uniform	274	335	none
36	LDOY_DP	ending DOY for winter dew point	Uniform	90	151	none
37	SLPRD	slope	Normal	0.23	0.53	
38	COEFHAR	K_{Rs}	Uniform	0.15	0.22	$ºC^{-0.5}$
39	Z_e	Z_e	Uniform	0.1	0.2	m
40	REW	*REW*	Uniform	2	10	mm
41	C_Kcb2	C_{Kcb2}	Normal	3.2	16.2	none
42	albedo	α_T	Uniform	0.15	0.9	none

Source: Output DTN: SN0701T0502206.043, file: *LHS_PD_SA.OUT*.

P1 and P2 represent minimum and maximum values for uniform distributions and 0.1% and 99.9% values for normal distributions. Values are natural log transformed for loguniform and lognormal distributions.

Stepwise regression analysis was performed on the mean net infiltration results considering both raw and rank transformed input parameters. The results of this analysis are shown in Table 7.1.4-2. The parameters are listed in order of decreasing influence.

Table 7.1.4-2. Results of Stepwise Regression Analysis on Raw and Rank Data for Infiltration Estimate on Watershed

	Stepwise Regression (linear)				Stepwise Regression (rank)			
Step	Variable	tot. R^2	inc. R^2	SRC	Variable	tot. R^2	inc. R^2	SRRC
1	SDepth4	0.61	0.61	−0.79	SDepth4	0.61	0.61	−0.79
2	Hc_579	0.78	0.17	−0.42	Hc_579	0.82	0.21	−0.46
3	K0wint	0.81	0.03	−0.17	K0wint	0.85	0.03	−0.18
4	Z_r	0.84	0.03	−0.18	Z_r	0.87	0.02	−0.15
5	Z_e	0.85	0.01	−0.11	lnKs_579	0.89	0.01	0.11
6	lnKs_579	0.86	0.01	0.10	Z_e	0.90	0.01	−0.10
7	PREC_LR	0.87	0.01	−0.08	Kc_min	0.90	0.00	−0.06
8	Kc_min	0.88	0.01	−0.07	lnRks_406	0.90	0.00	0.06
9	Sublim	0.88	0.00	−0.06				
10	lnRks_404	0.88	0.00	0.05				

Source: Output DTN: SN0701T0502206.044, file: \MIC 01_03_2007\BIG LHS\Stepwise\ *Stepwise_Analysis_Infiltration_01_08_2007.xls*.

The results of the extended parameter sensitivity study confirm that the initial parameter screening criteria used for the uncertainty analysis are valid. Approximately 80% of the variance in mean net infiltration in the set of 200 realizations can be accounted for by the uncertainty in the same two input parameters that describe most of the variability in the uncertainty analysis results (Soil depth of Soil Depth Class 4 and Holding Capacity of Soil Group 5/7/9). The other parameters explain less than 3% of the variance each and are therefore not considered to be as important for estimating mean net infiltration. It is worth noting that several of these other parameters were not screened into the uncertainty analysis (K0wint, lnKs_579, PREC_LR, Sublim, lnRks_404, and lnRks_406), however, none these other parameters account for more than 3% of the variance in net infiltration.

7.1.5 Summary of Confidence Building During Model Development

As discussed previously, a Level II validation requires that Level I validation items 1 through 6 from SCI-PRO-002 are satisfied. The validation activities described within this section satisfied all 6 items as follows:

1) *Evaluate and select input parameters and/or data that are adequate for the model's intended use* Input parameters and data selected to represent precipitation are described in Section 7.1.1. Input parameters and data selected to represent evapotranspiration are described in Section 7.1.2. Input parameters and data selected to represent run-on and runoff are described in Section 7.1.3. The results of an extended sensitivity study that allowed 42 uncertain parameters to be varied are described in Section 7.1.4. These sections describe the selection of parameters and data that demonstrate that they are adequate for the model's intended use.

2) *Formulate defensible assumptions and simplifications that are adequate for the model's intended use.* Defensible assumptions and simplifications described in Section 7.1 include: the simplification of precipitation patterns using Fourier series parameters; the simplification of vegetation properties into parameters K_{cb} and NDVI'; and the adjustments made to soil hydraulic conductivities in order to match model results to streamflow data. These assumptions and simplifications are defensible and have been shown to be adequate for the model's intended use.

3) *Ensure consistency with physical principles, such as conservation of mass, energy, and momentum, to an appropriate degree commensurate with the model's intended use.* MASSIF is a water balance model, and closure of the mass balance equation is ensured by the mass balance accounting processes built into the model. Eq. 6.4-1 in Section 6.4 describes the mass balance equation that is calculated for every grid cell and every day in each simulation. Runoff is calculated as the remainder of the mass balance equation. This approach ensures closure of the mass balance equation.

4) *Represent important future state (aleatoric), parameter (epistemic), and alternative model uncertainties to an appropriate degree commensurate with the model's intended use.* Both aleatoric and epistemic uncertainties are considered in the model and parameter development discussed in Sections 6.6 and 6.7.

5) *Ensure simulation conditions have been designed to span the range of intended use and avoid inconsistent outputs or that those inconsistencies can be adequately explained and demonstrated to have little impact on results.* Simulation conditions have been designed to span the range of intended use. Sensitive parameters have been determined in Sections 6.7 and 7.1.4, and parameter uncertainties have been captured in Section 6.6 to ensure that simulation conditions span the range of intended use.

6) *Ensure that model predictions (performance parameters) adequately represent the range of possible outcomes, consistent with important uncertainties and modeling assumptions, conceptualizations, and implementation.* The sensitivity studies described in Sections 6.7 and 7.1.4, and the results of the uncertainty simulations described in Section 6.6 ensure that model parameters adequately represent the range of possible outcomes.

7.2 POST MODEL-DEVELOPMENT VALIDATION

Post-development validation includes several methods listed in Paragraph 6.3.2) of SCI-PRO-006. The methods used to validate the infiltration model include (1) corroboration of model results with data (e.g., field data, analog studies) not previously used to develop or calibrate the model and (2) corroboration of model results with other alternative mathematical model results. In addition, post-development validation includes one method given in Paragraph 6.3.2b) of SCI-PRO-006, technical review by an external agency, and documented by the external agency. This review is the 1997 expert elicitation panel on unsaturated zone (UZ) flow model issues (CRWMS M&O 1997 [DIRS 100335]. Although this review was conducted 10 years ago, and the panel reviewed an entirely different infiltration model from that presented in this report, the conceptual models employed by the infiltration models are quite similar, and the conclusions of the expert elicitation project remain generally relevant in 2007.

Section 7.2.1 describes corroboration of the model results with data, Section 7.2.2 presents corroboration of the model results with alternative models, and Section 7.2.3 summarizes the conclusions and infiltration estimates from the 1997 expert elicitation panel on UZ flow model issues.

7.2.1 Corroboration of Model Results with Data and Relevant Observations

In Section 7.2.1, MASSIF predictions of infiltration are compared to limited field data collected, and relevant observations made at Yucca Mountain (Section 7.2.1.1), and compared to large-scale estimates of net infiltration or recharge for other locations in Nevada (Section 7.2.1.2.1), other locations in the southwestern United States (Section 7.2.1.2.2), and for other locations in the western United States (Section 7.2.1.2.3).

7.2.1.1 Corroboration of Model Results with Field Data

No measurements have ever been made at Yucca Mountain that directly quantify net infiltration under ambient conditions. Net infiltration, and recharge, are extremely difficult to directly measure in arid climates (Hogan et al. 2004 [DIRS 178487], page vii). Field data that were considered for comparison to MASSIF predictions in the report include 1) observations of seepage in the south ramp of the Exploratory Studies Facility (ESF) in the spring of 2005; 2)

estimates of net infiltration at borehole UZ#4 in Pagany Wash in the spring of 1998; and 3) estimates of net infiltration from neutron logging data. There are a variety of other field data that indirectly provide estimates of net infiltration below the root zone. Some of these datasets have been used for model validation of the 2000 net infiltration model (USGS 2001 [DIRS 160355]), and validation of the 2004 revision of the 2000 net infiltration model (BSC 2004 [DIRS 170007]) such as borehole temperature data, chloride mass balance data, calcite data, and perched water chemistry data.

However, in this report, data collected from depths greater than a few meters into the UZ were considered to be invalid for comparison to MASSIF predictions of net infiltration. The reason for this is that the validity of comparing point measurements from boreholes with model predictions with 30-m × 30-m grid cells are questionable for surface measurements due to extreme scale differences between borehole data and grid cell size. In addition, data collected from rock/water samples at greater than a few meters depth, especially at many tens of meters of depth additionally has been strongly influenced by its transit through the deep UZ. In addition, the validity of some of the UZ data and methods is questionable. For example, the 1997 expert elicitation panel did not embrace the use of temperature gradient and heat flux data to estimate percolation flux, and they viewed the chloride mass balance method as supportive of other methods but insufficient for obtaining independent estimates of percolation flux (CRWMS M&O 1997 [DIRS 100335], pp. 3-15 and 3-17). They also concluded that net infiltration is equivalent to percolation flux at the repository horizon, with some differences in spatial distribution, so their conclusions are relevant to validation of the net infiltration model (CRWMS M&O, 1997 [DIRS 100335], p. 3-5). Refer to Section 1.2 for additional discussion on the limitations of using data collected from the UZ for validation of the infiltration model.

The difficulty in comparing data from a point measurement to model predictions for a 30-m × 30-m grid cell is exacerbated by the paucity of soil depth data and soil hydraulic property data for the site. Without a good estimate of soil depth and soil hydraulic properties, comparison of point measurements to model grid cells is not reliable. Consider the comparison of model soil depth versus actual soil depth for 95 neutron logging boreholes located within the infiltration model domain. For this comparison, the grid cell IDs containing the 95 neutron logging boreholes were found using the Mathcad file *Infiltration at NL Boreholes (Preprocess).xmcd* located in Neutron Logging Boreholes folder in the Validation Analyses folder within the MASSIF calculation (Output DTN: SN0701T0502206.037). This file outputs the cell ID# for the 95 neutron logging boreholes. Borehole locations can be found in DTN: MO9906GPS98410.000 [DIRS 109059]. Soil depths can be found in three DTNs that include some qualified sources and some unqualified sources. These DTNs are listed below Figure 7.2.1.1-1. These data sources are compiled in an Excel file *Soil depth at NL boreholes.xls* located within the following path in the MASSIF calculation: (Output DTN: SN0701T0502206.037):

\\Welcome to Massif\Massif\Validation Analyses\Data\Borehole Locations\

Figure 7.2.1.1-1 shows the poor correlation between measured and modeled soil depth within each soil depth class region. This figure is included to demonstrate the difficulty in making comparisons between modeled infiltration data for a grid cell, compared to infiltration calculated from measured data collected at boreholes, particularly for the extreme case where measured soil

depths are close to zero, but modeled soil depth has a nominal value of 16.47 m (for Soil Depth Class 2). Note that none of the 95 boreholes are located in cells with Soil Depth Class 1 (95-m soil depth).

Notwithstanding the previous discussion, MASSIF was compared to measurements of net infiltration at Pagany Wash and to net infiltration calculated from neutron logging data. These comparisons do not generally provide conclusive validation of the infiltration model, but they are summarized in this report nonetheless. In addition, a discussion of some heat dissipation probe data that measure water potential (and can be converted into water content) is included below.

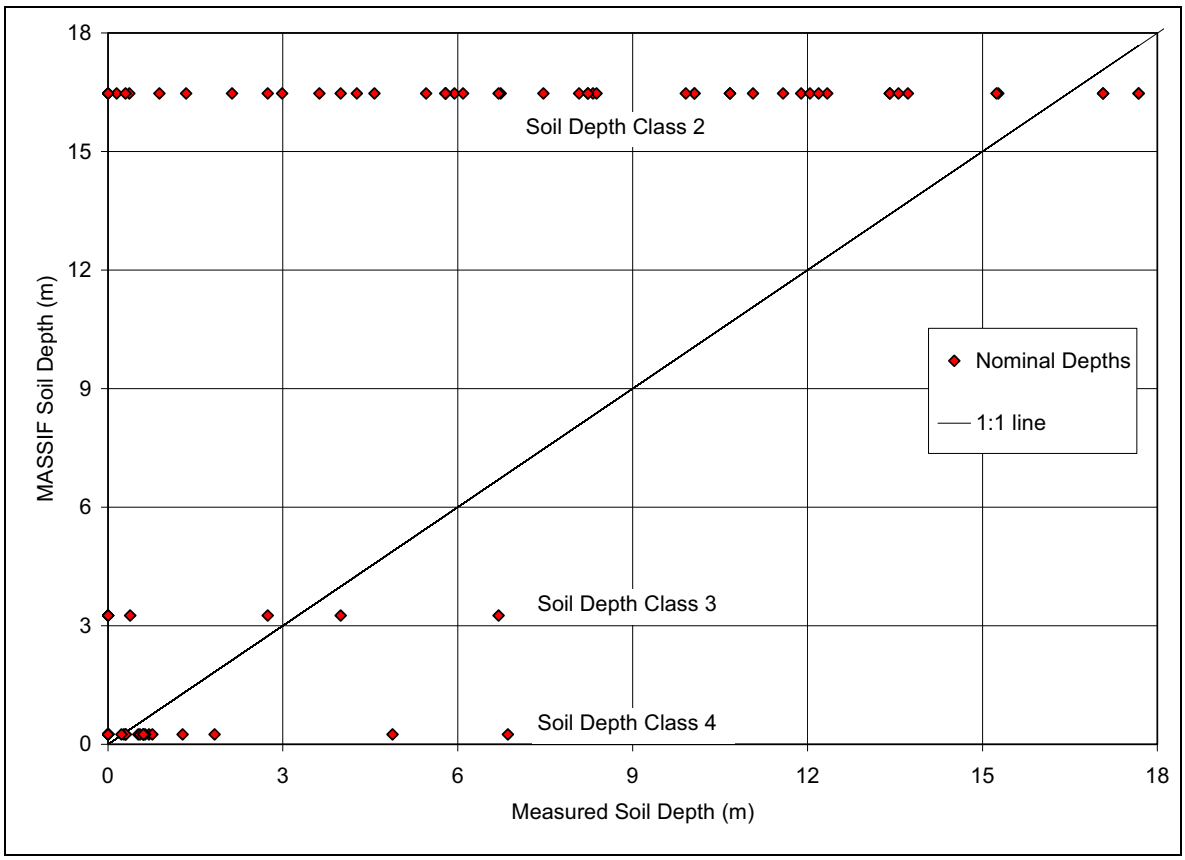

Source: Table 6.5.2.4-2 (modeled soil depths); Output DTN: SN0606T0502206.011 (soil depth class); DTNs: MO0004QGFMPICK.000 [DIRS 152554] (measured soil depth); MO0012MWDGFM02.002 [DIRS 153777]; and GS910808312212.001 [DIRS 175972].

Figure 7.2.1.1-1. Measured versus Modeled Soil Depth for 95 Neutron Logging Boreholes

7.2.1.1.1 Comparison of Model Predictions of Infiltration with Seepage Observations and Simulations above the South Ramp in 2005

During the 5-month period between October 2004 and February 2005, 324 mm (12.75 inches) of precipitation fell in the Yucca Mountain area. On February 28, 2005, YMP personnel working in the South Ramp of the ESF observed wet spots on the main drift's crown, ribs, and invert. This field observation is considered the first unambiguous evidence of seepage under ambient conditions. Based on several assumptions, it was estimated that 13% of a 5.1-m long drift section experienced seepage (Finsterle and Seol 2006 [DIRS 177754]).

Finsterle and Seol (2006 [DIRS 177754]) applied a Monte Carlo simulation using the *Seepage Model for PA Including Drift Collapse* (BSC 2004 [DIRS 167652]) in order to simulate the seepage fraction to resolve whether or not the observed seepage was an unexpected condition. Percolation flux was assumed to be equivalent to net infiltration flux, which was assumed to be on the order of 10% of precipitation, whose rate ranged from 393 mm/yr to 1309 mm/yr for November 2004, and February 2005, respectively. These precipitation rates are considerably higher than the long-term average value of 188.5 mm/yr reported by Finsterle and Seol (2006 [DIRS 177754], Table 1). Using probability distributions for fracture and capillary parameters and for net infiltration flux, it was estimated that seepage would occur along about 37% of the ESF South Ramp, compared with the observation that about 13% of the length exhibited wet spots. Therefore, these simulations confirm that the seepage observations in 2005 were not an unexpected condition, given the precipitation during this 5-month period (Finsterle and Seol 2006 [DIRS 177754], p. 17).

This section describes how MASSIF was used to corroborate the net infiltration fluxes assumed in Finsterle and Seol (2006 [DIRS 177754]). Although MASSIF results cannot be directly compared with quantitative field measurements of seepage, MASSIF infiltration can be compared to the ranges used by Finsterle and Seol (2006 [DIRS 177754]) in their seepage simulations. If MASSIF results are consistent with their infiltration ranges used to predict seepage, then this calculation provides additional model validation.

Monitor cells were identified at the ground surface directly above the areas identified as having seepage in the south ramp of the ESF. Precipitation and air temperature data for WY2004 and WY2005 were acquired for Site 8, located about 1.2 km east of the seepage observations. Since wind speed data were not collected at Site 8, wind speed data from Site 1 were used instead. Site 1 weather station has an elevation of only 12 m higher than the Site 8 station (CRWMS M&O 1997 [DIRS 100117], Table 2-1). MASSIF was used to calculate the average net infiltration for WY2005, with particular focus on monthly rates in November 2004 through February 2005.

MASSIF was run for WY 2004 and WY2005 (October 1, 2003 through September 2005). The sources for the weather data used in the simulation follows:

2003 weather data:

- Maximum and minimum air temperature and precipitation data from Site 8: DTN: MO0503SEPMMD03.001 [DIRS 176097].
- Wind speed data from Site 1: DTN: SN0608WEATHER1.005 [DIRS 177912].

2004 weather data:

- Maximum and minimum air temperature and precipitation data from Site 8: DTN: MO0607SEPMMD04.001 [DIRS 178311]
- Wind speed data from Site 1: DTN: SN0608WEATHER1.005 [DIRS 177912].

2005 weather data:

- Maximum and minimum air temperature and precipitation data from Site 8 and wind speed data from Site 1: DTN: MO0610METMND05.000 [DIRS 178328].

Note that the 2005 Site 8 precipitation dataset from DTN: MO0610METMND05.000 [DIRS 178328] is not complete. Missing data information was used for a storage gauge (DTN: MO0605SEPSGP05.000 [DIRS 178663]). The timing of the missing data is taken from Site 1: DTN: MO0610METMND05.000 [DIRS 178328]. See Excel file *Site 8 Pcp vs Site 1 Pcp.xls* in Output DTN: SN0701T0502206.037 for details on how Site 1 hourly data were scaled with a factor of 1.41 in order to replace Site 8 missing data.

Monitor cells were identified at the ground surface directly above the locations within the South Ramp of the ESF where seepage was observed in 2005. Three primary wet areas were identified in the ESF between stations 75+62 and 75+82, Stations 75+92 and 76+07, and Stations 77+48 to 77+53 (Finsterle and Seol 2006 [DIRS 177754], p. 1). These locations were converted into UTM coordinates using reference points and documented in the Excel file *seepage locations.xls* located in the South Ramp Infiltration folder within the MASSIF model Output DTN: SN0701T0502206.037. The Mathcad file *Locate cells above SR Seepage.xmcd* was used to locate the monitor cell IDs for these UTM coordinates. These three areas of observed seepage are directly beneath three monitor cells in the Drill Hole Wash watershed. Refer to Figure 7.1.3-1 for a map view of the infiltration watersheds, and the location of the South Portal and the grid cells below which seepage was observed. This figure also includes locations of other field data that are discussed later in Chapter 7.

MASSIF predicted net infiltration totals of 133 mm, 130 mm, and 113 mm for the three monitor cells for WY2005. This is equivalent to 31.4%, 30.7%, and 27.3% of precipitation for the three monitor cells. On a monthly basis, the infiltration/precipitation ratio ranged from 0.0 to 0.54. Refer to Table 7.2.1.1-1 for the results of the MASSIF simulations of infiltration above the South Ramp. These values are compared to the monthly values used in (Finsterle and Seol 2006 [DIRS 177754]).

Table 7.2.1.1-1. Summary of MASSIF Results for South Ramp Infiltration Simulations

		Precipitation (mm/yr)			
Month	Year	Finsterle & Seol 2006	MASSIF Cell1	MASSIF Cell2	MASSIF Cell3
October	2004	814.0	861.5	856.8	839.5
November	2004	393.0	419.2	416.9	408.5
December	2004	575.0	564.4	561.4	550.0
January	2005	865.0	894.5	889.6	871.7
February	2005	1309.0	1317.0	1309.8	1283.4

Table 7.2.1.1-1. Summary of MASSIF Results for South Ramp Infiltration Simulations (Continued)

Month	Year	Infiltration (mm/yr)			
		Finsterle & Seol 2006 LBNL	MASSIF Cell1	MASSIF Cell2	MASSIF Cell3
October	2004	81.4	143.3	136.0	107.9
November	2004	39.3	108.7	103.2	86.3
December	2004	57.5	242.7	238.9	210.4
January	2005	86.5	391.3	377.8	329.7
February	2005	130.9	714.7	698.4	619.9

Source: Output DTN: SN0701T0502206.037, file: \Welcome to Massif\Massif\Validation Analyses\South Ramp Seepage*South Ramp Results.xls*.

The results of this MASSIF calculation demonstrate that the estimate of net infiltration used as a boundary condition to predict seepage in the South Ramp by Finsterle and Seol (2006 [DIRS 177754]) was reasonable and in fact, considerably lower than the monthly infiltration predicted by MASSIF. Based on the assumption and conclusions in Finsterle and Seol (2006 [DIRS 177754]) and the MASSIF results in this section, observations of seepage in the South Ramp in 2005 were not unexpected.

However, the results of this MASSIF calculation beg the question of why wasn't more seepage observed in the south ramp if the seepage model predicted seepage along 37% of south ramp when about seepage along 13% of the south ramp was observed, and MASSIF predicts more infiltration than the boundary condition used by Finsterle and Seol (2006 [DIRS 177754]). One explanation is that Finsterle and Seol (2006 [DIRS 177754]) did not account for any delay of infiltration between the bottom of the root zone, and the ceiling of the south ramp, or for any change in storage or lateral flow in this zone that has a thickness ranging from 70 m to 40 m. This range in thickness is calculated in *Seepage Locations.xls* in the MASSIF calculation (Output DTN: SN0701T0502206.037). In addition, the seepage model did not account for evaporation effects in the ESF, which would have reduced their estimate of observed seepage in the ESF ceiling. These additional considerations would support the conclusion that the MASSIF results, the seepage model results, and the observed seepage in the ESF are not inconsistent.

7.2.1.1.2 Comparison of Model Predictions with Pagany Wash Infiltration Data from 1998

MASSIF was used to simulate infiltration at a monitor cell that contains the location of borehole UE-25 UZ #4 (also referred to as UZ #4). This is an instrumented borehole in Pagany Wash. The winter of 1997-1998 was an El Nino winter and therefore was considerably wetter than average winters. The total precipitation recorded at Site 3 for WY1998 was 402.6 mm (DTN: SN0608WEATHER1.005 [DIRS 177912]). In the spring of 1998, 183.4 mm of precipitation was recorded during 14 out of 23 days between February 2 and 24 (DTN: SN0608WEATHER1.005 [DIRS 177912]), and approximately 35,000 m^3 of runoff was recorded at the lower Pagany Wash streamflow gauge (see Table 7.1.3-1) during this 23-day period in February 1998 (DTN: GS960908312121.001 [DIRS 107375]). LeCain et al. (2002 [DIRS 158511]) describe infiltration data collected at this borehole during the spring of 1998. Borehole UZ #4 is located in the alluvial deposits of Pagany Wash, a stream-carved, dry channel. This borehole was instrumented with temperature, pressure, and water potential sensors in July

1995, in order to gain insight into infiltration through the alluvial deposits of the usually dry stream channels (LeCain et al. 2002 [DIRS 158511]). Refer to Figure 7.1.3-1 for a map view of the infiltration watersheds and the location of Pagany Wash and UZ #4.

LeCain et al. (2002 [DIRS 158511]) describe two methods for estimating infiltration in Pagany Wash based on data collected at UZ #4. The first is an analytical method in which the infiltration flux is calculated from soil saturated conductivity, porosity, and velocity of a wetting front observed to pass from a depth of 3.0 m to 6.1 m. The second method uses a numerical model to estimate infiltration flux given temperature data measured in UZ #4. The first method produced a percolation flux of 1.13 m while the second method produced a percolation flux of 1 to 2 m.

First, MASSIF was used with nominal input values to simulate infiltration at the monitor cell containing borehole UZ#4. Infiltration for WY1998 at UZ #4 was calculated to be 11.8 mm using precipitation data from the Site 6 station, and 28.3 mm using precipitation data from the Site 3 station. Second, soil and rock hydraulic conductivities (K_{sats}) for the grid cell containing borehole UZ #4 were adjusted to test the sensitivity of infiltration to K_{sat}, and to demonstrate that modeled infiltration can match the measured infiltration reported by LeCain et al. (2002 [DIRS 158511]) with adjustments to Ksats. Soil Ksat was increased by about one order of magnitude to a value of 7 m/s, and rock Ksat was increased to a value of 10^{-3} m/s so that it would not be a limiting factor on infiltration. The analytical method used by LeCain et al. (2002 [DIRS 158511]) to calculate infiltration flux from 3.0 to 6.1 m does not include rock hydraulic conductivity, so rock hydraulic conductivity should not be a limiting factor for a comparison with MASSIF. MASSIF calculated a total net infiltration for WY1998 at the grid cell containing UZ #4 of 414 mm and 375 mm for Site 3 and Site 6 stations, respectively. When soil Ksats were increased to 10^{-5} m/s, infiltration increased to 597 and 548 mm, for Site 3 and Site 6 precipitation, respectively. These MASSIF calculations can be found in the Pagany Wash Borehole folder in the Validation Analyses folder in the MASSIF calculation (Output DTN: SN0701T0502206.037, file: \Welcome to Massif\Massif\Validation Analyses\Pagany Wash Borehole*Pagany Wash Results.xls*.).

In the analytical method described by LeCain et al. (2002 [DIRS 158511]), if the value of soil porosity is changed from 0.31 to 0.157 m^3/m^3, which is the porosity assigned to the soil type in this grid cell, then the percolation flux would change from 1,130 to 573 mm (see file "PW infiltration analytical calculation.xmcd" in Output DTN: SN0701T0502206.037). This is very close to the net infiltration flux calculated by MASSIF when soil and rock Ksats are adjusted.

This comparison of percolation flux between MASSIF and an analytical method reported by LeCain et al. (2002 [DIRS 158511]) shows that MASSIF calculated approximately the same amount of infiltration at UZ #4, if soil Ksat for that grid cell is increased by ~1.5 orders of magnitude, and if rock hydraulic conductivity for that grid cell is increased so that it is not a limiting factor. Although this increase in soil Ksat is outside of the standard error range in soil Ksat for soil type 3 (Ksat range = 9.5 to 6.2×10^{-7} m/s) reported in *Data Analysis for Infiltration Modeling: Development of Soil Units and Associated Hydraulic Parameter Values* (BSC 2006 [DIRS 176335], Table 6-7), it is within the range of maximum and minimum values (1.7×10^{-7} to 1.7×10^{-5} m/s), and this adjusted soil Ksat may be more appropriate for the soil near the grid cell containing UZ #4 on Yucca Mountain. The soil Ksat values (BSC 2006 [DIRS 176335],

Table 6-7) are not directly measured, but are developed from Yucca Mountain textural data using pedotransfer functions (BSC 2006 [DIRS 176335], Section 6.4.5). Therefore, they are appropriate and defensible for large-scale assessments of infiltration at Yucca Mountain. However, they are likely to be inaccurate for comparison to borehole-scale infiltration estimates as we have seen in this validation calculation.

Although not referenced in *Data Analysis for Infiltration Modeling: Development of Soil Units and Associated Hydraulic Parameter Values* (BSC 2006 [DIRS 176335]), Hofmann et al. (2000 [DIRS 153709]) report measurements of soil saturated hydraulic conductivity at two locations at Yucca Mountain. These locations included a measurement in Pagany Wash near borehole UE-25 UZN #14 and a measurement on a stable terrace adjacent to Fortymile Wash at borehole UE-25 UZN #85, both using a prototype-automated-infiltrometer. They measured a saturated hydraulic conductivity of 17.79 cm/hr (4.94×10^{-5} m/s) for the location in Pagany Wash and 1.78 cm/hr (4.94×10^{-6} m/s) for the terrace location (Hofmann et al. 2000 [DIRS 153709], Table 4). The measurement in Pagany Wash corroborates the adjustments to soil conductivity that are required to match infiltration inferred at UZ #4.

7.2.1.1.3 Discussion of Water Content Data

Discussion of Neutron Logging Data

Neutron logging data were collected from mid-1989 through September 1995 at 99 boreholes. Ninety-five of the 99 boreholes are located within the current infiltration model domain. Refer to Figure 7.1.3-1 for a map view of the infiltration watersheds and the locations of the 95 neutron logging boreholes. All 95 boreholes are located within four watersheds; one borehole is located within Yucca Wash while the remaining 94 boreholes are located within Drill Hole Wash, Dune Wash, or Solitario Canyon 1 watersheds. Details of the neutron logging program and datasets can be found in *Technical Evaluation and Review of Results, Technical Procedures, and Methods Related to the Collection of Moisture Monitoring Data Using Neutron Probes in Shallow Boreholes* (BSC 2006 [DIRS 177083]), and by Flint and Flint (1995 [DIRS 100394]).

An uncertainty analysis of this dataset concluded that water content values from the neutron logging are accurate to approximately ±6% absolute water content within a 95% confidence interval (BSC 2006 [DIRS 177083], Section 5.3.2). Given a typical water content value of 20%, this uncertainty translates to a 30% relative error in the measured value. However, the precision of the measurement is higher (less than 2% relative difference), which suggests that estimates of changes in water content are more certain. This increased certainty is limited by the fact that precision errors associated with each log are additive when considering changes in water content over time.

The way neutron logging data has been used has changed over time on the Yucca Mountain Project. Neutron logging data were used to calibrate the 1996 USGS net infiltration model (Flint et al. 1996 [DIRS 100147]), however data-model comparisons are only shown for two of the 99 boreholes and the calibration method used and the results obtained are not adequately documented. Streamflow data (and no neutron logging data) were used to calibrate the 2000 USGS net infiltration model (USGS 2001 [DIRS 160355]). The 2004 revision of the 2000 USGS

net infiltration model (BSC 2004 [DIRS 170007]) only used neutron logging data for model validation.

This dataset was deemed to be of limited use for validation (or calibration) of the 2007 SNL net infiltration model for several reasons. First, the errors associated with water content derived from these measuements make direct comparison with simulated water contents problematic, especially since conditions at each borehole (such as soil depth and properties) are likely to differ from the average values assigned to the soil depth class and soil group assigned to the cell. Second, the field capacity modeling approach is a "lumped" approach and is therefore not intended to be used to match moisture profiles with depth in the soil. Third, flux estimates using the change in water content over an interval require an estimate of the root-zone depth, which is likely to vary for each location. Despite this limitation, fluxes were estimated assuming a constant root-zone depth and compared with net infiltration calculated over the same time interval (see below). The following comparisons between measured and modeled infiltration, and provides justification for its exclusion from model validation.

Neutron logging measures the number of reflected (thermalized) neutrons at depth intervals in a region surrounding a borehole. The count of neutrons is also affected by the integrated properties of the material (e.g., density, mineral composition, etc.) and in relatively homogeneous materials has successfully been used to estimate water content. Several researchers have estimated net infiltration fluxes from neutron logging data collected at time intervals during which water content profiles were changing (e.g., Looney and Falta (2000 [DIRS 154273], p. 457) and McElroy (1993 [DIRS 177910], p. 13)). However, many assumptions are required in order to estimate net infiltration flux from these measurements. Net infiltration flux can be estimated from the change in water content ($d\theta v$ in m^3/m^3), with time, multiplied by a given depth interval ($d\theta v*dz$), and then summing these changes, for depths below the root zone (Looney and Falta (2000 [DIRS 154273], p. 457) and McElroy (1993 [DIRS 177910], p. 13)). Net infiltration flux can also be calculated as the change in integrated water content below the root zone, between two time periods. This method was implemented with Mathcad in "Borehole Processing Nominal.xmcd" located in the "Neutron Logging Boreholes" folder in the "Validation Analyses" folder within the MASSIF calculation (Output DTN: SN0701T0502206.037), for the time period spanning the greatest increase in borehole water content between about January 1 and mid-March 1995. The root zone was assumed to be 2 m below the ground surface for soil depths of 2 m or greater, and the root zone was set equivalent to soil depth for soil depths less than 2 m.

The use of these methods for calculating flux from water content data has not been widely used, and limitations in the approach, as well as limitations within the dataset, should be acknowledged. For example, this approach assumes 1-D piston flow, with no lateral flow at the soil–bedrock interface. The MASSIF model assumes that lateral flow can be neglected for the purposes of estimating a water balance for a 30 × 30 m grid cell (Section 5). However, this assumption may not be appropriate for measurements occurring on the scale of a borehole, since the active fracture spacing in the bedrock is likely to be greater than the region measured by the neutron probe. In addition, single calibrations, independent of media, were developed for each neutron probe, and were applied to all the neutron measurements made in various media (e.g., soil, "rotten" tuff near the soil–bedrock interface, or intact tuff). Refer to *Technical Evaluation and Review of Results, Technical Procedures, and Methods Related to the Collection*

of Moisture Monitoring Data Using Neutron Probes in Shallow Boreholes (BSC 2006 [DIRS 177083]) for details of the neutron probe calibrations. Since calibrations provide the means of interpreting water contents, the consequence of using a single calibration for different media is that there may be systematic errors in water contents for media not used in the calibration. In addition, as a result of the drilling methods, preferential pathways for water flow along the annulus space between the borehole casing and the geologic media may have been inadvertently created, and formerly solid rock may have been extensively fractured.

Despite the limitations of the dataset, and the assumptions inherent in calculating infiltration from changes in water content, this six-year dataset represents the only YMP site-specific dataset that measured wetting front movement, depths of infiltration, and indirectly, net infiltration flux, over a large area of the infiltration model area, and over a period with wet years and dry years. Therefore, it is worthwhile to compare MASSIF predictions of infiltration at the grid cells containing the neutron logging boreholes, with the infiltration calculated from neutron logging data. Figure 7.2.1.1-2 shows such a comparison for a period of infiltration spanning the wet winter of 1995, using 3 precipitation stations with MASSIF. As the figure shows, the comparison is not good. Even the averaged infiltration for all boreholes was not good (67 mm for MASSIF using Site 6 precipitation versus 173 mm from neutron logging data). This figure is included to show that the borehole-scale neutron logging data do not match model predictions very well. This figure supports the argument given in Section 7.2.1.1 that MASSIF should not be expected to be able predict infiltration at the borehole-scale.

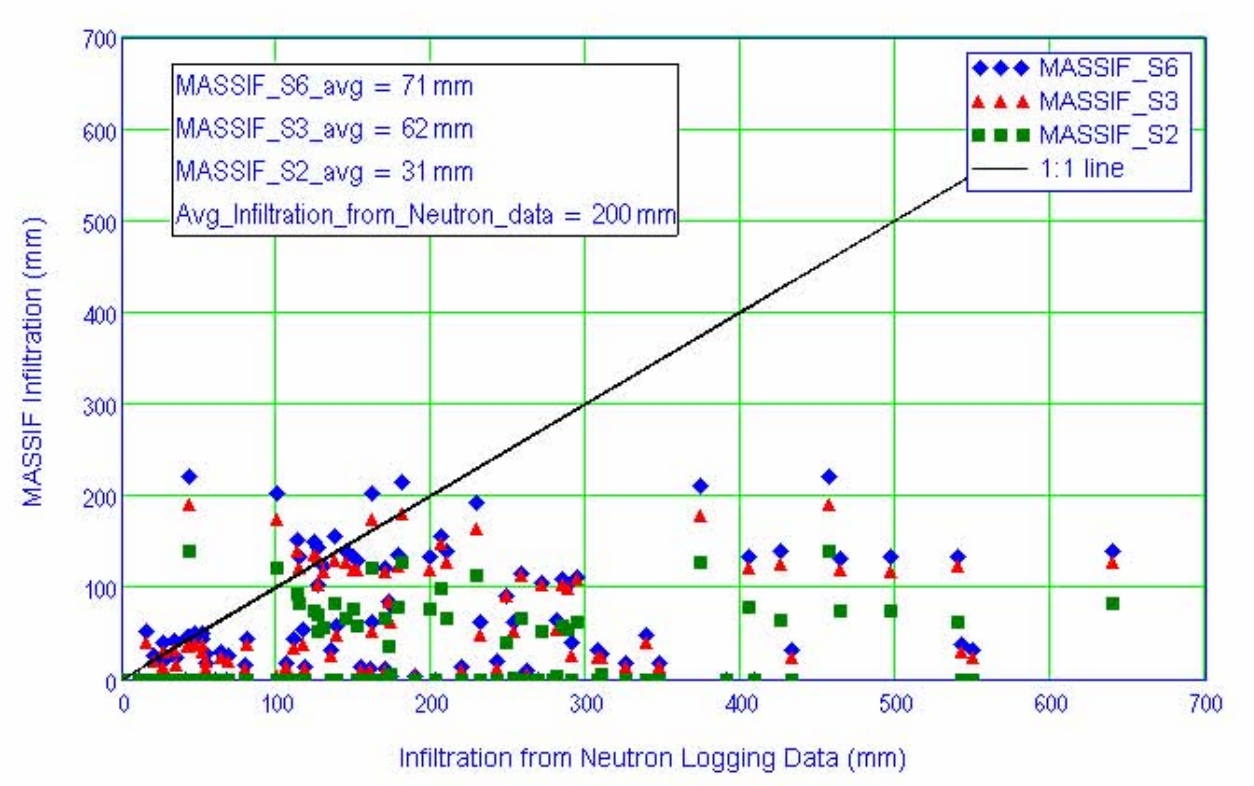

Source: Output DTN: SN0701T0502206.037, file: \Welcome to Massif\Massif\Validation Analyses\Neutron Logging Boreholes*Borehole_Processing_Nominal.xmcd*.

Figure 7.2.1.1-2. Comparison of Net Infiltration Calculated from Neutron Logging Data versus MASSIF Net Infiltration for Winter 1995

Discussion of Heat Dissipation Probe Data

Heat dissipation probe data, which measures water potential at different depths in the soil, are available for at least one location at Yucca Mountain (DTN: GS960908312211.004 [DIRS 146872]). Water potential data can be converted into water content data and then compared to model results using MASSIF, if the water retention properties of the soils are known. These data were not analyzed for additional model validation due to the problems with data traceability and the availability of site-specific soil property data needed to convert water potential to water content. However, if such soil property data could be found by additional soil sampling, then this dataset could be used for additional model validation in the future.

7.2.1.2 Comparison of Infiltration Estimates with Other Models and Data from Comparable Environments

In this section, MASSIF results for Present-Day, Monsoon, and Glacial Transition climates (Output DTNs: SN0701T0502206.034, SN0701T0502206.036, and SN0701T0502206.035, respectively) are compared to infiltration and/or recharge estimates from other models and data from comparable environments. These environments include other locations in Nevada (Section 7.2.1.2.1), the southwestern United States (Section 7.2.1.2.2), and the western United States (Section 7.2.1.2.3). Estimates from locations in the southwestern U.S. are approximately

analogous to the predicted recharge expected for the monsoon climate, based on the selection of analog climate sites in *Future Climate Analysis* (BSC 2004 [DIRS 170002], Table 6-1). And estimates from locations in the western are approximately analogous to the predicted recharge expected for the glacial-transition climate, based on the selection of analog climate sites in *Future Climate Analysis* (BSC 2004 [DIRS 170002], Table 6-1). Recharge and infiltration estimates for the Hanford site are briefly discussed in Section 7.2.1.2.3, although this site is quite dry and more analogous to Yucca Mountain under the present-day climate than the glacial-transition climate.

MASSIF results for Present-Day, Monsoon, and Glacial Transition climates (Output DTNs: SN0701T0502206.034, SN0701T0502206.036, and SN0701T0502206.035, respectively) are compared to several published models of infiltration and/or recharge versus precipitation and shown in Figure 7.2.1.2-1. The publication dates of these models span nearly 60 years and Figure 7.2.1.2-1 demonstrates the similarity of these models, despite the advances made in hydrologic sciences in the past 60 years. The step function of the Maxey-Eakin model (Maxey and Eakin 1950 [DIRS 100598], p. 40) is shown primarily for its historical significance as a well-recognized recharge model. A modified Maxey-Eakin model (Nichols 2000 [DIRS 178863], page C35), and a Maxey-Eakin model fit developed by Wilson and Guan (2004 [DIRS 172585], Equation 12) are also shown in this Figure. Figure 7.2.1.2-1 also shows MASSIF results compared to a model developed by Maurer and Berger (1997 [DIRS 177370], Equation 9) for west-central Nevada. The Maurer and Berger (1997 [DIRS 177370]) model predicts water yield based on precipitation in which water yield is defined as subsurface flow plus surface runoff, so it is not directly comparable to other models, but it is included for comparison purposes. Figure 7.2.1.2-1 also shows MASSIF results compared to a recent model developed by Faybishenko (2007 [DIRS 178766], Equation 16) for Yucca Mountain using analog meteorological data, and a fit to a dataset referred to as Davisson and Rose (Faybishenko (2007 [DIRS 178766], Figure 10). MASSIF results for three climate states are above the general trend of most of these models.

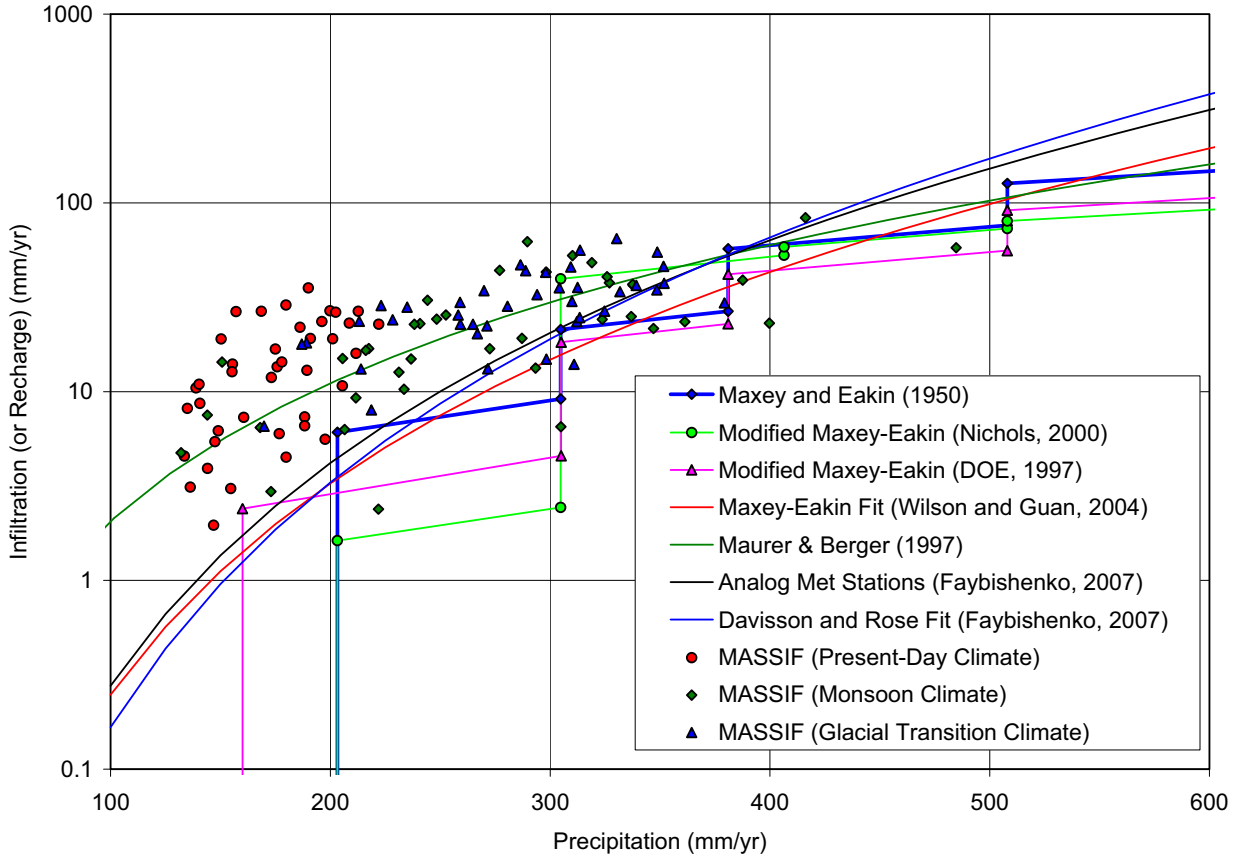

Source: Output DTNs: SN0701T0502206.034, SN0701T0502206.036, and SN0701T0502206.035; Validation Output DTN: SN0704T0502206.047.

NOTE: Vertical lines that extend to the horizontal axis associated with the Maxey-Eakin and Modified Maxey-Eakin models represent the precipitation amounts below which the models predict zero recharge.

Figure 7.2.1.2-1. Comparison of MASSIF Net Infiltration Results for Three Climates with Several Models

7.2.1.2.1 Infiltration Estimates for Other Locations in Nevada

The Nevada Division of Water Resources, Department of Conservation and Natural Resources and the U.S. Geological Survey have divided Nevada into 14 Hydrographic Regions or basins, which are used to compile information on water resources. These regions are further subdivided into 232 Hydrographic Areas (256 Hydrographic Areas and Sub-areas, combined) for more detailed study. A variety of technical publications have reported recharge estimates for Nevada Hydrographic Areas. Noteworthy examples include two series of publications by the Nevada Department of Conservation and Natural Resources: (1) the Groundwater Resources Reconnaissance Series; and (2) the Water-Resources Bulletins. In many cases, multiple recharge estimates using different methods, inputs and assumptions are available for the same area/subarea.

Thomas et al. (1989 [DIRS 177727], p. 15-16) estimated natural recharge for the Smith Creek Valley hydrographic area using both Maxey-Eakin and chloride mass balance methods and compared these results to a previous Maxey-Eakin estimate by another researcher (see Table 7.2.1.2-1). The two Maxey-Eakin estimates were approximately 15% and 45 % higher than the chloride mass balance estimate. The difference between the two Maxey-Eakin estimates was attributed to different altitude-precipitation relations and differences in delineation of recharge areas. The comparison illustrates that infiltration estimates can vary substantially between different methods or when the same method is applied by different researchers. However, when the results are expressed as recharge efficiency (recharge as a percentage of precipitation), all three the estimates compare fairly well.

Table 7.2.1.2-1. Recharge Estimates for Smith Creek Valley, Nevada [a]

Precipitation [b]		Recharge [b]		Efficiency	Method [c]
(acre-ft/yr)	(mm/yr)	(acre-ft/yr)	(mm/yr)	(%)	
92,000	75.3	9,600	7.9	10.4	ME
119,000	97.4	12,000	9.8	10.1	ME
92,000	75.3	8,300	6.8	9.0	CMB

[a] Thomas et al. 1989 [DIRS 177727], pp. 15-16.

[b] Precipitation and Recharge were reported in acre-ft/yr and converted to mm/yr using a basin area of 372,480 acres given in Horton 1998 [DIRS 174618], Appendix A-1.

[c] ME=Maxey-Eakin; CMB=chloride mass balance

Dettinger (1989 [DIRS 105384]) calculated chloride mass balance recharge estimates for a number of hydrographic areas/subareas in Nevada and compared them to Maxey-Eakin and water budget estimates obtained from Nevada Department of Conservation and Natural Resources Groundwater Resources Reconnaissance Reports and Water-Resources Bulletins (see Table 7.2.1.2-2). The basins were chosen to ensure a wide geographic coverage, a variety of areal extents and a variety of recharge efficiencies. Areal extents ranged from approximately 60,000 to 1,375,000 acres, with an average area of approximately 500,000 acres. Precipitation ranged from 29 mm/yr to 487 mm/yr. Recharge estimates from the three methods were generally in fair agreement. Estimated recharge efficiencies ranged from approximately 1% to 18%.

Avon and Durbin (1994 [DIRS 177200], Table 2) collected and evaluated basin-wide recharge estimates for a number of Nevada hydrographic areas/subareas. They developed comparisons between Maxey-Eakin estimates and water budget recharge estimates for 40 areas/subareas from studies published between 1946 and 1974 in the Nevada Department of Conservation and Natural Resources Groundwater Resources Reconnaissance Series and Water-Resources Bulletins (see Table 7.2.1.2-3). Estimates for five hydrographic areas/subareas (Duck Lake, Fish Lake, Penoyer, Southern Butte, and Northern Butte) were previously reported by Dettinger et al. (1989 [DIRS 105384]) and are not included in Table 7.2.1.2-3. The estimate for the eastern portion of the Honey Lake area was also excluded due to difficulty in determining an appropriate precipitation estimate. The basins studied covered a wide geographic area, a variety of areal extents, and a variety of recharge efficiencies. Areal extents ranged from approximately 6,000 to 1,240,000 acres, with an average area of approximately 320,000 acres. Precipitation ranged from 17 mm/yr to 476 mm/yr. Recharge estimates from the two methods were generally in fair agreement, with average differences of approximately 40% and a maximum difference of

approximately 200%. Estimated recharge efficiencies computed using the Maxey-Eakin method ranged from approximately 3% to 13%. Estimated recharge efficiencies computed from water budgets ranged from approximately 1% to 29%, with typical values below 12%.

Avon and Durbin (1994 [DIRS 177200], Table 3) also compared published Maxey-Eakin estimates and "model estimates" for 27 hydrographic areas/subareas. The "model estimates" were calculated using a variety of methods: (1) groundwater flow models; (2) a numerical infiltration model; (3) chloride mass balance; and (4) a deuterium-calibrated mixing-cell flow model. Table 7.2.1.2-4 lists the eight comparisons that do not overlap studies discussed above and for which precipitation estimates could be located. All eight comparisons include model estimates from the deuterium-calibrated mixing-cell flow model only. There is overlap between the studies used by Avon and Durban (1994 [DIRS 177200]) and those used in Dettinger (1989 [DIRS 105384]) and Thomas et al. (1989 [DIRS 177727], p. 15-16). In particular, all chloride mass balance estimates were obtained from Thomas et al (1989 [DIRS 177727], p. 15-16) and Dettinger (1989 [DIRS 105384]). The estimates are in fairly good agreement for each area. Recharge efficiencies for Maxey-Eakin estimates vary between approximately 3% and 7%, while the model estimated recharge efficiencies varied from approximately 2% to 14%.

Table 7.2.1.2-2. Recharge Estimates for Selected Nevada Hydrographic Areas/Subareas [a]

Number [b]	Name [b]	Size [b] (acres)	Precipitation [c]		Recharge [c] (mm/yr)			Efficiency (%)		
			(acre-ft/yr)	(mm/yr)	CMB	ME	WB	CMB	ME	WB
16	Duck Lake Valley	341,120	243,300	217	8.0	8.0	6.5	3.7	3.7	3.0
36	Independence Valley	220,800	251,410	347	13.4	22.4	16.8	3.9	6.5	4.8
56	Upper Reese River Valley	728,320	592,030	248	12.6	24.4	15.6	5.1	9.9	6.3
92	Lemmon Valley	59,520	30,818	158	8.3	8.3	8.3	5.3	5.3	5.3
117	Fish Lake Valley	451,840	251,410	170	18.1	22.4	18.1	10.6	13.2	10.6
122	Gabbs Valley	817,280	381,170	142	1.8	1.8	1.5	1.3	1.3	1.1
153	Diamond Valley	481,280	227,080	144	6.7	7.7	7.7	4.6	5.4	5.4
163	Mesquite Valley	151,040	30,007	61	3.3	3.3	4.9	5.4	5.4	8.1
170	Penoyer Valley	448,000	97,320	66	2.2	2.8	2.8	3.3	4.2	4.2
173A	Railroad Valley (Southern Part)	385,920	616,360	487	22.4	36.5	54.4	4.6	7.5	11.2
173B	Railroad Valley (Northern Part)	1,375,360	129,760	29	1.1	1.3	1.3	3.8	4.4	4.4
178A	Butte Valley (Northern Part)	173,440	48,660	86	4.3	7.1	15.7	5.0	8.3	18.3
178B	Butte Valley (Southern Part)	472,960	194,640	125	7.8	9.9	7.8	6.3	7.9	6.3
184	Spring Valley	1,063,040	786,670	226	17.7	21.6	21.2	7.8	9.6	9.4

[a] Dettinger 1989 [DIRS 105384], Table 2.
[b] Basin size given in Horton 1998 [DIRS 174618], Appendix A-1.
[c] Dettinger (1989 [DIRS 105384]) reported precipitation and recharge in cubic hectometers per year (hm^3/yr), which were converted to acre-ft/yr using a conversion factor of $1 hm^3/yr = 811$ acre-ft/yr given by Dettinger (1989 [DIRS 105384]). Precipitation and recharge converted to mm/yr using basin area.

Table 7.2.1.2-3. Maxey-Eakin and Water Budget Recharge Estimates for Selected Nevada Hydrographic Areas/Subareas [a]

Number [b]	Name [b]	Size [b] (acres)	Precipitation [c,d]		Recharge [d]				Efficiency	
					ME		WB		ME	WB
			(acre-ft/yr)	(mm/yr)	(acre-ft/yr)	(mm/yr)	(acre-ft/yr)	(mm/yr)	(%)	(%)
18	Painter Flat	19,840	31,000	476.3	1,300	20.0	1,200	6.3	3.6	2.8
21	Smoke Creek Desert	627,200	275,100	133.7	13,000	6.3	18,620	18.4	4.2	3.9
22	San Emidio Desert	195,200	47,900	74.8	2,100	3.3	3,200	9.0	4.7	6.8
24	Hualapai Flat	201,600	106,200	160.6	7,000	10.6	6,700	5.0	4.4	6.7
29	Pine Forest Valley	337,920	197,000	177.7	10,000	9.0	14,100	10.1	6.6	6.3
53	Pine Valley	641,280	654,000	310.8	45,500	21.6	24,000	12.7	5.1	7.2
55	Carico Lake Valley	240,640	86,600	109.7	4,300	5.4	4,500	11.4	7.0	3.7
71	Grass Valley	332,800	180,000	164.9	12,000	11.0	16,800	5.7	5.0	5.2
84	Warm Springs Valley	158,080	96,000	185.1	6,000	11.6	2,000	15.4	6.7	9.3
85	Spanish Springs Valley	48,640	16,000	100.3	600	3.8	1,000	3.9	6.3	2.1
86	Sun Valley	6,400	1,800	85.7	50	2.4	25	6.3	3.8	6.3
92	Lemmon Valley	59,520	43,400	222.3	1,800	9.2	900	1.2	2.8	1.4
95	Dry Valley	51,200	37,000	220.3	2,400	14.3	2,300	4.6	4.1	2.1
96	Newcomb Lake Valley	5,760	4,500	238.1	300	15.9	130	13.7	6.5	6.2
97	Honey Lake Valley	123,520	24,000	59.2	1,500	3.7	10,500	6.9	6.7	2.9
111A	Alkali Valley (Northern Part)	11,520	7027	185.9	400	10.6	300	7.9	5.7	4.3
113	Huntoon Valley	62,080	22,200	109.0	800	3.9	300	1.5	3.6	1.4
114	Teels Marsh Valley	206,720	38,400	56.6	1,300	1.9	1,400	2.1	3.4	3.6
118	Columbus Salt Marsh Valley	236,800	13,300	17.1	700	0.9	3,800	18.2	12.9	10.6
119	Rhodes Salt Marsh Valley	127,360	11,600	27.8	500	1.2	600	4.9	5.3	28.6
121	Soda Springs Valley/Eastern Part	240,640	19,600	24.8	700	0.9	430	1.4	4.3	5.2

Table 7.2.1.2-3. Maxey-Eakin and Water Budget Recharge Estimates for Selected Nevada Hydrographic Areas/Sub-Areas [a] (Continued)

Number [b]	Name [b]	Size [b] (acres)	Precipitation [c,d]		Recharge [d]				Efficiency	
					ME		WB		ME	WB
			(acre-ft/yr)	(mm/yr)	(acre-ft/yr)	(mm/yr)	(acre-ft/yr)	(mm/yr)	(%)	(%)
125-127	Stingaree Valley, Cowkick Valley, Eastgate Valley Area	236,160	94,100	121.5	6,000	7.7	6,000	0.5	3.6	2.2
128	Dixie Valley	833,920	116,200	42.5	6,000	2.2	9,200	7.7	6.4	6.4
132	Jersey Valley	90,880	16,970	56.9	800	2.7	800	3.4	5.2	7.9
133	Edwards Creek Valley	266,240	111,400	127.5	8,000	9.2	7,600	2.7	4.7	4.7
134	Smith Creek	372,480	92,000	75.3	9,600	7.9	7,000	8.7	7.2	6.8
136	Monte Cristo Valley	181,760	12,200	20.5	500	0.8	400	5.7	10.4	7.6
138	Grass Valley	380,800	211,000	168.9	13,000	10.4	13,000	0.7	4.1	3.3
150	Little Fish Lake Valley	277,760	181,000	198.6	11,000	12.1	10,000	10.4	6.2	6.2
153	Diamond Valley	481,280	319,000	202.0	21,000	13.3	21,000	11.0	6.1	5.5
156	Hot Creek	663,040	153,000	70.3	7,000	3.2	6,100	13.3	6.6	6.6
179	Steptoe Valley	1,242,880	810,000	198.6	85,000	20.8	70,000	2.8	4.6	4.0
183	Lake Valley	356,480	229,000	195.8	13,000	11.1	11,500	2.6	4.5	4.0
184	Spring Valley	1,063,040	791,000	226.8	75,000	21.5	74,000	9.8	7.9	8.6

[a] Avon and Durbin (1994 [DIRS 177200]), Table 2.
[b] Basin areas from Horton (1998 [DIRS 174618], Appendix A-1).
[c] Precipitation estimates from Lopes and Evetts (2004 [DIRS 175964], Appendix 1)
[d] Precipitation and recharge originally reported in acre-ft/yr were converted to mm/yr using basin areas reported by Horton (1998 [DIRS 174618], Appendix A-1).

Table 7.2.1.2-4. Maxey-Eakin and "Model" Recharge Estimates for Selected Nevada Hydrographic Areas/Sub-Areas [a]

Number [b]	Name [b]	Size [b] (acres)	Precipitation [c,d]		Recharge [d]				Efficiency (%)	
					ME [a]		Model Estimates [a]			
			(acre-ft/yr)	(mm/yr)	(acre-ft/yr)	(mm/yr)	(acre-ft/yr)	(mm/yr)	ME	Model
175	Long Valley	416,640	297,000	217.3	10,000	7.3	5,000	3.7	3.4	1.7
180	Cave Valley	231,680	206,000	271.0	14,000	18.4	12,000	15.8	6.8	5.8
181	Dry Lake Valley	564,480	118,000	63.7	5,000	2.7	6,700	3.6	4.2	5.7
182	Delamar Valley	245,120	34,000	42.3	1,000	1.2	1,800	2.2	2.9	5.3
206	Kane Springs Valley	149,760	10,000	20.4	500	1.0	1,000	2.0	5.0	10.0
208	Pahroc Valley	325,120	57,000	53.4	2,200	2.1	2,000	1.9	3.9	3.5
209	Pahranagat Valley	491,520	43,000	26.7	1,800	1.1	1,500	0.9	4.2	3.5
210	Coyote Springs Valley	420,480	39,000	28.3	2,100	1.5	5,300	3.8	5.4	13.6

[a] Avon and Durbin 1994 [DIRS 177200], Table 3.
[b] Basin areas from Horton 1998 [DIRS 174618], Appendix A-1.
[c] Precipitation estimates from Lopes and Evetts 2004 [DIRS 175964], Appendix 1.
[d] Precipitation and recharge originally reported in acre-ft/yr were converted to mm/yr using basin areas reported by Horton 1998 [DIRS 174618], Appendix A-1.

Lichty and McKinley (1995 [DIRS 100589], Tables 1 and 15) investigated groundwater recharge rates for 3-Springs and East Stewart basins, two small basins in central Nevada. Two independent modeling approaches were used at each site: water budget and chloride mass balance methods. Their results are presented in Table 7.2.1.2-5. The results for the East Stewart basin are included even though the precipitation in this basin is substantially higher than would be expected at Yucca Mountain, even for the glacial transition climate. One observes that for the 3-Springs basin, the chloride mass balance estimates are approximately three times higher than the water balance estimate. The recharge efficiency estimates vary from about 3% to 10%. The variation between the methods is much smaller for the East Stewart basin. The recharge efficiency for this basin is approximately 50%.

Table 7.2.1.2-5. Recharge to 3-Springs Basin, Central Nevada [a]

Basin	Area (km^2)	Precipitation (mm/yr)	Recharge (mm/yr)		Efficiency (%)	
			WB [b]	CMB [b]	WB [b]	CMB [b]
3-Springs	4.20	336.4	11.4	32.8	3.4	9.8
East Stewart	0.93	639.1	321.5	309.9	50.3	48.5

[a] Lichty and McKinley (1995 [DIRS 100589], Tables 1 and 15).
[b] WB= water balance; CMB = chloride mass balance.

Nichols (2000 [DIRS 178863]) estimated basin-scale recharge rates for 16 hydrographic basins in Nevada. These estimates, which used a modified Maxey-Eakin approach, are listed in Table 7.2.1.2-6. The basin areas used to calculate the annual precipitation in mm/yr are from Horton (1998 [DIRS 174618], Appendix A-1). These areas differ slightly from the areas reported by Nichols (2000 [DIRS 178863], Table C-19), however the differences are all less than 2%.

Table 7.2.1.2-6. Recharge Estimates for 16 Nevada Hydrographic Areas [a]

No. [b]	Name [b]	Area [b] (acres)	Precipitation [c]		Recharge [c]		Efficiency	Method [d]
			(acre-ft/yr)	(mm/yr)	(acre-ft/yr)	(mm/yr)	(%)	
150	Little Fish Lake Valley	276,482	236,430	261	9,628	10.6	4.1	MME
154	Newark Valley	509,282	515,470	309	49,092	29.4	9.5	MME
155	Little Smoky Valley	740,575	523,359	215	12,681	5.2	2.4	MME
156	Hot Creek Valley	658,501	424,067	196	5,756	2.7	1.4	MME
174	Jakes Valley	270,498	289,477	326	38,203	43.0	13.2	MME
175	Long Valley	419,844	452,368	328	47,740	34.7	10.6	MME
176	Ruby Valley	638,936	867,225	414	145,636	69.5	16.8	MME
177	Clover Valley	292,115	363,327	379	58,802	61.4	16.2	MME
178	Butte Valley	652,363	700,905	327	68,989	32.2	9.8	MME
179	Steptoe Valley	1,245,618	1,344,191	329	131,469	32.2	9.8	MME
184	Spring Valley	1,067,010	1,141,444	326	103,569	29.6	9.1	MME
185	Tippett Valley	221,574	211,904	291	12,389	17.0	5.8	MME
186	Antelope Valley	255,680	246,551	294	16,824	20.1	6.8	MME
187	Goshute Valley	612,169	592,875	295	40,911	20.4	6.9	MME

Table 7.2.1.2-6. Recharge Estimates for 16 Nevada Hydrographic Areas [a] (Continued)

No. [b]	Name [b]	Area [b] (acres)	Precipitation [c]		Recharge [c]		Efficiency	Method [d]
			(acre-ft/yr)	(mm/yr)	(acre-ft/yr)	(mm/yr)	(%)	
188	Independence Valley	360,670	394,415	333	50,065	42.3	12.7	MME
173B	Railroad Valley/Northern Part	1,369,671	1,089,249	242	61,083	13.6	5.6	MME

[a] Nichols 2000 [DIRS 178863], Chapter C.
[b] Basin area and number from Horton 1998 [DIRS 174618], Appendix A-1. The areas differ slightly from those listed in Nichols (2000 [DIRS 178863]). The differences are all less than 2% (see Output DTN SN0701T0502206.037, file: \Welcome to Massif\Massif\Validation Analyses\Excel Figures*Recharge_models_vs_MASSIF.xls*, sheet: "Nichols" for a comparison of this difference.
[c] Precipitation and recharge originally reported in acre-ft/yr by Nichols 2000 DIRS 178863], Table C-19, were converted to mm/yr using basin areas reported by Horton 1998 [DIRS 174618], Appendix A-1.
[d] MME = modified Maxey-Eakin.

The U.S. Geological Survey, in cooperation with the Nevada Division of Environmental Protection, has recently compiled estimates of natural recharge from published sources (Lopes and Evetts 2004 [DIRS 175964], Appendix 1). This report contains basin-wide estimates of average annual precipitation and recharge for basins in Nevada. These estimates of average annual precipitation and recharge for each basin are provided in Table 7.2.1.2-7. As with the report by Avon and Durbin (1994 [DIRS 177200]) there is some overlap between estimates reported by Lopes and Evetts (2004 [DIRS 175964], Appendix 1) and previous studies, so these estimates are excluded from the table. Also excluded are estimates for which no precipitation information was reported.

The recharge values reported in Table 7.2.1.2-7 are mainly Maxey-Eakin or modified Maxey-Eakin estimates, along with a much smaller number of water budget and chloride mass balance estimates. In many cases, Lopes and Evetts (2004 [DIRS 175964], Appendix 1) report multiple precipitation/recharge values for a single hydrographic area. Precipitation estimates for a single area can vary by a factor of 2 and as much as 4; recharge estimates for a single area can vary by as much as a factor of 5. Multiple methods and data sources were used to estimate these values, which is the primary reason for reporting multiple values and the source of the variability. However, irrespective of data source or estimation method, recharge values reported by Lopes and Evetts (2004 [DIRS 175964], Appendix 1) typically remain between 3% and 10% of precipitation. Estimates reported by Lopes and Evetts (2004 [DIRS 175964]) from Nichols (2000 [DIRS 178863]) are listed separately in Table 7.2.1.2-6.

Table 7.2.1.2-7. Recharge Estimates for Selected Nevada Hydrographic Areas/Subareas [a]

No. [b]	Name [b]	Area [b] (acres)	Precipitation [c]		Recharge [c]		Efficiency	Method [d]
			(acre-ft/yr)	(mm/yr)	(acre-ft/yr)	(mm/yr)	(%)	
1	Pueblo Valley	75,520	48,300	195	2,000	8.1	4.1	ME
2	Continental Lake Valley	136,960	254,200	566	11,000	24.5	4.3	ME
3	Gridley Lake Valley	124,800	97,900	239	4,500	11.0	4.6	ME
4	Virgin Valley	316,160	230,000	222	7,000	6.7	3.0	ME
6	Guano Valley	94,080	206,000	667	7,500	24.3	3.6	ME

Table 7.2.1.2-7. Recharge Estimates for Selected Nevada Hydrographic Areas/Subareas [a] (Continued)

No. [b]	Name [b]	Area [b] (acres)	Precipitation [c]		Recharge [c]		Efficiency	Method [d]
			(acre-ft/yr)	(mm/yr)	(acre-ft/yr)	(mm/yr)	(%)	
8	Massacre Lake Valley	112,640	88,200	239	3,500	9.5	4.0	ME
9	Long Valley	277,120	168,000	185	6,000	6.6	3.6	ME
11	Coleman Valley	32,640	28,000	261	1,000	9.3	3.6	ME
12	Mosquito Valley	20,480	14,300	213	700	10.4	4.9	ME
14	Surprise Valley	136,960	37,500	83	1,500	3.3	4.0	ME
15	Boulder Valley	56,320	50,400	273	2,000	10.8	4.0	ME
17	Pilgrim Flat	7,680	7,000	278	500	19.8	7.1	ME
19	Dry Valley	24,960	5,900	72	200	2.4	3.4	ME
20	Sano Valley	7,680	130	5	4	0.2	3.1	ME
23	Granite Basin	5,760	45,400	2,402	2,000	105.8	4.4	ME
24	Hualapai Flat	201,600	62,700	95	4,000	6.0	6.4	ME
25	High Rock Lake Valley	425,600	435,000	312	13,000	9.3	3.0	ME
26	Mud Meadow	316,800	130,600	126	8,000	7.7	6.1	ME
27	Summit Lake Valley	38,400	42,700	339	4,200	33.3	9.8	ME
28	Black Rock Desert	1,394,560	260,900	57	13,900	3.0	5.3	ME
30	Kings River Valley	264,320	260,000	300	15,000	17.3	5.8	ME
31	Desert Valley	673,280	100,000	45	5,000	2.3	5.0	ME
		673,280	110,000	50	7,000	3.2	6.4	ME
		673,280	110,000	50	3,300	1.5	3.0	CMB
32	Silver State Valley	200,320	35,000	53	1,400	2.1	4.0	ME
33	Quinn River Valley	783,360	880,000	342	62,000	24.1	7.0	ME
34	Little Owyhee River Area	458,240	357,000	237	2,700	1.8	0.8	ME
35	South Fork Owyhee River Area	838,400	1,004,000	365	28,000	10.2	2.8	ME
37	Owyhee River Area	341,120	458,000	409	17,000	15.2	3.7	ME
38	Bruneau River Area	328,960	497,000	460	26,000	24.1	5.2	ME
39	Jarbidge River Area	177,920	334,000	572	32,000	54.8	9.6	ME
40	Salmon Falls Creek Area	779,520	1,021,000	399	44,000	17.2	4.3	ME
41	Goose Creek Area	202,240	198,000	298	6,700	10.1	3.4	ME
46	South Fork Area	63,360	98,000	471	3,000	14.4	3.1	WB
47	Huntington Valley	503,680	554,000	335	14,000	8.5	2.5	WB
48	Dixie Creek-Tenmile Creek Area	250,880	235,000	286	13,000	15.8	5.5	WB
50	Susie Creek Area	142,720	147,000	314	9,700	20.7	6.6	ME
51	Maggie Creek Area	253,440	280,000	337	23,000	27.7	8.2	ME
52	Marys Creek Area	39,040	37,000	289	2,100	16.4	5.7	ME
53	Pine Valley	641,280	688,000	327	52,500	25.0	7.6	WB
		641,280	688,000	327	79,300	37.7	11.5	WB
		641,280	688,000	327	66,000	31.4	9.6	MME
54	Crescent Valley	481,280	200,000	127	14,000	8.9	7.0	Other
		481,280	446,000	282	25,200	16.0	5.7	WB
		481,280	446,000	282	26,200	16.6	5.9	WB

Table 7.2.1.2-7. Recharge Estimates for Selected Nevada Hydrographic Areas/Subareas [a] (Continued)

No. [b]	Name [b]	Area [b] (acres)	Precipitation [c]		Recharge [c]		Efficiency	Method [d]
			(acre-ft/yr)	(mm/yr)	(acre-ft/yr)	(mm/yr)	(%)	
		481,280	446,000	282	21,000	13.3	4.7	MME
55	Carico Lake Valley	240,640	239,000	303	18,700	23.7	7.8	WB
		240,640	239,000	303	20,400	25.8	8.5	WB
		240,640	239,000	303	18,000	22.8	7.5	MME
56	Upper Reese River Valley	728,320	803,000	336	71,400	29.9	8.9	WB
		728,320	803,000	336	110,000	46.0	13.7	WB
		728,320	803,000	336	93,000	38.9	11.6	MME
57	Antelope Valley	289,280	240,000	253	11,000	11.6	4.6	ME
		289,280	279,000	294	17,200	18.1	6.2	WB
		289,280	279,000	294	25,200	26.6	9.0	WB
		289,280	279,000	294	19,000	20.0	6.8	MME
58	Middle Reese River Valley	204,160	142,000	212	7,000	10.5	4.9	ME
		204,160	186,000	278	12,800	19.1	6.9	WB
		204,160	186,000	278	13,200	19.7	7.1	WB
		204,160	186,000	278	10,000	14.9	5.4	MME
59	Lower Reese River Valley	376,320	341,000	276	18,500	15.0	5.4	WB
		376320	341,000	276	19,000	15.4	5.6	WB
		376,320	341,000	276	13,000	10.5	3.8	MME
60	Whirlwind Valley	60,160	55,000	279	3,700	18.7	6.7	WB
		60,160	55,000	279	3,800	19.3	6.9	WB
		60,160	55,000	279	2,000	10.1	3.6	MME
61	Boulder Flat	348,160	291,000	255	14,000	12.3	4.8	ME
		348,160	308,000	270	19,100	16.7	6.2	WB
		348,160	308,000	270	19,300	16.9	6.3	WB
		348,160	308,000	270	11,000	9.6	3.6	MME
62	Rock Creek Valley	284,160	256,000	275	17,100	18.3	6.7	WB
		284,160	256,000	275	9,000	9.7	3.5	MME
		284,160	270,000	290	13,000	13.9	4.8	ME
63	Willow Creek Valley	259,200	279,000	328	20,000	23.5	7.2	ME
		259,200	280,000	329	27,500	32.3	9.8	WB
		259,200	280,000	329	28,000	32.9	10.0	MME
64	Clovers Area	460,800	401,000	265	17,900	11.8	4.5	WB
		460,800	401,000	265	18,400	12.2	4.6	WB
		460,800	401,000	265	13,000	8.6	3.2	MME
65	Pumpernickel Valley	191,360	169,000	269	8,800	14.0	5.2	WB
		191,360	169,000	269	9,000	14.3	5.3	WB
		191,360	169,000	269	7,500	11.9	4.4	MME
66	Kelly Creek Area	192,640	181,000	286	12,700	20.1	7.0	WB
		192,640	181,000	286	13,200	20.9	7.3	WB
		192,640	181,000	286	11,000	17.4	6.1	MME
67	Little Humboldt Valley	624,000	443,000	216	24,000	11.7	5.4	ME
68	Hardscrabble Area	106,880	115,000	328	9,000	25.7	7.8	ME

Table 7.2.1.2-7. Recharge Estimates for Selected Nevada Hydrographic Areas/Subareas [a] (Continued)

No. [b]	Name [b]	Area [b] (acres)	Precipitation [c]		Recharge [c]		Efficiency	Method [d]
			(acre-ft/yr)	(mm/yr)	(acre-ft/yr)	(mm/yr)	(%)	
69	Paradise Valley	384,000	121,000	96	10,000	7.9	8.3	ME
72	Imlay Area	493,440	82,000	51	4,000	2.5	4.9	ME
73	Lovelock Valley	406,400	60,000	45	3,200	2.4	5.3	ME
74	White Plains	104,960	100	0	3	0.0	3.0	ME
75	Bradys Hot Springs Area	113,920	4,800	13	160	0.4	3.3	ME
76	Fernley Area	76,800	13,000	52	600	2.4	4.6	ME
77	Fireball Valley	37,120	6,000	49	200	1.6	3.3	ME
78	Granite Springs Valley	618,880	97,600	48	3,500	1.7	3.6	ME
79	Kumiva Valley	213,120	28,000	40	1,000	1.4	3.6	ME
80	Winnemucca Lake Valley	237,440	61,000	78	2,900	3.7	4.8	ME
81	Pyramid Lake Valley	430,080	100,000	71	6,600	4.7	6.6	ME
82	Dodge Flat	58,880	21,000	109	1,400	7.2	6.7	ME
83	Tracy Segment	182,400	121,000	202	6,000	10.0	5.0	ME
85	Spanish Springs Valley	48,640	26,000	163	830	5.2	3.2	ME
		48,640	26,000	163	770	4.8	3.0	CMB
87	Truckee Meadows	129,920	161,000	378	27,000	63.3	16.8	ME
88	Pleasant Valley	24,960	46,000	562	10,000	122.1	21.7	ME
89	Washoe Valley	52,480	87,000	505	15,000	87.1	17.2	ME
91	Truckee CanyonSegment	53,760	110,000	624	27,000	153.1	24.5	ME
92	Lemmon Valley	59,520	44,000	225	1,500	7.7	3.4	ME
93	Antelope Valley	11,520	9,000	238	300	7.9	3.3	ME
94	Bedell Flat	33,920	27,000	243	1,100	9.9	4.1	ME
98	Skedaddle Creek Valley	27,520	17,680	196	600	6.6	3.4	ME
99	Red Rock Valley	37,120	7,700	63	900	7.4	11.7	ME
100	Cold Spring Valley	35,200	18,000	156	900	7.8	5.0	ME
101	Carson Desert	1,396,480	43,000	9	2,010	0.4	4.7	ME
102	Churchill Valley	307,200	32,000	32	1,300	1.3	4.1	ME
103	Dayton Valley	236,160	125,300	162	7,900	10.2	6.3	ME
		236,160	127,000	164	7,900	10.2	6.2	ME
		236,160	163,000	210	11,000	14.2	6.7	ME
		236,160	229,000	296	26,000	33.6	11.4	ME
104	Eagle Valley	44,160	58,000	400	8,700	60.0	15.0	ME
		44,160	67,000	462	8,000	55.2	11.9	WB
		44,160	67,000	462	10,000	69.0	14.9	WB
105	Carson Valley	268,160	254,000	289	25,000	28.4	9.8	ME
		268,160	350,000	398	49,000	55.7	14.0	ME
106	Antelope Valley	73,600	66,700	276	5,000	20.7	7.5	ME
107	Smith Valley	306,560	210,000	209	17,000	16.9	8.1	ME
108	Mason Valley	330,240	32,000	30	2,000	1.8	6.3	ME
109	East Walker Area	375,040	191,000	155	22,000	17.9	11.5	ME
110	Walker Lake Valley	864,000	101,000	36	6,500	2.3	6.4	ME
111	Alkali Valley	53,120	32,400	186	1,800	10.3	5.6	ME

Table 7.2.1.2-7. Recharge Estimates for Selected Nevada Hydrographic Areas/Subareas [a] (Continued)

No. [b]	Name [b]	Area [b] (acres)	Precipitation [c]		Recharge [c]		Efficiency	Method [d]
			(acre-ft/yr)	(mm/yr)	(acre-ft/yr)	(mm/yr)	(%)	
112	Mono Valley	17,280	16,000	282	700	12.3	4.4	ME
115	Adobe Valley	9,600	6,400	203	300	9.5	4.7	ME
116	Queen Valley	41,600	25,100	184	2,000	14.7	8.0	ME
120	Garfield Flat	58,880	9,400	49	300	1.6	3.2	ME
123	Rawhide Flats	145,280	5,000	10	150	0.3	3.0	ME
124	Fairview Valley	182,400	16,600	28	500	0.8	3.0	ME
		182,400	74,000	124	2,300	3.8	3.1	ME
125,6,7	Sum of HAs 125, 126, 127	236,160	171,000	221	6,700	8.6	3.9	ME
128	Dixie Valley	833,920	246,900	90	8,900	3.3	3.6	ME
130	Pleasant Valley	182,400	44,900	75	3,000	5.0	6.7	ME
		182,400	92,000	154	3,300	5.5	3.6	ME
132	Jersey Valley	90,880	41,000	138	1,400	4.7	3.4	ME
134	Smith Creek Valley	372,480	119,000	97	12,000	9.8	10.1	ME
135	Ione Valley	294,400	90,000	93	8,000	8.3	8.9	ME
137	Big Smoky Valley	1,872,640	741,000	121	77,000	12.5	10.4	ME
139	Kobeh Valley	555,520	110,000	60	11,000	6.0	10.0	ME
140	Monitor Valley	664,320	392,500	180	23,300	10.7	5.9	ME
141	Ralston Valley	621,440	340,000	167	16,000	7.8	4.7	ME
		621,440	115,000	56	5,000	2.5	4.3	ME
142	Alkali Spring Valley	200,320	2,800	4	100	0.2	3.6	ME
143	Clayton Valley	355,200	34,700	30	1,500	1.3	4.3	ME
144	Lida Valley	342,400	13,400	12	500	0.4	3.7	ME
145	Stonewall Flat	243,840	1,900	2	100	0.1	5.3	ME
146	Sarcobatus Flat	519,680	37,500	22	1,200	0.7	3.2	ME
147	Gold Flat	437,760	94,000	65	3,800	2.6	4.0	ME
148	Cactus Flat	257,920	15,000	18	600	0.7	4.0	ME
149	Stone Cabin Valley	630,400	362,000	175	16,000	7.7	4.4	ME
		630,400	103,000	50	5,000	2.4	4.9	ME
151	Antelope Valley	284,160	108,100	116	4,100	4.4	3.8	ME
152	Stevens Basin	10,880	8,500	238	200	5.6	2.4	ME
153	Diamond Valley	481,280	304,000	193	16,000	10.1	5.3	ME
154	Newark Valley	512,640	335,000	199	17,500	10.4	5.2	ME
155	Little Smoky Valley	741,120	140,000	58	5,400	2.2	3.9	ME
157	Kawich Valley	224,000	88,000	120	3,500	4.8	4.0	ME
158	Emigrant Valley	490,880	75,720	47	3,204	2.0	4.2	ME
159	Yucca Flat	195,200	19,300	30	700	1.1	3.6	ME
160	Frenchman Flat	296,320	3,200	3	100	0.1	3.1	ME
161	Indian Springs Valley	419,200	115,000	84	10,000	7.3	8.7	ME
163	Mesquite Valley	151,040	28,400	57	1,400	2.8	4.9	ME
164	Ivanpah Valley	208,640	13,350	20	700	1.0	5.2	ME
165	Jean Lake Valley	61,440	2,200	11	100	0.5	4.5	ME

Table 7.2.1.2-7. Recharge Estimates for Selected Nevada Hydrographic Areas/Subareas [a] (Continued)

No. [b]	Name [b]	Area [b] (acres)	Precipitation [c]		Recharge [c]		Efficiency	Method [d]
			(acre-ft/yr)	(mm/yr)	(acre-ft/yr)	(mm/yr)	(%)	
167	Eldorado Valley	339,200	37,000	33	1,100	1.0	3.0	ME
168	Three Lakes Valley	190,720	41,100	66	2,000	3.2	4.9	ME
169	Tikapoo Valley	638,720	115,000	55	6,000	2.9	5.2	ME
170	Penoyer Valley	448,000	97,300	66	13,500	9.2	13.9	ME
171	Coal Valley	294,400	62,000	64	2,000	2.1	3.2	ME
172	Garden Valley	315,520	137,000	132	10,000	9.7	7.3	ME
173	Railroad Valley	385,920	817,200	645	50,400	39.8	6.2	ME
175	Long Valley	416,640	297,000	217	10,000	7.3	3.4	ME
176	Ruby Valley	642,560	696,000	330	68,000	32.3	9.8	ME
177	Clover Valley	296,960	224,000	230	20,700	21.2	9.2	ME
180	Cave Valley	231,680	206,000	271	14,000	18.4	6.8	ME
181	Dry Lake Valley	564,480	118,000	64	5,000	2.7	4.2	ME
182	Delamar Valley	245,120	34,000	42	1,000	1.2	2.9	ME
185	Tippett Valley	220,800	114,000	157	6,900	9.5	6.1	ME
186	Antelope Valley	252,800	117,000	141	4,700	5.7	4.0	ME
188	Independence Valley	359,680	203,000	172	9,300	7.9	4.6	ME
189	Thousand Springs Valley	925,440	325,000	107	12,000	4.0	3.7	ME
190	Grouse Creek Valley	35,200	19,100	165	700	6.1	3.7	ME
191	Pilot Creek Valley	208,640	40,000	58	2,400	3.5	6.0	ME
192	Great Salt Lake Desert	324,480	77,600	73	4,800	4.5	6.2	ME
193	Deep Creek Valley	133,120	44,700	102	2,200	5.0	4.9	ME
197	Escalante Desert	67,840	76,000	341	2,300	10.3	3.0	ME
201	Spring Valley	183,680	177,000	294	10,000	16.6	5.6	ME
202	Patterson Valley	267,520	137,000	156	6,000	6.8	4.4	ME
206	Kane Springs Valley	149,760	10,000	20	500	1.0	5.0	ME
208	Pahroc Valley	325,120	57,000	53	2,200	2.1	3.9	ME
209	Pahranagat Valley	491,520	43,000	27	1,800	1.1	4.2	ME
210	Coyote Spring Valley	420,480	39,000	28	2,100	1.5	5.4	ME
211	Three Lakes Valley	199,040	56,000	86	6,000	9.2	10.7	ME
		199,040	56,000	86	7,300	11.2	13.0	MME
212	Las Vegas Valley	1,000,960	161,200	49	30,000	9.1	18.6	ME
		1,000,960	161,200	49	35,000	10.7	21.7	ME
		1,000,960	332,500	101	28,000	8.5	8.4	CMB
213	Colorado River Valley	360,320	5800	5	200	0.2	3.4	ME
214	Piute Valley	216,320	55,800	79	1,700	2.4	3.0	ME
215	Black Mountains Area	403,200	2,200	2	70	0.1	3.2	ME
216	Garnet Valley	99,840	11,000	34	400	1.2	3.6	ME
217	Hidden Valley	51,200	11,000	65	400	2.4	3.6	ME
218	California Wash	203,520	2,000	3	60	0.1	3.0	ME
220	Lower Moapa Valley	161,280	1,200	2	40	0.1	3.3	ME
221	Tule Desert	122,880	62,000	154	2,100	5.2	3.4	ME
222	Virgin River Valley	580,480	98,700	52	3,600	1.9	3.6	ME

Table 7.2.1.2-7. Recharge Estimates for Selected Nevada Hydrographic Areas/Subareas [a] (Continued)

No. [b]	Name [b]	Area [b] (acres)	Precipitation [c]		Recharge [c]		Efficiency	Method [d]
			(acre-ft/yr)	(mm/yr)	(acre-ft/yr)	(mm/yr)	(%)	
223	Gold Butte Area	341,120	27,600	25	1,000	0.9	3.6	ME
224	Greasewood Area	69,120	14,900	66	600	2.6	4.0	ME
225	Mercury Valley	70,400	5,200	23	250	1.1	4.8	ME
226	Rock Valley	52,480	900	5	30	0.2	3.3	ME
227	Fortymile Canyon	332,160	61,000	56	2,300	2.1	3.8	ME
228	Oasis Valley	294,400	33,500	35	1,000	1.0	3.0	ME
229	Crater Flat	116,480	6,700	18	220	0.6	3.3	ME
230	Amargosa Desert	573,440	90,000	48	1,500	0.8	1.7	ME
231	Grapevine Canyon	103,680	1,070	3	50	0.1	4.7	ME
232	Oriental Wash	116,480	8,500	22	300	0.8	3.5	ME

[a] Lopes and Evetts 2004 [DIRS 175964], Appendix 1.

[b] Basin areas from Horton 1998 [DIRS 174618], Appendix A-1.

[c] Precipitation and recharge originally reported in acre-ft/yr were converted to mm/yr using basin areas reported by Horton 1998 [DIRS 174618], Appendix A-1.

[d] CMB = chloride mass balance; ME=Maxey-Eakin; MME = modified Maxey-Eakin; WB = water budget.

Figure 7.2.1.2-2 summarizes the basin-scale, net infiltration estimates listed in Tables 7.2.1.2-1 through 7.2.1.2-7 and plots these data with the MASSIF net infiltration results for three climates. The Maxey-Eakin (1950 [DIRS 100598]) model (represented as a stepped line on the figure) is also shown for reference. Note that the Maxey-Eakin model line does not match the individual basin-scale Maxey-Eakin model net infiltration estimates, shown as black crosses on the figure. This is because each of these precipitation and recharge estimates is an area-weighted mean value derived from subareas of the basin in which precipitation is estimated locally. For each of these subareas an associated recharge amount is determined using the percent recharge values from Maxey-Eakin (1950 [DIRS 100598] p. 40). Thus the total precipitation and total recharge values are area-weighted mean values and vary depending on the precipitation patterns across the basin, which largely depend on the basin's topographic character. There is fairly good agreement among the methods for relatively low precipitation, but estimates tend to diverge as precipitation increases. The hydrographic areas closest to Yucca Mountain fall at the low end of the recharge scale (less than 10 mm/yr) and correspond well with the MASSIF net infiltration estimates for the Present-Day climate at Yucca Mountain. The MASSIF net infiltration estimates for the monsoon and glacial transition climates are generally within the range for the wetter Nevada basins.

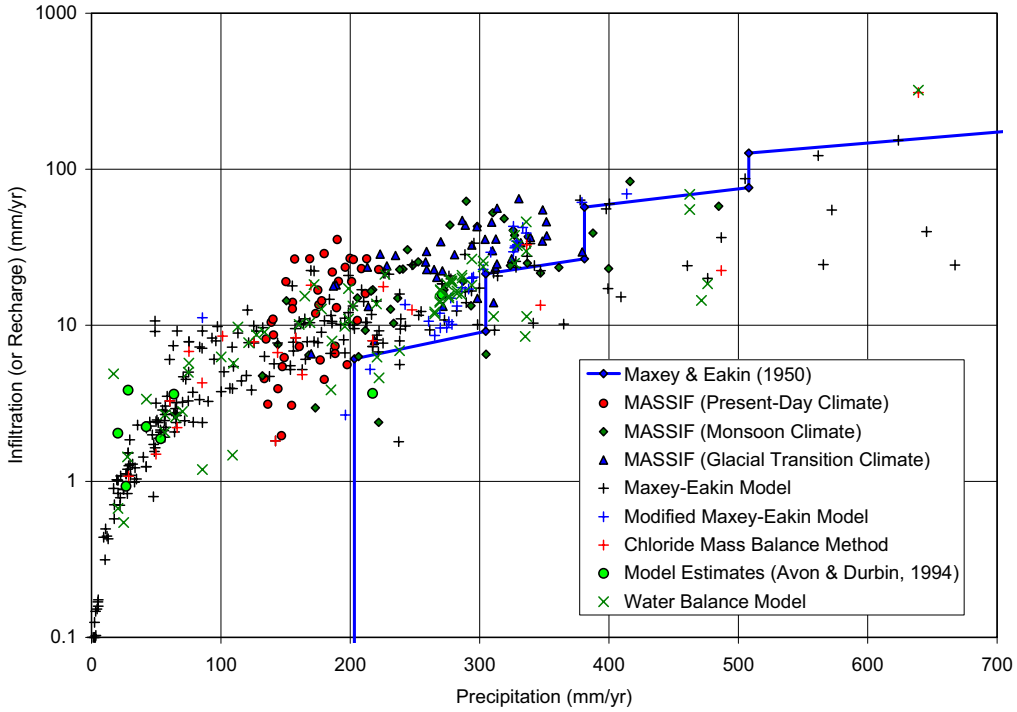

Source: Output DTNs: SN0701T0502206.034, SN0701T0502206.036, and SN0701T0502206.035, respectively (MASSIF results for Present-Day, Monsoon, and Glacial Transition climates). Data are from sources listed for Tables 7.2.1.2-1, 7.2.1.2-2, 7.2.1.2-3, 7.2.1.2-4, 7.2.1.2-5, and 7.2.1.2-6, which are also compiled in Validation Output DTN: SN0704T0502206.047.

NOTE: Vertical line that extends to the horizontal axis associated with the Maxey-Eakin model represents the precipitation amount below which the model predicts zero recharge.

Figure 7.2.1.2-2. Comparison of Recharge Estimates for Nevada Hydrographic Areas/Subareas with MASSIF Estimates of Net Infiltration at Yucca Mountain

7.2.1.2.2 Infiltration Estimates for Other Locations in the Southwestern United States

Infiltration data from the southwestern United States, including West Texas, New Mexico, and Arizona, are useful in assessing the model predictions for the monsoon climate. This region includes Hobbs, New Mexico and Nogales, Arizona (sites identified as average upper bound monsoon climate analogues in *Future Climate Analysis* (BSC 2004 [DIRS 170002], Table 6-1). Estimates for groundwater recharge in various locations in West Texas, New Mexico, and Arizona, and recharge estimates for other locations in the southwestern United States are shown in Table 7.2.1.2-8, which illustrates that recharge rates for the Southwestern United States, as a fraction of precipitation, remain consistent with Yucca Mountain and are typically between 0% and 10%. These data are compared with Yucca Mountain net infiltration rate predictions in Figure 7.2.1.2-3. A range of recharge rates for a site in northeastern Arizona, calculated using carbon-14 radiocarbon age dating combined with numerical modeling is also shown in Figure 7.2.1.2-3 even though this area is not a climate analog for Yucca Mountain under future climates (Zhu 2000 [DIRS 178539]).

Table 7.2.1.2-8. Recharge Estimates for West Texas, New Mexico, and Southeastern Arizona

Location	Precipitation (mm/yr)	Recharge (mm/yr)	Efficiency (%)	Method	Notes	Reference
Southeastern NM (Eddy County)	380	0.5	0.1	CMB	—	Shurbaji and Campbell 1997 [DIRS 178000]
	380	0.8	0.2			
	380	2.4	0.6			
Socorro, NM	200	7	3.5	Darcy's Law	pressure head data with harmonic mean conductivity	Stephens and Knowlton 1986 [DIRS 177281]
	200	36.6	18.3		pressure head data with geometric mean conductivity	
	200	37	18.5		Moisture content with unit hydraulic gradient	
Albuquerque, NM	510	23	4.5	regression of rainfall runoff data	Mountain block and mountain front recharge	Wilson and Guan 2004 [DIRS 172585], Table 2.
	510	66	12.9	regression of rainfall runoff data		
	510	31	6.1	CMB		
	510	132	25.9	basin model calibrated with inverse method		
	510	15	2.9	basin model calibrated with ^{14}C data		
Southern High Plains (Southeastern New Mexico and West Texas)	485	11	2.3	CMB	—	Wood and Sanford 1995 [DIRS 177304]
Heuco Bolson, West Texas (Chihuahuan Desert)	280	0.03	0.0	CMB	Range (.03 to .7) from 10 boreholes	Scanlon 1991 [DIRS 107233]
	280	0.7	0.3			

Table 7.2.1.2-8. Recharge Estimates for West Texas, New Mexico, and Southeastern Arizona (Continued)

Location	Precipitation (mm/yr)	Recharge (mm/yr)	Efficiency (%)	Method	Notes	Reference
Eagle Flat basin, West Texas (Chihuahuan desert)	320	0.03	0.0	CMB	Interdrainage (old eolian sheet)	Scanlon et al 1999 [DIRS 177852], Table 2.
	320	0.06	0.0		Interdrainage (young eolian sheet)	
	320	0.05	0.0		Interdrainage (young eolian sheet)	
	320	0.02	0.0		Interdrainage (alluvial fan)	
	320	0.03	0.0		Interdrainage (basin fill deposit)	
	320	0.02	0.0		Interdrainage (slope)	
	320	0.02	0.0		Interdrainage (10 m from fissure)	
Walnut Gulch Experimental Watershed, southeastern Arizona	124	7	5.6	Calibrated HYDRUS-1D simulations	(0.5 to 2m zone below surface), winter only	Scott et al. 2000 [DIRS 177853
	145	8	5.5			
	196	68	34.7			
	34	0	0.0			
	202	41	20.3			
	21	0	0.0			
	47	0	0.0			
	155	12	7.7			
	126	3	2.4			
	181	17	9.4			
	243	66	27.2			
	50	0	0.0			
	263	64	24.3			
	25	0	0.0			
	53	0	0.0			
	135	0	0.0			

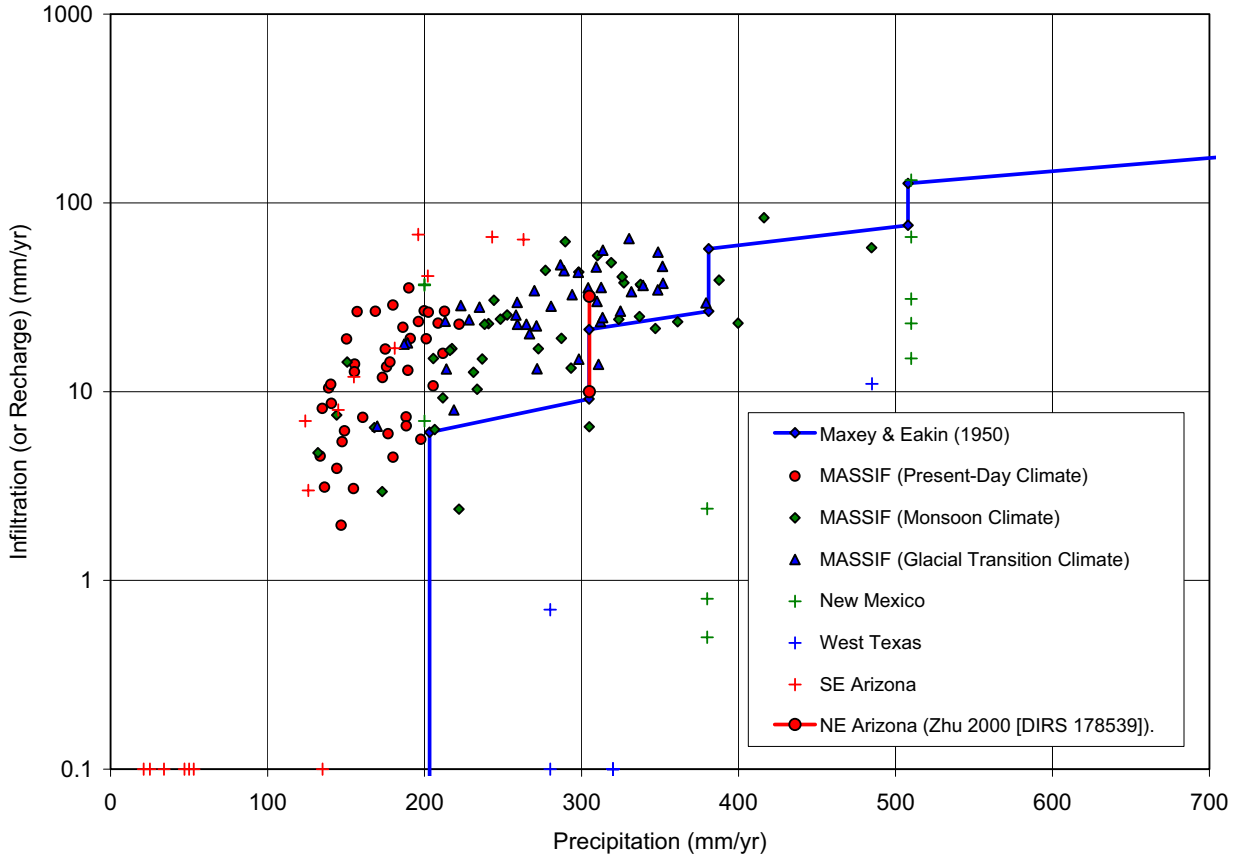

Source: Output DTNs: SN0701T0502206.034, SN0701T0502206.036, and SN0701T0502206.035, respectively (MASSIF results Present-Day, Monsoon, and Glacial Transition climates). Data points with <0.1 mm infiltration are plotted as 0.1 mm. All other data from Validation Output DTN: SN0704T0502206.047.

NOTE: Vertical line that extends to the horizontal axis associated with the Maxey-Eakin model represents the precipitation amount below which the model predicts zero recharge.

Figure 7.2.1.2-3. Comparison of Recharge Estimates for New Mexico, West Texas, and Arizona with MASSIF Estimates of Net Infiltration at Yucca Mountain.

7.2.1.2.3 Infiltration Estimates for Other Locations the Western United States

Future Climate Analysis (BSC 2004 [DIRS 170002], Table 6-1) identifies several sites on the Columbia Plateau in Eastern Washington (Spokane, Rosalia, and St. John) as average upper bound glacial transition climate analogs. Data from the Columbia Plateau in Washington State are therefore useful because they provide inferences into potential precipitation and recharge at Yucca Mountain during wetter climates. The Columbia Plateau's position in the rain shadow of the Cascade Mountains is also analogous to the Great Basin position behind the Sierra Nevada Mountains.

Model-derived estimates of average groundwater recharge to the Columbia Plateau regional aquifer system have been recently reported by Bauer and Vaccaro (1990 [DIRS 177726]). The deep-percolation model for estimating recharge used precipitation, temperature, streamflow, soils, land-use, and altitude data to calculate transpiration, soil evaporation, snow accumulation,

snowmelt, sublimation, and evaporation of intercepted moisture. Estimated annual average precipitation, and recharge rates for the various zones included in the Columbia Plateau study are shown in Table 7.2.1.2-9. The average annual precipitation for individual modeling zones ranges from approximately 168 to 410 mm/yr. Most precipitation values are clustered near the postulated range for the glacial transition lower bound mean annual precipitation (198 to 220 mm/yr). For these precipitation values, the recharge efficiency varies from about 0.1% to approximately 16%. The relatively fewer precipitation estimates that are near the postulated glacial transition upper bound exhibit the recharge efficiency varying from approximately 10% to 30%. Bauer and Vaccaro (1990 [DIRS 177726]) estimates are compared with predicted Yucca Mountain net infiltration rates in Figure 7.2.1.2-4. The Maxey-Eakin model is also shown in Figure 7.2.1.2-4 for reference.

Table 7.2.1.2-9. Recharge Estimates for Zones on the Columbia Plateau

Zone	Average Annual Precipitation (in/yr)	Average Annual Recharge (inch/yr)	Average Annual Precipitation (mm/yr)	Average Annual Recharge (mm/yr)	Efficiency (%)
1	7.29	0.43	185.2	10.9	5.9
2	8.91	1.25	226.3	31.8	14.0
3	9.34	1.37	237.2	34.8	14.7
4	6.61	0.38	167.9	9.7	5.7
5	8.77	1.18	222.8	30.0	13.5
6	8.64	0.66	219.5	16.8	7.6
7	8.26	1.31	209.8	33.3	15.9
8	6.95	0.3	176.5	7.6	4.3
9	7.64	0.43	194.1	10.9	5.6
10	7.93	0.45	201.4	11.4	5.7
11	7.76	0.44	197.1	11.2	5.7
12	7.41	0.15	188.2	3.8	2.0
13	8.19	0.47	208.0	11.9	5.7
14	7.95	0.23	201.9	5.8	2.9
15	6.98	0.13	177.3	3.3	1.9
16	8.31	0.39	211.1	9.9	4.7
17	8.09	0.26	205.5	6.6	3.2
18	12.05	1.3	306.1	33.0	10.8
19	10.09	0.83	256.3	21.1	8.2
20	9.19	0.87	233.4	22.1	9.5
21	17.27	5.39	438.7	136.9	31.2
22	22.75	10.52	577.9	267.2	46.2
23	22.32	6.01	566.9	152.7	26.9
24	9.64	0.57	244.9	14.5	5.9
25	10.33	1.36	262.4	34.5	13.2

Table 7.2.1.2-9. Recharge Estimates for Zones on the Columbia Plateau (Continued)

Zone	Average Annual Precipitation (in/yr)	Average Annual Recharge (inch/yr)	Average Annual Precipitation (mm/yr)	Average Annual Recharge (mm/yr)	Efficiency (%)
26	12.61	2.3	320.3	58.4	18.2
27	12.54	1.68	318.5	42.7	13.4
28	10.05	1.16	255.3	29.5	11.5
29	21.8	3.51	553.7	89.2	16.1
30	10.09	1.42	256.3	36.1	14.1
31	8.69	0.73	220.7	18.5	8.4
32	7.78	0.58	197.6	14.7	7.5
33	11.12	2.74	282.4	69.6	24.6
34	10.24	1.04	260.1	26.4	10.2
35	8.94	0.24	227.1	6.1	2.7
36	10.26	1.17	260.6	29.7	11.4
37	24.3	10.65	617.2	270.5	43.8
38	8.24	0.13	209.3	3.3	1.6
39	22.42	4.13	569.5	104.9	18.4
40	8.15	0.57	207.0	14.5	7.0
41	8.04	0.82	204.2	20.8	10.2
42	9.12	0.84	231.6	21.3	9.2
43	9.04	0.01	229.6	0.3	0.1
44	8.61	0.44	218.7	11.2	5.1
45	18.28	3.3	464.3	83.8	18.1
46	21.06	6.79	534.9	172.5	32.2
47	16.49	1.53	418.8	38.9	9.3
48	20.96	2.98	532.4	75.7	14.2
49	12.93	1.45	328.4	36.8	11.2
50	37.65	15.06	956.3	382.5	40.0
51	11.35	0.29	288.3	7.4	2.6
52	11.34	0.9	288.0	22.9	7.9
53	8.93	0.84	226.8	21.3	9.4

Source: Bauer and Vaccaro 1990 [DIRS 177726], Table 5.

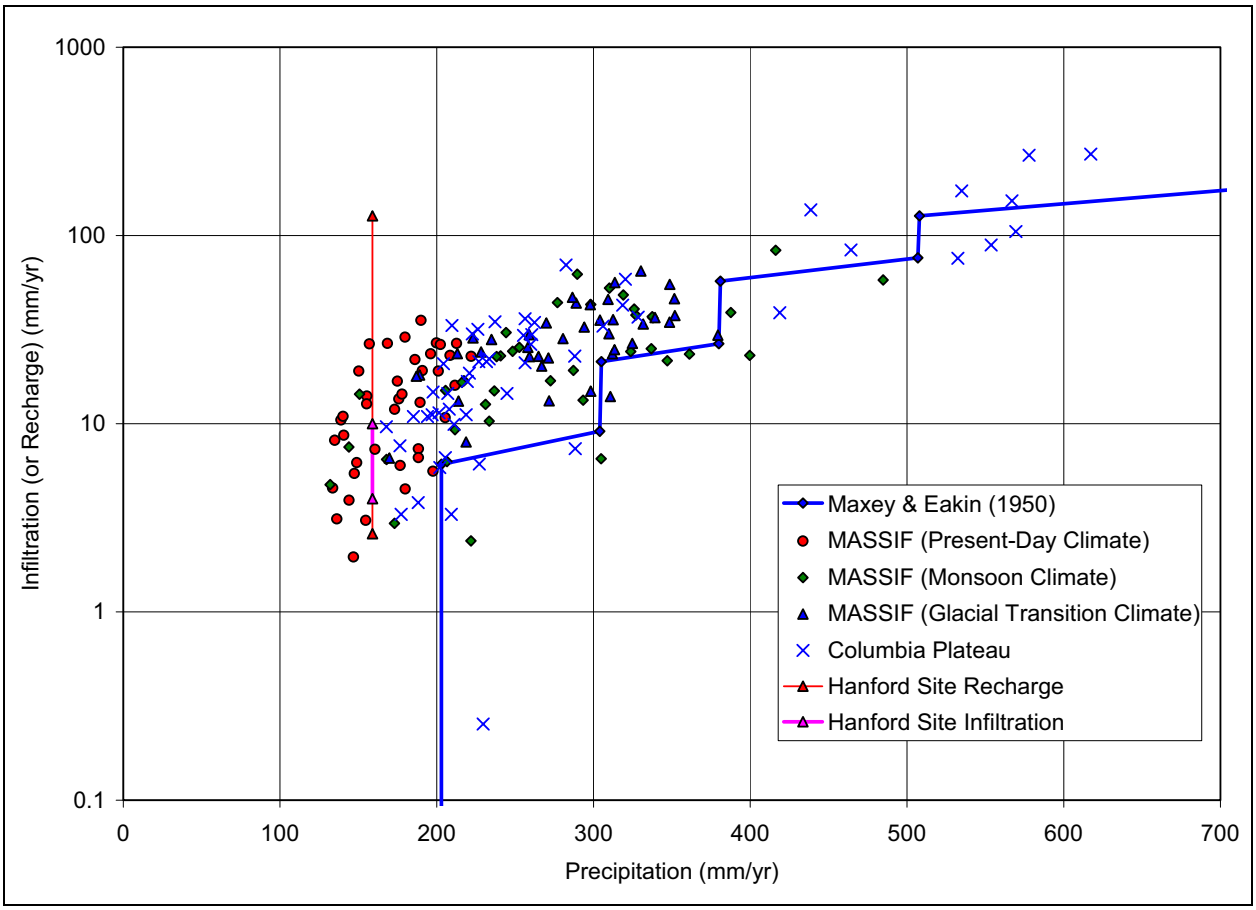

Source: Output DTNs SN0701T0502206.034, SN0701T0502206.036, and SN0701T0502206.035, respectively (MASSIF results for Present-Day, Monsoon, and Glacial Transition climates). All other data from Validation Output DTN: SN0704T0502206.047.

NOTE: Vertical line that extends to the horizontal axis associated with the Maxey-Eakin model represents the precipitation amount below which the model predicts zero recharge.

Figure 7.2.1.2-4. Comparison of Recharge Estimates for Columbia Plateau with MASSIF Estimates of Net Infiltration at Yucca Mountain

Fayer and Walters (1995 [DIRS 178191]) reported estimated recharge rates at the Hanford site in eastern Washington. They mapped soil type and vegetation/land use categories to measured or estimated recharge rates from a variety of sources (see Table 7.2.1.2-10). Estimation methods included lysimeter studies, chloride mass balance calculations, ^{36}Cl studies, and computer modeling. The long-term average recharge rates varied from 2.6 mm/yr for several soil and vegetation combinations to 127.1 mm/yr for basalt outcrop with no vegetation. The 30-year average annual precipitation value of 159 mm/yr for 1951 to 1980 is from the report by Fayer and Walters (1995 [DIRS 178191], Figure A.3). Maher et al. (2003 [DIRS 178540]) reported vadose zone infiltration rates of 4 to 10 mm/yr at the Hanford site. Their estimate was based on strontium isotope ratios measured in pore water, acid extracts, and sediments of a 70-m-thick vadose zone core.

Although average annual precipitation at the Hanford site is closer to the Yucca Mountain Present-Day climate than the Glacial Transition climate, the range in recharge rates from the report by Fayer and Walters (1995 [DIRS 178191], Table 4.1), and the range in infiltration rates from the report by Maher et al. (2003 [DIRS 178540]) are shown plotted in Figure 7.2.1.2-4 because the Hanford site is located in eastern Washington.

Table 7.2.1.2-10. Estimated Recharge Rates at the Hanford Site for Combinations of Soil Type and Vegetation/Land Use

Vegetation/Land Use		Recharge Rates (mm/yr)														
		Soil Types[a]														
Index	Description	Ri	Rp	He	Kf	Ba	E1	Ls	Eb	Ki	Wa	Sc	P	Qu	Rv	D
1	Shrub-steppe on slopes	3.4	8.6	2.6	2.6	2.6	2.6	3.4	2.6	3.4	3.4	3.4	3.4	3.4	8.6	8.6
2	Shrub-steppe on plain/uplands	3.4	8.6	2.6	2.6	2.6	2.6	3.4	2.6	3.4	3.4	3.4	3.4	3.4	8.6	8.6
3	Recovering shrub-steppe on plain/uplands	3.4	11.3	2.6	2.6	2.6	2.6	3.4	2.6	3.4	3.4	3.4	3.4	3.4	11.3	11.3
4	Bunchgrass on slopes	3.4	11.3	2.6	2.6	2.6	2.6	3.4	2.6	3.4	3.4	3.4	3.4	3.4	11.3	11.3
5	Hopsage/greasewood	3.4	8.6	2.6	2.6	2.6	2.6	3.4	2.6	3.4	3.4	3.4	3.4	3.4	8.6	8.6
6	Cheatgrass	4.8	25.4	3.4	3.4	2.6	4.9	4.8	4.9	4.8	4.8	4.8	4.8	4.8	25.4	25.4
7	Abandoned fields	4.8	25.4	3.4	3.4	2.6	4.9	4.8	4.9	4.8	4.8	4.8	4.8	4.8	25.4	25.4
10	Sand Dunes	55.4	55.4	55.4	55.4	55.4	55.4	55.4	55.4	55.4	55.4	55.4	55.4	55.4	55.4	55.4
11	Disturbed/Facilities	6.8	55.4	6.4	6.4	4.4	17.3	6.8	17.3	6.8	6.8	6.8	6.8	6.8	55.4	55.4
13	Basalt outcrops	86.7	86.7	86.7	86.7	86.7	86.7	127.1	86.7	86.7	86.7	86.7	86.7	86.7	86.7	86.7

Source: Table 4.1 in Fayer and Walters 1995 [DIRS 178191].

[a] Ri=Ritzville silt loam, Rp=Rupert sand, He=Hezel sand, Kf=Koehler sand, Ba=Burbank loamy sand, El=Ephrata sandy loam, Ls=Lickskillet silt loam, Eb=Ephrata stony loam, Ki=Kiona silt loam, Wa=Warden silt loam, Sc=Scootney stoney silt loam, P=Pasco silt loam, Qu=Esquatzel silt loam, Rv=Riverwash, D=Dune sand.

7.2.2 Corroboration of MASSIF Infiltration Model Using Alternative Model Approach

This section provides additional corroboration of the MASSIF infiltration model estimates. As discussed previously, there are no site-specific measurements of net infiltration that can be used for model validation. In this section, the model corroboration approach described in Step 6.2.1 of SCI-PRO-006 was used. The approach consists of corroborating model results with other model results obtained from the implementation of mathematical models. The alternative model considered is a one-dimensional unsaturated flow model based on Richards' equation. The computer code HYDRUS-1D (Simunek et al. 2005 [DIRS 178140]) was used to perform the simulations. Because HYDRUS-1D is unqualified software its use is limited (by SCI-PRO-006) to model corroboration and cannot be used to directly support model validation. The summary of this model corroboration activity is provided below. The details concerning modeling setup and supporting calculations are in Appendix K.

Four model scenarios were implemented with MASSIF and HYDRUS-1D in this coorboration analysis (see Figure 7.2.2-1). The four model scenarios represent one-dimensional homogeneous soil columns that are identical except for the depth of soil and roots in each column. The difference in the depths of the soil columns are as follows: Model 1 has a soil depth of 50 cm, Model 2 has a soil depth of 100 cm, Model 3 has a soil depth of 150 cm, and Model 4 has a soil depth of 200 cm. The plant rooting depth was assumed to be equal to the soil depth in each model scenario. The simulations were performed for one water year (365 days). These conceptual models were incorporated with MASSIF and HYDRUS-1D.

It was anticipated that significant infiltration would be generated in the case of Model 1 (thin soils) and negligible or zero infiltration would be generated in the case of the Model 4 (thick soils). This is consistent with the YMP site conceptual model according to which most infiltration occurs in the places where soils are thin or absent (bedrock outcrops). The corroboration can be considered successful if the cumulative infiltration estimates obtained with MASSIF and HYDRUS-1D are similar.

The same climate data were used as an atmospheric boundary condition in both MASSIF and HYDRUS-1D. The minimum and maximum daily temperatures, precipitation, and wind speed (wind speed is not used in HYDRUS-1D) for one water year were taken from *Weather Summary v2.1 for nominal of PD parameters.xls* located in *Present Day Precipitation* directory supplied with the MASSIF Package (Output DTN: SN0701T0502206.037). The climate data are for set 4 (representative year 952) with the probability of occurrence equal to 0.02. This set was selected because it has high total annual precipitation (471 mm) and consequently, may result in significant infiltration. This annual precipitation has 2% probability under the Present-Day climate at the YMP site.

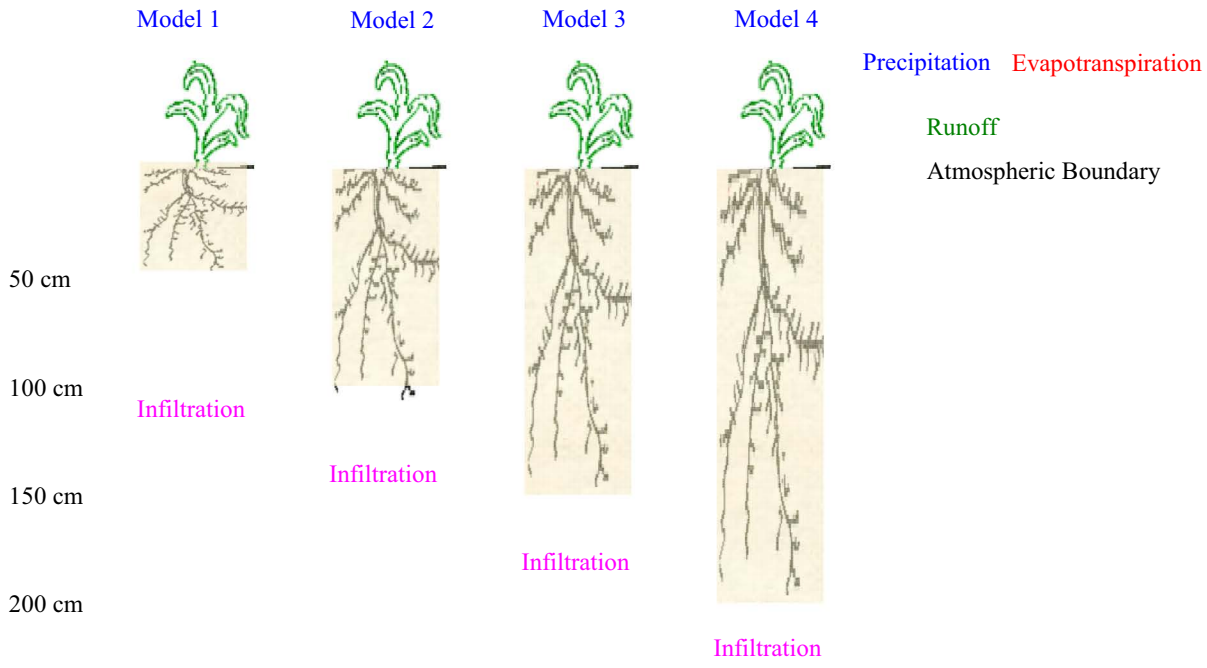

Figure 7.2.2-1. Conceptual Model Used in the Alternative Model Corroboration Analysis

Another input required at the atmospheric boundary is the limiting ET. Slightly different approaches are used in MASSIF and HYDRUS-1D to estimate the limiting ET. MASSIF uses the reference ET concept (Sections 6.3.3 and 6.4.4). Reference ET is calculated internally using the climate data. The default MASSIF parameters for the Present-Day climate (such as first and last day of winter) were used in calculating reference ET. HYDRUS-1D uses the concept of the potential ET. The potential ET is calculated externally using Hargreaves formula (Jensen et al. 1997 [DIRS 177103]). The details are presented in Appendix K. The potential evaporation and potential transpiration have to be specified separately to run HYDRUS-1D. The potential transpiration was calculated as the product of the potential ET and vegetation cover. The vegetation cover was assigned a value of 0.25 for both models. This is a reasonable assumption for the vegetation cover at the site (see Appendix D).

The atmospheric boundary conditions used in both codes are shown in Figure 7.2.2-2. As can be seen from this figure, the reference ET tends to be a little higher than the potential ET. This might be due to the fact that the reference ET accounts for the daily wind speed and the mean annual wind speed is higher than 2 m/s, and a value of 2 m/s characterizes the standard condition when the wind correction is not needed.

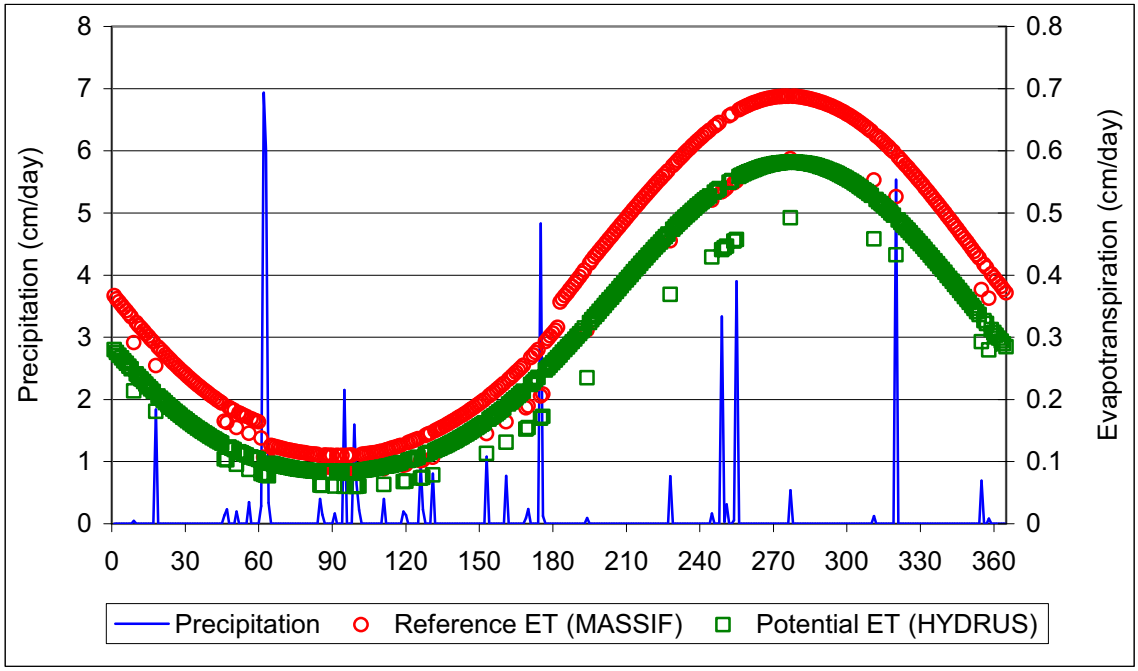

Source: Output DTN: SN0701T0502206.037; Validation Output DTN: SN0609T0502206.022 (HYDRUS 1D data).

Figure 7.2.2-2. Atmospheric Boundary Conditions Used in MASSIF and HYDRUS-1D

The lower boundary condition (the bottom of the soil profile) in MASSIF is incorporated through the bedrock layer. When the soil water holding capacity is exceeded, the bedrock drains the excess water at the rate equal to the bedrock saturated hydraulic conductivity. The lower boundary in HYDRUS-1D was defined as the seepage boundary. The seepage boundary condition assumes that a zero-flux boundary condition applies as long as the local pressure head at the bottom of the soil profile is negative. However, a zero pressure head will be used as soon as the bottom of the profile becomes saturated. This is conceptually close to, but not equivalent to the boundary condition in MASSIF. Note that this boundary condition does not require the presence of the lower soil or bedrock layer. Thus, the bedrock properties are not used in HYDRUS-1D modeling.

Different concepts are used in MASSIF and in HYDRUS-1D to calculate actual transpiration. MASSIF uses the K_{cb} function concept (Sections 6.3.3 and 6.3.4), and HYDRUS-1D uses the water stress function concept. The water stress function plays a role similar to K_{cb} function - it decreases the potential transpiration. The major difference is that water stress function reduces potential transpiration based on the pressure head (saturation) in the soil profile, and the K_{cb} function reduces potential transpiration based on the season of the year. Although the saturation is low during the dry season and high during the wet season, there is no direct translation from one function to another one.

The K_{cb} function is incorporated in MASSIF using two coefficients. The first coefficient (C_{kcb1}) represents the intercept and the second one (C_{kcb2}) represents the slope of the K_{cb} - *NDVI'* linear regression line (see Section 6.5.3). Both, C_{kcb1} and C_{kcb2} were set equal to MASSIF defaults for the Present-Day climate (-0.05 and 9.7, respectively).

The other transpiration and evaporation parameters in MASSIF were set equal to the defaults for the Present-Day climate as follow:

- Evaporation depth Z_e = 0.15 m
- Diffusive evaporation parameter K_{c_min} = 0
- Readily evaporable water parameter rew_1 = 6 mm
- Depletion factor parameter p = 0.65
- Plant height h_{plant} = 0.4 m.

There are no equivalents to these parameters in HYDRUS-1D. The actual ET in HYDRUS-1D is calculated based on the pressure and moisture within the soil profile.

The initial moisture conditions within the soil profile were set equal to 0.08 m^3/m^3 in both MASSIF and HYDRUS-1D.

The soil properties used in MASSIF are soil porosity, saturated hydraulic conductivity, field capacity, and wilting point. The additional parameter required is the bedrock saturated hydraulic conductivity. The most common soil grouping within the YMP site is soil group 5/7/9 with the saturated hydraulic conductivity of 6.82E-7 m/s. This group was selected for the analysis. The most common bedrock type selected for this analysis is bedrock type 405 with the saturated hydraulic conductivity of 1.1E-6 m/s. Minimum and maximum bedrock conductivities of 7.37E-7 m/s and 3.34E-6 m/s were used to see if the MASSIF estimates of infiltration would be affected by the type of the bedrock underlying the soil layer. Note that this range of conductivities for rock type 405 is different from the range of values reported in *Data Analysis for Infiltration Modeling: BedrockSaturated Hydraulic Conductivity Calculation* (BSC 2006 [DIRS 176355], Table 6-11) and used in the MASSIF net infiltration calculations.

The field capacity in MASSIF is considered to lie between the water contents at –1/3 bars and–1/10 bars (Section 6.5.2.3). The wilting point is defined as the water content at –60 bars. The water contents at –1/3 bars, –1/10 bars, and –60 bars were calculated using porosity, residual water content, and van Genuchten parameters *alpha* and *n* selected for HYDRUS-1D runs as described below. The details of these calculations are provided in Appendix K, but it should be noted that the resulting soil properties are not the same as defined for soil group 5/7/9 (Section 6.5.2.3) because the purpose of assigning parameter is to compare model results run with equivalent parameter inputs not to match Yucca Mountain soil data exactly. The resulting parameter values used in MASSIF are 0.173 m^3/m^3 (water content at –1/3 bars), 0.184 m^3/m^3 (water content at –1/10 bars), and 0.083 m^3/m^3 (water content at –60 bars). These parameters are close to the nominal properties of this soil group.

The soil parameters used in HYDRUS-1D are the parameters needed to define the moisture retention function and hydraulic conductivity–moisture relationship. The van Genuchten model in HYDRUS-1D was used to define these relationships. The input parameters are: residual water content, porosity, saturated hydraulic conductivity, and van Genuchten parameters *alpha* and *n*. The saturated hydraulic conductivity was set equal to the corresponding value in MASSIF. The van Genuchten parameter *alpha* and *n* were set equal to 0.002 cm^{-1} and 1.21. The residual water content and porosity were set equal to 0.022 and 0.19 m^3/m^3. Note that porosity is not used in MASSIF unless a significant runoff is generated (which should not be the case for the conceptual

models in consideration). As described above, these parameters result in the soil properties close to the nominal ones.

Four HYDRUS-1D models were developed using the initial and boundary conditions and modeling parameters described above. The inputs for these models are in Validation Output DTN: SN0609T0502206.021. The results of calculations are in Validation Output DTN: SN0609T0502206.022.

The MASSIF simulations were performed using an interface (*Alternative_Model.xmcd*) to MASSIF that was specifically designed for this purpose. This interface is provided as part of the MASSIF package (Output DTN: SN0701T0502206.037). The interface defines the MASSIF parameters described above, runs MASSIF calculations, and stores the results of the calculations. The interface calculates the soil water storage within the soil column, the daily cumulative infiltration, the total annual runoff, infiltration, and actual ET, and the change in storage. The interface reads the HYDRUS-1D results consisting of daily soil water storage and cumulative infiltration values. The interface displays the daily water storage and cumulative infiltration values calculated by MASSIF and HYDRUS-1D and calculates the mean root squared error between the MASSIF and HYDRUS-1D storage values to provide some basis for the comparison. The best match between the HYDRUS-1D and MASSIF results was obtained with the field capacity set equal to the water content at –1/10 bars (0.184 m^3/m^3).

The comparison between the water storage and cumulative infiltration calculated by MASSIF and HYDRUS-1D for the four models is presented in Figures 7.2.2-3 a through d).

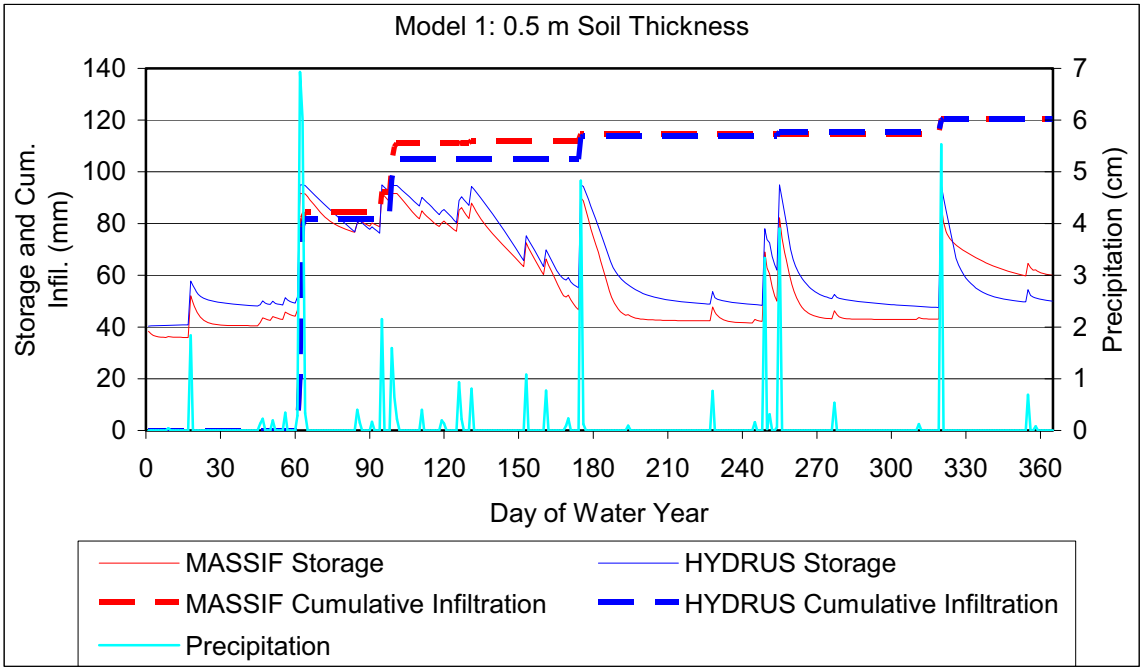

Source: Validation Output DTN: SN0609T0502206.022, *Alternative_Model_Outputs\Alternative_Model_Output.xls*.

Figure 7.2.2-3a. Soil Water Storage and Cumulative Infiltration for Model 1

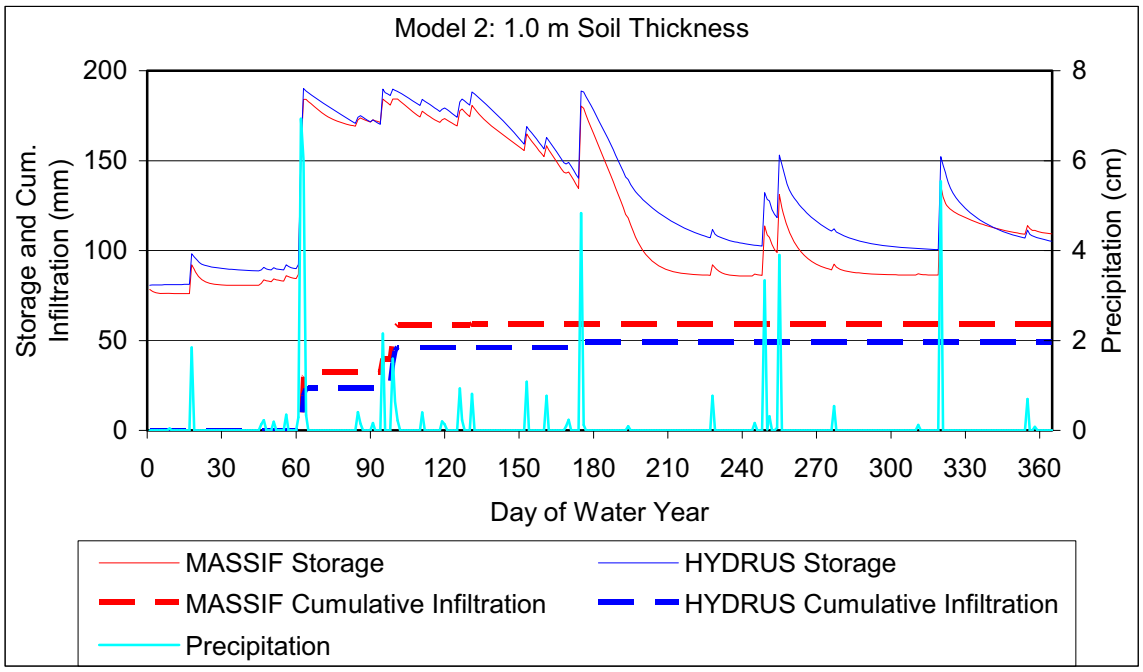

Source: Validation Output DTN: SN0609T0502206.022, *Alternative_Model_Outputs\Alternative_Model_Output.xls.*

Figure 7.2.2-3b. Soil Water Storage and Cumulative Infiltration for Model 2

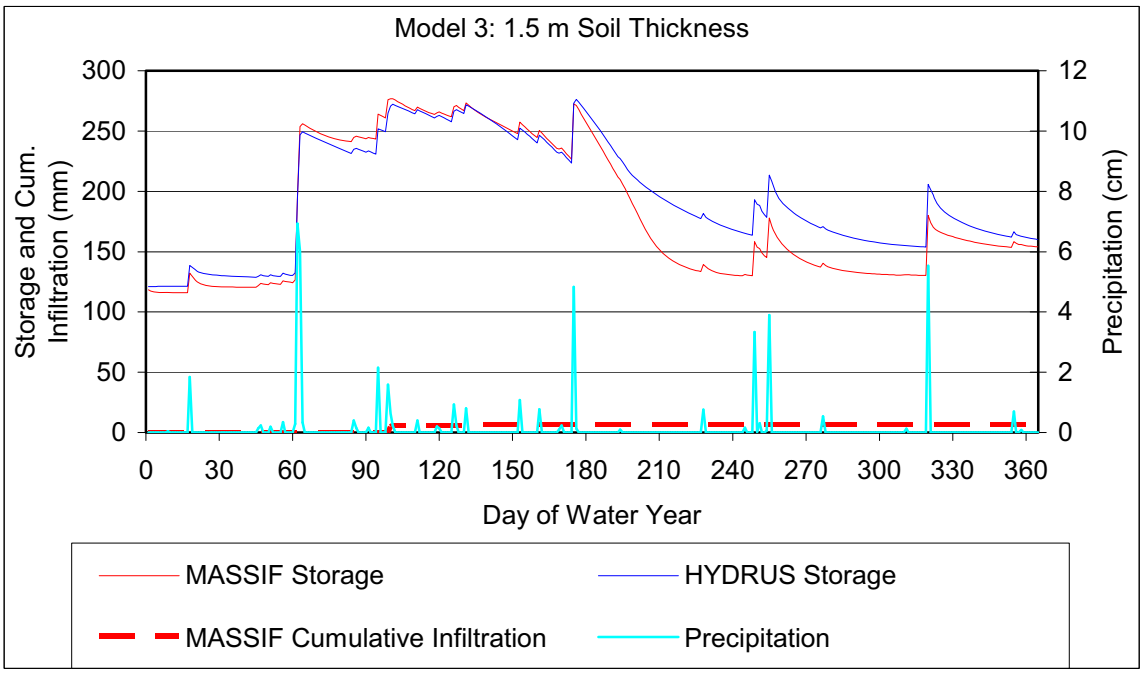

Source: Validation Output DTN: SN0609T0502206.022, *Alternative_Model_Outputs\Alternative_Model_Output.xls.*

Figure 7.2.2-3c. Soil Water Storage and Cumulative Infiltration for Model 3

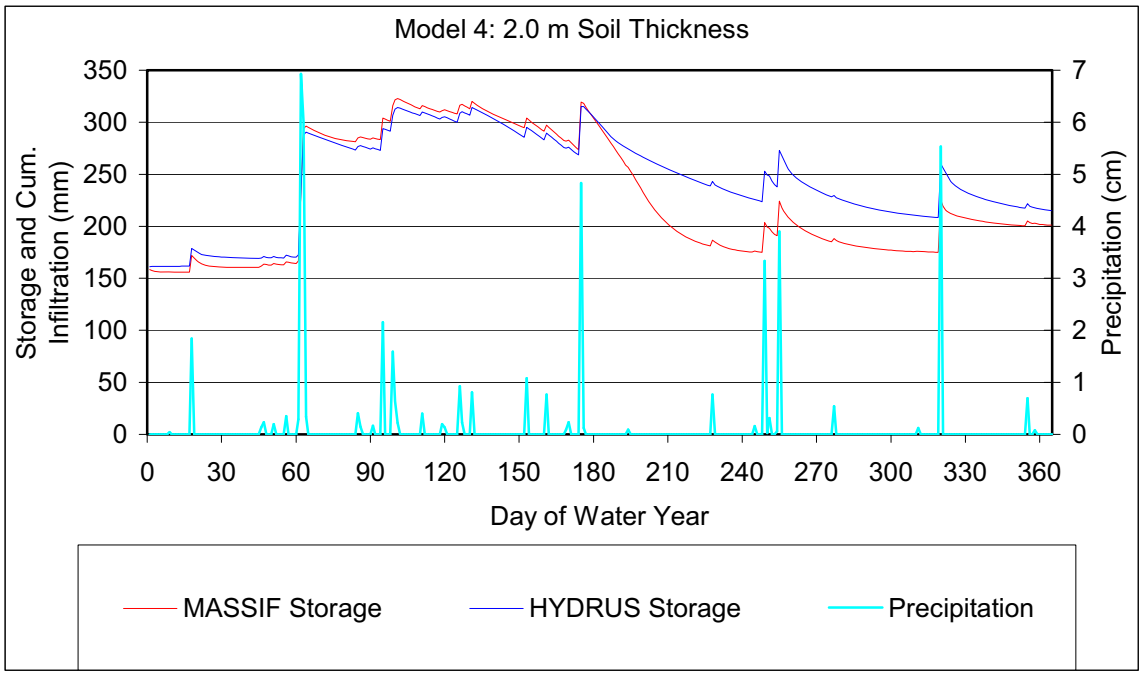

Source: Validation Output DTN: SN0609T0502206.022, *Alternative_Model_Outputs\Alternative_Model_Output.xls*.

Figure 7.2.2-3d. Soil Water Storage and Cumulative Infiltration for Model 4

The comparison between the annual values of the water balance components is presented in Figures 7.2.2-4 a through d. The summary of these results is in Table 7.2.2-1.

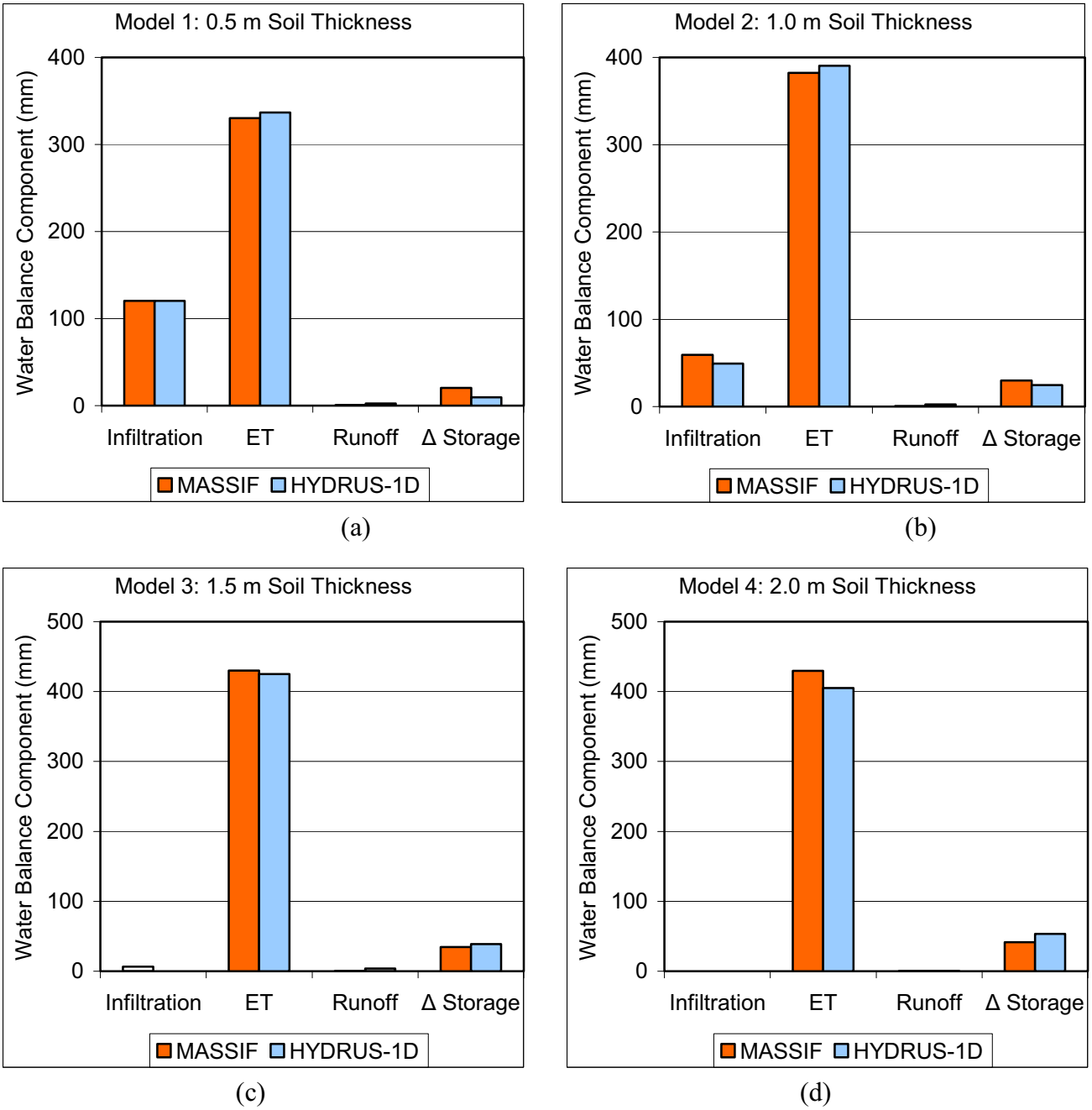

Source: Validation Output DTN: SN0609T0502206.022, *Alternative_Model_Outputs\Alternative_Model_Output.xls.*

Figure 7.2.2-4. Annual Water Balance Components for Alternative Model Comparison

Table 7.2.2-1. Summary of the Water Balance Results

		Annual Water Balance Constituents					
		Infiltration	Actual ET	Runoff	Change in Storage	Mean Root Squared Error	
Model	Code	mm	mm	mm	mm	mm	% Precipitation
Model 1	MASSIF	120.4	326.7	0.70	25.3	8.9	1.9
	HYDRUS-1D	120.5	336.8	2.5	9.6		
Model 2	MASSIF	63.9	377.8	0.70	30.8	17.1	3.6
	HYDRUS-1D	49.3	390.6	2.5	24.5		
Model 3	MASSIF	13.5	427.1	0.70	31.9	26.1	5.5
	HYDRUS-1D	0	425.1	3.7	39		
Model 4	MASSIF	0	437.5	0.70	35.0	33.4	7.1
	HYDRUS-1D	0	404.9	0.45	53.5		

Source: Validation Output DTN: SN0609T0502206.022, " *Alternative_Model_Outputs\Alternative_Model_Output.xls*.

As anticipated, Model 1 produced the highest infiltration. MASSIF and HYDRUS-1D calculated high total annual infiltration (120.4 mm from MASSIF and 120.5 mm from HYDRUS-1D), which constitutes 25% of the annual precipitation. As seen from Figure 7.2.2-3a, even the timing of the infiltration events is the same. The first infiltration event occurs at the time of the highest precipitation event. The soil moisture increases significantly and the following smaller precipitation events result in another infiltration event since the soil holding capacity is close to the maximum. A few following infiltration events coincide with the high precipitation events. The mean root squared difference between the MASSIF and HYDRUS-1D daily storage values is 8.9 mm (or 1.9% of the annual precipitation). The actual ET and runoff are in a close agreement as well (see Table 7.2.2-1).

The total annual infiltration calculated in Model 2 is 64 mm (MASSIF) and 49 mm (HYDRUS-1D). The timing of the infiltration events is the same. There are only two infiltration events in this case. The first infiltration event occurs at the time of the highest precipitation event. The second infiltration event occurs after a series of the smaller precipitation events during the period of time when the soil moisture content is high. The other high precipitation events do not result in infiltration as was in the case of Model 1 because the thicker soil was able to store all the moisture received. The mean root squared difference between the MASSIF and HYDRUS-1D daily storage values is 17.1 mm (or 3.6% of the annual precipitation). The actual ET and runoff are in a close agreement (see Table 7.2.2-1).

In the case of Model 3, MASSIF predicted one small infiltration event (13.75 mm) during the period of high moisture content that follows the highest precipitation event. The infiltration calculated by HYDRUS-1D is zero. The infiltration predicted by MASSIF in this case is a very small part (2.9%) of the annual precipitation. The mean root squared difference between the MASSIF and HYDRUS-1D daily storage values is 26.1 mm (or 5.5% of the annual precipitation). The actual ET and runoff are in a close agreement (see Table 7.2.2-1).

As anticipated, no infiltration occurs in the case of Model 4. Both, MASSIF and HYDRUS-1D predict zero infiltration. The mean root squared difference between the MASSIF and HYDRUS-1D daily storage values is 33.4 mm (or 7.1% of the annual precipitation). The actual ET and runoff are in a close agreement (see Table 7.2.2-1).

The difference between MASSIF and HYDRUS-1D results is slightly larger in the case when field capacity is defined at the water content at –1/3 bars. However, the agreement between these results is still good.

All four models were re-run with MASSIF, first using minimum and second using maximum values for the bedrock hydraulic conductivities. The estimates of all the balance constituents were identical to the cases when the hydraulic conductivity of the bedrock type 405 was used. This means that considering the seepage boundary condition in HYDRUS-1D (that does not require bedrock modeling) is appropriate. It also means that the conclusions made are not bedrock-specific.

Conclusions:

- The simplified water balance approach used in MASSIF produces annual infiltration estimates that are very close to the estimates obtained with physics based model such as HYDRUS-1D.

- MASSIF is capable of reproducing the same timing of the infiltration events as HYDRUS-1D. This means that the important physical processes resulting in infiltration are adequately represented in MASSIF.

- The other water balance components such as annual actual ET and annual runoff are in a good agreement with the HYDRUS-1D estimates as well.

- The mean root squared difference between the daily storage value calculated by MASSIF and HYDRUS-1D was in the range from 9 to 33 mm, which corresponds to 2% to 7% of the annual precipitation.

- Consequently, it can be concluded that corroboration of the MASSIF net infiltration model is successful. The corroboration criterion (close estimates of the cumulative infiltration calculated by MASSIF and HYDRUS-1D) was met.

7.2.3 Corroboration of Model Results with Infiltration and Percolation Estimates from 1997 Expert Elicitation Panel

In May 1997, an expert elicitation panel was convened in order to identify and assess the uncertainties associated with certain key components of the unsaturated zone flow system at Yucca Mountain. This assessment reviewed the data inputs, modeling approaches, and results of the unsaturated zone flow model and the infiltration model. In addition to data input and modeling issues, the assessment focused on percolation flux at the repository horizon. The seven panel members, who were experts from within and outside the Yucca Mountain project, represented a range of experience and expertise. The assessments and probability distributions

from this panel provide a reasonable aggregate representation of the knowledge and uncertainties about key issues regarding the unsaturated zone and the Yucca Mountain Site (CRWMS M&O 1997 [DIRS 100335], p. 1-1).

In order to provide a measure of the uncertainties associated with the estimates of net infiltration, the experts were asked to provide their judgments regarding the amount of net infiltration occurring at Yucca Mountain. Two of the 7 experts declined to give an assessment of net infiltration based on surface and near-surface data, citing inherent difficulties in attempting to model the area's highly complex and spatially variable surface and near-surface hydrologic system, as well as the paucity of data necessary to provide reliable estimates of episodic infiltration events (CRWMS M&O 1997 [DIRS 100335], p. 3-9).

For the five experts who provided an assessment of net infiltration, average infiltration rates in Table 3-1 ranged from 3.9 to 12.7 mm/yr, with an aggregate average of (7.4, 12.7, 8.4, 11.3, 3.9 mm/yr) = 8.7 mm/yr. Note that this range conflicts with the text of the report that cites a range of 3.9 to 11.3 mm/yr (CRWMS M&O 1997 [DIRS 100335], p. 3-10). All seven experts also provided a range for percolation flux at the repository horizon and noted that in most cases, net infiltration is equivalent to percolation flux at the repository horizon, although there may be perceived differences in their spatial distribution, and some experts used different methods to estimate the two quantities (CRWMS M&O 1997 [DIRS 100335], p. 3-5).

The experts predicted ranges of percolation fluxes at the repository horizon, and distribution types of those ranges. The combined average fluxes for all 7 experts yielded a mean value of 10.3 mm/yr, a median value of 7.2 mm/yr, and a 5th to 95th percentile range of 1.0 to 30 mm/yr (CRWMS M&O 1997 [DIRS 100335], Table 3-2). The cumulative distribution functions for the average of the experts' estimates, as well as the lower bound and upper bound CDFs are plotted on Figure 7.2.3-1. The CDF value corresponding to the experts' mean values were interpolated. MASSIF results for Present-Day climate for 40 LHS realizations are also plotted on this Figure. Note that with the exception of 3 of 40 data points, the MASSIF results fall between the experts' upper bound CDF and the experts' aggregate CDF. This comparison of results provides additional corroboration of the of the MASSIF results for the Present-Day climate.

Although the 1997 UZ expert elicitation panel convened nearly 10 years ago, their conclusions remain valid relative to the current infiltration model since it uses essentially the same conceptual model to that being developed in 1997. Therefore, it is relevant to highlight some of the panel's other conclusions with regard to infiltration and percolation flux, as follows.

Temporal Issues:

- The experts' general conclusion was that net infiltration is an episodic process linked to the occurrence of major storm events or sequences. The panel judged the average frequency of these episodic storm events to range from annual to approximately once every 20 years. Between these episodic infiltration events, there is little to no net infiltration.

- This conclusion is consistent with MASSIF predictions of net infiltration for Present-Day climate. Section 6.5.7.4 discusses the MASSIF predictions of net infiltration on a year-by-year basis and shows the small contribution of years with low to average precipitation to long-term mean net infiltration.

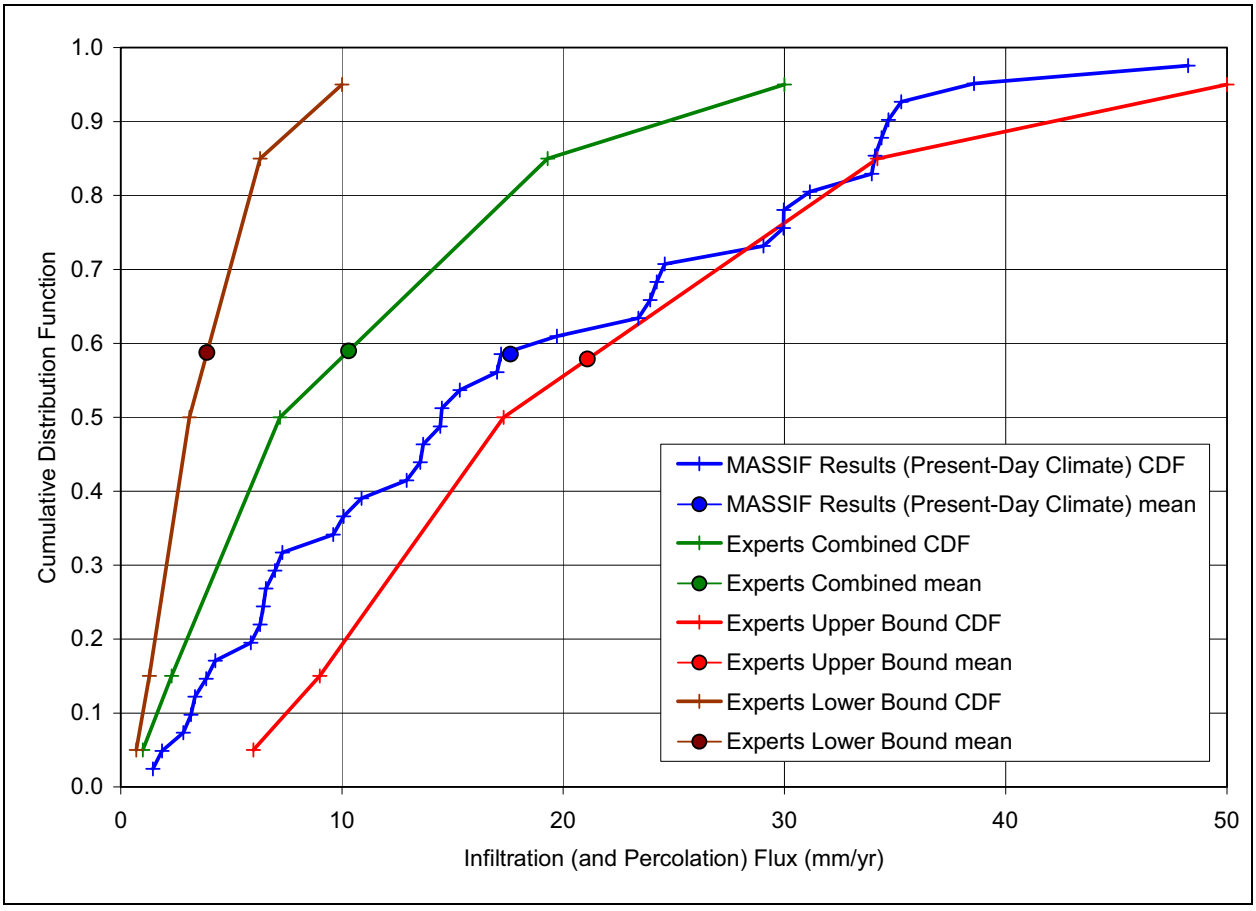

Source: Output DTN: SN0701T0502206.034 (MASSIF results for Present-Day climate); CRWMS M&O 1997 [DIRS 100335], Table 3-2 (Expert Elicitation Panel values).

NOTE: CDF values corresponding to mean values are interpolated.

Figure 7.2.3-1. MASSIF Net Infiltration Results for Present-Day Climate for the Repository Footprint Compared with Percolation Fluxes at the Repository Horizon from the 1997 Expert Elicitation Panel

Spatial Issues:

- All agreed that that the areas underlain by thick alluvial deposits likely experience the least infiltration because of the high storage capacity of the alluvium and the consequent opportunity for losses due to ET.

- This is consistent with MASSIF results.

- Some of the experts concluded that additional consideration of the potential for focused infiltration in washes and more explicit inclusion of surface runoff may lead to net infiltration estimates greater than those presented by USGS.

    - The conceptual model for surface water runoff in MASSIF is similar to the 2000 net infiltration model developed by the USGS, which was changed from the 1996 net infiltration model in response to this comment.

Modeling Issues:

- Some argued that the 1-D flow modeling is incapable of accounting for lateral flow at the soil–bedrock contact. However, another expert noted that the grid blocks used are too large to provide the spatial detail needed to take advantage of the additional information provided by a 2- or 3-D model.

    - Lateral flow is considered to be insignificant at the grid cell scale applied in MASSIF. Refer to the assumption on Interflow in Section 5.1.

- One expert placed low confidence in the "Bucket" model (field capacity model) used by the USGS (and implemented in MASSIF), concluding that it is inadequate for the level of detail considered in the analysis.

    - Given the lack of site-specific soil depth and soil hydraulic property data, the field capacity model is an appropriate model choice, rather than using a soil physics-based model that requires better soil depth and hydraulic property data.

7.3 VALIDATION AND CORROBORATION SUMMARY

Section 7.1 presented confidence building activities during model development. These activities included descriptions of MASSIF's abstraction of precipitation modeling using Fourier series parameters. MASSIF's ability to simulate ET and storage was demonstrated by comparing MASSIF output with lysimeter datasets from Area 5 at the Nevada Test Site, and Reynolds Creek, ID. These comparisons demonstrate that MASSIF can be applied to other sites to accurately predict water balance parameters such as ET. Section 7.1 also presented comparison of MASSIF predictions of streamflow with measured streamflow data. And Section 7.1 described the extended parameter sensitivity study (large LHS).

Section 7.2 presented post model development validation activities. These activities included comparison of MASSIF predictions of infiltration with seepage estimates observed in the South ramp of the ESF in the winter of 2005. MASSIF predictions of infiltration were qualitatively compared to borehole-scale estimates of infiltration, and this comparison was used to illustrate that MASSIF predictions of infiltration for a given grid cell cannot be accurately compared to borehole-scale estimates of infiltration due to the lack of site-specific Yucca Mountain soils data including soil depth data, and soil hydraulic property data.

Section 7.2 also compares MASSIF predictions of infiltration for Present-Day, Monsoon, and Glacial Transition climates for 40 realizations for each climate, with infiltration estimates from published models and data for the Yucca Mountain area, the southwestern United States, and the

western United States. The infiltration estimates from some southwestern sites is analogous to infiltration that could be expected during the monsoon climate state, and infiltration estimates from the Columbia River plateau sites is analogous to infiltration that could be expected during the glacial-transition climate state. These comparisons indicate that MASSIF predictions of infiltration for Present-Day, Monsoon, and Glacial Transition climates compare well to watershed-scale models and data for Nevada, and the southwestern and western United States.

Section 7.2 also describes an alternative model approach corroboration activity in which MASSIF results are compared to HYDRUS 1-D results for four different soil depths and using the same model inputs. These comparisons indicate that MASSIF and HYDRUS-1D give similar results. Finally, Section 7.2 summarizes some of the conclusions and infiltration and percolations estimates from the 1997 Expert Elicitation Panel on the UZ flow model. The MASSIF predictions of infiltration for Present-Day climate were almost entirely within the range between the mean and upper bounds of percolation flux predicted by the 1997 expert panel (who assumed that percolation flux was approximately equivalent to infiltration).

The results of calculations of net infiltration have been validated by applying acceptance criteria based on an evaluation of the model's relative importance to the potential performance of the repository system. Validation requirements defined in Technical Work Plan for: Infiltration Model Assessment, Revision, and Analyses of Downstream Impacts (BSC 2006 [DIRS 177492], Section 2.2.1) have been fulfilled (with the exceptions described in Section 1.4), including corroboration of model results with experimental data, and corroboration with alternative models. Activities requirements for confidence building during model development have also been satisfied. The model development activities and post-development validation activities described establish the scientific bases for the infiltration model. Based on this, the infiltration model used in this report is considered to be sufficiently accurate and adequate for the intended purpose.

Table 7.3-1 lists the Validation Output DTNs generated from model validation activities described in Section 7. These DTNs are not considered qualified product outputs.

Table 7.3-1. Validation Output Data Tracking Numbers

Title	Product Output DTN
Comparison of the calculated precipitation record with site data	SN0701T0502206.045
Analysis of soil water storage in Nevada Test Site (NTS) and Reynolds Creek Experimental Watershed (RCEW) lysimeters	SN0607T0502206.016
Recharge estimates used to validate the MASSIF model of net infiltration at Yucca Mountain	SN0704T0502206.047
Alternative infiltration model inputs	SN0609T0502206.021
Alternative infiltration modeling results	SN0609T0502206.022

INTENTIONALLY LEFT BLANK

8. CONCLUSIONS

8.1 SUMMARY AND FINDINGS

The purpose of the model documented in this report is to provide a spatial representation, including uncertainty, of the predicted average annual net infiltration at the Yucca Mountain site for three future climates predicted to occur at the site over the next 10,000 years. The resulting maps of average annual net infiltration provide input directly to the updated versions of the following model reports:

- *UZ Flow Models and Submodels* (BSC 2004 [DIRS 169861])
- *Calibrated Properties Model* (BSC 2004 [DIRS 169857])

The net infiltration model, MASSIF, presented in this report is a mass balance calculation of the surface and near surface water budget. Water enters the system as precipitation, which is simulated from a stochastic model of daily precipitation based on historical weather records from proxy climate sites identified in *Future Climate Analysis* (BSC 2004 [DIRS 170002]. The MASSIF infiltration model simulates processes occurring at the soil layer, including: flow through and storage of water in the soil layer, return of water vapor to the atmosphere by evaporation and plant transpiration (evapotranspiration), flow along the surface (runoff/run-on), and infiltration into the bedrock below the soil. Processes not included in the model are listed in Section 5.1.

The model documented in this report calculates net infiltration at the soil–bedrock interface without consideration of the properties of the rock at deeper locations. Instead of net infiltration, some authors call this parameter "deep drainage" or "potential recharge." *UZ Flow Models and Submodels* (BSC 2004 [DIRS 169861]) describes the method for calculating replenishment of the aquifer from the surface (i.e., recharge), taking into consideration the potential recharge and the make-up and orientation of the geologic strata, as well as other considerations.

The model documented in this report is valid only for the Yucca Mountain site for a 10,000-year period and for the climates specified in *Future Climate Analysis* (BSC 2004 [DIRS 170002], Section 7.1). For each climate, the model produces maps of average annual infiltration as a function of location, with no time dependence, although an examination of the nonaveraged results indicates that net infiltration in this environment is highly episodic (See Section 6.5.7). *UZ Flow Models and Submodels* (BSC 2004 [DIRS 169861]) provides the justification for characterizing net infiltration with non-episodic, time-averaged values. These output maps indicate the range of uncertainty in average annual steady-state net infiltration.

Infiltration predictions are limited by the uncertainty in future weather. Although a substantial body of literature supports the use of stochastic precipitation models, there are no records to validate our approach of extrapolation to 1000 years. Each available precipitation record, whether from the Yucca Mountain site, from a nearby weather station, or from a site representative of a future climate, covers periods of time much less than 100 years.

This model report documents the development and validation of a model for net infiltration of precipitation at the Yucca Mountain site and completely replaces the previous revision

(BSC 2004 [DIRS 170007] of this model report and model of net infiltration (BSC 2004 [DIRS 170007]). While the underlying conceptual model remains similar to the previous model, this revision increases confidence in the results by improving the traceability, transparency, and reproducibility of both the model development and the selection of inputs for calculations.

The results of this modeling work are the generation of 40 maps of net infiltration for each of the three future climates considered for the next 10,000 years (Output DTNs: SN0701T0502206.034, SN0701T0502206.036, and SN0701T0502206.035). For a given climate each of these 40 maps provides an equally probable outcome of net infiltration over the modeling domain. The range of net infiltration values within the set of 40 maps provides a reasonable estimate of the uncertainty in magnitude of net infiltration. This uncertainty is estimated using the structured Monte Carlo technique of Latin Hypercube sampling (see Sections 6.5.5 and 6.5.6). This method propagates uncertainty in a collection of input parameters to uncertainty in model outputs (net infiltration).

There are a number of ways that the results of this study could be used. First, for a given climate, the set of 40 maps could be ranked by net infiltration over some specified domain (e.g., full domain, UZ model domain, repository footprint) and predefined percentiles could be selected. Such a selection was done for the results in Section 6.5.7, where the 10th, 30th, 50th, and 90th percentiles are identified. A weight or probability of occurrence could be defined from the resulting empirical distribution. Second, the empirical distribution could be tested against a theoretical distribution (e.g., lognormal) and the representative maps could be defined from this "fitted" distribution. This was done in Section 6.6, where the results of each climate are compared and tested against lognormal distributions. Third, the results of this study can be used to estimate the nature and character of net infiltration at the site, including the timing and frequency of infiltration events and the relative importance of low-probability high precipitation years. Finally, the results of the sensitivity study can be used to define performance confirmation goals and identify sensitive parameters that could be the focus of possible future field studies at the site; however, this is not deemed necessary at this time.

The MASSIF model is validated using two of the methods available in SCI-PRO-006: (1) discussion of documented decisions and activities that are implemented during the model development process that build confidence and verify that a reasonable, credible, and technical approach using scientific and engineering principles was taken, and (2) postdevelopment model validation employing one of several methods described in Paragraph 6.3.2) of SCI-PRO-006. The first method is implemented by comparing certain model components (such as evapotranspiration, runoff, and precipitation) to field observations. The second method is to compare the results of the net infiltration calculations to independent regional measurements and estimates of net infiltration and recharge. Previous studies have used observations of steam flow measured at the site to calibrate models of net infiltration (BSC 2004 [DIRS 170007]). This methodology was considered invalid and not used in the present work. The reason for this lies in the fact that parameters that significantly influence surface run-off (e.g., soil hydraulic conductivity) in the model are not the same parameters that significantly influence net infiltration (e.g., soil depth and water holding capacity). As an alternative to model calibration, the MASSIF model was run with nominal input parameter values and compared to field observations of stream flow (Section 7.1.3), point estimates of net infiltration (Section 7.2.1), field observations from analogue sites (Sections 7.1.2 and 7.2.1), and infiltration model results from an alternative modeling approach (Section 7.2.2). Comparisons made in this model validation indicate that the

MASSIF model performs well, especially considering the uncertainty present in the input parameters.

The results of the uncertainty analysis for net infiltration are summarized in Section 8.2.

8.1.1 Data Tracking Numbers for Data Generated in This Report

The MASSIF model calculations of net infiltration are provided in Output DTN: SN0701T0502206.037. The results from the net infiltration model produced by these calculations are provided in the following output DTNs:

- SN0701T0502206.034 – present day net infiltration results (40 realizations)
- SN0701T0502206.036 – monsoon net infiltration results (40 realizations)
- SN0701T0502206.035 – glacial transition net infiltration results (40 realizations).

The complete list of developed output data generated in this report is listed by DTN in Table 8-1. In addition to the calculation and results DTNs, Table 8-1 includes developed data that provide input to the MASSIF net infiltration model and output resulting from the analysis of sensitivity and uncertainty. The flow of data associated with the net infiltration model, including both input data (from Table 4-1) and output data (from Table 8-1), is illustrated in Figure 8-1.

Appendix L discusses preliminary model outputs that are not considered the final technical product output of this report, but will be qualified in a separate data qualification report.

Table 8-1. Output Data Sets Generated in the Development and Application of the Net Infiltration Model

Description	Title	Product Output DTN
Results from the net infiltration model	Monsoon Net Infiltration Results, Rev 1	SN0701T0502206.036
	Present-Day Net Infiltration Results, Rev 1	SN0701T0502206.034
	Glacial Transition Net Infiltration Results, Rev 1	SN0701T0502206.035
Model calculation output	MASSIF Calculation of Net Infiltration at Yucca Mountain, Rev 1	SN0701T0502206.037
Developed input to the net infiltration model	Daily Precipitation for Water Years 1998, 2001, and 2002 – Sites 2, 3 & 4	MO0602SPAPRECP.000
	Daily Weather Data for Water Years 1998, 2001, 2002, Yucca Mountain Meteorological Site 1	MO0602SPAWEATH.000
	Reference Evapotranspiration (ET) for Yucca Mountain	MO0603SPAREFET.000
	Daily Weather Data for Spokane Washington	MO0605SPADAYWA.000
	Basal Transpiration Coefficients (K_{cb}) for Yucca Mountain Vegetation Associations (1993, 1991, and 1990 Water Years)	MO0606SPABASAL.001
	Transpiration Coefficients (K_{cb}) for a Bromus Tectorum Monoculture	MO0606SPATRANS.000

Table 8-1. Output Data Sets Generated in the Development and Application of the Net Infiltration Model (Continued)

Description	Title	Product Output DTN
Developed input to the net infiltration model (continued)	Cover Data for Vegetation Associations at Yucca Mountain (1990,1991, and 1993)	MO0606SPAVEGAS.001
	Total Annual Precipitation for Water Years 1990, 1991 and 1993 from Yucca Mountain Meteorological Sites 2, 3 and 4	MO0607SEPTOTAL.003
	Linear Regression Analysis for the MASSIF K_{cb} Versus NDVI Correlation	MO0610SPALINEA.000
	Solar Radiation and Reference Evapotranspiration (ET_0) on Inclined Surfaces	SN0602T0502206.003
	Calculated Daily Diffuse and Direct Solar Radiation from 2000 through 2004 and Measured at Desert Rock, Nevada	SN0602T0502206.004
	Evaluation of Hargreaves Solar Radiation Coefficient, K_{RS}, for Yucca Mountain	SN0602T0502206.005
	Evaluation of Published Diffuse and Total Solar Radiation Correlations for Yucca Mountain	SN0603T0502206.006
	Geospatial Inputs for Net Infiltration Model of Yucca Mountain	SN0606T0502206.011
	Daily Normalized Difference Vegetation Index (NDVI) Estimation for Selected Slopes/Azimuths at Yucca Mountain	SN0606T0502206.012
	Calculated Weather Summary for Present Day and Future Climates	SN0606T0502206.014
	Assembly Data for Geospatial Inputs to MASSIF Model of Yucca Mountain	SN0608ASSEMBLY.001
	Calibration Watersheds at Yucca Mountain Based on Pour Point Stream Gages	SN0608CWATSHED.001
	Drainage Delineation at Yucca Mountain	SN0608DRAINDYM.001
	Analysis Data Supporting Estimations of Normalized Difference Vegetation Index (NDVI) at Yucca Mountain, 1997–2002	SN0608NDVIANAL.001
	Auxiliary Data Used in Calculations of Daily Normalized Difference Vegetation Index (NDVI) Estimation for Selected Slopes/Azimuths at Yucca Mountain and Geospatial Inputs for Net Infiltration Model of Yucca Mountain	SN0608NDVIAUXD.001
	Normalized Difference Vegetation Index (NDVI) Derived from Calibrated and Geocorrected LANDSAT TM Data at Yucca Mountain, 1997–2002	SN0608NDVILSTM.001
	Normalized Difference Vegetation Index (NDVI) Imagery Derived from Calibrated and Georectified Quickbird Imagery of Yucca Mountain, August 31, 2002	SN0608NDVIQBIM.001
	Normalized Difference Vegetation Index (NDVI) on North and South Slopes and Supporting Data at Yucca Mountain, 1997–2002	SN0608NSSLOPES.001
	Potential Vegetation Response (PVR) at Yucca Mountain, 1997–2002	SN0608PVRATYMT.001
	Spatial Data Layers at Yucca Mountain	SN0701SPALAYER.002
	Temperature Model Fitting Parameters for Present-Day and Future Climate Proxy Sites	SN0608T0502206.019

Table 8-1. Output Data Sets Generated in the Development and Application of the Net Infiltration Model (Continued)

Description	Title	Product Output DTN
Developed input to the net infiltration model (continued)	Distribution of Slope on North-South Facing Terrain Slopes at Yucca Mountain	SN0609AZSLPHST.001
	Unsaturated Zone (UZ) Boundary and Repository Footprint	SN0612FTPRNUZB.002
	Thematic Mapper Processing Overview	SN0609LSTMPROC.001
	Precipitation Parameters Calculated using Fourier Analyses for Modern Interglacial and Future Climates	SN0609T0502206.023
	Calculated Weather Summary for Monsoon Climate, Rev 1	SN0701T0502206.041
	Calculated Weather Summary for Present Day Climate, Rev 1	SN0701T0502206.040
	Calculated Weather Summary for Glacial Transition Climate, Rev 1	SN0701T0502206.042
	Average Daily Wind Speed at 2 m Height above the Ground	SN0610T0502206.030
	Precipitation Duration Functions for the Present-Day, Monsoon, and Glacial Transition Climates for Infiltration Modeling at Yucca Mountain, NV	SN0610T0502206.031
LHS Files	Latin Hypercube Sample (LHS) Input and Output Files for MASSIF Calculation of Net Infiltration at Yucca Mountain, Rev 1	SN0701T0502206.043
Calculations supporting sensitivity analysis	Sensitivity Analysis of Average Net Infiltration for Three Climates	SN0701T0502206.044
Estimation of uncertainty for shallow soil depth	Estimation of Uncertainty on Upscaled Uniform Value for Soil Depth Class 4	SN0612T0502206.039
MASSIF verification	Independent Verification of MASSIF Infiltration Model	MO0703MASSIFIM.001

INTENTIONALLY LEFT BLANK

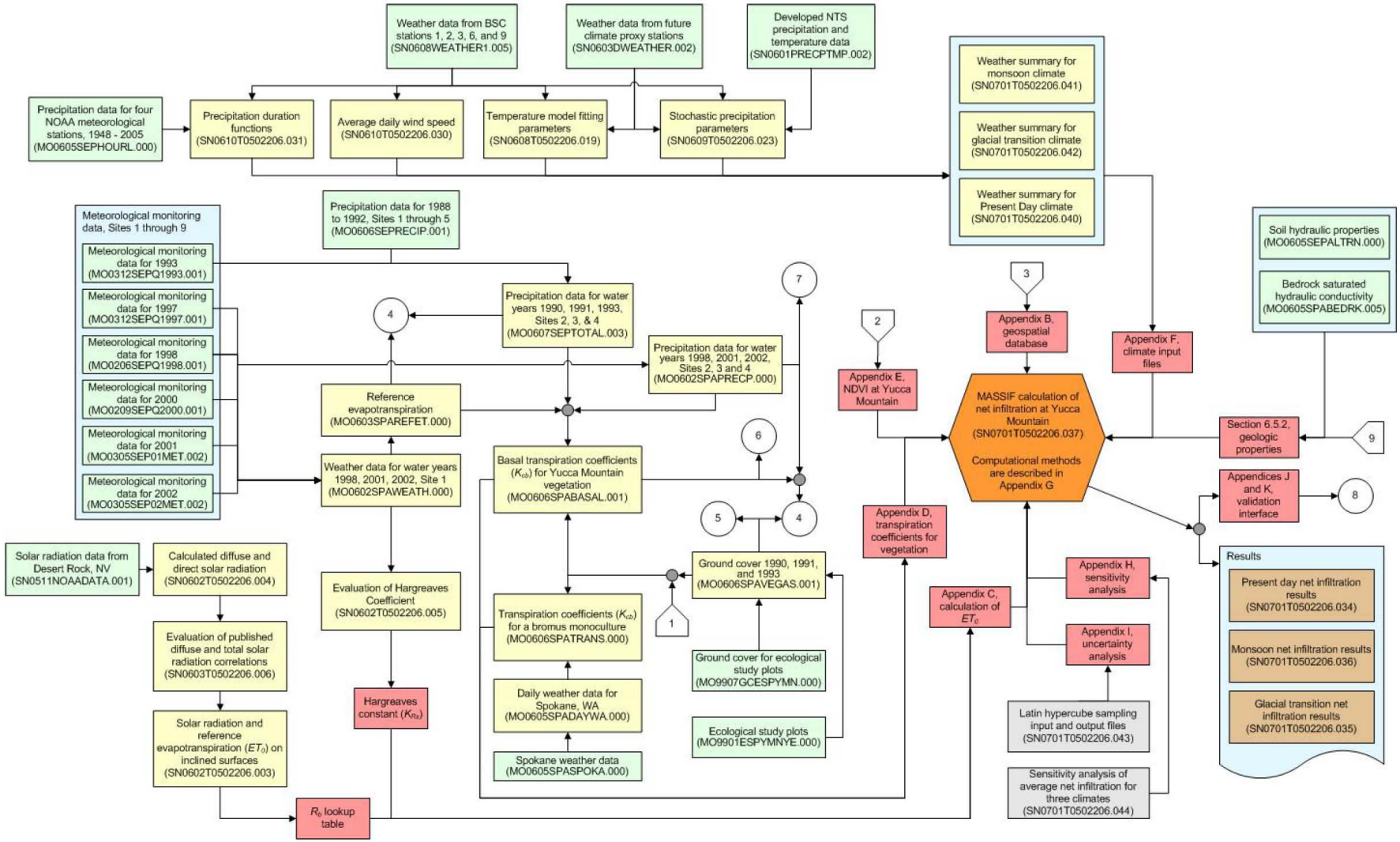

Figure 8-1. Data Flow for the MASSIF Net Infiltration Mode

INTENTIONALLY LEFT BLANK

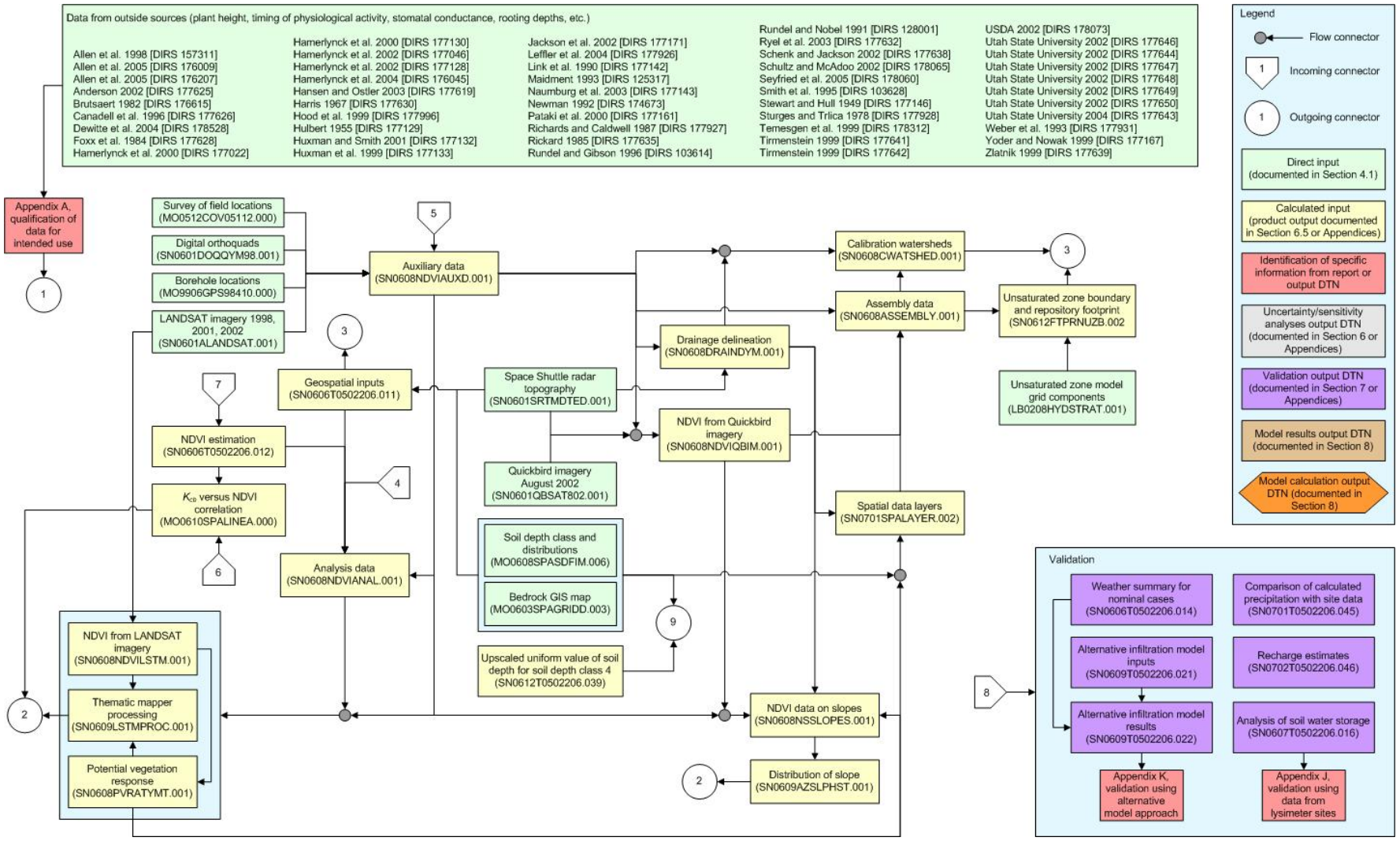

Figure 8-1. Data Flow for the MASSIF Net Infiltration Model (Continued)

INTENTIONALLY LEFT BLANK

8.2 MODEL UNCERTAINTY AND LIMITATIONS

The model documented in this report calculates net infiltration at the soil–bedrock interface without consideration of the properties of the bedrock at deeper locations. All water that enters the bedrock is assumed to be net infiltration. Instead of net infiltration, some authors call this parameter "deep drainage" or "potential recharge." Such terminology acknowledges that other mechanisms exist to move or remove water from the bedrock below the root zone. *UZ Flow Models and Submodels* (BSC 2004 [DIRS 169861]) describes the method used for simulating water flow from the bottom of the root zone through the unsaturated zone to the underlying aquifer (i.e., recharge), taking into consideration the potential recharge and the make-up and orientation of the geologic strata, as well as other considerations.

The model documented in this report is valid only for the Yucca Mountain site over a 10,000-year period and for the climates specified in *Future Climate Analysis* (BSC 2004 [DIRS 170002], Section 7.1). For each climate, the model produces maps of average annual infiltration as a function of location, with no time dependence. These output maps indicate the range of uncertainty in average annual net infiltration.

Infiltration predictions are limited by the uncertainty in future weather, and this uncertainty is accounted for in this model. Although a substantial body of literature supports the use of stochastic precipitation models, there are no records to support extrapolation to 1000 years. Each available precipitation record, whether from the Yucca Mountain site, from a nearby weather station, or from a site representative of a future climate, covers much less than 100 years.

Another significant uncertainty in the results of the net infiltration model is related to the spatial distribution of the net infiltration over the modeling domain. Sensitivity analyses presented in Sections 7.1.3 and 6.7 suggest that there may be insufficient characterization of soil properties (depth, holding capacity, and hydraulic conductivity) over the modeling domain to obtain accurate and detailed maps of net infiltration. Instead, results suggest that spatially averaged net infiltration estimates are more reliable than the resulting spatial distributions of net infiltration. This conclusion is supported by model validation comparisons of spatially averaged net infiltration model results with analogue site data from the region (Section 7.2).

8.3 YUCCA MOUNTAIN REVIEW PLAN CRITERIA ASSESSMENT

The general requirements to be satisfied by the TSPA are stated in 10 CFR 63 [DIRS 176544]. The acceptance criteria that will be used by the U.S. Nuclear Regulatory Commission to determine whether the technical requirements have been met are identified in *Yucca Mountain Review Plan*, *Final Report* (YMRP) (NRC 2003 [DIRS 163274]).

The acceptance criteria identified in Section 2.2.1.3.5.3 of the YMRP (NRC 2003 [DIRS 163274]) that are applicable to this report are included below along with a summary of where in this report each criterion is addressed.

Acceptance Criteria from Section 2.2.1.3.5.3, Climate and Infiltration.

Acceptance Criterion 1: ***System Description and Model Integration Are Adequate.***

(1) The total system performance assessment adequately incorporates, or bounds, important design features, physical phenomena, and couplings, and uses consistent and appropriate assumptions throughout the climate and net infiltration abstraction process.

This model, which feeds the TSPA through the UZ flow model, explicitly includes the following natural features and physical phenomena and couplings that control the processes of net infiltration in the area above the planned Yucca Mountain repository: 1) terrain elevation and contours (Section 6.5.2 and Appendices B and C); 2) site specific estimates of vegetation as a function of mean annual precipitation (Section 6.5.3 and Appendix D); 3) change of climate through time using inputs from the future climates model report (Section 6.5.1); and 4) appropriate soil and bedrock permeability estimates as discussed in Section 6.5.2.

(2) The aspects of geology, hydrology, geochemistry, physical phenomena, and couplings, that may affect climate and net infiltration, are adequately considered. Conditions and assumptions in the abstraction of climate and net infiltration are readily identified and consistent with the body of data presented in the description.

This model includes the effects of geology by distinguishing soil and bedrock types present in the model domain (Sections 6.5.2.2 and 6.5.2.5) and assigning properties to these units consistent with available data (Sections 6.5.2.3 and 6.5.2.6). In addition, soil depth is represented as distinct soil depth class regions in the model domain (Section 6.5.2.4). The effects of local surface water hydrology (i.e., stream flow) are captured in the methods used to estimate surface runoff and run-on and watershed discharge (as summarized in Section 6.4.3) and controlled by the representation of elevation over the domain (Section 6.5.2.1 and Appendix B). Physical phenomena and couplings that are included in the modeling include: 1) elevation adjustments to precipitation and temperature (Sections 6.4.1 and 6.4.5.3); 2) adjustments to incoming daily solar radiation as a function of slope, azimuth, elevation, and day of year (Section 6.4.5.3); and 3) a detailed approach to estimating evapotranspiration as a function of reference evapotranspiration, site-specific vegetation characteristics, and soil water contents that all vary with time (Section 6.4.4)

(3) The abstraction of climate and net infiltration uses assumptions, technical bases, data, and models that are appropriate and consistent with other related U.S. Department of Energy abstractions. For example, the assumptions used for climate and net infiltration are consistent with the abstractions of flow paths in the unsaturated zone (UZ) and flow paths in the saturated zone (SZ) (Sections 2.2.1.3.6 and 2.2.1.3.8 of the Yucca Mountain Review Plan, respectively). The descriptions and technical bases provide transparent and traceable support for the abstraction of climate and net infiltration.

This model uses input data from the following DOE reports, all of which summarize YMP-relevant data:

1. ANL-NBS-GS-000008, *Future Climate Analysis* (BSC 2004 [DIRS 170002])

2. ANL-MGR-MD-000015, *Analysis for Infiltration Modeling: Extracted Weather Station Data Used to Represent Present Day and Potential Future Climate Conditions within the Vicinity of Yucca Mountain* (BSC 2006 [DIRS 177081])

3. TDR-NBS-HS-000019, *Technical Evaluation and Review of Results, Technical Procedures, and Methods Related to the Collection of Moisture Monitoring Data Using Neutron Probes in Shallow Boreholes* (BSC 2006 [DIRS 177083])

4. ANL-NBS-HS-000054, *Data Analysis for Infiltration Modeling: Bedrock Saturated Hydraulic Conductivity Calculation* (BSC 2006 [DIRS 176355])

5. ANL-NBS-HS-000077, *Data Analysis for Infiltration Modeling: Technical Evaluation of Previous Soil Depth Estimation Methods and Development of Alternate Parameter Values* (BSC 2006 [DIRS 178819])

6. ANL-NBS-HS-000055, *Data Analysis for Infiltration Modeling: Development of Soil Units and Associated Hydraulic Parameter Values* (BSC 2006 [DIRS 176335]).

The outputs (net infiltration maps) from this model are used as feeds to the UZ models to ensure continuity of repository system-wide modeling approach. Outputs from this model are indirectly coupled to the SZ through the coupling in the UZ. Output from this model is also indirectly coupled through the UZ flow fields (generated in the UZ models) to the predictions of in-drift temperature and humidity as described in *Multiscale Thermohydrologic Model* (BSC 2005 [DIRS 173944]).

(4) Sufficient data and technical bases to assess the degree to which FEPs have been included for this abstraction are provided;

This report addresses three FEPs included in *Features, Events, and Processes in UZ Flow and Transport* (BSC 2005 [DIRS 174191]).

- *Infiltration and Recharge* (2.3.11.03.0A) includes the effects of infiltration into the subsurface as a boundary condition for groundwater flow.

- *Precipitation* (2.3.11.01.0A) includes the effects of precipitation on the estimated net infiltration. Daily precipitation is explicitly included in the MASSIF modeling of net infiltration for Yucca Mountain.

- *Surface runoff and flooding* (2.3.11.02.0A) includes both the processes of surface runoff and evapotranspiration. These processes are explicitly included in the MASSIF modeling of net infiltration for Yucca Mountain.

(5) Adequate spatial and temporal variability of model parameters and boundary conditions are employed to model the different parts of the system.

Spatially varying parameters are listed in Section 6.5.2 and Appendix B. These parameters are distributed onto a grid comprised of 30 × 30-m grid cells. Spatial variations at a scale smaller than 30 × 30 m are not explicitly represented. Parameters associated with the terrain include elevation, slope, azimuth, and latitude for each 30 × 30-m grid cell. Elevation is used to divide the entire domain into 11 distinct watersheds (Appendix B). Each grid cell is assigned to a soil group, a bedrock type, and a soil depth group. The properties of these groups are represented with property sets that are uniform for all cells in the group. These properties include: bedrock hydraulic conductivity, soil depth, soil properties (conductivity, field capacity, wilting point, and saturated water content). Values and uncertainties for these parameters are described in Section 6.5.2. Potential vegetation response (PVR) is a spatially varying parameter that indicates the potential for vegetation at a given location given sufficient precipitation. This variable was developed from satellite measurements made at the site during a set of three representative years. This parameter is discussed in Section 6.5.3 and Appendix E. In addition, elevation adjustments are made to daily values of precipitation and temperature (Sections 6.4.1 and 6.4.5.3).

(6) Average parameter estimates are used in process-level models over time and space scales that are appropriate for the model discretization.

The MASSIF model is built on parameter estimates to enable infiltration estimates that are tailored to the site-specific conditions, including climate, vegetation type and coverage, soil types, properties, and depths and bedrock permeability. Net infiltration estimates are developed for Present-Day, as well as future climates predicted for the next 10,000 years. The modeling domain for Yucca Mountain Project infiltration covers approximately 125 km^2 and is comprised of 139,092 30 × 30-m grid cells. Each of these grid cells must be assigned parameters of elevation, slope, azimuth, potential vegetation response, soil depth, soil properties, and bedrock conductivity. The large expanse of the model domain required that these parameters be grouped into spatial zones, most often contiguously, and average properties over each of the zones were assigned based on available data. The delineations of the various parameters are displayed in Figures B-6 through B-11.

(7) Projections of future climate change are based on evaluation of paleoclimate information over the past 500,000 years. For example, numerical climate models, if used for projection of future climate, are calibrated based on such paleoclimate data.

Future climate predictions are based in part on *Future Climate Analysis* (BSC 2004 [DIRS 170002], Section 7.1), which forecasts three distinct climate states during the next 10,000 years at Yucca Mountain based on an examination of paleoclimate information over the past 500,000 years. The Present-Day climate is estimated to persist for the next 400 to 600 years, followed by a warmer and much wetter Monsoon climate spanning 900 to 1,400 years, and then

followed by a cooler and wetter Glacial Transition climate that is expected to last until and beyond the 10,000-year mark. Climate conditions expected beyond 10,000 years are not explicitly stated in *Future Climate Analysis* (BSC 2004 [DIRS 170002]). Proxy sites representing upper and lower bounds for each of these climates are specified, and data from these sites has been compiled and analyzed. Relevant weather parameters (e.g., mean annual temperature and precipitation) have been derived from these data, and the parameters have been used to generate stochastic simulations of weather for each of the three climates. Weather inputs are discussed in *Analysis for Infiltration Modeling: Extracted Weather Station Data Used to Represent Present Day and Potential Future Climate Conditions within the Vicinity of Yucca Mountain* (BSC 2006 [DIRS 177081]). Parameter extraction methods and applications to generate stochastic future weather inputs are described in Section 6.5.1 and Appendix F.

(8) Guidance in NUREG–1297 and NUREG–1298 (Altman et al. 1988a,b [DIRS 103597 and 103750]), or other acceptable approaches for peer reviews and data qualification, is followed.

No peer reviews were conducted in support of this report. A summary of findings from an Expert Elicitation Panel is discussed in Section 7.2.3. All direct input data used for estimates of net infiltration were qualified for use according to applicable procedures.

Acceptance Criterion 2: *Data Are Sufficient for Model Justification.*

(1) Climatological and hydrological values used in the license application (e.g., time of onset of climate change, mean annual temperature, mean annual precipitation, mean annual net infiltration, etc.) are adequately justified. Adequate descriptions of how the data were used, interpreted, and appropriately synthesized into the parameters are provided.

Future climates predictions are based in part on *Future Climate Analysis* which forecasts three distinct climates during the next 10,000 years at Yucca Mountain (BSC 2004 [DIRS 170002], Section 7.1). The Present-Day climate should persist for the next 400 to 600 years, followed by a warmer and much wetter Monsoon climate spanning 900 to 1,400 years, and then by a cooler and wetter Glacial Transition climate that is expected to last until and beyond the 10,000-year mark. Proxy sites representing upper and lower bounds for each of these climates are specified, and data from these sites has been compiled and analyzed. Relevant weather parameters (e.g., mean annual temperature and precipitation) have been derived from these data, and the parameters have been used to generate stochastic simulations of weather for each of the three climates. Weather inputs are discussed in *Analysis for Infiltration Modeling: Extracted Weather Station Data Used to Represent Present Day and Potential Future Climate Conditions within the Vicinity of Yucca Mountain* (BSC 2006 [DIRS 177081]). Parameter extraction methods and applications to generate stochastic future weather inputs are described in Section 6.5.1 and Appendix F.

(2) Estimates of present-day net infiltration using mathematical models at appropriate time and space scales are reasonably verified with site-specific climatic, surface, and subsurface information.

Present-Day net infiltration estimates have been reasonably verified, as discussed in Section 7. The evapotranspiration model has been shown to accurately predict evapotranspiration from weighing lysimeters at a location on the Nevada Test Site located approximately 40 miles from the YMP (Section 7.1.2). Runoff has been shown to be adequately predicted, as described in Section 7.1.3, where several runoff events were recorded at the YMP during two relatively wet years. The stochastic simulations of weather are shown to be a good representation of the weather observed at the proxy sites for each climate in Section 7.1.1.

(3) The effects of fracture properties, fracture distributions, matrix properties, heterogeneities, time-varying boundary conditions, evapotranspiration, depth of soil cover, and surface-water run off and run on are considered, such that net infiltration is not underestimated.

Bedrock fracture and matrix properties, distributions, and uncertainties are developed in *Data Analysis for Infiltration Modeling: Bedrock Saturated Hydraulic Conductivity Calculation* (BSC 2006 [DIRS 176355]), and inputs to the MASSIF model based on this report are summarized in Section 6.5.2. Uncertainty in bulk bedrock conductivity includes the possibility that some portion of the filled bedrock fractures contain open conduits, and therefore, the potential for net infiltration is not underestimated.

Parameter ranges and distributions used to develop evapotranspiration estimates are discussed in Sections 6.5.3 and 6.5.4, Appendix D, and Appendix E. Uncertainties in these parameters ensure that the full range of uncertainty in evapotranspiration is captured and not overestimated, and therefore, net infiltration is not underestimated.

Soil depth estimates, including uncertainty and spatial variability are developed in D*ata Analysis for Infiltration Modeling: Technical Evaluation of Previous Soil Depth Estimation Methods and Development of Alternate Parameter Values* (BSC 2006 [DIRS 178819]) and are further summarized for the MASSIF model in Section 6.6. Assumptions are made (in Section 5) that state that soil depth and properties can be considered to be constant for the next 10,000 years. The inclusion of uncertainties in soil depth provides confidence that net infiltration results and is not underestimated. This is because soil depth is one of the most important parameters controlling net infiltration over the modeling domain.

As part of model validation, comparisons are made between observations and model predictions of runoff. Within the uncertainty range of input variables, these comparisons are quite consistent (Section 7.1.3). Therefore, there is no reason to believe that net infiltration is underestimated.

All of the parameters that influence infiltration are briefly discussed in Appendix I where they are screened for inclusion in the uncertainty analysis. Appendix H describes sensitivity analyses and identifies parameters that have the greatest influence on net infiltration. The most influential parameters are included in the uncertainty analysis. The range of predicted net infiltration reasonably represents the uncertainty in a manner that precludes that net infiltration is underestimated.

(4) Sensitivity or uncertainty analyses are performed to assess data sufficiency and determine the possible need for additional data.

Sensitivity analyses have been conducted to determine the influence of various parameters over their expected ranges, which include uncertainty, and these analyses are developed in Section 6.7. Sufficient data exist to enable credible and bounding predictions of infiltration. These studies show that soil depth in Depth Class 4 (shallow soils) and water holding capacity of soil group 5/7/9 are the most important physical parameters in the MASSIF model. In addition, the uncertainty related to future precipitation patterns is another significant source of uncertainty. While further data are not needed to develop sufficiently accurate estimates of infiltration for the purposes of TSPA, such data would serve to reduce the uncertainty in predicted infiltration ranges.

(5) Accepted and well-documented procedures are used to construct and calibrate numerical models;

The fundamental conceptual model is based on a mass-balance calculation where water enters a grid cell through precipitation (rain or snowmelt) and/or run-on and water leaves a cell through evapotranspiration, sublimation, runoff, and/or net infiltration. Mass balance implies that the sum of these fluxes equals zero. The mass balance approach is generally accepted and well documented. The primary sub-components upon which MASSIF is built are described in Section 6 and include: 1) FAO-56 methods to estimate evapotranspiration, and 2) Darcy's Law in conjunction with the field capacity concept for estimating water movement and storage in the soil. Both of these procedures are well accepted and well documented approaches. The actual physics controlling run-on and runoff processes are not represented in the model. Instead, runoff is routed along flow networks through the model domain during the course of the day with the constraint of mass balance being enforced. The only calibration done is in the definition of the parameters used to convert satellite data quantifying vegetation (NDVI') to ground measurements of basal crop coefficients (K_{cb}) at ecological study plots. A linear regression accounting for measurement uncertainties was performed for this purpose. The methods used are accepted and well-documented. See Section 6.5.3 for details.

(6) Reasonably complete process-level conceptual and mathematical models are used in this model report. In particular: (a) mathematical models provided are consistent with conceptual models and site characteristics; and (b) the robustness of results from different mathematical models is compared.

The conceptual and mathematical models used in this report are complete in the sense that they represent the complete near surface hydrologic system at the YMP. Section 6 describes the conceptual model development process, the mathematical model, and the use of the model to estimate net infiltration at the YMP. The use of the FAO-56 procedures in conjunction with satellite and ground-based measurements of vegetation at the YMP site ensure that the ET component of the calculation is customized for the YMP site. The generation of stochastic precipitation records is also entirely based on weather data collected in the vicinity of the YMP site and at other locations that represent the predicted range of future climates.

An alternative mathematical model (HYDRUS 1-D) was run, and results were compared with similar runs of the MASSIF model for the purpose of model corroboration. These comparisons are described in Section 7.2.2. In addition, the MASSIF model was run with historical weather data for the purpose of comparing model results with observations of ET, runoff, and net

infiltration at various locations both on and off the YMP site (Section 7). In general these comparisons indicate that the MASSIF model is valid for its intended use.

Number 7 under Acceptance Criterion 2 was listed in the TWP, but it is not included in present report because expert elicitation was not used to support model development.

Acceptance Criterion 3: ***Data Uncertainty Is Characterized and Propagated through the Model Abstraction.***

(1) Models use parameter values, assumed ranges, probability distributions, and bounding assumptions that are technically defensible, reasonably account for uncertainties and variabilities, and do not result in an under-representation of the risk estimate.

Each of the parameters that potentially influence infiltration is briefly discussed in Appendix I where it is evaluated and screened for inclusion in the uncertainty analysis. Parameters are screened into the uncertainty analysis if their relative standard uncertainty (standard deviation) is above 15% or they represent the properties of materials that cover more than 15% of the UZ domain. Parameter uncertainty is propagated to net infiltration by way of a Monte Carlo analysis using Latin Hypercube Sampling (LHS) (see Sections 6.5.5 and 6.5.6). The range of net infiltration is demonstrated to reasonably bound the estimates of infiltration in a manner to preclude under-representation of the risk estimate.

(2) The technical bases for the parameter values used in this abstraction are provided.

Each of the parameters that serve as input to the infiltration analysis have been technically evaluated and selected based on their appropriateness for use in calculating infiltration. Bedrock fracture and matrix properties and distributions are developed in *Data Analysis for Infiltration Modeling: Bedrock Saturated Hydraulic Conductivity Calculation* (BSC 2006 [DIRS 176355]) and inputs to the MASSIF model are summarized in Section 6.5.2.6, *Bedrock Saturated Conductivity*. Parameter ranges and distributions used to develop evapotranspiration estimates are discussed in Sections 6.5.3 and 6.5.4 and Appendix D. Soil depth estimates, including uncertainty and spatial variability are developed in D*ata Analysis for Infiltration Modeling: Technical Evaluation of Previous Soil Depth Estimation Methods and Development of Alternate Parameter Values* (BSC 2006 [DIRS 178819]) and are further summarized for the MASSIF model in Section 6.5.2.4. Soil hydraulic properties and associated uncertainties are developed in *Data Analysis for Infiltration Modeling: Development of Soil Units and Associated Hydraulic Parameter Values* (BSC 2006 [DIRS 176335]) and are further summarized for the MASSIF model in Section 6.5.2.3. Geographic parameters such as elevation and slope are presented in Appendix B, and summarized in Section 6.5.2.1. All of the parameters that influence infiltration are briefly discussed in Appendix I, where they are screened for inclusion in the uncertainty analysis.

(3) Possible statistical correlations are established between parameters in this abstraction. An adequate technical basis or bounding argument is provided for neglected correlations;

Correlations between parameters have been considered in order to constrain the LHS sample of input parameters to physically realistic combinations. The sample size of each probabilistic analysis was limited to 20. Up to fifteen parameters were sampled to generate the inputs for each of the 20 realizations. For the physical parameters (parameter related to physical properties of materials), no technical basis justifying imposing correlations between parameters was identified. Therefore, no correlations were applied.

For some of the stochastic precipitation parameters, two strong correlations have been identified between parameters. The first one is an actual correlation between two parameters (e.g., the annual average of average daily precipitation amount and annual average of average daily log of precipitation amount). These parameters are strongly correlated, as they are estimated from the same data (records of daily precipitation). As the relation between the two parameters has been shown to be linear, correlation has been taken into account by sampling one of the two parameters and estimating the other with a linear regression model as discussed in Section 6.5.5 and Appendix I. The second correlation identified is associated with a set of assumptions present in *Future Climate Analysis* (BSC 2004 [DIRS 170002]). For instance, it is stated that Monsoon Climate will experience series of years either with small amounts of rain, mainly in winter, or with a larger amount of rain, mainly in summer (BSC 2004 [DIRS 170002]). Therefore, the annual variation of the precipitation parameters was adjusted to match either of the two cases. This weather pattern has been taken into account by sampling one of the parameters controlling seasonal variation and estimating the other parameters using linear regression models as discussed in Section 6.5.5 and Appendix I. The purpose of including these two correlations is to ensure that the parameter inputs represent a realistic combination of parameter values.

(4) The hydrologic effects of future climate change that may alter the rates and patterns of present-day net infiltration into the UZ are addressed. Such effects may include changes in soil depths, fracture-fill material, and types of vegetation.

The potential for future climates to affect various parameters is captured in inputs including stochastic weather parameters and vegetation parameters. The variation of stochastic weather parameters including temperature and stochastic precipitation parameters for future climates is discussed in Section 6.5.1 and Appendix F. The response in vegetation to the predicted climate change is provided in Section 6.5.3. The amount of vegetation is directly related to the annual precipitation which varies with climate. In addition, vegetation parameters (maximum rooting depth and plant height) are given climate specific and appropriate values and distributions. Field observations of bedrock fracture filling indicate that these fillings were stable during previous wet climate cycles, and therefore, these fillings are expected to remain stable for the regulatory period of the repository. Potential variation in soil depth as a result of future climate change is assumed to be negligible (Section 5.4).

Acceptance Criterion 4: ***Model Uncertainty Is Characterized and Propagated through the Model Abstraction.***

(1) Alternate modeling approaches of FEPs, consistent with available data and current scientific understanding, are investigated. The results and limitation are appropriately considered in the abstraction.

Net infiltration results of an alternative conceptual and numerical model (HYDRUS-1D) are compared with the results of the MASSIF model in Section 7.2.2 and Appendix K. HYDRUS-1D is a model based on the Richards' equation and thus solves a different set of equations than MASSIF. The comparison demonstrated that while the models exhibit different transient net infiltration behaviors the results are very similar when summed over the year. Thus, since the purpose of the net infiltration calculation is to calculate a steady-state, long term average flux, both MASSIF and HYDRUS-1D provide comparable results, which corroborates the MASSIF model.

(2) The bounds of uncertainty created by process-level models are considered in this abstraction.

It is assumed in this analysis (Section 5) that net infiltration uncertainty caused by the selection of the model is not as significant as the uncertainty caused by the epistemic parameter uncertainty.

(3) Consideration of conceptual model uncertainty is consistent with available site characterization data, laboratory experiments, field measurements, natural analogue information and process-level modeling studies; and the treatment of conceptual model uncertainty does not result in an under-representation of the risk estimate.

The model uncertainties have been estimated by comparing model predictions to field observations and predictions of an alternative model (HYDRUS-1D). These comparisons are described in the model validation sections of the report (Section 7.2.2 and Appendices J and K).

Acceptance Criterion 5: ***Model Abstraction Output Is Supported by Objective Comparisons***

Number 1 under Acceptance Criterion 5 was listed in the TWP, but it is not included in present report because the output from this model is not a direct TSPA abstraction.

(2) Abstractions of process-level models may conservatively bound process-level predictions.

Net infiltration estimates presented in this report include the quantification of uncertainty which bounds these estimates. While it was not the intent of this analysis to provide a "conservative" estimate of net infiltration, the results of the analysis may be conservative (over-estimate) due to the lack of certain site-specific data to constrain the results. For example, as identified in Section 1.2, it is assumed in this analysis that there is no significant water loss below the soil-rock interface. If, in fact, a significant amount of water is lost from within the rock, then the net infiltration estimates from this analysis provide an upper bound on net infiltration.

(3) Comparisons are provided of output of abstracted models of climate and net infiltration with output of sensitivity studies, detailed process-level models, natural analogs, and empirical observations, as appropriate.

Section 7 includes: (a) comparisons of model outputs of precipitation to observed patterns of precipitation at the Yucca Mountain site as well as at analog meteorological sites used to represent future climate conditions (Section 7.1.1), (b) comparisons of model predictions of evapotranspiration to lysimeter observations (Section 7.1.2), (c) comparisons of simulated runoff to observations at Yucca Mountain monitoring stations (Section 7.1.3), (d) results of an extended sensitivity study examining the influence of parameter uncertainty on net infiltration uncertainty (Section 7.1.4), (e) comparison of net infiltration predictions with field estimates of net infiltration from the region (Section 7.2.1), (f) comparisons of net infiltration estimates with estimates calculated using an alternative, more detailed and mechanistic model (HYDRUS-1D) (Section 7.2.2), and (g) comparisons of net infiltration model predictions with the estimates provided as part of an expert elicitation (Section 7.2.3).

Acceptance Criteria from Section 2.2.1.1.3

(3) Technical Basis for Barrier Capability is Adequately Presented

The near-surface hydrologic system is part of the natural barrier capability of the repository design. The net infiltration model contributes to the natural barrier system by simulating the precipitation of water to the land surface and calculating the fraction of that water that enters the unsaturated zone as deep percolation. The representation of precipitation processes is described in Section 6.5.1 and Appendix F. Evapotranspiration is discussed in Section 6.5.3, 6.5.4, and Appendices C, D, and E.

INTENTIONALLY LEFT BLANK

9. INPUTS AND REFERENCES

The following is a list of the references cited in this document. Column 1 lists the Document Input Reference System number (DIRS). Column 2 lists the bibliographic citation.

9.1 DOCUMENTS CITED

176485 Allen, R.G. 1996. "Assessing Integrity of Weather Data for Reference Evapotranspiration Estimation." *Journal of Irrigation and Drainage Engineering, 122,* (2), 97-106. New York, New York: American Society of Civil Engineers. TIC: 258098.

176568 Allen, R.G. 1997. "Self-Calibrating Method for Estimating Solar Radiation from Air Temperature." *Journal of Hydrologic Engineering, 2,* (2), 56-67. New York, New York: American Society of Civil Engineers. TIC: 258131.

157311 Allen, R.G.; Pereira, L.S.; Raes, D.; and Smith, M. 1998. *Crop Evapotranspiration, Guidelines for Computing Crop Water Requirements.* FAO Irrigation and Drainage Paper 56. Rome, Italy: Food and Agriculture Organization of the United Nations. TIC: 245062.

176009 Allen, R.G.; Pereira, L.S.; Smith, M.; Raes, D.; and Wright, J.L. 2005. "FAO-56 Dual Crop Coefficient Method for Estimating Evaporation from Soil and Application Extensions." *Journal of Irrigation and Drainage Engineering, 131,* (1), 2-13. Reston, Virginia: American Society of Civil Engineers. TIC: 257869.

178493 Allen, R.G.; Pruitt, W.O.; Raes, D.; Smith, M.; and Pereira, L.S. 2005. "Estimating Evaporation from Bare Soil and the Crop Coefficient for the Initial Period Using Common Soils Information." *Journal of Irrigation and Drainage Engineering, 131,* (1), 14-23. Reston, Virginia: American Society of Civil Engineers. TIC: 258906.

176785 Allen, R.G.; Pruitt, W.O.; Wright, J.L.; Howell, T.A.; Ventura, F.; Snyder, R.; Itenfisu, D.; Steduto, P.; Berengena, J.; Yrisarry, J.B.; Smith, M.; Pereira, L.S.; Raes, D.; Perrier, A.; Alves, I.; Walter, I.; and Elliott, R. 2006. "A Recommendation on Standardized Surface Resistance for Hourly Calculation of Reference ET_o by the FAO56 Penman-Monteith Method." *Agricultural Water Management, 81,* 1-22. New York, New York: Elsevier. TIC: 258241.

176207 Allen, R.G.; Walter, I.A.; Elliott, R.L.; Howell, T.; Itenfisu, D.; and Jensen, M. 2005. *The ASCE Standardized Reference Evapotranspiration Equation.* Reston, Virginia: American Society of Civil Engineers. TIC: 257138.

103750 Altman, W.D.; Donnelly, J.P.; and Kennedy, J.E. 1988. *Qualification of Existing Data for High-Level Nuclear Waste Repositories: Generic Technical Position.* NUREG-1298. Washington, D.C.: U.S. Nuclear Regulatory Commission. TIC: 200652.

103597 Altman, W.D.; Donnelly, J.P.; and Kennedy, J.E. 1988. *Peer Review for High-Level Nuclear Waste Repositories: Generic Technical Position.* NUREG-1297. Washington, D.C.: U.S. Nuclear Regulatory Commission. TIC: 200651.

177625 Anderson, M.D. 2002. "Pinus Eulis." Washington, D.C.: U.S. Department of Agriculture, Forest Service. Accessed September 5, 2006. ACC: MOL.20060907.0013. URL: http://www.fs.fed.us/database/feis/plants/tree/pinedu/all.htm

176754 Asrar, G.; Myneni, R.B.; and Choudhury, B.J. 1992. "Spatial Heterogeneity in Vegetation Canopies and Remote Sensing of Absorbed Photosynthetically Active Radiation: A Modeling Study." *Remote Sensing of Environment, 41,* 85-103. New York, New York: Elsevier. TIC: 258219.

177200 Avon, L. and Durbin, T.J. 1994. "Evaluation of the Maxey-Eakin Method for Estimating Recharge to Ground-Water Basins in Nevada." *Water Resources Bulletin, 30,* (1), 99-111. Herndon, Virginia: American Water Resources Association. TIC: 255352.

127394 Barbour, M.G.; Burk, J.H.; and Pitts, W.D. 1980. *Terrestrial Plant Ecology.* Menlo Park, California: Benjamin/Cummings Publishing Company. TIC: 243042.

101486 Bauer, D.J.; Foster, B.J.; Joyner, J.D.; and Swanson, R.A. 1996. *Water Resources Data for Nevada Water Year 1995.* Water-Data Report NV-95-1. Carson City, Nevada: U.S. Geological Survey. ACC: MOL.20010721.0049.

177726 Bauer, H.H. and Vaccaro, J.J. 1990. *Estimates of Ground-Water Recharge to the Columbia Plateau Regional Aquifer System, Washington, Oregon, and Idaho, for Predevelopment and Current Land-Use Conditions.* Water-Resources Investigations Report 88-4108. Denver, Colorado: U.S. Geological Survey. ACC: MOL.20061115.0001.

178678 Baugh, W.M. and Groeneveld, D.P. 2006. "Broadband Vegetation Index Performance Evaluated for a Low-Cover Environment." *International Journal of Remote Sensing, 27,* (21-22), 4715 - 4730. New York, New York: Taylor & Francis. TIC: 259019.

177652 Bausch, W.C. and Neale, C.M.U. 1987. "Crop Coefficients Derived from Reflected Canopy Radiation: A Concept." *Transactions of the ASAE, 30,* (3), 703-709. St. Joseph, Michigan: American Society of Agricultural Engineers. TIC: 258520.

103356 Beatley, J.C. 1975. "Climates and Vegetation Pattern Across the Mojave/Great Basin Desert Transition of Southern Nevada." *American Midland Naturalist, 93,* (1), 53-70. Notre Dame, Indiana: University of Notre Dame. TIC: 241488.

102221 Beatley, J.C. 1976. *Vascular Plants of the Nevada Test Site and Central-Southern Nevada: Ecologic and Geographic Distributions.* TID-26881. Oak Ridge, Tennessee: Energy Research and Development Administration. TIC: 204727.

177995 Berg, N.H. 1986. "Blowing Snow at a Colorado Alpine Site: Measurements and Implications." *Arctic and Alpine Research, 18,* (2), 147-161. Boulder, Colorado: University of Colorado, Institute of Arctic and Alpine Research. TIC: 258763.

147076 Bevington, P.R. and Robinson, D.K. 1992. *Data Reduction and Error Analysis for the Physical Sciences.* 2nd Edition. New York, New York: McGraw-Hill. TIC: 243514.

176211 Bodhinayake, W. and Si, B.C. 2004. "Near-Saturated Surface Soil Hydraulic Properties under Different Land Uses in the St. Denis National Wildlife Area, Saskatchewan, Canada." *Hydrological Processes, 18,* 2835-2850. New York, New York: John Wiley & Sons. TIC: 257866.

176784 Bolstad, P.V.; Swift, L.; Collins, F.; and Régnière, J. 1998. "Measured and Predicted Air Temperatures at Basin to Regional Scales in the Southern Appalachian Mountains." *Agricultural and Forest Meteorology, 91,* 161-176. New York, New York: Elsevier. TIC: 258239.

127406 Bonham, C.D. 1989. *Measurements for Terrestrial Vegetation.* New York, New York: John Wiley & Sons. TIC: 242274.

160019 Brady, N.C. and Weil, R.R. 1999. *The Nature and Properties of Soils.* 12th Edition. Upper Saddle River, New Jersey: Prentice-Hall. TIC: 242178.

176615 Brutsaert, W. 1982. *Evaporation into the Atmosphere, Theory, History, and Applications.* Environmental Fluid Mechanics. Csanady, G.T., ed. Boston, Massachusetts: D. Reidel Publishing Company. TIC: 239388.

165991 BSC (Bechtel SAIC Company) 2003. *Analysis of Infiltration Uncertainty.* ANL-NBS-HS-000027 REV 01. Las Vegas, Nevada: Bechtel SAIC Company. ACC: DOC.20031030.0003.

168796 BSC 2003. *Risk Information to Support Prioritization of Performance Assessment Models.* TDR-WIS-PA-000009 REV 01 ICN 01 [Errata 001]. Las Vegas, Nevada: Bechtel SAIC Company. ACC: MOL.20021017.0045; DOC.20031014.0003.

165572 BSC 2003. *Underground Layout Configuration.* 800-P0C-MGR0-00100-000-00E. Las Vegas, Nevada: Bechtel SAIC Company. ACC: ENG.20031002.0007; ENG.20050817.0005.

169857 BSC 2004. *Calibrated Properties Model.* MDL-NBS-HS-000003 REV 02. Las Vegas, Nevada: Bechtel SAIC Company. ACC: DOC.20041006.0004.

170002 BSC 2004. *Future Climate Analysis.* ANL-NBS-GS-000008 REV 01. Las Vegas, Nevada: Bechtel SAIC Company. ACC: DOC.20040908.0005.

170029 BSC 2004. *Geologic Framework Model (GFM2000).* MDL-NBS-GS-000002 REV 02. Las Vegas, Nevada: Bechtel SAIC Company. ACC: DOC.20040827.0008.

167652 BSC 2004. *Seepage Model for PA Including Drift Collapse.* MDL-NBS-HS-000002 REV 03. Las Vegas, Nevada: Bechtel SAIC Company. ACC: DOC.20040922.0008; DOC.20051205.0001.

170007 BSC 2004. *Simulation of Net Infiltration for Present-Day and Potential Future Climates.* MDL-NBS-HS-000023 REV 00. Las Vegas, Nevada: Bechtel SAIC Company. ACC: DOC.20041109.0004.

180945 BSC 2004. *Technical Basis Document No. 1: Climate and Infiltration.* Revision 1. Las Vegas, Nevada: Bechtel SAIC Company. ACC: MOL.20040804.0292.

169861 BSC 2004. *UZ Flow Models and Submodels.* MDL-NBS-HS-000006 REV 02. Las Vegas, Nevada: Bechtel SAIC Company. ACC: DOC.20041101.0004; DOC.20050629.0003.

174191 BSC 2005. *Features, Events, and Processes in UZ Flow and Transport.* ANL-NBS-MD-000001 REV 04. Las Vegas, Nevada: Bechtel SAIC Company. ACC: DOC.20050809.0002.

173944 BSC 2005. *Multiscale Thermohydrologic Model.* ANL-EBS-MD-000049 REV 03. Las Vegas, Nevada: Bechtel SAIC Company. ACC: DOC.20050711.0001.

175539 BSC 2005. *Q-List.* 000-30R-MGR0-00500-000-003. Las Vegas, Nevada: Bechtel SAIC Company. ACC: ENG.20050929.0008.

176335 BSC 2006. *Data Analysis for Infiltration Modeling: Development of Soil Units and Associated Hydraulic Parameter Values.* ANL-NBS-HS-000055 REV 00. Las Vegas, Nevada: Bechtel SAIC Company. ACC: DOC.20060912.0006.

178819 BSC 2006. *Data Analysis for Infiltration Modeling: Technical Evaluation of Previous Soil Depth Estimation Methods and Development of Alternate Parameter Values.* ANL-NBS-HS-000077 REV 01. Las Vegas, Nevada: Bechtel SAIC Company. ACC: DOC.20060918.0009.

176355 BSC 2006. *Data Analysis for Infiltration Modeling: Bedrock Saturated Hydraulic Conductivity Calculation.* ANL-NBS-HS-000054 REV 00. Las Vegas, Nevada: Bechtel SAIC Company. ACC: DOC.20060710.0001.

177083 BSC 2006. *Technical Evaluation and Review of Results, Technical Procedures, and Methods Related to the Collection of Moisture Monitoring Data Using Neutron Probes in Shallow Boreholes.* TDR-NBS-HS-000019 REV 00. Las Vegas, Nevada: Bechtel SAIC Company. ACC: DOC.20060425.0005.

177492 BSC 2006. *Technical Work Plan for: Infiltration Model Assessment, Revision, and Analyses of Downstream Impacts.* TWP-NBS-HS-000012 REV 02. Las Vegas, Nevada: Bechtel SAIC Company. ACC: DOC.20060831.0006.

176736 Buschmann, C. and Nagel, E. 1993. "In Vivo Spectroscopy and Internal Optics of Leaves as Basis for Remote Sensing of Vegetation." *International Journal of Remote Sensing, 14,* (4), 711-722. New York, New York: Taylor & Francis. TIC: 258202.

177100 Campbell, M.D.; Gee, G.W.; Kirkham, R.R.; Phillips, S.J.; and Wing, N.R. 1991. "Water Balance Lysimetry at a Nuclear Waste Site." *Lysimeters for Evapotranspiration and Environmental Measurements, Proceedings of the International Symposium on Lysimetry, Honolulu, Hawaii, July 23-25, 1991.* Allen, R.G.; Howell, T.A.; Pruitt, W.O.; Walter, I.A.; and Jensen, M.E., eds. Pages 125-132. New York, New York: American Society of Civil Engineers. TIC: 258304.

177626 Canadell, J.; Jackson, R.B.; Ehleringer, J.R.; Mooney, H.A.; Sala, O.E.; and Schulze, E.-D. 1996. "Maximum Rooting Depth of Vegetation Types at the Global Scale." *Oecologia, 108,* 583-595. Berlin, Germany: Springer-Verlag. TIC: 258180.

176748 Carlson, T.N. and Ripley, D.A. 1997. "On the Relation between NDVI, Fractional Vegetation Cover, and Leaf Area Index." *Remote Sensing of Environment, 62,* 241-252. New York, New York: Elsevier. TIC: 258215.

174674 Carpenter, A.T. and Murray, T.A. [n.d.]. *Element Stewardship Abstract for Bromus Tectorum L (Anisantha Tectorum (L.) Nevski).* Arlington, Virginia: The Nature Conservancy. TIC: 257692.

177572 Chander, G.; Helder, D.L.; Markham, B.L.; Dewald, J.D.; Kaita, E.; Thorne, K.J.; Micjevic, E.; and Ruggles, T.A. 2004. "Landsat-5 TM Reflective-Band Absolute Radiometric Calibration." *IEEE Transactions on Geoscience and Remote Sensing, 42,* (12), 2747-2760. New York, New York: Institute of Electrical and Electronics Engineers. TIC: 258551.

176788 Chavez, P.S., Jr. 1988. "An Improved Dark-Object Subtraction Technique for Atmospheric Scattering Correction of Multispectral Data." *Remote Sensing of Environment, 124,* 459-479. New York, New York: Elsevier. TIC: 258249.

178132 Chen, J-S.; Drake, R.; Lin, Z.; and Jewett, D.G. 2002. "A Benchmarking Analysis for Five Radionuclide Vadose Zone Models (CHAIN, MULTIMED_DP, FECTUZ, HYDRUS, AND CHAIN 2D) in Soil Screening Level Calculations." *HLW, LLW, Mixed, Hazardous Restoration -- Working Towards a Cleaner Environment, WM'02 Proceedings, Feb. 24-28, 2002, Tucson, Arizona.* 1-17. Tucson, Arizona: WM Symposia. TIC: 258782.

177127 Cline, J.F.; Uresk, D.W.; and Rickard, W.H. 1977. "Comparison of Soil Water Used by a Sagebrush-Bunchgrass and a Cheatgrass Community." *Journal of Range Management, 30,* (3), 199-201. Denver, Colorado: Society for Range Management. TIC: 243506.

178314 Cohen, S.; Liepert, B.; and Stanhill, G. 2004. "Global Dimming Comes of Age." *Eos, 85,* (38), 382-383. Washington, D.C.: American Geophysical Union. TIC: 258567.

176487 Collares-Pereira, M. and Rabl, A. 1979. "The Average Distribution of Solar Radiation—Correlations Between Diffuse and Hemispherical and Between Daily and Hourly Insolation Values." *Solar Energy, 22,* 155-164. New York, New York: Pergamon Press. TIC: 258100.

102235 CRWMS (Civilian Radioactive Waste Management System) M&O (Management and Operating Contractor) 1996. *The Vegetation of Yucca Mountain: Description and Ecology.* B00000000-01717-5705-00030 REV 00. Las Vegas, Nevada: CRWMS M&O. ACC: MOL.19970116.0055.

100117 CRWMS M&O 1997. *Engineering Design Climatology and Regional Meteorological Conditions Report.* B00000000-01717-5707-00066 REV 00. Las Vegas, Nevada: CRWMS M&O. ACC: MOL.19980304.0028.

103155 CRWMS M&O 1997. *Meteorological Monitoring Program 1996 Summary Report.* B00000000-01717-5705-00072 REV 00. Las Vegas, Nevada: CRWMS M&O. ACC: MOL.19980210.0202.

100335 CRWMS M&O 1997. *Unsaturated Zone Flow Model Expert Elicitation Project.* Las Vegas, Nevada: CRWMS M&O. ACC: MOL.19971009.0582.

104589 CRWMS M&O 1998. *Classification and Map of Vegetation at Yucca and Little Skull Mountains, Nevada.* B00000000-01717-5705-00083 REV 00. Las Vegas, Nevada: CRWMS M&O. ACC: MOL.19990615.0237.

105031 CRWMS M&O 1999. *Final Report: Plant and Soil Related Processes Along a Natural Thermal Gradient at Yucca Mountain, Nevada.* B00000000-01717-5705-00109 REV 00. Las Vegas, Nevada: CRWMS M&O. ACC: MOL.19990513.0037.

115672 CRWMS M&O 1999. *Meteorological Monitoring Program 1997 Summary Report.* B00000000-01717-5705-00107 REV 00. Las Vegas, Nevada: CRWMS M&O. ACC: MOL.19990804.0287.

177096 Daly, C.; Gibson, W.P.; Taylor, G.H.; Johnson, G.L.; and Pasteris, P. 2002. "A Knowledge-Based Approach to the Statistical Mapping of Climate." *Climate Research, 22,* (2), 99-113. Oldendorf/Luhe, Germany: Inter-Research. TIC: 258404.

101557 Day, W.C.; Potter, C.J.; Sweetkind, D.S.; Dickerson, R.P.; and San Juan, C.A. 1998. *Bedrock Geologic Map of the Central Block Area, Yucca Mountain, Nye County, Nevada.* Miscellaneous Investigations Series Map I-2601. Washington, D.C.: U.S. Geological Survey. ACC: MOL.19980611.0339.

176858 Desotell, L.T.; Hudson, D.B.; Yucel, V.; and Carilli, J.T. 2006. *Use of Long-Term Lysimeter Data in Support of Shallow Land Waste Disposal Cover Design.* DOE/NV11718--1148. Las Vegas, Nevada: U.S. Department of Energy, Nevada Site Office. ACC: MOL.20060413.0159.

105384 Dettinger, M.D. 1989. "Reconnaissance Estimates of Natural Recharge to Desert Basins in Nevada, U.S.A., by Using Chloride-Balance Calculations." *Journal of Hydrology, 106,* 55-78. Amsterdam, The Netherlands: Elsevier. TIC: 236967.

178528 Dewitte, S.; Crommelynck, D.; Mekaoui, S.; and Joukoff, A. 2004. "Measurement and Uncertainty of the Long-Term Total Solar Irradiance Trend." *Solar Physics, 224,* 209-216. Berlin, Germany: Springer. TIC: 258937.

178133 Dho, N.Y.; Koo, J.K.; and Lee, S.R. 2002. "Prediction of Leachate Level in Kimpo Metropolitan Landfill Site by Total Water Balance." *Environmental Monitoring and Assessment, 73,* 207-219. Amsterdam, The Netherlands: Kluwer Academic. TIC: 258769.

178797 Di Sanza, E.F. 2006. "Yucca Mountain Project (YMP) Request for Area 5 Weighing Lysimeter Data." Memorandum from E.F. Di Sanza (DOE/NVO) to E.T. Smistad (YMP), January 26, 2006, WMD:1671.JC, with attachments. ACC: MOL.20060510.0140.

147785 DOE (U.S. Department of Energy) 1995. *Meteorological Monitoring Program Environmental Field Programs, 1993 Annual Summary Report.* Las Vegas, Nevada: Yucca Mountain Site Characterization Office. ACC: MOL.19950721.0152.

179958 DOE 2006. *Report for Surveillance OQA-SI-06-015 of Infiltration Model at Bechtel, SAIC Company, LLC in Las Vegas, Nevada, September 20-29, 2006.* Surveillance Report OQA-SI-06-015. Las Vegas, Nevada: U.S. Department of Energy, Office of Civilian Radioactive Waste Management. ACC: MOL.20070103.0116.

176786 Droogers, P. and Allen, R.G. 2002. "Estimating Reference Evapotranspiration Under Inaccurate Data Conditions." *Irrigation and Drainage Systems, 16,* 33-45. Dordrecht, The Netherlands: Kluwer Academic Publishers. TIC: 258242.

178498 Duchemin, B.; Hadria, R.; Erraki, S.; Boulet, G.; Maisongrande, P.; Chehbouni, A.; Escadafal, R.; Ezzahar, J.; Hoedjes, J.C.B.; Kharrou, M.H.; Khabba, S.; Mougenot, B.; Olioso, A.; Rodriguez, J.-C.; and Simonneaux, V. 2006. "Monitoring Wheat Phenology and Irrigation in Central Morocco: On the Use of Relationships Between Evapotranspiration, Crops Coefficients, Leaf Area Index and Remotely-Sensed Vegetation Indices." *Agricultural Water Management, 79,* 1-27. New York, New York: Elsevier. TIC: 258870.

176264 Duffie, J.A. and Beckman, W.A. 1980. *Solar Engineering of Thermal Processes.* New York, New York: John Wiley & Sons. TIC: 258031.

176616 Duffie, J.A. and Beckman, W.A. 1991. *Solar Engineering of Thermal Processes.* 2nd Edition. New York, New York: John Wiley & Sons. TIC: 258123.

176486 Erbs, D.G.; Klein, S.A.; and Duffie, J.A. 1982. "Estimation of the Diffuse Radiation Fraction for Hourly, Daily and Monthly-Average Global Radiation." *Solar Energy, 28,* (4), 293-302. New York, New York: Pergamon Press. TIC: 258099.

178766 Faybishenko, B. 2007. "Climatic Forecasting of Net Infiltration at Yucca Mountain Using Analogue Meterorological Data." *Vadose Zone Journal, 6,* 77-92. Madison, Wisconsin: Soil Science Society of America. TIC: 259076.

177499 Fayer, M.J. 2000. *UNSAT-H Version 3.0: Unsaturated Soil Water and Heat Flow Model, Theory, User Manual, and Examples.* PNNL-13249. Richland, Washington: Pacific Northwest National Laboratory. ACC: MOL.20060712.0224.

178191 Fayer, M.J. and Walters, T.B. 1995. *Estimated Recharge Rates at the Hanford Site.* PNL-10285. Richland, Washington: Pacific Northwest Laboratory. ACC: MOL.20061026.0075.

178173 Feddes, R.A.; Bresler, E.; and Neuman, S.P. 1974. "Field Test of a Modified Numerical Model for Water Uptake by Root Systems." *Water Resources Research, 10,* (6), 1199-1206. Washington, D.C.: American Geophysical Union. TIC: 258772.

156668 Fetter, C.W. 2001. *Applied Hydrogeology.* 4th Edition. Upper Saddle River, New Jersey: Prentice Hall. TIC: 251142.

177754 Finsterle, S. and Seol, Y. 2006. *Preliminary Evaluation of Seepage Observations from the ESF South Ramp Using the Drift Seepage Abstraction Model.* Albuquerque, New Mexico: Sandia National Laboratories. ACC: MOL.20060510.0330.

100147 Flint, A.L.; Hevesi, J.A.; and Flint, L.E. 1996. *Conceptual and Numerical Model of Infiltration for the Yucca Mountain Area, Nevada.* Milestone 3GUI623M. Denver, Colorado: U.S. Geological Survey. ACC: MOL.19970409.0087.

100394 Flint, L.E. and Flint, A.L. 1995. *Shallow Infiltration Processes at Yucca Mountain, Nevada—Neutron Logging Data 1984-93.* Water-Resources Investigations Report 95-4035. Denver, Colorado: U.S. Geological Survey. ACC: MOL.19960924.0577.

177628 Foxx, T.S.; Tierney G.D.; and Williams, J.M. 1984. *Rooting Depths of Plants on Low-Level Waste Disposal Sites.* LA-10253-MS. Los Alamos, New Mexico: Los Alamos National Laboratory. TIC: 228561.

101173 Freeze, R.A. and Cherry, J.A. 1979. *Groundwater.* Englewood Cliffs, New Jersey: Prentice-Hall. TIC: 217571.

163705 Gilbert, R.O. 1987. *Statistical Methods for Environmental Pollution Monitoring.* New York, New York: John Wiley & Sons. TIC: 252619.

176763 Gillies, R.R.; Carlson, T.N.; Cui, J.; Kustas, W.P.; and Humes, K.S. 1997. "A Verification of the 'Triangle' Method for Obtaining Surface Soil Water Content and Energy Fluxes from Remote Measurements of the Normalized Difference Vegetation Index (NDVI) and Surface Radiant Temperature." *International Journal of Remote Sensing, 18,* (15), 3145-3166. New York, New York: Taylor & Francis. TIC: 258232.

177128 Hamerlynck, E.P.; Huxman, T.E.; Charlet, T.N.; and Smith, S.D. 2002. "Effects of Elevated CO_2 (FACE) on the Functional Ecology of the Drought-Deciduous Mojave Desert Shrub, Lycium Andersonii." *Environmental and Experimental Botany, 48,* (2), 93-106. New York, New York: Elsevier. TIC: 257779.

177130 Hamerlynck, E.P.; Huxman, T.E.; Loik, M.E.; and Smith, S.D. 2000. "Effects of Extreme High Temperature, Drought and Elevated CO_2 on Photosynthesis of the Mojave Desert Evergreen Shrub, Larrea Tridentata." *Plant Ecology, 148,* (2), 183-193. Dordrecht, The Netherlands: Kluwer Academic Publishers. TIC: 257773.

176045 Hamerlynck, E.P.; Huxman, T.E.; McAuliffe, J.R.; and Smith, S.D. 2004. "Carbon Isotope Discrimination and Foliar Nutrient Status of Larrea Tridentata (Creosote Bush) in Contrasting Mojave Desert Soils." *Oecologia, 138,* 210-215. New York, New York: Springer-Verlag. TIC: 257872.

177022 Hamerlynck, E.P.; McAuliffe, J.R.; and Smith, S.D. 2000. "Effects of Surface and Sub-Surface Soil Horizons on the Seasonal Performance of Larrea Tridentata (Creosotebush)." *Functional Ecology, 14,* 596-606. Malden, Massachusetts: Blackwell Publishing. TIC: 257772.

177046 Hamerlynck, E.P.; McAuliffe, J.R.; McDonald, E.V.; and Smith, S.D. 2002. "Ecological Responses of Two Mojave Desert Shrubs to Soil Horizon Development and Soil Water Dynamics." *Ecology, 83,* (3), 768-779. Washington, D.C.: Ecological Society of America. TIC: 258371.

177619 Hansen, D.J. and Ostler, W.K. 2003. *Rooting Characteristics of Vegetation Near Areas 3 and 5 Radioactive Waste Management Sites at the Nevada Test Site.* DOE/NV/11718-595. Las Vegas, Nevada: U.S. Department of Energy, National Nuclear Security Administration. ACC: MOL.20060712.0208.

177508 Hanson, C.L. 2001. "Long-Term Precipitation Database, Reynolds Creek Experimental Watershed, Idaho, United States." *Water Resources Research, 37,* (11), 2831-2834. Washington, D.C.: American Geophysical Union. ACC: MOL.20060712.0230.

177509 Hanson, C.L.; Marks, D.; and Van Vactor, S.S. 2001. "Long-Term Climate Database, Reynolds Creek Experimental Watershed, Idaho, United States." *Water Resources Research, 37,* (11), 2839-2841. Washington, D.C.: American Geophysical Union. ACC: MOL.20060712.0231.

176787 Hargreaves, G.H. and Allen, R.G. 2003. "History and Evaluation of Hargreaves Evapotranspiration Equation." *Journal of Irrigation and Drainage Engineering, 129,* (1), 53-63. Reston, Virginia: American Society of Civil Engineers. TIC: 258243.

177630 Harris, G.A. 1967. "Some Competitive Relationships Between Agropyron Spicatum and Bromus Tectorum." *Ecological Monographs, 37,* (2), 89-111. Ithaca, New York: Ecological Society of America. TIC: 258196.

176151 Hay, J.E. 1979. "Calculation of Monthly Mean Solar Radiation for Horizontal and Inclined Surfaces." *Solar Energy, 23,* 301-307. New York, New York: Pergamon Press. TIC: 258030.

176740 Helder, D.L. and Ruggles, T.A. 2004. "Landsat Thematic Mapper Reflective-Band Radiometric Artifacts." *IEEE Transactions on Geoscience and Remote Sensing, 42,* (12), 2704-2716. New York, New York: Institute of Electrical and Electronics Engineers. TIC: 258206.

100583 Hillel, D. 1980. *Applications of Soil Physics.* New York, New York: Academic Press. TIC: 217649.

178856 Hillel, D. 2004. *Introduction to Environmental Soil Physics.* New York, New York: Elsevier. TIC: 259102.

153709 Hofmann, L.L.; Guertal, W.R.; and Flint, A.L. 2000. *Development and Testing of Techniques to Obtain Infiltration Data for Unconsolidated Surficial Materials, Yucca Mountain Area, Nye County, Nevada.* Open-File Report 95-154. Denver, Colorado: U.S. Geological Survey. TIC: 249343.

178487 Hogan, J.F.; Phillips, F.M.; and Scanlon, B.R., eds. 2004. "Preface." In *Groundwater Recharge in a Desert Environment: The Southwestern United States,* Hogan, J.F.; Phillips, F.M.; and Scanlon, B.R., eds, *Water Science and Application 9.* Washington, D.C.: American Geophysical Union. TIC: 256760.

177996 Hood, E.; Williams, M.; and Cline, D. 1999. "Sublimation from a Seasonal Snowpack at a Continental, Mid-Latitude Alpine Site." *Hydrological Processes, 13,* 1781-1797. New York, New York: John Wiley & Sons. TIC: 258621.

174618 Horton, G.A. 1998. *Abbreviations and Acronyms, Appendices, and Selected References.* Part 2 of *Water Words Dictionary.* 8th Edition. Carson City, Nevada: Nevada Division of Water Planning. TIC: 241350.

180680 Howell, David M.and Runkle, Gene E. 2007. *Root Cause Analysis Report In Response to Condition Report 5223 Regarding Emails Suggesting Noncompliance with Quality Assurance Requirements.* Las Vegas, NV: U.S. DOE Office of Civilian Radioactive Waste Management. ACC: LLR.20070504.008.

178317 Howell, T.A.; Evett, S.R.; Tolk, J.A.; and Schneider, A.D. 2004. "Evapotranspiration of Full-, Deficit-Irrigated, and Dryland Cotton on the Northern Texas High Plains." *Journal of Irrigation and Drainage Engineering, 130,* (4), 277-285. Reston, Virginia: American Society of Civil Engineers. TIC: 258627.

177190 Howell, T.A.; Schneider, A.D.; and Jensen, M.E. 1991. "History of Lysimeter Design and Use for Evapotranspiration Measurements." *Lysimeters for Evapotranspiration and Environmental Measurements, Proceedings of the International Symposium on Lysimetry, Honolulu, Hawaii, July 23-25, 1991.* Allen, R.G.; Howell, T.A.; Pruitt, W.O.; Walter, I.A.; and Jensen, M.E., eds. Pages 1-9. New York, New York: American Society of Civil Engineers. TIC: 258304.

176738 Huete, A.R. and Liu, H.Q. 1994. "An Error and Sensitivity Analysis of the Atmospheric- and Soil-Correcting Variants of the NDVI for the MODIS-EOS." *IEEE Transactions on Geoscience and Remote Sensing, 32,* (4), 897-905. New York, New York: Institute of Electrical and Electronics Engineers. TIC: 258204.

177129 Hulbert, L.C. 1955. "Ecological Studies of Bromus Tectorum and Other Annual Bromegrasses." *Ecological Monographs, 25,* (2), 181-213. Washington, D.C.: Ecological Society of America. TIC: 258184.

176048 Hunsaker, D.J.; Pinter, Jr., P.J.; Barnes, E.M.; and Kimball, B.A. 2003. "Estimating Cotton Evapotranspiration Crop Coefficients with a Multispectral Vegetation Index." *Irrigation Science, 22,* 95-104. New York, New York: Springer-Verlag. TIC: 257868.

178529 Hunsaker, D.J.; Pinter, P.J., Jr.; and Cai, H. 2002. "Alfalfa Basal Crop Coefficients for FAO-56 Procedures in the Desert Regions of the Southwestern U.S.." *Transactions of the ASAE, 45,* (6), 1799-1815. St. Joseph, Michigan: American Society of Agricultural Engineers. TIC: 258938.

177302 Hunsaker, D.J.; Pinter, P.J., Jr.; and Kimball, B.A. 2005. "Wheat Basal Crop Coefficients Determined by Normalized Difference Vegetation Index." *Irrigation Science, 24,* 1-14. New York, New York: Springer-Verlag. TIC: 258499.

129944 Hunter, R. 1991. "Bromus Invasions on the Nevada Test Site: Present Status of B. Rubens and B. Tectorum with Notes on Their Relationship to Disturbance and Altitude." *Great Basin Naturalist, 51,* (2), 176-182. Provo, Utah: Brigham Young University. TIC: 245250.

177132 Huxman, T.E. and Smith, S.D. 2001. "Photosynthesis in an Invasive Grass and Native Forb at Elevated CO_2 During an El Niño Year in the Mojave Desert." *Oecologia, 128,* 193-201. Berlin, Germany: Springer-Verlag. TIC: 257774.

177133 Huxman, T.E.; Hamerlynck, E.P.; and Smith, S.D. 1999. "Reproductive Allocation and Seed Production in Bromus Madritensis Ssp. Rubens at Elevated Atmospheric CO_2." *Functional Ecology, 13,* 769-777. Malden, Massachusetts: Blackwell Publishing. TIC: 257771.

176861 Irmak, S.; Howell, T.A.; Allen, R.G.; Payero, J.O.; and Martin, D.L. 2005. "Standardized ASCE Penman-Monteith: Impact of Sum-of-Hourly vs. 24-Hour Timestep Computations at Reference Weather Station Sites." *Transactions of the ASAE, 48,* (3), 1063-1077. St. Joseph, Michigan: American Society of Agricultural Engineers. TIC: 258278.

177171 Jackson, R.B.; Banner, J.L.; Jobbagy, E.G.; Pockman, W.T.; and Wall, D.H. 2002. "Ecosystem Carbon Loss with Woody Plant Invasion of Grasslands." *Nature, 418,* (6898), 623-626. New York, New York: Nature Publishing Group. TIC: 258009.

177103 Jensen, D.T.; Hargreaves, G.H.; Temesgen, B.; and Allen, R.G. 1997. "Computation of ETo Under Nonideal Conditions." *Journal of Irrigation and Drainage Engineering, 123,* (5), 394-400. Reston, Virginia: American Society of Civil Engineers. TIC: 258407.

160001 Jensen, M.E.; Burman, R.D.; and Allen, R.G., eds. 1990. *Evapotranspiration and Irrigation Water Requirements.* ASCE Manuals and Reports on Engineering Practice No. 70. New York, New York: American Society of Civil Engineers. TIC: 246697.

176743 Ji, L. and Peters, A.J. 2003. "Assessing Vegetation Response to Drought in the Northern Great Plains Using Vegetation and Drought Indices." *Remote Sensing of Environment, 87,* 85-98. New York, New York: Elsevier. TIC: 258210.

176742 Justice, C.O.; Vermote, E.; Townshend, J.R.G.; Defries, R.; Roy, D.P.; Hall, D.K.; Salomonson, V.V.; Privette, J.L.; Riggs, G.; Strahler, A.; Wolfgang, L.; Myneni, R.B.; Knyazikhin, Y.; Running, S.W.; Nemani, R.R.; Wan, Z.; Huete, A.R.; van Leeuwen, W.; Wolfe, R.E.; Giglio, L.; Muller, J.-P.; Lewis, P.; and Barnsley, M.J. 1998. "The Moderate Resolution Imaging Spectroradiometer (MODIS): Land Remote Sensing for Global Change Research." *IEEE Transactions on Geoscience and Remote Sensing, 36,* (4), 1228-1249. New York, New York: Institute of Electrical and Electronics Engineers. TIC: 258208.

177998 Kattelmann, R. and Elder, K. 1991. "Hydrologic Characteristics and Water Balance of an Alpine Basin in the Sierra Nevada." *Water Resources Research, 27,* (7), 1553-1562. Washington, D.C.: American Geophysical Union. TIC: 258622.

176760 Kenea, N.H. 2001. "Influence of Desert Varnish on the Reflectance of Gossans in the Context of Landsat TM Data, Southern Red Sea Hills, Sudan." *International Journal of Remote Sensing, 22,* (10), 1879-1894. New York, New York: Taylor & Francis. TIC: 258230.

176823 Kerr, Y.H.; Imbernon, J.; Dedieu, G.; Hautecoeur, O.; Lagouarde, J.P.; and Seguin, B. 1989. "NOAA AVHRR and its Uses for Rainfall and Evapotranspiration Monitoring." *International Journal of Remote Sensing, 10,* (4 and 5), 847-854. Philadelphia, Pennsylvania: Taylor & Francis. TIC: 258269.

177191 Kirkham, R.R.; Rockhold, M.L.; Gee, G.W.; Fayer, M.J.; and Campbell, M.D. 1991. "Lysimeters: Data Acquisition and Analysis." *Lysimeters for Evapotranspiration and Environmental Measurements, Proceedings of the International Symposium on Lysimetry, Honolulu, Hawaii, July 23-25, 1991.* Allen, R.G.; Howell, T.A.; Pruitt, W.O.; Walter, I.A.; and Jensen, M.E., eds. Pages 362-370. New York, New York: American Society of Civil Engineers. TIC: 258304.

176152 Klein, S.A. 1977. "Calculation of Monthly Average Insolation on Tilted Surfaces." *Solar Energy, 19,* 325-329. New York, New York: Pergamon Press. TIC: 258029.

176484 Klein, S.A. and Theilacker, J.C. 1981. "An Algorithm for Calculating Monthly-Average Radiation on Inclined Surfaces." *Journal of Solar Energy Engineering, 103,* 29-33. New York, New York: American Society of Mechanical Engineers. TIC: 258097.

177134 Klemmedson, J.O. and Smith, J.G. 1964. "Cheatgrass (Bromus Tectorum L.)." *The Botanical Review, XXX,* 226-262. Bronx, New York: New York Botanical Garden. TIC: 258182.

176757 Kustas, W.P.; Perry, E.M.; Doraiswamy, P.C.; and Moran, M.S. 1994. "Using Satellite Remote Sensing to Extrapolate Evapotranspiration Estimates in Time and Space Over a Semiarid Rangeland Basin." *Remote Sensing of Environment, 49,* 275-286. New York, New York: Elsevier. TIC: 258221.

158511 LeCain, G.D.; Lu, N.; and Kurzmack, M. 2002. *Use of Temperature, Pressure, and Water Potential Data to Estimate Infiltration and Monitor Percolation in Pagany Wash Associated with the Winter of 1997–98 El Niño Precipitation, Yucca Mountain, Nevada.* Water Resources Investigations Report 02-4035. Denver, Colorado: U.S. Geological Survey. TIC: 252641.

177926 Leffler, J.A.; Ivans, C.Y.; Ryel, R.J.; and Caldwell, M.M. 2004. "Gas Exchange and Growth Responses of the Desert Shrubs Artemisia Tridentata and Chrysothamnus Nauseosus to Shallow- Vs. Deep-Soil Water in a Glasshouse Experiment." *Environmental and Experimental Botany, 51,* 9-19. New York, New York: Elsevier. TIC: 258768.

178535 Lei, S.A. 1999. "Gradient Analysis of Pinyon-Juniper Woodland in a Southern Nevada Mountain Range." *USDA Forest Service Proceedings, Odgen, Utah. RMRS-P-9,* 64-68. Washington, D.C.: U.S. Department of Agriculture, Forest Service. ACC: MOL.20061214.0118.

163183 Levitt, D.G.; Lohrstorfer, C.F.; Sully, M.J.; and Ginanni, J.M. 1996. "An Arid Zone Lysimeter Facility for Performance Assessment and Closure Investigations at the Nevada Test Site." *HLW, LLW, Mixed Wastes and Environmental Restoration — Working Towards a Cleaner Environment, WM '96, Proceedings, February 25-29, 1996, Tucson, Arizona.* Tucson, Arizona: Laser Options. TIC: 254421.

177521 Levitt, D.G.; Sully, M.J.; Dozier, B.L.; and Lohrstorfer, C.F. 1999. "Determining the Performance of an Arid Zone Radioactive Waste Site Through Site Characterization, Modeling and Monitoring." *HLW, LLW, Mixed Wastes and Environmental Restoration — Working Towards a Cleaner Environment, WM'99, Proceedings, February 28-March 4, 1999, Tucson, Arizona.* Tucson, Arizona: WM Symposia. TIC: 250888.

177166 Li-Cor 1989. *LI-1600 Steady State Porometer Instruction Manual, Revision 6.* Lincoln, Nebraska: Li-Cor. TIC: 258419.

100589 Lichty, R.W. and McKinley, P.W. 1995. *Estimates of Ground-Water Recharge Rates for Two Small Basins in Central Nevada.* Water-Resources Investigations Report 94-4104. Denver, Colorado: U.S. Geological Survey. ACC: MOL.19960924.0524.

178081 Lide, D.R., ed. 2006. *CRC Handbook of Chemistry and Physics.* 87th Edition. Boca Raton, Florida: CRC Press. TIC: 258634.

178313 Liepert, B.G. and Romanou, A. 2005. "Global Dimming and Brightening and the Water Cycle." *Bulletin of the American Meteorological Society, 86,* (5), 622-623. Boston, Massachusetts: American Meteorological Society. TIC: 258566.

177142 Link, S.O.; Gee, G.W.; and Downs, J.L. 1990. "The Effect of Water Stress on Phenological and Ecophysiological Characteristics of Cheatgrass and Sandberg's Bluegrass." *Journal of Range Management, 43,* (6), 506-513. Denver, Colorado: Society for Range Management. TIC: 258327.

176739 Liu, H.Q. and Huete, A. 1995. "A Feedback Based Modification of the NDVI to Minimize Canopy Background and Atmospheric Noise." *IEEE Transactions on Geoscience and Remote Sensing, 33,* (2), 457-465. New York, New York: Institute of Electrical and Electronics Engineers. TIC: 258205.

176821 Lo Seen Chong, D.; Mougin, E.; and Gastellu-Etchegorry, J.P. 1993. "Relating the Global Vegetation Index to Net Primary Productivity and Actual Evapotranspiration Over Africa." *International Journal of Remote Sensing, 14,* (8), 1517-1546. Bristol, Pennsylvania: Taylor & Francis. TIC: 258271.

176789 Lookingbill, T.R. and Urban, D.L. 2003. "Spatial Estimation of Air Temperature Differences for Landscape-Scale Studies in Montane Environments." *Agricultural and Forest Meteorology, 114,* 141-151. New York, New York: Elsevier. TIC: 258240.

154273 Looney, B.B. and Falta, R.W., eds. 2000. *Vadose Zone, Science and Technology Solutions.* Two volumes. Columbia, Ohio: Battelle Press. TIC: 249256.

175964 Lopes, T.J. and Evetts, D.M. 2004. *Ground-Water Pumpage and Artificial Recharge Estimates for Calendar Year 2000 and Average Annual Natural Recharge and Interbasin Flow by Hydrographic Area, Nevada.* Scientific Investigations Report 2004-5239. Carson City, Nevada: U.S. Geological Service. ACC: MOL.20060116.0023.

177164 Mack, R.N. 1981. "Invasion of Bromus Tectorum L. into Western North America: An Ecological Chronicle." *Agro-Ecosystems, 7,* 145-165. Amsterdam, The Netherlands: Elsevier. TIC: 258181.

177141 Mack, R.N. and Pyke, D.A. 1983. "The Demography of Bromus Tectorum: Variation in Time and Space." *Journal of Ecology, 71,* 69-93. London, England: British Ecological Society. TIC: 258422.

178540 Maher, K.; DePaolo, D.J.; Conrad, M.E.; and Serne, R.J. 2003. "Vadose Zone Infiltration Rate at Hanford, Washington, Inferred from Sr Isotope Measurements." *Water Resources Research, 39,* (8), SBH 3-1-SBH 3-14. Washington, D.C.: American Geophysical Union. TIC: 259095.

125317 Maidment, D.R., ed. 1993. *Handbook of Hydrology.* New York, New York: McGraw-Hill. TIC: 236568.

177362 Markham, B.L. and Barker, J.L. 1987. "Thematic Mapper Bandpass Solar Exoatmospheric Irradiances." *International Journal of Remote Sensing, 8,* (3), 517-523. Elmont, New York: Taylor & Francis. TIC: 258864.

177512 Marks, D. 2001. "Introduction to Special Section: Reynolds Creek Experimental Watershed." *Water Resources Research, 37,* (11), 2817. Washington, D.C.: American Geophysical Union. ACC: MOL.20060712.0232.

177504 Marks, D.; Cooley, K.R.; Robertson, D.C.; and Winstral, A. 2001. "Long-Term Snow Database, Reynolds Creek Experimental Watershed, Idaho, United States." *Water Resources Research, 37,* (11), 2835-2838. Washington, D.C: American Geophysical Union. ACC: MOL.20060712.0227.

178523 Mata-González, R.; McLendon, T.; and Martin, D.W. 2005. "The Inappropriate Use of Crop Transpiration Coefficient (K_c) to Estimate Evapotranspiration in Arid Ecosystems: A Review." *Arid Land Research and Management, 19,* 285-295. Philadelphia, Pennsylvania: Taylor & Francis. TIC: 258847.

177370 Maurer, D.K. and Berger, D.L. 1997. *Subsurface Flow and Water Yield from Watersheds Tributary to Eagle Valley Hydrographic Area, West-Central Nevada.* Water-Resources Investigations Report 97-4191. Carson City, Nevada: U.S. Geological Survey. ACC: MOL.20060808.0017.

100598 Maxey, G.B. and Eakin, T.E. 1950. *Ground Water in White River Valley, White Pine, Nye, and Lincoln Counties, Nevada.* Water Resources Bulletin No. 8. Carson City, Nevada: State of Nevada, Office of the State Engineer. TIC: 216819.

177910 McElroy, D.L. 1993. *Soil Moisture Monitoring Results at the Radioactive Waste Management Complex of the Idaho National Engineering Laboratory, FY-1993.* EGG-WM-11066. Idaho Falls, Idaho: EG&G Idaho, Idaho National Engineering Laboratory. ACC: MOL.20061016.0249.

178204 MDH Engineered Solutions 2003. *Evaluation of Computer Models for Predicting the Fate and Transport of Salt in Soil and Groundwater, Phase I Report.* Pub. No: T/403. Edmonton, Alberta, Canada: Alberta Environment, Science and Standards Branch. TIC: 258784.

176887 Moreno, J.M. and Oechel, W.C., eds. 1995. *Global Change and Mediterranean-Type Ecosystems.* Ecological Studies, Vol. 117, Analysis and Synthesis. Lange, O.L. and Mooney, H.A., eds. New York, New York: Springer. TIC: 258254.

178316 Mutziger, A.J.; Burt, C.M.; Howes, D.J.; and Allen, R.G. 2005. "Comparison of Measured and FAO-56 Modeled Evaporation from Bare Soil." *Journal of Irrigation and Drainage Engineering, 131,* (1), 59-72. Reston, Virginia: American Society of Civil Engineers. TIC: 258629.

177143 Naumburg, E.; Housman, D.C.; Huxman T.E.; Charlet, T.N.; Loik, M.E.; and Smith, S.D. 2003. "Photosynthetic Responses of Mojave Desert Shrubs to Free Air CO_2 Enrichment are Greatest During Wet Years." *Global Change Biology, 9,* 276-285. Malden, Massachusetts: Blackwell Science. TIC: 258423.

174673 Newman, D. 1992. *Element Stewardship Abstract for Bromus Rubens.* Arlington, Virginia: The Nature Conservancy. TIC: 257691.

178863 Nichols, W.D. 2000. *Regional Ground-Water Evapotranspiration and Ground-Water Budgets, Great Basin, Nevada.* U.S. Geological Survey Professional Paper 1628. Reston, Virginia: U.S. Geological Survey. ACC: LLR.20070213.0076.

178674 NOAA (National Oceanic and Atmospheric Administration) 2002. *Monthly Station Normals of Temperature, Precipitation, and Heating and Cooling Degree Days 1971-2000, 02 Arizona.* Climatography of the United States No. 81. Asheville, North Carolina: National Oceanic and Atomspheric Administration. ACC: MOL.20070125.0051.

178676 NOAA 2002. *Monthly Station Normals of Temperature, Precipitation, and Heating and Cooling Degree Days 1971-2000, 26 Nevada.* Climatography of the United States No. 81. Asheville, North Carolina: National Oceanic and Atmospheric Administration. ACC: MOL.20070125.0053.

178675 NOAA 2002. *Monthly Station Normals of Temperature, Precipitation, and Heating and Cooling Degree Days 1971-2000, 29 New Mexico.* Climatography of the United States No. 81. Asheville, North Carolina: National Oceanic and Atmospheric Administration. ACC: MOL.20070125.0052.

178677 NOAA 2002. *Monthly Station Normals of Temperature, Precipitation, and Heating and Cooling Degree Days 1971-2000, 42 Utah.* Climatography of the United States No. 81. Asheville, North Carolina: National Oceanic and Atmospheric Administration. ACC: MOL.20070125.0054.

178673 NOAA 2002. *Monthly Station Normals of Temperature, Precipitation, and Heating and Cooling Degree Days 1971-2000, 45 Washington.* Climatography of the United States No. 81. Asheville, North Carolina: National Oceanic and Atmospheric Administration. ACC: MOL.20070125.0050.

160500 Nobel, P.S. 1983. "Plants and Fluxes." *Biophysical Plant Physiology and Ecology.* Pages 461-523. New York, New York: W.H. Freeman and Company. TIC: 252952.

159953 Nobel, P.S. 1983. "Temperature—Energy Budgets." *Biophysical Plant Physiology and Ecology.* Pages 339-386. New York, New York: W.H. Freeman and Company. TIC: 253519.

163274 NRC (U.S. Nuclear Regulatory Commission) 2003. *Yucca Mountain Review Plan, Final Report.* NUREG-1804, Rev. 2. Washington, D.C.: U.S. Nuclear Regulatory Commission, Office of Nuclear Material Safety and Safeguards. TIC: 254568.

102160 O'Farrell, T.P. and Collins, E. 1984. *1983 Biotic Studies of Yucca Mountain, Nevada Test Site, Nye County, Nevada.* EGG 10282-2031 S-764-R. Goleta, California: EG&G Energy Measurements. ACC: HQS.19880517.1810.

176483 Orgill, J.F. and Hollands, K.G.T. 1977. "Correlation Equation for Hourly Diffuse Radiation on a Horizontal Surface." *Solar Energy, 19,* 357-359. New York, New York: Pergamon Press. TIC: 258101.

177161 Pataki, D.E.; Huxman, T.E.; Jordan, D.N.; Zitzer, S.F.; Coleman, J.S.; Smith, S.D.; Nowak, R.S.; and Seemann, J.R. 2000. "Water Use of Two Mojave Desert Shrubs Under Elevated CO_2." *Global Change Biology, 6,* 889-897. Malden, Massachusetts: Blackwell Science. TIC: 258767.

177091 Phillips, D.L.; Dolph, J.; and Marks, D. 1992. "A Comparison of Geostatistical Procedures for Spatial Analysis of Precipitation in Mountainous Terrain." *Agricultural and Forest Meteorology, 58,* 119-141. Amsterdam, The Netherlands: Elsevier. TIC: 258405.

177503 Pierson, F.B.; Slaughter, C.W.; and Cram, Z.K. 2001. "Long-Term Stream Discharge and Suspended-Sediment Database, Reynolds Creek Experimental Watershed, Idaho, United States." *Water Resources Research, 37,* (11), 2857-2861. Washington, D.C.: American Geophysical Union. ACC: MOL.20060712.0226.

178131 Ravi, V. and Williams, J.R. 1998. *Estimation of Infiltration Rate In the Vadose Zone: Compilation of Simple Mathematical Models.* EPA/600/R-97/128a. Volume 1. Cincinnati, Ohio: U.S. Environmental Protection Agency. ACC: MOL.20061030.0075.

177336 Ray, S.S. and Dadhwal, V.K. 2001. "Estimation of Crop Evapotranspiration of Irrigation Command Area Using Remote Sensing and GIS." *Agricultural Water Management, 49,* 239-249. New York, New York: Elsevier. TIC: 258486.

176480 Reindl, D.T.; Beckman, W.A.; and Duffie, J.A. 1990. "Evaluation of Hourly Tilted Surface Radiation Models." *Solar Energy, 45,* (1), 9-17. New York, New York: Pergamon Press. TIC: 258102.

103450 Resource Concepts 1989. *Soil Survey of Yucca Mountain Study Area, Nye County, Nevada.* NWPO EV 003-89. Carson City, Nevada: Resource Concepts. TIC: 206227.

176482 Revfeim, K.J.A. 1976. "Solar Radiation at a Site of Known Orientation on the Earth's Surface." *Journal of Applied Meteorology, 15,* 651-656. Boston, Massachusetts: American Meteorological Society. TIC: 258104.

177165 Rice, K.J.; Black, R.A.; Radamaker, G.; and Evans, R.D. 1992. "Photosynthesis, Growth, and Biomass Allocation in Habitat Ecotypes of Cheatgrass (Bromus Tectorum)." *Functional Ecology, 6,* 32-40. Malden, Massachusetts: Blackwell Publishing. TIC: 258322.

177927 Richards, J.H. and Caldwell, M.M. 1987. "Hydraulic Lift: Substantial Nocturnal Water Transport Between Soil Layers by Artemisia Tridentata Roots." *Oecologia, 73,* 486-489. Berlin, Germany: Springer-Verlag. TIC: 258563.

177635 Rickard, W.H. 1985. "Shoot Production and Mineral Nutrient Assimilation in Cheatgrass Communities." *Northwest Science, 59,* (3), 169-179. Pullman, Washington: Washington State University Press. TIC: 258186.

176758 Rivard, B.; Arvidson, R.E.; Duncan, I.J.; Sultan, M.; and El Kaliouby, B. 1992. "Varnish, Sediment, and Rock Controls on Spectral Reflectance of Outcrops in Arid Regions." *Geology, 20,* 295-298. Boulder, Colorado: Geological Society of America. TIC: 258227.

176741 Rivard, B.; Petroy, S.B.; and Miller, J.R. 1993. "Measured Effects of Desert Varnish on the Mid-Infrared Spectra of Weathered Rocks as an Aid to TIMS Imagery Interpretation." *IEEE Transactions on Geoscience and Remote Sensing, 31,* (1), 284-291. New York, New York: Institute of Electrical and Electronics Engineers. TIC: 258207.

177738 Rodríguez, E.; Morris, C.S.; Belz, J.E.; Chapin, E.C.; Martin, J.M.; Daffer, W.; and Hensley, S. 2005. *An Assessment of the SRTM Topographic Products.* D-31639. Pasadena, California: Jet Propulsion Laboratory. ACC: MOL.20061011.0062.

178583 Rose, C.W. 1968. "Evaporation from Bare Soil Under High Radiation Conditions." Chapter 7 of *Transactions.* Volume 1. Pages 57-66. New York, New York: Elsevier. TIC: 258919.

177526 Rosenberg, N.J.; Blad, B.L.; and Verma, S.B. 1983. *Microclimate, The Biological Environment.* 2nd Edition. New York, New York: John Wiley & Sons. TIC: 222878.

178534 Roundy, B.A. and Vernon, J.L. 1999. "Watershed Values and Conditions Associated with Pinyon-Juniper Communities." *USDA Forest Service Proceedings, Odgen, Utah. RMRS-P-9,* 172-187. Washington, D.C.: U.S. Department of Agriculture, Forest Service. ACC: MOL.20061214.0117.

177246 Rouse, J.W., Jr.; Haas, R.H.; Schell, J.A.; and Deering, D.W. 1974. "Monitoring Vegetation Systems in the Great Plains with ERTS." *Third Earth Resources Technology Satellite-1 Symposium, Volume I: Technical Presentations, Section A, Proceedings of a Symposium held by Goddard Space Flight Center, Washington, D.C., December 10-14, 1973.* Freden, S.C. and Mercanti, E.P., eds. Paper A 20. Pages 309-317. Washington, D.C.: National Aeronautics and Space Administration. ACC: MOL.20060501.0105.

103614 Rundel, P.W. and Gibson, A.C. 1996. *Ecological Communities and Processes in a Mojave Desert Ecosystem: Rock Valley, Nevada.* New York, New York: Cambridge University Press. TIC: 223005.

128001 Rundel, P.W. and Nobel, P.S. 1991. "Structure and Function in Desert Root Systems." *Plant Root Growth, An Ecological Perspective, Special Publication Number 10,* 349-378. London, England: Blackwell Scientific Publications. TIC: 242299.

176819 Running, S.W. and Nemani, R.R. 1991. "Regional Hydrologic and Carbon Balance Responses of Forests Resulting from Potential Climate Change." *Climatic Change, 19,* (4), 349-368. Dordrecht, The Netherlands: Kluwer Academic Publishers. TIC: 258228.

177632 Ryel, R.J.; Caldwell, M.M.; Leffler, A.J.; and Yoder, C.K. 2003. "Rapid Soil Moisture Recharge to Depth by Roots in a Stand of Artemisia Tridentata." *Ecology, 84,* (3), 757-764. Washington, D.C.: Ecological Society of America. TIC: 258010.

176569 Sanchez, A. 2006. Conducting Confirmatory Field Observations for Special Infiltration Project [partial submittal]. Scientific Notebook SN-M&O-SCI-053-V1. Pages 1-83. ACC: MOL.20060306.0186.

107233 Scanlon, B.R. 1991. "Evaluation of Moisture Flux from Chloride Data in Desert Soils." *Journal of Hydrology, 128,* 137-156. Amsterdam, The Netherlands: Elsevier. TIC: 224126.

177213 Scanlon, B.R.; Christman, M.; Reedy, R.C.; Porro, I.; Simunek, J.; and Flerchinger, G.N. 2002. "Intercode Comparisons for Simulating Water Balance of Surficial Sediments in Semiarid Regions." *Water Resources Research, 38,* (12), 59/1-59/16. Washington, D.C.: American Geophysical Union. TIC: 255363.

178109 Scanlon, B.R.; Keese, K.; Reedy, R.C.; Simunek, J.; and Andraski, B.J. 2003. "Variations in Flow and Transport in Thick Desert Vadose Zones in Response to Paleoclimate Forcing (0-90 kyr): Field Measurements, Modeling, and Uncertainties." *Water Resources Research, 39,* (7), 3/1-3/6. Washington, D.C.: American Geophysical Union. TIC: 258648.

177852 Scanlon, B.R.; Langford, R.P.; and Goldsmith, R.S. 1999. "Relationship Between Geomorphic Settings and Unsaturated Flow in an Arid Setting." *Water Resources Research, 35,* (4), 983-999. Washington, D.C.: American Geophysical Union. TIC: 252295.

175977 Scanlon, B.R.; Levitt, D.G.; Reedy, R.C.; Keese, K.E.; and Sully, M.J. 2005. "Ecological Controls on Water-Cycle Response to Climate Variability in Deserts." *Proceedings of the National Academy of Sciences of the United States of America, 102,* (17), 6033-6038. Washington, D.C.: National Academy of Sciences of the USA. TIC: 257888.

142228 Scanlon, B.R.; Tyler, S.W.; and Wierenga, P.J. 1997. "Hydrologic Issues in Arid, Unsaturated Systems and Implications for Contaminant Transport." *Reviews of Geophysics, 35,* (4), 461-490. Washington, D.C.: American Geophysical Union. TIC: 246881.

177638 Schenk, H.J. and Jackson, R.B. 2002. "Rooting Depths, Lateral Root Spreads and Below-Ground/Above-Ground Allometries of Plants in Water-Limited Ecosystems." *Journal of Ecology, 90,* 480-494. Oxford, England: Blackwell Publishing. TIC: 257985.

178754 Schroeder, P.R. and Peyton, R.L. 1987. *Verification of the Lateral Drainage Component of the HELP Model Using Physical Models.* EPA/600/2-87/049. Cincinnati, Ohio: U.S. Environmental Protection Agency, Hazardous Waste Engineering Research Laboratory. ACC: MOL.20070126.0113.

178857 Schroeder, P.R. and Peyton, R.L. 1988. *Verification of the Hydrologic Evaluation of Landfill Performance (HELP) Model Using Field Data.* EPA/600/S-2-87/050. Washington, D.C.: U.S. Government Printing Office. ACC: LLR.20070213.0075.

178136 Schroeder, P.R.; Lloyd, C.M.; Zappi, P.A.; and Aziz, N.M. 1994. *The Hydrologic Evaluation of Landfill Performance (HELP) Model, User's Guide for Version 3.* EPA/600/R-94/168a. Washington, D.C.: U.S. Environmental Protection Agency, Office of Research and Development. ACC: MOL.20060831.0163.

178065 Schultz, B. and McAdoo, K. 2002. *Common Sagebrush in Nevada.* Special Publication SP-02-02. Reno, Nevada: University of Nevada, Reno, Cooperative Extension. TIC: 258542.

104181 Scott, R.B. and Bonk, J. 1984. *Preliminary Geologic Map of Yucca Mountain, Nye County, Nevada, with Geologic Sections.* Open-File Report 84-494. Denver, Colorado: U.S. Geological Survey. ACC: HQS.19880517.1443.

177853 Scott, R.L.; Shuttleworth, W.J.; Keefer, T.O.; and Warrick, A.W. 2000. "Modeling Multiyear Observations of Soil Moisture Recharge in the Semiarid American Southwest." *Water Resource Research, 36,* (8), 2233-2247. Washington, D.C.: American Geophysical Union. TIC: 252313.

176764 Seevers, P.M. and Ottmann, R.W. 1994. "Evapotranspiration Estimation Using a Normalized Difference Vegetation Index Transformation of Satellite Data." *Hydrological Sciences Journal, 39,* (4), 333-345. Wallingford, Oxfordshire, England: International Association of Hydrological Sciences. TIC: 258233.

176824 Sellers, P.J.; Berry, J.A.; Collatz, G.J.; Field, C.B.; and Hall, F.G. 1992. "Canopy Reflectance, Photosynthesis, and Transpiration. III. A Reanalysis Using Improved Leaf Models and a New Canopy Integration Scheme." *Remote Sensing of Environment, 42,* (3), 187-216. New York, New York: Elsevier. TIC: 258268.

177480 Sevruk, B. 1982. *Methods of Correction for Systematic Error in Point Precipitation Measurement for Operational Use.* Operational Hydrology Report No. 21. WMO - No. 589. Geneva, Switzerland: World Meteorological Organization. TIC: 258537.

177501 Seyfried, M.; Harris, R.; Marks, D.; and Jacob, B. 2001. "Geographic Database, Reynolds Creek Experimental Watershed, Idaho, United States." *Water Resources Research, 37,* (11), 2825-2829. Washington, D.C.: American Geophysical Union. ACC: MOL.20060712.0225.

177505 Seyfried, M.S.; Flerchinger, G.N.; Murdock, M.D.; Hanson, C.L.; and Van Vactor, S. 2001. "Long-Term Soil Temperature Database, Reynolds Creek Experimental Watershed, Idaho, United States." *Water Resources Research, 37,* (11), 2843-2846. Washington, D.C.: American Geophysical Union. ACC: MOL.20060712.0228.

177515 Seyfried, M.S.; Hanson, C.L.; Murdock, M.D.; and Van Vactor, S. 2001. "Long-Term Lysimeter Database, Reynolds Creek Experimental Watershed, Idaho, United States." *Water Resources Research, 37,* (11), 2853-2856. Washington, D.C.: American Geophysical Union. ACC: MOL.20060821.0215.

177506 Seyfried, M.S.; Murdock, M.D.; Hanson, C.L.; Flerchinger, G.N.; and Van Vactor, S. 2001. "Long-Term Soil Water Content Database, Reynolds Creek Experimental Watershed, Idaho, United States." *Water Resources Research, 37,* (11), 2847-2851. Washington, D.C.: American Geophysical Union. ACC: MOL.20060712.0229.

178060 Seyfried, M.S.; Schwinning, S.; Walvoord, M.A.; Pockman, W.T.; Newman, B.D.; Jackson, R.B.; and Phillips, F.M. 2005. "Ecohydrological Control of Deep Drainage in Arid and Semiarid Regions." *Ecology, 86,* (2), 277-287. Washington, D.C.: Ecological Society of America. TIC: 258561.

178000 Shurbaji, A.-R. and Campbell, A.R. 1997. "Study of Evaporation and Recharge in Desert Soil Using Environmental Tracers, New Mexico, USA." *Environmental Geology, 29,* (3/4), 147-151. New York, New York: Springer-Verlag. TIC: 258630.

150228 Slate, J.L.; Berry, M.E.; Rowley, P.D.; Fridrich, C.J.; Morgan, K.S.; Workman, J.B.; Young, O.D.; Dixon, G.L.; Williams, V.S.; McKee, E.H.; Ponce, D.A.; Hildenbrand, T.G.; Swadley, W C; Lundstrom, S.C.; Ekren, E.B.; Warren, R.G.; Cole, J.C.; Fleck, R.J.; Lanphere, M.A.; Sawyer, D.A.; Minor, S.A.; Grunwald, D.J.; Laczniak, R.J.; Menges, C.M.; Yount, J.C.; Jayko, A.S.; Mankinen, E.A.; Davidson, J.G.; Morin, R.L.; and Blakely, R.J. 2000. *Digital Geologic Map of the Nevada Test Site and Vicinity, Nye, Lincoln and Clark Counties, Nevada, and Inyo County, California, Revision 4; Digital Aeromagnetic Map of the Nevada Test Site and Vicinity, Nye, Lincoln, and Clark Counties, Nevada, and Inyo County, California; and Digital Isostatic Gravity Map of the Nevada Test Site and Vicinity, Nye, Lincoln, and Clark Counties, Nevada, and Inyo County, California.* Open-File Report 99-554—A, —B, and —C. Denver, Colorado: U.S. Geological Survey. TIC: 248049; 251985; 251981.

177354 Slaughter, C.W.; Marks, D.; Flerchinger, G.N.; Van Vactor, S.S.; and Burgess, M. 2001. "Thirty-Five Years of Research Data Collection at the Reynolds Creek Experimental Watershed, Idaho, United States." *Water Resources Research, 37,* (11), 2819–2823. Washington, D.C.: American Geophysical Union. TIC: 258491.

177358 Smith, B. and Sandwell, D. 2003. "Accuracy and Resolution of Shuttle Radar Topography Mission Data." *Geophysical Research Letters, 30,* (9), 20-1-20-4. Washington, D.C.: American Geophysical Union. TIC: 258765.

179904 Smith, R.B. 2004. "Mountain Meteorology and Regional Climates." Chapter 9 of *Atmospheric Turbulence and Mesoscale Meteorology: Scientific Research Inspired by Doug Lilly.* Fedorovich, E.; Rotunno, R.; and Stevens, B., eds. Pages 193-222. New York, New York: Cambridge University Press. TIC: 259247.

103628 Smith, S.D.; Herr, C.A.; Leary, K.L.; and Piorkowski, J.M. 1995. "Soil-Plant Water Relations in a Mojave Desert Mixed Shrub Community: A Comparison of Three Geomorphic Surfaces." *Journal of Arid Environments, 29,* (3), 339-351. New York, New York: Academic Press. TIC: 240834.

103636 Smith, S.D.; Monson, R.K.; and Anderson, J.E. 1997. *Physiological Ecology of North American Desert Plants.* New York, New York: Springer-Verlag. TIC: 242260.

177081 SNL (Sandia National Laboratories) 2006. *Data Analysis for Infiltration Modeling: Extracted Weather Station Data Used to Represent Present-Day and Potential Future Climate Conditions in the Vicinity of Yucca Mountain.* ANL-MGR-MD-000015 REV 00. Las Vegas, Nevada: Sandia National Laboratories. ACC: DOC.20070109.0002.

176745 Song, C.; Woodcock, C.E.; Seto, K.C.; ax Lenney, M.; and Macomber, S.A. 2001. "Classification and Change Detection Using Landsat TM Data: When and How to Correct Atmospheric Effects?" *Remote Sensing of Environment, 75,* 230-244. New York, New York: Elsevier. TIC: 258212.

176751 Spatz, D.M. and Taranik, J.V. 1989. "Regional Analysis of Tertiary Volcanic Calderas (Western U.S.) Using Landsat Thematic Mapper Imagery." *Remote Sensing of Environment, 28,* 257-272. New York, New York: Elsevier. TIC: 258217.

177281 Stephens, D.B. and Knowlton, R., Jr. 1986. "Soil Water Movement and Recharge Through Sand at a Semiarid Site in New Mexico." *Water Resources Research, 22,* (6), 881-889. Washington, D.C.: American Geophysical Union. TIC: 258458.

177146 Stewart, G. and Hull, A.C. 1949. "Cheatgrass (Bromus Tectorum L.) - An Ecologic Intruder in Southern Idaho." *Ecology, 30,* (1), 58-74. Ogden, Utah: Ecological Society of America, Duke University Press. TIC: 258421.

176705 Stothoff, S.A.; Or, D.; Groeneveld, D.P.; and Jones, S.B. 1999. "The Effect of Vegetation on Infiltration in Shallow Soils Underlain by Fissured Bedrock." *Journal of Hydrology, 218,* 169-190. New York, New York: Elsevier. TIC: 257887.

177928 Sturges, D.L. and Trlica, M.J. 1978. "Root Weights and Carbohydrate Reserves of Big Sagebrush." *Ecology, 59,* (6), 1282-1285. Tempe, Arizona: Ecological Society of America. TIC: 258560.

106958 Sweetkind, D.S.; Verbeek, E.R.; Geslin, J.K.; and Moyer, T.C. 1995. *Fracture Character of the Paintbrush Tuff Nonwelded Hydrologic Unit, Yucca Mountain, Nevada.* Administrative Report. Denver, Colorado: U.S. Geological Survey. ACC: MOL.19960311.0125.

106959 Sweetkind, D.S.; Verbeek, E.R.; Singer, F.R.; Byers, F.M., Jr.; and Martin, L.G. 1995. *Surface Fracture Network at Pavement P2001, Fran Ridge, Near Yucca Mountain, Nye County, Nevada, Draft.* Administrative Report. Denver, Colorado: U.S. Geological Survey. ACC: MOL.19960603.0119.

176735 Szilagyi, J. 2000. "Can a Vegetation Index Derived from Remote Sensing be Indicative of Areal Transpiration?" *Ecological Modelling.* 127. 65-79. New York, New York: Elsevier. TIC: 258201.

176840 Szilagyi, J. 2002. "Vegetation Indices to Aid Areal Evapotranspiration Estimations." *Journal of Hydrologic Engineering, 7,* (5), 368-372. Reston, Virginia: American Society of Civil Engineers. TIC: 258267.

176839 Szilagyi, J.; Rundquist, D.C.; Gosselin, D.C.; and Parlange, M.B. 1998. "NDVI Relationship to Monthly Evaporation." *Geophysical Research Letters, 25,* (10), 1753-1756. Washington, D.C.: American Geophysical Union. TIC: 258266.

177653 Tasumi, M.; Allen, R.G.; Trezza, R.; and Wright, J.L. 2005. "Satellite-Based Energy Balance to Assess Within-Population Variance of Crop Coefficient Curves." *Journal of Irrigation and Drainage Engineering, 131,* (1), 94-109. Reston, Virginia: American Society of Civil Engineers. TIC: 258519.

177620 Tausch, R.J.; Wigand, P.E.; and Burkhardt, J.W. 1993. "Viewpoint: Plant Community Thresholds, Multiple Steady States, and Multiple Successional Pathways: Legacy of the Quaternary?." *Journal of Range Management, 46,* (5), 439-447. Wheat Ridge, Colorado: Society for Range Management. TIC: 258420.

178312 Temesgen, B.; Allen, R.G.; and Jensen, D.T. 1999. "Adjusting Temperature Parameters to Reflect Well-Watered Conditions." *Journal of Irrigation and Drainage Engineering, 125,* (1), 26-33. New York, New York: American Society of Civil Engineers. TIC: 258490.

177727 Thomas, J.M.; Carlton, S.M.; and Hines, L.B. 1989. *Ground-Water Hydrology and Simulated Effects of Development in Smith Creek Valley, a Hydrologically Closed Basin in Lander County, Nevada.* U.S. Geological Survey Professional Paper 1409-E. Denver, Colorado: U.S. Geological Survey. ACC: MOL.20061115.0002.

109462 Thompson, R.S.; Anderson, K.H.; and Bartlein, P.J. 1999. *Atlas of Relations Between Climatic Parameters and Distributions of Important Trees and Shrubs in North America - Introduction and Conifers.* Professional Paper 1650-A. Washington, D.C.: U.S. Geological Survey. TIC: 245909.

177641 Tirmenstein, D. 1999. "Artemisia Tridentata Spp. Tridentata." Washington, D.C.: U.S. Department of Agriculture, Forest Service. Accessed September 5, 2006. ACC: MOL.20060907.0010. URL: http://www.fs.fed.us/database/feis/plants/shrub/arttri/all.html

177642 Tirmenstein, D. 1999. "Chrysothamnus Nauseosus." Washington, D.C.: U.S. Department of Agriculture, Forest Service. Accessed September 5, 2006. ACC: MOL.20060907.0011. URL: http://www.fs.fed.us/database/feis/plants/shrub/chrnau/all.html

178315 Tolk, J.A. and Howell, T.A. 2001. "Measured and Simulated Evapotranspiration of Grain Sorghum Grown with Full and Limited Irrigation in Three High Plains Soils." *Transactions of the ASAE, 44,* (6), 1553-1558. St. Joseph, Michigan: American Society of Agricultural Engineers. TIC: 258632.

177149 Upadhyaya, M.K.; Turkington, R.; and McIlvride, D. 1986. "The Biology of Canadian Weeds. 75. Bromus Tectorum L." *Canadian Journal of Plant Science, 66,* 689-709. Ottawa (Ontario), Canada: Agricultural Institute of Canada. TIC: 258324.

178073 USDA (U.S. Department of Agriculture) 2002. "Big Sagebrush, Artemisia Tridentata Nutt." *Plant Fact Sheet.* Washington, D.C.: U.S. Department of Agriculture, Natural Resources Conservation Service. ACC: MOL.20060712.0207.

173916 USDA 2004. *Soil Survey of Nye County, Nevada, Southwest Part.* Two parts. Washington, D.C.: U.S. Department of Agriculture. ACC: MOL.20050614.0146.

160355 USGS (U.S. Geological Survey) 2001. *Simulation of Net Infiltration for Modern and Potential Future Climates.* ANL-NBS-HS-000032 REV 00 ICN 02. Denver, Colorado: U.S. Geological Survey. ACC: MOL.20011119.0334.

177649 Utah State University 2002. "Indian Ricegrass." *Range Plants of Utah.* Logan, Utah: Utah State University, Cooperative Extension. Accessed July 11, 2006. TIC: 258428. URL: http://extension.usu.edu/rangeplants/Grasses/indianricegrass.htm

177648 Utah State University 2002. "Needle-and-Thread." *Range Plants of Utah.* Logan, Utah: Utah State University, Cooperative Extension. Accessed July 11, 2006. TIC: 258429. URL: http://extension.usu.edu/rangeplants/Grasses/needleandthread.htm

177646 Utah State University 2002. "Pinyon Pine." *Range Plants of Utah.* Logan, Utah: Utah State University, Cooperative Extension. Accessed July 11, 2006. TIC: 258431. URL: http://extension.usu.edu/rangeplants/Woody/pinyonpine.htm

177644 Utah State University 2002. "Rubber Rabbitbrush." *Range Plants of Utah.* Logan, Utah: Utah State University, Cooperative Extension. Accessed July 11, 2006. TIC: 258432. URL: http://extension.usu.edu/rangeplants/Woody/rubberrabbitbrush.htm

177647 Utah State University 2002. "Sandberg Bluegrass." *Range Plants of Utah.* Logan, Utah: Utah State University, Cooperative Extension. Accessed July 11, 2006. TIC: 258430. URL: http://extension.usu.edu/rangeplants/Grasses/sandbergbluegrass.htm

177650 Utah State University 2002. "Squirreltail." *Range Plants of Utah.* Logan, Utah: Utah State University, Cooperative Extension. Accessed July 11 2006. TIC: 258427. URL: http://extension.usu.edu/rangeplants/Grasses/squirreltail.htm

177643 Utah State University 2004. "Utah Juniper, Juniperus Osteosperma, Cupressaceae or the Cypress Family." *Utah Trees and Forests.* Logan, Utah: Utah State University, Cooperative Extension. Accessed July 11, 2006. TIC: 258426. URL: http://extension.usu.edu/forestry/utahforests/treeid/juos.htm

176050 van der Kamp, G.; Hayashi, M.; and Gallen, D. 2003. "Comparing the Hydrology of Grassed and Cultivated Catchments in the Semi-Arid Canadian Prairies." *Hydrological Processes, 17,* 559-575. New York, New York: John Wiley & Sons. TIC: 257865.

176481 Vignola, F. and McDaniels, D.K. 1986. "Beam–Global Correlations in the Pacific Northwest." *Solar Energy, 36,* (5), 409-418. New York, New York: Pergamon Press. TIC: 258103.

176746 Vogelmann, J.E.; Helder, D.; Morfitt, R.; Choate, M.J.; Merchant, J.W.; and Bulley, H. 2001. "Effects of Landsat 5 Thematic Mapper and Landsat 7 Enhanced Thematic Mapper Plus Radiometric and Geometric Calibrations and Corrections on Landscape Characterization." *Remote Sensing of Environment, 78,* 55-70. New York, New York: Elsevier. TIC: 258213.

176752 Walter-Shea, E.A.; Privette, J.; Cornell, D.; Mesarch, M.A.; and Hays, C.J. 1997. "Relations Between Directional Spectral Vegetation Indices and Leaf Area and Absorbed Radiation in Alfalfa." *Remote Sensing of Environment, 61,* 162-177. New York, New York: Elsevier. TIC: 258218.

176737 Walthall, C.L.; Norman, J.M.; Welles, J.M.; Campbell, G.; and Blad, B.L. 1985. "Simple Equation to Approximate the Bidirectional Reflectance from Vegetative Canopies and Bare Soil Surfaces." *Applied Optics, 24,* (3), 383-387. Washington, D.C.: Optical Society of America. TIC: 258203.

178108 Walvoord, M.A.; Plummer, M.A.; Phillips, F.M.; and Wolfsberg, A.V. 2002. "Deep Arid System Hydrodynamics 1. Equilibrium States and Response Times in Thick Desert Vadose Zones." *Water Resources Research, 38,* (12), 44/1-44/15. Washington, D.C.: American Geophysical Union. TIC: 255212.

176761 Wang, J.; Rich, P.M.; and Price, K.P. 2003. "Temporal Responses of NDVI to Precipitation and Temperature in the Central Great Plains, USA." *International Journal of Remote Sensing, 24,* (11), 2345-2364. New York, New York: Taylor & Francis. TIC: 258231.

177931 Weber, D.J.; Hess, W.M.; Bhat, R.B.; and Huang, J. 1993. "Chrysothamnus: A Rubber-Producing Semi-Arid Shrub." *Proceeding of the Second National Symposium NEW CROPS-Exploration, Research, and Commercialization, Indianapolis, Indiana, October 6-9, 1991.* Janick, J. and Simon, J.E., eds. Pages 355-357. New York, New York: John Wiley & Sons. TIC: 258559.

178536 West, N.E. 1999. "Distribution, Composition, and Classification of Current Juniper-Pinyon Woodlands and Savannas Across Western North America." *USDA Forest Service Proceedings, Odgen, Utah. RMRS-P-9,* 20-23. Washington, D.C.: U.S. Department of Agriculture, Forest Service. ACC: MOL.20061214.0119.

160442 Whelan, J.F.; Paces, J.B.; and Peterman, Z.E. 2002. "Physical and Stable-Isotope Evidence for Formation of Secondary Calcite and Silica in the Unsaturated Zone, Yucca Mountain, Nevada." *Applied Geochemistry, 17,* (6), 735-750. New York, New York: Elsevier. TIC: 253462.

177113 Wight, J.R. and Hanson, C.L. 1990. "Crop Coefficients for Rangeland." *Journal of Range Management, 43,* (6), 482-485. Denver, Colorado: Society for Range Management. TIC: 258409.

177104 Wight, J.R.; Hanson, C.L.; and Cooley, K.R. 1986. "Modeling Evapotranspiration from Sagebrush-Grass Rangeland." *Journal of Range Management, 39,* (1), 81-85. Denver, Colorado: Society for Range Management. TIC: 258408.

177624 Wills, C.A. and Ostler, W.K. 2001. *Ecology of the Nevada Test Site: An Annotated Bibliography.* DOE/NV/11718–594. Las Vegas, Nevada: U.S. Department of Energy, National Nuclear Security Administration. ACC: MOL.20060712.0222.

172585 Wilson, J.L. and Guan, H. 2004. "Mountain-Block Hydrology and Mountain-Front Recharge." In *Groundwater Recharge in a Desert Environment: The Southwestern United States,* Hogan, J.F.; Phillips, F.M.; and Scanlon, B.R., eds, *Water Science and Application 9.* Pages 113-137. Washington, D.C.: American Geophysical Union. TIC: 256760.

177304 Wood, W.W. and Sanford, W.E. 1995. "Chemical and Isotopic Methods for Quantifying Ground-Water Recharge in a Regional, Semiarid Environment." *Ground Water, 33,* (3), 458-468. Dublin, Ohio: Ground Water Publishing. TIC: 258473.

176108 Woolhiser, D.A. and Pegram, G.G.S. 1979. "Maximum Likelihood Estimation of Fourier Coefficients to Describe Seasonal Variations of Parameters in Stochastic Daily Precipitation Models." *Journal of Applied Meteorology, 18,* 34-42. Boston, Massachusetts: American Meteorological Society. TIC: 257886.

165987 WRCC (Western Regional Climate Center) 2002. *Western U.S. Historical Summaries by State [Arizona, California, Idaho, Nevada, New Mexico, Oregon, Utah, and Washington]*. Reno, Nevada: Western Regional Climate Center, Desert Research Institute. TIC: 253357.

162307 WRCC 2003. "Nogales 6N, Arizona, NCDC 1971-2000 Monthly Normals." Reno, Nevada: Desert Research Institute, Western Regional Climate Center. Accessed March 4, 2003. TIC: 253915. http://www.wrcc.dri.edu/cgi-bin/cliNORMNCDC2000.pl?aznoga

152233 WRCC 1997. "Spokane, Washington: Normals, Means, and Extremes." Reno, Nevada: Desert Research Institute, Western Regional Climate Center. Accessed August 23, 2000. TIC: 248857. http://www.wrcc.dri.edu/cgi-bin/clilcd.pl?wa24157

177167 Yoder, C.K. and Nowak, R.S. 1999. "Soil Moisture Extraction by Evergreen and Drought-Deciduous Shrubs in the Mojave Desert During Wet and Dry Years." *Journal of Arid Environments, 42,* 81-96. San Diego, California: Academic Press. TIC: 258179.

178539 Zhu, C. 2000. "Estimate of Recharge from Radiocarbon Dating of Groundwater and Numerical Flow and Transport Modeling." *Water Resources Research, 36,* (9), 2607-2620. Washington, D.C.: American Geophysical Union. TIC: 252313.

177639 Zlatnik, E. 1999. "Juniperus Osteosperma." Washington, D.C.: U.S. Department of Agriculture, Forest Service. Accessed September 5, 2006. ACC: MOL.20060907.0012. URL: http://www.fs.fed.us/database/feis/plants/tree/junost/all.html

9.2 CODES, STANDARDS, REGULATIONS, AND PROCEDURES

176544 10 CFR 63. 2006. Energy: Disposal of High-Level Radioactive Wastes in a Geologic Repository at Yucca Mountain, Nevada. Internet Accessible.

178394 70 FR 53313. Implementation of a Dose Standard After 10,000 Years. Internet Accessible.

157394 ANSI/NCSL Z540-2-1997. 1997. *American National Standard for Calibration — U.S. Guide to the Expression of Uncertainty in Measurement.* Boulder, Colorado: NCSL International. TIC: 251472.

153195 ASME PTC 19.1-1998. *Test Uncertainty, Instruments and Apparatus.* New York, New York: American Society of Mechanical Engineers. TIC: 249327.

151762 IEEE/ASTM SI 10-1997. 1997. *Standard for Use of the International System of Units (SI): The Modern Metric System.* New York, New York: Institute of Electrical and Electronics Engineers. TIC: 240989.

IM-PRO-003, Rev. 02, ICN 0. *Software Management*. Washington, DC: U.S. Department of Energy, Office of Civilian Radioactive Waste Management. ACC: DOC.20070228.0002.

SCI-PRO-001, Rev. 02, ICN 0. *Qualification of Unqualified Data*. Washington, DC: U.S. Department of Energy, Office of Civilian Radioactive Waste Management. ACC: DOC.20070522.0016.

SCI-PRO-002, Rev. 02, ICN 0. *Planning for Science Activities*. Washington, DC: U.S. Department of Energy, Office of Civilian Radioactive Waste Management. ACC: DOC.20070320.0001.

SCI_PRO-006, Rev. 02, ICN 00. *Models.* Washington, DC: U.S. Department of Energy, Office of Civilian Radioactive Waste Management. ACC: DOC.20070420.0001.

9.3 SOURCE DATA, LISTED BY DATA TRACKING NUMBER

151139 GS000308315121.003. Meteorological Stations Selected to Represent Future Climate States at Yucca Mountain, Nevada. Submittal date: 03/14/2000.

176317 GS011208312212.004. SN-USGS-SCI-113 V1: Empirical Calculation of Soil Thickness Based on Field Measurements. Submittal date: 01/24/2002.

175972 GS910808312212.001. Geohydrologic Data Collected from Shallow Neutron-Access Boreholes and Resultant Preliminary Geohydrologic Evaluations, Yucca Mountain Area, Nye County, Nevada. Submittal date: 08/09/1991.

107374 GS941208312121.001. Surface-Water Discharge Data for the Yucca Mountain Area, Southern Nevada and Southern California, 1994 Water Year. Submittal date: 11/30/1994.

107375 GS960908312121.001. Surface-Water Discharge Data for the Yucca Mountain Area, Southern Nevada and Southern California, 1995 Water Year. Submittal date: 10/10/1996.

146872 GS960908312211.004. Heat Dissipation Probe Data: Bleach Bone Ridge 3/95 - 11/95. Submittal date: 09/19/1996.

107128 GS971208314221.003. Revised Bedrock Geologic Map of the Central Block Area, Yucca Mountain, Nevada. Submittal date: 12/30/1997.

174491 LB0208HYDSTRAT.001. 2002 UZ Model Grid Components. Submittal date: 08/26/2002.

146848 MO0003COV00095.000. Coverage: Scotbons. Submittal date: 03/01/2000.

152554 MO0004QGFMPICK.000. Lithostratigraphic Contacts from MO9811MWDGFM03.000 to be Qualified Under the Data Qualification Plan, TDP-NBS-GS-000001. Submittal date: 04/04/2000.

153777 MO0012MWDGFM02.002. Geologic Framework Model (GFM2000). Submittal date: 12/18/2000.

166731 MO0206SEPQ1998.001. Meteorological Monitoring Data for 1998. Submittal date: 06/26/2002.

166730 MO0209SEPQ2000.001. Meteorological Monitoring Data for 2000. Submittal date: 09/09/2002.

166164 MO0305SEP01MET.002. Meteorological Monitoring Data for 2001. Submittal date: 05/21/2003.

166163 MO0305SEP02MET.002. Meteorological Monitoring Data for 2002. Submittal date: 05/21/2003.

176092 MO0312SEPQ1993.001. Meteorological Monitoring Data for 1993. Submittal date: 12/24/2003.

167116 MO0312SEPQ1997.001. Meteorological Monitoring Data for 1997. Submittal date: 12/24/2003.

176097 MO0503SEPMMD03.001. Meteorological Monitoring Data for 2003. Submittal date: 03/03/2005.

175064 MO0508SEPFEPLA.002. LA FEP List and Screening. Submittal date: 08/22/2005.

177249 MO0512COV05112.000. Special Infiltration Project - Survey of Field Observation Locations. Submittal date: 12/12/2005.

177236 MO0601GSCSPINF.000. Special Infiltration Project Position of Field Observation Locations of Ecological Study Plot Corners and Streamflow Gauges. Submittal date: 01/30/2006.

176585 MO0603GSCGEOMP.000. Digital Geologic Map of Nevada Test Site and Vicinity, Nye, Lincoln, and Clark Counties, Nevada, and Inyo County, California. Submittal date: 03/09/2006.

179889 MO0603SEPSTREA.000. Surface Water Discharge Data Collected During Water Year 1998 from Streamflow Gauge Stations 102512531, 102512533 and 102512537. Submittal date: 03/22/2006.

177121 MO0603SPAGRIDD.003. Gridded Infiltration Model Input File Showing Infiltration Hydrogeologic Units. Submittal date: 03/06/2006.

178089 MO0605SEPALTRN.000. Alternative Soil Units, Hydraulic Parameters, and Associated Statistics for Infiltration Modeling at Yucca Mountain, NV. Submittal date: 05/31/2006.

177237 MO0605SEPHOURL.000. Hourly Precipitation Data for Four NOAA Meteorological Stations for the Years 1948 through 2005. Submittal date: 05/17/2006.

178663 MO0605SEPSGP05.000. Storage Gauge Precipitation 2005. Submittal date: 05/19/2006.

179890 MO0605SEPSURFC.000. Surface Water Discharge Data Collected During WY 1993 from Streamflow Gauge Station No. 102512533 (Pagany Wash No. 1), and During WY 1995 from Streamflow Gauge Station No. 1025125372 (Lower Split Wash). Submittal date: 05/15/2006.

177122 MO0605SPABEDRK.005. Bedrock Saturated Hydraulic Conductivity for Infiltration Hydrogeologic Units. Submittal date: 05/25/2006.

180539 MO0605SPAFABRP.004. Supporting Calculation Files for the Assessment of Bedrock Saturated Hydraulic Conductivity. Submittal date: 05/25/2006.

177135 MO0605SPASPOKA.000. Spokane Weather Data - Daily Values. Submittal date: 05/19/2006.

177136 MO0606SEPRECIP.001. Precipitation Data Collected at Yucca Mountain Meteorological Sites 1 through 5 for the Period January 1, 1988 through December 31, 1992. Submittal date: 06/01/2006.

178079 MO0607SEPMED94.000. Air Temperature Data from Meteorological Data Acquisition (MEDA) Station 05 for 1994 - 2004. Submittal date: 07/12/2006.

178311 MO0607SEPMMD04.001. Meteorological Monitoring Data for 2004. Submittal date: 07/18/2006.

178082 MO0608SPASDFIM.006. Soil Depth Input File for Use in Infiltration Modeling. Submittal date: 8/31/2006.

178328 MO0610METMND05.000. Meteorological Monitoring Data for 2005. Submittal date: 09/18/2006.

177247 MO9901ESPYMNYE.000. Ecological Study Plots at Yucca Mountain, Nye County, Nevada. Submittal date: 01/04/1999.

116056 MO9903CLIMATOL.001. Climatological Tables from 1986-1997 Meteorological Data from Site 1 through Site 9 EFPD Meteorological Sites. Submittal date: 03/23/1999.

150118 MO9905VMMDAJ90.000. Validated Meteorological Monitoring Data, April - June 1990. Submittal date: 05/21/1999.

150056 MO9905VMMDJM90.000. Validated Meteorological Monitoring Data, January - March 1990. Submittal date: 05/21/1999.

150119 MO9905VMMDJS90.000. Validated Meteorological Monitoring Data, July - September 1990. Submittal date: 05/21/1999.

150120 MO9905VMMDOD90.000. Validated Meteorological Monitoring Data, October - December 1990. Submittal date: 05/21/1999.

109059 MO9906GPS98410.000. Yucca Mountain Project (YMP) Borehole Locations. Submittal date: 06/23/1999.

157659 MO9907GCESPYMN.000. Ground Cover Data for Ecological Study Plots at Yucca Mountain, Nevada. Submittal date: 07/29/1999.

177169 MO9907SADESYYM.000. Soil Analysis Data for Ecological Study Plots at Yucca Mountain, Nevada. Submittal date: 07/28/1999.

177238 SN0511NOAADATA.001. NOAA and SORAD Meteorological and Solar Radiation Data Measured at Desert Rock, Nevada. Submittal date: 11/22/2005.

177239 SN0601ALANDSAT.001. Landsat Imagery of Yucca Mountain from January 1998 to August 2002. Submittal date: 02/07/2006.

177240 SN0601DOQQYM98.001. Digital Ortho Quarter Quad (DOQQ), Yucca Mountain 06/01/1998 - 08/18/1998. Submittal date: 01/24/2006.

176122 SN0601PRECPTMP.002. Developed Precipitation Data at NTS Sites from 1959-2004, and Precipitation and Temperature Data at Amargosa Farms-Garey from 1965-2005.Submittal date: 01/16/2006.

177241 SN0601QBSAT802.001. Quickbird (QB) Satellite Imagery, Yucca Mountain, 31 August 2002. Submittal date: 04/25/2006.

177242 SN0601SRTMDTED.001. Shuttle Radar Topography Mission (SRTM) Digital Terrain Elevation Data (DTED) of Yucca Mountain, February 2000. Submittal date: 01/23/2006.

177917 SN0603DWEATHER.002. Developed Weather Station Data for Beowawe, NV (1982-2004), Delta, UT (1968-2004), Hobbs, NM (1947-2004), Nogales, AZ (1948-1983), Rosalia, WA (1949-2004), St. John, WA (1963-2004), and Spokane, WA (1948-2004). Submittal date: 03/20/2006.

179875 SN0608T0502206.020. Climate Data, Geospatial Information, and Soil Moisture and Property Data for Reynolds Creek Experimental Watershed (RCEW), Idaho. Submittal date: 08/21/2006.

177912 SN0608WEATHER1.005. Temperature, Precipitation, Wind Speed, Relative Humidity, Dew Point Temperatures, and Barometric Pressure Data Collected from 1993-2004 Measured at Yucca Mountain Weather Stations 1,2,3,6, and 9. Submittal date: 08/23/2006.

9.4 DEVELOPED DATA, LISTED BY DATA TRACKING NUMBER

MO0602SPAPRECP.000. Daily Precipitation for Water Years 1998, 2001, and 2002 – Sites 2, 3 & 4. Submittal date: 02/16/2006.

MO0602SPAWEATH.000. Daily Weather Data for Water Years 1998, 2001, 2002, Yucca Mountain Meteorological Site 1. Submittal date: 02/16/2006.

MO0603SPAREFET.000. Reference Evapotranspiration (ET) for Yucca Mountain. Submittal date: 03/01/2006.

MO0605SPADAYWA.000. Daily Weather Data for Spokane Washington. Submittal date: 05/24/2006.

MO0606SPABASAL.001. Basal Transpiration Coefficients (K_{cb}) for Yucca Mountain Vegetation Associations (1993, 1991, and 1990 Water Years). Submittal date: 06/28/2006.

MO0606SPATRANS.000. Transpiration Coefficients (K_{cb}) for a Bromus Tectorum Monoculture. Submittal date: 06/05/2006.

MO0606SPAVEGAS.001. Cover Data for Vegetation Associations at Yucca Mountain (1990,1991, and 1993). Submittal date: 06/26/2006.

MO0607SEPTOTAL.003. Total Annual Precipitation for Water Years 1990, 1991 and 1993 from Yucca Mountain Meteorological Sites 2, 3 and 4. Submittal date: 07/13/2006.

MO0610SPALINEA.000. Linear Regression Analysis for the MASSIF K_{cb} Versus NDVI Correlation. Submittal date: 10/19/2006.

MO0703MASSIFIM.001. Independent Verification of MASSIF Infiltration Model. Submittal date: 03/05/2007.

SN0602T0502206.003. Solar Radiation and Reference Evapotranspiration (ET_0) on Inclined Surfaces. Submittal date: 02/20/2006.

SN0602T0502206.004. Calculated Daily Diffuse and Direct Solar Radiation from 2000 through 2004 and Measured at Desert Rock, Nevada. Submittal date: 03/13/2006.

SN0602T0502206.005. Evaluation of Hargreaves Solar Radiation Coefficient, K_{RS}, for Yucca Mountain. Submittal date: 02/28/2006.

SN0603T0502206.006. Evaluation of Published Diffuse and Total Solar Radiation Correlations for Yucca Mountain. Submittal date: 03/13/2006.

SN0606T0502206.011. Geospatial Inputs for Net Infiltration Model of Yucca Mountain. Submittal date: 05/31/2006.

SN0606T0502206.012. Daily Normalized Difference Vegetation Index (NDVI) Estimation for Selected Slopes/Azimuths at Yucca Mountain. Submittal date: 05/31/2006.

SN0606T0502206.014. Calculated Weather Summary for Present Day and Future Climates. Submittal date: 06/07/2006.

SN0607T0502206.016. Analysis of Soil Water Storage in Nevada Test Site (NTS) and Reynolds Creek Experimental Watershed (RCEW) Lysimeters. Submittal date: 08/24/2006.

SN0608ASSEMBLY.001. Assembly Data for Geospatial Inputs to MASSIF Model of Yucca Mountain. Submittal data: 08/15/2006.

SN0608CWATSHED.001. Calibration Watersheds at Yucca Mountain Based on Pour Point Stream Gages. Submittal date: 08/15/2006.

SN0608DRAINDYM.001. Drainage Delineation at Yucca Mountain. Submittal date: 08/15/2006.

SN0608NDVIANAL.001. Analysis Data Supporting Estimations of Normalized Difference Vegetation Index (NDVI) at Yucca Mountain, 1997–2002. Submittal date: 08/15/2006.

SN0608NDVIAUXD.001. Auxiliary Data Used in Calculations of Daily Normalized Difference Vegetation Index (NDVI) Estimation for Selected Slopes/Azimuths at Yucca Mountain and Geospatial Inputs for Net Infiltration Model of Yucca Mountain. Submittal date: 08/15/2006.

SN0608NDVILSTM.001. Normalized Difference Vegetation Index (NDVI) Derived from Calibrated and Geocorrected LANDSAT TM Data at Yucca Mountain, 1997–2002. Submittal date: 08/15/2006.

SN0608NDVIQBIM.001. Normalized Difference Vegetation Index (NDVI) Imagery Derived from Calibrated and Georectified Quickbird Imagery of Yucca Mountain, August 31, 2002. Submittal date: 08/15/2006.

SN0608NSSLOPES.001. Normalized Difference Vegetation Index (NDVI) on North and South Slopes and Supporting Data at Yucca Mountain, 1997–2002. Submittal date: 08/15/2006.

SN0608PVRATYMT.001. Potential Vegetation Response (PVR) at Yucca Mountain, 1997–2002. Submittal date: 08/15/2006.

SN0608T0502206.019. Temperature Model Fitting Parameters for Present-Day and Future Climate Proxy Sites. Submittal date: 08/16/2006.

SN0609AZSLPHST.001. Distribution of Slope on North-South Facing Terrain Slopes at Yucca Mountain. Submittal date: 09/18/2006.

SN0609LSTMPROC.001. Thematic Mapper Processing Overview. Submittal date: 09/21/2006.

SN0609T0502206.021. Alternative Infiltration Model Inputs. Submittal date: 09/18/2006.

SN0609T0502206.022. Alternative Infiltration Modeling Results. Submittal date: 09/18/2006.

SN0609T0502206.023. Precipitation Parameters Calculated using Fourier Analyses for Modern Interglacial and Future Climates. Submittal date: 09/07/2006.

SN0609T0502206.024. Monsoon Net Infiltration Results. Submittal date: 09/18/2006. [Preliminary]
SN0609T0502206.025. Calculated Weather Summary for Monsoon Climate. Submittal date: 09/21/2006. [Preliminary]

SN0609T0502206.026. Calculated Weather Summary for Present-Day Climate. Submittal date: 09/21/2006. [Preliminary]

SN0609T0502206.027. Calculated Weather Summary for Glacial Transition Climate. Submittal date: 09/21/2006. [Preliminary]

SN0609T0502206.028. Present-Day Net Infiltration Results. Submittal date: 09/22/2006. [Preliminary]
SN0609T0502206.029. Glacial Transition Net Infiltration Results. Submittal date: 09/28/2006. [Preliminary]
SN0610T0502206.030. Average Daily Wind Speed at 2 m Height above the Ground. Submittal date: 10/09/2006.

SN0610T0502206.031. Precipitation Duration Functions for the Present-Day, Monsoon, and Glacial Transition Climates for Infiltration Modeling at Yucca Mountain, NV. Submittal date: 10/09/2006.

SN0610T0502206.032. MASSIF Calculation of Net Infiltration at Yucca Mountain. Submittal date: 10/31/2006. [Preliminary]

SN0610T0502206.033. Latin Hypercube Sample (LHS) Input and Output Files for MASSIF Calculation of Net Infiltration at Yucca Mountain. Submittal date: 10/20/2006. [Preliminary]

SN0612FTPRNUZB.002. Unsaturated Zone (UZ) Boundary and Repository Footprint. Submittal date: 12/14/2006.

SN0612T0502206.039. Estimation of Uncertainty on Upscaled Uniform Value for Soil Depth Class 4. Submittal date: 12/06/2006.

SN0701SPALAYER.002. Spatial Data Layers at Yucca Mountain. Submittal date: 01/16/2007.

SN0701T0502206.034. Present-Day Net Infiltration Results, Rev 1. Submittal date: 01/11/2007.

SN0701T0502206.035. Glacial Transition Net Infiltration Results, Rev 1. Submittal date: 01/11/2007.

SN0701T0502206.036. Monsoon Net Infiltration Results, Rev 1. Submittal date: 01/11/2007.

SN0701T0502206.037. MASSIF Calculation of Net Infiltration at Yucca Mountain, Rev 1. Submittal date: 02/13/2007.

SN0701T0502206.040. Calculated Weather Summary for Present Day Climate, Rev 1. Submittal date: 01/10/2007.

SN0701T0502206.041. Calculated Weather Summary for Monsoon Climate, Rev 1. Submittal date: 01/10/2007.

SN0701T0502206.042. Calculated Weather Summary for Glacial Transition Climate Rev 1. Submittal date: 01/10/2007.

SN0701T0502206.043. Latin Hypercube Sample (LHS) Input and Output Files for MASSIF Calculation of Net Infiltration at Yucca Mountain. Submittal date: 01/11/2007.

SN0701T0502206.044. Sensitivity Analysis of Average Net Infiltration for Three Climates. Submittal date: 01/18/2007.

SN0701T0502206.045. Comparison of the Calculated Precipitation Record with Site Data. Submittal date: 01/23/2007.

SN0704T0502206.047. Recharge Estimates Used to Validate the Massif Model of Net Infiltration at Yucca Mountain. Submittal date: 04/19/2007

9.5 SOFTWARE CODES

176015 ArcGIS Desktop V. 9.1. 2005. WINDOWS XP. STN: 11205-9.1-00.

178783 ENVI+IDL V. 4.2. 2005. XP. STN: 11204-4.2-00.

139422 INFIL VV2.0. 2001. PC, Windows NT 4.0. 10307-2.0-00.

147608 Infil VVA_2.a1. 2001. DEC Alpha, VMS AXP V7.2-1. 10253-A_2.a1-00.

178784 LHS V. 2.51. 2006. OPENVMS 8.2. STN: 10205-2.51-01.

173438 MVIEW V. 4.0. 2005. WINDOWS 2000. STN: 10072-4.0-00.

178228 Šimùnek, J.; Šejna, M.; and van Genuchten, M.Th. 1999. *The HYDRUS-2D Software Package for Simulating the Two-Dimensional Movement of Water, Heat, and Multiple Solutes in Variably-Saturated Media.* Version 2.0. Riverside, California: U.S. Salinity Laboratory, U.S. Department of Agriculture. ACC: MOL.20061101.0023.

178140 Šimùnek, J.; van Genuchten, M.Th.; and Šejna, M. 2005. *The HYDRUS-1D Software Package for Simulating the One-Dimensional Movement of Water, Heat, and Multiple Solutes in Variably-Saturated Media.* Version 3.0. Riverside, California: University of California, Department of Environmental Sciences. ACC: MOL.20060828.0051.